

**TOXIC SPECIES AND PARTICULATE EMISSIONS FROM WOOD
AND POOL FIRES**

By

Bintu Grema Mustafa

**Submitted in accordance with the requirements for the Degree of Doctor
of Philosophy**

The University of Leeds

School of Chemical and Process Engineering

December, 2019

The candidate confirms that the work submitted is her own, except where work which has formed part of jointly-authored publications has been included. The contribution of the candidate and the other authors to this work has been explicitly indicated below. The candidate confirms that appropriate credit has been given within the thesis where reference has been made to the work of others.

- I. Mustafa B.G., Mat Kiah M.H., Andrews G.E., Phylaktou H.N., Li H.(2019) **Smoke particle size distribution in pine wood fires**, Proceedings of the ninth International Seminar on Fire and Explosion Hazards, St. Petersburg (April, 2019)

(Included in Chapter 4)

All the experimental work, analysis of results and writing up of the publication were carried out by Bintu Grema Mustafa. Miss H. Mat Kiah participated in carrying out the experimental procedures, Dr. Phylaktou, Prof. Andrews and Dr. Hu Li supervised the research work and proof-read the publication

- II. Bintu G. Mustafa, Miss H. Mat Kiah, Juma Al-Nahdi, Gordon E. Andrews, Herodotos N. Phylaktou, Hu Li (2019) **Toxic Emissions from Processed Wood in Cone Calorimeter Tests** (Submitted to Fire and Materials) Under review.

(Included in Chapter 4)

All the experimental work, analysis of results and writing up of the publication were carried out by Bintu Grema Mustafa. Miss H. Mat Kiah assisted with experimental procedures, Juma Al-Nahdi (MSc. student) participated in one of the tests, Dr. Phylaktou, Prof. Andrews and Dr. Hu Li supervised the research work and proof-read the publication

- III. Bintu Grema Mustafa, Miss H. Mat Kiah, Gordon E. Andrews, Herodotos N. Phylaktou, Hu Li (2020) **Toxic Gas Emissions from Plywood Fires**, Wood and Fire Safety 2020; 9th International Scientific Conference, Strbske Pleso, Slovakia May, 2020

(Included in Chapter 4)

All the experimental work, analysis of results and writing up of the publication were carried out by Bintu Grema Mustafa. Miss H. Mat Kiah participated in carrying out the experimental procedures, Dr. Phylaktou, Prof. Andrews and Dr. Hu Li supervised the research work, and proof-read the publication.

- IV. B.G. Mustafa, M. H. Mat Kiah, A. Irshad, G.E. Andrews, H.N. Phylaktou, H. Li and B.M. Gibbs (2019) **Rich Biomass Combustion: Gaseous and Particle Number Emissions**, Fuel, July 2019

(Included in chapter 5)

All the experimental work, analysis of results and writing up of the publication were carried out by Bintu Grema Mustafa. Miss H. Mat Kiah participated in carrying out the experimental procedures, A. Irshad participated in the experimental procedure and setup, Dr. Phylaktou, Prof. Andrews and Dr. Hu Li supervised the research work and proof-read the publication, B.M. Gibbs had an input on the analysis of the results.

- V. Bintu G. Mustafa, Rosmawati Zahari, Yangfu Zeng, Miss H. Mat Kiah, Gordon E. Andrews and Herodotos N. Phylaktou (2020) **Pine Wood Crib Fires: Toxic Gas Emissions Using a 5m³ Compartment Fire**, Wood and Fire Safety 2020; 9th International Scientific Conference, Strbske Pleso, Slovakia May, 2020

(Included in Chapter 6)

All the experimental work, analysis of results and writing up of the publication were carried out by Bintu Grema Mustafa. Miss H. Mat Kiah participated in carrying out the experimental procedures, Rosmawati Zahari and Yanfu Zeng (MSc. Students) participated in the tests, Dr. Phylaktou and Prof. Andrews supervised the research work, and proof-read the publication.

Dedication

This thesis is dedicated to my father

Grema Mustafa

who isn't here to witness this achievement

and to my mother

Yamoduram Grema Mustapha

who always believed in me

Acknowledgement

All praises and adoration are due to Allah, the Beneficent, the most Merciful.

My sincere appreciation goes to my supervisors Dr. Herodotos N. Phylaktou, Prof. Gordon Andrews and Dr. Hu Li for their constant support, guidance and encouragement throughout the PhD programme.

I would also like to thank the SCAPE laboratory technicians; Ed Woodhouse, David Instrell, Gurdev Bhogal, Adrianne Cunliffe and Karine Alves Thorne for their time and support during the experiments.

The support and encouragement of my colleagues and friends: Miss Hasimawaty Binti Mat Kiah, Dr. Aysha Irshad, Jackie Chan, James Hammerton, Yanlong Wu, Ebikienmo Peters, Francis Olanrewaju, Dr. Zainab Adiya, Dr. Sergio Ramirez, Yabalu Zakari and Habiba M. Sani is greatly appreciated. Many thanks to Aishajane Saidu, Rahila Saidu and Hadiza Aliyu for making my stay in Leeds a memorable one.

Special thanks to Ibrahim Ibrahim for the help and words of encouragement.

The Petroleum Technology Development Fund (PTDF Nigeria) and the University of Maiduguri are greatly acknowledged for the sponsorship and study fellowship.

Lastly, my gratitude goes to my family, especially my mother for instilling in me a sense of dedication and hard work and for the constant prayer. Amina, Umar, Hafsat, Ramatu, Fatima, Bilkisu, Falmata, Aisha, Tijjani and Mustafa Grema Mustapha; thank you for the love, care, support and prayers throughout this journey. Thank you aunt Falmata B. Modu for always being there.

Abstract

Fire fatalities in the UK are attributed to smoke inhalation especially in dwellings. Another serious issue of great concern is the exposure to respirable particles of sizes less than 0.1μ in diameter found in smoke and soot and these have not been given much attention despite the health hazards associated with them. The main aim of this research was to quantitatively look at the toxic emissions (toxic gases and particulates) under different fire conditions for wood based materials relevant to residential fires and in pool fires relevant to industrial scenarios.

Different classes of wood (Natural, Processed and Plywoods) used in construction and furnishings were investigated under free ventilation conditions and restricted ventilation conditions using the standard cone calorimeter and the controlled atmosphere cone calorimeter modified to enable raw gas sampling. Pool fires (Diesel, Lubricating oil and olive oil) were also investigated using the freely ventilated standard cone calorimeter.

Pine wood crib and diesel pool of different sizes were investigated in a 5m^3 fire test compartment at varying ventilation rates. Toxic concentrations were measured through a heated sampling line using a heated FTIR analyser, calibrated for 65 species.

An important finding was the overwhelming toxic gases produced by low temperature smouldering fires exceeding the impairment of escape threshold and the lethality threshold by a factor of 60-10 000 on an impairment of escape basis and a factor of 4-100 on lethal basis.

The real-time particle size, number and mass distribution from the burning fuels was obtained using the DMS 500 particle size analyser and this showed a bimodal distribution, representing a nucleation mode and an agglomeration/accumulation mode. The particle size distribution on a number basis showed a peak of 20 nm in the nano particle size range and a peak of 200 nm in the agglomeration range for most fires. These nano particles (20 nm) will penetrate the lungs in the event of fire, potentially leading to impairment of escape and eventually death due to the effects that fine particles have on the lungs thereby making them a major toxic hazard in fires. To the knowledge of the

author, this is the first time that particulates in this size range (20nm and less) have been quantified from burning materials.

The modified cone calorimeter proved to be a good technique for realistic determination of toxic yields and particle size distributions when used with the heated FTIR and the DMS 500 analysers.

Table of Contents

Dedication	iv
Acknowledgement	v
Abstract	vi
Table of Contents	viii
List of Figures	xvi
List of Tables	xxvi
Glossary of Terms and Symbols	xxviii
Chapter 1 Introduction	1
1.1 Fire Fatalities and Injuries- Statistics	1
1.2 The Influence of the Materials in the Fire Load	3
1.3 Some Relevant Historical Fires	6
1.3.1 The Cleveland Clinic Fire 1929	6
1.3.2 The MGM Grand Fire, 1980	7
1.3.3 The Rose Park Nursing Home Fire 2004	7
1.3.4 The Grenfell Tower Fire 2017	8
1.3.5 Piper Alpha 1988.....	9
1.3.6 Buncefield 2005	9
1.4 Particulates in Smoke – Longer term effects.....	10
1.5 General Legislative Background.....	13
1.6 Aim and Objectives of this Work.....	14
Chapter 2 Literature Review	15
2.1 Fire Chemistry	15
2.2 Types of fires.....	16
2.2.1 Solid Materials.....	16
2.2.1.1 Wood	16
2.2.2 Pool Fires	17
2.3 Compartment Fires.....	18
2.4 ISO19706 Characterisation of Fire Stages	19
2.4.1 Non-flaming Combustion.....	20
2.4.2 Well-Ventilated Flaming Fires	21
2.4.3 Low/Under Ventilated Fires	22
2.4.4 Post Flashover Fires	22

2.5	Hazards From Fire	23
2.5.1	Heat	23
2.5.1.1	Hyperthermia:.....	23
2.5.1.2	Body Surface Burns:.....	24
2.5.1.3	Burns to the Respiratory Tract:.....	24
2.5.2	Smoke.....	24
2.6	Toxic Combustion Products.....	25
2.6.1	Asphyxiant Gases	25
2.6.1.1	Carbon Monoxide	26
2.6.1.2	Hydrogen Cyanide.....	26
2.6.2	Irritants	27
2.7	Influence of Ventilation on Fires	31
2.8	Factors Determining Toxic Hazard	37
2.8.1	Equivalence Ratio:	37
2.8.1.1	Air-to- Fuel Ratio	37
2.8.2	Heat Release Rate:.....	39
2.8.3	Yield	41
2.9	Sampling of Fire Gases	44
2.10	Review of Methods for Studying Toxic Effluents	45
2.10.1	Bench-Scale Methods for Generating Toxic Effluents.....	45
2.10.1.1	The Smoke Density Chamber.....	46
2.10.1.2	The Controlled Atmosphere Cone Calorimeter (CACC)	48
2.10.1.3	The steady state tube furnace (SSTF).....	51
2.11	Particulates.....	52
2.11.1	Health and Environmental Impacts of Particulate Matter	53
2.11.2	Characteristics of Smoke Aerosol Formation in Fires	54
2.11.3	Particle and Aerosol Characteristics:	55
2.11.3.1	Particle Size and Shape	55
2.11.3.2	Particle Size Distribution.....	57
2.11.3.3	Mass and Number Concentration	58
2.11.3.4	Particulate Chemical Composition.....	59
2.11.4	Particulate Yield/ Emission Index	60
2.11.5	Techniques for Sampling and Analysis of Particulates/Aerosol in Fire Effluents	61

2.11.5.1 Gravimetric Sampling Method of Total Particle Mass Concentration	62
2.11.5.2 Cascade Impactor:	62
2.11.5.3 Low Pressure Impactor:.....	63
2.11.5.4 Electrical Low Pressure Impactor (ELPI):	63
2.11.5.5 Electrical Low Pressure Impactor Plus (ELPI+):	64
2.11.5.6 Differential Mobility Spectrometer (DMS 500):.....	64
2.11.6 Sampling Train and Sampling Line	66
2.11.7 Particulate Measurement Studies	67
2.12 Fire Hazard Analysis/ Toxicity Assessment.....	72
2.12.1 Calculation of Fractional Effective Dose.....	73
2.12.1.1 Levin's N-GAS Model	73
2.12.1.2 Purser's LC ₅₀ Model.....	75
2.12.1.3 Fractional Irritant Concentration (FIC) Model.....	76
2.12.2 Other Methods for Toxicity Assessment:.....	77
2.12.2.1 Safe Exposure Limits.....	78
2.12.2.2 Impairment of escape:	79
2.12.2.3 Incapacitation Exposure Limits	80
2.12.2.4 Lethal Exposure Limits:	80
Chapter 3 Methodology	83
Introduction	83
3.1 Analytical Experiments	83
3.1.1 Elemental Analysis.....	83
3.1.2 Proximate Analysis.....	84
3.1.3 Bomb Calorimeter	85
3.2 Description of Experimental Rigs	86
3.2.1 The 5 m ³ Fire Compartment:.....	86
3.2.1.1 5m ³ Compartment Modification	88
3.2.1.2 Temperature Measurements	89
3.2.1.3 Ventilation Area	91
3.2.2 The Standard Cone Calorimeter	92
3.2.3 The Controlled Atmosphere Cone Calorimeter	93
3.3 Principle of the Fourier Transform Infra-red Spectrometer (FTIR):..	96
3.3.1 Gas Analysis Description:	98
3.3.2 Paramagnetic Oxygen Analyser.....	99

3.4	The DMS 500 Particle Size Analyser.....	100
3.5	Soot Sampling Equipment (Smoke Meter)	102
3.6	Analysis Techniques.....	103
3.6.1	Heat Release Rate Calculation	103
3.6.2	Air to Fuel Ratio and Equivalence Ratio ϕ	104
3.6.3	Toxic Gas Yields	105
3.6.4	Combustion Efficiency.....	105
3.6.5	Particle Size Calculation	106
3.6.6	Soot Deposition.....	106
3.6.7	Toxicity Assessment	107
3.7	Research Materials.....	108
3.8	General Experimental Procedure for the Cone Calorimeter	117
3.9	General Experimental Procedure for the 5m ³ Compartment.....	118
Chapter 4 Freely Ventilated Test Results on the Cone Calorimeter		119
4.1	General Burning Characteristics.....	119
4.1.1	Natural Wood:	120
4.1.1.1	Mass Loss, Equivalence Ratio and Heat Release Rates (HRR)	120
4.1.2	Processed Wood:.....	122
4.1.2.1	Mass Loss, Equivalence Ratio and Heat Release Rates (HRR)	122
4.1.3	Plywood:	123
4.1.3.1	Mass Loss, Equivalence Ratio and Heat Release Rates (HRR)	123
4.2	Toxicity of Different Wood Samples	124
4.2.1	Natural Wood	125
4.2.1.1	Toxic Gas Concentration	126
4.2.1.2	Total Fire Toxicity N on an LC ₅₀ and COSHH 15min Basis.....	127
4.2.1.3	Toxic Gas Yields.....	129
4.2.1.4	Combustion Efficiency and Heat Release Rate Correction	131
4.2.2	Processed Wood.....	133
4.2.2.1	Toxic Gas Concentration	133
4.2.2.2	Total Fire Toxicity N on an LC ₅₀ and COSHH _{15min} Basis	134

4.2.2.3	Toxic Gas Yields.....	137
4.2.2.4	Combustion Efficiency and Heat Release Rate Correction	138
4.2.3	Plywood	139
4.2.3.1	Toxic Gas Concentration	139
4.2.3.2	Total Fire Toxicity N on an LC ₅₀ and COSHH _{15min} Basis	141
4.2.3.3	Toxic Gas Yields.....	144
4.2.3.4	Combustion Efficiency and Heat Release Rate Correction	146
4.3	Particulate Emissions from Wood Samples.....	147
4.3.1	Natural Wood	148
4.3.1.1	Particle Number Concentration.....	148
4.3.1.2	Particle Mass Concentration.....	150
4.3.1.3	Particle Emission Index	152
4.3.2	Processed Wood.....	153
4.3.2.1	Particle Number Concentration.....	153
4.3.2.2	Particle Mass Concentration.....	155
4.3.2.3	Particle Emission Index	157
4.3.3	Plywood	158
4.3.3.1	Particle Number Concentration.....	158
4.3.3.2	Particle Mass Concentration.....	160
4.3.3.3	Particle Emission Index	162
4.4	Comparison Between the Natural Wood and Processed Wood ...	163
4.4.1	Mass Loss, Equivalence Ratio and Heat Release Rates (HRR).....	164
4.4.2	Toxic Gas Concentrations	166
4.4.3	Total Toxicity	169
4.4.4	Toxic Gas Yields	170
4.5	Summary	172
Chapter 5 Controlled Atmosphere Test Results on the Cone Calorimeter		175
5.1	General Burning Characteristics.....	176
5.1.1	Pine Wood.....	176
5.1.1.1	Mass Loss Rate and Equivalence Ratio	177
5.1.1.2	Heat Release Rate	178

5.1.2	Block Board Wood	179
5.1.2.1	Ignition.....	180
5.1.2.2	Mass Loss Rate and Equivalence Ratio	181
5.1.2.3	Heat Release Rate	182
5.2	The Influence of Airflow Rate on Toxic Gas Emissions	184
5.2.1	Toxic Gas Concentration.....	184
5.2.2	Total Fire Toxicity N on an LC ₅₀ and COSHH 15min Basis .	186
5.2.3	Toxic Gas Yields	189
5.2.4	Combustion Efficiency and Heat Release Rate Correction .	192
5.3	The Influence of Heat flux on Toxic Gas Emissions	193
5.3.1	Toxic Gas Concentration.....	194
5.3.2	Total Fire Toxicity N on an LC ₅₀ and COSHH _{15min} Basis	197
5.3.3	Toxic Gas Yields	200
5.3.4	Combustion Efficiency and Heat Release Rate Correction .	204
5.4	Particulate Emissions from Wood Samples in Controlled Atmosphere Cone Calorimeter	205
5.4.1	Pine Wood.....	206
5.4.1.1	Particle Number Concentration.....	206
5.4.1.2	Particle Mass Concentration.....	210
5.4.1.3	Particle Emission Index	213
5.4.2	Block Board Wood	215
5.4.2.1	Particle Number Concentration.....	215
5.4.2.2	Particle Mass Concentration.....	218
5.4.2.3	Particle Emission Index	220
5.5	Comparison Between the Controlled Atmosphere Cone Calorimeter and the Freely Ventilated Setup	222
5.5.1	Mass Loss and Heat Release Rates (HRR).....	223
5.5.2	Toxicity, CO, Hydrocarbon, Fire Equivalence Ratio and Combustion Efficiency.....	224
5.5.3	Particle Number Concentration	226
5.5.4	Particle Number Comparison	227
5.6	Summary	229
Chapter 6 5m³ Compartment Test Results		232
6.1	General Burning Characteristics.....	232
6.1.1	Small Wood Crib	232

6.1.1.1	Mass Loss Rate, Mean Ceiling Temperature and Heat Release Rate (HRR).....	232
6.1.2	Medium Wood Crib	236
6.1.2.1	Mass Loss Rate, Mean Ceiling Temperature, Oxygen. Equivalence Ratio and Heat Release Rate (HRR)	236
6.1.3	Large Wood Crib	239
6.1.3.1	Mass Loss Rate, Mean Ceiling Temperature, Oxygen. Equivalence Ratio and Heat Release Rate (HRR)	239
6.2	Toxic Gas Emissions from Wood Crib Tests	242
6.2.1	Medium Wood Crib	243
6.2.1.1	Toxic Gas Concentration	243
6.2.1.2	Total Fire Toxicity N on an LC ₅₀ and COSHH _{15min} Basis	244
6.2.2	The Large Wood Crib.....	245
6.2.2.1	Toxic Gas Concentration	245
6.2.2.2	Total Fire Toxicity N on an LC ₅₀ and COSHH _{15min} Basis	247
6.2.3	Toxic Gas Yields	248
6.3	Particulate Emissions from Wood Crib Tests	250
6.3.1	Small Wood Crib	250
6.3.1.1	Particle Number Concentration.....	250
6.3.1.2	Particle Mass Concentration.....	251
6.3.2	Medium Wood Crib	252
6.3.2.1	Particle Number Concentration.....	252
6.3.2.2	Particle Mass Concentration.....	254
6.3.3	Large Wood Crib	255
6.3.3.1	Particle Number Concentration.....	255
6.3.3.2	Particle Mass Concentration.....	255
6.3.4	Gravimetric Soot Sampling.....	256
6.3.4.1	Soot Particulate Mass Concentration	256
6.3.4.2	Soot Particulate Yield	257
6.4	SEM Analyses on Soot Samples.....	259
6.5	Summary.....	261
	Chapter 7 Pool Fires	263
7.1	Cone Calorimeter Pool Tests	263

7.1.1	General burning Characteristics: Mass Loss, Mass Loss Rate, Heat Release Rates, Equivalence Ratio and Oxygen	264
7.2	Toxic Gas Concentrations from Cone Calorimeter Pool Fires	266
7.2.1	Total Fire Toxicity N on an LC ₅₀ and COSHH 15min Basis.	268
7.2.2	Toxic Gas Yields	271
7.2.3	Combustion Efficiency and Heat Release Rate Correction.	273
7.3	5m ³ Pool Tests	275
7.3.1	The Effect of Pool Size.....	276
7.3.1.1	Toxic Gas Concentrations	279
7.3.1.1.1	Total Toxicity N on an LC ₅₀ and COSHH _{15min} Basis	280
7.3.1.2	Toxic Gas Yield and Combustion Efficiency	282
7.3.1.3	Particulate Emissions	285
7.3.1.3.1	Soot Yield.....	286
7.3.2	The Effect of Ventilation	287
7.3.2.1	Toxic Gas Concentrations	289
7.3.2.1.1	Total Toxicity N on an LC ₅₀ and COSHH _{15min} Basis	290
7.3.2.2	Toxic Gas Yield	291
7.3.2.3	Particulate Emissions	292
7.3.2.3.1	Soot Yield.....	294
7.4	Tests without Orifice Plate.....	294
7.4.1	Toxic Gas Concentrations.....	295
7.4.2	Soot Deposit.....	296
7.5	SEM Analyses on Soot Samples.....	296
7.6	Summary.....	299
	Chapter 8 Conclusions and Future Work.....	301
8.1	Main Findings and Conclusions.....	301
8.2	Recommendations and Future Work.....	302
	References.....	304

List of Figures

Figure 1-1 Causes of fire deaths, Great Britain, 2018/2019 [5].....	4
Figure 1-2 Causes of fire deaths, USA 2011-2013 [9]	4
Figure 1-3 Fire Deaths in the UK (1955-2013) [8].....	5
Figure 1-4 Fire Deaths and Injuries in Poland (2000-2016) [10]	5
Figure 1-5 Total fire-related fatalities in dwellings or other fires, England; 1981/82 to 2017/18 [13].....	6
Figure 1-6 The MGM Grand Fire [19].....	7
Figure 1-7 The Grenfell Tower Fire [4].....	8
Figure 1-8 The Piper Alpha Fire [20].....	9
Figure 1-9 The Buncefield Fire [21].....	10
Figure 2-1 The Fire Triangle	15
Figure 2-2 Charring of Wood [42].....	17
Figure 2-3 Hot layer gases in an enclosure	19
Figure 2-4 Stages of fire Development within a compartment [53].....	23
Figure 2-5 Incomplete Combustion Products	29
Figure 2-6 Yield Data Comparison extracted from Alarifi [87]	36
Figure 2-7 CO Yield extracted from Aljumaiah [85].....	36
Figure 2-8 The Smoke Density Chamber [109].....	48
Figure 2-9 The Controlled Atmosphere Cone Calorimeter [109].....	50
Figure 2-10 The Steady State Tube Furnace [109].....	51
Figure 2-11 The deposition of particles in the respiratory system [8].....	53
Figure 2-12 Formation of Particles in Fires	55
Figure 2-13 Examples of size distributions a) Histogram b) Log-normal distribution curve [137].....	58
Figure 2-14 Cascade Impactor.....	63
Figure 2-15 Low Pressure Impactor.....	63
Figure 2-16 Electrical Low Pressure Impactor Plus (ELPI +)	64
Figure 2-17 SEM Images of Aggregate Particles Generated from: (a) Non- flaming and (b) Flaming Douglas-fir Wood; (c) Non-flaming and (d) Flaming SBR Rubber; (e) Non-flaming and (f) Flaming Polypropylene; (g) Flaming Coal; and TEM Images of (h) Flaming Coal and (i) Flaming PVC Rubber extracted from [31].....	68
Figure 2-18 Particle Mass Size Distributions extracted from [133, 151].....	70
Figure 2-19 Number Size Distributions for Mass Size Distributions shown in Fig. 2-14 extracted from [133, 151].....	70

Figure 2-20 Particle Number Distribution as a Function of Size for Pellets A and Fuel Oil with a Comparison with a Euro 2 Diesel Operated on Rape Seed Oil extracted from [154]	71
Figure 2-21 Particle Mass Concentration as a Function of Time [156].....	72
Figure 3-1 A schematic diagram of the 5m ³ compartment.....	87
Figure 3-2 Multi Hole X-probe for the 5m ³ Compartment	88
Figure 3-3 Sampling point for all analysers (a) Particle Size analyser (b)	89
Figure 3-4 Arrangement of Thermocouples in the 5m ³ Compartment.....	91
Figure 3-5 The air inlet sizes; fully open (0.15 m ² ; K _{in} = 5%) (a); two square holes (0.03m ² ; K _{in} = 1%) (b); and closed (K _{in} = 0%) (c)	92
Figure 3-6 The standard Cone Calorimeter Setup	93
Figure 3-7 The Controlled Atmosphere Cone Calorimeter and Setup.....	96
Figure 3-8 Schematic of the Gas analysers	99
Figure 3-9 DMS500 Classifier extracted from [147]	101
Figure 3-10 The DMS500 Particle size analyser.....	102
Figure 3-11 The schematic of the Smoke Meter	103
Figure 3-12 The collection of soot deposits	107
Figure 3-13 Pine Wood Cribs.....	115
Figure 4-1 Mass loss rate (a) and Equivalence Ratio (b)	121
Figure 4-2 Primary HRR (a) and HRR based on Mass Loss Rate (b).....	121
Figure 4-3 Mass loss rate (a) and Equivalence Ratio (b)	122
Figure 4-4 Primary HRR (a) and HRR based on Mass Loss Rate	123
Figure 4-5 Mass Loss Rate (a) and Equivalence Ratio (b)	124
Figure 4-6 Primary HRR (a) and HRR based on Mass Loss Rate (b).....	124
Figure 4-7 Toxic gas concentrations; CO (a), Total Hydrocarbon (b), Benzene (c), Formaldehyde (d), Acrolein (e), Hydrogen Cyanide (f), NO (g) and NO ₂ (h)	127
Figure 4-8 Total N relative to LC ₅₀ (a) and COSHH _{15min} (b)	128
Figure 4-9 N-Gas Composition (LC ₅₀) PWS (a) and SB (b)	128
Figure 4-10 N-Gas Composition (COSHH _{15min}) PWS (a) and SB (b).....	129
Figure 4-11 Toxic gas yields; CO (a), Total Hydrocarbon (b), Benzene (c), Formaldehyde (d), Acrolein (e) and Hydrogen Cyanide (f)	131
Figure 4-12 Combustion Efficiency	132
Figure 4-13 Mass, HRR based on the mass loss rate, adjusted HRR, based on inefficiency of combustion for; Pine Wood (a) and Scaffolding Board (b)	132

Figure 4-14 Toxic gas concentrations; CO (a), Total Hydrocarbon (b), Benzene (c), Formaldehyde (d), Acrolein (e) and Hydrogen Cyanide (f).	134
Figure 4-15 Total toxicity N relative LC ₅₀ (a) and relative to COSHH _{15 min} (b)	135
Figure 4-16 N-Gas Composition (LC ₅₀) OSB (a) Chipboard (b) and MDF (c)	136
Figure 4-17 N-Gas Composition (LC ₅₀) OSB (a) Chipboard (b) and MDF (c)	136
Figure 4-18 Toxic yields of CO (a) and Total Hydrocarbon (b).	137
Figure 4-19 Combustion Efficiency	138
Figure 4-20 Mass, HRR based on the mass loss rate, adjusted HRR, based on inefficiency of combustion for; OSB (a) CFM (b) and MDF (c).....	139
Figure 4-21 Toxic gas concentrations; CO (a), Total Hydrocarbon (b), Benzene (c), Formaldehyde (d), Acrolein (e) and Hydrogen Cyanide (f).	141
Figure 4-22 Total toxicity N relative LC ₅₀ (a) and relative to COSHH _{15 min} (b)	142
Figure 4-23 Species Contribution relative to LC ₅₀ : PW A (a) PW B (b) DPW (c) and LPW (d)	143
Figure 4-24 Species Contribution relative to COSHH _{15min} : PW A (a) PW B (b) DPW (c) and LPW (d)	144
Figure 4-25 Toxic gas yields; CO (a), Total Hydrocarbon (b), Benzene (c), Formaldehyde (d), Acrolein (e) and Hydrogen Cyanide (f)	146
Figure 4-26 Combustion Efficiency for Plywood.....	146
Figure 4-27 Mass, HRR based on the mass loss rate, adjusted HRR, based on inefficiency of combustion for; PW A (a) PW B (b) DPW (c) and LPW (d).....	147
Figure 4-28 Particle Number and Size Distribution; PWS (a) and SB (b)...	149
Figure 4-29 Particle Number and Size Distribution at Different times; PWS (a) and SB (b)	149
Figure 4-30 20 nm and 200 nm sizes particle number; PWS (a) and SB (b)	150
Figure 4-31 Particle Mass and Size Distribution; PWS (a) and SB (b).....	151
Figure 4-32 Particle Mass and Size Distribution at Different times; PWS (a) and SB (b).....	151
Figure 4-33 20 nm and 200 nm Sizes Particle Mass; PWS (a) and SB (b)	152
Figure 4-34 Particle Number per Mass of Fuel Burnt for 20 nm and 200 nm Particles; PWS (a) and SB (b)	153

Figure 4-35 Particle Mass per Mass of Fuel Burnt for 20 nm and 200 nm Particles; PWS (a) and SB (b)	153
Figure 4-36 Particle Number and Size Distribution; OSB.....	154
Figure 4-37 Particle Number and Size Distribution at Different times; OSB	154
Figure 4-38 20 nm and 200 nm sizes particle number; OSB	155
Figure 4-39 Particle Mass and Size Distribution; OSB.....	156
Figure 4-40 Particle Mass and Size Distribution at Different times; OSB...	156
Figure 4-41 20 nm and 200 nm Sizes Particle Mass; OSB	157
Figure 4-42 Particle Number and Mass per Mass of Fuel Burnt for 20 nm and 200 nm Particles; OSB.....	157
Figure 4-43 Particle Number and Size Distribution; PW A (a) and PW B (b)	158
Figure 4-44 Particle Number and Size Distribution at Different times; PW A (a) and PW B (b).....	159
Figure 4-45 20 nm and 200 nm sizes particle number; PW A (a) and PW B (b)	160
Figure 4-46 Particle Number per Volume Compared with the Equivalence Ratio Variation with Time; PW A (a) and PW B (b)	160
Figure 4-47 Particle Mass and Size Distribution; PW A (a) and PW B (b) .	161
Figure 4-48 Particle Mass and Size Distribution at Different times; PW A (a) and PW B (b)	161
Figure 4-49 20 nm and 200 nm Sizes Particle Mass; PW A (a) and PW B (b)	162
Figure 4-50 Particle Number per Mass of Fuel Burnt for 20 nm and 200 nm Particles; PW A (a) and PW B (b)	163
Figure 4-51 Particle Mass per Mass of Fuel Burnt for 20 nm and 200 nm Particles; PW A (a) and PW B (b)	163
Figure 4-52 Mass loss rate (a), Equivalence ratio (b) and Heat release rate (HRR) (c)	166
Figure 4-53 Toxic gas concentrations; CO (a), Total Hydrocarbon (b), Benzene (c), Formaldehyde (d), Acrolein (e) and Hydrogen Cyanide (f).	168
Figure 4-54 Total toxicity N relative LC ₅₀ (a) and relative to COSHH _{15 min} (b)	170
Figure 4-55 Toxic Gas Yields; CO (a), Total Hydrocarbon (b), Benzene (c), Formaldehyde (d), Acrolein (e) and Hydrogen Cyanide (f).	171
Figure 5-1 Mass Loss Rate (a) and Equivalence Ratio (b)	178
Figure 5-2 Heat Release Rates; Total HRR by Oxygen Consumption (a), HRR by Mass Loss Rate (b) and Primary HRR (c).	179

Figure 5-3 Block Board Wood; Mass Loss (a), Mass Loss Rate (b) and Equivalence Ratio (c).....	182
Figure 5-4 Heat Release Rates; Total HRR by O ₂ Consumption (a), by Mass Loss Rate (b) and Primary Heat Release Rate (c).....	184
Figure 5-5 Toxic gas concentrations; CO (a), Total Hydrocarbon (b), Benzene (c), Formaldehyde (d), Acrolein (e) and Hydrogen Cyanide (f)	186
Figure 5-6 Total N relative to LC ₅₀ (a) and COSHH _{15min} (b)	187
Figure 5-7 N-Gas Composition (LC ₅₀) PWS; 59 kW/m ² _{air} (a) 112 kW/m ² _{air} (b) and 174 kW/m ² _{air} (c)	188
Figure 5-8 N-Gas Composition (COSHH _{15min}) PWS; 59 kW/m ² _{air} (a) 112 kW/m ² _{air} (b) and 174 kW/m ² _{air} (c).....	189
Figure 5-9 Toxic Gas Yields; CO (a), Total Hydrocarbon (b), Benzene (c), Formaldehyde (d), Acrolein (e) and Hydrogen Cyanide (f)	192
Figure 5-10 Combustion Efficiency for Pine Wood.....	192
Figure 5-11 Mass, HRR based on the mass loss rate, adjusted HRR, based on inefficiency of combustion for; 59 kW/m ² air (a) 112 kW/m ² air (b) 174 kW/m ² air (c)	193
Figure 5-12 Toxic gas concentrations; CO (a), Total Hydrocarbon (b), Benzene (c), Formaldehyde (d), Acrolein (e) and Hydrogen Cyanide (f)	196
Figure 5-13 Total N relative to LC ₅₀ (a) and COSHH _{15min} (b)	198
Figure 5-14 Species Contribution relative to (LC ₅₀) BBW; 25 kW/m ² (a) 30 kW/m ² (b) 35 kW/m ² (c) 40 kW/m ² (d) and 50 kW/m ² (e).....	199
Figure 5-15 Species Contribution relative to (COSHH _{15min}) BBW; 25 kW/m ² (a) 30 kW/m ² (b) 35 kW/m ² (c) 40 kW/m ² (d) and 50 kW/m ² (e)	200
Figure 5-16 Toxic Gas Yields; CO (a), Total Hydrocarbon (b), Benzene (c), Formaldehyde (d), Acrolein (e) and Hydrogen Cyanide (f)	203
Figure 5-17 Combustion Efficiency for Block Board Wood	204
Figure 5-18 Mass, HRR based on the mass loss rate, adjusted HRR, based on inefficiency of combustion for; 59 kW/m ² (a) 112 kW/m ² (b) 174 kW/m ² (c)	205
Figure 5-19 Particle Number and Size Distribution; 59 kW/m ² _{air} (a) 112 kW/m ² _{air} (b) and 174 kW/m ² _{air} (c).....	208
Figure 5-20 Particle Number and Size Distribution at Different times; 59 kW/m ² _{air} Compared with Diesel [192] and Biomass Pellet [154] (a) 112 kW/m ² _{air} (b) and 174 kW/m ² _{air}	209
Figure 5-21 20 nm (a) and 200 nm (b) Particle Size Concentration as a Function of Time	210
Figure 5-22 Particle Mass and Size Distribution; 59 kW/m ² _{air} (a) 112 kW/m ² _{air} (b) and 174 kW/m ² _{air} (c)	212

Figure 5-23 Particle Mass and Size Distribution at Different times; 59 kW/m ² _{air} (a) 112 kW/m ² _{air} (b) and 174 kW/m ² _{air} (c).....	212
Figure 5-24 20 nm (a) and 200 nm (b) Particle Size Mass as a Function of Time.....	213
Figure 5-25 Particle Number per Mass of Fuel Burnt for 20 nm (a) and 200 nm (b) Particles.....	214
Figure 5-26 Particle Mass per Mass of Fuel Burnt for 20 nm (a) and 200 nm (b) Particles.....	214
Figure 5-27 Particle Number and Size Distribution; 25 kW/m ² (a) 35 kW/m ² (b) and 50 kW/m ² (c).....	216
Figure 5-28 Particle Number and Size Distribution at Different times; 25 kW/m ² (a) 35 kW/m ² (b) and 50 kW/m ² (c).....	217
Figure 5-29 Nuclei and Accumulation mode sizes particle number for; 25 kW/m ² (a) 35 kW/m ² (b) and 50 kW/m ²	217
Figure 5-30 Particle Mass and Size Distribution; 25 kW/m ² (a) 35 kW/m ² (b) and 50 kW/m ² (c)	219
Figure 5-31 Particle Mass and Size Distribution at Different Times; 25 kW/m ² (a) 35 kW/m ² (b) and 50 kW/m ² (c)	219
Figure 5-32 Nuclei and Accumulation Mode Sizes Particle Mass for; 25 kW/m ² (a) 35 kW/m ² (b) and 50 kW/m ² (c).....	220
Figure 5-33 Particle Number per Mass of Fuel Burnt for nucleation mode and Accumulation mode particles for; 25 kW/m ² (a) 35 kW/m ² (b) and 50 kW/m ² (c)	221
Figure 5-34 Particle Number per Mass of Fuel Burnt for nucleation mode and Accumulation mode particles for; 25 kW/m ² (a) 35 kW/m ² (b) and 50 kW/m ² (c)	222
Figure 5-35 Mass loss rate (a) and primary heat release rate (b).	224
Figure 5-36 Oxygen in the cone outlet chimney	224
Figure 5-37 Total LC ₅₀ FEC toxicity	224
Figure 5-38 CO yield (a) and HC yield (b).....	225
Figure 5-39 Equivalence ratio (a) and Combustion efficiency (b).....	226
Figure 5-40 Particle number concentration and size distribution; (a) restricted (b) freely ventilated.	226
Figure 5-41 20 nm particle number concentration (a) and 200 nm particle number concentration (b).....	227
Figure 5-42 Comparison of particle number distribution with that of Hertzberg [133] using the ELPI aerodynamic size separation instrument for restricted (a) and freely ventilated (b).	228
Figure 6-1 Mass Loss (a) Mass Loss Rate (b) Mean Ceiling Temperature (c) and Heat Release Rate HRR (d)	233

Figure 6-2 Picture Showing Ceiling Impingement during the Small crib Test	234
Figure 6-3 Picture showing the final stage of the small crib combustion....	235
Figure 6-4 Residue after the Small Crib Tests	235
Figure 6-5 Mass Loss (a) Mass Loss Rate (b) Oxygen (c) Equivalence Ratio (d) Mean Ceiling Temperature (e) and Heat Release Rate HRR (f) ..	237
Figure 6-6 Fire development stages for medium crib 1	238
Figure 6-7 Fire development stages for medium crib 2	238
Figure 6-8 The Burnt Cribs	239
Figure 6-9 Mass Loss (a) Mass Loss Rate (b) Oxygen (c) Equivalence Ratio (d) Mean Ceiling Temperature (e) and Heat Release Rate HRR (f) ..	240
Figure 6-10 Large Wood Crib Flaming Pool Fire.....	241
Figure 6-11 Large Wood Crib Smouldering Combustion	242
Figure 6-12 Char and Ashes at the end of the Large Crib Test	242
Figure 6-13 Toxic gas concentrations; CO (a), Total Hydrocarbon (b), Benzene (c), Formaldehyde (d), Acrolein (e) and Hydrogen Cyanide (f)	244
Figure 6-14 Total N relative to LC ₅₀ (a) and COSHH _{15min} (b)	244
Figure 6-15 N-Gas Composition (LC ₅₀) Medium Crib 1 (a) and Medium Crib 2 (b)	245
Figure 6-16 N-Gas Composition (COSHH _{15min}) Medium Crib 1 (a) and Medium Crib 2 (b)	245
Figure 6-17 Toxic gas concentrations; CO (a), Total Hydrocarbon (b), Benzene (c), Formaldehyde (d), Acrolein (e) and Hydrogen Cyanide (f)	247
Figure 6-18 Total N relative to LC ₅₀ (a) and COSHH _{15min} (b)	247
Figure 6-19 N-Gas Composition (LC ₅₀) (a) and (COSHH _{15min}) (b)	248
Figure 6-20 Toxic Gas Yields; Medium Crib 1 (a), Medium Crib 2 (b) and Large Crib (c).....	249
Figure 6-21 Comparison of CO Yield with Literature [87].....	249
Figure 6-22 Particle Number and Size Distribution; Small Crib 1 (a) and 2 (b)	251
Figure 6-23 Particle Number and Size Distribution at Different times; Small Crib 1 (a) and 2 (b)	251
Figure 6-24 Particle Mass and Size Distribution; Small Crib 1 (a) and 2 (b)	252
Figure 6-25 Particle Mass and Size Distribution at Different times; Small Crib 1 (a) and 2 (b)	252

Figure 6-26 Particle Number and Size Distribution; Medium Crib 1 (a) and 2 (b)	253
Figure 6-27 Particle Number and Size Distribution at Different times; Medium Crib 1 (a) and 2 (b)	253
Figure 6-28 Particle Mass and Size Distribution; Medium Crib 1 (a) and 2 (b)	254
Figure 6-29 Particle Mass and Size Distribution at Different times; Medium Crib 1 (a) and 2 (b)	254
Figure 6-30 Large Crib Particle Number Concentration and Size Distribution at Different times.....	255
Figure 6-31 Large Crib Particle Mass Concentration (a) and Size Distribution at Different times (b)	256
Figure 6-32 Comparison of Filter Paper Mass Concentration with Literature [156].....	257
Figure 6-33 Soot Deposits on Filter Paper (a) medium crib 1 (b) medium crib 2 and (c) Large crib.....	257
Figure 6-34 Soot Particulate Yield as a Function of Equivalence Ratio	258
Figure 6-35 Soot Particulate as a Function of Time	258
Figure 6-36 Small Crib 1 SEM Analysis on Smoke Meter Sample.....	259
Figure 6-37 Small Crib 1 SEM Analysis on Window Sample	259
Figure 6-38 Small Crib 1 SEM Elemental Analysis on Smoke Meter Sample	260
Figure 6-39 Small Crib 1 SEM Elemental Analysis on Window Sample	260
Figure 7-1 Normalised Mass Loss (a) Mass Loss Rate (b) Equivalence Ratio (c) Heat Release Rate HRR (d) and Oxygen (e).....	266
Figure 7-2 Toxic gas concentrations; CO (a), Total Hydrocarbon (b), Benzene (c), Formaldehyde (d), Acrolein (e) and Hydrogen Cyanide (f)	267
Figure 7-3 Total N relative to LC ₅₀ (a) and COSHH _{15min} (b)	268
Figure 7-4 Species Contribution (LC ₅₀); Diesel (a) Lube oil (b) Olive oil (c)	270
Figure 7-5 Species Contribution (COSHH _{15min}); Diesel (a) Lube oil (b) Olive oil (c)	270
Figure 7-6 Toxic gas yields; CO (a), Total Hydrocarbon (b), Acrolein (c), Formaldehyde (d), Benzene (e) and Hydrogen Cyanide (f)	272
Figure 7-7 Combustion Efficiency	273
Figure 7-8 Mass, HRR based on the mass loss rate, adjusted HRR, based on inefficiency of combustion for; Diesel (a) Lube oil (b) and olive oil (c)	274

Figure 7-9 Oxygen (a) Ceiling Temperature (b) and Equivalence Ratio (c) for tests with different pool fire size.....	277
Figure 7-10 200 x 200 mm pool tray Figure 7-11 Fire burning at the corner.....	278
Figure 7-12 Pulsing Phenomenon (400 mm ($K_{in}=1\%$) Test)	279
Figure 7-13 Toxic Gas concentrations; CO (a) THC (b) Benzene (c) Formaldehyde (d) Acrolein (e)	280
Figure 7-14 Total N relative to LC_{50} (a) and $COSHH_{15min}$ (b)	281
Figure 7-15 Species Contribution (LC_{50}); Diesel 400 mm ($K_{in}=1\%$) Test (a) and 200 mm ($K_{in}=1\%$) Test (b).....	282
Figure 7-16 Species Contribution ($COSHH_{15min}$); Diesel 400 mm ($K_{in}=1\%$) Test (a) and 200 mm ($K_{in}=1\%$) Test (b)	282
Figure 7-17 Toxic gas yields; CO (a), Total Hydrocarbon (b), Acrolein (c), Formaldehyde (d), Benzene (e) and Hydrogen Cyanide (f)	284
Figure 7-18 Combustion Efficiency	284
Figure 7-19 CO Yield Comparison with Aljumaiah's [85]	284
Figure 7-20 Particle Number and Size Distribution; 400 mm ($K_{in}=1\%$)Test (a) and 200 mm ($K_{in}=1\%$)Test (b).....	285
Figure 7-21 Particle Number and Size Distribution; 400 mm ($K_{in}=1\%$)Test (a) and 400 mm ($K_{in}=1\%$)Test (b).....	286
Figure 7-22 The Discharged Soot Yield for Tests 7 and 8	287
Figure 7-23 Ceiling Temperature (a) and Equivalence Ratio (b).....	288
Figure 7-24 Toxic Gas Concentrations; CO (a) THC (b) Benzene (c) Formaldehyde (d) and Acrolein (e)	290
Figure 7-25 Total N relative to LC_{50} (a) and $COSHH_{15min}$ (b)	291
Figure 7-26 Species Contribution Diesel 200 mm ($K_{in}=5\%$) Test; LC_{50} (a) and $COSHH_{15min}$ (b).....	291
Figure 7-27 Toxic Gas Yields for tests with different ventilation factor; CO (a) THC (b) Benzene (c) Formaldehyde (d) and Acrolein (e)	292
Figure 7-28 200 mm ($K_{in}=5\%$)Test Particle Number and Size Distribution (a) and Mass Concentration (b).....	293
Figure 7-29 Comparison of Particle Number and Size Distribution at Different times; 200 s (a) and 600 s (b)	293
Figure 7-30 Sample Tray Temperatures as a Function of Time.....	295
Figure 7-31 Total N relative to LC_{50} (a) and $COSHH_{15min}$ (b)	296
Figure 7-32 Diesel Pool 200 mm ($K_{in}=0\%$) SEM Analysis on Smoke Meter Sample.....	297
Figure 7-33 Diesel Pool 200 mm ($K_{in}=0\%$) SEM Analysis on Window Sample	297

Figure 7-34 Diesel Pool 200 mm ($K_{in}=0\%$) SEM Elemental Analysis on Smoke Meter Sample	297
Figure 7-35 Diesel Pool 200 mm ($K_{in}=0\%$) SEM Elemental Analysis on Window Sample.....	298

List of Tables

Table 2-1 Effects of Exposure of heat to the skin [56].....	24
Table 2-2 Summary of fire effluents and their effect [63]	30
Table 2-3 Summary of the Main Techniques for Measurement of Particulates in Fire [144].....	65
Table 2-4 Constants and LC ₅₀ Concentrations for Levin N-Gas Model [157]	74
Table 2-5 30-min LC ₅₀ Values used in Purser's Model [127]	76
Table 2-6 Classification of Threshold Levels of Fire Toxicity Assessment...	78
Table 3-1 Distance and Position of Thermocouples in the Compartment ...	90
Table 3-2 Air Flow Rate Conversion	95
Table 3-3 The 51 Gases FTIR was Calibrated to Measure	97
Table 3-4 Some Toxic Threshold Limits and their Comparison	108
Table 3-5 Wood Samples for the Cone Calorimeter Tests.....	110
Table 3-6 Measured Properties of Wood Test Materials.....	112
Table 3-7 Other Properties of Wood	114
Table 3-8 Pine wood Crib properties.....	116
Table 3-9 Measured Properties of Liquid Pool.....	117
Table 4-1 Toxic Gas Yields.....	130
Table 4-2 Toxic Gas Yields for Plywood	144
Table 5-1 Ignition Times for Burning Pine Wood at Different Ventilation Conditions.....	177
Table 5-2 Ignition Times for Burning Pine Wood at Different Ventilation Conditions.....	180
Table 5-3 Toxic Gas Yields for Pine Wood Restricted Ventilation.....	190
Table 5-4 Toxic Gas Yields for Pine Wood Restricted Ventilation.....	201
Table 6-1 Toxic Gas Yields.....	250
Table 6-2 Small Crib 1 SEM Elemental Analysis on Smoke Meter Sample	260
Table 6-3 Small Crib 1 SEM Elemental Analysis on Window Sample.....	261
Table 7-1 Combustion Period	263
Table 7-2 Toxic Gas Yields.....	271
Table 7-3 Summary of the 5m ³ Pool Tests	275
Table 7-4 The Average Results of the Tests with Different Pool Fire Size.	276
Table 7-5 Total Soot Yield	287

Table 7-6 The Average Results of the Burning Characteristics at Different Ventilation	288
Table 7-7 Total Soot Yield Comparison	294
Table 7-8 The Average Results of the Burning Characteristics of Tests Without Orifice Plate	294
Table 7-9 Yield of Soot Deposited on the Walls of the Compartment	296
Table 7-10 Diesel Pool 200 mm ($K_{in}=0\%$) SEM Elemental Analysis on Smoke Meter Sample	298
Table 7-11 Diesel Pool 200 mm ($K_{in}=0\%$) SEM Elemental Analysis on Window Sample.....	298

Glossary of Terms and Symbols

Abbreviation	Meaning
ACGIH	American Conference of Government Industrial Hygienists
ADB	Approved Document B
AEGL	Acute Exposure Guideline Levels
AFR	Air to Fuel Ratio
BS	British Standard
CACC	Controlled Atmosphere Cone Calorimeter
CFM	Chipboard faced with melamine
CO	Carbon monoxide
COHb	Carboxyhaemoglobin
COSHH	Control of Substances Hazardous to Health
DMS	Differential Mobility Spectrometer
DPW	Dark Plywood
EI	Emission Index
FEC	Fractional Effective Concentration
FED	Fractional Effective Dose
FIC	Fractional Irritant Concentration
FID	Flame Ionisation Detector
FTIR	Fourier Transform Infrared
GC-MS	Gas Chromatography Mass Spectrometer
HBr	Hydrogen Bromide
HCl	Hydrogen Chloride
HCN	Hydrogen Cyanide
HF	Hydrogen fluoride
HRR	Heat Release Rate
HSE	Health and Safety Executive
IDLH	Immediately Dangerous to Life or Health
ISO	International Standards Organisation
LC50	Lethal Concentration affecting 50% of the population
LPW	Light Plywood
MDF	Medium density fibreboard
MFR	Mass Flow Rate
MLR	Mass Loss Rate
MW	Molecular Weight
N	Total Toxicity
NIOSH	National Institute for Occupational Safety and Health (USA)
NIST	National Institute for Standards and Technology (USA)
O ₂	Oxygen
OSB	Oriented Strand Board
OSHA	Occupational Safety and Health Administration
PEL	Permissible Exposure Limit
PM ₁₀	Particulate Matter (10µm and below)

PVC	Polyvinyl chloride
PW	Plywood
PWS	Pine Wood Sticks
SB	Scaffolding Board
SEM	Scanning Electron Microscope
SO ₂	Sulphur dioxide
STELs	Short Term Exposure Limits
TGA	Thermo-gravimetical Analysis
THC	Total amount of Hydrocarbons
TLV	Threshold Limit Value
TMB	Trimethylbenzene
TWA	Time Weighted Average
VOC	Volatile Organic Compound
WELs	Work Exposure Limits

Symbols:

Symbol	Meaning
D_p	Particle diameter
\dot{m}	Mass burning rate
\dot{m}''	Mass burning rate flux
ΔH_c	Heat of combustion
\dot{Q}	Heat release rate
L	Length
A_f	Horizontal burning area of the fuel
V	Volume
A/F	Air to fuel ratio
M	Molecular weight
Φ	Equivalence ratio
Y	Yield
T_{ig}	Time to ignition
K_{in}	Ventilation parameter
A_{in}	Air inlet flow area (m ²)
$V^{2/3}$	Mean enclosure cross sectional area (m ²)
η	Combustion efficiency

Chapter 1 Introduction

Uncontrolled accidental fires are hazardous to life and property, create atmospheric pollution through gaseous and particulate emissions and cause water and land contamination from fire-fighting water run-off and airborne ground deposition of fire toxins.

Heat and flames from fires are the obvious hazards but the effect of toxic gases and smoke being the less obvious may pose the greatest danger as they may prevent or slow down escape and some (e.g. CO and HCN) may cause death [1]. In the past few decades, production of toxic gases from fire has become a recognised serious threat to people and as such started receiving considerable public attention. Some notable fire deaths include [2] the 1929 Cleveland Hospital fire with 125 fatalities, the Beverly Hills supper club fire (1977) with 164 fatalities, the MGM Grand Hotel fire (1980) with 85 fatalities, the white Plains Stouffers Inn fire (1980) with 26 fatalities, the Houston west chase Hilton fire (1982) with 12 fatalities. More recent examples include of the blaze at the Rose Park Nursing home in Edinburgh, 2004 with 14 fatalities [3] and the Grenfell Tower fire in London, 2017 with 71 fatalities [4]. Escape impairment through the inhalation of toxic gases from the fire has been attributed to most of these deaths.

1.1 Fire Fatalities and Injuries- Statistics

It is now a known fact that the biggest cause of fire deaths and injury is the toxicity of fire effluents [5] . Widely used synthetic polymers, derived from oil, burn more quickly and also produce more toxic effluents, especially when they contain fire retardants (halogens) [6, 7]. Although there's a reduction in the overall number of deaths in the UK, there has been a gradual shift in the cause of death from 'burns' to 'overcome by toxic gas or smoke' from 1955 to 2013 (Fig. 1-3) [8]. It appears therefore that both relatively and absolutely, gas or smoke is the major factor of importance to the occurrence of fatal and non-fatal casualties in fires. A similar trend of cause of fire death shown in Fig. 1-2 was also observed in the USA with smoke inhalation accounting for the majority of fire fatalities. In the US,

death as a result of smoke inhalation accounted for 85% of the total fire fatalities (13,125 fatalities/year) from 2011-2013 with 39% accounting for smoke inhalation only and 46% for smoke and burns [9]. Fires still continue to claim lives and cause injuries at an unacceptable level in many parts of Europe. The Polish fire deaths and injuries statistics [10] show twice the UK's number of fatalities per head of population (Fig. 1-4) while a factor of 10 more fire deaths was observed in Latvia, Estonia and Lithuania [8]. The current Polish incidence of deaths is similar to that in the UK during the 1970s and 1980s, before the introduction of the furniture flammability regulations in 1988 [11] and the rise in the use of smoke alarms [12], and approximately 3 times the current UK figure, while that of injuries is approximately 2 times those in the UK. According to Giebułtowicz et al. [10], there may be a number of contributory factors responsible for these differences, including life-style and cultural differences, inadequate publicity and awareness about hazards associated with fire in the home, and lower rates of smoke alarm installations. The particular UK requirements for furniture flammability may have played a significant role in the difference, which is absent in Poland.

Although residential fires receive less public attention than fires in industry and public places, they happen more often than the industrial fires. This is because there is hardly any residential fire responsible for a large number of deaths. The UK fire statistics of April 2018 to March 2019 [5] showed that 77 % (196) of fire-related fatalities, occurred in dwelling fires in 2018/19. This compares with the figures obtained in 2017/18, 264 (78%), 217 (78%) in the previous five years, 2013/14 and 255 (79%) ten years previously in 2008/09. There were 263 fire-related fatalities in dwelling fires recorded in 2017/18 (Fig. 1-5). This was an increase of 23% as compared with 214 in the previous year. The figure obtained in 2017/18 includes the 71 fire-related fatalities from the Grenfell Tower fire. A number of dwelling fire death cases studied for a period of 8 years (2003-2011) in the Mazowieckie region of Poland [8] indicated that the majority of the fire deaths were in the room of fire origin and around half were found close to burned upholstered furniture. The majority of the victims were incapacitated as a result of inhalation of smoke including CO and other toxic gases while about 80% of the victims were reported to have had soot in their airways [8].

Non-fatal fire injuries are significantly higher than the fatalities and include various degrees of burns, damage to the lungs, and respiratory problems. The number of non-fatal casualties in fires in England has also been on the decline since the mid-1990s, more than halving from a peak of around 14,800 in 1996/97 down to around 7,100 in 2016/17. The decline, however, has slowed in recent years and there was an increase in the number of non-fatal casualties in 2017/18 by three per cent from the previous year, to around 7,300 [13].

1.2 The Influence of the Materials in the Fire Load

Different materials produce different mixtures of toxic gases on burning. In this Thesis the toxicity from wood burning materials is examined mainly in relation to residential fires and of hydrocarbon liquid pool fires in reference to some common industrial fires.

Wood and other cellulosic materials are extensively used in the construction of homes and other buildings [14]. Processed wood such as plywood, MDF, block board and laminated veneer are used in modern buildings for surface finishing, furniture, flooring, scaffolding, ceilings, shelves and partitioning and these are studied in the present work. Wood is the most dominant fire load in homes and other buildings accounting for approximately 70% of CO₂ emissions and 65% of CO emissions [15]. There is hardly any building, be it residential, industrial or any public building that does not have anything made of wood. The fire size, burning rate, duration and the damages, injuries and deaths it causes relates directly to the quantity of the fire load and toxic gases released in fires.

In an attempt to reduce the flammability of synthetic polymeric materials e.g. plastics, flame retardants were introduced. Unfortunately, these retardants contain halides, nitrogen, phosphorous and sulphur compounds, leading to the production of additional irritant toxic gases, SO₂, HCl, HF, HBr and HCN during combustion. They also cause the problem of combustion inefficiency leading to an increase in the yield of CO, HCN and other irritant gases. Thus although fire retardants decrease the risk of the start of a fire, if a fire occurs elsewhere and engulfs the fire retarded material then fire retardants can make the fire toxicity worse.

Industrial fires do not occur very often, but when they do, they come with a lot of casualties that will generate a public outcry. An example of industrial fire is pool fires such as diesel pool, other hydrocarbon pool and oil pool fires. Pool fires can generate large amount of smoke which presents extreme hazards. Diesel is a common material in offshore platforms and factories, and the hazards posed by accidental pool fires are an important aspect of safety cases [16]. The loss of hydrocarbon containment can arise from mechanical failure, damage or procedure failures. The leakage rates and their time dependence, hydrocarbon type, storage and discharge conditions greatly influence the nature and extent of a fire [17]. One of the major pool fire events that occurred in recent times was the Buncefield fire at the Hertfordshire oil storage terminal. Although the storage tanks were outside and therefore the fire in the open, the satellite photo showed that a black smoke cloud was formed after the initial explosion. However, small hydrocarbon spillage fires inside refineries occur more frequently, forming an enclosure pool fire. This work determined the fire gas toxicity and particulate emissions that people would experience when exposed to different wood materials and pool fires both in a compartment fire and in freely ventilated open fires.

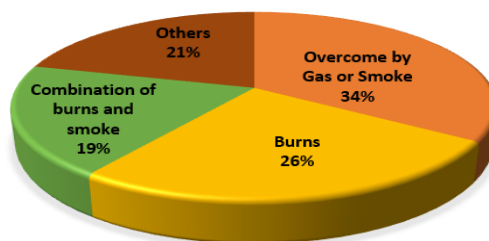


Figure 1-1 Causes of fire deaths, Great Britain, 2018/2019 [5]

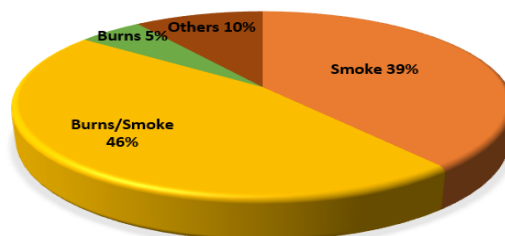


Figure 1-2 Causes of fire deaths, USA 2011-2013 [9]

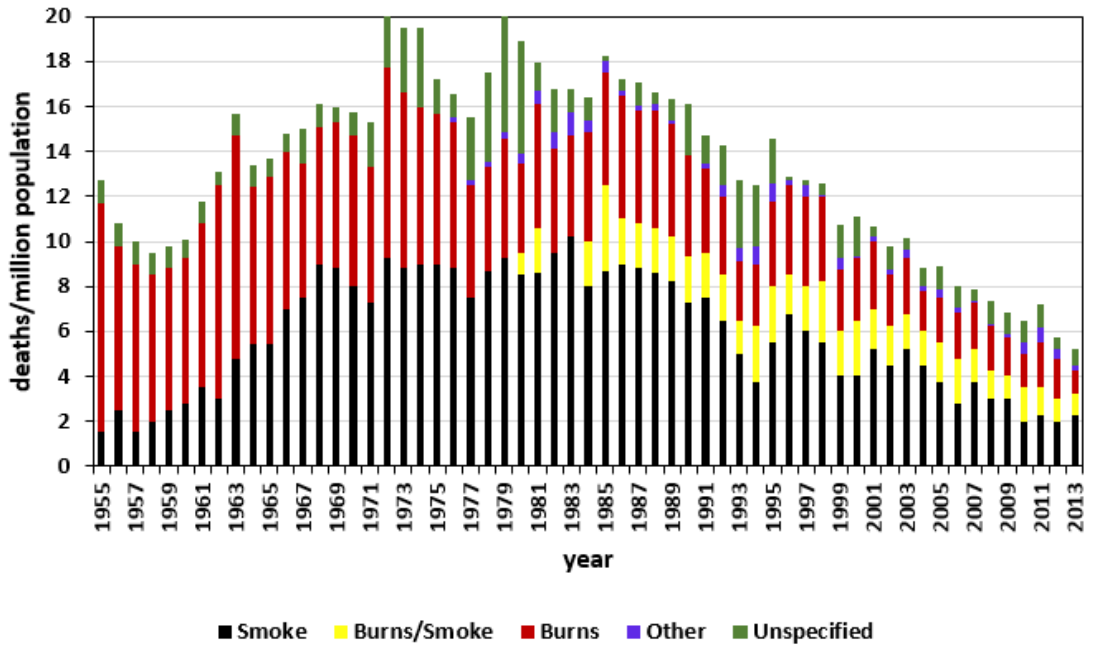


Figure 1-3 Fire Deaths in the UK (1955-2013) [8]

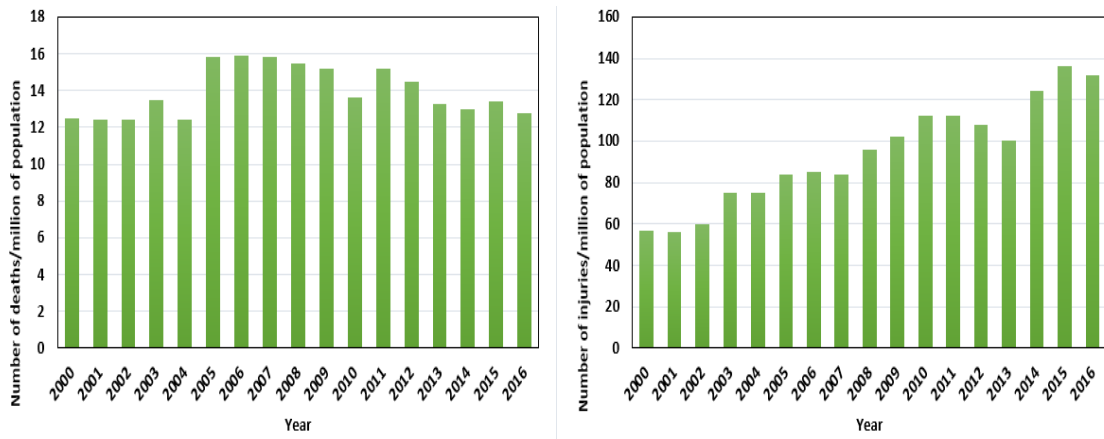


Figure 1-4 Fire Deaths and Injuries in Poland (2000-2016) [10]

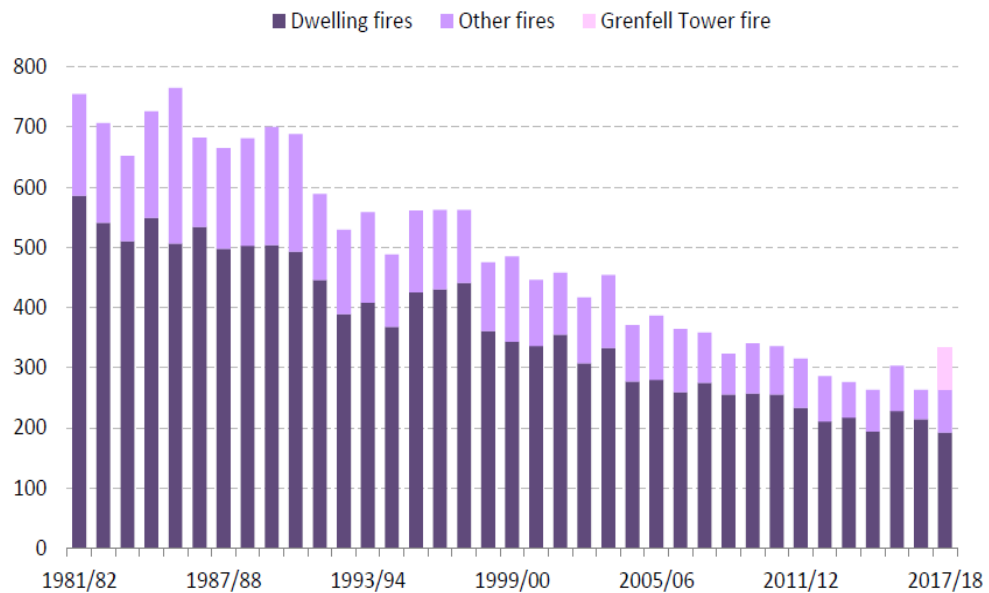


Figure 1-5 Total fire-related fatalities in dwellings or other fires, England; 1981/82 to 2017/18 [13]

1.3 Some Relevant Historical Fires

A few fire incidents whereby fire victims died as a result of smoke inhalation are discussed below.

1.3.1 The Cleveland Clinic Fire 1929

The Cleveland clinic fire occurred on the 15th of May, 1929 at approximately 11.30 a.m. The clinic was a 4-storey fire proof structured building of doctor’s offices surrounded by a small atrium. The fire started at the basement of the building where a pile of x-ray films were stored and was believed to have been triggered when x-ray film came too close to an incandescent light bulb of 100 Watt. The X-ray film was made of Nitro-cellulose, a highly flammable compound often called guncotton. Three tons of the x-ray film caught fire and released a deadly yellowish-brown poisonous gas that filled the waiting room of the floors above. At the time of the fire, 225 people were in the clinic, 123 died and 92 were injured. People that died had their faces turning yellowish-brown within minutes after death. Deadly nitrous peroxide filled everywhere and fatalities increased as a result of the inhalation of the poisonous gas and not the actual fire. All 123 deaths were as a result of inhalation of the poisonous gas.

The absence of air in the room prevented the fire from burning freely thereby increasing the quantity of the gas that was formed [18].

1.3.2 The MGM Grand Fire, 1980

The MGM Grand fire happened on the 21st of November, 1980 at MGM Grand Hotel and Casino in Nevada, USA at about 7.05 a.m. As at the time of the fire, there were about 5,000 people in the hotel. The cause of the fire was reported to be an electrical ground fault inside a wall in the hotel restaurant known as 'The Deli'. The presence of combustible furnishings, interior finishes, foam padding and moulding, air supply and a very large undivided area in the casino contributed greatly to the spread of the fire and production of heavy smoke. 85 people were killed by the fire and 650 were sent to the hospital. Out of the 85 fatalities, 1 jumped out of the building, 4 died as a result of burns while the remaining 80 died as a result of smoke inhalation and carbon monoxide. The fire mainly damaged the ground floor casino and other adjacent restaurants but most of the deaths occurred as a result of smoke inhalation on the upper floors of the hotel. Only 18 people died on the casino floor while 67 died on floors 16 through floor 26. The toxic smoke spread throughout the building through stairways, elevator hoist ways, open vertical shafts, impaired smoke dampers etc. all the way to the top floors [19]. MGM Grand fire is the worst fire disaster that has happened in Nevada and the third worst hotel fire in modern USA .



Figure 1-6 The MGM Grand Fire [19]

1.3.3 The Rose Park Nursing Home Fire 2004

The Rose Park nursing home is a 43-bed home for the elderly and infirm. The nursing home had 40 residents as at the time of the fire which occurred on the night of January 31, 2004 at about 4.30 a.m. Following the Fatal Accident Inquiry

(FAI) in 2010, Colin Hird from the Scottish Government explained that the fire started in a cupboard along a corridor, following an electrical fault [3]. It is thought that materials in the form of aerosols stored in the cupboard exploded, with the force of the blast blowing open some nearby fire doors along the corridor. Materials directly outside the cupboard including chairs, wallpaper, timber handrails ignited, causing heat and smoke to spread. Some of the residents had their doors open during the fire incidence and had their rooms filled up with smoke. Residents in bedrooms along two corridors were exposed to high concentration of toxic gases [3]. Ten (10) people died of smoke inhalation at the scene, within 11 minutes while four others died at the hospital.

1.3.4 The Grenfell Tower Fire 2017

The Grenfell Tower was a 24-storey tower block with 129 apartments housing up to 600 people in North Kensington, inner London. The tower had only a single central staircase. It underwent a renovation from 2012-2016 having new claddings and insulation. The fire started in the early hours of Wednesday the 14th of June, 2017 and was reported to have begun on the fourth floor. The fire was put out six minutes after the alarm but the flames rose up the exterior of the building and continued to spread very fast engulfing the whole of the upper floors. Residents got trapped in the building because they were incapacitated. As of 27th September 2017, the police estimated the death of 72 people. It was also reported that some survivors were treated for smoke inhalation with about three treated for hydrogen cyanide poisoning which was probably from the burning of the building exterior compounds [4]. Although the investigation into the fire incidence has not been concluded, it is most likely that people were incapacitated as a result of the inhalation of toxic gases and particulates which led to their death eventually.



Figure 1-7The Grenfell Tower Fire [4]

1.3.5 Piper Alpha 1988

Piper Alpha was a large oil production platform located in the North Sea, north east of Aberdeen, Scotland which on 6 July 1988 ignited as a result of gas leak, causing an explosion, followed by large intense oil pool fires. The leak was a condensate of almost entirely propane, which is heavier than air and hence the leak was concentrated at a low level. A total of 167 people were killed, 61 workers survived while 30 bodies were never recovered [20]. Most of the victims suffocated in toxic fumes which developed after a gas leak that led to the blasts and the ensuing fire. The total insured loss was about £1.7 billion [20]. Dense smoke was released into the atmosphere indicating the presence of toxic gases and particulates.



Figure 1-8 The Piper Alpha Fire [20]

1.3.6 Buncefield 2005

The Buncefield incident happened on the night of 10th December 2005 at the Hertfordshire oil storage, part of the Buncefield oil storage depot. This happened as a result of overfilling of one of the storage tanks, eventually leading to large quantities of petrol overflow from the top of the tank. A petrol vapour cloud of about 120,000 m² was formed, which ignited causing a massive explosion and a fire that lasted five days. The ensuing fire engulfed over 20 large fuel storage tanks to ignite, each of which was a hydrocarbon pool fire [21] with air and fuel in abundance. Damage claims by insurance companies, small businesses and families of about £700 million was estimated to have been caused by this disaster. The smoke plume covered the majority of south-east England and emitting huge amounts of particulate emissions and gaseous emissions into the atmosphere, with warnings announced to avoid going outside to reduce the risk of both emissions [21].



Figure 1-9 The Buncefield Fire [21]

1.4 Particulates in Smoke – Longer term effects

Smoke comprises mixture of gases, vapours and particulates. Particulates are any material collected on a filter paper after cooling the sample to 50°C. They comprise condensed volatile material, carbon and ash. Particulates comprise both micro droplets formed from condensed organic vapours and carbonaceous agglomerated structures (known as soot) consisting of spherical primary particles ranging from hundreds to many thousands [22]. Depending on the amount and location of deposition within the respiratory tract, several hazards are associated with the inhalation of smoke aerosols. The particle size determines how deep the particles are going to penetrate into the lungs and their likelihood of being exhaled while the extent of damage depends on the quantity of the deposited particles which in turn is related to the concentration of the smoke aerosol, shape and toxicity [22]. The effect of the damage can be immediate, such as cough or long term, such as cancer.

The key to survival during a fire incident is escape from the fire. Escape can only be possible if there is sufficient time, suitable escape routes and unaffected capabilities. Fires pose a great threat to life safety due to different physiological and behavioural effects as a result of the inhalation of hot air and toxic fire gases. Helplessness, lack of coordination, defective judgement, confusion, vision obscuration and fear may occur. This then tends to delay or prevent the escape of occupants which eventually leads to injury or death because of the increase in time being exposed to the toxic gases and/or hot air [2].

The awareness of health and environmental impact of particles generated from fires has increased in recent years. The significance of carcinogens as long-term

fire toxicants is becoming a great concern as a result of recent findings that fire fighters have twice the rate of cancer deaths of the civilian population [8]. A recent study by National Institute for Occupational Safety and Health (NIOSH) [23] affirmed that there's a very strong connection between firefighting and cancer. The study evaluated almost 30 000 firefighters employed between 1950-2009 and found that there was increase in cancer deaths and cancer incidence cases which comprised mainly of digestive and respiratory cancers within the period of study. Apart from the asphyxiants, irritants, allergens and carcinogens, another serious issue receiving great attention is the exposure to respirable particles of sizes less than 0.1 μ in diameter found in smoke and soot. These fine particles also increase the risk of having cardiovascular diseases, affecting the heart and the blood vessels.

In the mid-1990s, epidemiological data in the USA and UK showed that 1% extra deaths occurred for every 10 $\mu\text{g}/\text{m}^3$ of PM_{10} in ambient air within days of the high particulates [24-26]. Epidemiological studies have linked fine particulates in air pollution with cardiopulmonary mortality. The only medical explanation of this effect is that particles <50 nm must be present [27] as they cause alveolar inflammation and blood thickening [28], which reduces lung function and places a strain on the heart. This epidemiological data is based on correlations of PM_{10} in the atmosphere and hospital admissions and asthma drug demand. The medical explanation [27] involves the presence of solid nano-particles in the alveolar region of the lungs and the composition of these particles is not significant [27]. However, other evidence of health effects of fine particles include allergic reactions, chronic obstruction pulmonary disease (COPD), pulmonary fibrosis and lung cancer [29], indicate that the chemicals absorbed on the particles may also be part of the health effects of ultra-fine particles.

There is currently no standard or legislation that directly requires carcinogens from burning materials to be quantified [8]. There is also no limit on materials producing lethal quantities of carcinogens during a fire [8]. It is well known that fire fighters have the potential of experiencing acute and/or chronic respiratory health effects during firefighting activities.

Despite the health hazards associated with particulates generated during combustion in buildings/compartments or in the open, very little research has been done on fine particulate exposure in fires, especially on soot particulates generated from air starved fires or vitiated combustion. Earlier studies have shown investigations on smoke/soot production and particulates but not on fine particulates. Tewarson [30] examined emissions of smoke from various fire sizes and fuels for fully ventilated combustion and came up with a correlation between the average smoke emission rate and yields which holds for particulate dominated smoke in the presence of H and OH atoms provided by other fuels or ignition sources. Perera and Litton [31] studied smoke particles produced from a range of flaming and non-flaming combustible materials and determined the fractal aggregates using light scattering and light extinction. They [31] also determined the morphology using SEM and TEM. Tsuchiya and Mathieu [32] conducted an experiment of plywood under a depleted oxygen atmosphere using the Ohio State University (OSU) heat release rate (HRR) apparatus and used the experimental data to calculate the release rate and the total release of heat, carbon monoxide and smoke and the mean mass loss rate. Barakat et al. [33] analysed the smoke generated by four of the most commonly used oils in the Electricite de France production unit as well as heating oil and found that these fuels have the high propensity of generating soot particles. Haynes et al. [34] investigated soot formation in flat, premixed flames of ethylene, benzene, and pyridine with air using laser light scattering and fluorescence and extinction measurements. Most importantly, there exists a gap in the knowledge of fine particle size distribution of the smoke/soot particles generated during compartment fires. It is important to have a knowledge of the smoke yield, smoke size distribution and transport and deposition processes in order to develop a model of smoke deposition resulting from fires [22].

The development of safe building designs and safety strategies undoubtedly need effective assessment, measurement and quantification of toxic hazards to which humans can be exposed to in the event of a fire. This research seeks to look into toxicity of the gases and the size distribution of particulates emitted during the combustion of different solid materials and pool fires in compartments under different ventilation conditions.

1.5 General Legislative Background

As mentioned previously, smoke (comprising both toxic gases and particulates) inhalation accounts for over 60% of deaths in fires. Both toxic gases and particulates emitted during compartment fires and in the open are a serious threat to human health and the environment. Despite the serious threat fire effluents (toxic gases and particulates) pose to the human health and the environment, scientific understanding of particles associated with fires occurring in buildings remains poor. No specific requirements, standard or legislation on toxic products released from burning materials exist at the moment except in specific applications such as passenger vessels (trains and ships) with no evidence of wider adoption.

Current fire test guidance like Approved Document B ADB [35], BS 9991 [36] and BS 476 [37] mainly provide guidance and standards for the fire tests of building materials in terms of combustibility and fire propagation [38]. Although there is a requirement for measurement on smoke production, it is only defined by optical obscuration while the chemical analysis of smoke is not required. The reason for measuring optical obscuration is that the smoke can obscure vision, so that people caught up in a fire would not be able to recognize the emergency lighting and the exits, thereby leading to the impairment of escape from fires. However, the composition and yield either for soot, toxic gases or particulates in smoke, which actually kill people, are not required to be analysed. Under the current legislations, many materials or product with low flame propagation, such as some flame retardant and thermal insulation products, could pass the relevant fire test even though they generate extremely high amounts of toxic effluent. Smoke production is related to toxic gas production in that high smoke production would generally indicate high concentration of toxic gases species. There is therefore the need for toxicity assessment and measurements, but the methodology needs to be relevant and workable within a regulatory framework.

1.6 Aim and Objectives of this Work

The main aim of this research is to quantitatively study the toxic emissions (toxic gases and particulates) and the different fire conditions for wood based materials relevant to residential fires and in pool fires relevant to industrial scenarios.

The specific objectives include:

- Review all the available data on combustion, fire toxicity and toxic gas particulate yields.
- Develop a methodology for the analysis of particulate sizes using the cone calorimeter and the 5m³ fire rig test compartment.
- Carry out experiments to investigate the products of incomplete combustion in limited and free ventilation fires, including particulates.
- Investigate the size distributions of particulates generated during the combustion of certain fuel loads such as wood, and pool fires.
- Provide a set of yield data for the toxic gases and particulates yield that can be used to develop a model of smoke deposition resulting from fire.
- Carry out a toxicity assessment of the toxic species based on their lethality and irritancy.

Chapter 2 Literature Review

2.1 Fire Chemistry

As a process, fire can take many forms, all of which involves chemical reaction between combustible species and oxygen in the air. A fire can in general terms be also referred to as “Uncontrolled Combustion”. The process of combustion can be described in a simple form using the fire triangle in Fig. 2-1. The fire triangle shows the three components (Fuel, Heat and Air) necessary for a fire to occur. If any one of the components is absent or depleted, fire will not occur or cannot continue.

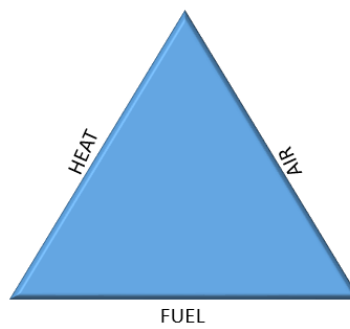


Figure 2-1 The Fire Triangle

A number of physical and chemical events take place before an ignition occurs. Flame is a gas phase phenomenon and therefore flaming combustion of liquid and solid fuels does not occur without their conversion into gaseous form [39]. For flaming combustion to occur in solid organic materials (e.g. wood or synthetic polymer), energy is required at the initial stage to thermally break the chemical bonds in the material. The first step is therefore for the material to get heated through radiation, convection or conduction which raises its temperature of the material depending on the thermal properties of the material [40]. Once the pyrolysis temperature of the material is reached, pyrolysis sets in. Pyrolysis produces volatile fragments and solid char in some cases. When the pyrolysis gases mix with oxygen, a combustible mixture is formed. With a suitable concentration of the combustible mixture (above the lower flammable limit) and a high enough temperature the material auto-ignites or the material can be ignited by pilot ignition. The surface temperature of burning solids is typically

300°C for many cellulose [39]. For burning liquids, flaming combustion occurs by evaporative boiling at the surface, producing gases that mix with oxygen to form a combustible mixture

2.2 Types of fires

Different types of substances or materials have the ability to burn. These substances include liquids (starting as pools, jet releases and aerosols), solids (starting as solid objects or dust particles) and gases. In this study, test fires are carried with solid objects (wood) and the liquid pools.

2.2.1 Solid Materials

The burning of solid materials almost always requires the pyrolysis of the solid to give off volatile fuel gases from the surface and burn in the flame. As this thesis is largely concerned with the toxic emissions from the combustion of solid and liquid pool fires, only the macroscopic behaviour of the materials on fire will be considered and not the chemical reactions involved in this process. The macroscopic behaviour of a solid, say a wooden stick, may be determined using some method of calorimeter, e.g. the cone calorimeter [39], which is one of the equipment used in this work, and this type of testing is usually adequate to define the material properties without a detailed investigation of the chemical processes involved [41]. While different forms of combustible solids exist, only wood (natural and processed) will be considered here.

2.2.1.1 Wood

Wood is a dominant type of fuel load in buildings as it is widely used in furniture and in construction of structure, flooring, fencing, decking, cladding, etc. Wood and other cellulosic solids burn through the process of pyrolysis, where the solid does not burn out completely but leaves a residue known as char.

When exposed to radiant heat of sufficient energy, wood begins to undergo pyrolysis where volatiles come off the surface of the wood. These volatiles are fuel gases and their mass flow rate from the solid wood depends on the intensity of the incident flux. With sufficient quantities of the fuel gases and available air, a flammable fuel/air mixture is formed, which can be ignited by the introduction of an ignition source such as a pilot flame or a spark and if the autoignition

temperature is reached, it can self-ignite without any pilot ignition. Once ignited, the burning of fuel introduces heat energy to the solid wood in addition to the incident flux. This increased energy raises the rate of volatiles released and the rate of combustion.

The release of more volatiles from the surface of the wood leads to the formation of a char layer on the surface of the wood which builds up as the pyrolysis penetrates deeper into the inner part of the wood to release more volatiles. The char layer formed serves as an insulation to the surface of the wood thereby reducing the intensity of the heat reaching the inner part of the wood for pyrolysis. This also reduces the rate of pyrolysis and therefore the rate of heat released from the burning. At around 300°C [42], the char layer begins to shrink, crack and break down allowing more volatiles to be released from the surface for the burning process to continue (as shown in Fig. 2-2). The process continues until all the volatiles are given off from the wood at which point flaming combustion stops and the char begins glowing. The formation of a char indicates that the volatiles produced in burning are different as burning progresses.

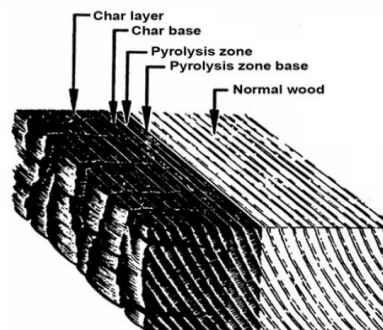


Figure 2-2 Charring of Wood [42]

2.2.2 Pool Fires

Pool fires are defined as turbulent diffusion flames established over horizontal fuel surfaces with defined boundaries under conditions where the fuel has zero or low initial momentum [17, 43]. For liquid fuel, the depth of the pool is identified through the accumulation of fuel in the prescribed area.

A key feature of pool fires is the degree of feedback between the fire and the fuel. The heat transferred back from the fire to the pool determines the rate at

which the pool evaporates, and hence the fire size and other characteristics including the toxic emissions [17].

The pool fuel may be contained (confined by the physical barrier providing confinement) or running/spreading fire (in the case of spill or leak) [17, 43]. The contained pool fires can burn for a very long period of time, provided the fuel is available and burning at a very high rate, mostly guaranteed by the effective limit on heat losses to the substrate [44]. Spill fires are difficult to accurately define because of the way they spread along surfaces, with the dimensions of the spread being controlled by the physical properties of the fuel and the nature of the substrate. However, local build-up of fuel tends to be small having thin layers and losses to the substrate are similarly larger. Hence, spill fires are anticipated to have short flame height and duration with large effective diameter. The large diameters indicate poor entrainment, thus higher soot production [45].

Pool fires represent an important element of the risks linked with major accidents on offshore and onshore physical and chemical processing installations, particularly installations that may have large liquid hydrocarbon inventories such as storage and distribution depots. This work studies the toxic emissions from pool fires.

2.3 Compartment Fires

A compartment fire can be defined as a fire which is confined within a room or similar enclosure within a building [39]. The development of fire in an enclosure or compartment depends on various factors and these include the enclosure geometry, the ventilation (size and location of openings) and the type of fuel, amount and surface area. The existence of walls and ceilings in compartment fires makes them somewhat different from those fires burning in the open air [46]. In free space or open air fires, most of the generated heat and smoke would be lost to the ambient quickly while in compartment fires, the generated heat and smoke would be confined in the upper part of the compartment or ceiling and then lost to the environment through exits from the room. The hot gases trapped inside the compartment and the heated upper compartment boundaries, will also radiate heat back to the fuel surfaces increasing thus the burning rate compared

to an open fire, while the limitation of air-flow through the compartment openings will impose an upper limit in the burning rate.

At the onset of fire in an enclosure, the fire is said to be fuel-controlled or highly ventilated whereby the enclosure itself has no effect on the fire. The fire burns freely at this stage as it would in the open. As the fire grows, its behaviour changes, the room openings supply air into the compartment and the fire plume develops. The ceiling interrupts this plume, forming a hot gas layer. As the hot gas layer descends below the top of the opening, fire gases that flow out are replaced by new air that flows into the room with the new air providing fresh oxygen to the fire, allowing it to burn more vigorously and increasing the quantity of heat and fire gases [47]. This clearly describes a well ventilated fire as shown in Fig. 2-3 below.

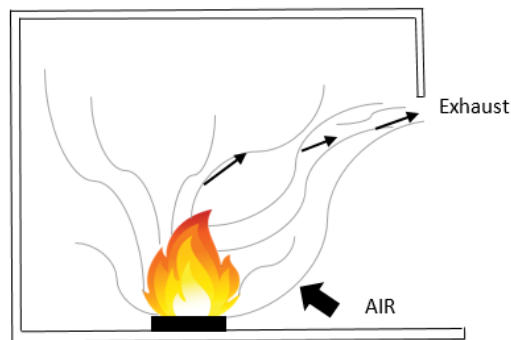


Figure 2-3 Hot layer gases in an enclosure

2.4 ISO19706 Characterisation of Fire Stages

In order to gain a better understanding on the production of toxic gases, it is important to classify the stages of fire growth so as to know the role they play in the production of toxic gases and the hazards they pose to individuals. ISO [48] classifies these stages in terms of heat flux, temperature, oxygen concentration, CO₂:CO ratio, equivalence ratio and combustion efficiency. The nature of the fire differs for every fire incident, some may remain relatively constant while some often develop through series of stages each involving a different set of combustion conditions [49]. ISO 19706 [48] classifies fires as follows:

1. Non-flaming Combustion
 - a. Self-sustaining (Smouldering)

- b. Oxidative pyrolysis from externally applied radiation
- c. Anaerobic pyrolysis from externally applied radiation
- 2. Well-Ventilated flaming fires
- 3. Under-Ventilated flaming fires
 - a. Small localised fire, generally in a poorly ventilated compartment
 - b. Post-flashover

2.4.1 Non-flaming Combustion

Non-flaming is the initiating event of any fire and occurs when a material/polymer undergoes a thermal decomposition as a result of an endothermic reaction through the application of an external source of heat or self-heating. This causes a thermal breakdown of the structure of the polymer. At this stage the heat flux is zero with the oxygen level remaining constant without being lowered. **Stage 1a** only occurs with porous materials such as foam or other cellular structures or residues such as char from burning wood. This type of fire has the exothermic oxidation of the porous material driving the endothermic thermal decomposition of the adjacent undecomposed material making the overall product yields depend on the combined effects of the two processes. **Stage 1b** is the most common form of thermal decomposition in fires. Here, reaction with oxygen occurs on the surface of the material and also possibly in the gas phase when air is present. In the absence of large ignition sources, stage 1b is often the antecedent to flaming combustion. Most materials undergo oxidative thermal decomposition at temperature above 300°C. **Stage 1c** is the simplest pyrolysis that occurs in the event of fire. This occurs in an inert atmosphere when the temperature is high enough to produce thermal breakdown of the polymer structure. These fires may not be immediately hazardous but can lead to toxic concentration of CO and other irritants over time. The equivalence ratio in this stage of fire is close to zero.

Toxic gas emissions from smouldering fires are significantly different to those from flaming fires. First, there is a much lower emissions rate per unit area and also a different chemistry [50]. Smouldering is typically an incomplete combustion, releasing species and quantities that are substantially different from

that in stoichiometric and complete combustion. For example, the CO/CO₂ ratio which signifies the incompleteness of a combustion is ~0.4 in smouldering but ~0.1 in flaming combustion [50]. The release of pyrolysate, which does not burn without a flame being present, significantly contributes to the production of a complex gaseous mixture including volatile organic compounds (VOC), polyaromatic hydrocarbons (PAH), other hydrocarbons and particulate matter (PM). Although the yield of toxic species is larger in smouldering fires than in flaming fires [51], the rate of production, which is proportional to the rate of spread, is much lower. This implies that a smouldering fire of long duration inside an enclosure or compartment, (from 1-3 hours for a single bedroom size compartment [52]) can lead to a lethal dose of toxicity, especially CO [50]. But there is still insufficient data on the toxicity of smouldering materials to conclusively resolve the issue of life hazards.

2.4.2 Well-Ventilated Flaming Fires

Flaming fires are always well ventilated at the initial stage and will remain well ventilated as long as the fire is small in comparison to the size of the compartment it is burning in and the air supplied to it is enough. The compartment geometry plays an important role at this stage of the fire.

In small compartments, at the early stage of the flaming fire, hot gases of smoke is formed below the ceiling and the heat from the smoke is radiated back to the fire to accelerate the intensity of the fire producing heat, carbon dioxide, water and sooty smoke until flashover or fully developed fire is reached. The yield of CO is usually very low except for materials such as foams, polyvinyl chloride (PVC) etc.

In large compartments, such as shopping malls with atriums or warehouses, the fire continues to grow while remaining well ventilated. The main hazard here is the heat from spreading fire and the upper layer smoke. Well ventilated fires are the least important in terms of toxicity because they hardly generate sufficient concentration of effluent to cause harm except in a very small enclosed space. At this stage, escape and extinguishment are often possible.

Most fire tests have been carried out under well ventilated conditions and therefore most of the available data on fire tests and toxicity were obtained under these conditions.

2.4.3 Low/Under Ventilated Fires

Modern buildings and transport vehicles consist of enclosed compartments with low ceilings or a number of compartments interconnected by open doors. In these types of buildings, vitiated fires are the most common. As the fire grows, the ceiling is filled with hot gases and smoke until the upper layer starts to descend thereby increasing the proportion of the flames. The rate at which the fire grows determines how fast the upper layer is filled. The mass of air entrained per unit mass of fuel is decreased. The global equivalence at this stage is greater than unity with a vitiated and incomplete combustion taking place. The yield of CO₂ and NO_x becomes very low while the yield of other products of incomplete combustion such as CO, VOCs and smoke particulates increase. The incomplete or inefficient combustion decreases the heat of combustion and when the upper layer descends to the base of the fire, the fire is extinguished.

The hazard to occupants arising from this stage of fire is mainly from inefficient combustion which give rise to high yields of asphyxiant gases (CO and HCN) and irritant smoke.

2.4.4 Post Flashover Fires

The availability of fuel load and ventilation are the conditions necessary for flashover to be attained. When the temperature of the hot layer is high enough to be fully reactive (between 500-600°C), heat is radiated downwards to ignite all combustible materials in the enclosure causing a widespread growth of fire (**Flashover**). If enough ventilation is available, the fire continues to burn until all the fuel is consumed. The smoke layer at this stage descends to provide an under-ventilated combustion. If the building remains without collapsing and is enclosed, such fires fill up all open areas with smoke enriched with toxic products within a very short time. Exposure to such smoke can cause incapacitation very

quickly and be lethal within a short period. The fire may then continue to burn slowly or self-extinguish depending on the leaks available in the enclosure/compartment.

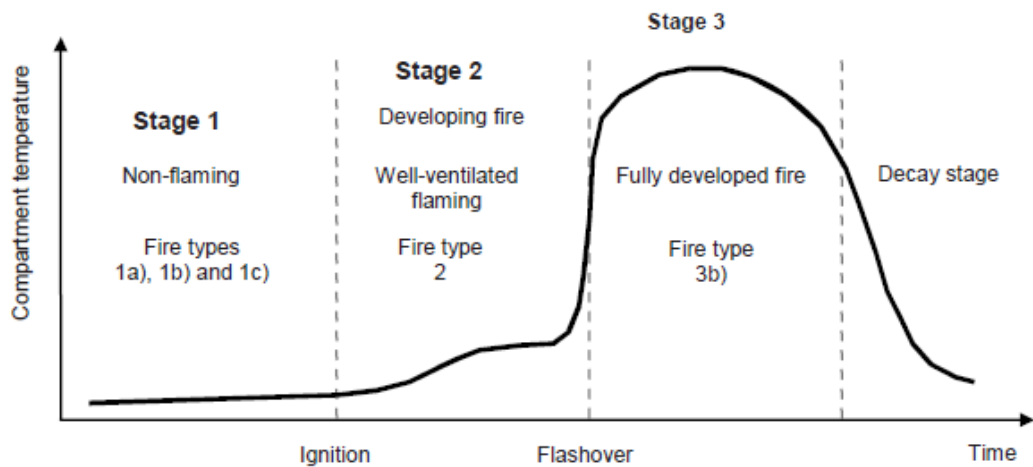


Figure 2-4 Stages of fire Development within a compartment [53]

2.5 Hazards From Fire

A number of toxic hazards are associated with fire and the inability of victims to escape from fire environments result from being exposed to heat, visual obscuration as a result of smoke, narcosis due to the inhalation of toxic gases and irritation of the respiratory tract [54]. These hinder escape and frequently cause death to those who manage to escape but have damaged lungs as a result of the exposure [55].

2.5.1 Heat

Exposure to heat can be life threatening in three ways and these include hyperthermia, body surface burns and respiratory tract burns [55].

2.5.1.1 Hyperthermia:

this is an elevation in body temperature whereby the body produces or absorbs more heat than it dissipates. When predicting life threat due to heat exposure in fires, only the threshold of second degree burns and the exposure where hyperthermia is enough to cause mental deterioration which in turn become a threat to the survival of people need to be considered [55].

2.5.1.2 Body Surface Burns:

when considering the exposure of skin to heat, the smoke layer temperature should not exceed 200°C which is approximately 2.5 kW/m² radiant heat flux. Anything above 200°C or 2.5 kW/m² will lead to untenable conditions and make escape impossible [56]. Below 200°C or 2.5 kW/m², exposure can be tolerated for 30 min or even longer without having an effect on the time available for escape [55].

Table 2-1 Effects of Exposure of heat to the skin [56]

Types and Period of Exposure	Effect	Temperature (°C)
Radiation	Severe skin pain	200
Conduction-metal (1 second)	Skin burns	60
Convection (30 minutes)	Hyperthermia	100
Convection (< 5 minutes)	Skin/lungs burns by hot gases	120
Convection (< 1 minute)	Skin/lungs burns by hot gases	190

2.5.1.3 Burns to the Respiratory Tract:

as a result of inhalation of dry air, usually < 10% water vapour are accompanied with burns to the skin or the face [55]. Air above 60°C saturated with vapour can burn the respiratory tract when inhaled.

2.5.2 Smoke

Smoke can be defined as an aerosol of solid or liquid particles usually resulting from incomplete combustion followed by various fire gases and dictated by burning or heated material. The production of smoke depends on various factors such as the chemical make-up or composition of the fuel, the temperature of the burning process, the amount of oxygen supporting the combustion process and the existence or lack of ventilation. The smoke produced during a fire is a

collection of particulates, superheated air and toxic chemical compounds [57]. Purser [58] showed that the main toxic products in most fires are CO, HCN and irritant or acidic gases and the amount of each depends on the thermal decomposition of the fuel, which also depends on the temperature and oxygen supply. The increase in the use of synthetic polymeric materials in commercial and residential buildings has contributed to differences in combustion and fire behaviour and the smoke production during a fire. These synthetic materials are majorly carbon based bonded with different atoms such as hydrogen, nitrogen, chlorine, and sulphur. Synthetic substances easily ignite and burn fast causing rapidly developing fires and producing toxic smoke [57]. The accumulation of smoke in an enclosure makes it very difficult for occupants to find their way. This difficulty results in an increase in the time required for escape. As the intensity of the smoke increases, the vision becomes impaired thereby making the occupants unaware of their location despite being familiar with the surrounding. The time when such occurs represents the upper limit for the time available for escape due to smoke obscuration. Estimates have shown that confrontation with a fuel mass loss concentration of 20 gm^{-3} for well ventilated fires or 10 gm^{-3} for under-ventilated fires results in occupants literally not seeing their hands in front of their faces and hence becoming disoriented [55].

2.6 Toxic Combustion Products

The toxic combustion products can be classified into two: The asphyxiant gases and the irritant gases [55]. A classification of the toxic combustion products is shown in Fig. 2-5. Table 2-2 shows a summary of the toxic effluents and their effects.

2.6.1 Asphyxiant Gases

Sometimes called narcotic gases are those gases that prevent the uptake of oxygen by cells. This is accompanied by central nervous system depression, loss of consciousness and eventually death. The dose of the gases inhaled determines the severity of their effect as the higher the dose the higher the severity [1]. This means that the concentration and the time of exposure play a

key role in the effects of these toxicants. The main asphyxiants are carbon monoxide and hydrogen cyanide. Low oxygen concentration can lead to asphyxiation and carbon dioxide can affect asphyxiation [55].

2.6.1.1 Carbon Monoxide

Carbon monoxide is a tasteless, odourless and colourless gas that is lighter than air. It has a toxic effect of lowering the oxygen carrying capacity of the blood even when the partial pressure of oxygen and the rate of blood flow are normal. Carbon monoxide binds with oxygen in the red blood cells to form carboxyhaemoglobin COHb. Carboxyhaemoglobin is 200 times more stable than oxyhaemoglobin which leads to difficulty in the transportation of oxygen from the lungs to cells in the body. This then causes a deterioration in mental and muscular performance [55]. CO also combines with myoglobin in the muscle cell ruining distribution of oxygen to cardiac and skeletal muscles [58]. At different concentrations, the inhalation of carbon monoxide impairs individual's ability to escape causing different effects at different concentrations. A 10 ppm carbon monoxide exposure for short periods cause impairment of judgement and visual perception, 100 ppm exposure causes dizziness, headache and weariness, loss of consciousness occurs when exposed to 250 ppm, and inhalation of 1000 ppm results in quick death. Low levels of carbon monoxides are suspected of causing respiratory and heart system disorders when a person is exposed to it for a very long time [59].

2.6.1.2 Hydrogen Cyanide

Hydrogen cyanide is a colourless liquid or gas with a characteristic odour (bitter almond-like odour). It is a very volatile liquid that boils at 26°C. Hydrogen cyanide is 25 times more toxic than carbon monoxide due to the formation of cyanide ion as a result of hydrolysis in the blood [1]. The only materials that yield HCN are the nitrogen-containing materials which require very high temperature for that [1]. Hydrogen cyanide differs from carbon monoxide in the sense that the cyanide ion formed is distributed throughout the body fluid and is in contact with the cells of tissues and organs whereas Carbon monoxide remains primarily in the blood [1]. Cyanide is said to be toxic in two ways. First it combines with ferric ion in the mitochondrial cytochrome oxidase inhibiting the transport of electron in the

cytochrome system and inhibiting the cells' oxygen use. Secondly, it causes a brief stimulation, then severe depression of respiratory frequency follows leading to starvation of body oxygen which then results in convulsions, respiratory arrest and death [60]. Inhalation of HCN causes incapacitation thereby preventing escape. The quantification of CN^- in the blood of fire victims is very expensive and therefore not carried out most of the time [55]. HCN also decays very rapidly in the blood and thus assessment by post-mortem can be unreliable [55]. This makes it difficult to know the contribution of hydrogen cyanide to the death of fire victims [55]. Hydrogen Cyanide is more complex than Carbon monoxide.

2.6.2 Irritants

Combustion toxicologists have considered irritant effects to be of two types [1], sensory irritation including irritation of the eyes and upper respiratory tract, and pulmonary irritation affecting the lungs including coughing and bronchoconstriction. Most fires produce symptoms of both. Unlike asphyxiants, irritants are more complex because they can't be found in the blood of fire victims. They can lead to incapacitation and also prevent escape. In most cases the cause of death will be attributed to elevated level of carboxyhaemoglobin but in reality, they must have been exposed to some irritants which impaired their escape leading directly or indirectly to death. Irritant fire effluents affect the eyes, nose, throat and upper respiratory tract causing uneasiness and severe pain. The effects of irritants are numerous and include: tears and reflex blinking of the eyes, pain in the nose, throat, and chest, breath-holding, coughing, excessive secretion of mucus, bronchoconstriction and laryngeal spasms [58]. Most irritants have the tendency to penetrate deep into the lungs when attached to submicron sized particles such as soot causing pulmonary irritation, leading to respiratory discomfort and distress and death, which can be after a few hours or several days, due to flooding of the lungs (Pulmonary oedema) [61]. Irritant gases comprise; halogen acids e.g. HCl, nitrogen oxides, sulphur oxides, acrolein and aldehydes e.g. formaldehyde. The greatest danger associated with irritant gases is reducing the speed of egress during the evacuation of people in the event of a fire occurring.

Purser [62] presented that in most fires the key toxic products are CO, HCN and irritant or acidic gases and the amount of each depends on the thermal decomposition of the fire load, which again depends on the temperature and oxygen supply. However, HCN, HCl and HBr are typically low except if the fire load contains N, Cl, or Br. This applies to wood and pure hydrocarbon fire. Low levels of HCN (but at toxic levels) can potentially occur through hydrocarbon reactions with nitrogen in the air in rich zones.

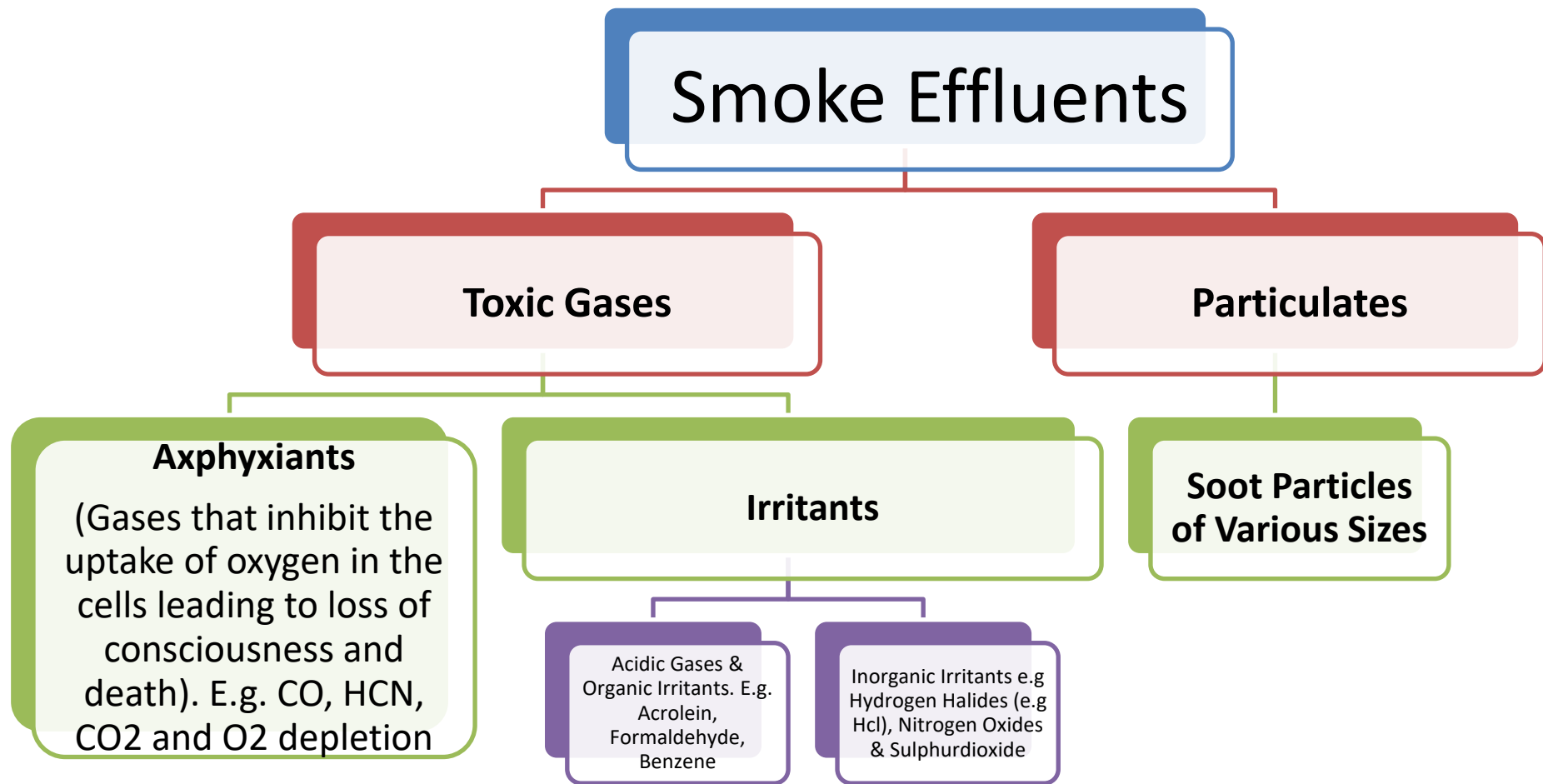


Figure 2-5 Incomplete Combustion Products

Table 2-2 Summary of fire effluents and their effect [63]

Type of Component	Examples of Compounds	Sources	Risks
Inorganic Gases	CO ₂	All fires	Acute: Asphyxia
	CO	All fires	Acute: Asphyxia
	HCN	Nitrogen containing fuels, e.g. Nylon	Acute: Asphyxia
	NO, NO ₂ , (NO _x)	Nitrogen containing fuels, e.g. Nylon	Acute: Asphyxia Sublethal: Lung damages
	NH ₃	Nitrogen containing fuels, e.g. Nylon	Acute: Asphyxia
	HCl	Chlorine containing fuels e.g. PVC	Acute: Asphyxia
	HF	Fluorine containing fuels e.g. PTFE	Acute: Asphyxia
	HBr	Bromine containing fuels, e.g. Br-flame retarded material	Acute: Asphyxia
	SO ₂	Sulphur containing fuels, e.g. wool	Acute: Asphyxia
Volatile Organic Compounds	Isocyanates	Nitrogen Containing fuels e.g. PUR, mineral wool	Acute: Irritation
	Phenol	General for many fires	Sublethal: Asthma, Cancer
	Styrene	Polystyrene	Acute: Irritation
	Benzene	General for all fires	Acute: Irritation Sublethal: Cancer
Semi-Volatile/Condensed phase organics	PAH	General for all fires, particularly aromatic fuels	Sublethal: cancer
	Dioxins/furans	Fires with fuels containing chlorine or bromine	Sublethal: Cancer, immune toxicity, etc.
Particles	Soot particles of various sizes	All fires	Acute: Visual obscuration,

2.7 Influence of Ventilation on Fires

Despite the number of deaths every year as a result of the inhalation of toxic gases during fire incidents and the importance of fire incidents which occurred in an air-starved enclosure (e.g. Rose Park Nursing Home Fire), the experimental study on air starved fires has not been much and most of the publications available for toxic yields in fires have been for highly ventilated fires. Andrews et al. [64-66] carried out a review on the experimental fire ventilation data available and this showed that most data was for an enclosure with a door either wide open or at least partly open.

Wieczorek [67] studied species generation and transport from enclosure fires with a half-scale ISO 9705 enclosure. A 6.1 m long hallway was connected to the compartment in a head-on configuration for the transport study. Limited ventilation compartment fire was generated using a continuously fed n-hexane burner. A range of heat release rates ranging from 50 kW to 500 kW, along with four ventilation conditions with an opening area of 0.06, 0.15, 0.2, and 0.54 m² were used for the experiment. Utiskul and others [68-70] conducted an experiment using the reduced scale enclosure RSE (40 x 40 x 40 cm), fitted with top and bottom vents to examine the behaviour of fully developed compartment fires. Utiskul [68] examined different fire behaviour characteristics such as extinction, oscillation, fire area shrinkage, and response of fuel to thermal and oxygen effect in ventilation-controlled fires. A major project on limited ventilation of hydrocarbon fires was conducted by NIST [71, 72], which was aimed at generating detailed information on ventilation controlled pool fires, useful for validating fire CFD models. Different fire experiments at different fire conditions were conducted in 1.4 m³ reduced scale enclosure, equivalent to a 2/5 scale compartment, based on the ISO-9705 room having two open door configurations of 0.388, and 0.194 m² area. Gas species and soot measurements were obtained from two locations in the upper layer of the compartment. The fuels considered, heptane, toluene, and polystyrene, generate highly smoky fires over a range of natural ventilation condition.

Fire tests with controlled ventilation have often been investigated in test rigs that have open window or door situations where passive fire protection can be applied to limit the supply of air to the fire [64-66]. The fire legislations require windows and doors to be closed, as such, opening windows and doors is not a very realistic way of determining the toxic gases from a fire (but rather closed window and doors). In a situation where the opening is quite small such as door leakage areas, the inadequate supply of oxygen will cause incomplete combustion, leading to a decrease in the amount of fuel burnt, which in turn causes the energy release rate to decrease while the concentration of unburnt gases increases. Generally CO is considered to cause the greatest number of fire deaths [55]. In most fires, carbon monoxide and carbon dioxide are not the only gases present. There are always a large number of other substances present in smoke which include particulates. When considering the time to incapacitation of victims, several factors need to be looked at, including the duration of CO exposure, level of victim activity and the age of victim. This present work investigates fires in a freely ventilated environment and an under-ventilated enclosure with doors and windows closed where CO, other toxic gases and particulates would be investigated.

Fire legislation require doors and windows be closed in rooms for passive fire protection and energy conservation. Therefore a room adhering to these legislation will have a fire resulting in very low ventilation rates like the leakage rates of smoke in the design of fire doors. However, the development of the fire is slow as it is well known that heat release rates and fire temperatures in enclosed fires are mainly dependent on the air ventilation rates.

Fire resistance testing seem to be an adequate approach under well-ventilated fires with high fire temperatures because they create the worst case fire scenarios in terms of loss of compartmentation but seem to be inappropriate for fire toxicity studies as they do not create the worst case scenario, apart from CO and sometimes CO₂ toxicity. It is known that oxygen deprived fires generate high levels of CO, unburnt hydrocarbons and other potentially dangerous species including particulates. This work investigates products of incomplete combustion of different materials with emphasis on smoke particulate emissions under different fire conditions. In rich fires where the supply of air is through an open

door, the fire temperature is high and the yield of CO level is usually well below equilibrium unless the temperature is very high [64, 66]. The presence of high hydrocarbons in oxygen deprived fires generate acidic and irritant toxic gases due to the partial oxidation products of hydrocarbons.

A ventilation parameter K_{in} was introduced by Andrews et al. [64-66] and is described as the air in leakage equivalent open area, A_v , divided by the cross-sectional area of a cubic room of equivalent volume (V) to the test room. The parameter K_{in} allows air in leakage to be assessed for any shape of room. This can be expressed mathematically as $K_{in} = A_v/V^{2/3}$.

K_{in} was shown by Andrews et al. to range from 0.09% to 0.6% for designs that comply with the regulations of passive fire protection where fire doors and windows are closed. Before the work of Andrews et al. [73], Sugawa et al. [74] determined K_{in} value of 1.32%, Peatross and Beyler [75] determined 1.7% and Auduoin et al. [76] studied K_{in} value of 1.9%.

The experiments with a door or window open recorded K_{in} of 4.4% by Gottuk et al. [77] [78], Peatross and Beyler [75] studied K_{in} of 2.7 and 6.8%, Fleischmann, C.M. and Parkes, A.R. [79] studied a K_{in} of 9.2% while Chamberlain [16] studied K_{in} of 9.4 and 26% in a much larger enclosure. A similar test facility to one used by Andrews et al. [73], but with conventional open fire doors was used by Ohmiya et al. [80] to study K_{in} of 19%, 28.5% and 38%. These values can only be obtained with a door that is very large in a small room or a double door in a normal sized domestic lounge. Ohmiya et al. also determined a range of K_{in} from 4% to 16% in a smaller cubic fire enclosure. Both experiments were shown to be ventilation controlled, having heat release rate controlled by the air flow even though it was very large. Utiskul et al. [70] investigated the fire behaviour of heptane pool fires in a small-scale 40 x 40 x 40 cm³ compartment with wall vents at the ceiling and the floor. The total area of the vents was varied from 2 to 240 cm² which translated to a K_{in} of 0.1% to 15%. A room that is about 40 m³ in volume with a completely open door has K_{in} of the order of 17% and an open window has a K_{in} of about 5%. A major project on limited ventilation of hydrocarbon fires was conducted by NIST [71, 72], aimed at generating detailed information on ventilation controlled pool fires, useful for validating fire CFD

conducted in 1.4 m³ reduced scale enclosure having two open door configurations of 0.388, and 0.194 m² areas. These ventilation configurations resulted in a K_{in} of 31% and 15%. Most enclosed fire investigations have been carried out using the open window and door scenarios of fire ventilation [73]. Smoke control standards have permissible gaps that convert to a K_{in} of 0.06% which would give about 9 air changes an hour in the test facility of 1.56 m³ used by Andrews et al. [64-66].

The construction of a 1.56 m³ combustion rig test facility was initiated by Andrews, Ledger and Phylaktou to carry out experiments with known flow rates in a repeatable way. Many experiments were carried out in the rig using different fuel types and fire loads at varying ventilation rates. The authors Andrews et al. [64-66, 73] showed that the situation in enclosed fires with closed doors (air starved fires) is quite different from compartment fires having doors open. They found the richest fire equivalence ratio to be 0.55 for 2.7 air changes per hour and 0.75 for 30 air changes per hour. The flow of 2.7 air changes per hour was 9% and 8% for the higher airflow. The peak mean ceiling fire temperatures were 250°C and 450°C respectively. These fire temperatures were not high enough to achieve CO or un-burnt hydrocarbon (UHC) oxidation and CO and UHC levels were found to be very high at 3000 and 2500 ppm, respectively, for the low airflow and increased to 1% for the higher airflow. Comparing with the CO yields of other investigators [77, 78] using the same fire equivalence ratio showed yields of 50-200 g/kg for the low ventilation low temperature fires, as with 10-50 g/kg in the higher ventilated higher temperature fires obtained in the literature, where fires in rooms with airflow similar to that of an open door were studied. The available literature on the influence of ventilation on fires all show higher levels of CO than equilibrium in the lean equivalence ratio region and close to equilibrium in the rich fire region [77, 78].

The study of carbon monoxide yield by Gottuk et al. [77, 78] showed an identification of a correlation between the emission yield and equivalence ratio. They found out that carbon monoxide yields increased with equivalence ratio while the carbon dioxide level decreased. The work carried out by Andrews et al. [64-66] showed that the yield of toxic products in fires is a function of the fire equivalence ratio. Purser [81] also showed that using the BRE tube furnace

which he compared with the large scale fires of Tewarson [82]. Pitts [83] also found that high levels of CO are formed in enclosure fires which are under-ventilated. Pitts [83] identified that one mechanism responsible for the formation of CO is the quenching of a fire plume upon entering an upper layer of rich combustion products. The combustion products generated by this process have been shown to have a strong correlation with the upper-layer equivalence ratio. Experiments show that the correlations depend on the upper-layer temperature, but that well-defined correlations exist for low ($< \sim 700$ K) and high ($> \sim 900$ K) temperatures. Andrews et al. [73] in their study, found out that the tabulations of fire product yields measured in the standard cone calorimeter which is a freely ventilated equipment may not represent the actual yields in enclosed air starved fires.

Tewerson [84] used the ASTM E2058 fire propagation apparatus FPA to produce his fire toxicity yields database for many common fuels, which was in a well-ventilated condition. Aljumaiah [85] investigated the toxic gas yield produced from 4.6 kg wood crib fire under several ventilation conditions using a 1.6 m³ fire rig test compartment. They concluded that the amount of toxic yield produced in wood fire depends highly on the ventilation condition where higher yield of CO and total hydrocarbons were obtained for the ventilation-controlled fire. The result were consistent with the data provided by Tewarson [84] with richer mixtures having higher yield of CO. Gottuk et al. [77] used a 2.2 m³ compartment to report CO yield data from wood and Beyler [86] used a 1.6 m³ hood controlling the air supply to achieve varying equivalence ratios. Both results [77] and [86] show strong dependence of yield on equivalence ratio as shown in Fig. 2-6.

Alarifi [87] compared the result from wood pellet tests in his full-scale experiments with that of [77, 84-86] in Fig. 2-6. His [87] results show good agreement between Tewarson's correlation and Aljumaiah's data at the lower ventilation rate. But, for a significant amount of data for seemingly larger compartments and/or larger ventilation rates there was a significant deviation from Tewarson's correlation which starts at equivalence ratio of 0.5 and higher where the correlation significantly underpredicts the data. However, there was good agreement between his data and those of Gottuk and Beyler for equivalence ratios of 0.5 to 1.3. Their data does not extend beyond Φ of 1.6 while

Alarifi's extend up to Φ of approximately 2, where yields of CO close to 0.3 were measured. Some of Aljumaiah's data at the highest ventilation rate gave comparable yields but at much higher Φ of 2.5. Aljumaiah measured the yield of CO from four different pool fires (Diesel, Heptane, Toluene and Kerosene) and compared them as shown in Fig. 2-7. Heptane produced the highest yield of CO followed by toluene, diesel and then kerosene.

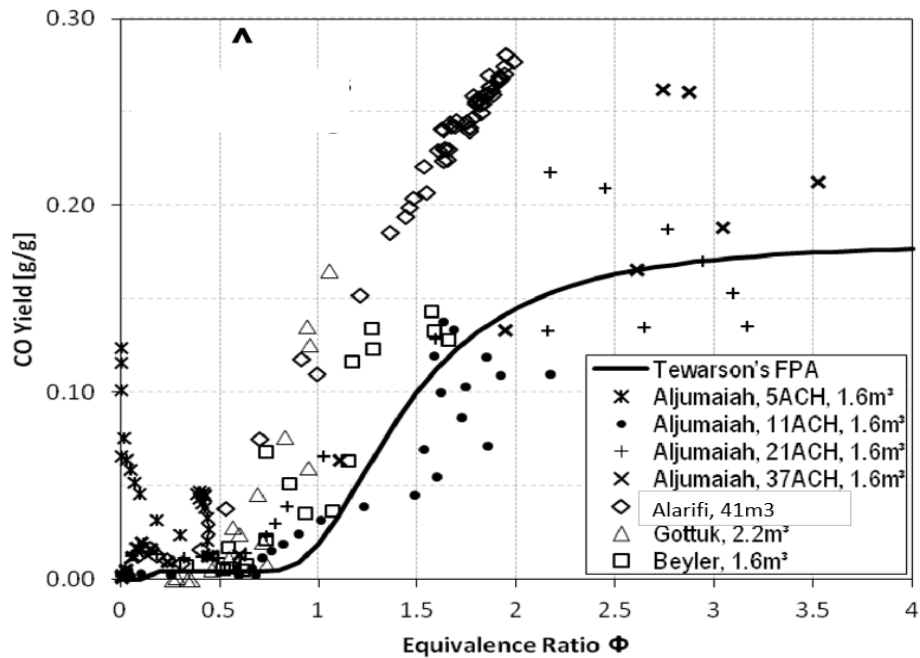


Figure 2-6 Yield Data Comparison extracted from Alarifi [87]

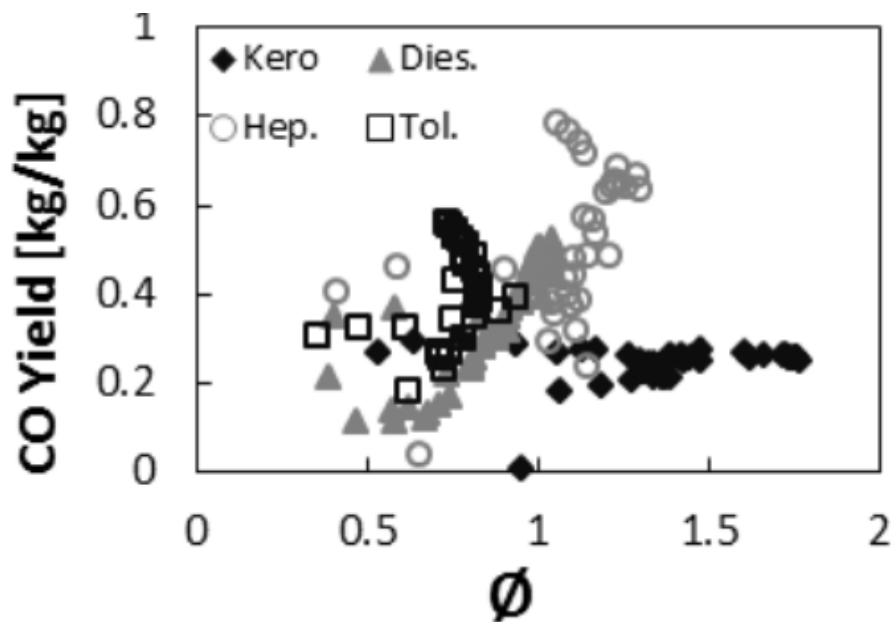


Figure 2-7 CO Yield extracted from Aljumaiah [85]

2.8 Factors Determining Toxic Hazard

2.8.1 Equivalence Ratio:

Equivalence ratio, denoted as ϕ is very important in defining the fire conditions and the production of toxic gases. Equivalence ratio can be defined as the ratio between the mass of air needed for complete combustion of a unit mass of fuel and the actual mass of air and fuel involved in the reaction. The mass of fuel is referred to as the stoichiometric ratio. Stoichiometric refers to that condition where there is just enough oxygen for a complete combustion. Equivalence ratio is defined so that a ratio of less than unity indicates an over-ventilated, fuel-lean or fuel-limited fire, while an equivalence ratio greater than unity indicates an under-ventilated, fuel-rich or ventilation-limited fire while an equivalence ratio equal to unity indicates a stoichiometric condition. Equivalence ratio can be presented mathematically as shown in equation 2-1.

$$\begin{aligned}\phi &= \frac{\textit{Actual fuel to air ratio}}{\textit{Stoichiometric fuel to air ratio}} \\ &= \frac{\textit{Stoichiometric air to fuel ratio}}{\textit{Actual air to fuel ratio}}\end{aligned}\quad 2-1$$

If: $\phi < 1$ -----fire is well ventilated or fuel lean

$\phi > 1$ -----fire is vitiated/ under-ventilated or fuel rich

$\phi = 1$ -----Stoichiometric fire

2.8.1.1 Air-to- Fuel Ratio

A full gas composition carbon balance was carried out in the work of Aljumaiah et al. [88] and Mustafa et al. [89] to determine the air/fuel ratio by mass, which together with the fuel mass loss rate from a load cell, gives the air consumption by the fire using the 1.6 m³ fire rig constructed by Andrews et al. The calculation of the air/fuel ratio by mass (A/F) from the gas composition Aljumaiah et al. [88] and Mustafa et al. [89] used involved the CO/CO₂ ratio which is similar to the CO/CO₂ ratio developed by [90] and [91] however an improved version because the unburned hydrocarbons are included. For full carbon balance A/F ratio to be achieved, the elemental composition of the fuel has to be known or assumed. For pure hydrocarbon fires, Spindt equation [92] for A/F is suitable for use but

seems unsuitable for fuels with high oxygen content such as methanol or wood as a more general computation procedure is required. A relevant A/F calculation procedure for these fuels have been developed by Chan [93].

The air/fuel ratio is important and needed when converting gas concentrations from a volume to mass basis and when converting particulate measurements from g/m³ to a mass yield per mass of fuel burnt. Fire toxic gas emissions and soot are usually expressed as a fire yield in terms of kg of fire load consumed. By expressing them as yields, different fire loads and fire materials can easily be compared under real fire conditions which then makes it a better way of ranking the fire materials for their toxic gas release than the standard methods, such as the standard cone calorimeter, which do not simulate the real air/fuel ratios of fires [66]. Andrews et al. [66] used the equation below as the conversion equation.

$$\text{Gas Concentration kg / kg fuel} = \text{Constant} \times \text{volume concentration (\%)} \left[1 + \frac{A}{F} \right] \quad 2-2$$

Where: the constant in the equation represents the ratio of the species molecular mass to the molecular mass of the fire product gases. However, the fire product gases can adequately be taken as air because it was found to be accurate with an error of less than 2% [94], else the calculation becomes rather cumbersome. In fire research, these emissions are referred to as fire product yield, and as an emission index (normally in units of g/kg) in pollution legislation.

The air to fuel ratio on mass basis is obtained by dividing the measured entrainment of air into the fire chamber by the mass loss rate as shown below;

$$\text{Mass AFR} = \left[\frac{\text{Air flow (kg/s)} / 3.6}{\text{Fuel mass loss rate (g/s)}} \right] \quad 2-3$$

The air to fuel ratio calculation by mass loss rate is not very accurate and can be misleading because it assumes that all the air entrained is used up by the fire. Because of this reason, Chan's method is more preferable due to its accuracy. Chan's method determines the air to fuel ratio based on the gas emission analysis. Chan's method considers a general formula for the composition of a fuel represented as $C_{\alpha}H_{\beta}O_{\gamma}N_{\delta}$ and the oxidizer which is air (comprising of

78.09% N₂, 20.94% O₂, 0.93% Ar and 0.04% CO₂) to arrive at the AFR as shown in the equation below:

$$AFR_{Chan} = \frac{138.324A^*}{12.011\alpha + 1.008\beta + 15.999\gamma + 14.007\delta} \quad 2-4$$

Where:

A* represents the wetness in air

2.8.2 Heat Release Rate:

The heat release rate can be defined as the amount of heat released per unit time and measures the potential of a material to contribute to a fire. It describes how big a fire is. It can also be defined as the rate at which combustion reactions produce heat. The most common method used in measuring HRR is known as “oxygen consumption calorimetry (ASTM E1354)”. This method is based on the assumption that most gases, liquids, and solids release a constant amount of energy for each unit mass of oxygen consumed. This constant was found to be 13,100 kJ/kg oxygen consumed and is considered to have an accuracy of within ±5 percent for most hydrocarbon fuels [95]. After ignition has occurred, a hood is then used to collect all of the combustion products and removed through an exhaust duct where the flow rate and composition of the gases is then measured to determine how much oxygen has been used for combustion. The HRR can then be calculated using the constant relationship between oxygen consumed and energy released.

Another method that is commonly used in assessing HRR is by measuring the burning rate, also known as the mass loss rate. This measurement is done by weighing the fuel as it burns, using weighing devices or load cells. This method of estimating the HRR based on the mass loss rate needs knowledge of the effective heat of combustion [96]. The HRR can then be calculated using equation 2-5 below:

$$\dot{Q} = \dot{m}\Delta H_{eff} \quad 2-5$$

Where;

\dot{Q} = heat Release rate (kW)

\dot{m} = mass loss rate (kg/s)

ΔH_{eff} = effective heat of combustion (kJ/kg)

When wood undergoes thermal degradation, some combustible volatiles are produced. These volatiles are responsible for flaming combustion and heat release [97]. The heat release rate of combustion of the volatile pyrolysis products of untreated and fire-retardant-treated ponderosa pine wood was calculated by Browne and Brenden [98] using an oxygen bomb calorimeter. After determining the heat of combustion of the whole wood and the partially pyrolysed wood (char residue), the authors, found that the heat of combustion of the volatile product of pyrolysis varied with the degree of volatilization (pyrolysis) [98]. The volatile products had heat of combustion less than that of the original wood while the heat of combustion of the residual char was higher than that of the original wood. As a result of the difference between the heat of combustion of the volatile product and the whole wood, one cannot estimate heat release rate based on mass loss rate as can be done with ideal gases, liquids and other non-charring solid materials [97].

The heat release determined by Andrews et al. [64] in enclosed fires was by using the fire load mass loss rate with the fire load resting on load cells which they preferred to oxygen consumption calorimetry as it does not require the mass flow of the exhaust gases to be determined, just like the case of the cone calorimeter and whole room fire calorimetry [99, 100]. Andrews, et al. [64] developed a method of using oxygen consumption calorimetry by determining the air consumption mass flow rate from the gas analysis based air/fuel mass ratio and the measured fuel mass loss rate.

The heat release rates of air-starved/under-ventilated enclosure fires depend on the air consumption rates of the fire. The heat release rates are usually measured indirectly with various assumptions concerning window or door air flow

coefficients together with calculation of the hot/cold gas neutral plane [79] and this is because of the difficulty in carrying out the direct measurement. Gottuk et al. [77, 78] studied the direct measurement of the air velocity at a fire enclosure air inlet with a separate upper fire product exit. The direct and indirect measurement both have the drawback of measuring the air entrained into the enclosure instead of the air consumed by the fire. It is known that the initial stages of fire always have enough air in the enclosure, therefore there is no need for air entrainment and its importance depends on the ratio of the mass of air in the enclosure to fire load mass. In the later stages of fire, the heat release rate turns out to be limited by the air entrainment and for steady state fires the air entrainment can equal the air consumption. This tends to underestimate the air consumption by a fire in the early stages and an overestimate of the global fire equivalence ratio.

2.8.3 Yield

Yields as referred to in the field of fire toxicity or emission index or factor as referred to in the field of environmental pollution can be defined as the ratio between mass discharge rate of the specific gas from the combustion reaction and the mass burning rate of the fuel in $g_{\text{species}}/g_{\text{fuel}}$ or $g_{\text{species}}/kg_{\text{fuel}}$. The toxic yields depend on the composition (elemental composition and organic) of the materials [101] [49] and the conditions of the fire. For flaming combustion, the most important factor is the fuel:air ratio, although other factors such as the concentration in the compartment can also affect the yields [55]. Toxic emissions produced from fires can be quantified by yield values. Yield depends on the development of the fire and is considered as a fire characteristic that develops as the fire grows and changes with other fire characteristics such as temperature. Changing the sampling point location during a toxicity test generally does not change the yield data except if a post-oxidation reaction occurs. This significant quality is essential for reporting data from experimental tests at different scales. Yields are normally obtained on the basis of the concentration measurements and then later on converted to mass based ratio e.g. grams of gas emitted per gram of fuel burnt or kg of gas emitted per kg of fuel burnt.

There are two most common methods of calculating yields in the literature. One of the methods is presented in ISO 19700 [102] and BS7990 [103]. This method was presented to be used specifically for the tube furnace test but with little modifications, it can be used for other small scale tests with fixed flow rates. The second method is the one used by Gottuk and Lattimer [104], Tewarson [105] and others [106, 107] which depends on the air to fuel ratio instead of the fixed flow rate of the exhaust. Method 1 gives two options for obtaining yield; mass charge yield and mass loss yield. While the mass charge option is useful for ranking and comparing materials, because it takes into account the reactivity of the specimen, the mass loss method is most useful for the actual representation of the combustion and more useful for fire toxicity scaling and modelling. ISO 19700 [102] and BS 7990 [103] outline the following steps for the calculation of yield:

Step 1: Calculation of yield using the mass charge concentration

$$C_{m.charge} = \frac{\dot{m}}{\dot{a}} \quad 2-6$$

Where;

$C_{m.charge}$ is the mass charge concentration in $g.m^{-3}$

\dot{m} is the rate of introduction of the test specimen mass into the furnace in $mg.min^{-3}$

\dot{a} is the total airflow rate through the mixing and measurement chamber in $L.min^{-1}$

The mass charge yield can then be calculated thus;

$$Y_i(t) = \left(\frac{g_i(t)}{C_{m.charge}(t)} \right) \times \frac{M_{W,i}}{V_{ideal\ gas}} \times 10 \quad 2-7$$

Where:

$Y_i(t)$ is the gas yield in g_i/g_{fuel} for species i at time t , $g_i(t)$ is the gas i concentration at time t in % (l_i/l_{air}), $C_{m.charge}(t)$ is the mass charge concentration in $g_{fuel}.m_{air}^{-3}$ (grams of fuel per cubic metre of dispersed space), $M_{W,i}/V_{ideal\ gas}$ is in $g_i.l_i^{-1}$, $10 = 100(l_{air}.m_{air}^{-3})/100\%$

Step 2: Calculation of yield using mass-loss concentration

1: calculate the mass loss per unit length, m_{loss} in $mg.mm^{-1}$ using;

$$m_{loss} = m_{load} - m_{res} \quad 2-8$$

Where; m_{load} is the test-specimen mass loading in $mg.mm^{-1}$ and m_{res} is the test-specimen residue mass loading in $mg.mm^{-1}$

2: Calculate the mass loss concentration $C_{m.loss}$ in $mg.mm^{-1}$ using

$$\dot{m}_{loss} = m_{loss} \times \dot{b} \quad 2-9$$

Where; \dot{b} is the combustion boat advance rate in $mg.mm^{-1}$

3: Calculate the mass loss concentration $C_{m.loss}$ in $g.m^{-3}$ using

$$C_{m.loss} = \frac{\dot{m}_{loss}}{\dot{a}} \quad 2-10$$

Where: \dot{a} is the total airflow rate through the mixing and measurement chamber in $L.min^{-1}$.

The yield can then be calculated as follows:

$$Y_i(t) = \left(\frac{g_i(t)}{C_{m.loss}(t)} \right) \times \frac{M_{W.i}}{V_{ideal\ gas}} \times 10 \quad 2-11$$

The disadvantage of these formulas is that a constant flow rate of effluents is needed just like in the case of the ISO 19700 [102] Tube Furnace test where 50 L/min is required and the ISO 5660 [108] Cone Calorimeter where 24 L/min is required. Full scale experiments without hoods will have a limitation in using the equation as they won't have a constant flow rate.

Gottuk and Lattimer [104], Tewarson [105] and others [106, 107] presented an alternative method of calculating the yield as shown in equation 2-12

$$Y_i(t) = [g_i(t)] \times \frac{M_{W.i}}{M_{W_{mix}}} \times \{1 + AFR(t)\} \quad g/g \quad 2-12$$

Where:

$Y_i(t)$ is gas yield in (g_i/g_{fuel}) at time t , $M_{W_{mix}}$ is the molecular weight of the mixture assumed to be that of air which is 28.9 g/mol, $M_{W.i}$ is the molecular weight of the

gas in g/mol, $g_i(t)$ is the concentration of the gas at time t (ppm vol) $\times 10^{-6}$ or in (% vol) $\times 10^{-2}$, AFR(t) is the mass based actual air to fuel ratio in $g_{\text{air}}/g_{\text{fuel}}$.

The method by the authors above does not need a defined flow rate of effluents rather it requires the actual air to fuel mass ratio and this was used in this work.

2.9 Sampling of Fire Gases

Due to the transient nature of fires, the characterisation of gases from fire becomes complicated. In the course of the fire, some compounds in the smoke plume may change from ppm-level to %-level. Fire gases are also hot at the sampling point most of the time which may lead to further chemical reactions or the cold parts of the sampling equipment having condensed gases, or on surfaces in the test apparatus. High concentrations of carbon dioxide, water and other gaseous compounds found in fire gases make quantification of fire gases difficult especially with the use of spectroscopic methods. High concentration of particles is also a problem during sampling. Therefore, the method of sampling for the characterisation of fire gases is an important part of the overall measurement strategy.

Since the main objective of sampling is to collect a representative amount of the fire gases for further analysis, the analyser must be designed in such a way that the objective is achieved. The sampling equipment for gases therefore consists of a sampling probe, a particulate filter, tubing and a pump [63]. The particulate filter and the sample line/tubing are usually heated to avoid condensation.

The most commonly applied technique for sampling of toxic gases has been to extract samples from a smoke collection duct or hood. Sampling from a duct, where the smoke gases are well mixed, is the traditional and most controlled situation, however the gases are diluted with the entrained air before getting to the duct, which reduces the concentration of the toxic gases. The general principle is that the fire gases are adequately well mixed at a distance of five times the duct-diameter [63] and that, in such cases, a single-hole probe can be used.

The fire gases exiting the opening of an enclosure are more concentrated and not as well mixed as in a smoke collection duct. Hence, the sampling conditions are more severe in the former case. To sample at the exit of an enclosure, raw gas sampling, heated sample systems are required to obtain extra information regarding the specific composition of the fire gases as they exit the enclosure. The basis for this sampling strategy is to minimise the effects of any likely postfire reactions of the combustion products prior to the sampling location especially from poorly ventilated combustion. Additionally, the proper measurement of the ventilation conditions in the enclosure does not require any dilution of the fire gases which should be avoided. An advantage of raw gas sampling is the reduction of possible losses of gases due to condensation in the hood/duct system. Even though raw gas sampling has numerous advantages, only a few researchers have used it for toxic gas research. It will be shown later that this work used the raw gas sampling method for toxic gases sampling using a heated sampling line.

2.10 Review of Methods for Studying Toxic Effluents

This section reviews the most common and relevant bench scale methods for generating toxic effluents.

2.10.1 Bench-Scale Methods for Generating Toxic Effluents

Bench-scale methods used for generating toxic effluents have played an important role in toxicity research, but have their disadvantages. Some of the methods are incapable of properly reproducing the most toxic under-ventilated fire condition, where the yields of carbon monoxide and hydrogen cyanide are highest, while other methods have shown good agreement with large scale test data [109]. Bench-scale methods used for generation of toxic fire effluents should ideally be able to replicate individual fire stages or combustion conditions, that can be input into models of combustion toxicity. Full-scale fires simultaneously are transient and involve different fire stages in different places, which are changing with time. Some bench-scale methods allow the combustion conditions to change in the course of the test, however, these methods are much more difficult to relate to full-scale fires, because the duration of each fire condition is not known, and the behaviour of fires change on scale-up [109]. Most bench

scale methods have non-uniform combustion conditions, examples of which include the closed chambers exposed to a fixed source of heat (smoke density chamber (SDC) (ISO 5659–2 2012)), and static tube furnace tests (NF X 70–100 (2006)). Those with uniform combustion conditions are more appropriate for generating data suitable for comparison and modelling. The steady state tube furnace (SSTF) (ISO/TS 19700 2013) has been specifically designed for this purpose. Other methods are just in-between these two methods and include those that can generate quasi-steady combustion conditions, such as the cone calorimeter (ISO 5660–1 2002) with a non-standardised modification (controlled atmosphere attachment (CACC)), and the fire propagation apparatus (ISO 12136 2011). The problem of reproducing the conditions of fully developed under-ventilated flaming on a bench-scale is caused by numerous issues:

- The equivalence ratio Φ depends on the mass loss rate of the sample and the available air available for combustion; for most methods one or both are unknown;
- Φ will be increased by an unknown factor if there is a feedback of fire products into the flame zone.
- The rapid change of the equivalence ratio Φ experienced in some apparatus does not give enough time for sampling and measurement of mass loss and emission composition at a specific value of Φ , resulting in errors and uncertainties.
- A constant heat flux is applied in some bench-scale methods, and often inadequate to sustain flaming at low oxygen concentrations;
- Additionally, there is a problem of unknown quantity of fresh air bypassing the fire plume, so that the ventilation condition, and hence Φ , remain unknown.

Each method is described briefly in the following section.

2.10.1.1 The Smoke Density Chamber

This is the most widely used fire-test apparatus, specified in smoke regulations in most countries of the developed world (ISO 5659–2 2012) given in Fig. 2-8. Because of its widespread use and availability, it has been adapted for toxic gas generation and assessment. The standard identifies four test conditions, but has failed to link them to particular fire scenarios. The conditions specified are: 25

kWm^{-2} without piloted ignition; 25 kWm^{-2} with piloted ignition; 50 kW m^{-2} without piloted ignition; and 50 kW m^{-2} with piloted ignition. The smoke density chamber uses a sample size of $75 \times 75 \text{ mm}^2$ solid sheet and the results are only valid at the thickness of 1-4 mm as stated in the smoke measurement standard. The thickness of the sample determines the ventilation condition in the chamber (fixed volume of 0.51 m^3) in the sense that a thin sample will burn under well ventilated conditions assuming a complete combustion with minimum release of toxic products while a thick sample is expected to produce a high yield of CO and other products of incomplete combustion. The transport industries have modified the procedure for toxicity testing in the aircraft (EN2826 2011), maritime (Fire Test Procedure Code 2010), and railway tests (CEN/TS 45545–2 2009). Some of these procedures try to deal with the change through the fire stages by monitoring the formation of toxic gases with time, as the oxygen concentration drops, and the ventilation changes from well-ventilated to under-ventilated. However, in contrast to a real fire, the heat flux remains fixed, therefore when the oxygen concentration drops, the flame may be extinguished. The transport industries have embraced the smoke density chamber ISO 5659–2 (2012) and ASTM E662, for toxic product yields quantification (Fire Test Procedure Code 2010; CEN/TS 45545–2 2009) using simple pass/fail chemical detection (e.g. Draeger tubes), conventional infrared spectroscopy or Fourier transform infrared spectroscopy (FTIR) gas analysis, regardless of significant issues of reproducibility. It has been proposed that the reproducibility problems are due to the single point measurement, that is, the tip of the probe may be in the centre of the plume, below it, or if there's efficient mixing, the upper layer may be recirculated through the flame, or the timing of the effluent sampling may cause instabilities (for instance an initial proposal to sample after 8 min was substituted by a proposal to sample when the smoke density reached its peak). The reviewed procedure is based on continuous sampling of the fire effluent.

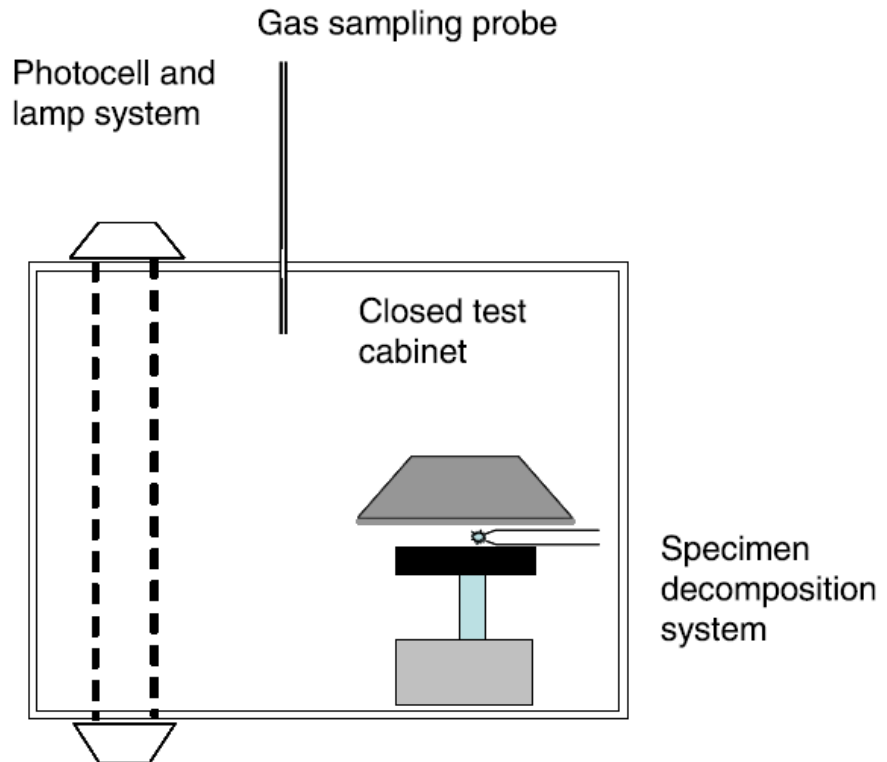


Figure 2-8 The Smoke Density Chamber [109]

2.10.1.2 The Controlled Atmosphere Cone Calorimeter (CACC)

The cone calorimeter (ISO 5660) [108] is a standard bench scale piece of equipment designed to measure the heat release rate and flammability properties of materials. The cone calorimeter reproduces the oxidative pyrolysis stage (class 1b) and well ventilated flaming fires (class 2) classification of ISO 19706 [48] where a fire would be too small to generate toxicants at harmful concentrations but in very small enclosures. The cone calorimeter uses test samples of 100 × 100 mm of up to 50 mm thick, in both the horizontal and vertical orientation. In an attempt to simulate oxygen-depleted conditions of a fully developed fire and the fuel-rich post flashover fire, a non-standard modification of the apparatus has been developed, enclosing the fire model in a ventilation controlled chamber. The controlled atmosphere cone calorimeter standardised setup has not been defined yet. Efforts are being made to establish an ISO standard for using CACC for toxicity measurements but the final version is yet to be produced. Therefore, the design of the device differs from one laboratory to the other. The controlled atmosphere cone calorimeter was first introduced by

Babrauskas et al. [110]. In the modification, the controlled atmosphere cone calorimeter (CACC) [110], shown in Fig. 2-9, a conical heater, sample holder and load cell is enclosed in a heat resistant glass chamber (400 mm high with 300 × 300 mm base) so that the air flow around the sample may be controlled by diluting the oxygen content with nitrogen thereby facilitating the recirculation of combustion products over the sample surface. In some cases, secondary flaming is experienced whereby the effluent continues to burn as it emerges from the chamber (Fig. 2-9) eventually giving well-ventilated flaming. In others, under low oxygen concentrations, the fuel lifts from the surface, but does not ignite [111]. In the last two decades, a few number of designs have been reported that described vitiated cone calorimeter approaches. Babrauskas and Mulholland [110, 112], Christy and Petrella [111, 113], and Leonard [114] each, reported a different controlled-atmosphere cone calorimeter. Mikkola [115] in 1993 introduced a ventilation-controlled cone calorimeter that was adopted for some works that became commercially available. Hietaniemi [116, 117], Gomez and Janssens [118-120], Marquis [121, 122], and Guillaume [123] reported their work on vitiated cone calorimeter studies using similar design setups used by Mikkola. However, Mikkola's ventilation-controlled cone calorimeter and all latter setups based on this design differed from those reported by Babrauskas and Mulholland, Petrella and Christy, or Leonard. Although the controlled-atmosphere cone calorimeter setups are mostly closed, the ventilation-controlled cone calorimeter has an open connection between the cone calorimeter's exhaust hood and a controlled-atmosphere chamber mounted underneath the exhaust hood. Nonetheless, the ventilation-controlled cone calorimeter allows the ventilation conditions to be controlled and therefore, it is rather a controlled atmosphere cone calorimeter than a ventilation-controlled cone calorimeter. A chimney was sometimes proposed by Hietaniemi et al. [117] to be used on the top of the cone heater to prevent backflow of ambient air and to avoid effluent burning in ambient air as it emerges from the combustion chamber ultimately giving well-ventilated flames. Hietaniemi et al. [117] used the controlled atmosphere cone calorimeter, but argue that an instantaneous "effective" global equivalence ratio, ϕ_{eff} , should be used, instead of an averaged local equivalence ratio, based on the oxygen supply to the chamber, his reason being the

occurrence of a secondary flame outside the test chamber in some experiments, such that the amount of oxygen available for combustion surpassed the amount that was supplied to the enclosed chamber. Marquis et al. [124] used the controlled atmosphere cone calorimeter to study its effects under ambient and non-ambient oxygen conditions. Numerous designs were investigated using Poly(methyl) methacrylate (PMMA) as the test material. Marquis et al. concluded that results differ from one design to the other.

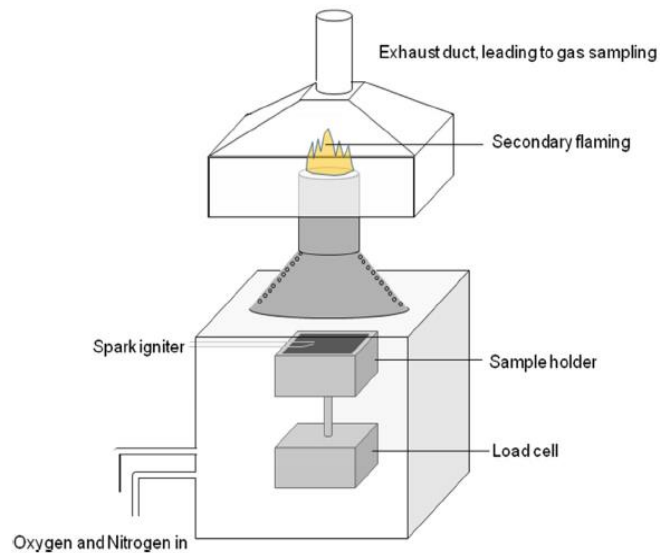


Figure 2-9 The Controlled Atmosphere Cone Calorimeter [109]

The main advantage the CACC has over the standard cone calorimeter is the ability to control the combustion conditions in accordance with ISO 19706 classifications. The greatest concern when it comes to toxicity measurement using this setup is the dilution occurring outside the burning chamber before the diluted sampling point, this problem can be fixed by introducing raw sampling [87]. Another concern is the effect of using inert atmosphere on the HRR measurements through the principle of oxygen consumption as the reference oxygen should not use standard 20.95 %vol. of oxygen in air, more discussion and details of solutions to the issue are presented by Werrel [125]. Werrel [125] introduced a new approach for determining the oxygen baseline value taking varying dilution ratios into account. He [125] also derived a set of modified equations for the HRR calculation. Werrel showed that neglecting changes in the dilution ratio may lead to an overestimation of the HRR with an error of up to 30%. As a function of the adjusted concentration of oxygen in the enclosure box,

the deviation is systematic and rises to a significant order of magnitude of 5% once the enclosure oxygen mole fraction is decreased below 20 %vol. Irshad [126] in her PhD thesis modified the controlled atmosphere cone calorimeter to include a chimney and an orifice plate to solve some of the problems mentioned above.

This work uses the controlled atmosphere cone calorimeter with some modifications as reported in Irshad's [126] work to avoid some of the problems mentioned and is shown in Chapter 3.

2.10.1.3 The steady state tube furnace (SSTF)

The steady state tube furnace [102], shown in Fig. 2-10, operates by feeding the sample (pellets, strips or granules) into its hot zone at a fixed rate and controlled air supply, inside a horizontal silica tube having a diameter of 48 mm, which allows adequate mixing of fuel and oxidant. Combustion occurs by sending the sample into a furnace of increasing heat flux at a fixed rate, so that several tests could be run with the same material at different ventilation conditions. This allows each fire stage to be replicated by steady state burning. The fire products produced in the flame zone then move to the heated furnace tube, maintaining a high temperature, just as obtained in the upper layer of a compartment fire. The data obtained during the steady state burn period such as the gas concentrations and mass feed rate can then be used to quantify the toxic product yields. This bench scale equipment was designed to generate data for input to fire hazard assessments, using the methodology in [127] and [128], mainly in relation to the ISO fire stages.

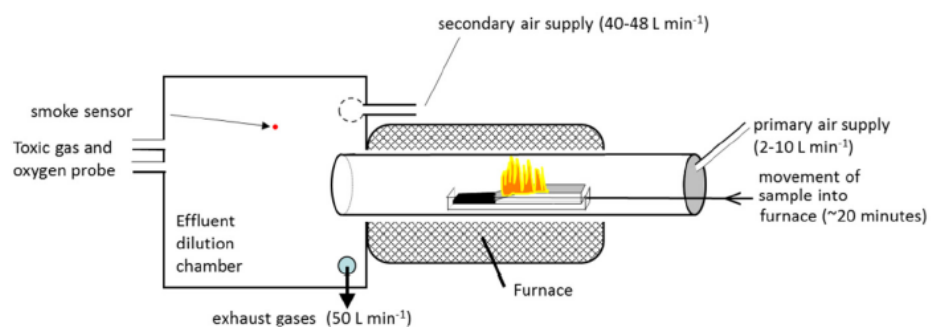


Figure 2-10 The Steady State Tube Furnace [109]

Many researchers have used the tube furnace method to determine the yield of toxic products, generating a very useful database of toxic emission [129-131].

The steady state tube furnace has a few limitations regarding the smoke produced and measured; firstly, condensation and loss of products is likely to occur as a result of the low temperature at the end of quartz tube before the dilution chamber, as detailed in [132]. Ideally this temperature should be above 200°C. Secondly, Mass loss rate (MLR) can only be obtained from the mass charge rate obtained from the feeding rate because, it cannot be measured instantaneously. For unpyrolysed char residue to be considered for the yield (g/g) measurements, the average MLR is used [103], which is satisfactory if the steady state phase is realised immediately, but in the steady state tube furnace, the steady state phase is much shorter than the total test time which starts from feeding the sample into the furnace and continues until the end of the test. Thirdly, the sample is very small; the low production of fire effluents during the test limits the sampling process to diluted only. The low flow rate of primary air feed may be a potential problem by having the secondary air supplied to the dilution chamber drawn into the quartz tube.

2.11 Particulates

Smoke contains particulates which have their own health hazards. Smoke particulates are so small that they pose a respiratory hazard. Particulates include both micro-droplets formed as a result of organic vapour condensation and carbonaceous agglomerated structures (soot) which consist of hundreds to thousands of nearly spherical primary particles [22]. Very few investigations have been made regarding the size, distribution and composition of particulates despite them being generated in large quantity during fire incidents [130]. Factors responsible for the particle size distribution include the material or fuel load, the temperature and the fire conditions (well ventilated or limited ventilation). Particle sizes are generally of the order of 1µm from spherical droplets of smouldering fires while those of irregular soot particulates found at the flaming combustion stage are even larger and difficult to determine and basically depend on the measuring technique and sampling position [55].

Particles generally affect the respiratory system by creating a release of fluid and inflammation, thereby preventing the exchange of gas in the alveolae. The bronchioles when inflamed can lead to a complete blockage. The excess fluid in

the lungs then prevents the flow of oxygen through the blood-gas barrier [133]. Particles of size $< 0.5 \mu\text{m}$ penetrate between the surface of the alveolae and the blood capillaries causing interstitial and luminal oedema [55]. These small particles can also go beyond the blood-gas barrier and go into the bloodstream leading to dangerous immune responses from the white blood cells such as polymer fume fever, increased platelet stickiness which can lead to heart attacks [55]. Particulates aid in the transport of other poisonous molecules deep into the lungs. Figure 2-11 shows the respiratory system with where each particle size is deposited.

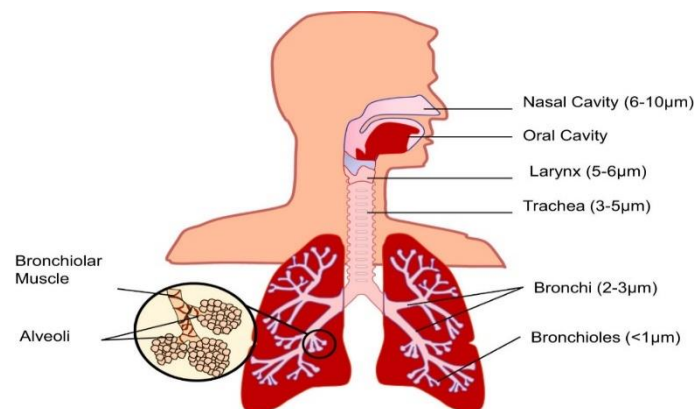


Figure 2-11 The deposition of particles in the respiratory system [8]

2.11.1 Health and Environmental Impacts of Particulate Matter

Fire generated aerosols/particulates can be a fire threat to people and the environment in numerous ways:

1. Small respirable particles are released in a fire and can penetrate deep into the lung structure. Due to the irritating nature of inhaled particles, the ability of people to escape from fire is reduced.
2. These particles have the ability to adsorb and/or absorb toxic and irritant gases and vapours, providing a means for transport beyond the respiratory tract natural defences and deep into the lungs.
3. The concentration of toxic gases and vapours in the fire effluent may be reduced by even less or non-respirable particles and can deposit them on surfaces.
4. Aerosols /particles may obscure vision, possibly reducing the ability of people to move effectively toward safety.
5. Particles settled on vegetation block their stomata resulting in the withering of plants.

2.11.2 Characteristics of Smoke Aerosol Formation in Fires

It is important to know the character of particulate matter as it emerges from the fire to gain more understanding of how conditions within lungs can be assessed. A number of processes are involved in the formation and growth of soot. The first step involves the fuel pyrolysing from the surface as the fuel fragments. At high flame temperatures the fuel fragments react to form acetylene, benzene and radical species including H, OH and small hydrocarbon radicals [22]. The one-ring benzene undergoes a series of reactions involving acetylene and the radical species, leading to the formation of polycyclic aromatic hydrocarbons (PAHs). The PAHs formed continue growing to eventually form the smallest soot particles which are on the order of a few nanometres [134]. The subsequent particle growth occurs as a result of surface addition of acetylene and particle-particle collision (coagulation), followed by coalescence into a single particle. At this step the particle may have a size of 0.02 μm to 0.05 μm . Subsequent growth of particles arises as a result of the agglomeration of these primary particles. The flame region and the post flame region are the two regions in a fire development where agglomeration process takes place. In the flame region, agglomeration occurs when some of the primary particles are partially fused while in the post flame region, agglomeration occurs when the particles are held together by dispersion forces. The cooling of the smoke leaving the flame causes the PAHs to condense on the surfaces of soot particles. For over-ventilated fires, the amount of condensed organics is usually less than 20% whereas for under-ventilated fires it can rise as high as 50%, forming agglutinated agglomerates [135]. Smaller molecules comprising water, benzene, other hydrocarbons and acid gases may absorb on the surface of the agglomerates. The surface area of a smoke particle and the chemical functionalities on it play an important role in the particle's subsequent growth and movement and contribute to its capability to absorb water and toxic gases [22]. Figure 2-12 summarises the formation of particles in fires.

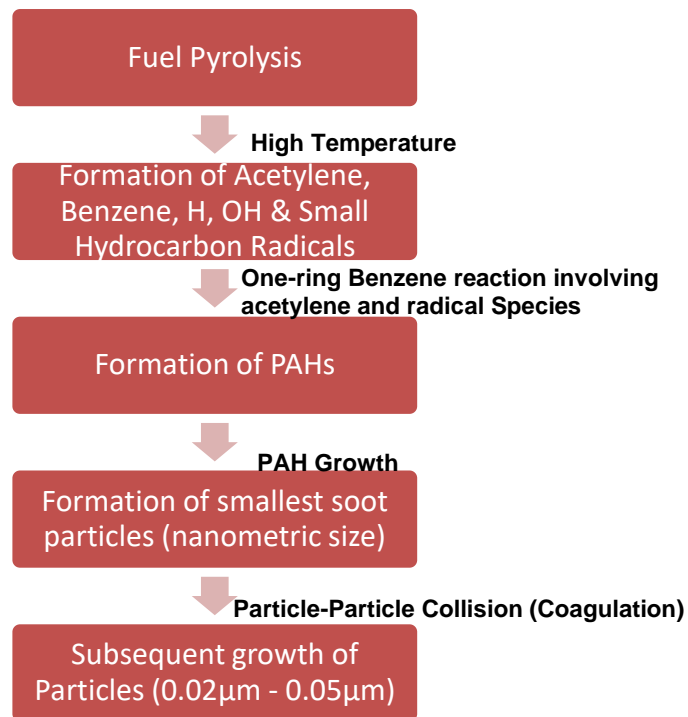


Figure 2-12 Formation of Particles in Fires

2.11.3 Particle and Aerosol Characteristics:

Particles from fires exhibit an extremely wide range of particle sizes, shapes, densities, concentrations and chemical composition. Particles react in different ways to various forces applied over the aerosol according to their individual characteristics which can be used for their classification and characterisation. This also contributes towards the very high sensitivity shown by the aerosol to sampling and measuring conditions, transport, changes in temperature, dilution, etc. This section describes particle and aerosol characteristics and properties that determine the aerosol behaviour.

2.11.3.1 Particle Size and Shape

At the time of their formation, aerosol droplets are spherical in shape and remain spherical as they grow by aggregation or condensation. The diameters of the droplets range from 1 nm- >100 µm. Carbonaceous particles on the other hand are spherical when initially formed with diameter D_p , are homogeneous and have a varying size ranging between 10nm-50 nm. Such particles normally exhibit a

Gaussian form of frequency distribution [136]. However, as these small particles adhere to each other to form larger particles, the aged and agglomerated carbon particles in fire effluents are rarely spherical, their fractal structure being a result of the growth process. As such, it is important to characterize the sizes using parameters other than those used to describe a sphere. The description of particle size has gone beyond the optical appearance of the particles. Based on the different behaviour of the particles under the influence of various forces, diffusion, aerodynamic, electrical and optical equivalent diameters have been defined, each representing a measurable index of the particle. The two main parameters used to characterize the sizes are the aerodynamic diameter and the electric mobility diameter. Other additional diameters such as the volume equivalent diameter, gyration diameter, aggregate diameter etc. exist but this section will focus on the two main definitions.

Aerodynamic Diameter:

This diameter D_a represents that of a sphere having a density of 1 g/cm^3 with the same settling velocity in calm air as that of the considered particle. For an unspecified particle, the Eqn. 2-13 links this diameter to the mass median diameter of the distribution.

$$D_a = \sqrt{\frac{\rho}{x}} \cdot d_{50} \tag{2-13}$$

Electrical Mobility:

This diameter represents that of a sphere having the same electrical mobility Z_p as that of the particle being considered. The relationship is given below;

$$D_m = \frac{Cc}{3\pi\mu B} \tag{2-14}$$

Where:

C_c is the Cunningham correction factor

B is the dynamic mobility, which characterizes forces produced by surrounding gas on the particle.

The electrical mobility equivalent diameters mentioned in this section will be used throughout this work.

2.11.3.2 Particle Size Distribution

The size distribution of aerosol is a statistical representation of the total particle sizes contained in a sampled aerosol. A monodisperse aerosol is characterised by a single parameter since all particles are identical. On the other hand, polydisperse aerosols have individual particles within a range of sizes. Fire aerosols are polydisperse and their diameter may range over two to three decades. The size distribution can be a representation of any concentration measurement contained in separate size ranges, or as a continuous function of the particle size.

A graphical representation of the size distribution is frequently done as a histogram (Fig. 2-13a) with the discrete concentration contained in a size bar or "bin". Several instruments produce binned data, examples include; cascade impactors, scanning mobility particle sizers, optical particle sizers, etc. A more convenient way of representing the size distribution is by using a frequency distribution or cumulative distribution curve (Fig. 2-13b) because the mathematical properties allow for computation of size related information of interest. From a cumulative distribution the fraction above or below a fixed size can be readily determined.

Most aerosols with long tails at larger sizes have an asymmetrical shape of frequency distribution and in some cases they are multimodal. In contrast to normal distribution, the mode, median and mean sizes are different and the particle diameter distributions are in the hierarchy of smaller to larger values of the mode, median and mean. The mode is the most recurrent size, the median is the size that cuts the distribution into two equal areas, and the mean is the average value. Because larger sizes have a skewed distribution consisting of a long tail, aerosol size distributions are most often represented by a log-normal distribution. This is the same as a normal distribution of the logarithm of the particle size.

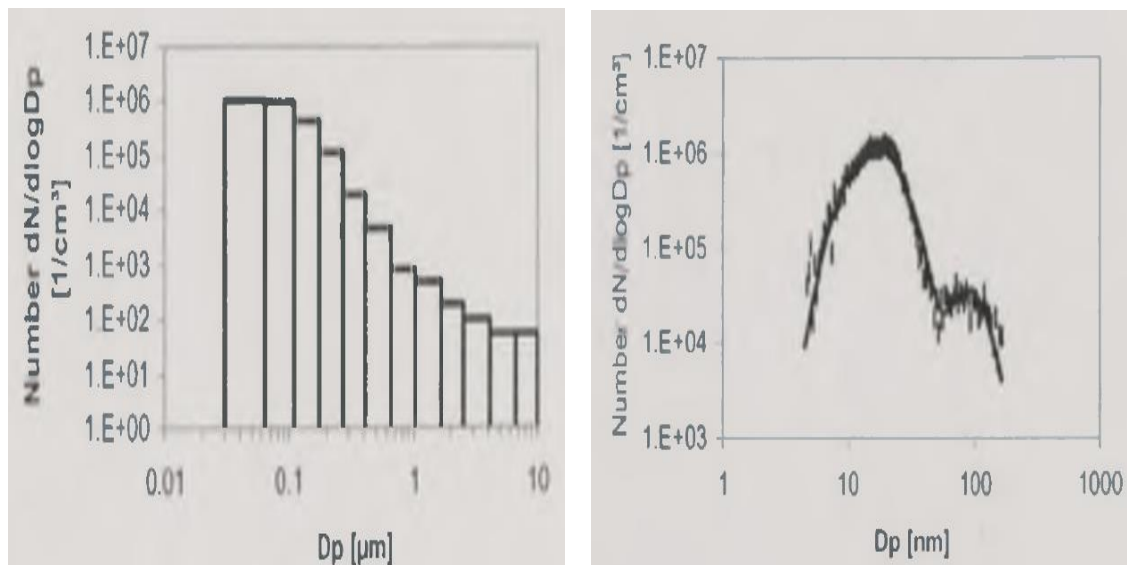


Figure 2-13 Examples of size distributions a) Histogram b) Log-normal distribution curve [137]

2.11.3.3 Mass and Number Concentration

The concentration of an aerosol can be defined as some integrated measure per unit volume. Regardless of size, the aerosol number concentration is the total number of particles per unit volume while the mass concentration is the total aerosol mass per unit volume. Other concentration measurements consist of: aerosol diameter, surface area, light scattering, and electrical charge per unit volume. Measurement devices commonly provide a single concentration measurement over a wide range or a concentration measurement over a number of sizes within a certain range. Optical particle counters give the number concentration and the particle size distribution for particles greater than about 300 nm. Condensation particle counters measure the number concentration for particles greater than about 10 nm. The gravimetric method of aerosol sampling provides mass concentration measurements of particles below a certain size through inertial impaction of large particles.

A few large particles can be significant and dominating to the mass concentration, surface area concentration, or light scattering concentration. On the other hand, under-counting, or not sampling a small number of large particles may not have any significant effect on the number distribution. Similarly, not weighing a large amount of very small particles may not affect the mass concentration significantly.

Depending on the type of instrument used, the aerosol concentration measured may be an average value over a time interval, or time resolved. Time averaging over a test is usually necessary when a limiting amount is specified, such as the total smoke production from a burning sample, or when a yield is calculated from the total sample mass loss. For a gravimetric filter sampling to be accurate, it may require time averaging in order to collect sufficient mass deposit to weigh. Similarly, gravimetric cascade impactor sampling must be over a time interval adequate enough to accumulate enough mass on the separate stages, associated with the size range of interest.

2.11.3.4 Particulate Chemical Composition

Aerosols can be characterized chemically after an appropriate sampling procedure. The nature of the surface on which the aerosols have been collected (e.g. a filter) is an important factor to be considered in chemical analysis of aerosol particles or droplets. When granulometric analysis indicates the presence of a polydispersed aerosol, it is likely that the various granulometric size ranges may each have a different chemical nature. It is thus essential in these cases to carry out a particle or droplet size range determination.

Aerosols generated in fires can contain mineral-based fillers or other additives, depending on the type of combustible material. Examples of such fillers include; titanium oxides, aluminium trioxides and clays. Samples collected on filters can be analysed qualitatively and semi quantitatively for elements and crystal structures by X-Ray fluorescence and X-Ray scattering characterization technique. Metals present in aerosols on the other hand can be analysed by the use of selective solvents on the trapping filter followed by treatment with acid, e.g., regal solution or sulphuric acid. The solution formed can be analysed by ion liquid chromatography, inductively coupled plasma (ICP), or atomic absorption. Quantitative analysis is also possible. It should be noted that some metals can be reduced or oxidized in a flame, leading to the formation of compounds that cannot be measured by this technique.

In the case of filter paper sampling, a “blank” analysis of the filter is essential to differentiate it from the actual compounds obtained from the various techniques.

Other compounds that may be present can be analysed on the basis of a knowledge of the likely combustion products from a fire. But this can be difficult, as these products may differ from those expected from the nature of the fuels, due to the combustion conditions and other interactions.

2.11.4 Particulate Yield/ Emission Index

Yield of particulates as referred to in fire toxicity and emission index or emission factor in environmental pollution is measured in mass or number of particles per unit mass of fuel burned (g/kg or number/kg). These values help to give a better understanding of the impacts of burning any fuel on human health, global and climate change and can be used to model smoke particle production and release into the atmosphere. The impacts of particulates on humans depends largely on the dose received and the scope of area covered by the emissions whereas the impact to the environment depend on the amount of particles released to the atmosphere that can affect the radiation balance, acidification of cloud, rain and fog [138].

There have been reports of PM_{2.5} emission factors of different species of trees in the literature. Hays et.al [139] studied an open burning of mixed hardwood forest foliage in United States and found an emission factor of 10.8 ± 3.9 g/kg. Fine et al. [140] found an emission factor ranging from 2.7 to 5.7 g/kg for hardwoods and 3.7 to 11.4 g/kg for softwoods grown in the North-eastern United States. A similar study of woods grown in the Southern United States by Fine et al. [141] yielded 3.3 to 6.8 g/kg for hardwoods and 1.6 to 3.7 g/kg for softwoods. Emission factors of 2.9 to 9 g/kg for softwoods and 2.3 to 8.3 g/kg for hardwood were obtained from a study aimed at characterising emissions from wood burning in a fireplace [142]. Hedberg et al. [143] obtained 0.1 to 2.6 g/kg from the burning of birch wood in a stove.

There are no studies conducted to measure the particle number emission factors except particle mass emission factors in fire research to the knowledge of the author and only limited studies in atmospheric research. This research seeks to obtain the particle emission factors/index or yields from a range of materials.

2.11.5 Techniques for Sampling and Analysis of Particulates/Aerosol in Fire Effluents

A major hazard from both diesel exhausts and fire is the aerosol particles. The smaller particles known as PM 10s and PM 2.5 have the capability of penetrating deep into the lung, leading to a flooding of the lung known as pulmonary oedema. They also have the capability of acting as vehicles for transporting other toxicants to evade the body's normal defences. The techniques required for sampling and analysing particulates/aerosols in fire effluents differ from those used for gases and vapours. Four main properties characterise solid and liquid particulates in fire effluents [144] and these include:

- The Concentration of the particles
- The size distribution of the particles
- The chemical nature of the particles, which may also depend on the size of particle
- Morphology (form and structure of the particulates)

The sampling process for particulates must try to preserve all the properties of the particulates. The analyser must therefore be designed in such a way that these properties are preserved. These can be achieved by designing the sampling probe to operate at a velocity set to provide isokinetic sampling (that is, the velocity of sampling is the same as the sampled effluent flow, thus avoiding any change in concentration or particle characteristics through use of the probe) [144]. The material and temperature of the probe and sampling are also very important as well as the pressure. The physical and chemical nature of the particulates can be preserved before analysis after sampling it by dilution as concentrated solid aerosol particulates and liquid droplets tend to agglomerate into larger particles or droplets with time [144]. Current research is geared towards nanometric particulates which have extremely small particles. The various techniques available for measuring the characteristics of particulates are based on the use of optical benches (light transmission, light scattering), or on a separation technique (based on particulate diameter or mobility diameter) coupled with a device for measuring the mass or number of particulates. The characterisation of particles/aerosols by mass size concentration and particle number concentration can be done using several pieces of equipment such as the cascade impactor, low pressure cascade impactor, Electrical Low Pressure

Impactor, Electrical low pressure Impactor plus and the DMS 500 etc. A summary of the most common techniques used for measuring particulates generated from fires is given in Table 2-3 below.

2.11.5.1 Gravimetric Sampling Method of Total Particle Mass Concentration

This is the basic method used to measure mass concentrations of particulate matter off-line in flue gases. The sampling is done on quartz or glass fibre filters that have been in a desiccator or a room with controlled humidity before sampling. The gravimetric sampling method gives total mass concentration. The gravimetric method has an option of gathering mass concentration of specific size fraction in combination with a pre-cyclone with a cut off of say 10 μm or 2.5 μm resulting in PM_{10} or $\text{PM}_{2.5}$. The disadvantage of filter sampling is that it enables typical time resolution of 15 minutes and up and hence does not allow the identification of fast processes [145]. However, there is the advantage of being able to carry out further chemical analysis on particles since they are available on filter paper.

2.11.5.2 Cascade Impactor:

The cascade impactor shown in Fig. 2-14 is an apparatus used to measure aerodynamic diameter [146]. The device has a compartment that has a series of collection platforms known as stages in which the aerosol enters. This works with inertial forces. The inertial forces transport particles perpendicular to the streamlines of the velocity field in the compartment with a rate dependant on parameters including flow field, size and density, causing particles in successively smaller ranges to impact on successive stages.



Figure 2-14 Cascade Impactor

2.11.5.3 Low Pressure Impactor:

This is a low pressure cascade impactor (Fig. 2-15) that classifies airborne particles into 13 size fractions, starting from 30 nm to 1 μm with evenly distributed impactor stages. This is achieved by progressively decreasing the nozzle diameter.



Figure 2-15 Low Pressure Impactor

2.11.5.4 Electrical Low Pressure Impactor (ELPI):

The ELPI measures real time particle sizes from 0.01-10 μm in diameter and particle concentrations. ELPI has a simple point type unipolar diode charger that charges the particles unipolarly to a well-defined level. The charged particles are then fractionated into sizes in a 13 stage multi jet low pressure impactor that is equipped with electrically insulated stages according to the aerodynamic equivalent diameter.

2.11.5.5 Electrical Low Pressure Impactor Plus (ELPI+):

The ELPI+ (Fig. 2-16) is a modification of the cascade impactor which measures the particle size distribution and number concentration of aerosols in real-time. It has three main operating parts that perform the following functions: electrical particle charging, classification of sizes by the cascade impactor and charged particles detection by sensitive electrodes. When the particles enter the instrument, they are first charged by a corona before they enter the cascade impactor. In the cascade impactor, the particles are then separated according to their aerodynamic diameter. The ELPI+ can collect particle sizes ranging from 10 μm – 6 nm. It can be applied in a broad range of aerosol measurement.



Figure 2-16 Electrical Low Pressure Impactor Plus (ELPI +)

2.11.5.6 Differential Mobility Spectrometer (DMS 500):

The DMS 500 was first launched in the year 2002. It is not very popular in the fire toxicity industry as very few researchers have used it for particulates analysis. It is more common for measurements from engine exhausts. It works by combining electrical mobility measurements of particles with sensitive electrometer detectors which allows particle size/number distributions to be generated in real-time [147]. These outputs can further be processed to give simultaneous outputs of particle size, number and mass. The DMS 500 measures particle size distribution from 5 nm up to 2.5 μm allowing measurement of PM_{2.5}. This research used the DMS 500 for the analysis of particles due to the numerous advantages it has over other analysers. The DMS500 has the following advantages:

- Measures aerosol size spectrum from 5 nm to 1.0 µm or 5 nm to 2.5 µm for both solid particles and liquid droplets
- It has a fast time response
- Real-time measurement
- Enhanced sensitivity

Table 2-3 Summary of the Main Techniques for Measurement of Particulates in Fire [144]

Name	Principle of Measurement	Information provided	Range (µm)	Uses in hazard assessment
Light Extinction	Attenuation of a light beam is linked to soot concentration	Extinction coefficient, soot concentration and soot yield	0.1-1	Visual observation
Light Scattering	Scattering of a light beam across smoke is measured at fixed angles	Extinction coefficient, particle size distribution	>1	
Direct gravimetric method	Soot is deposited on a filter at a fixed mass flow and filter is weighed after collection	Soot main concentration and soot yield	Total	Carbon balance
Cascade Impactor	Soot is classified by aerosol aerodynamic diameter and measured by gravimetric method	Mass distribution (aerodynamic diameter)	0.3-30 ^a 0.02-30 ^b	Effect on lung function
Electrical Low Pressure cascade impactor (ELPI)	Same as cascade impactor, but quantification is made continuously by electrostatic measurement	Time-dependent number distribution (aerodynamic diameter)	0.02-30	Changes during transport, e.g. agglomeration
Scanning mobility particle sizer (SMPS)	Aerosol is separated in a diffusion mobility analyser (DMA)	Number distribution	0.01-1	

	followed by measurement of electric mobility diameter by condensation nucleus counter (CNC)	(electrical mobility diameter)		
Aerodynamic particle sizer (APS)	Aerosol is accelerated and a double laser beam measures velocity. Acceleration is a function of the aerodynamic diameter of the aerosol	Granulometric distribution (aerodynamic diameter)	0.5-20	

2.11.6 Sampling Train and Sampling Line

Typically, direct concentration measurements are performed on extracted fire aerosol samples drawn into an instrument, or onto a filter. *In situ* measurements tend to be indirect measurements, such as by light extinction. The benefit of an *in situ* measurement like light extinction is its simplicity and the fact that it does not disturb the aerosol or flow. However, light extinction is spatially averaged over a path length. Extractive sampling may disturb flows, and is subject to biases due to non-isokinetic sampling, diffusive losses in sampling lines, sedimentation and impaction losses, and electrostatic losses depending on sampling line materials and aerosol electrical charge [136]. In general, particle losses in sampling tubes must be considered for any aerosol measurements. The design of the experimental setup, and the sampling system should be tailored to minimize the losses of particles in the size range of interest. For instance, beyond the shortest possible sampling lines, metallic or conductive plastic tubing will minimize electrostatic losses, large radius bends and short horizontal lines will reduce impaction and sedimentation losses, and large volumetric flow rates will reduce diffusion losses. The temperature and humidity of the aerosol as it flows to instrumentation and gets mixed with any dilution air

may affect its particle size distribution. Heated lines will reduce condensation when extracting fire aerosols at temperatures above the ambient. Dilution air at the same temperature and relative humidity will reduce evaporation and condensation of volatiles and water [136].

2.11.7 Particulate Measurement Studies

Different measurement and combustion conditions have yielded different results of particle size distribution in previous studies. Earlier studies have shown investigations on smoke/soot production and particulates but not on fine particulates. Tewarson [30] examined emissions of smoke from various fire sizes and fuels for fully ventilated combustion and came up with a correlation between the average smoke emission rate and yields which holds for particulate dominated smoke in the presence of H and OH atoms provided by other fuels or ignition sources. Perera and Litton [31] studied smoke particles produced from a range of flaming and non-flaming combustible materials and determined the fractal aggregates using light scattering and light extinction. They [31] also determined the morphology using SEM and TEM as shown in Fig. 2-17. Perera and Litton concluded that all of the aerosols generated were fractal aggregates, but there exist significant differences in their morphology and size both as a function of combustion source and combustion mode leading to different fractal properties. The smoke produced from open flaming fires were fractal aggregates with rather small primary particles and elongated, chain-like morphologies, while those formed from non-flaming fires had larger primary particles and clumped or more densely packed morphologies [31]. Tsuchiya and Mathieu [32] conducted an experiment of plywood under a depleted oxygen atmosphere using the Ohio State University (OSU) heat release rate (HRR) apparatus and used the experimental data to calculate the release rate and the total release of heat, carbon monoxide and smoke and the mean mass loss rate. Barakat et al. [33] analysed the smoke generated by four of the most commonly used oils in the Electricite de France production unit as well as heating oil and found that these fuels have the high propensity of generating soot particles. Haynes et al. [34] investigated soot formation in flat, premixed flames of ethylene, benzene, and pyridine with air using laser light scattering and fluorescence and extinction measurements.

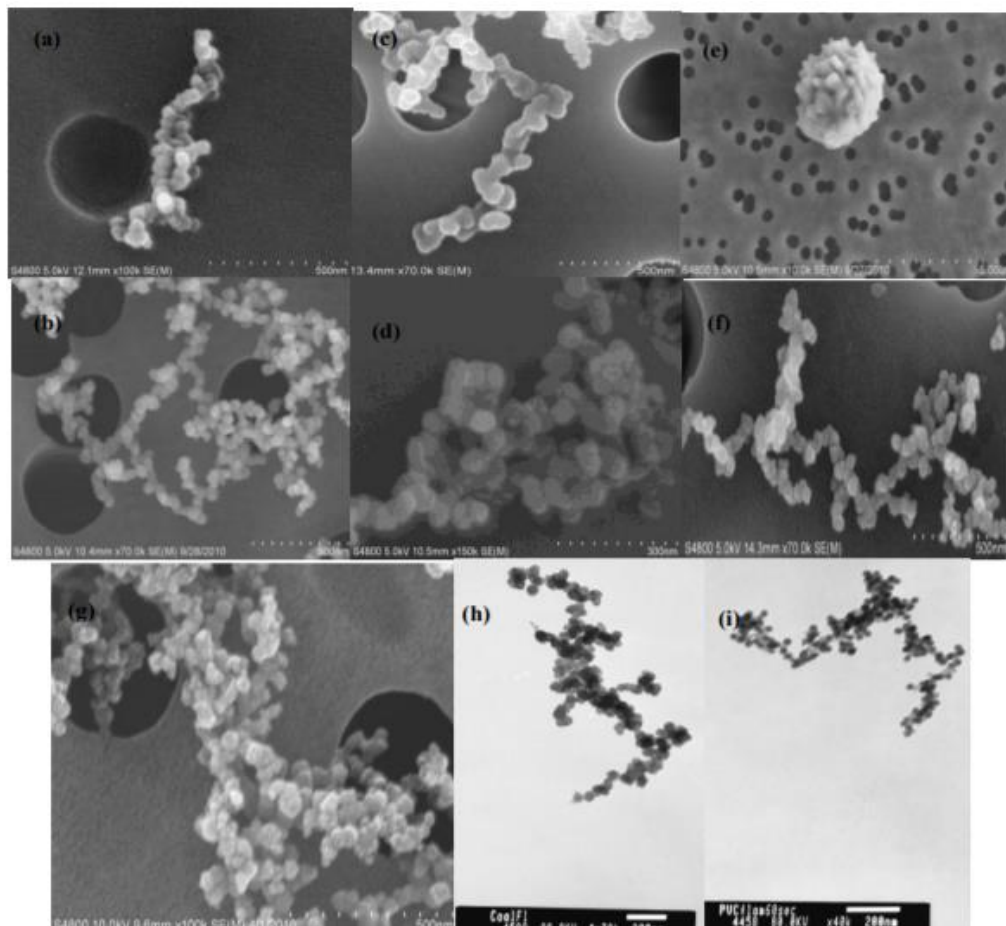


Figure 2-17 SEM Images of Aggregate Particles Generated from: (a) Non-flaming and (b) Flaming Douglas-fir Wood; (c) Non-flaming and (d) Flaming SBR Rubber; (e) Non-flaming and (f) Flaming Polypropylene; (g) Flaming Coal; and TEM Images of (h) Flaming Coal and (i) Flaming PVC Rubber extracted from [31]

Hays et al. [139] simulated combustion of fuel in a field using an enclosure of about 28 m³. They reported a unimodal distribution of particle sizes using the SMPS with a geometric mean diameter of 0.1-0.2 μm. This may be as a result of condensation and coagulation of particles in the enclosure. Le Canut et al. [148] used a laser optical particle counter to measure particle size distributions of savanna fire. Their result was a bimodal distribution of particles with the first mode in the 0.2-0.3 μm range and the second mode above 2 μm. Chakrabarty et al. [149] used SMPS and image analysis to measure the particle size distribution of eight different fuels. They reported that the diameter peaks ranged from 30-200 nm for wet and dry fuels. Hosseini et al. [150] studied the characteristics of particle size distribution in chaparral fires. They used a well

diluted laboratory scale enclosure for their tests and the size distribution was measured with FMPS and APS. They reported a size distribution of 29 to 52 nm for most of the fuel tested and a particle mass distribution of 0.5 to 10 μm for PM_{10} . They also found out that most fuels produced unimodal distribution during the flaming phase and bimodal distribution during the smouldering phase of the fire. Hertzberg et al. [133, 151], studied particles and Isocyanates from fires in Sweden. Most of the experiments were carried out on a small scale using the cone calorimeter (ISO 5660), though some were performed at an intermediate scale using the SBI method, EN 13823, and at full scale using the room corner, ISO 9705. The authors carried out the experiment using different building materials (24 of them) and measured the particle size distribution using a low pressure impactor. The authors found that fire retarded materials produced more particles than the materials which are not fire retarded (See Fig. 2-18 below). Figure 2-19 shows the result of the particle number distribution of some of the materials in Fig. 2-18 including wood which was compared with the present work. Blomqvist et al. [130, 152] carried out tests using polyurethane, FR (fire retardant) polyethylene cable insulation materials, polyvinylchloride (PVC) carpet and wood board in the purser furnace (ISO 19706 tube furnace) under different ventilation conditions and concluded that particle sizes are smaller in well ventilated fires than vitiated fires. Loo et al. [153] tested two grades of heptane and dodecane (pure and technical grade) in a 1 m^3 mechanically ventilated compartment at 5 ACH and 8 ACH. The particle size was analysed using the DMS 500 particle size analyser. The authors found out that the technical grade dodecane had the highest soot while the pure n-heptane produced the least. They also found that the soot sizes of all four grades were having a diameter of about 200 nm. Altaher et al. [154] investigated the particulate mass and size distribution for a biomass wood-pellet air heater, which they compared with the equivalent number size distribution for the fuel oil fired heater and for a Euro 2 6 cylinder 6L TCIC diesel engine that was operated on 100% rape seed oil as shown in Fig. 2-20. They [154] found that the peak of the number distribution pellets A was 5×10^8 number/ cm^3 occurring at 25 nm. This was higher than for the fuel oil burner, which had a peak number at 100 nm,

indicating more particle coagulation. The diesel engine had a diesel size distribution with a peak number at 50 nm.

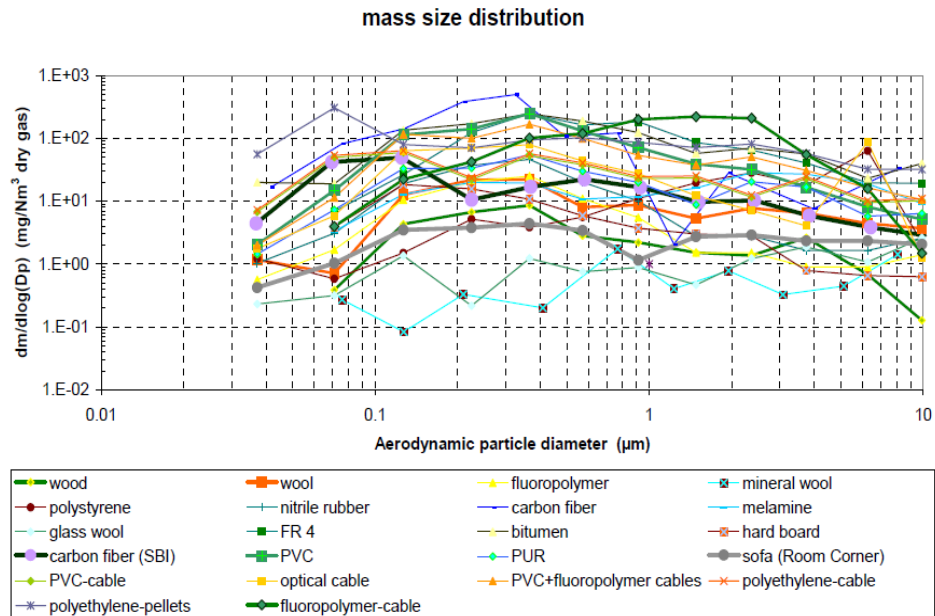


Figure 2-18 Particle Mass Size Distributions extracted from [133, 151]

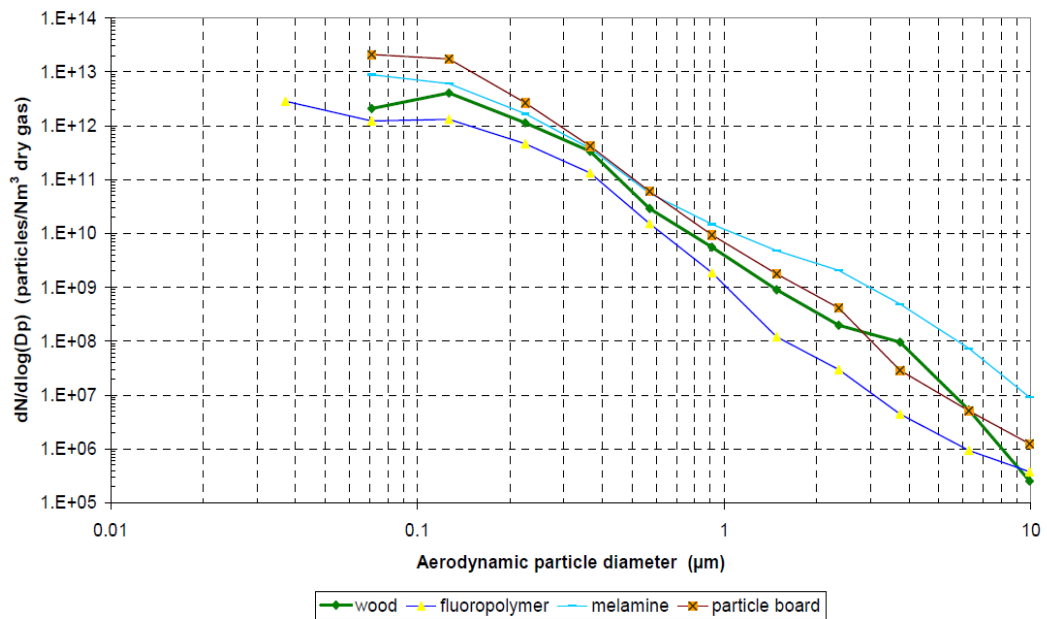


Figure 2-19 Number Size Distributions for Mass Size Distributions shown in Fig. 2-14 extracted from [133, 151]

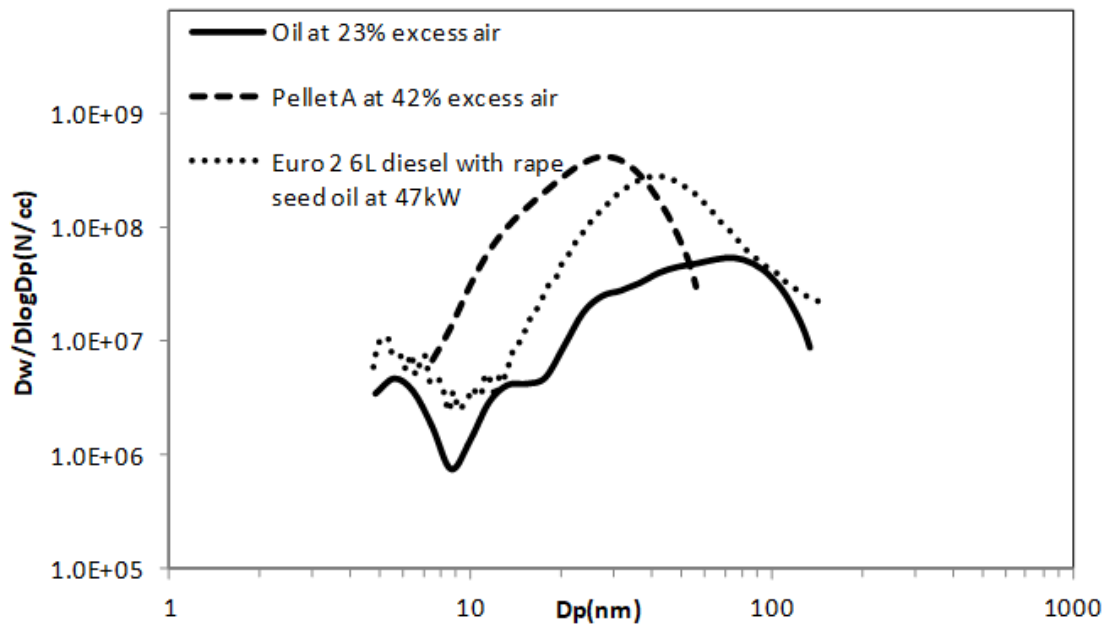


Figure 2-20 Particle Number Distribution as a Function of Size for Pellets A and Fuel Oil with a Comparison with a Euro 2 Diesel Operated on Rape Seed Oil extracted from [154]

Goo [155] studied wood and polypropylene (PP) in the steady-state tube furnace (ISO 19700) for each fire stage and measured the size distribution of smoke particulates in real-time using an electric low pressure impactor (ELPI+). Their morphologies were analysed using the transmission electron microscopy (TEM). He [155] found that the number concentration and shape of smoke particles differ between fire stages and combustion materials. From his findings, wood and PP have different number concentration distributions for fire stages 1b and 2 (ISO 19706 classification). Wood generated a large volume of soot in stage 1b while PP produced dense soot in large volume in stage 2. Andrews et al. [156] investigated particle mass concentration from diesel, wood crib and kerosene in a 1.6m^3 rig and compared them as shown in Fig. 2-21. Soot samples were collected gravimetrically using filter paper particulate sampler. They found that the diesel produced more particle mass concentration, followed by wood crib and then kerosene.

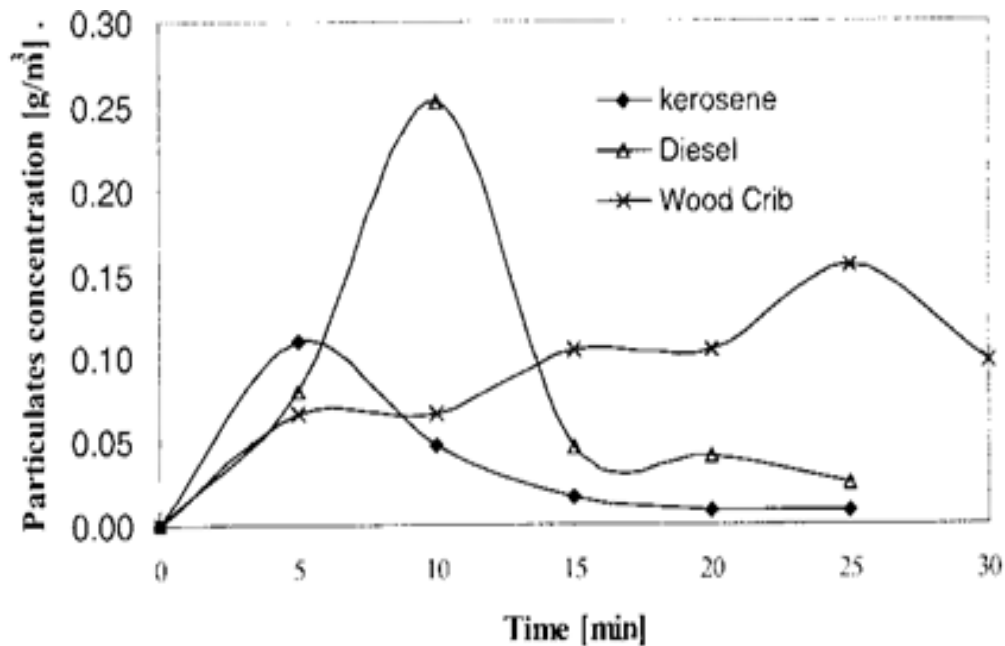


Figure 2-21 Particle Mass Concentration as a Function of Time [156]

2.12 Fire Hazard Analysis/ Toxicity Assessment

The exposure of humans to fire effluents has a significant effect on them. The effect is proportional to the concentration of the substance exposed to and its potency. This applies to visual obscuration due to smoke and the exposure to irritants. For asphyxiant gases, the effect depends on the dose inhaled. It takes time for the effect of asphyxiant to develop and it depends on the concentration of the substance inhaled and the time over which it is inhaled [157]. A threshold concentration or exposure dose known as the effective concentration or exposure dose can be used to predict serious effects for a given toxic or physiological end point. For toxic hazards calculations, the concept of fractional effective concentration (FEC) or dose (FED) is used whereby the concentration or dose being exposed to at any point during a fire is expressed as a fraction of the predicted exposure concentration or dose capable of producing a given effect such as incapacitation or death [157]. This effect can be estimated by exposing animals directly to the effluents to estimate the effects of the effluents on the animals or it can be done indirectly from tables of concentrations causing a particular effect, such as limit below which 50% of the population will be incapacitated or dead. The use of animals is not permitted in Europe, as such other chemical analysis must be used for fire toxicity testing. ISO 13344:2015

has recommended a methodology for estimating the Fractional Effective Dose (FED) which is based on lethal concentration of 50% of the population which were derived from rat lethality data.

2.12.1 Calculation of Fractional Effective Dose

The two equations recommended by ISO 13344:2015 for the estimation of the 30-minutes lethality FED from the chemical composition of the environment in the physical fire model begin with the precept that fractional lethal doses of most gases are additive [158]. The two equations were developed by Levin et al and Purser.

2.12.1.1 Levin's N-GAS Model

A seven gas N-GAS model was introduced by Levin [159] and Babrauskas et al. [160, 161] for toxicity assessment. This model was based on toxicological interactions of 7 gases (both asphyxiants and irritants), CO, CO₂, HCN, NO₂, low O₂, HCl and HBr with the hypothesis that a small number ('N') of gases in the smoke accounts for a large percentage of the observed toxic potency. Animal tests using rats were used to predict the toxicity of the gases in terms of their lethality and an approximate LC₅₀ value was determined. Levin's model assumes that carbon dioxide enhances the lethal toxicity of carbon monoxide with a maximum effect at a concentration of 5% carbon dioxide. When carbon dioxide exceeds 5%, the enhancement of carbon monoxide decreases. This effect was corrected in the N-gas equation using constants m and b which represent the slope and the intercepts of the combination gas toxicity curve. Corrective terms were also added in the equation for the protective effect of nitrogen dioxide on hydrogen cyanide toxicity. The equation is given thus:

$$N - Gas = \frac{m[CO]}{[CO_2]-b} + \frac{21-[O_2]}{21-[LC_{50,O_2}]} + \left(\frac{[HCN]}{LC_{50,HCN}} \times \frac{0.4[NO_2]}{LC_{50,NO_2}} \right) + \frac{0.4[NO_2]}{LC_{50,NO_2}} + \frac{[HCl]}{LC_{50,HCl}} + \frac{[HBr]}{LC_{50,HBr}} \quad 2-15$$

Purser [162] recommended the values below to be used for the Levin's N-gas model where m and b depend on the concentration of CO₂:

Table 2-4 Constants and LC₅₀ Concentrations for Levin N-Gas Model [157]

Gas	LC ₅₀ Concentrations for 30min exposures plus 14 days post-exposure period
For $[CO_2] \leq 5\%$	$m = -18, b = 122\ 000$
For $[CO_2] \geq 5\%$	$m = 23, b = 38\ 600$
Hypoxia – oxygen depletion	(21 – 5.4 = 15.6% depletion)
HCN	150 ppm
HCl	3700 ppm
HBr	3000 ppm
NO ₂	200 ppm

Although Levin's model was a major achievement in the fire industry, it has some drawbacks which include:

- Carbon dioxide correction was only applied to carbon monoxide with the assumption that carbon monoxide is likely to be the major toxic gas present even though carbon dioxide has been shown to employ synergistic effects on the toxicity of several other gases.
- The correction of hydrogen cyanide toxicity for the protective effect of nitrogen dioxide as shown in the equation applies to 200 ppm nitrogen dioxide only. A low level of nitrogen or negligible nitrogen will undermine the hydrogen toxicity which is not correct while at level higher than 200 ppm, the equation tends to enhance it, which is also not correct. In the real sense, nitrogen dioxide is present at low concentrations during fires and the major oxide species is nitric oxide [163].
- Organic irritants are omitted from the analysis (these are major causes of lung inflammation and death).
- The model assumed that the effect of low oxygen hypoxia is linearly related to decreased oxygen concentration, when in practice it is known to be non-linear [157].

2.12.1.2 Purser's LC₅₀ Model

The Purser model was developed mainly by fitting the rat LC₅₀ data obtained by Levin et al. [164] and Kaplan and Hartzell [165]. Purser introduced a multiplication factor V_{CO_2} for CO₂ driven hyperventilation to account for the increased respiration rate caused as a result of the inhalation of carbon dioxide on the increased uptake of harmful effect of other toxic species which increase the contribution of FED from all the toxic species [166]. An acidosis factor A was also introduced in the equation to account for CO₂ on its own. Purser explained that a FED of unity predicts death, and the mass loss exposure dose for the gases-producing materials is then equal to the LC₅₀ for the material decomposed in the same test conditions. Purser's model is more adequate because all possible toxic effect are included.

$$L_{FED} = \left[\frac{[CO]}{LC_{50,CO}} + \frac{[CN] - [NO_x]}{LC_{50,HCN}} + \frac{[X]}{LC_{50,X}} + \frac{[Y]}{LC_{50,Y}} \right] \times V_{CO_2} \times A + \frac{1}{\text{hypoxia function}}$$

2-16

Where:

[CN] is the concentration of cyanide

[NO_x] is the sum of [NO] concentration and [NO₂]

[X] is the Concentration of each acid gas

[Y] is the concentration of each organic irritant

LC_{50,X} is the LC₅₀ of each acid gas irritant

LC_{50,Y} is the LC₅₀ of each organic irritant

[CO₂] is the CO₂ concentration

V_{CO_2} is a multiplication factor for CO₂-driven hyperventilation and is equal to:

$$V_{CO_2} = 1 + \frac{\exp(0.14[CO_2]) - 1}{2} \quad 2-17$$

A is an acidosis factor equal to $([CO_2] \times 0.05) - 0.02$

Hypoxia function = $\exp(8.13 - 0.54 \times [21-O_2])$

The 30-min LC₅₀ values used in the Purser's model are given in table 2-4 below:

Table 2-5 30-min LC₅₀ Values used in Purser's Model [127]

Fire Effluent Gas	30-min LC ₅₀ (µl/l)
CO	5700
HCN	165
HCL	3800
HBr	3800
HF	2900
SO ₂	1400
NO ₂	170
Acrolein	150
Formaldehyde	750

2.12.1.3 Fractional Irritant Concentration (FIC) Model

This model has been developed for the estimation of irritant potency of an atmosphere based on the fractional effective concentration concept. The fractional irritant concentration (FIC) model assumes that each component contributes additively to the overall irritancy of a mixture. The concept of this model was developed by Purser [167] to assess the combined effects of irritants. The concentration (FIC) of each irritant is expressed as a fraction, having the concentration of the irritant present in the atmosphere as the numerator and the concentration likely to impair escape or considered likely to cause incapacitation as the denominator. The FICs for each irritant are then added up to give a total FIC. When the total FIC reaches unity, it is predicted that the smoke would be highly irritant and is enough to slow down escape attempts but if the FIC reaches 4 or more then it is predicted that escape would most likely not occur. The FIC can be calculated thus using equation (2-18):

$$FIC = FIC_{HCl} + FIC_{HF} + FIC_{SO_2} + FIC_{NO_2} + FIC_{CH_2CHO} + FIC_{CH_2O} + \sum FIC_x$$

2-18

Where $\sum FIC_x = FICs$ for any other irritants present.

This method is commonly used to assess the possible or likely effects of mixtures of toxic gases for industrial hygiene purposes and has the advantage of being reasonably conservative.

A detailed guidance is given in the EU COSHH procedures on how to handle the overall toxicity of a mixture of toxic gases, such as those in the products of fires [168]. It follows the same procedure as the fire N gas model and the FICs in that the concentration of each gas is divided by the toxic limit to present an **n** value for that toxic gas. All the toxic gases are then added up to give an overall toxicity with a value of **N**. The most significant gases can then be identified by using the ratio **n/N**. Two important pieces of information relevant to fire engineering can be derived from the measurement of **N** in compartment fires with realistic ventilation;

- A material's toxic behaviour can be estimated on a scale larger than the Purser tube test and larger than the cone calorimeter, but under realistic ventilation and fire temperatures.
- The value of **N** can be used in fire CFD modelling as the reduction of **N** by dilution since the fire smoke gases escaping from a fire room that mix with the air in the rest of the building can be predicted [169].

2.12.2 Other Methods for Toxicity Assessment:

Toxicity assessment has been a major issue in fire studies. There has always been a problem of uncertainty in identifying the toxic components because of the limited availability of information on irritants in toxic smoke. Most models available are based on lethality, as anything lower than the lethal point is not considered. Irritation and incapacitation effects are important hazards in fire smoke especially when considering escape.

Several bodies in Europe, and North America have come up with gases exposure threshold limits that have helped in shedding more light on toxic fire effluent. These bodies include U.S Environmental Protection Agency with Acute Exposure Guideline Levels (AEGL), The UK Health and Safety Commission with Work Exposure Limits (WELs) in Control of Substances Hazardous to Health (COSHH), OSHA with PEL [170], ACGIH with TLV [171], NIOSH with IDLH [172],

AEGL [173], ISO with IC₅₀ [128] and LC₅₀ [127], and SFPE with impairment of escape, incapacitation, and lethality exposure limits [7, 174]. The gases exposure limits are approved by Medical Committees and show that irritant species play an important role in impairment of escape and fire casualties.

Alarifi [87] in his thesis titled 'Compartment Fire Toxicity: Measurements and Aspects of Modelling', reviewed the available threshold (13 datasets) by the various bodies mentioned above and proposed four threshold levels to be used for different levels of fire toxicity assessment. Alarifi categorised the different threshold levels under 'Safe', 'Impairment of Escape', 'Incapacitation' and 'lethal'. The classifications are given in Table 2-6 below:

Table 2-6 Classification of Threshold Levels of Fire Toxicity Assessment

SAFE	IMPAIRMENT OF ESCAPE	INCAPACITATION	LETHAL
OSHA-PEL (STEL)	SFPE _{escape} Impairment	ISO-IC ₅₀	SFPE _{30min.Lethal}
TLV (STEL)	0.3 x SFPE _{escape} Impairment	SFPE _{incapacitaion}	ISO-LC ₅₀
COSHH (STEL)	IDLH		AEGL-3 _{30min}
AEGL-1 _{10min}	AEGL-2 _{10min}		

The various thresholds are defined thus;

2.12.2.1 Safe Exposure Limits

- a) WELs: these are work exposure limits (OELs) set under COSHH so that the health of workers are protected. EH40/2005 defines WEL as follows; 'WELs are concentrations of hazardous substances in the air, averaged over a specified period of time referred to as a time-weighted average (TWA)'. Two time periods are used : Long term and short term, based on 8 hours and 15 minutes respectively [168]. Short term exposure limits (STELs) are set to help prevent effects such as eye irritation, which may occur following exposure for a few minutes. STEL for COSHH is published by the UK Health and Safety Executive (HSE) to regulate Control of Substances Hazardous to Health in workplaces and considered the legal

limit in the UK for short term exposures (15 minutes) of an employee to a chemical substance. Alarifi recommended the STEL 15 min exposure for the exposure limits.

- b) OSHA-PEL (STEL): this is equivalent of COSHH obtained in the US. It is the approved safe exposure limit to toxic gases established by the Occupational Safety and Health Administration (OSHA). OSHA provides an extensive database for Permissible Exposure Limits (PELs) for different chemical substances. Alarifi recommended the STEL 15 min exposure for the exposure limits.
- c) TLV: TLV values are published by a private, not for profit and non-governmental scientific association called American Conference of Government Industrial Hygienists (ACGIH). Threshold Limit Values (TLVs) refer to 'airborne concentrations of chemical substances and represent conditions under which it is believed that nearly all workers may be repeatedly exposed, day after day, over a working lifetime, without adverse effects'. Alarifi recommended the STEL 15 min exposure for the exposure limits.
- d) AEGL-1_{10min}: this is one of the exposure guideline levels published by the US environmental Protection Agency. It can be defined as 'the airborne concentration, expressed as parts per million or milligrams per cubic metre (ppm or mg/m³) of a substance above which it is predicted that the general population including susceptible individuals could experience notable discomfort, irritation or certain asymptomatic non sensory effects. However the effects are not disabling and are transient and reversible upon cessation of exposure'. Alarifi recommended to use the level 1-10 min exposure limit for the safe exposure limits.

2.12.2.2 Impairment of escape:

- a) AEGL-2_{10min}: this can be define as 'the airborne concentration expressed as parts per million or milligrams per cubic metre (ppm or mg/m³) of a substance above which it is predicted that the general population including susceptible individuals could experience irreversible or other serious, long lasting adverse health effects or an impaired ability to

escape'. Alarifi recommended to use the level 2-10 min exposure limit to be classified under the impairment of escape exposure limits.

- b) SFPE Impairment of escape: these values are presented by Purser [7] in the SFPE handbook. These values represent the predicted concentrations that can lead to impairment of escape of half the population exposed. Alarifi suggested these values to be best classified under the impairment of escape threshold values.
- c) $0.3 \times$ SFPE Impairment of escape: Purser [7], recommended impairment of escape threshold to be multiplied by 0.3 to allow 'for the escape of nearly all exposed individuals'. Alarifi considered it to be appropriate under the impairment of escape classification.
- d) IDLH: Immediately dangerous for life or health (IDLH) are values published by the National Institute for Occupational Safety (NIOSH) of the US. IDLH condition is "one that poses a threat of exposure to airborne contaminants when that exposure is likely to cause death or immediate or delayed permanent adverse health effects or prevent escape from such an environment " [172]. This definition is not very clear as all the exposure levels are mentioned in the definition. Though it was classified under the impairment of escape, it needs to be used with caution [87]

2.12.2.3 Incapacitation Exposure Limits

- a) ISO-IC₅₀: IC₅₀ was introduced by the International Standards Organisation (ISO) and published in ISO 13571. It can be defined as 'the concentration that is expected to seriously compromise occupants' ability to take effective action to accomplish escape'.
- b) SFPE incapacitation: Purser [7] presented these values in the SFPE handbook to show the predicted concentrations that can cause incapacitation to half of the population that are exposed.

2.12.2.4 Lethal Exposure Limits:

- a) SFPE 30min Lethal: Purser presented these values showing the concentrations in which half of the population exposed die.
- b) ISO-LC₅₀: these values were published by the International Standard Organisation in ISO 13344 [175]. 'The LC₅₀ values are those that have

been statistically determined from independent experimental data to produce lethality in 50% of test animals (rats) within a 30-min exposure plus a 14-day post -exposure period' [175].

- c) AEGL-3_{30minutes}: AEGL-3 is 'the airborne concentration expressed as parts per million or milligrams per cubic metre (ppm or mg/m³) of a substance above which it is predicted that the general population including susceptible individuals could experience life-threatening health effects or death'. Purser [7] recommended that the AEGL-3 for 10 minutes and 30 minutes be used for lethal fire hazard assessment. Alarifi considered the 30 minute exposure limit for level 3 most appropriate for the lethal classification for fire effluents exposure threshold.

Andrews et al. [73] have previously argued that the COSHH 15 minute limits are more appropriate for fire toxic emissions evaluation, as levels above this will impair a person's ability to escape when exposed. The LC₅₀ is appropriate for predicting when half of the people exposed die in a fire from toxic gas inhalation. The occupational exposure data has a much wider range of toxic substances than the LC₅₀ data. In the work of Andrews et al. [73], the EU 15 min maximum exposure COSHH data was primarily used together with STEL limit for gases without a COSHH limit. Andrews et al. have shown that any assessment of toxicity in fires depends on which toxicity limit data is being used as any analysis of relative toxicity in gas mixtures will always place much more emphasis on CO using LC₅₀ data than COSHH 15 minute limits and on the other hand COSHH will always place much more emphasis on acrolein.

Andrews et al. [73, 176] found that the main toxic species found in pine wood crib fires are acrolein, formaldehyde, CO and benzene. They also found that CO and benzene were low contributors while more than 80% of the toxicity was from acrolein and formaldehyde.

Summary;

From the literature review, this study was initiated based on the following reasons:

1. Knowledge of particle size distribution and emission factors from compartment fires is still limited.

2. There is little information on particle number emission factors during fires.
3. Knowledge of PAHs from fires is limited, especially compartment fires.
4. Fire deaths as a result of smoke inhalation is still high which means the problem of fire toxicity is far from over and requires more investigations on the products of incomplete combustion arising from fires.

Chapter 3 Methodology

Introduction

Chapter 3 describes in detail the experimental methods, methods for analysing data and toxicity assessment methods used by the Author. The analytical tests conducted to determine the characteristics of the fuel used are described in detail in the first section of this chapter, followed by the main experimental equipment (cone calorimeter and the 5 m³ compartment) described in section 3.2, while the gas and particulate analysis equipment are described in section 3.3. Finally, the mathematical equations and gas analysis techniques are also presented as well as the toxicity assessment methods used.

3.1 Analytical Experiments

In this work analytical laboratory tests and techniques were used mainly to get the characteristics of fuels used, giving a rough idea of what to expect as toxic gases during combustion. It also enabled the determination of the stoichiometric air-fuel ratio of each fuel. Other analytical tests were carried out on soot samples collected on filter paper.

3.1.1 Elemental Analysis

The fuels for the experiments were characterised in terms of elemental composition and combustible content. Elemental analysis, mostly referred to as CHNS analysis determines the weight percentage of Carbon, Hydrogen, Nitrogen and Sulphur in a sample. The CHNS analysis provides useful information about the combustion characteristics of an unknown material tested under different fire conditions. It also helps in predicting the possible products of combustion under different testing conditions and their interactions [177].

The elemental analysis of the fuels was carried out using Flash 2000 Thermo Scientific analyser. The analyser consists of a single reactor with a temperature of 1800°C for the detection of Carbon, Hydrogen, Nitrogen and Sulphur. Oxygen was obtained by subtracting the total of the CHNS percentages from 100% as shown in Eqn. 3-1. The Flash 2000 elemental analyser requires samples in

powdered form or finely grinded in order to improve the reactivity for a complete combustion in the test chamber. Therefore, wood samples were milled into powdered form before the analysis was carried out. Prior to the loading of the samples into the analyser, the samples are placed in tin capsules and weighed. At a pre-set time, the tin capsules are then placed inside the Thermo scientific MAS 200R autosampler and then released into an oxidation/reduction reactor having a temperature of 900-1000°C. The actual amount of oxygen needed for the optimum combustion of the sample to occur is introduced into the combustion reactor at a specific time. Oxygen reacts with the tin capsules at an elevated temperature thereby generating an exothermic reaction and raising the temperature to about 1800°C for a few seconds. At this elevated temperature, the organic and inorganic substances in the sample are converted into gases comprising carbon dioxide, water, nitric oxides and sulphides. The combustion products produced, after further reduction, are then separated by a chromatographic column and detected by the thermal conductivity detector (TCD). This further generates an output signal proportional to the concentration of the elemental oxides present in the mixture. Table 3-6 shows the measured composition of the fuel used in this work obtained from the CHNS analyser and the TGA analyser.

$$\% O = 100 - (\% C + \% H + \% N + \% S + \% \text{Moisture} + \% \text{Ash}) \quad \mathbf{3-1}$$

3.1.2 Proximate Analysis

The Shimadzu TGA-60W was used to analyse the samples for moisture, volatile and fixed carbon content. The ash content was determined by difference. In this analyser, samples were subjected to high temperatures in an inert atmosphere to heat and remove moisture and volatiles from the sample, after which the atmosphere is changed to oxygen to allow combustion and conversion of fixed carbon, leaving ash as the final weight. Table 3-6 shows the proximate analysis of all the fuel used in the experiments.

The TGA analysis involved the following steps:

1. Samples were heated up under nitrogen atmosphere from ambient temperature to 110°C at the rate of 10°C/min and was held at this temperature for 10 minutes to remove the moisture content completely

from the sample, hence providing the mass of moisture in the sample by weight loss.

2. The temperature was increased from 110°C to 910°C at the rate of 25°C/min and was held at this temperature for 10 min to get the weight of the volatile loss.
3. The sample was then heated from 910°C to 920°C at the rate of 10°C/min and O₂ was introduced at this point causing a reaction with fixed carbon in the char. The sample was held at 920°C for 10 minutes. Thus the mass loss here represents the fixed carbon content of the material. What is remaining is the ash content, and this is obtained by difference.

3.1.3 Bomb Calorimeter

The Parr 6200 Oxygen Bomb Calorimeter measures calorific values (CV) of fuels and other combustible samples. This instrument was used in this work to determine the Gross and Net Calorific Value of the samples. The instrument works by combusting a weighed sample in a pressure vessel (the 'bomb'), filled with pure oxygen and surrounded by a 'bucket' containing a known weight of water. The resulting temperature rise of water is used to compute the CV of the sample. The calorimeter is calibrated by combusting a standard material of known CV, usually benzoic acid, in the same way.

In this work, the powdered wood sample (about 1g) was first pelletised using hydraulic manual press to avoid explosion. This pellet was then weighed into the crucible and placed into the sample holding ring attached to one of the electrodes that was held in the bomb lid. A loop of the fused wire was placed just above the sample (close enough to the sample) without touching the sample and the crucible. Bomb lid was placed in the bomb cylinder and screwed tightly to prevent air leakage. The bomb was then filled with oxygen to a pressure of 25 bar. The bucket was filled with 2000 g of deionized water and placed in the calorimeter consisting of a thermistor and stirrer. The bomb was then placed in the bucket of water and the lid of the calorimeter was covered. Ignition was activated through the fused wire. Sample was burnt in the high-pressure oxygen atmosphere (25 bar) within the bomb. The energy released during the combustion process is absorbed within the calorimeter and the resulting temperature change was recorded and used for the measurement of the sample's heating value.

3.2 Description of Experimental Rigs

3.2.1 The 5 m³ Fire Compartment:

One of the pieces of equipment used for this work is the University of Leeds 5 m³ compartment. The 5 m³ compartment was built by Deansfield fabrications in 1996 but has been modified and upgraded over the years. Though a 5 m³ compartment, the compartment can be converted to different volumes by making some modifications such as providing air sealed walls inside the compartment to create a desired internal volume. Previous experiments [64, 156, 178] were carried out in the reduced scale of 1.6 m³ which was achieved by providing air sealed walls in the compartment to come up with three adjacent compartments of equal sizes (1.4 m x 0.96 m x 1.25 m) where only the centre compartment has been used. Al-jumaiah et al. [85] modified the reduced 1.6 m³ compartment by including an online FTIR system to analyse gases. In this work, the 1.6 m³ compartment has been modified by removing the air sealed walls in the compartment to get a room scale compartment of 5 m³ for the first time. Other modifications were also done to allow for gas analysis, soot sampling and particulate analysis as described in the sections below.

The enclosed fire testing rig is made up of a 5 m³ compartment having a size of 1.4 m x 2.88 m x 1.5 m (as shown in Fig. 3-1). An air distribution plenum that is 1.4 m x 0.96 m x 0.25 m is located below the compartment. The compartment is internally lined with 25 mm thick Triton Kaowool 1260 insulation board to prevent heat loss by radiation. The door/observation window is at the centre of the compartment and was covered with another door having the same insulation material. Natural ventilation was used to provide air into the compartment which was achieved by opening the air distribution plenum below the compartment door, or closing it, to achieve the desired inlet ventilation factor K_{in} . The air then finds its way to the compartment through the 10 slots in the compartment. Inside the compartment, at the centre, a suspended ceiling of 0.825 m by 1.21 m was used. It was positioned 1.12 m above the compartment floor and 5 cm below the enclosed compartment roof with leakage gaps by the sides of the suspended ceiling. The smoke generated from the fire hits the ceiling and allows for mixing before finding its way to the exhaust through the leakage gaps. An exhaust port

having a diameter of 152 mm was located above the suspended ceiling and centrally positioned on the roof of the compartment. A multi-hole X gas sample probe shown in Fig. 3-2 was located within the exhaust port. This sample probe had 36 sample holes on centres of equal area which allowed sampling of combustion gases.

A large hood of 3 m x 1.5 m was situated 90 mm above the roof of the compartment into which the products of combustion leaving the compartment through the chimney were discharged. The chimney was 202 mm high and had a diameter of 381 mm through which the extraction system was used to convey the products of combustion to the atmosphere. The extraction was enabled by a 381 mm bifurcated fan manufactured by Halifax Fan Manufacturing Company Limited with an air flow rate of 1.24 m³/s and a maximum speed of 1425 rpm.

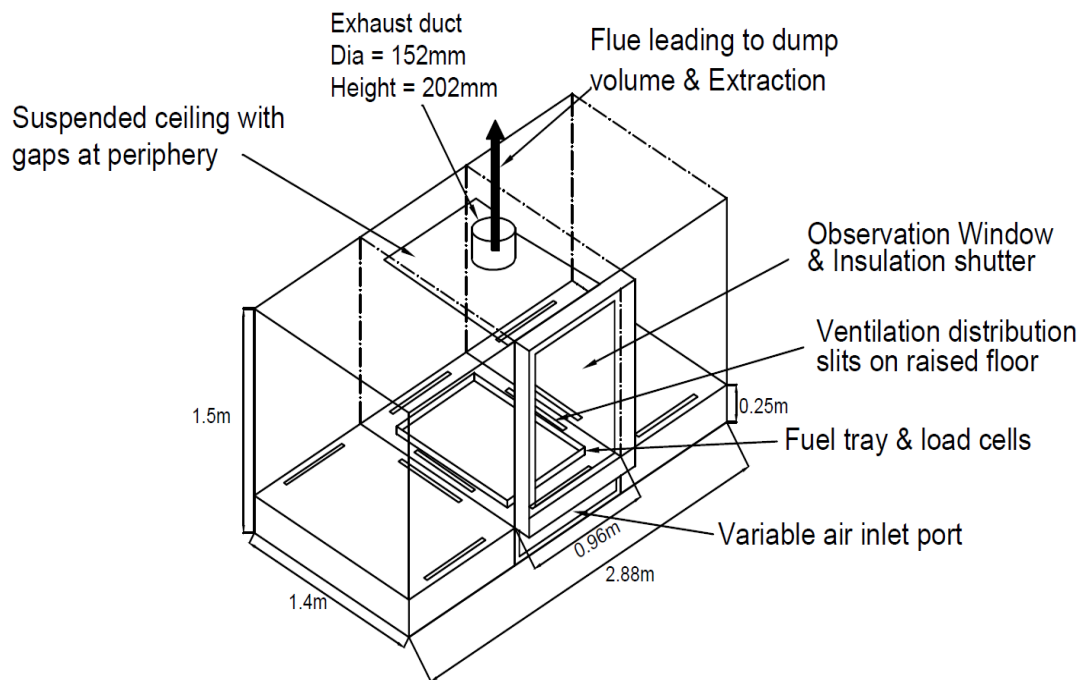


Figure 3-1 A schematic diagram of the 5m³ compartment



Figure 3-2 Multi Hole X-probe for the 5m³ Compartment

3.2.1.1 5m³ Compartment Modification

In developing this experimental method it was found that the airflow was controlled by the exhaust thereby introducing excessive air into the compartment as observed in the first few tests conducted (chapter 7). The chimney with 15.2 cm diameter and 20.2 cm length resulted in an outlet ventilation factor K_{out} factor of 0.62 %. It was expected that the inlet air to the compartment would enter through the opening at the bottom, so that the air supplied to the combustion would be totally controlled by the area of the opening, and the chimney would only act as the exhaust for the fire smoke. However, in the first few tests, the oxygen reading from the analyser didn't show any oxygen consumption which was not reasonable. This was as a result of the large amount of air backflow into the chimney, which affected the air supply to the combustion, thereby diluting the raw fire gases. To take care of the problem, an orifice plate (Fig. 3-3 a) of 73 mm diameter was placed above the chimney to restrict the backflow of air into the compartment. The outlet ventilation factor K_{out} , became 0.14% with the orifice plate.

The FTIR sampling point was also changed to a stainless steel tube placed directly inside the chimney to get the raw sample and this was connected to the FTIR heated sample line.

To get a dilute sample for the particle size analyser, a sampling tube was designed to fit within the extraction vent so that gases leaving the compartment

would be diluted before sampling. Figure 3-3 b shows a picture of the sampling tube design for the fire rig. The top tube just fits within the extraction vent bore and lies about 100 mm within the vent. It has 8 holes of 1/16" diameter that are placed equidistant about the extraction centreline so that a mean sample can be obtained. Pitch dimension between the holes is 70 mm giving a total spread of 490 mm (the extraction vent has an inside diameter of 590 mm).

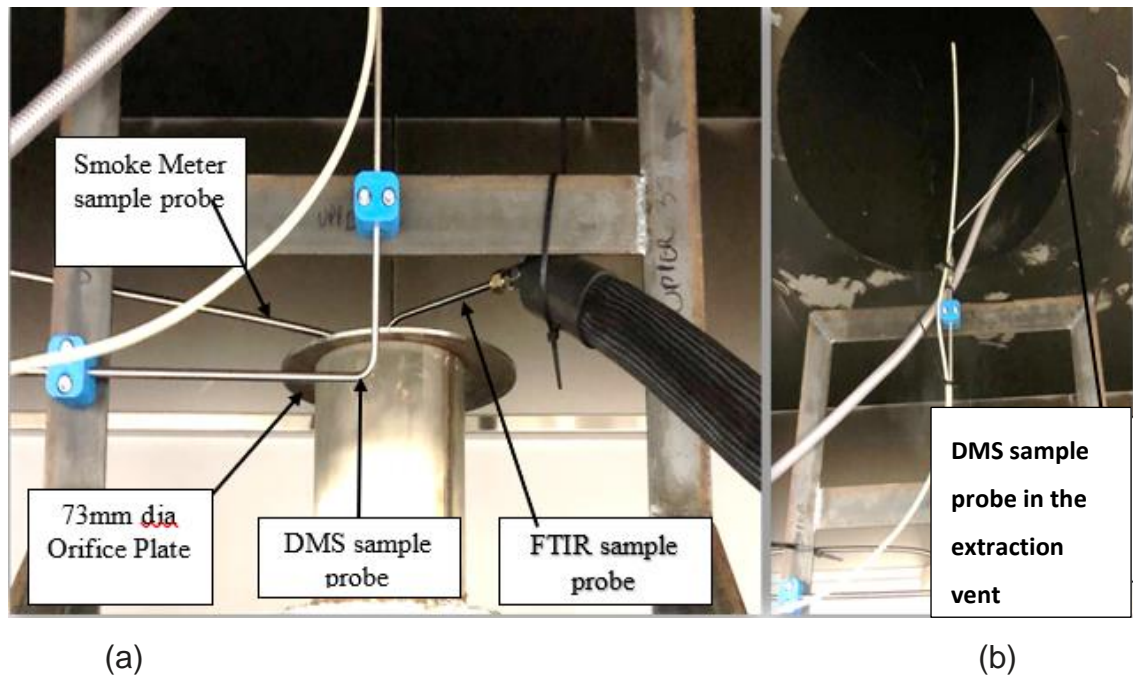


Figure 3-3 Sampling point for all analysers (a) Particle Size analyser (b)

3.2.1.2 Temperature Measurements

Temperatures in the compartment were measured using 30 type K mineral insulated exposed hot junction, 1.5 mm bead, 613 stainless steel sheathed thermocouples from TC Ltd. company. The arrangement of the thermocouples are described thus; and shown in Fig. 3-4 and Table 3-1 below. The temperature measurements were not corrected for radiation losses and poor convective heat transfer; this is expected to result in an experimental error of about 5% [179] considering the burning conditions used (enclosed compartment). Wall temperatures and gas velocity measurements in the thermocouple region were not possible in this work, thus, the measured values were accepted with this uncertainty.

The thermocouples were positioned in the compartment to measure the upper layer temperature (measured by the Top Row thermocouples), the ceiling

temperature (in the case of pine wood crib test) or sample tray temperature (in the case of the pool fire), the wall temperatures and the exhaust temperature. The exact position of each thermocouple based on the X, Y, and Z value of the compartment dimension is shown in Fig. 3-4.

Table 3-1 Distance and Position of Thermocouples in the Compartment

Thermocouple	X-value (cm)	Y-value (cm)	Z-value (cm)
Centre 1	70	48	46
Centre 2	70	48	60
Centre 3	70	48	74
Centre 4	70	48	88
Centre 5	70	48	102
Centre 6	70	48	116
Centre 7	70	48	130
Top Row 1	121	48	142
Top Row 2	105	48	142
Top Row 3	89	48	142
Top Row 4	51	48	142
Top Row 5	35	48	142
Top Row 6	19	48	142
Exhaust 1	70	120	142
Exhaust 2	70	168	142
Sample Tray	70	144	40
Wall 1	132	48	130
Wall 2	132	48	116
Wall 3	132	48	102
Wall 4	132	48	88
Wall 5	132	48	74
Wall 6	132	48	60
Wall 7	132	48	46
Wall 8	15	240	130
Wall 9	15	240	116
Wall 10	15	240	102
Wall 11	15	240	88
Wall 12	15	240	74
Wall 13	15	240	60
Wall 14	15	240	46

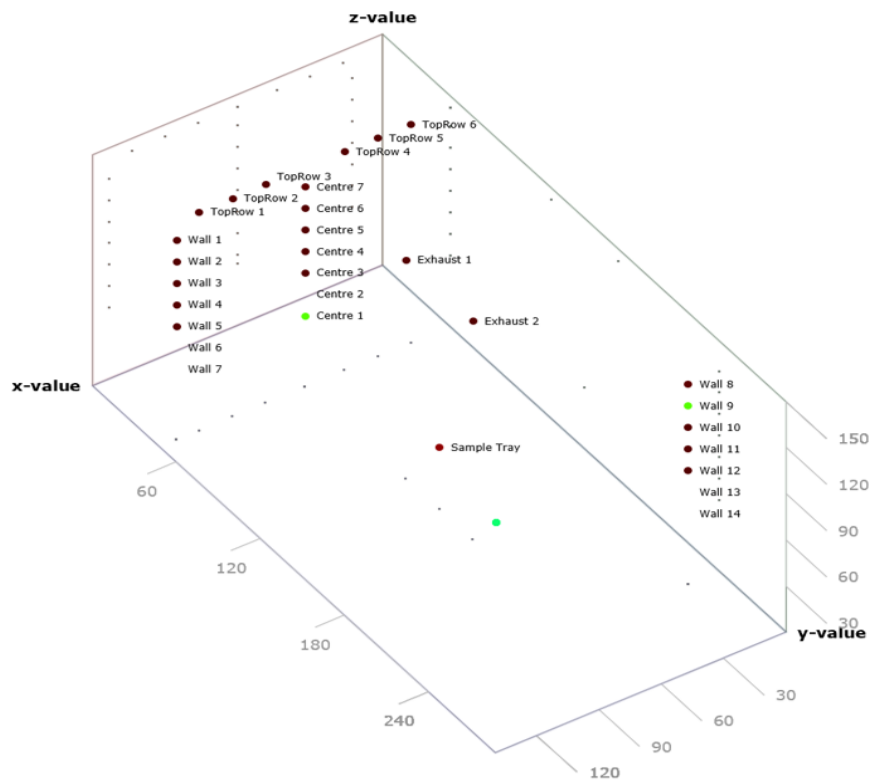


Figure 3-4 Arrangement of Thermocouples in the 5m³ Compartment

3.2.1.3 Ventilation Area

As mentioned earlier, the opening below the compartment was used as an air inlet. A cardboard sheet was used to seal the opening and a desired size of opening is made in the cardboard to determine the air inlet area and the ventilation factor. Three different sizes were used in this work for the wood crib and pool fires and these are shown in Fig. 3-5:

1. The fully open, without closure which is 0.15 m² and translates to a K_{in} factor of 5 %.
2. The completely sealed or no hole (except a small hole of 25 mm x 10 mm where the cable for the load cell gets through) with a K_{in} of 0 % and
3. Two square openings with a total area of 0.03 m², translating to 1 %.

The K_{in} was calculated using the equation introduced by [64, 65], $K_{in} = A_v/V^{2/3}$.

where A_v is the air in leakage equivalent open area and V is the volume of the test room.

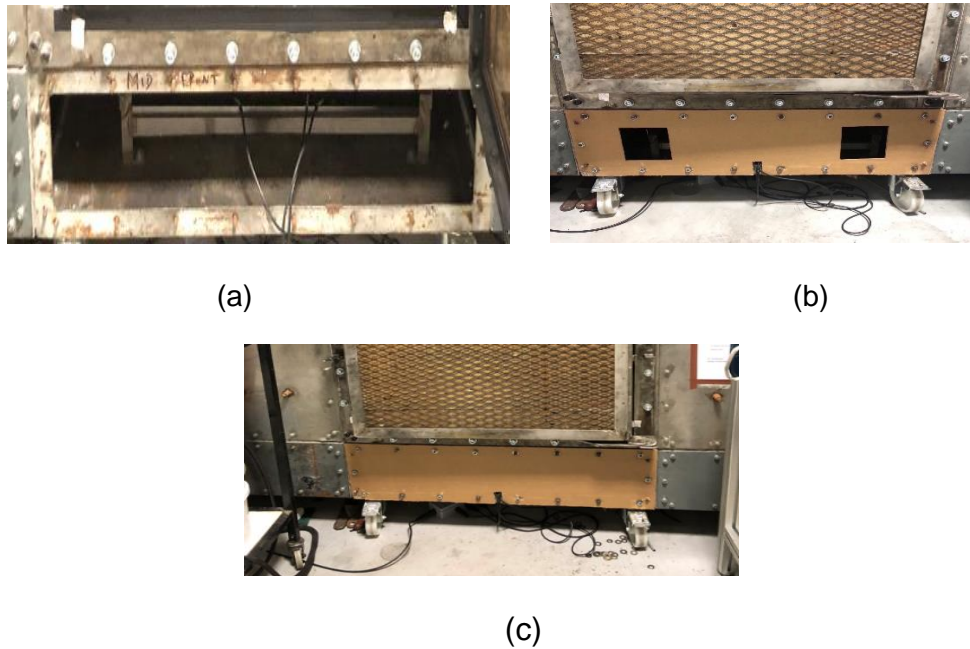


Figure 3-5The air inlet sizes; fully open (0.15 m^2 ; $K_{in} = 5\%$) (a); two square holes (0.03 m^2 ; $K_{in} = 1\%$) (b); and closed ($K_{in} = 0\%$) (c)

3.2.2 The Standard Cone Calorimeter

The standard cone calorimeter (ISO 5660), designed to measure the heat release rate and flammability properties of materials, was used for toxicity measurements in this work. The cone calorimeter replicates the oxidative pyrolysis stage (class 1b) and well ventilated flaming fires (class 2) classification of the ISO 19706 [48] where a fire would be too small to generate toxicants at harmful concentrations, unless in very small enclosures. The standard cone calorimeter (ISO 5660) [108] was adopted with modification for freely ventilated experiments. The cone calorimeter experimental setup was modified to enable a raw gas (predilution) sample to be obtained from the exit of the cone. A 20-hole X sample probe was mounted on top of the exit plane of the cone heater for the sampling of the mean composition of the raw gases. The X probe was mounted in a 76 mm diameter duct with flanges joining the cone heater exit to the chimney. This gas sample probe duct was 40 mm long. An 80 mm diameter chimney, i.e. the same diameter as the cone outlet, and 210 mm long, was mounted on top of the sample probe and the total chimney length was 250 mm. To avoid the

backflow of air down the chimney, a grid plate restrictor was placed at the chimney exit to increase the exhaust flow pressure loss, which then prevented backflow of air down to the sample probe. This orifice plate on the chimney had five holes each of 6.3 mm diameter. An insulation board was also placed in the sample holder underneath the test specimen to prevent heat losses to the supporting metal cylinder leading to the load cell heating. The airflow introduced to the combustion chamber was from the laboratory environment. Figure 3-6 shows the standard cone calorimeter setup with the modification.

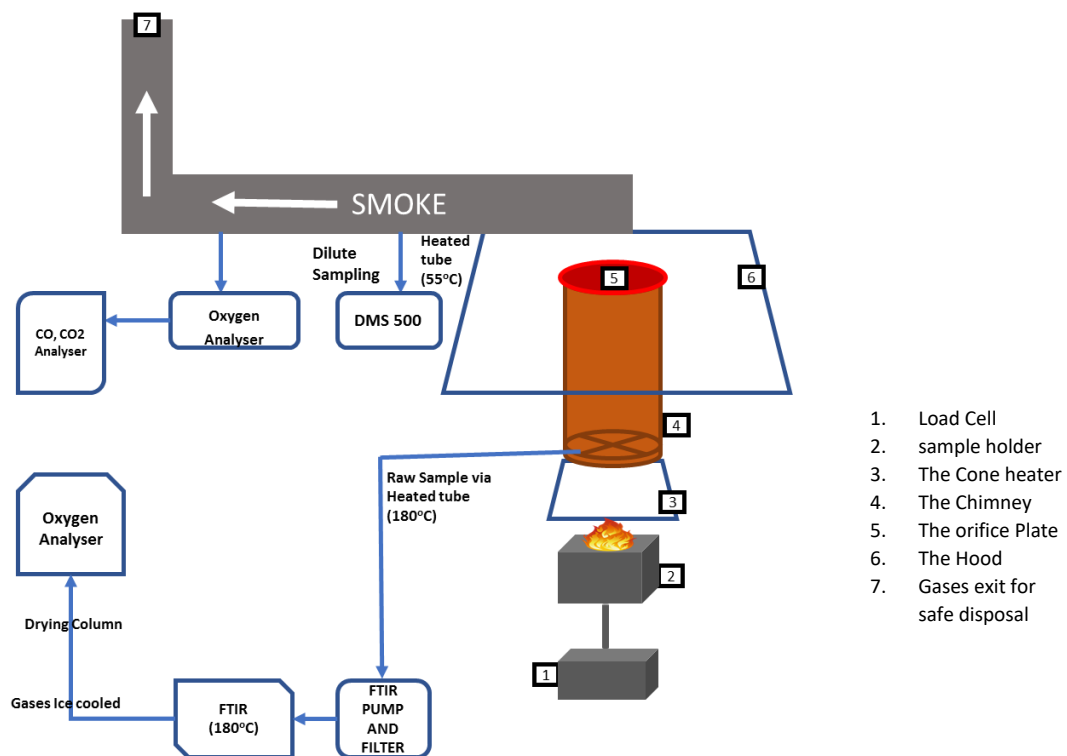


Figure 3-6 The standard Cone Calorimeter Setup

3.2.3 The Controlled Atmosphere Cone Calorimeter

The controlled atmosphere cone calorimeter is a modification of the standard cone calorimeter ISO 5660 [108] to create a vitiated (oxygen reduced environment) environment. The standard cone calorimeter setup (ISO 5660) can generate a combustion condition that will be in accordance with class 1b (oxidative pyrolysis) and class 2 (well ventilated flaming fires) based on the classification of fire stages in ISO 19706 [48]. This is not ideal for toxicity tests as it does not create the worst-case scenario but is suitable for material testing where the maximum heat release is required. The introduction of the enclosure

makes the controlled atmosphere cone calorimeter apparatus capable of creating the combustion conditions 1c (anaerobic pyrolysis) and both 3a (low ventilated fires) and 3b (post flashover fires) according to the classifications given in the ISO 19706 [48]. The controlled atmosphere cone calorimeter can create all the stages of fire except for class 1a (self-sustained smouldering fires).

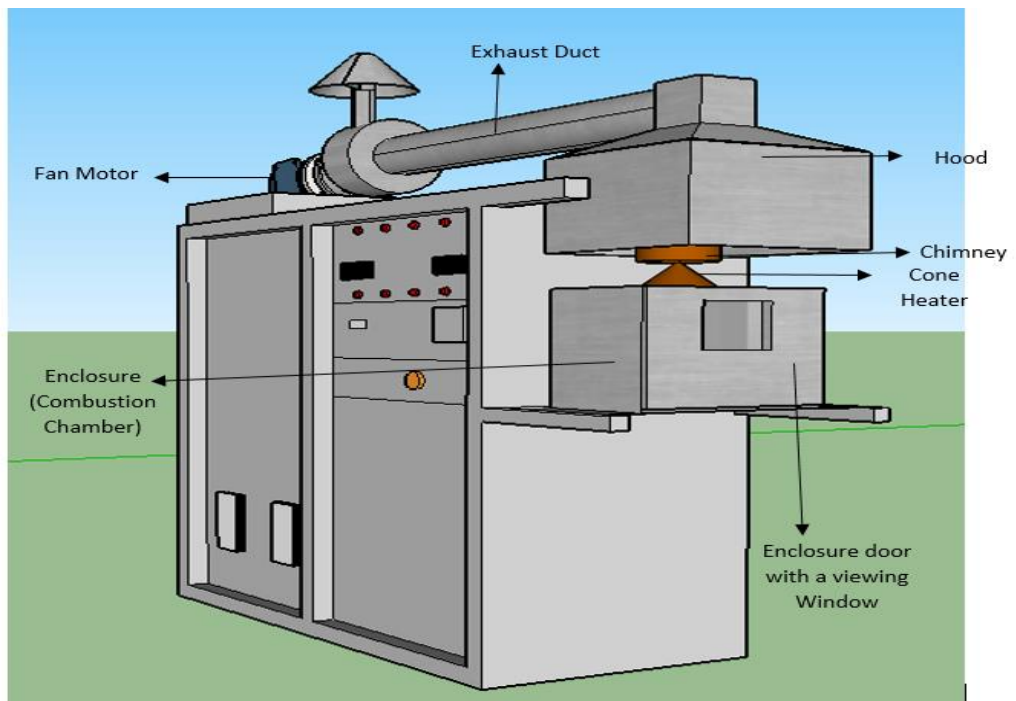
The cone calorimeter was used with an airtight stainless-steel box specially constructed to create vitiated conditions which enclosed the balance/sample holder and the cone heater. The airtight box was 38 cm long, 30 cm wide and 33 cm high. The airtight box was insulated from the inside and the door from the outside using an insulation board to avoid heat loss as a result of heating the stainless steel. The cone calorimeter enclosure also had a glass window for the observation of the combustion. The global equivalence ratio Φ of the combustion was obtained by supplying the box with a metered air flow. Two openings at the bottom of the steel box were used to supply the metered primary air to the steel box. The airflow to the combustion chamber was measured using a variable air flow meter and the air flow could be varied from 6 – 28 l/min (0.1 l/min accuracy or about 1%) from a compressed air supply, which is 0.12 – 0.56 g/s air mass flow and the air mass flow per exposed surface area of the test specimen (0.01 m²) is 12 – 56 g/sm². Another way of looking at the combustion conditions is to use the fact that for all HCON fuels there are 3.05 MJ [95] of heat release per kg of air and this converts the air mass flow range into a combustion HRR range of 0.37 – 1.71 kW and in terms of the exposed surface area of the wood is 37 – 171 kW/m². Three different flow rates were used in this work and results presented in kW/m² of air. Table 3-2 shows the conversions of the airflow rates used.

The sample was placed in a 100 mm square test holder and mounted on a load cell which enabled the A/F by mass to be determined as the test was proceeding. The load cell was cooled by water as the test was going on to avoid damaging the load cell because of the heat.

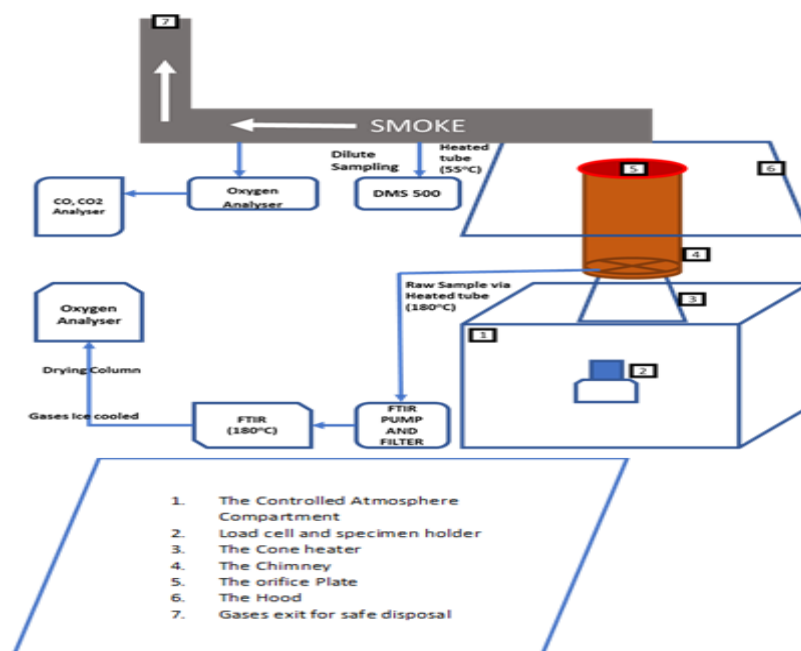
A multi hole X sample probe was mounted on top of the cone heater for the sampling of raw gases. Mounted on top of the sample probe is a chimney of 21 cm high and 8 cm diameter covered with an orifice plate to transport the gases to the exhaust as well as prevent post oxidation by gases within the chimney.

Table 3-2 Air Flow Rate Conversion

Unit	Air Flow Rate		
l/min	9.4	18	28
g/s	0.1919	0.3675	0.5717
$g_{air}/(m^2s)$	19.2	36.8	57.2
Air Change per hour (ACH)	18.8	36	56
kW/m^2_{air} using $3.05 MJ/kg_{air}$	59	112	174



(a)



(b)

Figure 3-7 The Controlled Atmosphere Cone Calorimeter and Setup

3.3 Principle of the Fourier Transform Infra-red Spectrometer (FTIR):

The FTIR equipment is a CR-Series portable FTIR manufactured by TEMET GASMET. The FTIR equipment is based on the principle of infra-red spectroscopy and is used for analysing chemical compounds. The infra-red radiation passes through the sample of gaseous molecules. Part of the radiation is transmitted through the sample while the rest is absorbed by the sample, producing an infra-red spectrum. Since each gas molecule has a molecular structure with a unique combination of atoms, each of the gas molecules produces a unique infra-red spectrum. From this, the gas can be identified and analysed. Because chemical functional groups absorb light at specific frequencies, the make-up of the sample of gas can easily be identified. The FTIR equipment available at the University of Leeds gives a typical 2 ppm resolution having an accuracy of 2% and a precision that is 0.01% of the measurement range.

The detector cell, sample line, pump and filter all need to be heated to about 180°C so that no species is lost during the analysis and so that high molecular

weight hydrocarbons can be detected. The three parts of the detection cell (sample cell body and 2 mirrors) have a special rhodium coating that makes it resist corrosion. The FTIR equipment is calibrated by the manufacturers to detect 51 species simultaneously using reference gas concentrations, for all the significant species that are present in fire exhaust samples. Most of the significant gases have their peak vibration in the wavelength range 2.5-16 μm which is equivalent to a wave number range of 4000-625 cm^{-1} . The zero had to be set using nitrogen before the experiment commences. The FTIR calibration for the range of gases is presented in Table 3-3 below.

Table 3-3 The 51 Gases FTIR was Calibrated to Measure

Species	Range		Species	Range	
Water vapour	50	%	1,3,5-trimethylbenzene	500	ppm
CO ₂	30	%	Ethylbenzene	*200	ppm
CO	20000	ppm	Indene	*500	ppm
N ₂ O	500	ppm	Methanol	500	ppm
NO	2000	ppm	Ethanol	500	ppm
NO ₂	1000	ppm	Propanol	500	ppm
SO ₂	1000	ppm	Butanol	*200	ppm
COS	200	ppm	MTBE	500	ppm
NH ₃	500	ppm	Dimethyl Ether	*200	ppm
HCN	500	ppm	Formaldehyde	500	ppm
HCl	500	ppm	Acetaldehyde	200	ppm
HF	200	ppm	Formic acid	200	ppm
Methane	1000	ppm	Acetic acid	500	ppm
Ethane C ₂ H ₆	500	ppm	Acrolein	500	ppm
Propane C ₃ H ₈	500	ppm	Naphthalene	500	ppm

Butane C ₄ H ₁₀	500	ppm	1-ethylnaphthalene	500	ppm
Pentane C ₅ H ₁₂	500	ppm	Sulphur hexafluoride	50	ppm
Iso-pentane C ₅ H ₁₂	*200	ppm	i-Butane	*100	ppm
Hexane C ₆ H ₁₄	500	ppm	1-Butene	*500	ppm
Heptane C ₇ H ₁₆	500	ppm	Tran-2-Butene	*100	ppm
Octane C ₈ H ₁₈	*200	ppm	Cis-2-Butene	*150	ppm
Iso-octane C ₈ H ₁₈	*500	ppm	i-ButeneC ₄ H ₈	*150	ppm
Cetane C ₁₆ H ₃₄	*200	ppm	PenteneC ₅ H ₁₀	*250	ppm
Acetylene C ₂ H ₂	500	ppm	HexeneC ₆ H ₁₂	*500	ppm
Ethylene C ₂ H ₄	500	ppm	HepteneC ₇ H ₁₄	*500	ppm
Propene C ₃ H ₆	500	ppm	Octene C ₈ H ₁₆	*500	ppm
1,3-Butadiene	500	ppm	Nonene C ₉ H ₁₈	*500	ppm
Benzene	500	ppm	Cyclopropane C ₃ H ₆	*500	ppm
Toluene	500	ppm	Cyclohexane C ₆ H ₁₂	*500	ppm
m-xylene	500	ppm	Alpha-pinene	*500	ppm
o-xylene	500	ppm	NOx	3000	ppm
p-xylene	500	ppm	THC	1000	ppm
1,2,3-trimethylbenzene	500	ppm	TMB	1500	ppm
1,2,4-trimethylbenzene	500	ppm	* = Generic libraries used		

3.3.1 Gas Analysis Description:

The sample gas transport system to the gas analysers is shown schematically in Fig. 3-8. A heated 180°C sample line was used to transport the gases from the exhaust to a 180°C heated pump (3 lpm) and filter and then there was another heated line to transport the gases to the 180°C heated Gaset FTIR. The FTIR

gas analyser has been calibrated by the manufacturers for 51 gaseous species and has been used for many research studies on toxicity at the University of Leeds [66, 73, 88, 169, 176, 180]. The raw gas sample prevented any post oxidation of species by dilution of the gases with ambient air, as the gases were entrained into the cone calorimeter diluted flow metering section or the 5 m³ compartment. Also, it prevented any losses of condensable gases that would occur if the exhaust was simply thermally cooled [181]. The gas sample from the FTIR outlet was transported via a PTFE tube to a refrigeration cooler of about 2°C and a silica gel column for the removal of water vapour before entering a paramagnetic oxygen analyser and then was discharged through the cone calorimeter discharge duct.

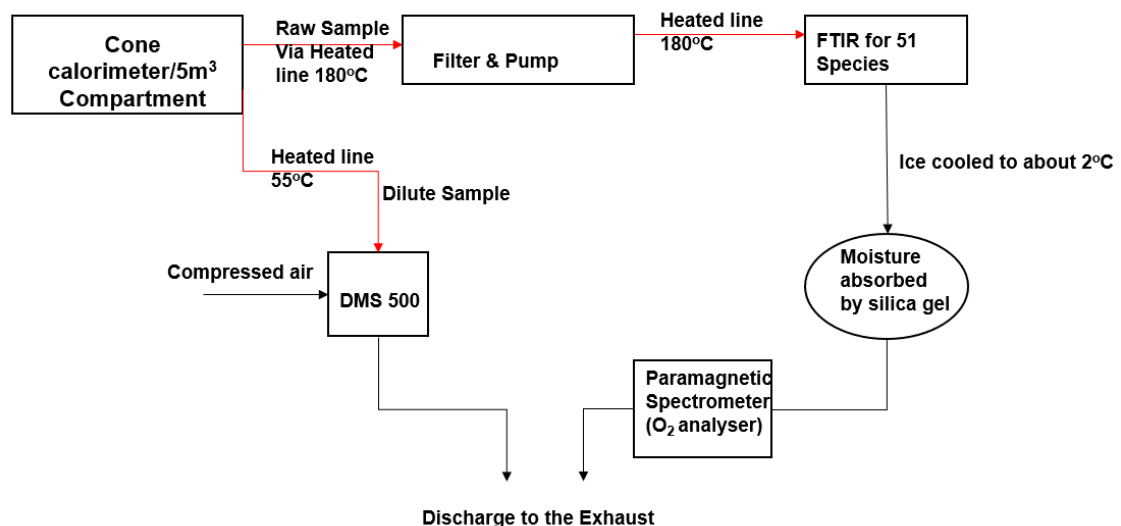


Figure 3-8 Schematic of the Gas analysers

3.3.2 Paramagnetic Oxygen Analyser

The paramagnetic oxygen analyser comprises the following components; a magnetic field, diamagnetic substance (nitrogen), turning dumbbell (having two glass spheres filled with nitrogen and a mirror fixed in the middle of the rod), light source and light receiver (photocell). This work used it to analyse oxygen. A magnetic field is created by the pair of magnets across the gas cell where the sample is introduced. The dumbbell remains static when oxygen is not available in the gas cell as the nitrogen (diamagnetic substance) inside the spherical glass

on both ends of the dumbbell is going to be held in the middle by the magnetic field whereby the photocell detects that based on the light reflected in the mirror. Because oxygen is magnetic, once it is introduced to a magnetic field, its dipole will align with the field and strengthen it. The concentration of oxygen is presented as a percentage with a resolution of 0.01%. The detector measurements are taken from dry analysis, as such they need to be converted to wet analysis if they are to be used for comparison.

3.4 The DMS 500 Particle Size Analyser

The DMS500 manufactured by CAMBUSTION is a real time nanoparticle size spectrometer and this was used for the analysis of particulates. The DMS500 uses a classifier column which operates at 0.25 bar absolute with an external vacuum pump connected to the DMS 500 via a reinforced hose. Another hose is connected from the pump to the extractor to get rid of the exhaust from the pump. A dry, oil free compressed air is fed to the analyser from its rear, via a PTFE ¼ inch tube directly from the main supply set at 2 bar to drop the dew point of exhaust gas. The metered compressed air flows out through a 6 mm push-fit connector at the front of the analyser and into the primary diluter for dilution. The sample inlet located on the front of the instrument was connected to a heated sample line of 5 m and a primary diluter. The heated sample line includes a primary or 1st diluter using compressed air metered by the DMS500 to provide a controlled dilution ratio and a heated tube to transport the sample to the instrument. This was mounted and clamped on the front door of the DMS500, and the electrical connector, sample pipe and the dilution air pipe connected on the front of the instrument. The use of the heated line was to allow dilution of the sample gas which serves to lower the dew point of the air so that condensation does not occur within the instrument. The remote cyclone assembly in which the dilution occurs is heated to minimise hydrocarbon condensation and water condensation at cold start. The heated line then transports the diluted gas to the DMS500. Particles greater than 1000 nm (> 1000 nm) are removed by a cyclone separator to reduce the need for cleaning. Two optional stages of software controlled dilution (1st dilution ratio and 2nd dilution ratio) are applied prior to the sample gas passing through a corona discharge charger and into a classifier

column. It uses a unipolar corona discharge to place a prescribed charge on each particle proportional to its surface area. After the aerosol is charged, it moves into a strong radial electrical field inside a classifier column. This field causes the charged particles to flow via a particle-free sheath flow which is a uniform, cylindrical laminar column of air designed to carry the charged particles to the electrometer detectors [147].

Depending on the electrical mobility, particles are then detected at different distances down the column. The outputs from the 22 electrometer rings are then processed in real time to provide spectral data in 38 or 48 size classes together with other desired parameters (see Fig. 3-9). This piece of equipment was connected to the dilute sampling point of the cone calorimeter and the 5 m³ fire rig test facility to get the samples of particulates that were analysed via a heated sample line of about 55°C.

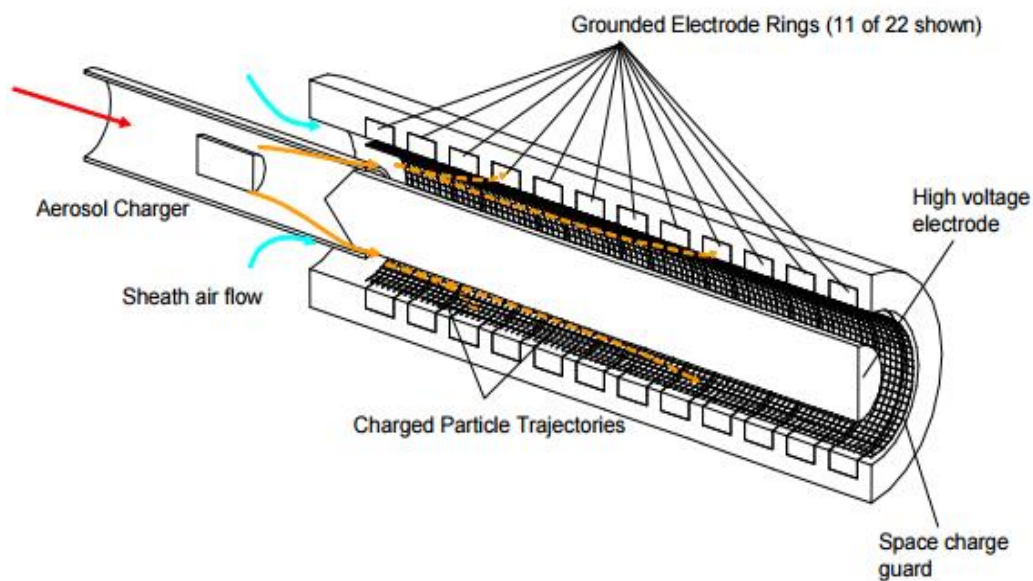


Figure 3-9 DMS500 Classifier extracted from [147]



Figure 3-10 The DMS500 Particle size analyser

3.5 Soot Sampling Equipment (Smoke Meter)

The Richard Oliver heated filter paper soot sample system was used for gravimetric measurement of particulates. The system uses a pump to take specified volumes of exhaust products at controlled flow rates through a filter paper in a heated oven. The particulate mass and concentration was obtained through this process. The particulate obtained on the filter can then be further analysed to get the chemical composition of the particulates which makes it possible for the identification of polycyclic aromatic hydrocarbons (PAHs) and other cancer causing compounds. A single-hole 1/4 " sample probe was placed inside the chimney to collect the raw soot from the smoke meter via 150°C heated sample line. The sample then gets to the oven, where a temperature of 47°C is maintained to avoid water vapour condensation and loss of toxic species. The soot sample was collected on a filter paper placed in the filter paper sample holder at a flow rate of 10 litres/min at intervals. A burst filter paper indicates that too much soot was collected and the sample time was reduced. Prior to the test, filter papers were placed in a desiccator to remove any moisture. Filter papers were weighed before and after the test.

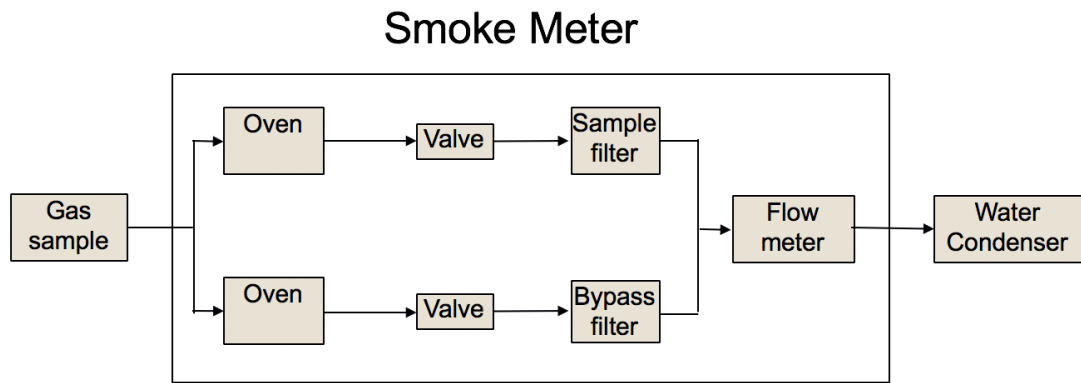


Figure 3-11 The schematic of the Smoke Meter

3.6 Analysis Techniques

3.6.1 Heat Release Rate Calculation

The heat release rate HRR was calculated using two methods; the oxygen consumption calorimetry using the air mass flow rate and the oxygen concentration and the mass loss rate based HRR using the calorific value of the sample. Oxygen consumption calorimetry works based on a constant amount of heat released per kg of oxygen consumed for the complete combustion of liquid/solid fuels. This constant was found by Huggett [95] to be 13.1 kJ/g of oxygen with an accuracy of $\pm 5\%$. The HRR equation is given below [182].

$$q = E(m_a Y^a_{O_2} - \dot{m}_e Y^e_{O_2})$$

3-2

Where \dot{q} - Heat release rate, kW; E - Heat release per mass unit of oxygen consumed, 13.1kJ/g; \dot{m}_a - Mass flow rate of the inlet air, \dot{m}_e - Mass flow rate of the exhaust gases, $Y^a_{O_2}$ - Mass fraction of the combustion air, 0.232 g/g air; $Y^e_{O_2}$ - Mass fraction of the exhaust gases

The relationship between the heat release rate and mass loss rate is given by:

$$\text{HRR} = \Delta h_c \times \text{MLR}$$

3-3

where

Δh_c = net heat of combustion (kJ/g)

3.6.2 Air to Fuel Ratio and Equivalence Ratio ϕ

The air-to-fuel ratio was calculated using Chan's equation [93] by carbon balance as shown in Eqn. 3-4. Another method of obtaining the air-to-fuel ratio is on mass basis (Eqn. 2-3).

$$A/F_{Chan} = \left(\frac{1}{12.011\alpha + 1.008\beta + 15.999\gamma + 14.007\delta} \right) \times \left[\frac{\alpha A_1 - \gamma + \left(\frac{\beta K(CO_2)}{2A_2} \right) - \left(\frac{\alpha A_3 A_4}{2A_2} \right)}{2.0038 + A_5 - \left(\frac{A_5 K(CO_2)}{A_2} \right) + \left(\frac{0.0019 A_3 A_4}{2A_2} \right) - 0.0019 A_1} \right]$$

3-4

Where:

$$K = \exp \left[2.743 - \frac{1.761}{0.001 T_{eq}} - \frac{1.611}{(0.001 T_{eq})^2} + \frac{0.2083}{(0.001 T_{eq})^3} \right]$$

T_{eq} = Equilibrium temperature

$$A_1 = \frac{[CO] + 2[CO_2] + 2[O_2] + [NO] + 2[NO_2]}{[CO] + [CO_2] + [HC]}$$

$$A_2 = K[CO_2] + [CO]$$

$$A_3 = \frac{K[CO_2]}{[CO]([CO] + [CO_2] + [HC])}$$

$$A_4 = x[HC][CO]$$

$$A_5 = 4.7755 \frac{P_v}{P_A - P_v}$$

X = Ratio of Elemental Hydrogen to Elemental Carbon

[] = Volumetric concentrations in %

P_A = Atmospheric Pressure (atm)

P_v = Pressure of water vapour (atm)

The equivalence ratio was calculated thus:

$$\text{Equivalence ratio, } \phi = \frac{F/A_{actual}}{F/A_{stoichiometric}} \quad 3-5$$

Or

$$\phi = \frac{A/F_{Stoichiometric}}{A/F_{Actual}}$$

Where:

F/A_{actual} = fuel to the air ratio by mass for the actual combustion

$F/A_{stoichiometric}$ = fuel to the air ratio by mass for the complete combustion

3.6.3 Toxic Gas Yields

The toxic gas yields were calculated using the Eqn. 3-6 from the gases measured by the FTIR.

$$Y_i = C_{g_i} \times \frac{MW_i}{MW_{air}} \times \left(1 + \frac{A}{F}\right) \quad (\text{gi/gf}) \quad 3-6$$

where, C_{g_i} is the *concentration* of the toxic gas specie (which if measured in ppm or %, should be multiplied by 10^{-6} or 10^{-2} respectively), and

$\frac{MW_i}{MW_{air}}$ is ratio of molecular weight of the toxic species to the molecular weight of air.

3.6.4 Combustion Efficiency

In an under ventilated combustion, the insufficient supply of oxygen to the burning process leads to an incomplete combustion, with the release of CO_2 , CO and a substantial amount of unburnt hydrocarbons, often not considered in the estimation of the combustion efficiency [85]. These products of incomplete combustion result in a low combustion efficiency and therefore it is better to take in account the unburnt hydrocarbon emissions when estimating the combustion efficiency. The combustion efficiency was used to correct the heat release rates calculated by mass loss rate for inefficiencies, where it is assumed that the combustion is complete and all the energy is released.

The combustion inefficiency was calculated using Eqn. 3-7 below, taking into consideration emissions of unburnt hydrocarbon, CO, and soot.

$$1 - \eta = \left(Y_{CO} \times \frac{CV_{CO}}{CV_{Fuel}}\right) + \left(Y_{UHC} \times \frac{CV_{UHC}}{CV_{Fuel}}\right) + \left(Y_{Soot} \times \frac{CV_{Soot}}{CV_{Fuel}}\right) \quad 3-7$$

Where, Y is the yield of CO, UHC or soot (g/g),

CV_i is the calorific value of CO, UHC or soot (MJ/kg),

The CV of unburnt fuel was taken to be same as the fuel.

3.6.5 Particle Size Calculation

The particle size was measured by DMS 500 as mentioned above. The number concentration was obtained and was corrected for dilution using Eqn. 3-8. This was converted to particulate mass in g/m^3 using Eqn. 3-9, assuming the particles to be spherical in shape and having a density of 1000 kg/m^3 . This enabled the yield to be obtained using Eqn. 3-10.

$$\text{Dilution Ratio: } \frac{MFR \text{ g/s}}{MLR + MFR_{\text{inlet air}} \text{ g/s}} \quad 3-8$$

Where MFR is the mass flow rate of the exhaust gas set as 24 l/s (29 g/s) for the cone calorimeter.

MLR is the mass loss rate of the fuel and $MFR_{\text{inlet air}}$ is the mass flow rate of the inlet air in g/s.

Dilution ratio for the 5 m^3 compartment was obtained by performing two separate tests with different sampling points (Dilute and raw sampling). The ratio of the nitrogen oxides obtained in both tests was used to obtain the dilution ratio. A second method used was the ratio of their equivalence ratio.

$$\text{Particulate Mass: } P\text{Mass} = V \times D \times N \quad 3-9$$

Where PMass is the Particulate Mass in g/m^3

V is the volume of a sphere, D is the density of water droplet (1000 kg/m^3) and N is the number concentration (Number/cm^3)

$$\text{Particulate Yield or Emission Index: } EI = [P\text{Mass}/1180](1 + A/F) \quad 3-10$$

Where 1180 is the ambient density of the sample gas which is taken to be that of air (g/m^3)

A/F is the Air-to-Fuel ratio of the sample

3.6.6 Soot Deposition

To obtain the amount of soot deposited in the 5 m^3 compartment, samples were collected from the glass window as shown in Fig. 3-12. Samples were taken from the top and bottom of the window. The sizes of the sample area and the weight of the sample were measured and the deposition mass per m^2 was obtained by dividing the soot mass by the sample area. It was assumed that the deposited

soot was distributed uniformly across the compartment, hence the estimation of total mass of soot deposition was based on that for each experiment.

$$M_{Soot\ Deposition} = S \times \frac{m}{A} \quad (g) \quad 3-11$$

$$Y_{Soot\ Deposition} = \frac{M_{Soot\ Deposition}}{M_{Fuel}} \quad (g/g) \quad 3-12$$

where, S is the surface area of deposited soot (m^2),

m is the mass of sample collected (g) and,

A is the area of sample collected (m^2),

M_{Fuel} is the mass of fuel (g).



Figure 3-12 The collection of soot deposits

3.6.7 Toxicity Assessment

The toxicity of the various materials tested was assessed based on two criteria of fire toxicity assessment; lethality based on LC_{50} and impairment of escape based on $COSHH_{15min}$. Some of the threshold limits are shown in Table 3-4. The method for obtaining the total toxicity N is described in Chapter 2. The equations below were used to obtain the total toxicity:

$$N - LC_{50} = \frac{[CO]}{LC_{50,CO}} + \frac{[HCl]}{LC_{50,HCl}} + \frac{[HBr]}{LC_{50,HBr}} + \frac{[HF]}{LC_{50,HF}} + \frac{[SO_2]}{LC_{50,SO_2}} + \frac{[NO_2]}{LC_{50,NO_2}} + \frac{[Acrolein]}{LC_{50,Acrolein}} + \frac{[Formaldehyde]}{LC_{50,Formaldehyde}} + \sum \frac{Species[i]}{LC_{50,Species\ i}} \quad 3-13$$

Where;

$LC_{50, \text{Species } i}$ = the lethal threshold concentration of toxic gases provided in [127]

i = the measured concentration of the gas by FTIR

$$N - COSHH_{15} = \frac{[CO]}{COSHH_{15,CO}} + \frac{[NO]}{COSHH_{15,NO}} + \frac{[HBr]}{COSHH_{15,HBr}} + \frac{[HF]}{COSHH_{15,HF}} + \frac{[SO_2]}{COSHH_{15,SO_2}} + \frac{[NO_2]}{COSHH_{15,NO_2}} + \frac{[Acrolein]}{COSHH_{15,Acrolein}} + \frac{[Formaldehyde]}{COSHH_{15,Formaldehyde}} + \sum \frac{Species[i]}{LC_{50,Species i}} \quad 3-14$$

Where;

$COSHH_{15, \text{Species } i}$ = the threshold concentration of toxic gases that cause impairment of escape [168]

$[i]$ = the measured concentration of the gas by FTIR

Table 3-4 Some Toxic Threshold Limits and their Comparison

Gases	Chemical Formula	LC ₅₀	AEGL	COSHH	AEGL	LC ₅₀ /AEGL2	LC ₅₀ /COSHH ₁₅
			30 min.		10 min.		
			3	15 Min.	2		
Carbon monoxide	CO	3,000	600	200	420	7	15
Hydrogen cyanide	HCN	135	21	10	17	8	13.5
Hydrogen fluoride	HF		62	3	95		
Hydrogen chloride	HCl	3,700	210	5	100	37	740
Hydrogen bromide	HBr		250	3	250		
Nitrogen dioxide	NO ₂	350	25	5	20	17.5	70
Sulfur dioxide	SO ₂	500	30	5	0.75	667	100
Acrolein	C ₃ H ₅ O	135	2.5	0.3	0.44	307	450
Formaldehyde	CH ₂ O	250	70	2	14	18	125
Benzene	C ₆ H ₆	10,000	5600	3	2000	5	3333

3.7 Research Materials







Wood as a building material possesses a lot of environmental benefits. It is not only the most widely used building material but also one with characteristics that make it appropriate for a wide range of applications. One of the greatest features

of wood is that it is renewable. Over the past decade, the public has become aware of the concept of green building¹ because of the potential environmental benefits of this alternative to conventional construction. Green building focuses more on reducing a building's energy consumption (e.g. better insulation, more efficient appliances and heating, ventilation, and air-conditioning systems) and reducing negative human health impacts (such as controlled ventilation and humidity to reduce mould growth). However, choosing building materials that exhibit positive environmental attributes is also something to take into account. In an attempt to go green, various wood-based composites are manufactured in the timber industry ranging from fibreboard to laminated beams. These composites are used for a number of non-structural and structural applications in product lines ranging from panels for interior covering purposes to panels for exterior uses and in furniture and support structures in buildings (such as plywood, oriented strand board, particleboard, fibre board, structural composite lumber, doors, windows and frames, and factory-laminated wood products). Unfortunately, wood-based composites are manufactured with adhesives and other additives which contribute to the toxic gases released in the event of fire. Wood might not necessarily be the cause of fire but it will contribute to the fire load and the toxicity. It will be shown later that the glued surface and the manufacturing processes introduce nitrogen compounds into the fuel and this produced HCN in the toxic gases.

Wood is one of the most common fire material with about 50% of all fires involving wood as main fuel. In residential buildings, almost 80% of furniture is wood. For this reason, a range of wood types used in construction and furniture were investigated in the present research. Pool fires were also investigated relevant to industrial scenarios of oil spillages leading to a pool fire. These materials investigated include pine wood (PWS), scaffolding board (SB), oriented strand board (OSB), chipboard faced with melamine (CFM), medium density fibreboard (MDF), block board wood (BBW), plywood, diesel, lubricating oil and olive oil. Pine wood crib of three different sizes, small, medium and big were built and used as the fire load for this research in the 5m³ compartment. Materials were sourced commercially from building materials suppliers. Table 3-5 and

Fig.3-13 show some of the test materials used in this work. Table 3-7 shows the properties of the wood crib built for this work.

Table 3-5 Wood Samples for the Cone Calorimeter Tests

 <p>Oriented strand board (OSB)</p>	 <p>Chipboard faced with melamine (CFM)</p>
 <p>Medium density fibreboard (MDF)</p>	 <p>Plywood B (PW B)</p>
 <p>Plywood A (PW A)</p>	 <p>Pine wood sticks (PWS)</p>



Block board wood (BBW)



Scaffolding board (SB)



Light plywood (LPW)



Dark plywood (DPW)

Table 3-6 Measured Properties of Wood Test Materials

Sample	Volatile Matter (wt. %) (Daf)	Fixed Carbon (wt. %) (Daf)	Carbon (wt.%) (Daf)	Hydrogen (wt. %) (Daf)	Nitrogen (wt. %) (Daf)	Sulphur (wt. %) (Daf)	Oxygen (wt. %) (Daf)	Stoichiometric A/F by Carbon balance	Gross Calorific Value (MJ/kg)	Moisture (as received) (%)	Ash (as received) (%)
Pine Wood Sticks (PWS)	86.54	13.46	53.95	6.79	0.11	0	39.15	5.89	18.9	6.18	2.27
Block Board Wood (BBW)	83.92	16.08	51.13	6.56	1.02	0	41.29	5.42	19.1	6.22	2.18
Plywood A (PW A)	79.47	20.53	52.00	6.56	0.38	0	41.06	5.35	18.8	6.68	3.42
Chipboard Faced with Melamine (CFM)	82.87	17.13	49.11	6.50	4.39	0	40.01	5.17	18.7	4.21	4.14
Dark Plywood (DPW)	84.23	15.77	45.88	5.94	1.74	0	46.45	4.50	18.6	4.58	3.27
Light Plywood (LPW)	82.64	17.36	50.03	6.66	3.51	0	39.80	5.35	18.4	5.02	3.30
Medium Density	83.19	16.81	50.61	6.80	5.04	0	37.55	5.63	19.1	2.73	4.45

Fibreboard (MDF)											
Oriented Strand Board (OSB)	84.27	15.73	50.32	6.36	0.41	0	42.91	5.38	19.5	6.18	0.74
Plywood B (PW B)	80.81	19.19	47.39	6.22	6.43	0	39.97	4.83	18.3	6.91	1.68
Scaffolding Board (SB)	86.89	13.11	52.99	7.46	0.08	0	39.47	5.82	19.1	5.62	4.34

Table 3-7 Other Properties of Wood

Sample	Mass (g)	Thickness (mm)	Density (kg/m³)	Number of Layers
Pine Wood Sticks (PWS)	127.4	21	610	Not applicable
Block Board Wood (BBW)	135.3	18	752	Not applicable
Plywood A (PW A)	108.9	20	545	7
Chipboard Faced with Melamine (CFM)	94.9	15	633	Not applicable
Dark Plywood (DPW)	66.8	11	607	7
Light Plywood (LPW)	61.4	11	558	7
Medium Density Fibreboard (MDF)	103.3	18	574	Not applicable
Oriented Strand Board (OSB)	110.3	18	613	Not applicable
Plywood B (PW B)	97.8	18	543	11
Scaffolding Board (SB)	139.6	35	399	Not applicable

SMALL CRIB 20 x 20 x 200 mm



20 x 20 x 400 mm

MEDIUM CRIB



BIG CRIB 44 x 44 x 400 mm



Figure 3-13 Pine Wood Cribs

Table 3-8 Pine wood Crib properties

Wood Crib	Pine Wood Stick Properties			Wood Crib Dimension						Energy in the Wood Crib (MJ)	Fire Loading (MJ/m ²)	Fire Loading (MJ/m ³)
	(W X D X L) in mm	Gross Calorific Value (MJ/kg)	CHO Composition	Gap Between Stick (mm)	Layer of Wood Stick	Number of sticks per layer	Total No. of Sticks	Height (mm)	Weight (g)			
Small Crib 1	20 x 20 x 200 (Stick 1)	20.0121	CH _{1.51} O _{0.54}	100	12	3 (2 stick for the top bottom layer)	35	240	1802.1	36.1	8.9	7.2
Small Crib 2	20 x 20 x 200 (Stick 1)	20.0121	CH _{1.51} O _{0.54}	100	12	3 (2 stick for the top bottom layer)	35	240	1761.6	35.3	8.7	7.1
Medium Crib 1	20 x 20 x 400 (Stick 2)	18.9571	CH _{1.63} O _{0.78}	100	13	5 (2 stick for the top bottom layer)	62	260	6220	117.9	29.2	23.6
Medium Crib 2	20 x 20 x 400 (Stick 2)	18.9571	CH _{1.63} O _{0.78}	100	13	5 (2 stick for the top bottom layer)	62	260	5900	111.8	27.7	22.4
Big Crib	44 x 44 x 400 (Stick 3)	18.9571	CH _{1.63} O _{0.78}	73	6	4 (2 stick for the top bottom layer)	24	497	14211	269.4	66.8	53.9
	63 x 38 x 400 (Stick 4)	18.9571	CH _{1.63} O _{0.79}	80	4	4 (2 stick for the top most layer)	12					

Liquid Pool:

The materials used for the pool fire experiments were diesel, lubricating oil and olive oil. The diesel and lubricating oil were sourced from a local BP garage in Leeds, while the olive oil was sourced from a local store in Leeds. The diesel used for the experiments was the same batch of diesel and thus had the same properties. The measured properties of the liquid pool obtained using the CHNS analyser are presented in Table 3-9.

Table 3-9 Measured Properties of Liquid Pool

Sample	Carbon (%)	Hydrogen (%)	Nitrogen (%)	Sulphur (%)	Oxygen (%)	Gross Calorific Value (MJ/kg)
Diesel	75.44	10.44	0.11	0	14.01	42.8
Lubricating Oil	84.73	14.82	0.26	0	0.19	43.0
Olive oil	77.20	12.16	0.22	0	10.43	41.7

3.8 General Experimental Procedure for the Cone Calorimeter

1. Wood samples were placed in a sample holder or sample tray in the case of pool fire and weighed before the start of the test.
2. The analysers and FTIR were cleaned and calibrated before the start of each test. The cone heater was then switched on and temperature set to the desired heat flux already determined by the heat flux meter.
3. When the temperature for the desired heat flux was reached, the desired controlled airflow into the compartment was regulated by a flow meter (in the case of the controlled atmosphere cone calorimeter). For freely ventilated fires, the air was natural from the laboratory environment.
4. The sample holder is then mounted on the load cell with a 25 mm gap allowance between the surface of the sample and the cone heater.
5. Door of the compartment was closed (for controlled atmosphere cone calorimeter), shutters were closed and the heating of the sample begins.

6. The load cell measures the changes in mass as the experiment progresses for the duration of the test.
7. After the test, the sample holder or tray is removed and allowed to cool. Results output in Excel were obtained and analysed.

3.9 General Experimental Procedure for the 5m³ Compartment

1. The analysers and FTIR were cleaned and calibrated before the start of each test and connections made.
2. The samples, pine wood crib or diesel pool (in a sample tray of different size) were placed on the load cell in the centre of the compartment.
3. The samples were then ignited using a blow torch (for the diesel) and an accelerant and blow torch for the pine wood crib.
4. Door of the compartment was closed and the fire was observed through the door and test was allowed to run until flameout.
5. The load cell measures the changes in mass as the experiment progresses for the duration of the test.
6. After the test, the debris or tray is removed and allowed to cool. Results output in Excel were obtained and analysed.

Chapter 4 Freely Ventilated Test Results on the Cone Calorimeter

This Chapter presents analyses and discusses the results from the cone calorimeter freely ventilated experiments of different wood samples. The experimental setup and fuel characteristics for each experiment have been presented in detail in Chapter 3. The wood samples were grouped into 3 and analyses are presented in sections based on;

- Natural Wood (Pine wood and Scaffolding Board)
- Processed Wood (Chipboard faced with Melamine (CFM), OSB and MDF)
- Plywood (4 different plywoods)

The analyses focused on the toxic gas and particulate emission measurements that were taken from these tests. Additionally heat release rate values are estimated using mass burning rates and calorific value concept.

4.1 General Burning Characteristics

Wood and other cellulosic materials are widely used in the construction of homes and other buildings. Wood-based composites such as plywood, MDF, block board and laminated veneer are used in modern buildings for surface finishing, furniture, flooring, scaffolding, ceilings, shelves and partitioning. Wood being the most dominant fire load in homes and other buildings, accounts for approximately 70% of CO₂ emissions and 65% of CO emissions [15]. Toxic effluents released from fires reduce visibility and contain irritant gases that impair vision and cause respiratory problems. Irritant gases may impair escape, increasing the risk of a lethal exposure to asphyxiant gases, leading to the death of those managing to escape. Despite the dangers of toxic fire effluents, the knowledge has in general not been adequately captured in the fire community or in standards or codes. There are no toxic gas requirements to be met for fires in any material used in buildings except in specific applications such as passenger vessels. Only light obscuration by smoke in standard fire tests is required for building materials and these smoke production regulations have no requirements to measure the composition of the smoke either for soot particle size or toxic gases. It is therefore important to understand the burning characteristics of the

wood samples to gain more understanding of the toxic emissions from these samples.

4.1.1 Natural Wood:

The mass loss rate, equivalence ratio and the heat release rates for pine wood and scaffolding board are presented in this section.

4.1.1.1 Mass Loss, Equivalence Ratio and Heat Release Rates (HRR)

Pine wood and scaffolding board freely ventilated fires are compared at 35 kW/m² cone radiant heating and both had a gas sample for toxic gas and oxygen analysis taken as a raw heated mean gas sample from the chimney fitted on the cone exit. Figure 4-1 shows that the ignition delay was much shorter for the scaffolding board (40 s) compared to the pine wood (192 s). Both samples burned lean throughout the combustion with the pine wood having an equivalence ratio of 0.35 and the scaffolding board 0.32 at the steady state burning phase as shown in Fig. 4-1 (b). Figure 4-1 (a) shows the mass loss rate for the two tests. Pine wood showed a mass loss rate at steady state of 0.07 g/s, with a much slower burn rate during the char burn phase from 1200 s while the scaffolding board burned for a longer period of time, with a slower burn rate of 0.04 g/s at steady state. This difference in burn time is as a result of the thickness of the wood, with scaffolding board having a thickness of 35 mm and pine wood having a thickness of 21 mm. Two peaks were observed in the mass burn rate. The 1st peak was as a result of the pyrolysis of gases and the initial combustion forming a thin layer on the surface of the sample and increasing the mass loss with time until its maximum value was reached. The release of the pyrolysis products was blocked as a result of a thick char layer formed, thereby decreasing the mass loss rate. The mass loss rate continued decreasing until it remained constant for a period of time at the steady state combustion phase. When the heat got deeper into the sample, the mass loss rate increased again as a result of the release of more combustion products or depletion of the sample and hence the 2nd peak. The two peaks in the mass burn rates will be shown to be associated with peaks in toxic gas emissions and in particulate emissions.

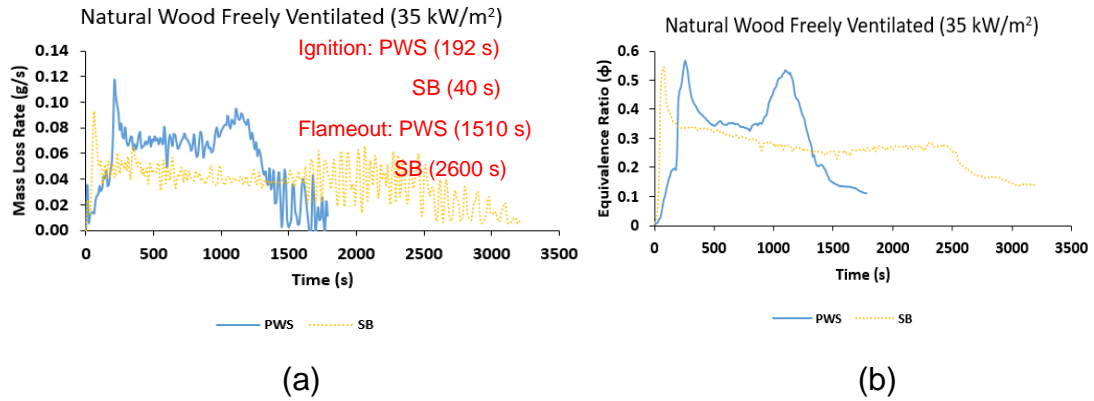


Figure 4-1 Mass loss rate (a) and Equivalence Ratio (b)

The oxygen mass consumption based heat release rate (HRR), shown in Fig. 4-2 (a), was computed from cone outlet chimney oxygen analysis, downstream of the FTIR while the heat release rate (HRR) based on the mass loss rate and the calorific value (CV) of the wood is shown in Fig. 4-2 (b). This evaluation of the HRR based on the mass loss rate effectively assumes complete combustion and release of all the available energy. Both tests showed that the HRR peaked immediately after ignition and remained steady at 130 kW/m² (Pine Wood), and about 80 kW/m² (Scaffolding Board). This was due to the low burn rate and much leaner burning that occurred during the scaffolding board combustion. The heat release rate based on mass loss rate was higher than the one based on the oxygen consumption during the initial phase of the combustion, where the yields of CO and unburnt total hydrocarbon were high. Ideally if the burning of biomass fuel is complete, HRR by mass loss rate should be equal to HRR by oxygen consumption which was what happened during the steady state combustion where the combustion efficiency was almost 100 %.

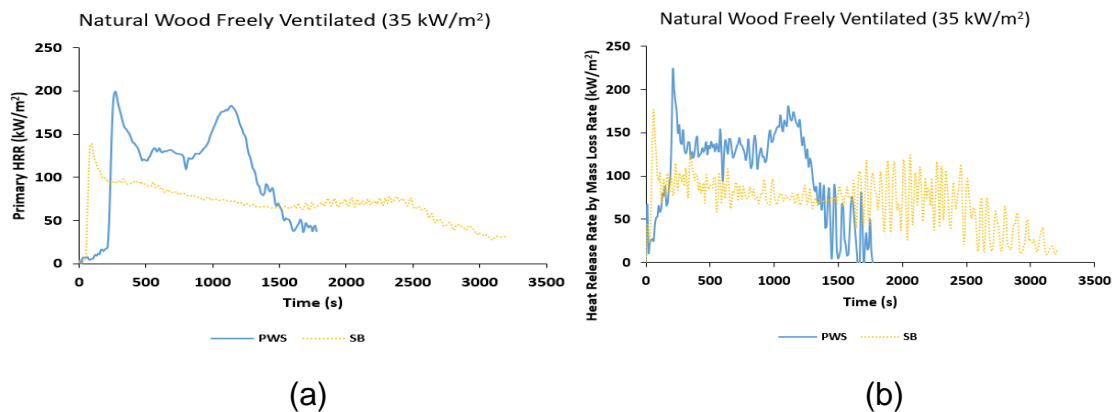


Figure 4-2 Primary HRR (a) and HRR based on Mass Loss Rate (b)

4.1.2 Processed Wood:

Processed wood such as plywood, MDF, OSB and laminated veneer are used in modern buildings for surface finishing, furniture, flooring, scaffolding, ceilings, shelves and partitioning. These processed woods are manufactured with adhesives and other additives which contribute to the toxic gases released in the event of fire. The burning characteristics of 3 different types of processed wood (OSB, MDF and chipboard faced with Melamine (CFM)) are presented in this section.

4.1.2.1 Mass Loss, Equivalence Ratio and Heat Release Rates (HRR)

The results presented are based on the raw gases sampled directly from the chimney. Figure 4-3 (a) shows that the ignition delay was much shorter for the MDF fire, due to the richer mixtures during the delay period, as shown in Fig. 4-3 (b). The substrates covered by melamine prolonged the ignition delay for the chipboard faced with melamine. All tests showed a mass loss rate at steady state of 0.06 g/s with a much slower burn rate during the char burn phase from around 1100 s. Carbon balance equivalence ratios showed that rich mixtures occurred in some of the tests, indicating that some features of confinement were found in the raw gas analysis. These rich mixtures produced high concentrations of toxic gases as will be shown in section 4.2.2.

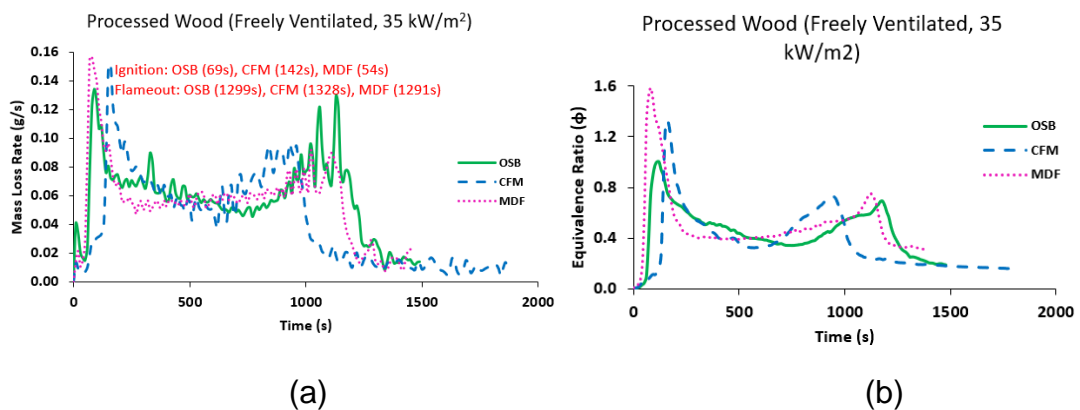


Figure 4-3 Mass loss rate (a) and Equivalence Ratio (b)

The 3 samples had similar peak HRR (180-200 kW/m²), but the time variation of HRR was different with the chipboard faced with melamine having a slower growth of the fire to peak HRR. The substrates covered by melamine or maple,

organic improvers, wax, and resin appear to have a chemical flame retardation effect that delayed the initial combustion.

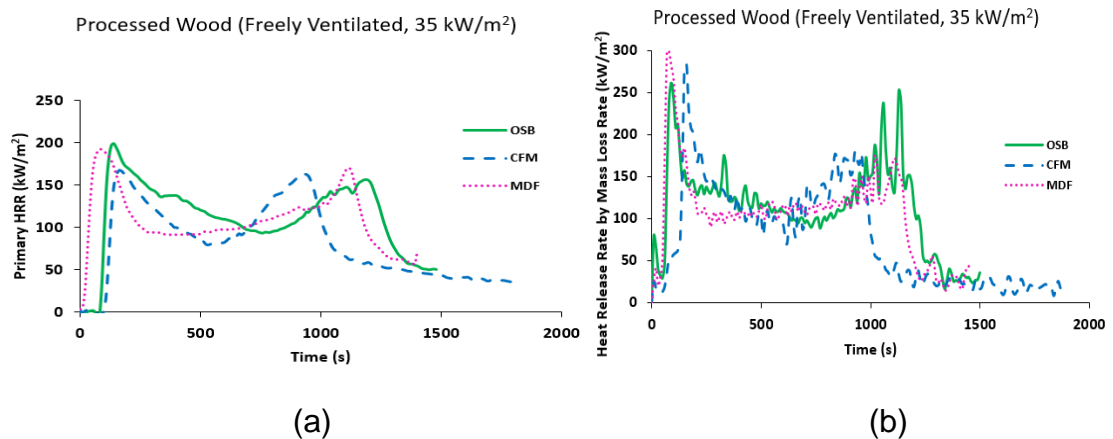


Figure 4-4 Primary HRR (a) and HRR based on Mass Loss Rate

4.1.3 Plywood:

Plywood can be defined as a panel product built up wholly or primarily of sheets of veneer called plies [42]. Its construction is with an odd number of layers with the grain direction of adjacent layers oriented perpendicular to one another. Plywood panels are used for different purposes, such as; construction sheathing, furniture, and cabinet panels. Four different types of plywood were investigated for toxic emissions.

4.1.3.1 Mass Loss, Equivalence Ratio and Heat Release Rates (HRR)

Each plywood sample was exposed to the conical heater of the cone calorimeter radiating at 35 kW/m² and the ignition delay for the 4 samples was 54 s (Plywood A), 53 s (Plywood B), 73 s (Dark Plywood) and 49 s (Light Plywood), respectively. The mass loss rate at steady state for all the samples was about 0.06 g/s, with a much slower burn rate during the char burning phase. The equivalence ratios from carbon balance showed that rich mixtures occurred in some of the tests, indicating that some features of confinement were found in the raw gas analysis. Most of the samples had rich mixtures at the initial stage of the combustion except for Plywood B which burnt lean at the initial stage until the second burning phase. All the Plywoods had initial rich mixtures and a second burning phase. These rich mixtures produced high concentrations of toxic gases.

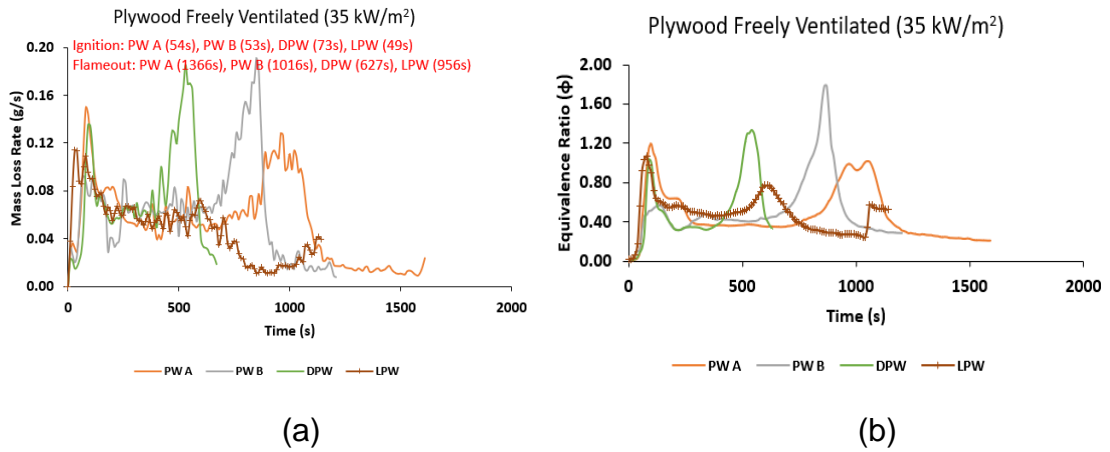


Figure 4-5 Mass Loss Rate (a) and Equivalence Ratio (b)

The 4 samples had different peak HRR, but similar steady state HRR. The time variation of HRR was different with the Plywood B having a slower growth of the fire. The difference in the HRR was as a result of the different ignition times and the composition of the different plywoods as each plywood had a different composition. The steady state heat release rate by oxygen consumption and mass loss rate was similar for all plywood but the peak heat release rates by mass loss rate was higher (170-350 kW/m²) than that obtained based on oxygen consumption (100-200 kW/m²). The peak heat release rates were found to correspond to the rich burning phases of the combustion.

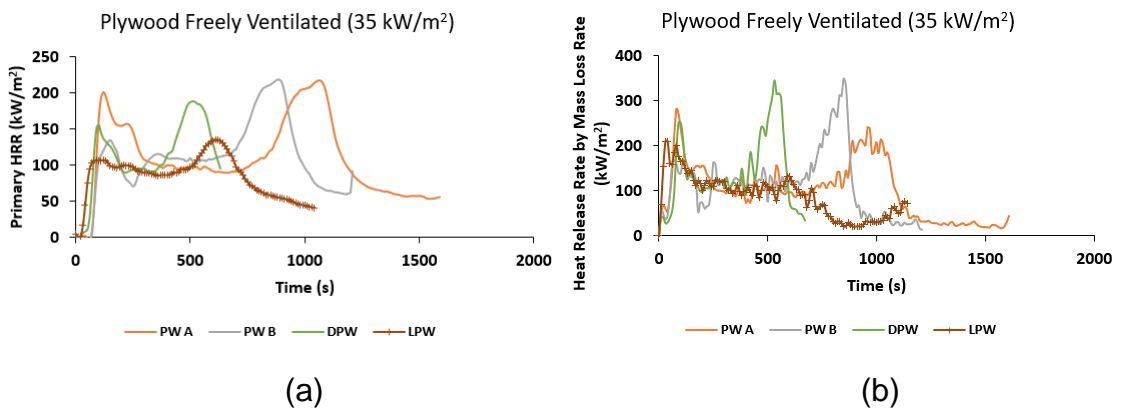


Figure 4-6 Primary HRR (a) and HRR based on Mass Loss Rate (b)

4.2 Toxicity of Different Wood Samples

Inhalation of toxic smoke from fires is responsible for over 60% of fire deaths as described in chapter 1 and its effect can be lethal [6, 167, 183, 184]. This lethal

effect is normally measured by the LC₅₀ toxic limits [6, 167, 183, 184] for 50% deaths after 30 minutes exposure. However, survivors of fires often describe toxic gases as acidic and/or irritant gases and these slow the movement of people eventually leading to their death [6, 167, 183, 184] through the impairment of escape. Purser [183] has shown that the main toxic products in most fires are CO, HCN and irritant or acidic gases and the concentration of each depends on the thermal decomposition of the fire load, which also depends on the temperature and oxygen supply. The present work used heated Fourier Transform Infra-Red spectroscopy (FTIR) specifically to investigate the toxic gases (asphyxiant and irritant/acidic gases) in wood fires. There are several methods of assessing the toxicity of fire products. The most common is the LC₅₀ 30 min exposure concentration which aims at predicting the concentrations at which 50% of the people will die in the fire if exposed to the gas concentration for 30 minutes [6]. The statutory law in Europe on occupational exposure limits is COSHH [168], equivalent to the US short term exposure limits. The COSHH_{15 min} toxic gas concentration represents a safe condition for 15 minutes where there will be no impairment of escape. The Acute Exposure Guideline Levels (AEGL) [6] are the USA guidelines having three different exposure levels: AEGL 1 is for non-disabling and is basically like the COSHH 8-hour levels; AEGL 2 is the COSHH_{15min} levels equivalent for disabling and impairment of escape based on 10 minute exposure, and AEGL 3 for lethality which are similar to LC₅₀.

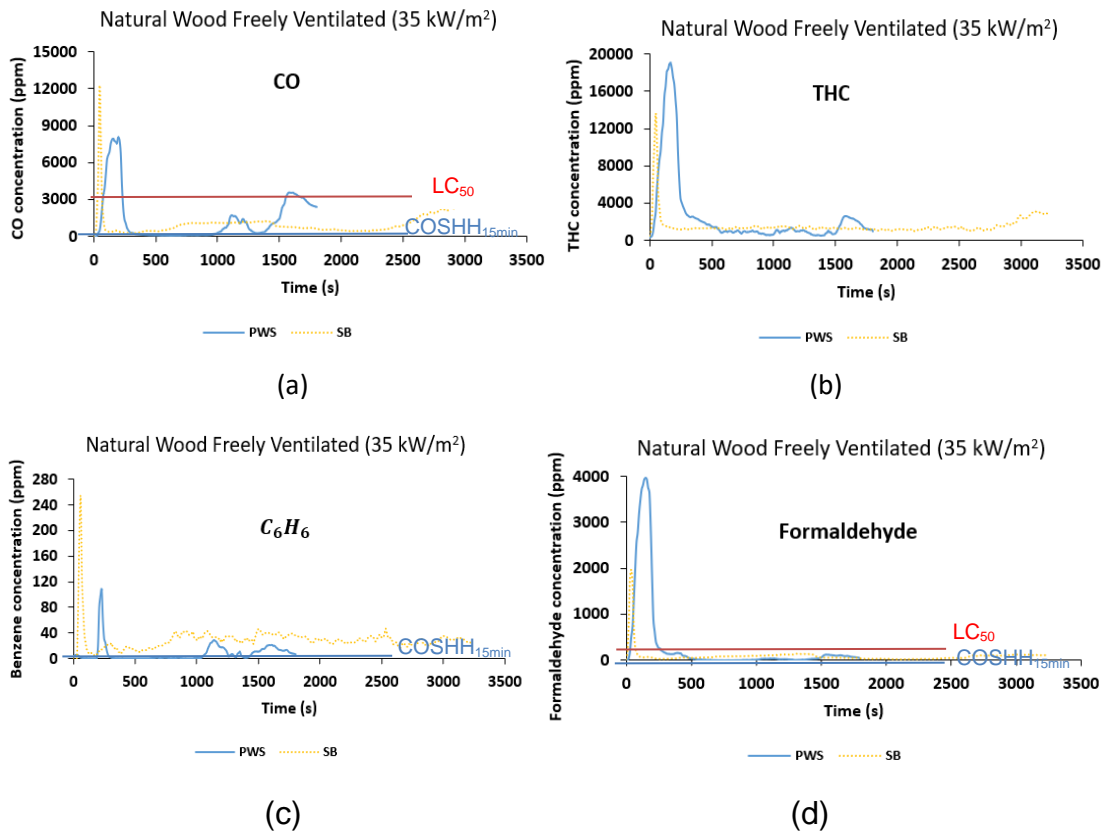
All the measured species from the 60 species analysed using the FTIR were normalized to their COSHH_{15min} or LC₅₀ concentration where available to give **n** for each toxic gas. Then all the individual **n** were summated to give an overall total **N** for all toxic species that were detected. The toxic species were then ranked by dividing the toxic gas specie **n** by the total **N** to express the toxicity as a percentage of the total. This enabled the most important toxic gases to be identified. This data will be expressed in the results as the %**N** as a function of time for the most important toxic gases.

4.2.1 Natural Wood

The toxic gases and total toxicity from pine wood and scaffolding board are presented in this section.

4.2.1.1 Toxic Gas Concentration

Some of the important toxic gases are presented in Fig. 4-7. Both samples showed high concentration of toxic gases during the ignition delay periods. Most of the toxic gases showed high concentrations for the pine wood test, except for CO, benzene and HCN, even though the nitrogen content is slightly higher in the pine wood. The low concentration of HCN in the pine wood may be due to higher temperature that led to the oxidation of HCN to other oxides of nitrogen such as NO_2 [185]. The acrolein concentration in pine wood fire was a factor of 5 higher than the scaffolding board fire while the formaldehyde concentration in the pine wood test was double that obtained with the scaffolding board. On LC_{50} and $\text{COSHH}_{15\text{ min}}$ basis CO and formaldehyde concentration limits were exceeded for both fires. Only the $\text{COSHH}_{15\text{ min}}$ concentration limits for the impairment of escape were exceeded for all gases in both fires. This shows that the gases that are of importance to lethality are different from that of impairment of escape.



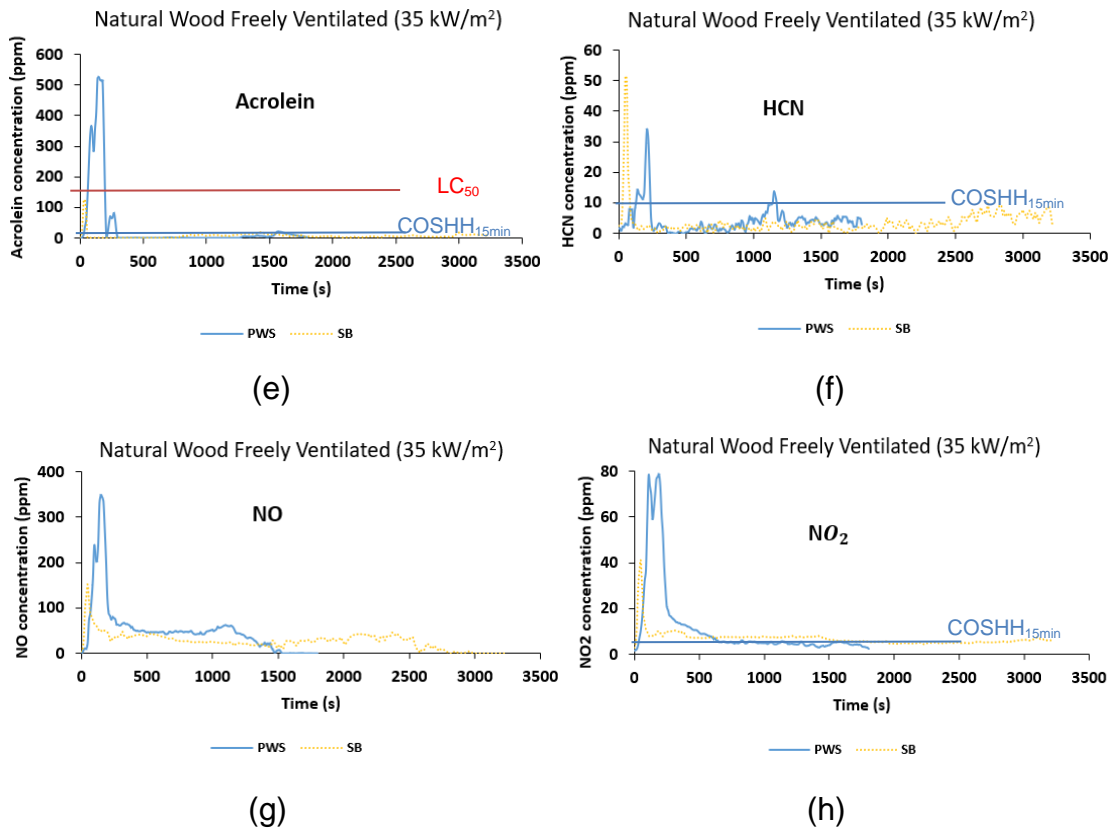


Figure 4-7 Toxic gas concentrations; CO (a), Total Hydrocarbon (b), Benzene (c), Formaldehyde (d), Acrolein (e), Hydrogen Cyanide (f), NO (g) and NO₂ (h)

4.2.1.2 Total Fire Toxicity **N** on an LC₅₀ and COSHH 15min Basis

The total toxicity **N** for LC₅₀ and COSHH_{15min} are shown as a function of time in Fig. 4-8 for pine and scaffolding board. Both methods of deriving **N** showed similar shapes of the dependence of **N** on time for the two wood samples. Despite the differences in relative toxicity, the two methods for calculating **N** indicate the same time in the fire where the peak toxicity occurs. These results show that the pine wood had by far the highest total toxicity with an LC₅₀ of 22, while the scaffolding board had 12. Scaffolding board had a single peak of **N**, due to flaming combustion while pine wood had a second small peak. For the highest toxicity for pine wood nearly 40% of the energy in the fuel was not released in the fire and emerged via high CO and HC, this occurring during the long ignition delay period of 192 s. This indicates poor mixing of the fire products with the surrounding air.

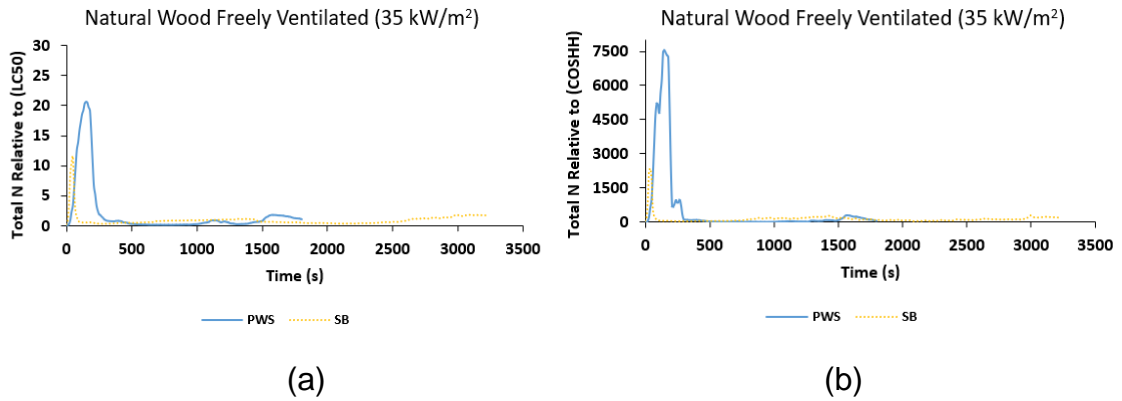


Figure 4-8 Total N relative to LC₅₀ (a) and COSHH_{15min} (b)

The % contribution of the most toxic gases to the total N (Figs. 4-9 and 4-10) shows that CO was the dominant toxic gas for LC₅₀, with formaldehyde as the next most important for both fires. In the early stages of the fire during the flame development phase and throughout the combustion, formaldehyde had a high contribution to N. For COSHH_{15min} impairment of escape toxicity for both fires, acrolein was the dominant toxic gas during the flaming phase of the fire. Formaldehyde was the next most important gas. This is in agreement with what was obtained by Mustafa et. al [89] in their work on pine wood cribs. The complex nature of materials as a result of wide differences in composition makes it difficult to compare their overall toxicity.

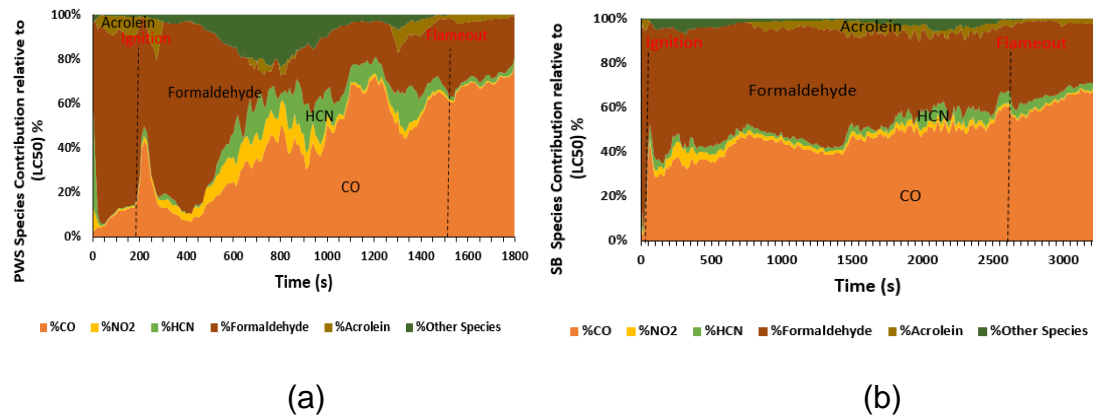


Figure 4-9 N-Gas Composition (LC₅₀) PWS (a) and SB (b)

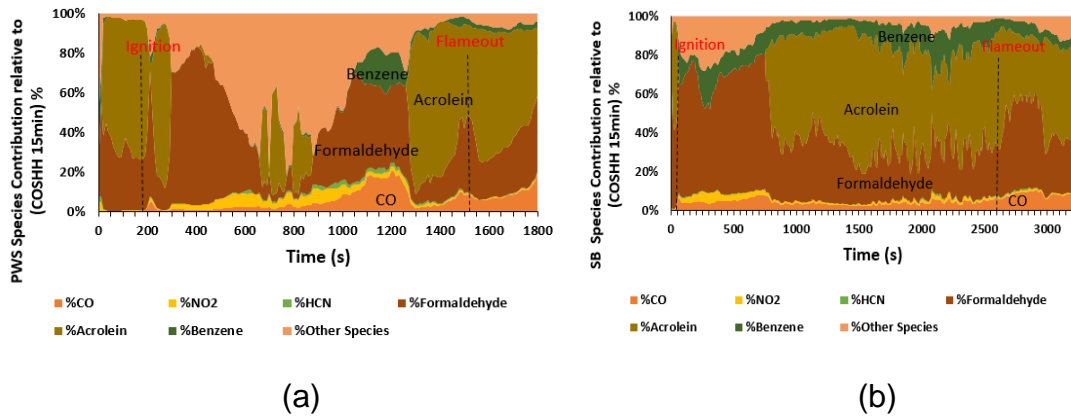


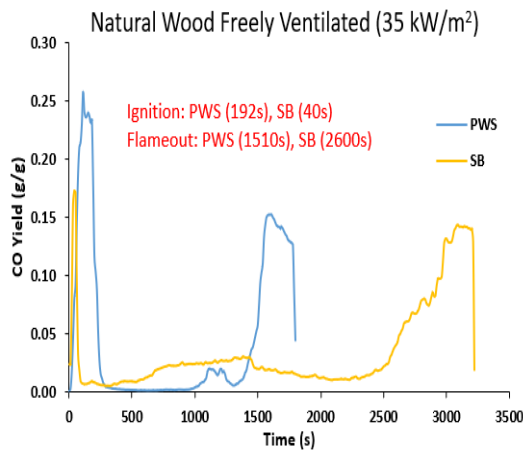
Figure 4-10 N-Gas Composition (COSHH_{15min}) PWS (a) and SB (b)

4.2.1.3 Toxic Gas Yields

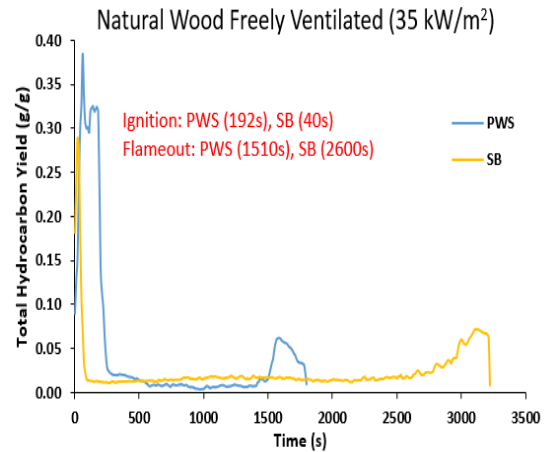
The yields of the important gases are shown as a function of time in Fig. 4-11 for the two natural woods; pine wood sticks (PWS) and scaffolding board (SB). PWS and SB produced their peak CO yield during the ignition delay period, when the fire was rich and the mass loss rate and HRR were at their peak at 110 s (0.26 g/g) for PWS and at 50 s (0.17 g/g) for SB. A fairly constant yield of the unburnt total hydrocarbon was observed for both fuel after ignition with the highest peak during the ignition delay (PWS (0.39 g/g), SB (0.29 g/g)) and another peak just at flameout time. Acrolein and formaldehyde peak toxic yields were also produced during the ignition delay periods for all the fires, with pine wood producing the highest yield of both gases. Benzene yield was produced throughout the combustion period with the highest yield during the ignition delay period where the richer mixtures were formed and the oxygen level was at its minimum. HCN yield was produced throughout the combustion period but was highest during the ignition delay and smouldering phase, with the scaffolding board having the highest HCN yield. The yields of the toxic gases are very high even though they burned lean in both cases. The high yields of CO and THC are due to inefficient combustion. A summary of the peak yields and the time to reach the peak yield are presented in Table 4-1.

Table 4-1 Toxic Gas Yields

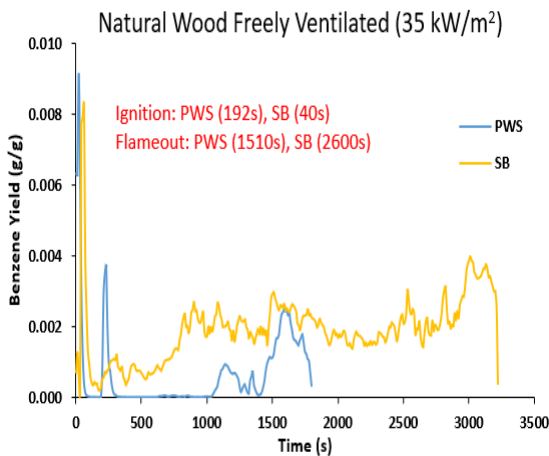
Toxic Gas	Peak Yield and Time to Peak yield	
	PWS g/g	SB g/g
CO	0.26 (110 s)	0.17 (50 s)
THC	0.39 (60 s)	0.29 (20 s)
Acrolein	0.04 (90 s)	0.017 (20 s)
Formaldehyde	0.18 (60 s)	0.16 (20 s)
Benzene	0.009 (20 s)	0.008 (60 s)
HCN	0.0008 (20 s)	0.0012 (10 s)



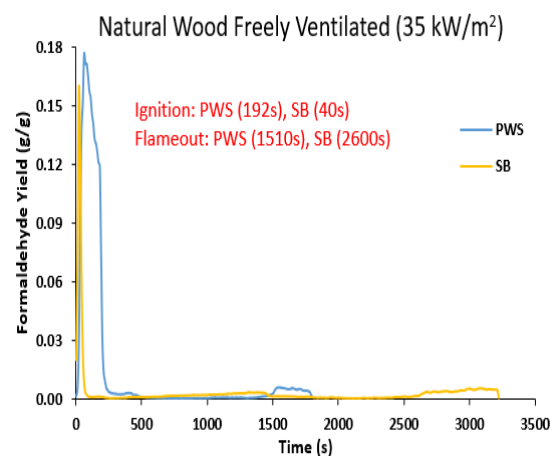
(a)



(b)



(c)



(d)

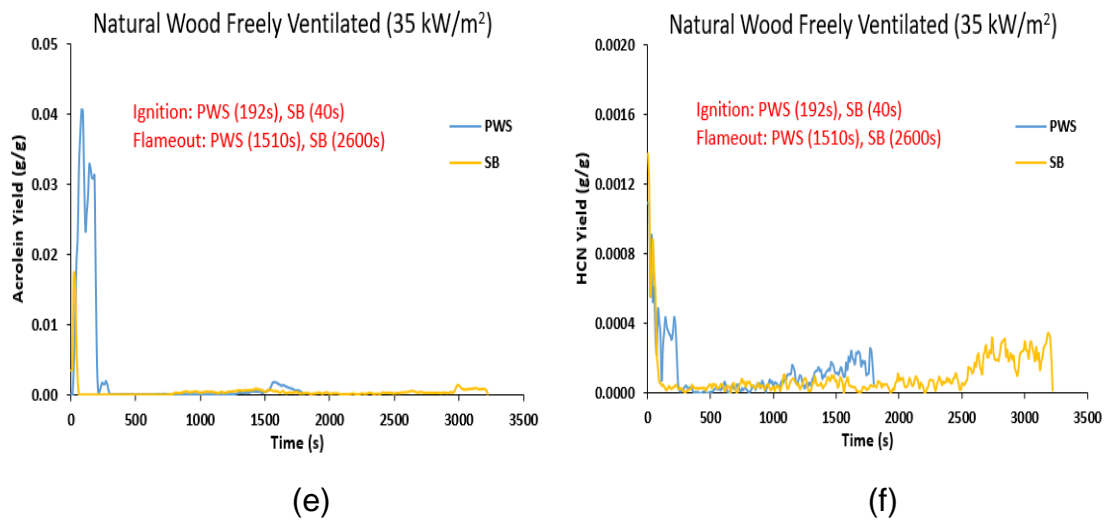


Figure 4-11 Toxic gas yields; CO (a), Total Hydrocarbon (b), Benzene (c), Formaldehyde (d), Acrolein (e) and Hydrogen Cyanide (f)

4.2.1.4 Combustion Efficiency and Heat Release Rate Correction

The combustion efficiency was determined by summing the CO and THC yields using the calorific value of CO and taking HC as methane. This is shown in Fig.4-12. For the pine wood fire the combustion efficiency was < 60 % during the ignition delay and increased to > 95 % after the first 180 s following autoignition, when the HRR was still increasing. For the scaffolding board, the CO and HC emissions were lower, resulting in a slightly higher combustion efficiency than the pine wood with about > 60 % efficiency during the ignition delay. The combustion efficiency deteriorates during the smouldering combustion, as shown in Fig. 4-12. The combustion efficiency increased to > 95 % following autoignition of the sample and flaming combustion.

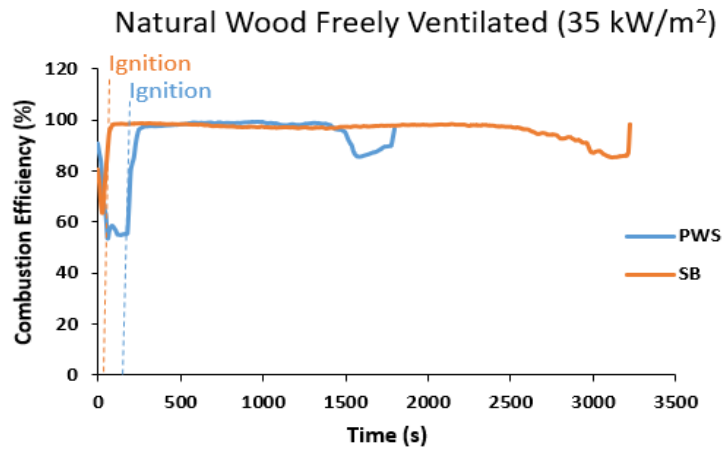


Figure 4-12 Combustion Efficiency

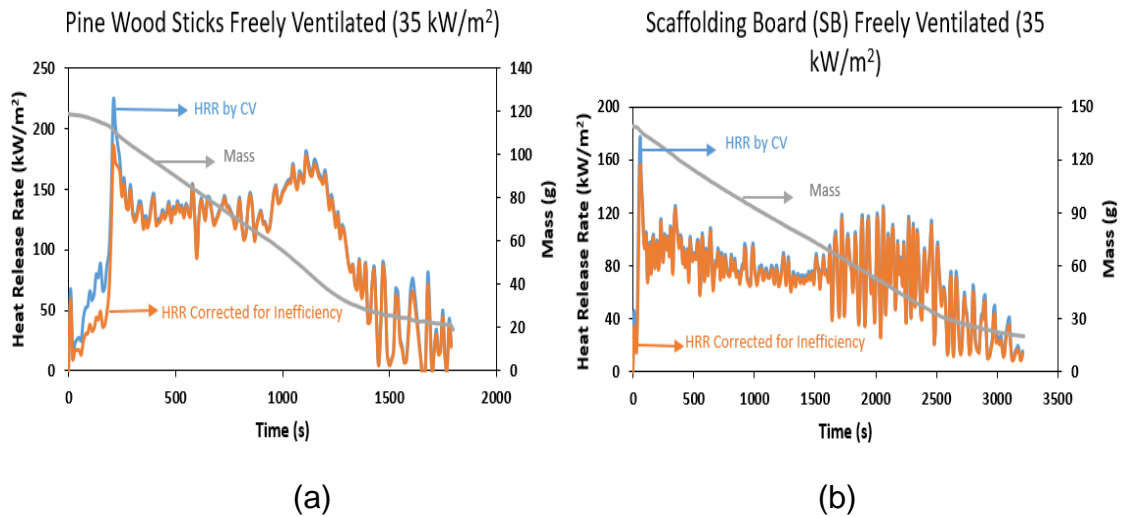


Figure 4-13 Mass, HRR based on the mass loss rate, adjusted HRR, based on inefficiency of combustion for; Pine Wood (a) and Scaffolding Board (b)

The mass loss rate and calorific value (CV) based heat release rate (HRR) for the two (2) wood samples is shown in Fig. 4-13. This heat release rate by mass loss rate assumes complete combustion and release of all the available energy. CO, total unburnt hydrocarbons, THC and soot are all indication of incomplete combustion and therefore unreleased energy, which is measured as the combustion inefficiency. For soot yields to be significant, they need to be $> 1\%$. The present work did not determine the soot yield, the combustion efficiency was determined based on the CO and total hydrocarbons by procedures used for engine emissions [107].

Aljumaiah et al. [88] showed that in under-ventilated wood crib fires, total hydrocarbons (unburnt hydrocarbon) were particularly significant in correctly evaluating the heat release rate HRR.

The CO and total hydrocarbon yields in Fig. 4-11 a and b were used in the present work to correct the heat release rate HRR shown in Fig.4-13. The heat release rate by mass loss rate showed an over-estimation of the corrected heat release at stages of the fire where the combustion efficiency was low.

4.2.2 Processed Wood

The toxic gases and total toxicity from 3 different types of processed wood (OSB, MDF and Chipboard faced with melamine (CFM)) are presented in this section.

4.2.2.1 Toxic Gas Concentration

The most important toxic gases are compared in Fig. 4-14. High concentrations of the gases were released during the ignition delay and when the HRR was at its peak for all the test fires due to the rich mixture at the initial stage of the fire. The melamine coating was responsible for the delay in igniting the chipboard. OSB had formaldehyde and acrolein concentration higher than the 2 wood samples by a factor of 4. The most important toxic species were CO, acrolein, formaldehyde, benzene and HCN on both an LC₅₀ and COSHH_{15min} basis, which is used as an indicator of impairment of escape.

HCN concentration was very low for OSB which is expected, looking at the nitrogen content in the OSB (0.41%) as compared to chipboard (4.39%) and MDF (5.04%). The high nitrogen content in the chipboard (CFM) and MDF was due to their composite structure with glued chips, particles or fibres. All concentrations exceeded the toxic limits in terms of LC₅₀ and COSHH_{15 min} except for benzene and acrolein which have an LC₅₀ concentration limit of 10,000 ppm and 300 ppm and these were not reached.

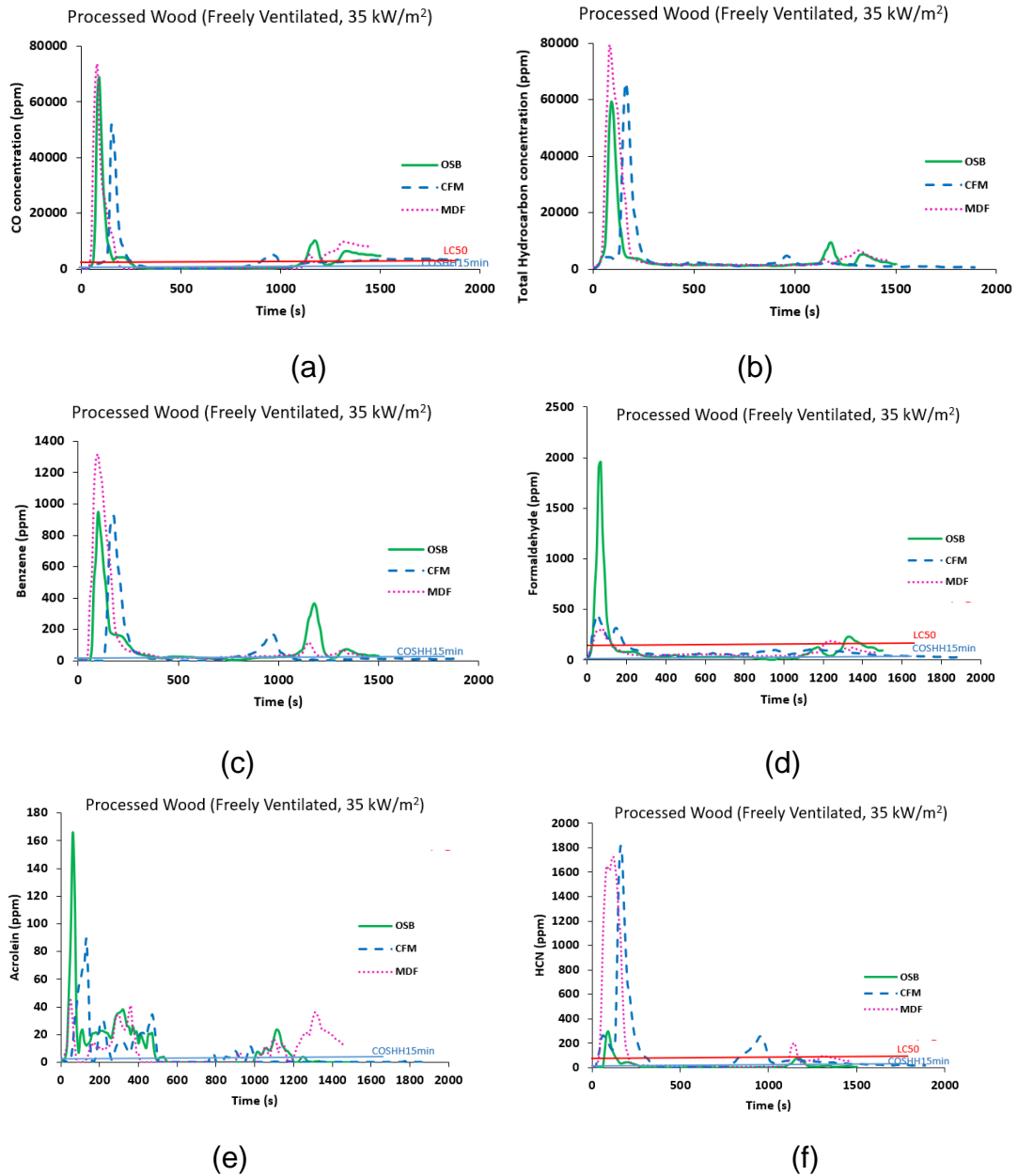


Figure 4-14 Toxic gas concentrations; CO (a), Total Hydrocarbon (b), Benzene (c), Formaldehyde (d), Acrolein (e) and Hydrogen Cyanide (f).

4.2.2.2 Total Fire Toxicity N on an LC₅₀ and COSHH_{15min} Basis

The total toxicity **N** for the 3 wood samples is shown in Fig. 4-15 as a function of time. The results show similar variation of **N** with time for the COSHH_{15min} and LC₅₀ toxic assessments. At the early combustion stage (140-200 s), lethal levels of 30-minute exposure toxicity were produced in these wood fires and the COSHH_{15min} toxicity levels indicate that the concentrations would impair escape for the entire duration of the fire even though the fire burned lean for most of the

time. The dilution required to prevent 30-minute LC₅₀ exposure levels from being lethal was about 30-40 indicating that people exposed to these gases would be at risk of death. Impairment of escape would be a much more significant effect as these toxic gases need to be diluted by over 1000 for chipboard faced with melamine fire and over 2000 for OSB and MDF before these gases would not impair escape.

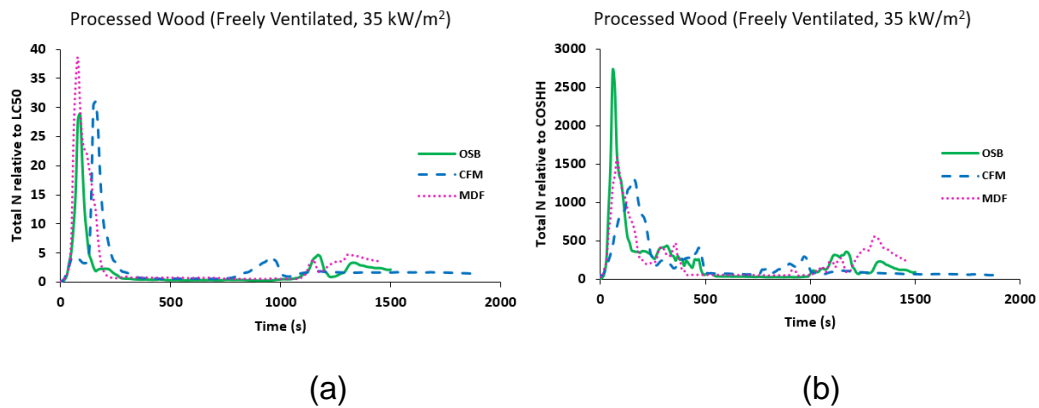
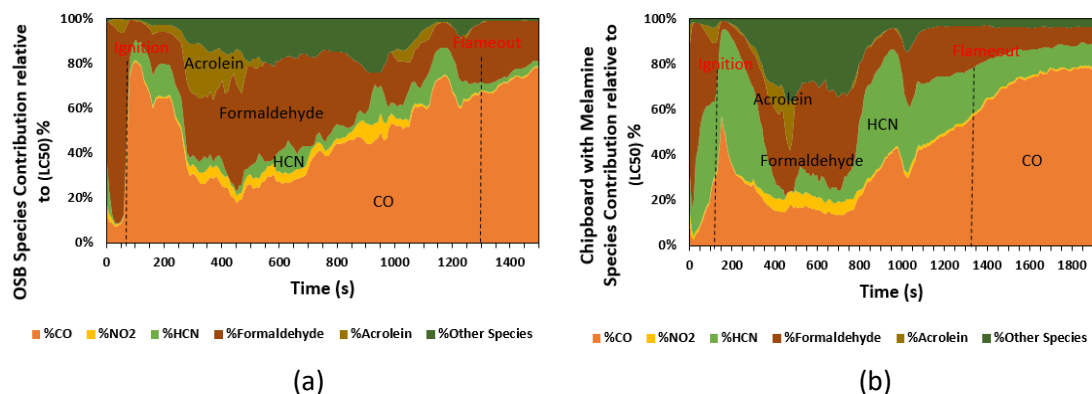
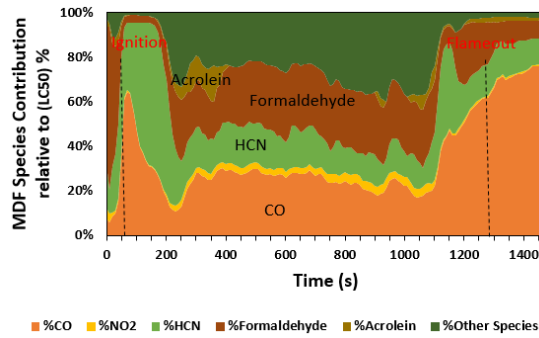


Figure 4-15 Total toxicity N relative LC₅₀ (a) and relative to COSHH_{15 min} (b)

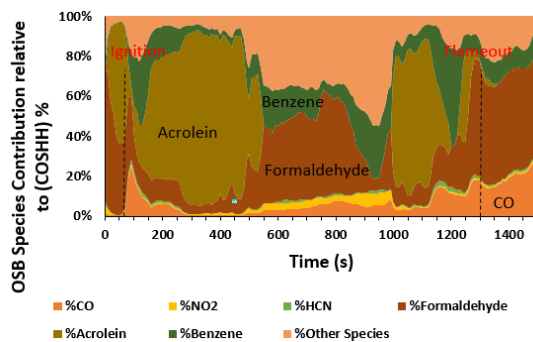
Figure 4-15 shows that the peak toxicity on a COSHH_{15min} and LC₅₀ basis occurred early in the fires for chipboard faced with melamine and MDF and this was due to the high nitrogen content of the binder used in the wood products for chipboard and MDF, but the high initial toxicity peak for OSB was due to formaldehyde. This rapid release of the highest toxicity soon after the onset of the fires is of concern as these gases will be produced in fires involving these materials during the initial escape period.



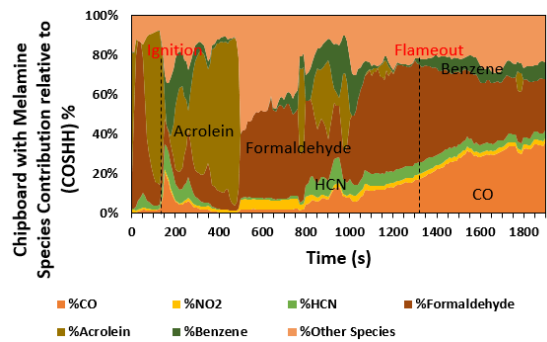


(c)

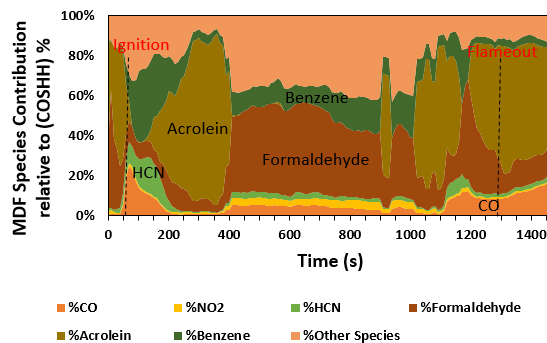
Figure 4-16 N-Gas Composition (LC₅₀) OSB (a) Chipboard (b) and MDF (c)



(a)



(b)



(c)

Figure 4-17 N-Gas Composition (LC₅₀) OSB (a) Chipboard (b) and MDF (c)

Figures 4-16 and 4-17 show the key toxic gases that would cause death and impair escape involving the processed wood fires. On LC₅₀ basis, the key gases were found to be CO, NO₂, HCN, formaldehyde and acrolein while on COSHH_{15min} basis, the most important toxic gases were CO, NO₂, HCN, formaldehyde, acrolein and benzene. This shows that for both toxicity

assessment methods, most of the gases were common except for benzene which the LC₅₀ does not give much importance. CO is the most dominant toxic gas in terms of LC₅₀ while formaldehyde and acrolein are the most dominant in terms of COSHH_{15 min}.

4.2.2.3 Toxic Gas Yields

The yields for CO and unburnt total hydrocarbon and their variations with time are shown in Fig.4-18. CO yield was higher in the initial stages with a reduced yield during the char burning phase as shown in Fig. 4-18a. OSB had the highest CO yield with a peak of 0.5 g/g (500 g/kg) followed by MDF with a yield of 0.32 g/g (320 g/kg) and CFM (Chipboard faced with Melamine) and pine produced similar yield of 0.25 g/g (250 g/kg). The total unburnt hydrocarbon yields are shown in Fig. 4-18b. These were much higher in the initial volatile burning phase and lower in the char burning phase. These yields were used to estimate the combustion efficiency and correct the heat release rate for inefficiencies. Other toxic yields are compared with natural wood (pine wood) in section 4.4.

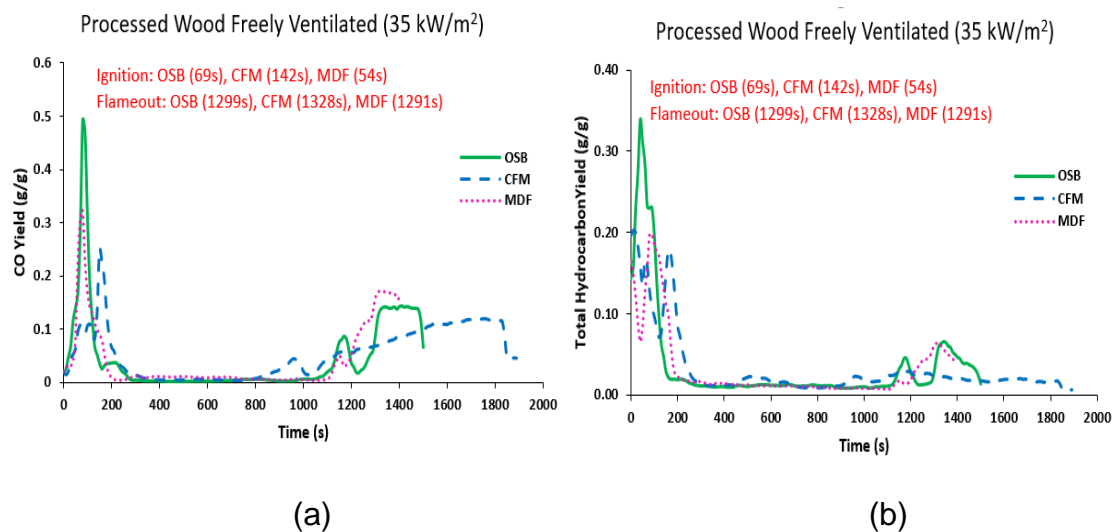


Figure 4-18 Toxic yields of CO (a) and Total Hydrocarbon (b).

4.2.2.4 Combustion Efficiency and Heat Release Rate Correction

The combustion efficiency is shown in Fig.4-19. For the OSB wood fire the combustion efficiency was about 60% during the ignition delay but decreased to about 50% just after ignition at around 90 s and increased to about 98% afterwards with a slight decrease during the smouldering combustion phase. The MDF, showed a slightly higher combustion efficiency than the OSB wood with about > 60% efficiency during the ignition delay.

The combustion efficiency deteriorates during the smouldering combustion, as shown in Fig. 4-19. The combustion efficiency increased to > 95% following autoignition of the sample and flaming combustion. The chipboard followed a similar trend but had the highest combustion efficiency of 70% during the ignition delay. This is as a result of the much lower yield of CO and total unburnt hydrocarbon produced by CFM. The efficiency during the steady flaming combustion was similar for all the processed woods.

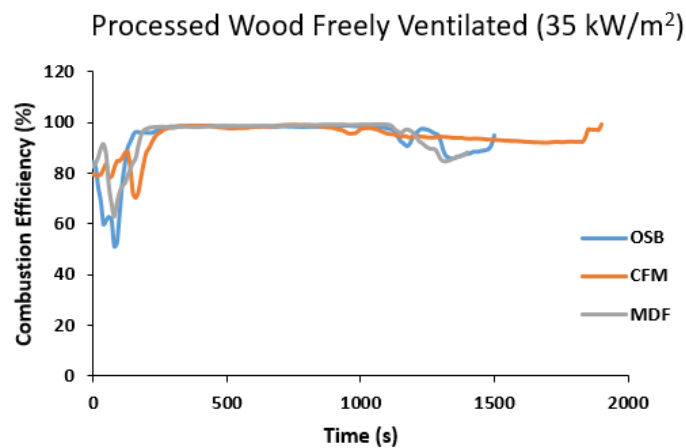
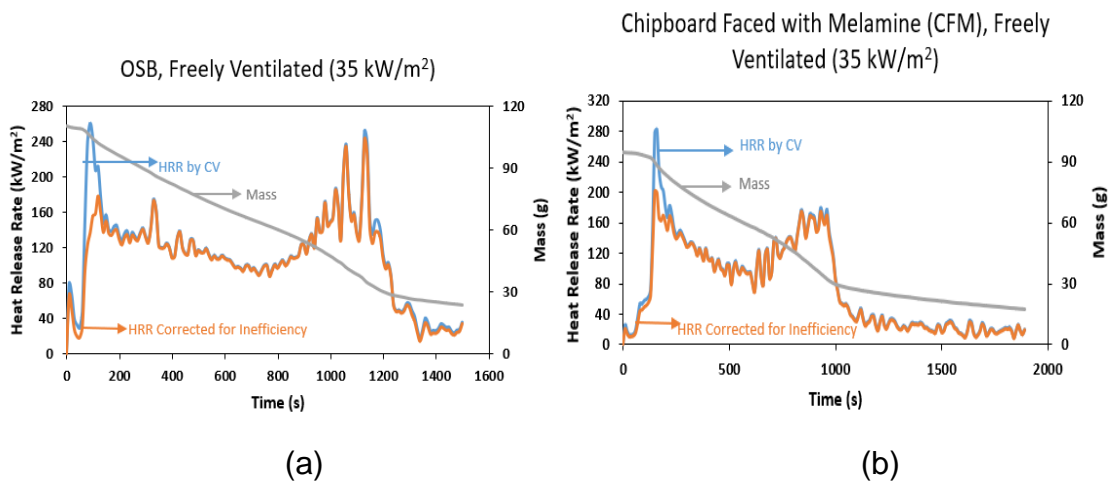
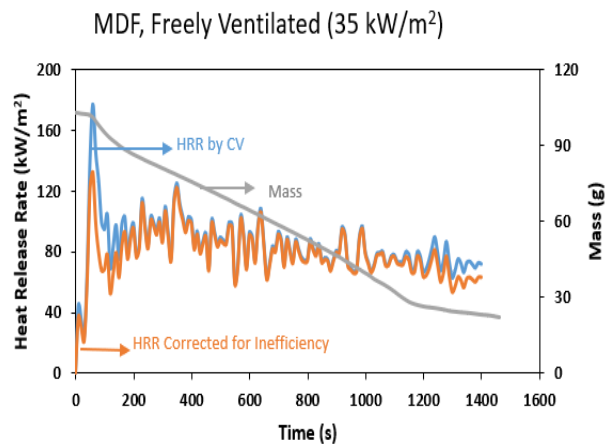


Figure 4-19 Combustion Efficiency



(a)

(b)



(c)

Figure 4-20 Mass, HRR based on the mass loss rate, adjusted HRR, based on inefficiency of combustion for; OSB (a) CFM (b) and MDF (c)

Figure 4-20 shows the heat release rates corrected for inefficiencies, using the yields of CO and total unburnt hydrocarbons. This shows that there was an overestimation of the heat release rates calculated based on the mass loss rate and the calorific values, where it is assumed all the energy released is consumed in the combustion. These differences in heat release rates occurred when the combustion efficiencies were low in all cases.

4.2.3 Plywood

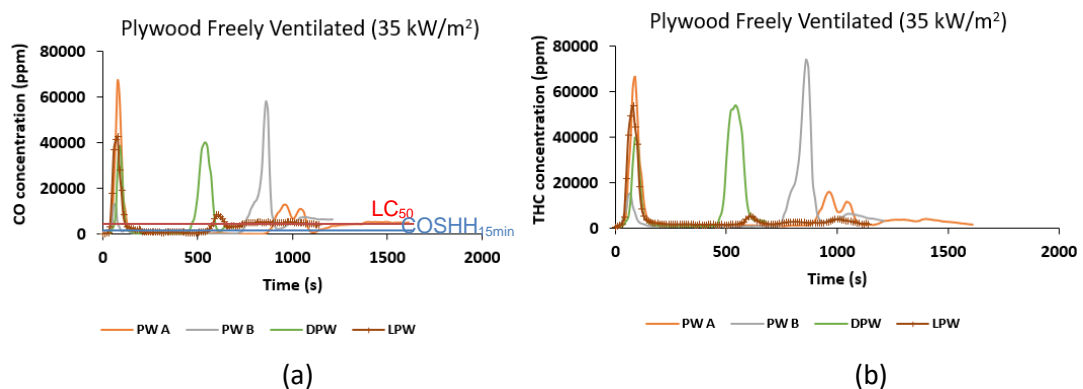
The toxic gases and total toxicity from 4 different types of plywood (Plywood A (PW A), Plywood B (PW B), Light plywood (LPW) and dark plywood (DPW)) are presented in this section.

4.2.3.1 Toxic Gas Concentration

The most important toxic gas emissions are shown in Fig. 4-21 with their toxic limits shown. The LC₅₀ toxic limits reflect conditions that will cause death and the COSHH_{15min} limits reflect conditions that will impair escape. The CO concentrations for the plywood B fire were lower than the rest of the plywood at the 1st flaming phase of the fire, but increased by a factor of 4 at about 860 s during the 2nd flaming combustion and an almost zero CO emission during the steady burning phase. Plywood A and the light plywood had their peak CO concentration during the 1st flaming phase with a much lower peak (about 5 times

lower) in the 2nd phase. Dark plywood had 2 peaks of almost the same CO concentration in both phases of flaming combustion.

All plywood samples had an almost zero concentration of CO during the steady state burning phase. The highest concentration of each of the toxic gases released occurred during the rich combustion, indicating that a bit of confinement was experienced even though the experiments were freely ventilated. The highest concentration of benzene was released by plywood A, followed by the dark plywood, plywood B and the light plywood. There were significant differences in the concentration of the toxic gases presented in Fig. 4-21 (CO, Benzene, Formaldehyde, Acrolein, HCN), both in terms of magnitude and the time the peak concentrations occurred. The toxicity was higher the richer the fire became, and the toxicity peaked during the period the fire HRR increased to its maximum value. The elemental analysis of the four samples showed that they had different nitrogen content, indicating different glues were used. Plywood B had the highest Nitrogen content of 6.43%, which resulted in the highest HCN concentration by a factor of 2-4. All toxic gases concentration levels were considerably higher than the LC₅₀ limit except for acrolein and benzene but all the toxic gas emissions were above the COSHH_{15min}, with each type of plywood having different concentrations of toxic gases. These results indicate that plywood should be selected based on their toxic emissions performance in fires.



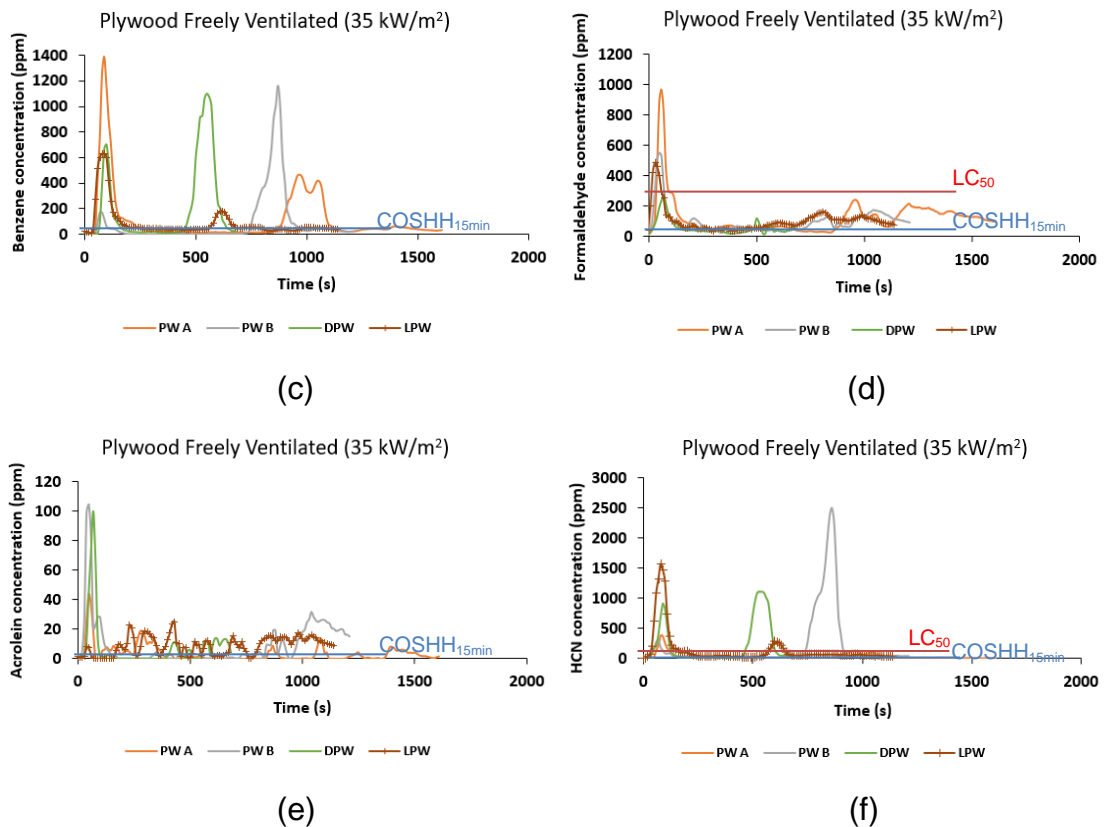


Figure 4-21 Toxic gas concentrations; CO (a), Total Hydrocarbon (b), Benzene (c), Formaldehyde (d), Acrolein (e) and Hydrogen Cyanide (f).

4.2.3.2 Total Fire Toxicity N on an LC₅₀ and COSHH_{15min} Basis

The most important toxic species were CO, HCN, acrolein, formaldehyde and benzene on both an LC₅₀ and COSHH_{15min} basis, which is used as an indicator of lethality and impairment of escape. The results showed that the **N** for LC₅₀ toxic assessment were all > 20 and were different, both in terms of the magnitude and the time when the peak toxicity occurred. The total **N** on a COSHH_{15min} basis gives values of > 900. This means that the toxic gases need to be diluted with fresh air by a factor of about 900-1500 before escape is not impaired and it has to be diluted by a factor of > 20 before it doesn't kill anybody in 30 mins. The two methods of deriving **N** show that the dependence of **N** on time were very similar for all the plywood. This shows that the two methods for determining **N** locate the same time in the fire where the peak toxicity occurs.

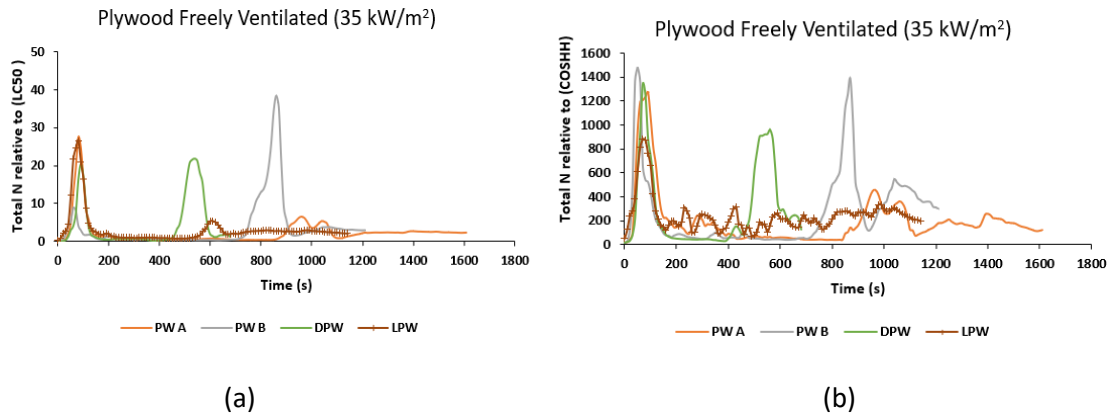


Figure 4-22 Total toxicity N relative LC₅₀ (a) and relative to COSHH_{15 min} (b)

The major contribution to the total toxicity are shown on an LC₅₀ and COSHH_{15min} basis in Figs. 4-23 and 4-24 for the 4 plywood fires. For PW A the toxicity was dominated by CO, followed by formaldehyde, HCN and acrolein on an LC₅₀ basis and formaldehyde, acrolein, benzene, CO and HCN on a COSHH_{15min} basis. HCN was the third most important toxic gas, but its contribution never exceeded 10% on an LC₅₀ basis. For the PW B the toxicity was dominated by CO, HCN, formaldehyde and acrolein on an LC₅₀ basis, but formaldehyde was more significant on a COSHH_{15min} basis, followed by acrolein, HCN, benzene and CO. For the DPW the toxicity was dominated by CO, HCN, formaldehyde on an LC₅₀ basis, with < 10 % contribution of acrolein. On a COSHH_{15min} basis, formaldehyde dominated the toxicity, followed by acrolein, benzene, CO and HCN. The LPW fire was also dominated by CO, HCN, formaldehyde on an LC₅₀ basis, with < 10 % contribution of acrolein. Acrolein was the most important toxic gas on COSHH_{15min} basis followed by formaldehyde, benzene, CO and HCN. The results showed that benzene was also a significant contribution to the toxicity in these plywood fires.

The differences between LC₅₀ and COSHH_{15min} toxic assessments in these fires show that the relative importance of the four toxic gases for death are different from that of impairment of escape. For these plywood fires CO dominates in relation to death and for impairment of escape the other three gases are more important and each plywood had different toxic gases dominating more than the other. This further shows that plywood should be selected based on its toxic emissions performance in fires. These toxic emissions were similar to those for

pine wood crib compartment fires [88, 89, 178] with the added significance of HCN emissions from the glues used in plywood construction.

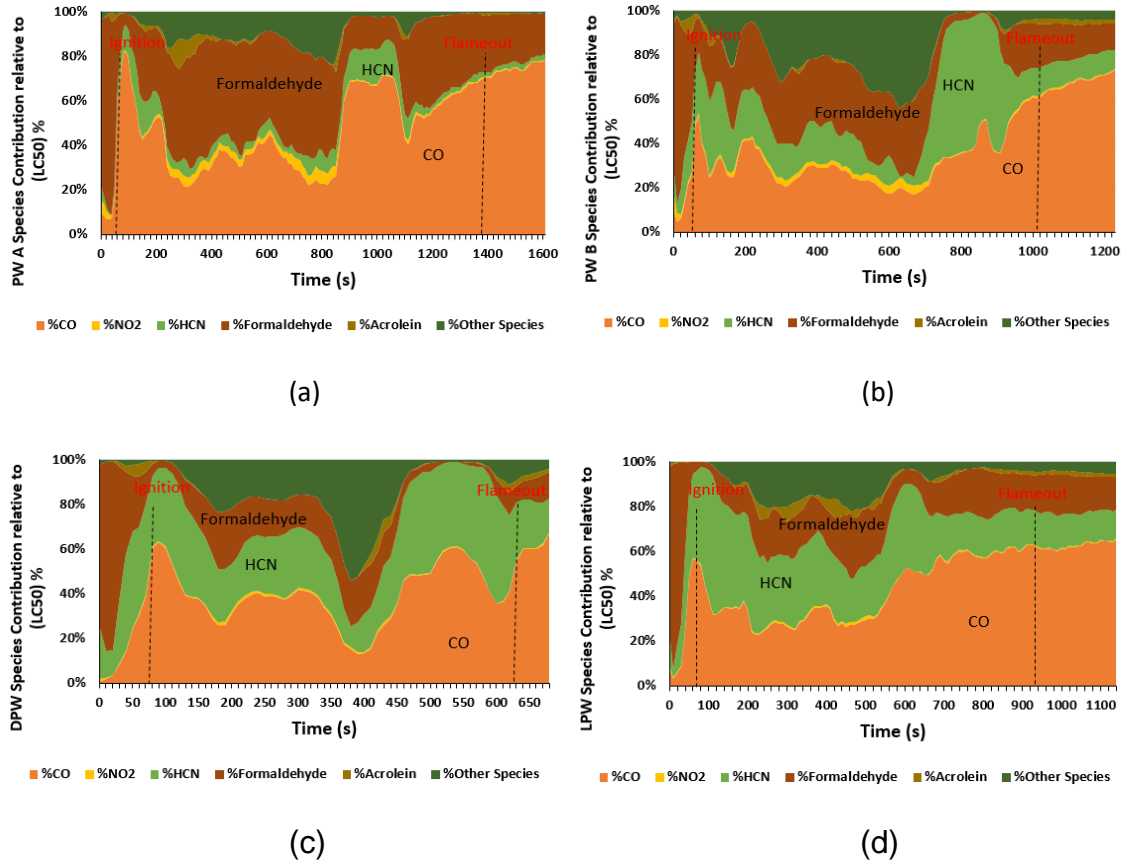
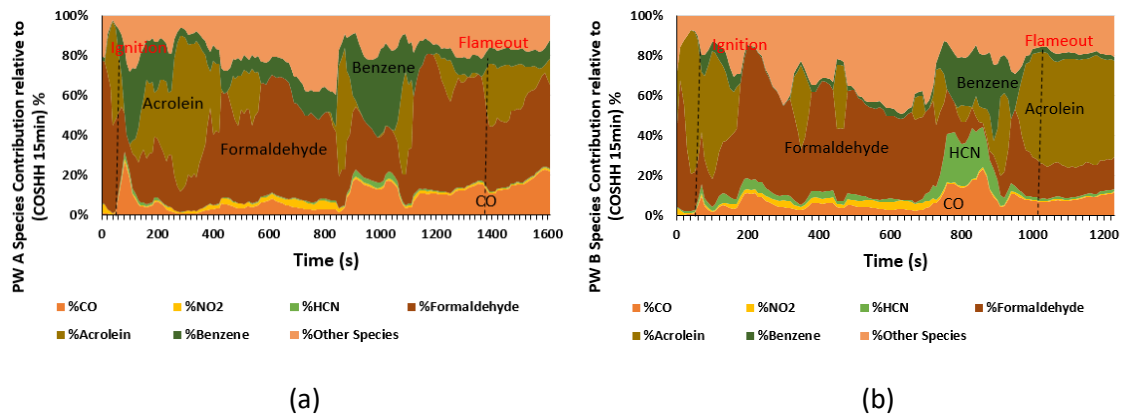


Figure 4-23 Species Contribution relative to LC₅₀: PW A (a) PW B (b) DPW (c) and LPW (d)



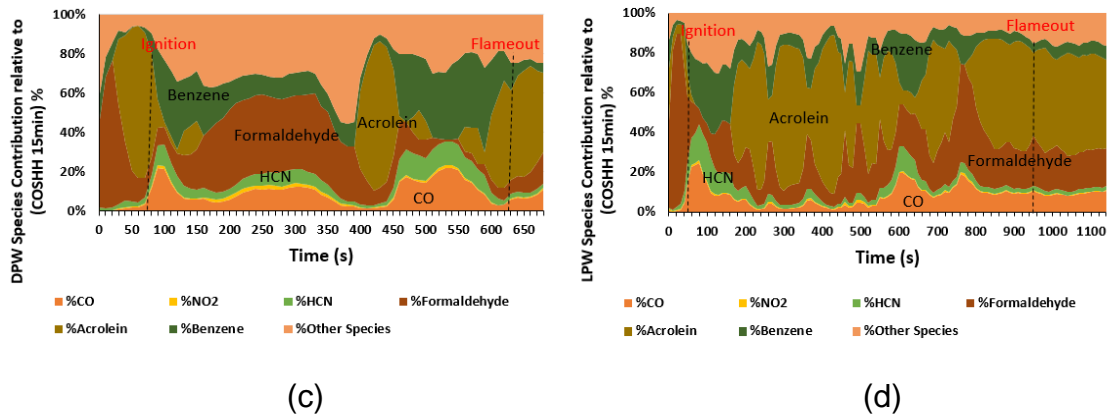


Figure 4-24 Species Contribution relative to COSHH_{15min}: PW A (a) PW B (b) DPW (c) and LPW (d)

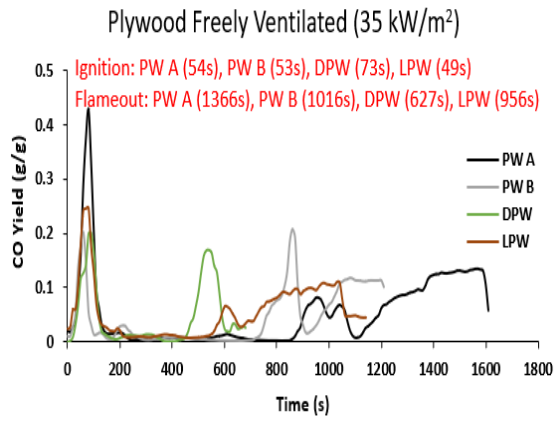
4.2.3.3 Toxic Gas Yields

The most important toxic gas yields are shown in Fig. 4-25. All plywood samples had an almost zero yield of CO during the steady state burning phase. The highest yield of each of the toxic gases released occurred during the early rich combustion, indicating that entrainment of air into the fire gases was not sufficient to produce overall lean mixtures, even though the experiments were freely ventilated. The total unburnt hydrocarbon yield was also high (0.2-0.25 g/g) during the early rich combustion indicating that the combustion efficiency will be low at that period. The highest yield of benzene was released by plywood A, followed by the dark plywood, plywood B and the light plywood. There were significant differences in the yields of the toxic gases (CO, total unburnt hydrocarbon, Benzene, Formaldehyde, Acrolein, HCN), both in terms of magnitude and the time the peak yields occurred. The yields were higher for richer fires, and the toxicity peaked at maximum HRR. Plywood B had the highest nitrogen content of 6.43%, which resulted in the highest HCN yield. Table 4-2 shows a summary of the peak toxic yields.

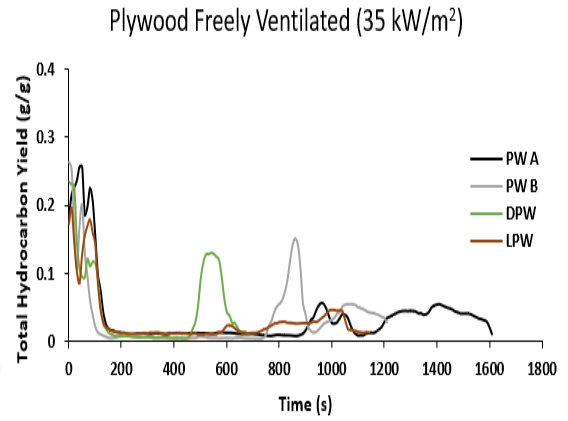
Table 4-2 Toxic Gas Yields for Plywood

Toxic Gas	Peak Yield and Time to Peak yield			
	PW B g/g	PW A g/g	DPW g/g	LPW g/g
CO	0.428 (80 s)	0.202 (60 s)	0.201 (90 s)	0.248 (80 s)
THC	0.257 (50 s)	0.252 (10 s)	0.228 (20 s)	0.195 (10 s)
Acrolein	0.011 (40 s)	0.010 (40 s)	0.005 (60 s)	0.0006 (10 s)

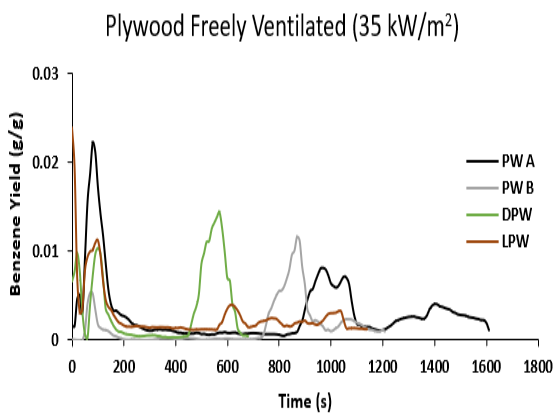
Formaldehyde	0.095 (40 s)	0.200 (50 s)	0.022 (30 s)	0.073 (20 s)
Benzene	0.022 (80 s)	0.011 (880 s)	0.014 (570 s)	0.024 (10 s)
HCN	0.002 (80 s)	0.009 (850 s)	0.009 (40 s)	0.009 (90 s)



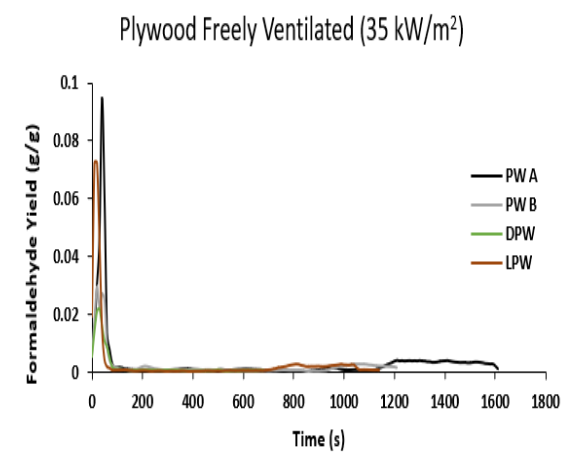
(a)



(b)



(c)



(d)

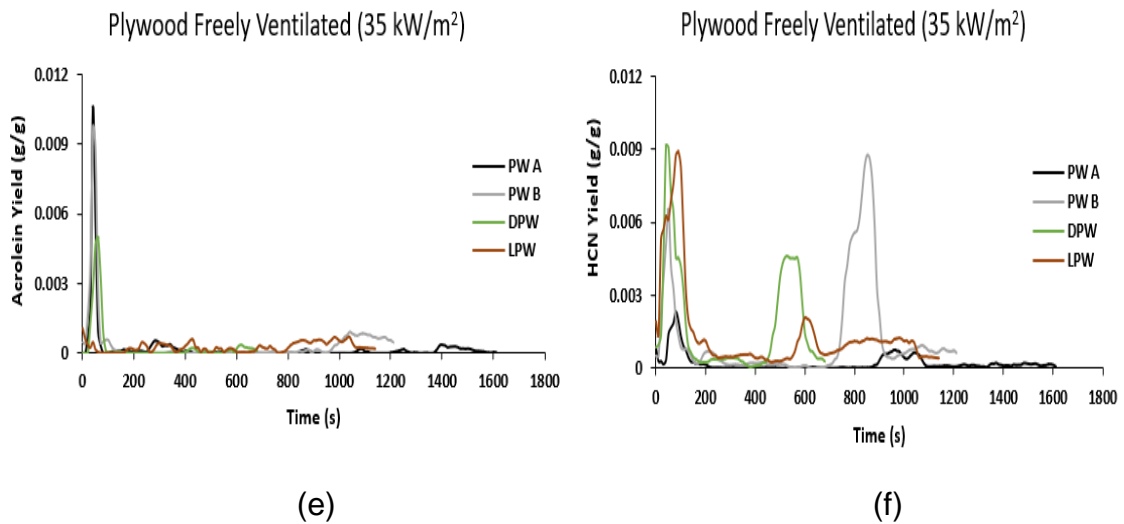


Figure 4-25 Toxic gas yields; CO (a), Total Hydrocarbon (b), Benzene (c), Formaldehyde (d), Acrolein (e) and Hydrogen Cyanide (f)

4.2.3.4 Combustion Efficiency and Heat Release Rate Correction

Figure 4-26 shows the combustion efficiency for the different plywoods. PW A with the highest yield of CO and unburnt total hydrocarbon had the lowest combustion efficiency of about 55% at around 80 s. PW B and LPW had a combustion efficiency of 70% at about the same time as the PW A with DPW having a slightly higher combustion efficiency of 77% at about the same time. The combustion efficiency increased to 98% during the steady flaming combustion with a slight decrease during the smouldering combustion phase. This is as a result of the much lower yield of CO and total unburnt hydrocarbon during the flaming combustion.

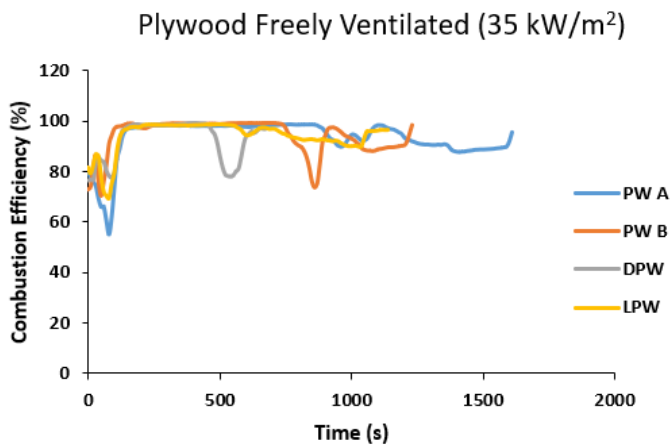


Figure 4-26 Combustion Efficiency for Plywood

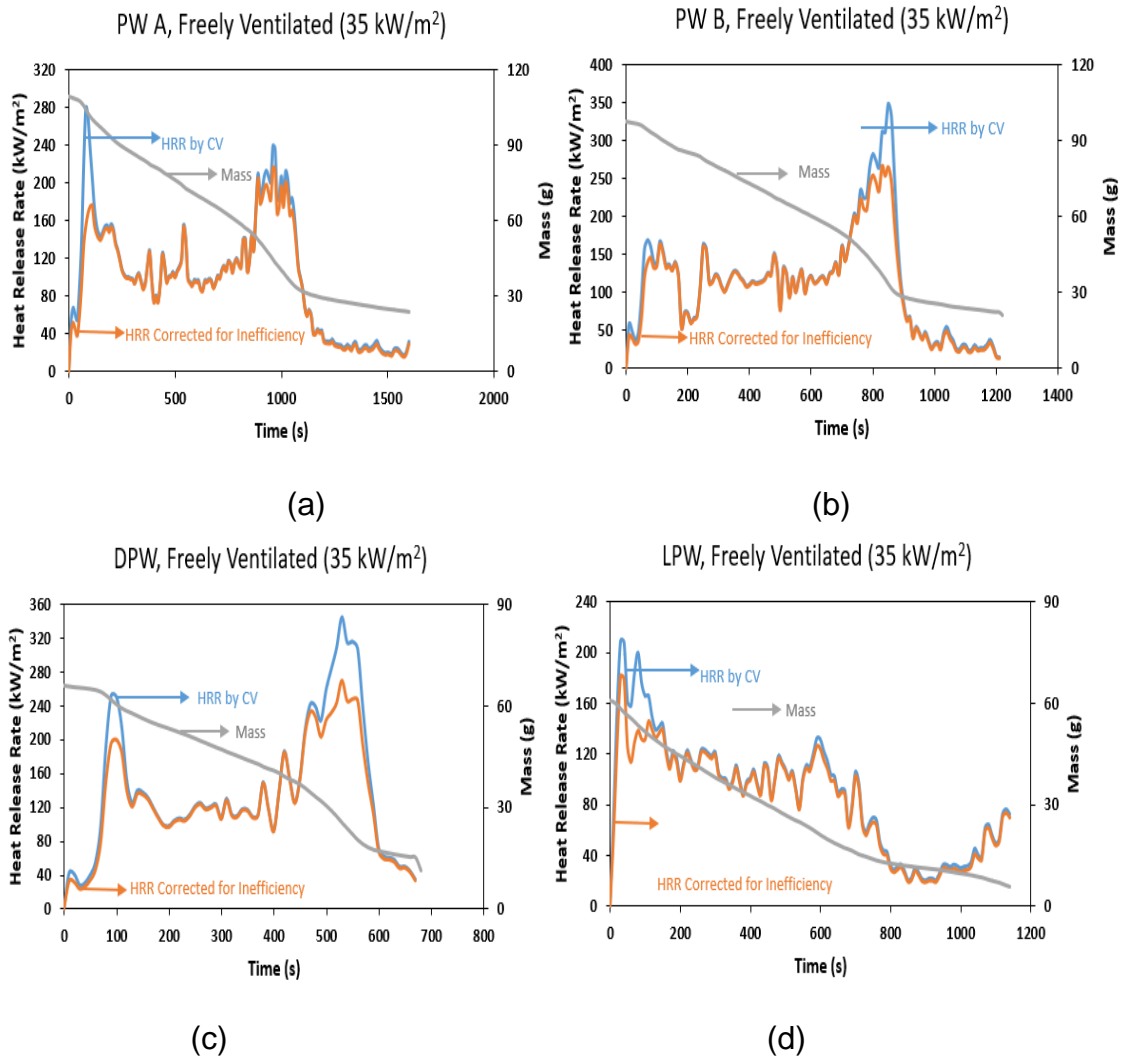


Figure 4-27 Mass, HRR based on the mass loss rate, adjusted HRR, based on inefficiency of combustion for; PW A (a) PW B (b) DPW (c) and LPW (d)

Figure 4-27 shows the heat release rates corrected for inefficiencies, using the yields of CO and total unburnt hydrocarbons. This shows that there was an overestimation of the heat release rates calculated based on the mass loss rate and the calorific values, at periods where the combustion efficiency was low and the CO and total hydrocarbon yields were high. The heat release rate was fairly similar during the steady flaming phase of the combustion where the efficiency was almost 100%.

4.3 Particulate Emissions from Wood Samples

Smoke production in legislated testing is measured by optical obscuration and is related to visibility and impairment of escape through lack of line of sight to

escape doors. The smoke regulations are generally not there because of the toxicity of smoke. The smoke production regulations have no requirement to measure the composition of the smoke either for soot particle size or toxic gases. The victims and some of the survivors of the Grenfell Tower fire in London had black lungs and some of those who survived had to have black particles flushed out of their lungs. The size of particles that reach the alveolar region of the lungs is < 50 nm and particles of this size have no effect on light obscuration [136] and so are not measured in the traditional fire smoke tests. There have been few studies of the ultra-fine particles generated in fires and they are not discussed in the fire literature as a cause of impairment of escape as discussed in Chapter 2. In this section, the results of particles generated during the combustion of the different types of wood are presented. Only the OSB particles result would be shown under the processed wood and only plywood A and B will be presented under the plywood category due to the absence of the particle size analyser during the tests.

4.3.1 Natural Wood

4.3.1.1 Particle Number Concentration

The particle number concentration as a function of size and time is shown in Figs. 4-28 and 4-29. A bimodal distribution of the particle sizes was observed indicating the nucleation mode and accumulation mode of the particle size distribution. The nuclei mode for both fires was found to peak at 20 nm. For the accumulation mode, the pine wood fire peaked at 200 nm throughout the combustion but the scaffolding board fire showed a smaller peak of the accumulation mode of about 500 nm between 500–1000 s at a low concentration before having a peak of 200 nm. The particle concentrations were highest at the peak HRR of 200 kW/m² for the pine wood and 140 kW/m² for the scaffolding board fires. Both fires showed a fairly constant concentration of particle number at the steady state burning phase.

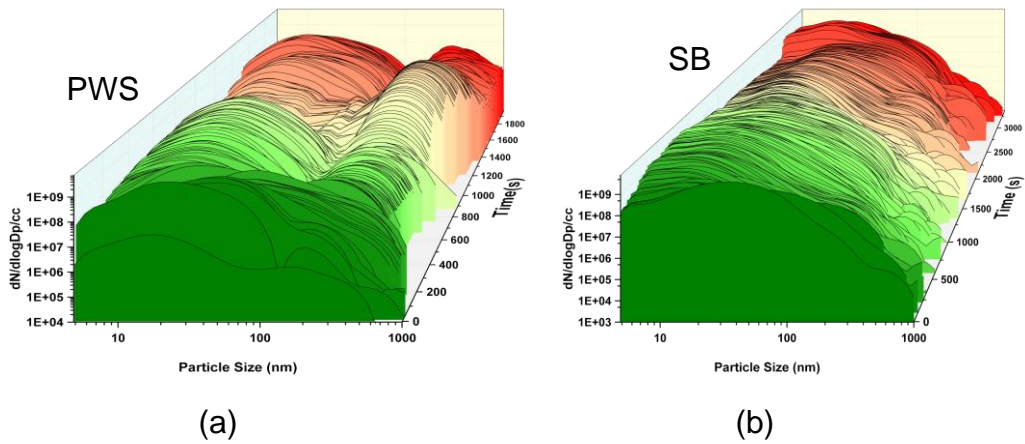


Figure 4-28 Particle Number and Size Distribution; PWS (a) and SB (b)

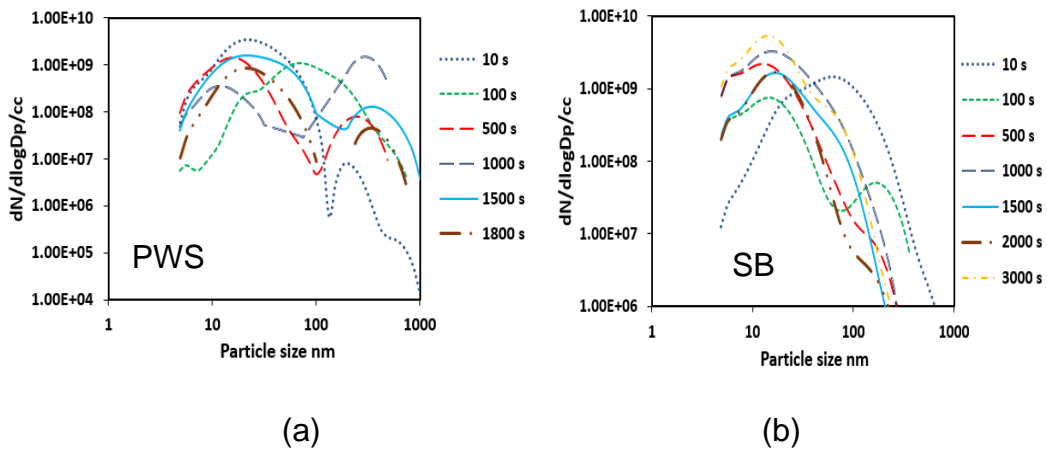


Figure 4-29 Particle Number and Size Distribution at Different times; PWS (a) and SB (b)

The number of particles for the two modes (nucleation and accumulation) 20 nm and 200 nm are compared in Fig. 4-30 as a function of time for both fires. The pine wood, 20 nm nuclei particle number was $10^9/cc$ at the start of the test but decreased after about 40 s and increased immediately after ignition (192 s) to maintain its peak at $10^9/cc$ for the first 900s. There was then a reduction to $1.4 \times 10^7/cc$ from 900 – 1400 s and then an increase to $1.5 \times 10^9/cc$ just around the flame out time. High numbers of 20 nm particles continued to be produced in the char burning phase, but there was a much-reduced accumulative mode particle number. The scaffolding board, 20 nm nuclei particle number was also $10^9/cc$ at the start of the test but there was a slight decrease after about 20 s and increased immediately after ignition to maintain its peak at $10^9/cc$ throughout the flaming combustion and a further increase after the flameout at 2600 s. High numbers of 20 nm particles continued to be produced in the char burning phase, but there was a much-reduced accumulative mode particle number. For both fires, the 20

nm particle number produced was 10^6 higher than those reported at the road side (1.8×10^4 to 3.4×10^4 / cm^3) [186] where the health hazards are known to be high. These results show that ultra-fine particulate emissions in fires from wood burning are a potential serious toxic impairment of escape hazard and materials should be evaluated for their propensity to form ultra-fine particles in fires.

The 200 nm accumulation mode particles for pine wood fire were produced at 1×10^8 /cc before the ignition and then reduced to 1×10^7 /cc after the ignition from 192 s to 900 s. There was then an increase at 900 – 1400 s to 1×10^9 /cc but decreased during the char burning phase. The scaffolding board produced 200 nm particles throughout the flaming phase in the range of 1×10^5 /cc – 1×10^6 /cc and then reduced to $< 1 \times 10^6$ /cc in the smoldering phase of the combustion. Particles 30 nm – 100 nm had lower concentrations than the 20 nm particles for both fires. The small size found in the present work is of great concern as that is where the greatest health hazard occurs. Particle number concentrations were highest when the heat release was at its peak and gradually decreased after the flameout.

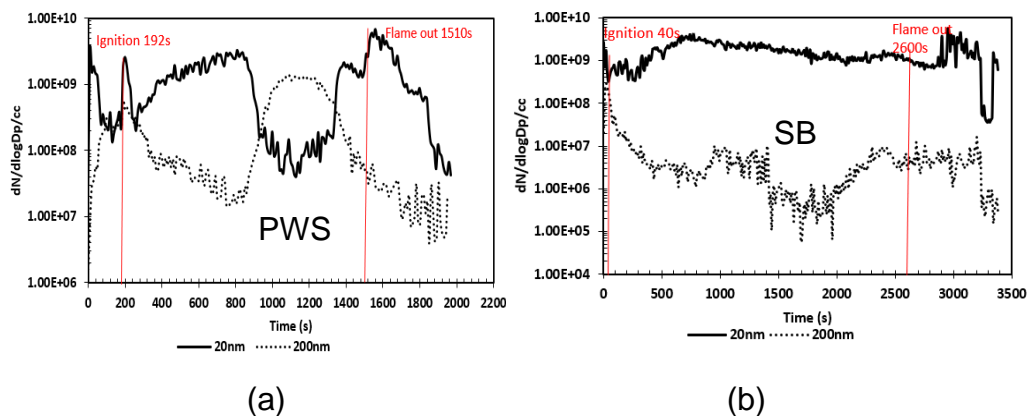


Figure 4-30 20 nm and 200 nm sizes particle number; PWS (a) and SB (b)

4.3.1.2 Particle Mass Concentration

The equivalent mass distributions for pine wood and scaffolding board fires are shown in Figs. 4-31 and 4-32. Figures 4-31 and 4-32 show that there was less mass in the ultrafine particle region as compared to the larger particles >100 nm. In terms of number, small particles in the nucleation mode constitute the majority of particles. However because of their small sizes, their contribution to the total mass of aerosols are very small and therefore that will mitigate potential significance of human health impact. Conversion from particle number to mass

involves assuming spherical particles of constant density of 1000 kg/m^3 , which gives high values of the bigger particles.

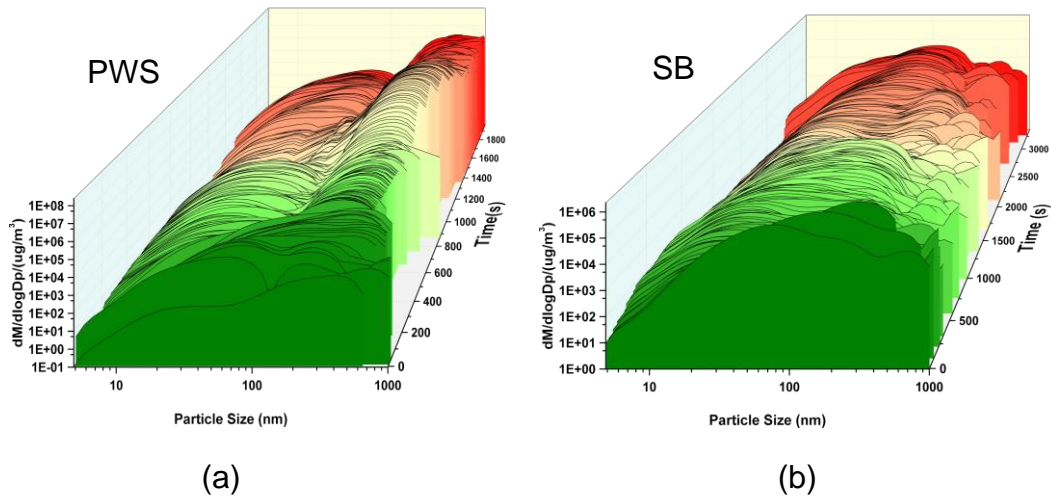


Figure 4-31 Particle Mass and Size Distribution; PWS (a) and SB (b)

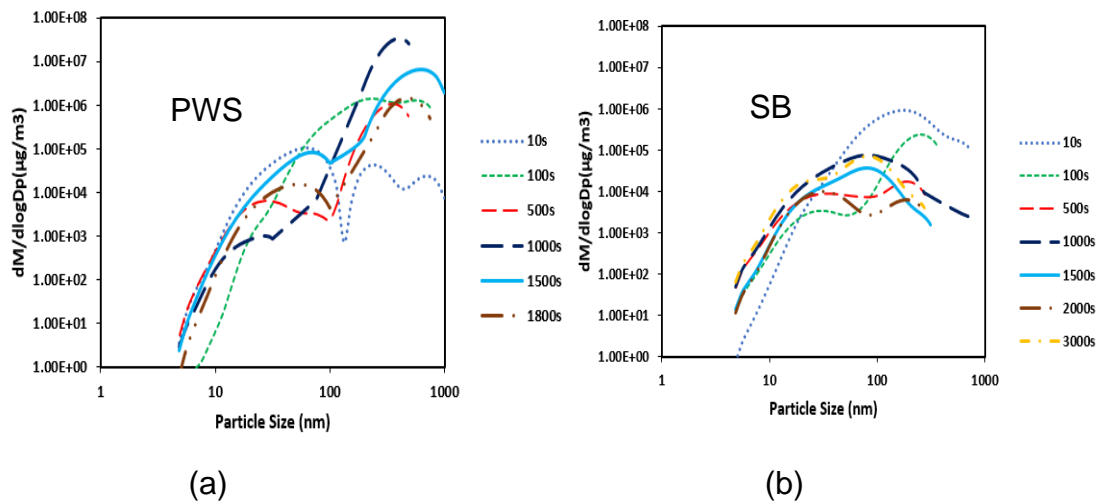


Figure 4-32 Particle Mass and Size Distribution at Different times; PWS (a) and SB (b)

Figure 4-33 shows that the pine wood 20 nm particle size had a mass of about 0.01 g/m^3 and that the 200 nm mode had a mass of 10 g/m^3 during the flaming phase of the combustion. The scaffolding board 20 nm and 200 nm particle size had similar mass of about 0.01 g/m^3 during the flaming phase of the combustion. It is also clear in Fig. 4-32 that for the pine wood, there is more particle mass above the 1000 nm upper measurement range of the Cambustion DMS500. In air quality legislation for particulate emissions the European 24 hour limit for $\text{PM}_{2.5}$ is $50 \mu\text{g}/\text{m}^3$ and the annual limit is $40 \mu\text{g}/\text{m}^3$. The 24 hour limit is a total particulate loading, for an average human breathing 10 m^3 of air per day, of 0.5

mg/day. Exposure to the present pine wood fires would give a lung loading of 0.1 g per day of 20 nm particles and 100 g per day of 200 nm particles while exposure to the scaffolding board would give a lung loading of 0.1 g per day for both particle sizes. This represents a major health risk to people who breathe wood based particulates in fires.

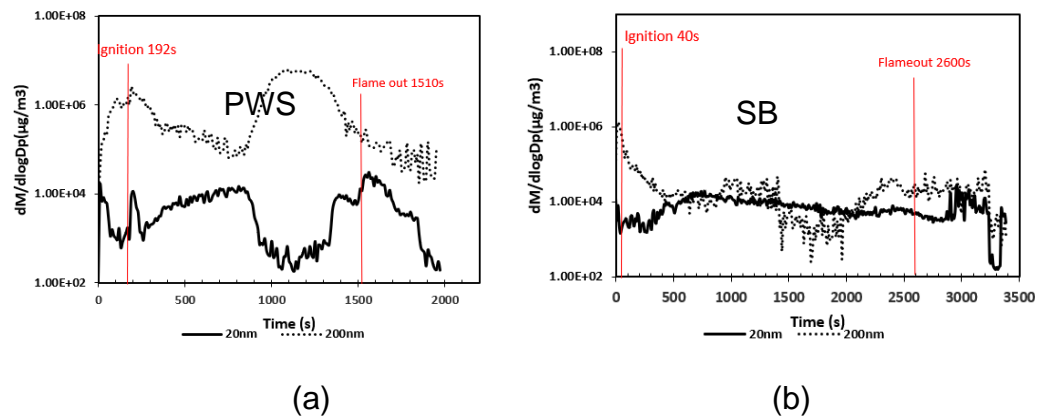


Figure 4-33 20 nm and 200 nm Sizes Particle Mass; PWS (a) and SB (b)

4.3.1.3 Particle Emission Index

Figure 4-34 shows the particle number for 20 nm and 200 nm particles as a function of the mass of wood burnt for the natural wood. This shows that for both particle sizes the particle number has a fairly constant relationship with the fuel mass burn rate. Figure 4-1b is responsible for the trends in particle number. Only in the smouldering combustion phase of the fire were the trends in particle number different for 20 and 200 nm, with an increase in yield of 20 nm particles and a decrease with 200 nm particles. The higher yield of the 20 nm particles was produced in both fires with the 20 nm particle for pine wood having a yield of between 4.4×10^{14} number/kg to 2×10^{18} number/kg while the 200 nm yield was between 1.2×10^{14} number/kg to 1.6×10^{16} number/kg. The scaffolding board produced a 20 nm yield of between 5×10^{15} number/kg to 1.2×10^{18} number/kg while the 200 nm yield was between 1.8×10^{13} number/kg to 8×10^{16} number/kg. The pine wood produced more particles than the scaffolding board.

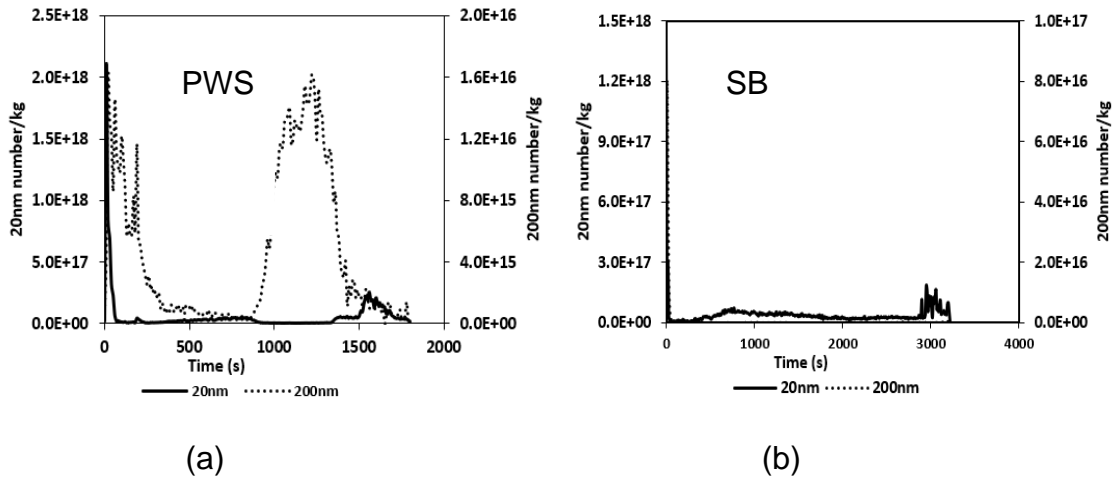


Figure 4-34 Particle Number per Mass of Fuel Burnt for 20 nm and 200 nm Particles; PWS (a) and SB (b)

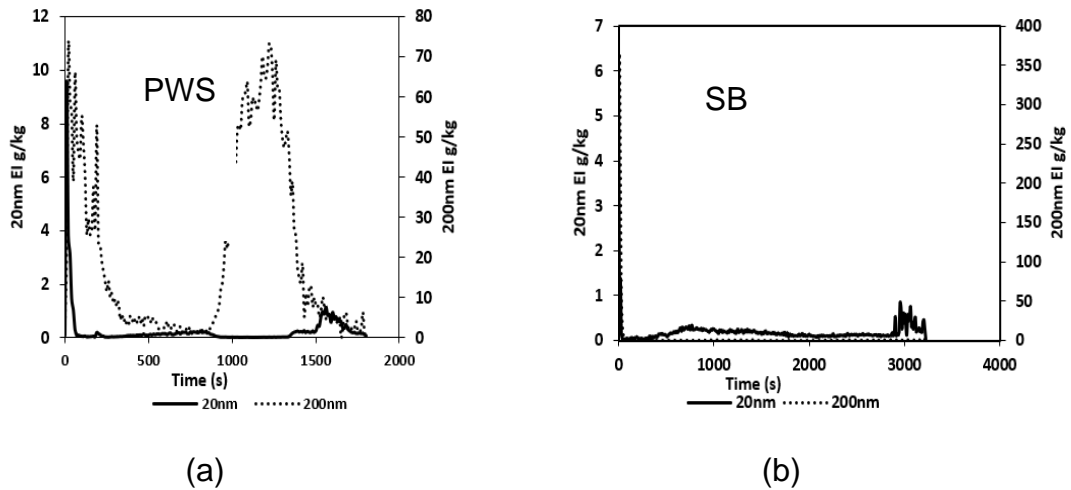


Figure 4-35 Particle Mass per Mass of Fuel Burnt for 20 nm and 200 nm Particles; PWS (a) and SB (b)

The particle mass per unit mass of fuel burned shows the 20 nm particle for pine wood having a yield of between 0.006 g/kg to 9.5 g/kg while the 200 nm yield was between 0.6 g/kg to 73 g/kg. The scaffolding board produced a 20 nm yield of between 0.1 g/kg to 6 g/kg while the 200 nm yield was between 0.02 g/kg to 360 g/kg.

4.3.2 Processed Wood

4.3.2.1 Particle Number Concentration

The particle number concentration as a function of size and time for OSB from the start of the test to the end of sampling is shown in Fig. 4-36. Figure 4-37 shows some individual size distributions at defined times, where it is easier to

read the particle number. A bimodal distribution of the particle sizes was observed indicating the nucleation mode and accumulation mode of the particle size distribution. The initial particle size distribution during the ignition delay period (69 s) showed nano particles with a peak at 10 nm and the larger particles with a peak of 300 nm. After about 200 s, the nuclei mode was found to peak at 20 nm and the accumulation mode peaked at 200 nm. The number based size distribution was reasonably consistent from 300 to 1000s, which falls within the main flaming combustion period. The particle concentrations were highest at the peak HRR of 200 kW/m². There were differences in size distribution in the char burning phase of the fire, with a reduction in the number of accumulation mode particles.

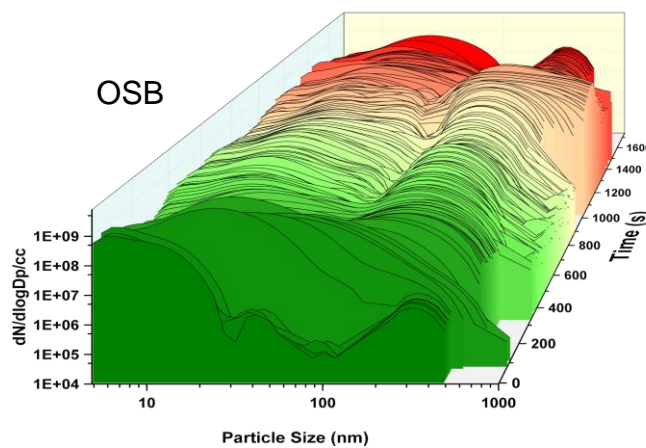


Figure 4-36 Particle Number and Size Distribution; OSB

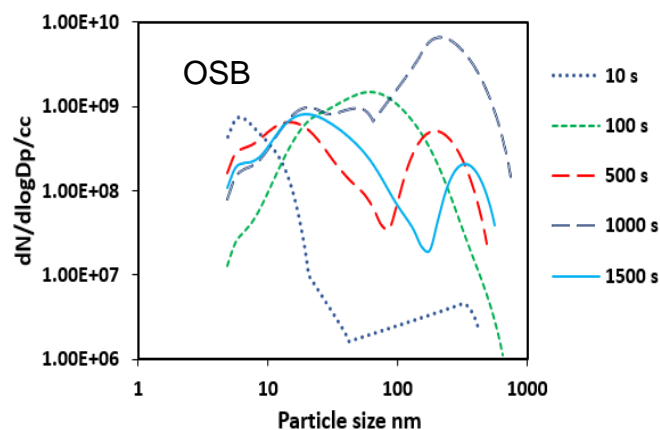


Figure 4-37 Particle Number and Size Distribution at Different times; OSB

The number of particles for the two modes (nucleation and accumulation) 20 nm and 200 nm are compared in Fig. 4-38 as a function of time. The 20 nm nuclei particle number was $10^9/\text{cc}$ at the start of the test but decreased about 30 s after ignition (120 s) to $10^8/\text{cc}$ for about 500 s and maintained its peak of $10^9/\text{cc}$ afterwards. There was then a reduction to $3.5 \times 10^8/\text{cc}$ from 1070 – 1240 s and then an increase to $1.4 \times 10^9/\text{cc}$ just around the flame out time. High 20 nm particles continued to be produced in the char burning phase, but there was a much-reduced accumulative mode particle number. These results show that ultra-fine particulate emissions in fires from wood burning are a potential serious toxic impairment of escape hazard and materials should be evaluated for their propensity to form ultra-fine particles in fires.

The 200 nm accumulation mode particles were not produced until after ignition and these were produced at $1 \times 10^8/\text{cc}$ with an increase to $1 \times 10^9/\text{cc}$ from 700 s to 1200 s. There was then a decrease to $1 \times 10^7/\text{cc}$ during the char burning phase. The small size found in the present work is of great concern as that is where the greatest health hazard occurs. Particle number concentrations were highest when the heat release was at its peak and gradually decreased after the flameout.

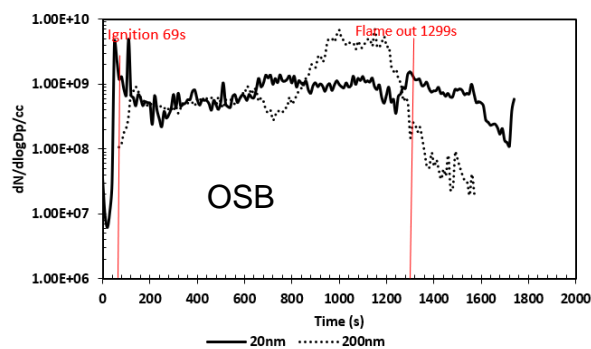


Figure 4-38 20 nm and 200 nm sizes particle number; OSB

4.3.2.2 Particle Mass Concentration

Figure 4-39 shows the mass distribution of OSB as a function of size and time. This shows that there was less mass of the smaller particles as compared to the larger particles and therefore that will mitigate potential significance of human health impact. Some individual mass distribution at defined times is presented in Fig. 4-40.

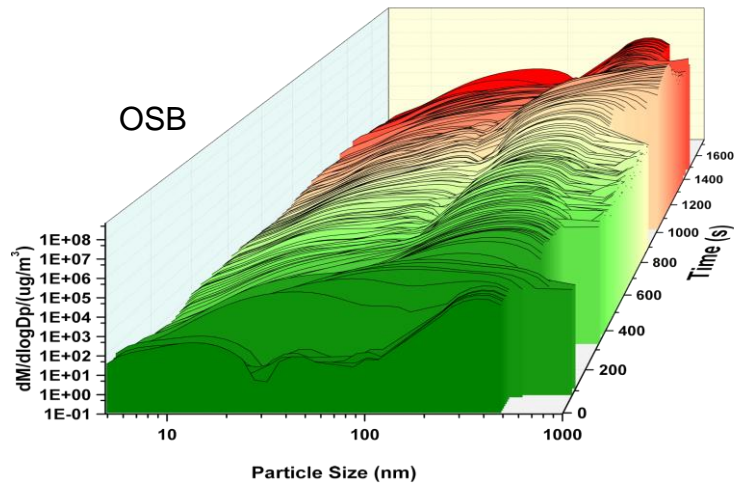


Figure 4-39 Particle Mass and Size Distribution; OSB

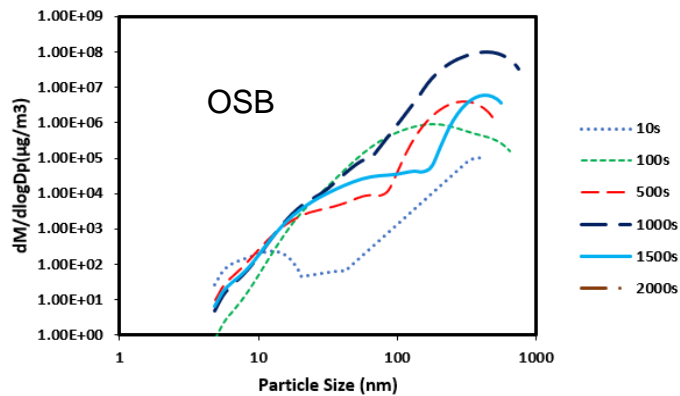


Figure 4-40 Particle Mass and Size Distribution at Different times; OSB

Figure 4-41 shows that the 20 nm particle size had a mass of about 0.02 g/m³ for the first 100 s and then reduced to 0.0045 g/m³ throughout the flaming combustion. The particle mass reduced during the char burning phase. The 200 nm accumulation mode particles were not produced until after ignition and these produced a mass of 3.8 g/m³ with an increase to 22 g/m³ from 700 s to 1200 s. There was then a decrease to 0.1 g/m³ at the end of sampling. The processed wood also produced particles that represents a major health risk to people who breathe wood based particulates in fires.

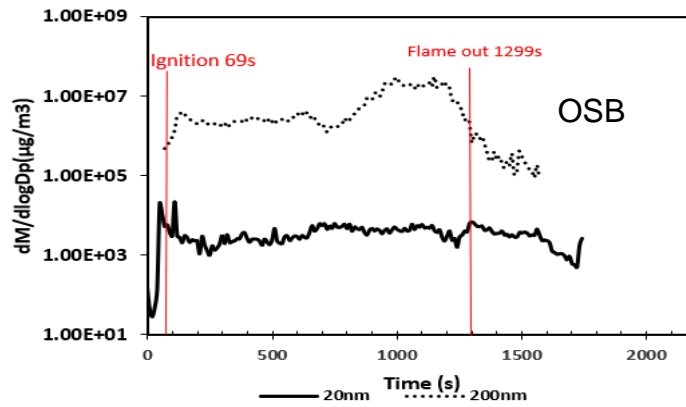


Figure 4-41 20 nm and 200 nm Sizes Particle Mass; OSB

4.3.2.3 Particle Emission Index

Figure 4-42 shows the particle number for 20 nm and 200 nm particles as a function of the mass of wood burnt. This shows that for both particle sizes the particle number has a fairly constant relationship with the fuel mass burn rate. The equivalence ratio is responsible for the trends in particle number. The two modes 20 nm and 200 nm showed different times when the maximum yield was produced, with the 20 nm particle size having its highest yield at the ignition delay period while the 200 nm particle size having its highest yield at the 2nd peak of the mass burn rate. At the smouldering combustion phase of the fire, 20 nm yield was slightly higher than the 200 nm yield. A higher yield of the 20 nm particles was produced, of about 4.3×10^{17} number/kg during the ignition delay period while the 200 nm yield was about 6.2×10^{16} number/kg. These high yields of ultrafine particles can lead to the impairment of escape when a fire occurs.

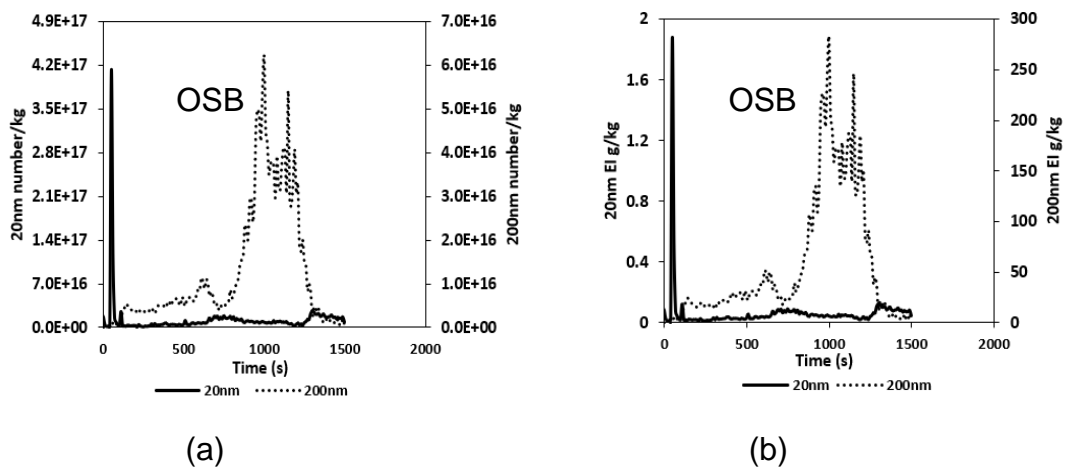


Figure 4-42 Particle Number and Mass per Mass of Fuel Burnt for 20 nm and 200 nm Particles; OSB

The particle mass per unit mass of fuel burned shows the 20 nm particle for OSB wood having a yield of 2 g/kg at the ignition delay period while the 200 nm yield was about 280 g/kg.

4.3.3 Plywood

4.3.3.1 Particle Number Concentration

Figure 4-43 shows the particle number concentration and size distributions for plywood A and plywood B from the start of the test to the end of sampling. Some individual size distribution at defined times and easier to read are shown in Fig. 4-44. The initial particle size distribution during the ignition delay period showed only nano particles with a peak at 20 nm for both plywood A and plywood B. These are likely to be liquid hydrocarbon aerosols and the high peak in THC in this period supports this. Once flaming combustion started there was a bimodal size distribution of nuclei particles centered on 20 nm and accumulation mode particles centered on 200 nm. The number-based size distribution for plywood A was reasonably consistent from 200 to 1360 s, which is the main flaming combustion period while in plywood B, it was consistent from 200 to 1000 s also representing the main flaming combustion period. There were differences in size distribution in the char burning phase of the fire, with a reduction in the number of accumulation mode particles.

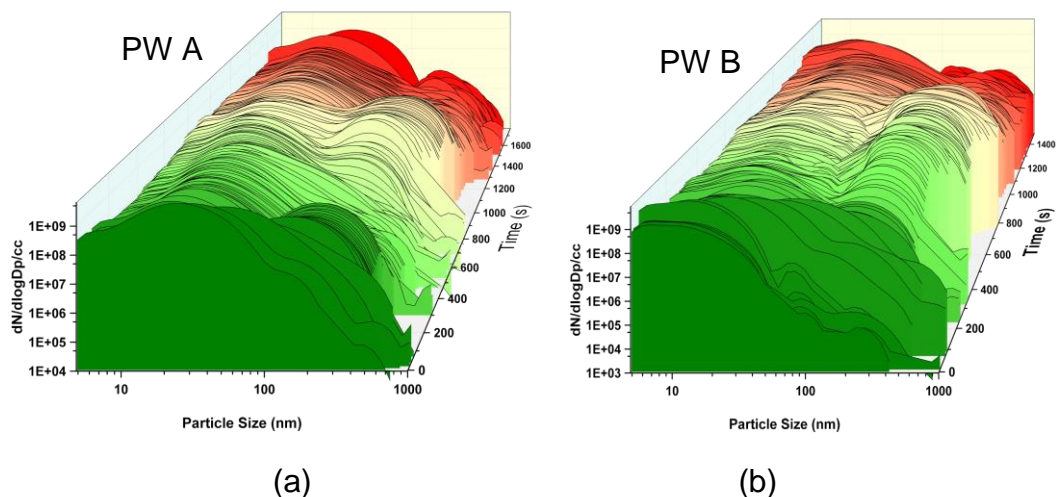


Figure 4-43 Particle Number and Size Distribution; PW A (a) and PW B (b)

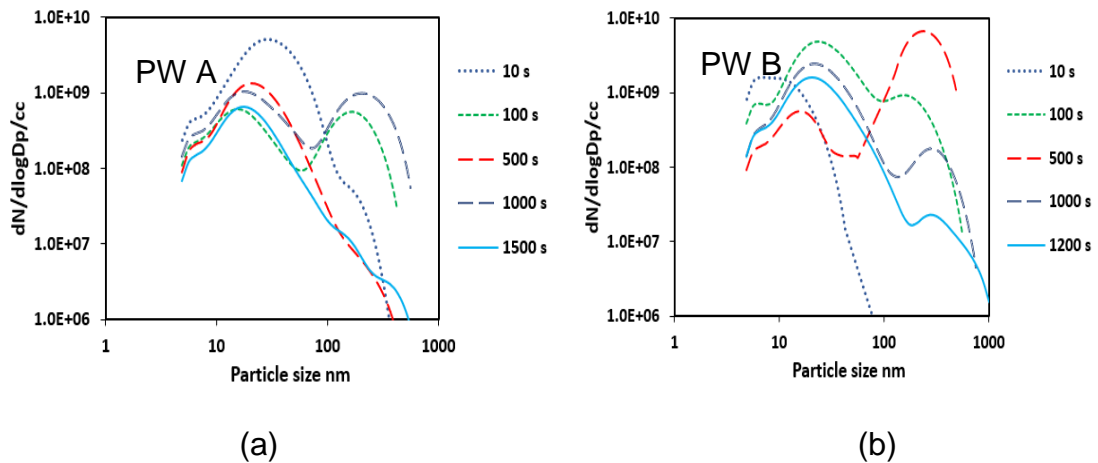


Figure 4-44 Particle Number and Size Distribution at Different times; PW A (a) and PW B (b)

Figure 4-45 shows as a function of time, the 20 nm and 200 nm sizes particle number, as characteristic of the nuclei and accumulative mode particles for the two wood samples. The 20 nm nuclei particle number for plywood A decreased from $10^9/cc$ to $10^8/cc$ after ignition (54 s) but increased after about 200 s to maintain $10^9/cc$. There was then a reduction to $10^8/cc$ just before the flame out. High 20 nm particles continued to be produced in the char burning phase, but there was a much-reduced accumulative mode particle number. Plywood B also produced 20 nm nuclei particle number of $> 10^9/cc$ during the ignition delay phase but decreased in number after ignition for a short period of time and then increased for 100 s before decreasing to $10^8/cc$ from 320 to 600 s. It increased and maintained the $10^9/cc$ until the char burning phase where the particle number was reduced but still very high.

The 200 nm accumulation mode particles for plywood A were produced at $1 \times 10^8/cc$ during the ignition delay period, but decreased to $> 1 \times 10^6/cc$ throughout the steady state burning phase and then an increase to $> 1 \times 10^8/cc$ after 600 s which lasted for 200 s. There was a decrease in the smouldering phase of the combustion to $> 1 \times 10^6/cc$. Particles 30 nm – 100 nm had lower concentrations than the 20 nm particles. The 200 nm accumulation mode particles for plywood B were produced at $> 1 \times 10^4/cc$ during the ignition delay period, but increased to $> 1 \times 10^8/cc$ for 90 s and then decreased to $> 1 \times 10^6/cc$ with a sudden increase to $> 1 \times 10^9/cc$ from 300 to 850 s. The 200 nm particle decreased to $> 1 \times 10^6/cc$ during the char burning phase. As in the case of plywood A, particles

30 nm – 100 nm had lower concentrations than the 20 nm particles. These plywood samples produced ultra-fine particles of great concern as that is where the greatest health hazard occurs. Particle number concentrations were highest when the heat release was at its peak and gradually decreased after the flameout. Figure 4-46 shows how the equivalence ratio is responsible for the trends in particle number. Plywood B produced more particles than plywood A.

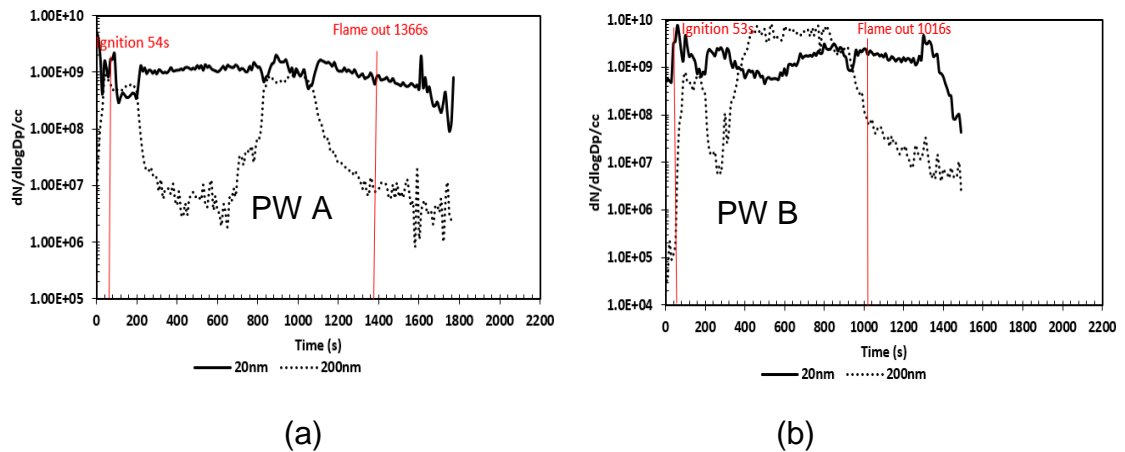


Figure 4-45 20 nm and 200 nm sizes particle number; PW A (a) and PW B (b)

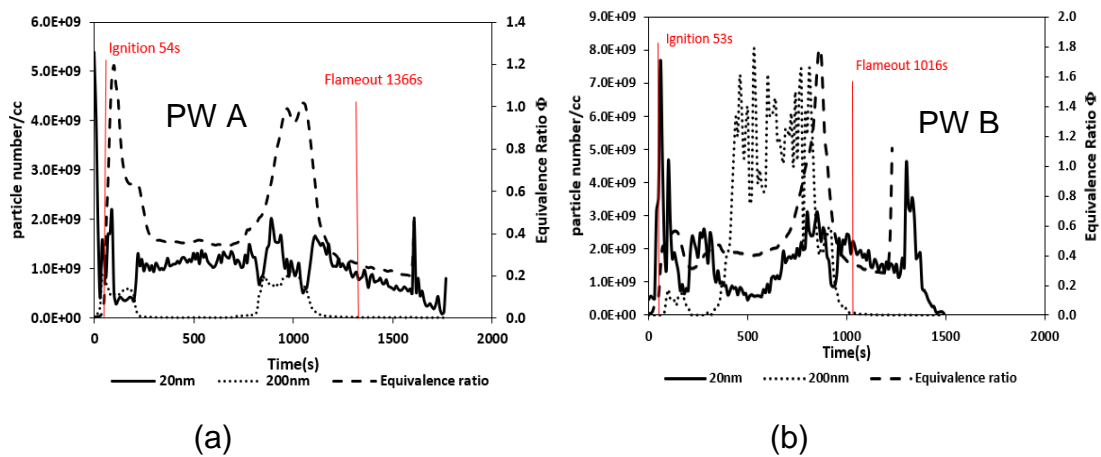


Figure 4-46 Particle Number per Volume Compared with the Equivalence Ratio Variation with Time; PW A (a) and PW B (b)

4.3.3.2 Particle Mass Concentration

Figure 4-47 to 4-49 show that the plywood A 20 nm particle size had a mass of about 0.01 g/m³ and that the 200 nm mode had a mass of 5 g/m³ during the flaming phase of the combustion. The plywood B 20 nm and 200 nm particle size had mass of about 0.01 g/m³ and 30 g/m³ during the flaming phase of the combustion. It is also clear in Fig. 4-49 that for the plywood B, there is more

particle mass above the 1000 nm upper measurement range of the Cambustion DMS500. Plywood B produced a higher mass of 200 nm particles than plywood A by a factor of 6 as a peak production value. This shows that different plywoods may produce different concentrations of particles even though they were tested under the same burning condition.

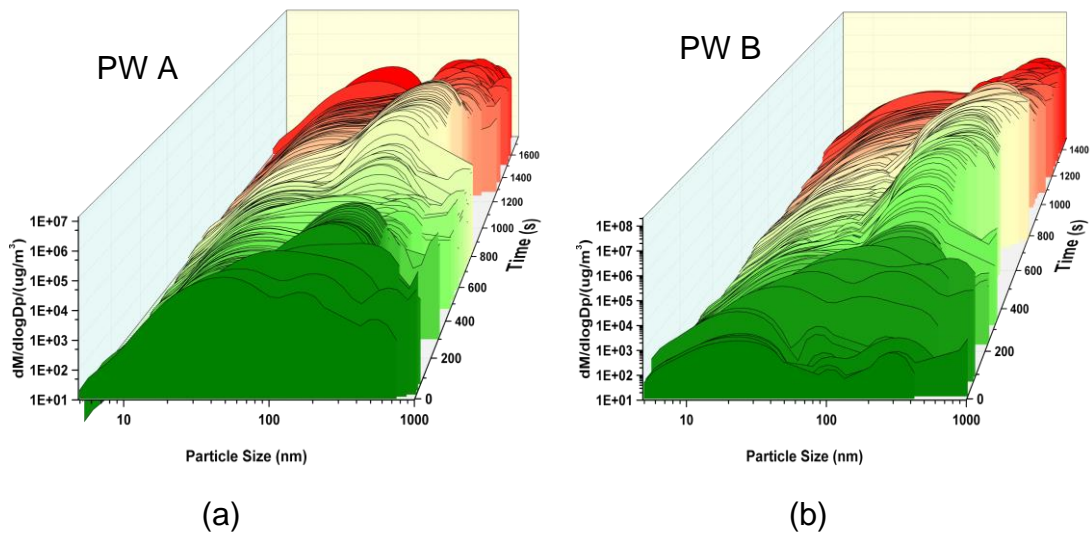


Figure 4-47 Particle Mass and Size Distribution; PW A (a) and PW B (b)

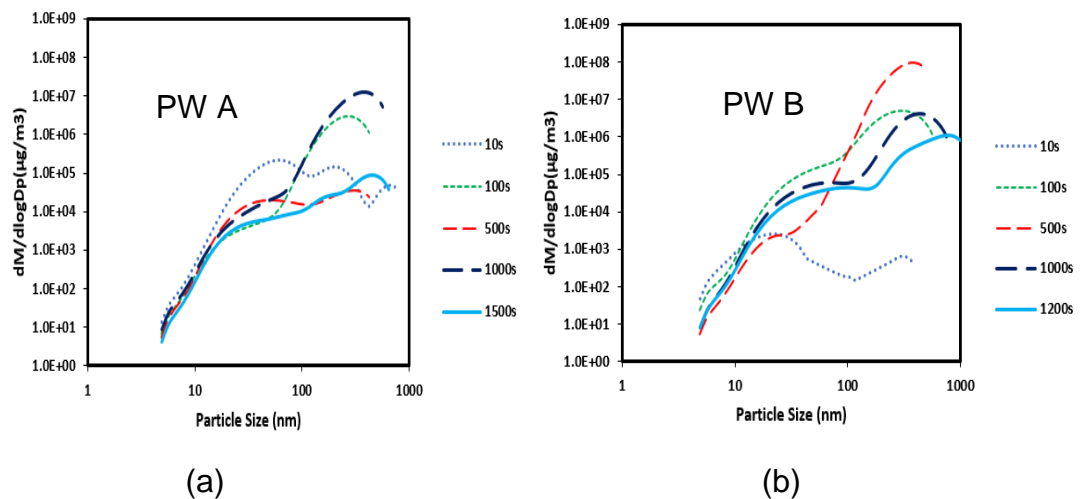


Figure 4-48 Particle Mass and Size Distribution at Different times; PW A (a) and PW B (b)

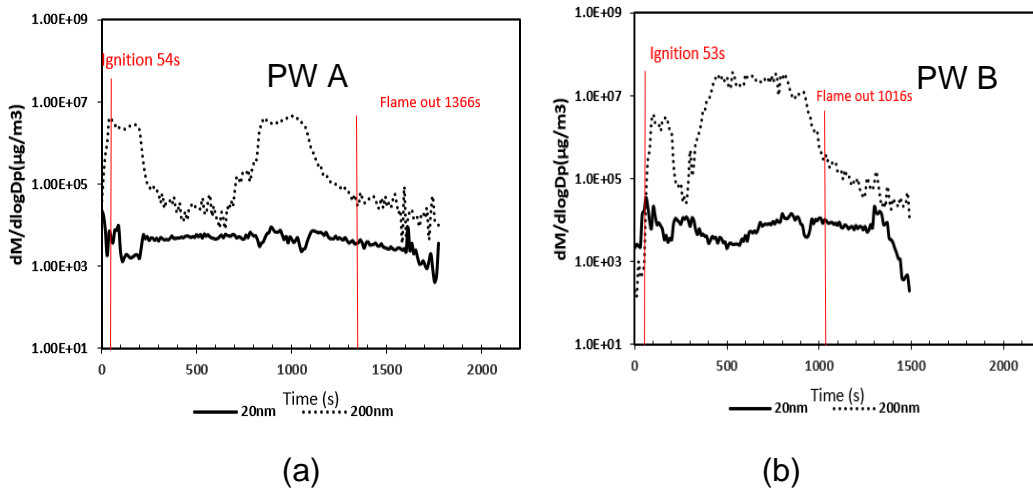


Figure 4-49 20 nm and 200 nm Sizes Particle Mass; PW A (a) and PW B (b)

4.3.3.3 Particle Emission Index

Figure 4-50 shows the particle number for 20 nm and 200 nm particles as a function of the mass of wood burnt for plywood A and B. This shows that for both particle sizes the particle number has a fairly constant relationship with the fuel mass burn rate. Only in the smouldering combustion phase of the fire were the trends in particle number different for 20 and 200 nm, with an increase in yield of 20 nm particles and a decrease with 200 nm particles. Higher yield of the 20 nm particles was produced in both fires at the ignition delay period with the 20 nm particle for plywood A having a yield of 3.1×10^{18} number/kg while the 200 nm yield was between 1.55×10^{17} number/kg. Plywood B produced a 20 nm yield of about 2.2×10^{17} number/kg during the ignition delay while the 200 nm yield was low. Higher yield of 200 nm particles was produced of about 8.8×10^{16} number/kg, corresponding to the time the heat release rate was at its peak.

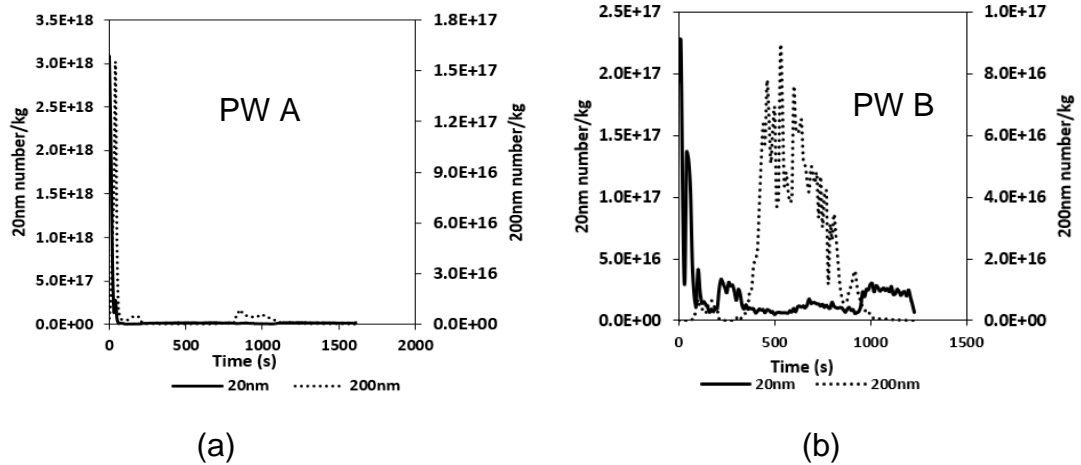


Figure 4-50 Particle Number per Mass of Fuel Burnt for 20 nm and 200 nm Particles; PW A (a) and PW B (b)

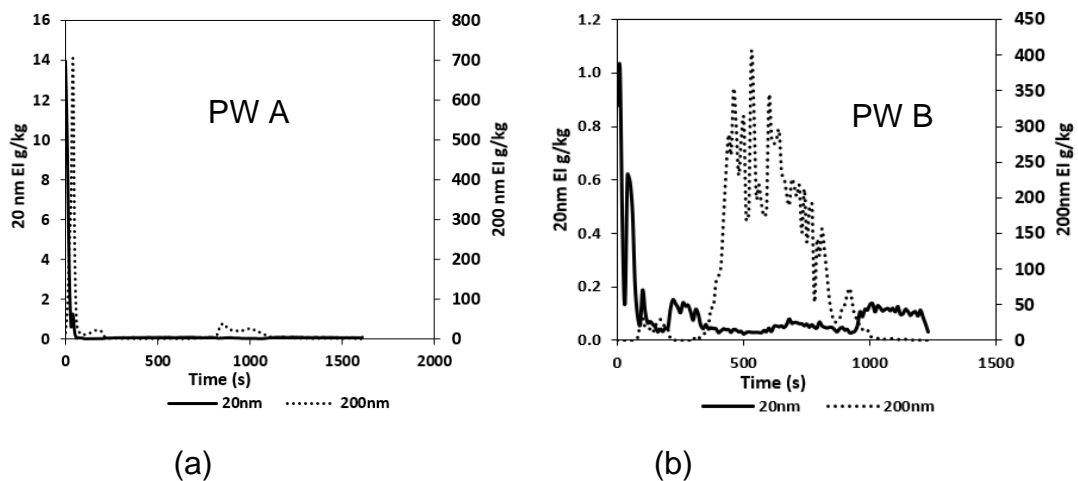


Figure 4-51 Particle Mass per Mass of Fuel Burnt for 20 nm and 200 nm Particles; PW A (a) and PW B (b)

The particle mass per unit mass of fuel burned in Fig. 4-51 shows the 20 nm particle for plywood A having a yield of 14 g/kg while the 200 nm yield was about 700 g/kg, both during the ignition delay period. The plywood B however produced a 20 nm yield of about 1 g/kg during the ignition delay period and a much lower yield during the steady burning phase, while the 200 nm yield was as high as 400 g/kg at the time the heat release rate and mass burn rate were at their peak.

4.4 Comparison Between the Natural Wood and Processed Wood

This work investigated the toxic gas emissions from three different types of processed wood; Oriented Strand Board (OSB), Medium density fiberboard

(MDF) and Chipboard faced with white melamine (CFM). Construction pine wood sticks (PWS) were used as a non-processed wood comparison. The standard cone calorimeter was used with “raw” (pre-dilution) hot gas sampling, using an 80 mm diameter chimney mounted on top of the cone heater exit. Heated gas sampling and heated Gasmeter FTIR toxic gas analysis was used with a 20-hole mean gas sample probe at the conical heater outlet plane. Each wood sample was exposed to the conical heater of the cone calorimeter radiating at 35 kW/m² and the ignition delay for the 4 samples was 69 s (OSB), 142 s (CFM), 54 s (MDF) and 192 s (PWS). The much longer ignition delay for pine wood compared with the processed woods OSB and MDF was shown to result in earlier toxic gas release in these processed woods. Also it was shown that significant toxic gases were released from pine wood prior to the auto-ignition time. The early release of toxic gases in these fires is of concern as if this occurred in a real fire then toxic gases would be released during the period of escape. The fires continued until flaming combustion ceased and there was only char burning. It was shown that this transition from flaming combustion to char smouldering combustion was associated with a change in the release of toxic gases.

4.4.1 Mass Loss, Equivalence Ratio and Heat Release Rates (HRR)

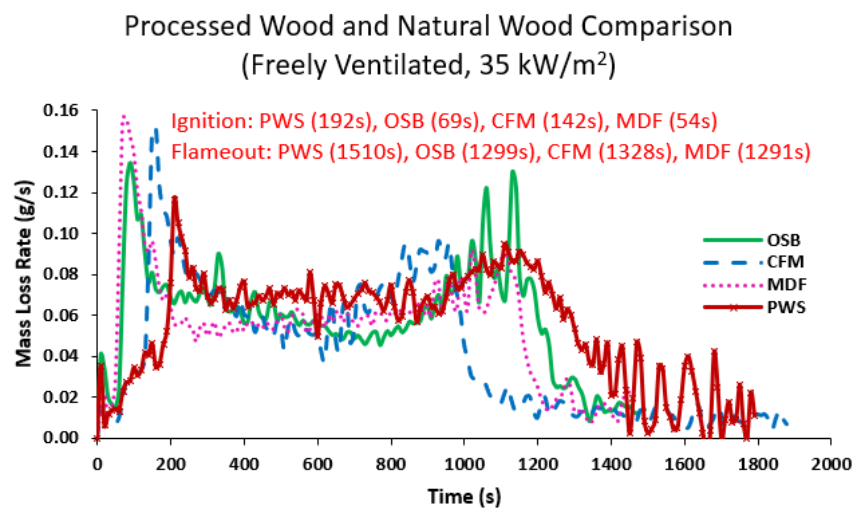
Figure 4-52 shows that the ignition delay was much shorter for the MDF fire, due to the richer mixtures during the delay period, as shown in Fig. 4-52b. The chipboard faced with melamine (CFM) and the reference pine wood sample (PWS) had a prolonged ignition delay of 142 s and 192 s respectively compared with 54 and 69 s for MDF and OSB respectively. The melamine facing delayed the thermal decomposition of the processed wood and thermal conduction in pine slowed the surface heating rate, where the initial volatiles were released. All the process wood materials had a mass loss rate at steady state of 0.05 - 0.06 g/s with a much slower burn rate during the char burn phase from around 1100 s. Pine wood at steady state burning had the highest mass loss rate of 0.07 g/s.

Carbon balance equivalence ratios showed that rich mixtures occurred in MDF and CFM processed woods early after ignition. This was due to their rapid release of volatiles, shown by the high mass loss rate early in the fires. These rich mixtures indicate that some features of confinement of fires were found in

the raw cone exit gas analysis. These rich mixtures produced high concentrations of toxic gases, as shown in Fig. 4-53.

The primary heat release rate (HRR) in the cone calorimeter was determined from the measured chimney oxygen concentration. The chimney flow rate was determined from the overall cone calorimeter equivalence ratio by carbon balance, together with the raw gas equivalence ratio which enable the dilution ratio to be determined. The cone calorimeter mass flow is controlled by the cone calorimeter and so the total mass of chimney flow can be determined. As the fuel mass consumption rate is measured, this enables the entrained air flow into the primary cone combustion to be determined and hence the inlet oxygen mass flow determined. The chimney oxygen measurement and chimney mass flow then enabled the oxygen mass consumption and the primary HRR to be determined.

The 4 samples had similar total peak HRR ($180\text{--}200\text{ kW/m}^2$), but the time variation of HRR was different with the CFM and PWS having a slower growth of the fire to the peak HRR than CFM and PWS. This was due to the longer ignition delays for CFM and PWS. Figure 4-52c shows two peaks in the primary HRR for all materials tested.



(a)

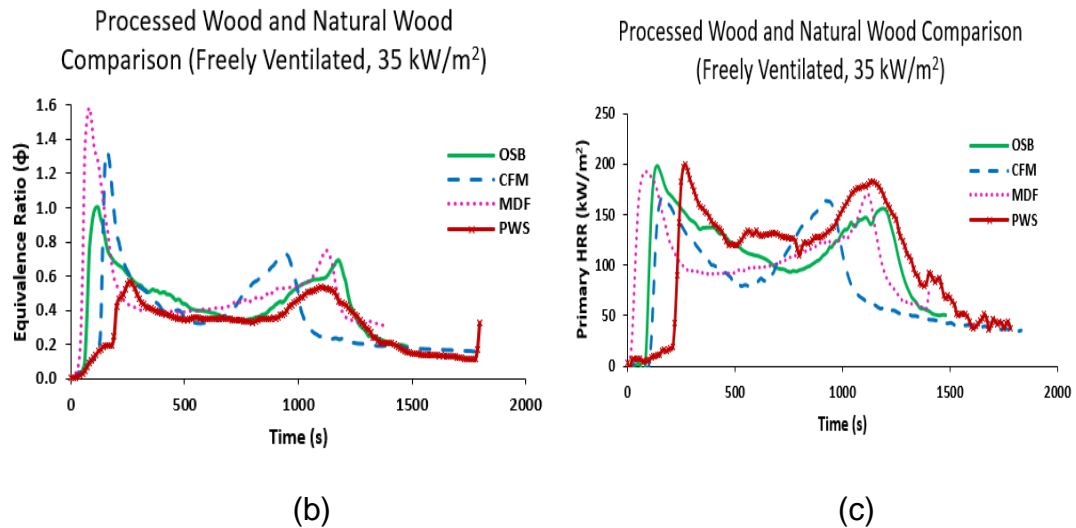


Figure 4-52 Mass loss rate (a), Equivalence ratio (b) and Heat release rate (HRR) (c)

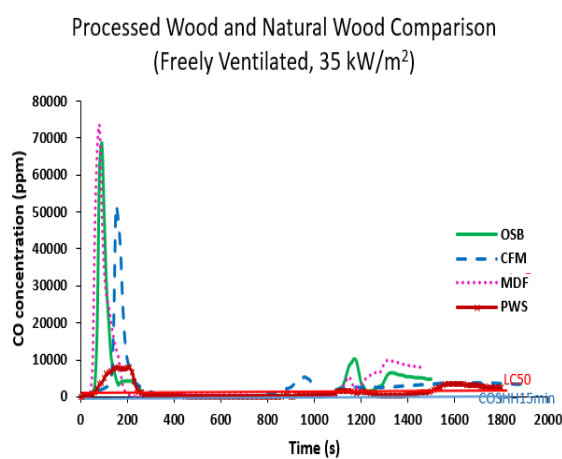
The mass loss rate in Fig. 4-52a and the equivalence ratio in Fig. 4-52b both show two peaks at the same time as the two peaks in primary HRR. The first peak was the combustion of the volatiles released from the processed woods and from pine. This was earlier for all the processed woods than for pine wood, which could be due to the composition of the woods. The second primary HRR peak in Fig. 4-52c was always lower than the first peak and occurred later in the fire just before flame combustion ceased. Pine wood (PWS) had the highest primary HRR in this second fire phase. This second HRR peak occurred because of the combustion of char with its higher GCV than wood as a whole. However, once the fire had propagated through the unburnt material to the rear face there was no more release of volatiles and flame combustion of char ceased and there was a transition to smouldering char combustion with much lower HRR. It will be shown that the toxic gases were primarily associated with the first flaming combustion phase of the fire. There was a second toxicity peak with the second peak in HRR, but this was of much lower importance than the first peak.

4.4.2 Toxic Gas Concentrations

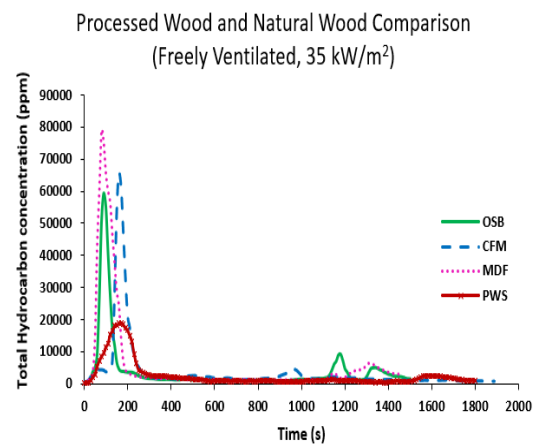
The six most important toxic gases are compared for the four wood samples in Fig. 4-53. This shows that for all materials and for all toxic gases the peak toxicity occurred in the flaming combustion phase of the fires over the first 300 s of the fires. The initial flaming fire burnt the volatiles released early in the fires. There was a second much smaller peak in toxicity that occurred at the second peak in

HRR in Fig. 4-52c. This early release of toxic gases for all fires is of concern as this will occur during the period of escape from fires, whereas the second smaller peak in toxicity is of less concern as evacuation of the building should be complete before this toxic gas release occurs.

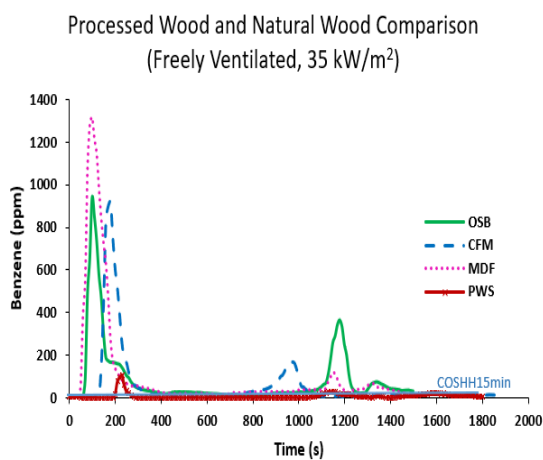
High concentrations of toxic gases were released during the ignition delay where pyrolysis gases were being released without combustion, this was particularly the case for pine wood (PWS) with the longest ignition delay. Toxic gases for all the processed woods and pine wood were high during the first peak in the primary HRR, due to the occurrence of the richest mixtures in the initial phase of the fire. OSB had formaldehyde and acrolein concentrations higher than the other samples by a factor of four. The most important toxic species were: CO, acrolein, formaldehyde, benzene and HCN, on both an LC₅₀ and COSHH_{15min} basis, which is used as an indicator of impairment of escape.



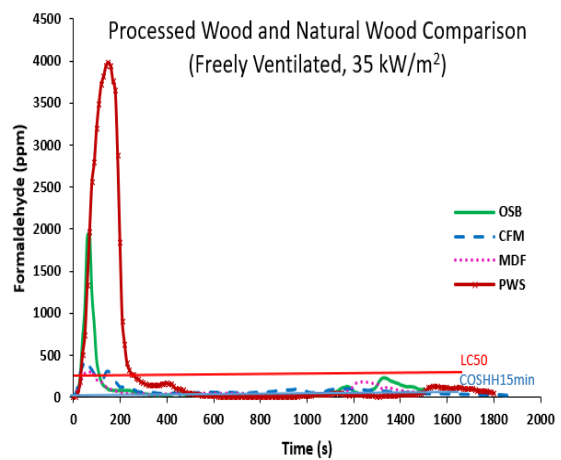
(a)



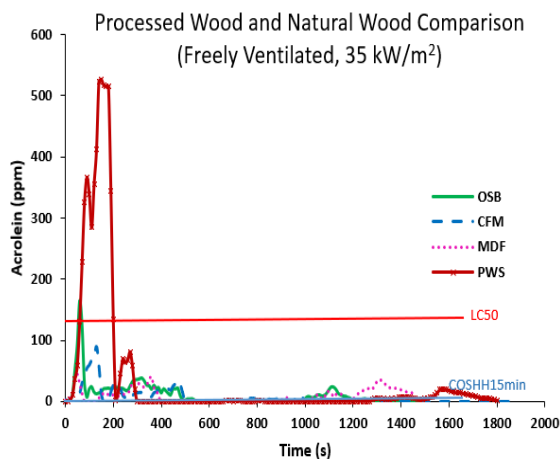
(b)



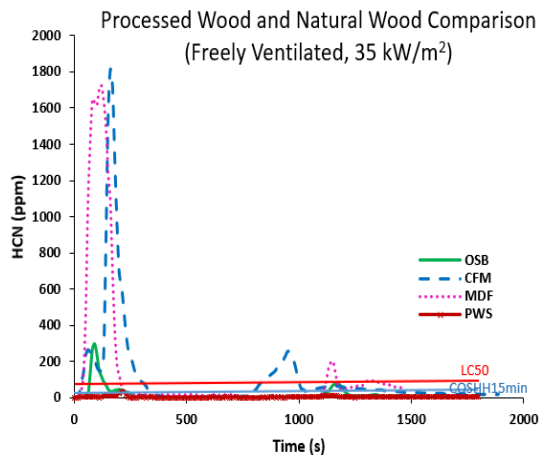
(c)



(d)



(e)



(f)

Figure 4-53 Toxic gas concentrations; CO (a), Total Hydrocarbon (b), Benzene (c), Formaldehyde (d), Acrolein (e) and Hydrogen Cyanide (f).

HCN concentration was very low for OSB and PWS which was expected from the low nitrogen content in Table 3-6. The CFM and MDF had high organic nitrogen in Table 3-6 and high HCN in Fig. 4-53f. The high nitrogen content in the CFM and MDF was due to their composite structure with glued chips, particles or fibres. All concentrations exceeded the toxic limits in terms of LC₅₀ and COSHH_{15 min} for all toxic species in Fig. 4-53, except for benzene LC₅₀ which is a concentration limit of 10,000 ppm.

An unexpected feature of the results was the quite different toxic gas importance for pine wood (PWS) compared with the processed woods which was due to the long ignition delay that led to high concentration of formaldehyde and acrolein. Figure 4-53 shows that PWS had much higher toxic emissions of formaldehyde and acrolein than processed woods and much lower emissions of the other four toxic gases. This resulted in PWS being the most toxic material on COSHH_{15min} impairment of escape basis.

4.4.3 Total Toxicity

The total toxicity **N** for the 4 wood samples are shown in Fig. 4-54 as a function of time. This shows a similar variation of **N** with time for the COSHH_{15min} and LC₅₀ toxic assessments and both assessment methods show that the initial flaming combustion phase of the fire dominates the total toxicity in terms of death risk and impairment of escape risks. At the early combustion stage (140-200 s), lethal levels of 30-minute exposure toxicity were produced in these wood fires and the COSHH_{15min} toxicity levels indicate that impaired escape would occur for the entire duration of the fire, even though the fire burned lean for most of the time. The dilution required to prevent 30-minute LC₅₀ exposure levels from being lethal was about 30-40 indicating that people exposed to these gases would be at risk of death. Impairment of escape would be a much more significant effect as these toxic gases need to be diluted by over 1000 for the CFM fire and over 2000 for OSB and MDF before these gases would not impair escape.

Pine wood (PWS) had the worst **N** for impairment of escape, roughly three times higher than for the nearest processed woods. This was because of the much high formaldehyde and acrolein emissions for pine wood. In terms of risk of death pine wood was safer than all the processed woods, but was still a significant risk in the early stage of the fires. Later in the fires the total toxicity was much lower, but still lethal in the period around the second peak in primary HRR. Also impairment of escape **N** was higher than unity for all times in the fire, and over 100 in the second primary HRR peak time region.

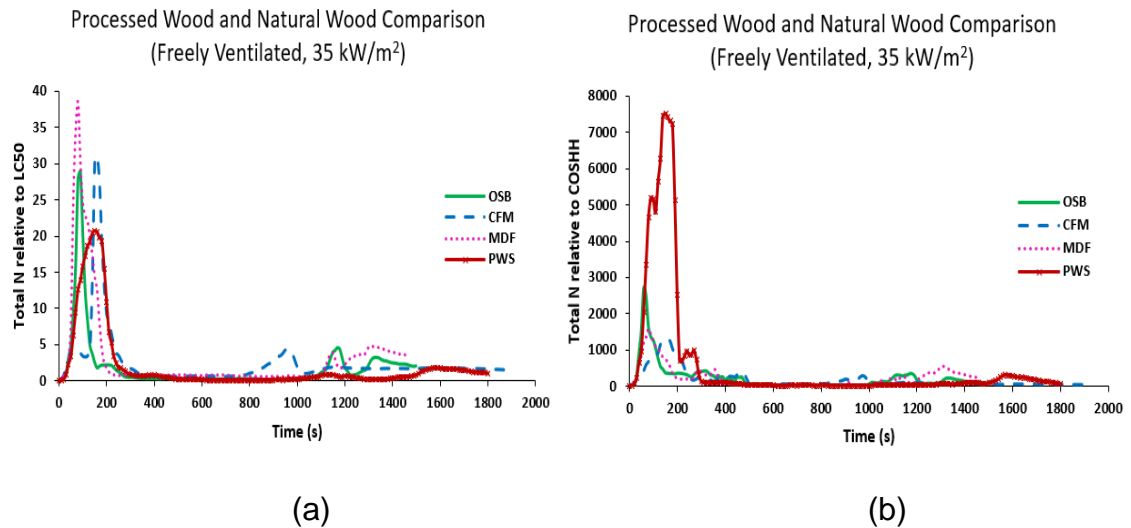
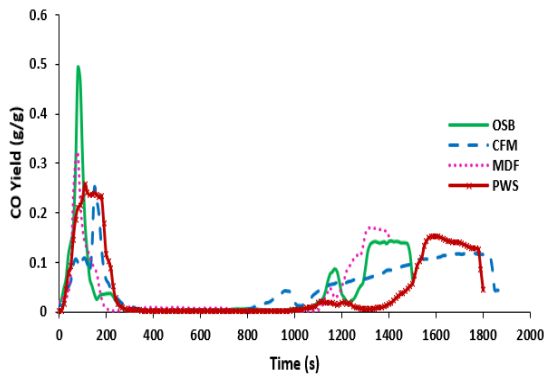


Figure 4-54 Total toxicity N relative LC₅₀ (a) and relative to COSHH_{15 min} (b)

4.4.4 Toxic Gas Yields

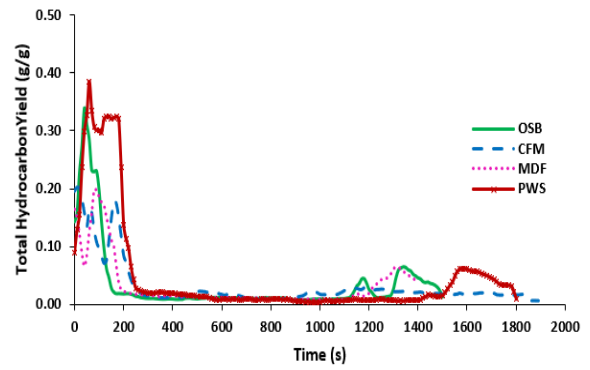
The yields for the key toxic gases and their variations with time are shown in Fig. 4-55. CO yield was higher in the initial stages with a reduced yield during the char burning phase as shown in Fig. 4-55a. OSB had the highest CO yield with a peak of 0.5 g/g (500 g/kg) followed by MDF with a yield of 0.32 g/g (320 g/kg) and CFM and pine produced similar yield of 0.25 g/g (250 g/kg). The total unburnt hydrocarbon yields are shown in Fig. 4-55b. These were much higher in the initial volatile burning phase and lower in the char burning phase. The processed wood produced higher yield of benzene as compared to the pine wood and these were produced at the initial stage of the combustion and the char burning phase and were relative to the glues and resins used in the production of these materials. High yields of acrolein and formaldehyde were produced by pine during its ignition delay of 192 s as compared to the processed woods but once flaming combustion started, and during the char burning phase, yields became very low. The nitrogen in the binders gave rise to the production of HCN with the CFM having the highest yield of HCN of about 0.017 g/g (17 g/kg) followed by MDF with a yield of 0.009 g/g (9 g/kg) and OSB with a yield of 0.002 g/g (2 g/kg). Comparing the yield of HCN with pine wood shows that pine produced a very low yield of HCN as expected because of the low nitrogen content of pine wood.

Processed Wood and Natural Wood Comparison
(Freely Ventilated, 35 kW/m²)



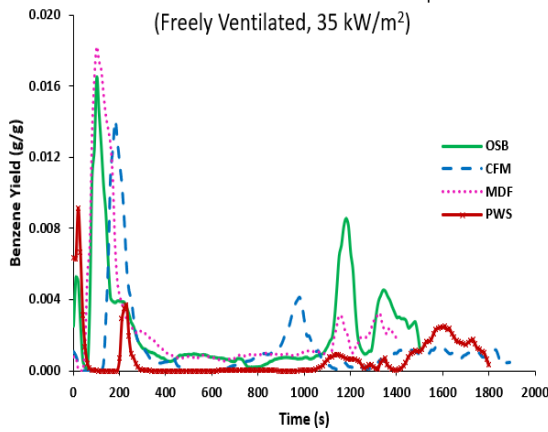
(a)

Processed Wood and Natural Wood Comparison
(Freely Ventilated, 35 kW/m²)



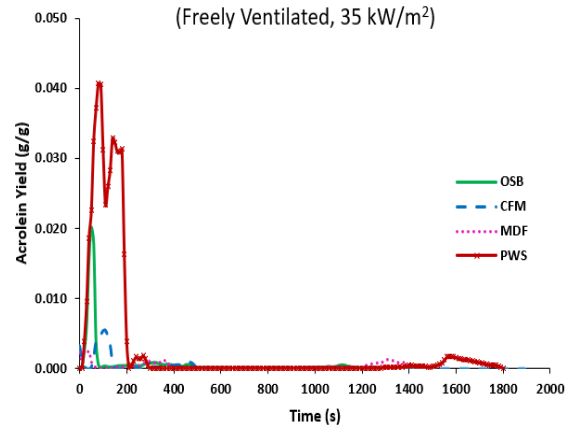
(b)

Processed Wood and Natural Wood Comparison
(Freely Ventilated, 35 kW/m²)



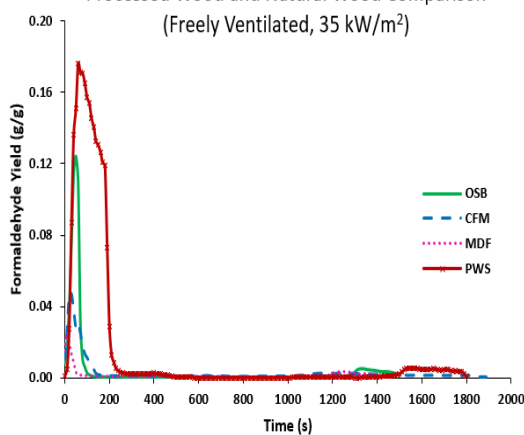
(c)

Processed Wood and Natural Wood Comparison
(Freely Ventilated, 35 kW/m²)



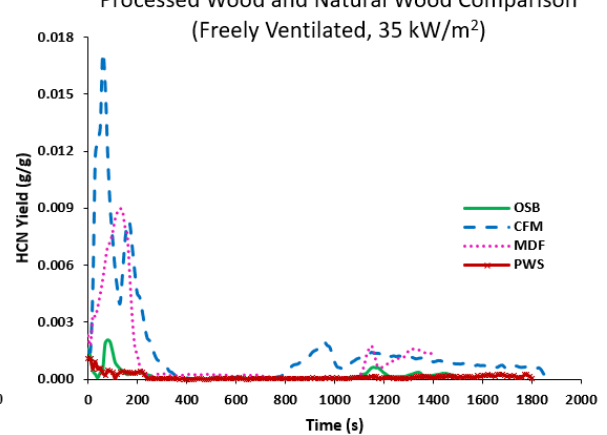
(d)

Processed Wood and Natural Wood Comparison
(Freely Ventilated, 35 kW/m²)



(e)

Processed Wood and Natural Wood Comparison
(Freely Ventilated, 35 kW/m²)



(f)

Figure 4-55 Toxic Gas Yields; CO (a), Total Hydrocarbon (b), Benzene (c), Formaldehyde (d), Acrolein (e) and Hydrogen Cyanide (f).

Very high concentrations of toxic gases that would impair escape and potentially lead to death were released by the processed wood fires and the baseline pine wood fire. The flame retarding properties of melamine prolonged the ignition delay of the CFM, but the longest ignition delay was for pine wood.

The glue and resins used in the manufacture of wood-based composites are a potential toxicity hazard as they release high concentrations of HCN and benzene. However, in spite of up to 5% organic N in CFM and MDF, HCN was not the most important toxic gas in the mixture.

4.5 Summary

The tests with the freely ventilated set-up of the standard cone calorimeter resulted in the following main findings.

Natural Wood:

- Pine wood showed high concentrations of most of the toxic gases except for CO and benzene. Acrolein concentration in pine wood fire was a factor of 5 higher than the scaffolding board while formaldehyde was double that obtained in scaffolding board. This was as a result of the lean combustion by the scaffolding board
- The main toxic gases produced in these tests were CO, Acrolein, Formaldehyde, Benzene and a low concentration of HCN.
- The fire products in these tests were of extreme toxicity exceeding the lethal exposure dose (LC₅₀), and the irritancy threshold (COSHH_{15min}). For example the LC₅₀ limit for CO in pine was exceeded by a factor of 2 while that of COSHH_{15min} was exceeded by a factor of 40. The scaffolding board exceeded the LC₅₀ limit by a factor 4 while that of COSHH_{15min} was exceeded by a factor of 60
- On an LC₅₀ (lethality) basis, the ranking for both pine and scaffolding were: CO > Formaldehyde > HCN > Acrolein.
- On COSHH_{15min} (irritancy) basis, the ranking for both pine and scaffolding board were: Formaldehyde > Acrolein > CO > Benzene, and scaffolding board is: Formaldehyde > Acrolein > Benzene > CO

- Bimodal distribution of the particles were produced in both fires with the nuclei mode centred at 20 nm. The accumulation mode centred at 200 nm for pine wood while the scaffolding board peaked between 200 nm – 500nm. Most of the particulates produced are in the size range where they can be easily transported into the alveolar regions of the respiratory tract and the blood stream.
- The number yield and mass yield of the 2 sizes were reported to be high. In atmospheric particulate pollution, the mass concentration is an annual 24 hr average of PM₁₀ of 40 µg/m³ but in this work 0.01 g/m³ of particle mass with number yield 1.8 x 10³ – 2 x 10⁸ number/kg and mass yield of 0.006 – 9.5 g/kg was obtained.

Processed Wood

- The raw gas sampling showed there was confinement at the initial stage of the fire, creating rich mixtures and this created high levels of toxic gases.
- Very high concentrations of toxic gases that would impair escape and lead to death were released by the processed wood fires because of the adhesives and resins used in their manufacture.
- The glue and resins used in the manufacture of wood-based composites are a potential toxicity hazard as they release high concentrations of HCN and benzene. However, in spite of up to 5 % organic N in CFM and MDF, HCN was not the most important toxic gas in the mixture.
- On LC₅₀ basis, the key gases were found to be CO, NO₂, HCN, formaldehyde and acrolein while on COSHH_{15min} basis, the most important toxic gases were CO, NO₂, HCN, formaldehyde, acrolein and benzene
- The particles produced by the OSB fire were also bimodal, centred at 20 nm and 200 nm representing the nuclei mode and the accumulation mode. These were produced at very high concentrations at 1 x 10⁹ /cc .

A comparison between the processed wood and natural wood:

- The chipboard faced with melamine (CFM) and the reference pine wood sample (PWS) all tested at 35 kW/m² had a prolonged ignition

delay of 142 s and 192 s respectively compared with 54 and 69 s for MDF and OSB respectively.

- An unexpected feature of the results was the quite different toxic gas importance for pine wood (PWS) compared with the processed woods. PWS had much higher toxic emissions of formaldehyde and acrolein than processed woods and much lower emissions of the other four toxic gases. This resulted in PWS being the most toxic burning material on an impairment of escape basis,
- Pine wood (PWS) had the worst total toxicity **N** for impairment of escape, roughly 3 times higher than for the nearest processed woods. This was because of the much high formaldehyde and acrolein emissions for pine wood. In terms of risk of death pine wood was safer than all the processed woods, but was still a significant risk in the early stage of the fires

Plywood:

- High concentrations of toxic gases that would impair escape were produced in the initial stage of the fire, where escape is occurring in a fire.
- The 4 plywoods had different compositions indicating that the manufacturing processes were different and hence released different concentrations of the toxic gases. Toxic gas regulation for plywoods should be introduced to control this.
- All toxic gases concentration levels were considerably higher than the LC₅₀ limit except for acrolein and benzene but all the toxic gas emissions were above the COSHH_{15min}.
- The initial particle size distribution during the ignition delay period showed only Nano particles with a peak at 20 nm for both plywood A and plywood B.
- These plywood samples produced ultra-fine particles of great concern as that is where the greatest health hazard occurs.
- Particle number concentrations were highest when the heat release was at its peak and gradually decreased after the flameout.

Chapter 5 Controlled Atmosphere Test Results on the Cone Calorimeter

The Cone Calorimeter is one of the most common bench scale piece of equipment in fire research, where it is used to determine certain parameters of a test material such as the ignition heat flux and the heat release rate, as well as the toxic gas production [187, 188]. One of the most common fire materials is wood, as about 50% of all fires involve wood as the main fuel. In residential buildings, almost 80% of furniture in homes is wood.

The controlled atmosphere cone calorimeter, a modification of the standard cone calorimeter ISO 5660 [108] was used to create a vitiated (oxygen reduced environment) environment (described in chapter 3). The standard cone calorimeter (ISO 5660) generates combustion conditions in accordance with class 1b (oxidative pyrolysis) and class 2 (well ventilated flaming fires) based on the classification of fire stages in ISO 19706 [48]. This is not ideal for toxicity tests as it does not create the conditions of compartment fires, where toxicity levels are much higher than for freely ventilated fires. The standard cone calorimeter is suitable for material testing where the maximum heat release or ignition radiant heat is required. In real compartment fires, temperature, ventilation and equivalence ratio all depend on each other. The introduction of the enclosure makes the controlled atmosphere cone calorimeter apparatus capable of creating the combustion conditions 1c (anaerobic pyrolysis) and both 3a (low ventilated fires) and 3b (post flashover fires) according to the classifications given in the ISO 19706 [48]. The controlled atmosphere cone calorimeter can create all the stages of fire except for class 1a (self-sustained smouldering fires). In this chapter, the results of pine wood sticks at varying air mass flow rates and how they affect the production of toxic gases and particulates are presented.

The conical radiant heater in the cone calorimeter is used for two purposes: firstly, to determine the minimum radiant ignition energy of the test material; and secondly, to enable combustion of a small test specimen of material to be undertaken in the presence of radiation from a larger fire and it is this use of the cone calorimeter that is most important in the present work. Obviously the choice

of the radiant heat intensity is significant and higher radiant heat essentially simulates a hotter fire. The influence of the heat flux on the combustion of block board wood in a restricted ventilation compartment was investigated and also presented in this chapter.

5.1 General Burning Characteristics

5.1.1 Pine Wood

Five 100 x 20 x 20 mm (L x W x H) rectangular shaped pine sticks were arranged in the 100 x 100 mm square sample holder of the cone calorimeter and tested in a horizontal orientation with the top surface exposed to the applied radiant heat flux. The pine wood was exposed to the conical heater of the cone calorimeter radiating at 35 kW/m² with varying air mass flow for each test. This is the recommended standard heat flux recommended by British Standards [108] for use in material evaluation for performance in fires using the standard cone calorimeter [108]. Also, 35 kW/m² was recommended by Flecknoe-Brown et al. [189]. Herzberg and Blomqvist, [133] noted that 35 kW/m² was a "trade-off between a lower value, which possibly would have caused materials to pyrolyse only, and a higher value which might have provoked an unrealistically clean burning behaviour". The three (3) airflow rates varied in this test are; 54 kW/m²_{air}, 112 kW/m²_{air} and 174 kW/m²_{air}. The initial weights of the wood were determined by the load cell as 127 g, 136 g and 128 g. The load cell was checked with reference weights at the start of each test programme and was very stable. The 35 kW/m² radiant heat flux caused the thermal decomposition of the samples leading to auto-ignition of the evolved gases and the auto-ignition delay time was determined in the tests at 29 s, 27 s and 51 s. This was a very small part of the much longer burn time. The fire continued until flaming combustion ceased and there was only char burning. It will be shown that this transition from flaming combustion to char smouldering combustion was associated with a change in the toxic gas emissions and particle size distribution.

Table 5-1 Ignition Times for Burning Pine Wood at Different Ventilation Conditions

Air Flow Rate (kW/m²_{air})	Ignition Time (s)	Flameout Time (s)
59	29	1500
112	27	1650
174	51	1450

5.1.1.1 Mass Loss Rate and Equivalence Ratio

The mass loss rate for the pine wood during the process of fire development in the controlled atmosphere cone calorimeter is shown in Fig. 5.1a as a function of time. The tests showed that the ignition delay was much shorter for the 54 kW/m²_{air} ventilation fire, due to the richer mixtures during the delay period, shown in Fig. 5.1b followed by the 112 kW/m²_{air} fire which was not as rich. The 174 kW/m²_{air} fire had a longer ignition delay because of the lean mixture. Figure 5.1a shows an initial high mass loss rate followed by a slower mass loss rate at the wood burn out stage which coincided with the transition between the flaming combustion and the char combustion. It will be shown that most of the fire gas toxicity and the particulates occurred in this period. The mass loss rate for the three tests were similar at 0.07-0.075 g/s with the 174 kW/m²_{air} test having a slightly higher mass loss rate at the steady state burning phase. This is as a result of the high airflow rate which increased the burn rate as seen in the heat release rate of Fig. 5-2.

The fire equivalence ratio in the ventilation-controlled compartment is shown in Fig. 5-1b as a function of time. This is the equivalence ratio based on the ratio of the stoichiometric A/F by mass to that of the measured A/F mass ratio of the metered air flow and the mass loss rate of wood in the fire. This shows that for 59 kW/m²_{air} and 112 kW/m²_{air}, the combustion was rich or ventilation controlled throughout the flaming combustion phase, but was lean or fuel controlled in the char burning phase. The 174 kW/m²_{air} fire burned at stoichiometric at the beginning of the fire but burned lean throughout the steady burning phase. Figure 5-1b shows that there were two periods with mixtures richer than the mean and this was the first phase of flaming combustion up to 200 s and the 1000 – 1250

s period towards the last phase. It is possible that this last phase of rich combustion was due to oxidation of char. As the air flow was held constant in each test, the variation in equivalence ratio was due to the variation in the rate of fuel mass loss.

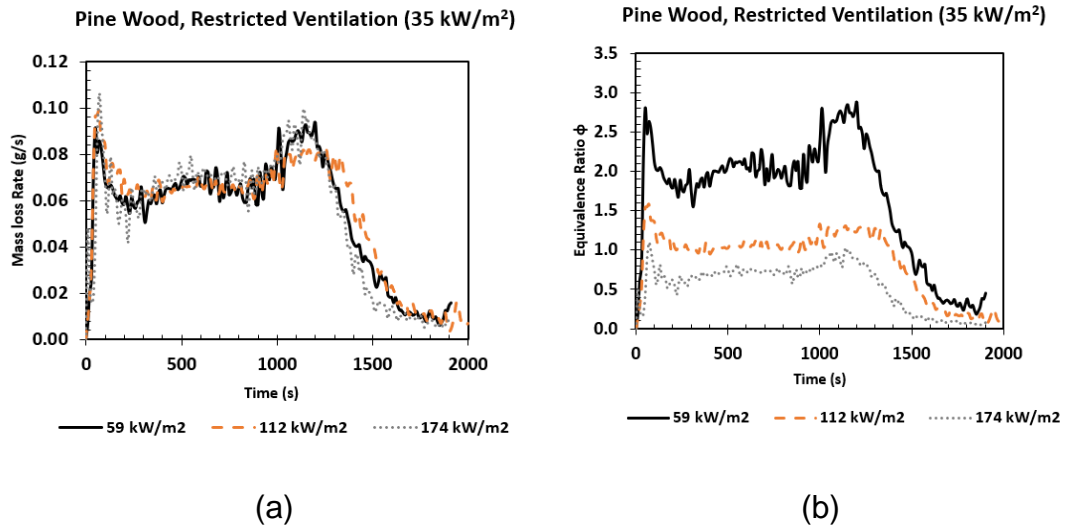


Figure 5-1 Mass Loss Rate (a) and Equivalence Ratio (b)

5.1.1.2 Heat Release Rate

The oxygen consumption overall or total heat release rates (HRR) results are shown as a function of time in Fig. 5-2, together with the primary HRR by oxygen consumption and the HRR derived from the mass loss rate times the gross calorific value GCV of pine. The ignition delays at a radiant heating of 35 kW/m² were 29 s, 27 s and 51 s as shown in Table 5-1. At a heat flux of 35 kW/m² the total HRR was about 50 kW/m² throughout the flaming combustion phase from 200 to 1000 s for the 59 kW/m²_{air} fire. The difference between the total and primary HRR was very small and was only significant between 1000 s and 1500 s just before flameout. This small difference shows that there was little secondary combustion as the entrained cold air cooled the discharge from the chimney and stopped CO and HC oxidation.

The HRR by mass loss rate was about 130 kW/m² at steady state combustion phase for all tests. The reason for this difference, from the lower values in Fig. 5-2 for the primary HRR by oxygen consumption, is that the aim of the primary zone is to burn the fuel rich and pass rich product gases to the secondary zone. The difference is the potential HRR in a properly designed second stage burner.

The heat release rates are given in Fig. 5-2. At a heat flux of 35 kW/m² the 174 kW/m²_{air} test had the highest heat release rate of 90 kW/m² at 1300 s because of the intense burning caused by the high rate of inlet air. The 59 kW/m²_{air} and the 112 kW/m²_{air} test maintained a similar heat release pattern having a peak of slightly > 50 kW/m² and 60 kW/m² throughout the flaming combustion phase.

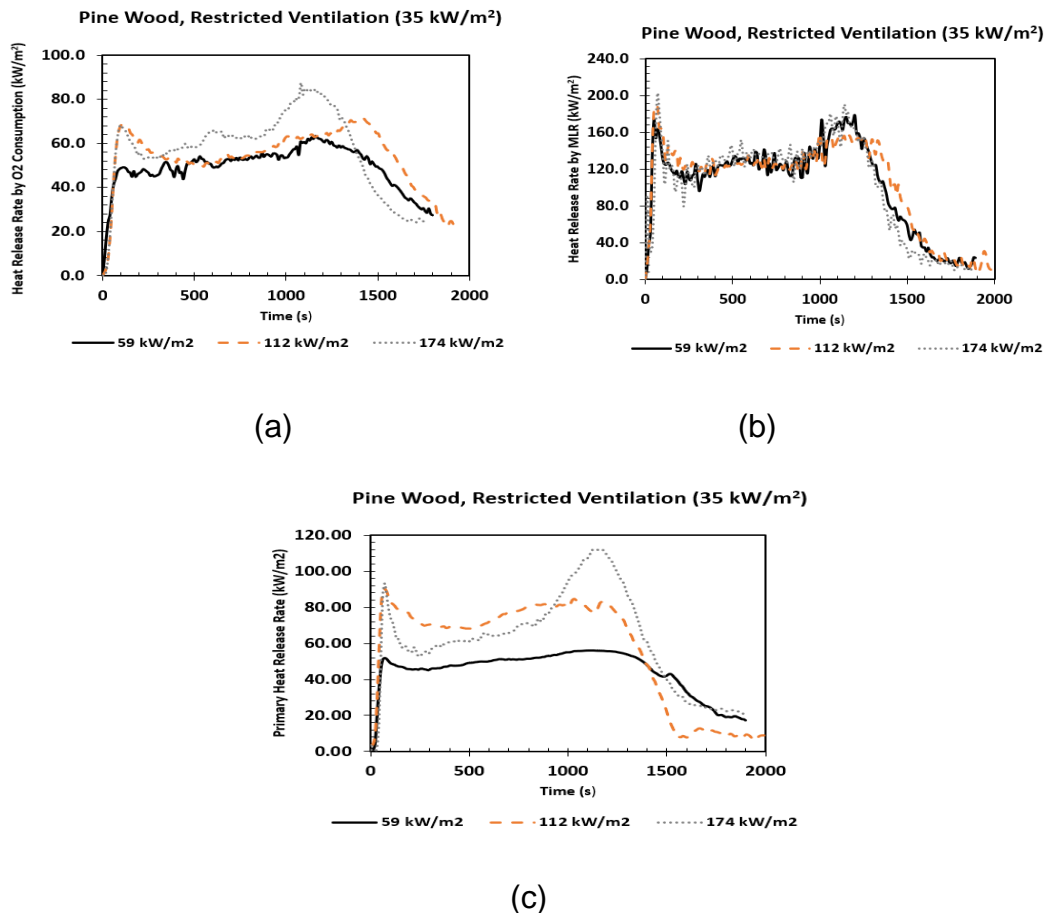


Figure 5-2 Heat Release Rates; Total HRR by Oxygen Consumption (a), HRR by Mass Loss Rate (b) and Primary HRR (c).

5.1.2 Block Board Wood

Construction block board wood of 100 x 100 x 18 mm was tested in the controlled atmosphere cone calorimeter in a horizontal orientation. Five (5) different samples were tested at different heat fluxes to determine the minimum ignition flux for the material, heat release rates, mass loss rates and the toxic emissions from these tests. The air flow was kept constant at 174 kW/m²_{air} and the radiant heat flux was varied from 25 kW/m² to 50 kW/m².

5.1.2.1 Ignition

A series of physical and chemical events are responsible for ignition as discussed in chapter 2. This involves heating a material by means of radiation, convection or conduction. The type of material and its thermal properties determine the rate at which the temperature rises. Once the pyrolysis temperature is reached, decomposition sets in and volatiles are released. These volatiles mix with surrounding air and form a combustible mixture. Ignition occurs when the concentration of the combustible mixture is right i.e. greater than the lower flammability limit, and the temperature is high enough. This work focused on the auto ignition of wood where the fire was initiated without an external heat source. The initial mass of the samples at the start of the test and the ignition and flameout times are given in Table 5-2.

Table 5-2 Ignition Times for Burning Pine Wood at Different Ventilation Conditions

Heat Flux (kW/m²)	Radiant Temperature (°C)	Mass (g)	Ignition Time (s)	Flameout Time (s)
25	568	143	No ignition	-
30	610	140	118	1628
35	645	135	85	1480
40	695	132	31	1445
50	760	148	20	1230

The block board wood test at 25 kW/m² lasted for 1500 s but did not ignite. At a heat flux of 30 kW/m² the sample ignited at 118 s into the test. The sample tested at 35 kW/m² ignited at 85 s into the test. The 40 and 50 kW/m² tests ignited at 31 and 20 s respectively.

Vertical panels of ponderosa pine with a thickness of 6.4 mm were examined by Moran [190] using an electrical radiant panel and found the minimum radiant ignition to be 25 kW/m². Shoub and Bender's [191] results of tests done on 13 mm plywood using an electrical radiant panel showed that wood will ignite at 4.3 kW/m² if exposed for hours not minutes. Various factors such as the type of wood or material and the conditions under which the test was performed can affect the

ignitability of the material. Since the aim of this research is not the auto ignition of wood, further research was not carried out.

The 50, 40, 35 and 30 kW/m² test had flaming combustion that lasted for 1230, 1445, 1480 and 1628 s. This was expected as the higher the heat exposed to the sample, the faster the volatiles released are burnt out.

5.1.2.2 Mass Loss Rate and Equivalence Ratio

The normalised mass loss percentage and the mass loss rate for the five block board wood tests are shown in Fig. 5-3a and b as a function of time. Figure 5-3a showed that 100% of the sample was burnt during the 50 kW/m² test and about 70-80% of the wood sample was burnt during the other tests with the exception of the 25 kW/m² test which did not ignite but smouldered for 1500 s and about 56 % of the sample was burnt. At the beginning of the test, a thin char layer formed on the sample surface, increasing the mass loss with time until its maximum value was reached. The release of pyrolysis products was blocked as the char layer became thicker, thereby decreasing the mass loss rate. The mass loss rate continued decreasing until it remained constant for a period of time at the steady state combustion phase. When the heat got deeper into the sample, the mass loss rate increased again. The mass loss rate decreased at the char burning phase as a result of the depletion of the sample. This explains the 2 peaks obtained in Fig. 5-3b. The 25 kW/m² test did not ignite and the test was stopped at 1500 s but had a mass loss rate of 0.04 g/s. The 50 kW/m² test burned faster than all the tests as expected because of the high heat flux at a mass loss rate of 0.085 g/s during the steady burning phase. This was followed by the 40 kW/m² test which had a mass loss rate of 0.074 g/s. At 30 kW/m², the fire burned at a rate of 0.071 g/s, but a slower burning rate was observed when the wood was tested at 35 kW/m² burning at the rate of 0.063 g/s. The 35 kW/m² test did not follow the expected trend of the higher the heat flux, the higher the mass loss rate.

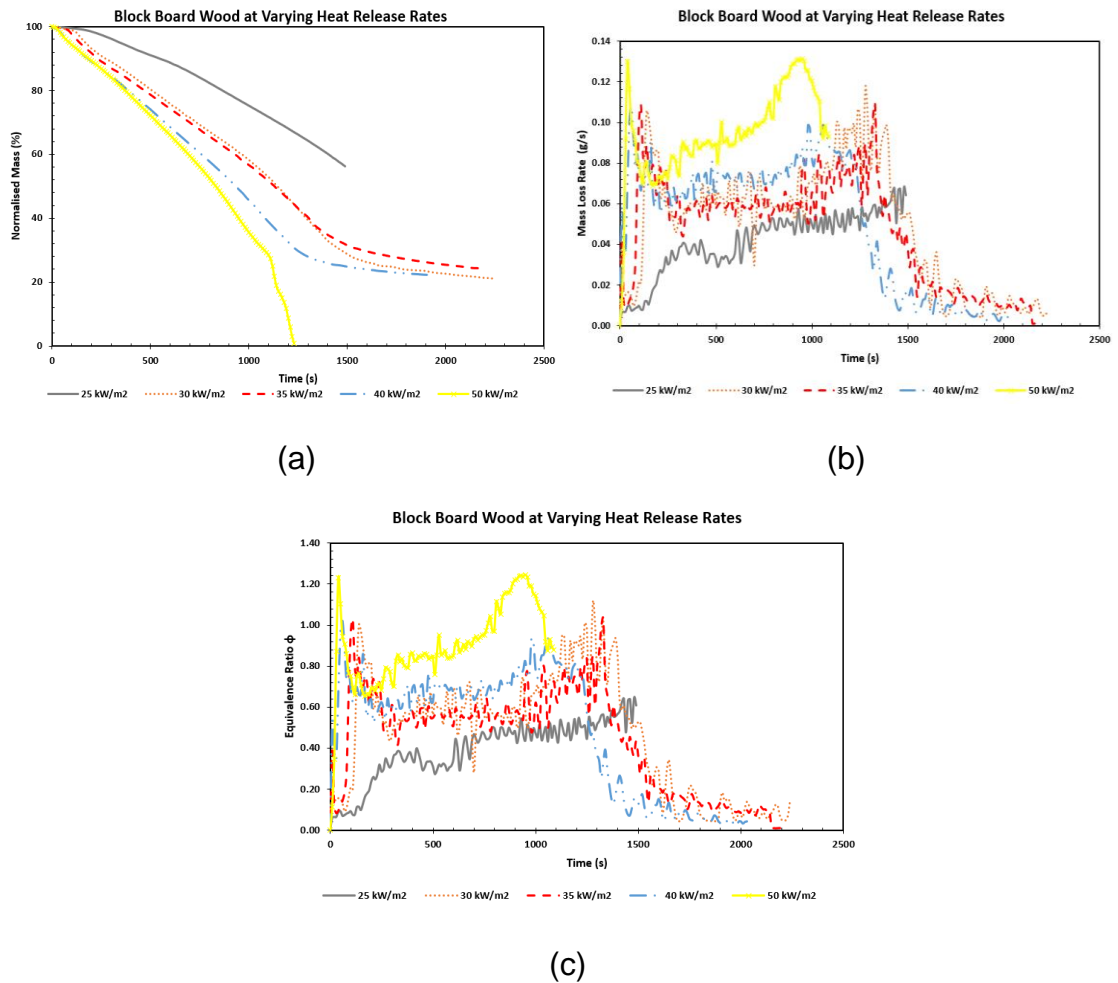


Figure 5-3 Block Board Wood; Mass Loss (a), Mass Loss Rate (b) and Equivalence Ratio (c)

The metered equivalence ratio is shown in Fig. 5-3c as a function of time. All the tests with the exception of the 25 kW/m² fire burned at stoichiometric or rich at the beginning of the fire but burned lean throughout the steady burning phase and the char burning phase. The 25 kW/m² burned lean throughout the test because it did not ignite. Figure 5-3c shows that there were two periods with mixtures richer than the mean and this was the first phase of flaming combustion and the last phase. It is possible that this last phase of rich combustion was due to oxidation of char. As the air flow was held constant the variation in equivalence ratio was due to the variation in the rate of fuel mass loss.

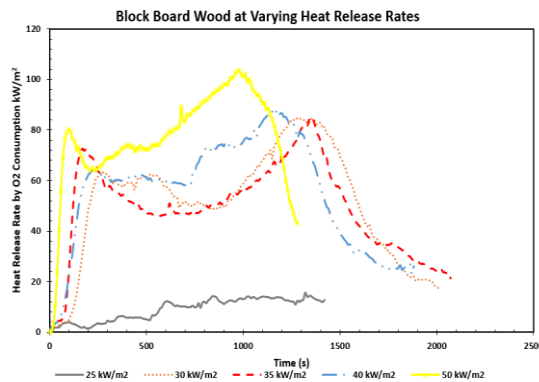
5.1.2.3 Heat Release Rate

The oxygen consumption overall or total heat release rate (HRR) results are shown as a function of time in Fig. 5-4, together with the primary HRR by oxygen

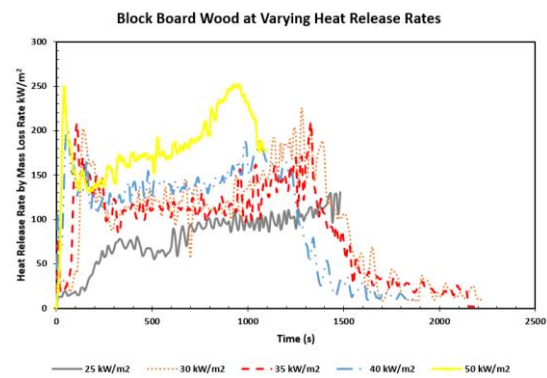
consumption and the HRR derived from the mass loss rate times the GCV, 19.1 MJ/kg of the block board wood. From Fig. 5-4, it can be seen that apart from the 25 kW/m² test which did not ignite, all the test that ignited follow the stages of combustion; ignition, growth stage reaching a peak value, steady state, and decay period before extinction.

The 50 kW/m² test had the highest heat release rate, as expected. At a heat flux of 50 kW/m² the total HRR was about 72 kW/m² throughout the flaming combustion phase from 170 to 600 s. The rest of the tests with the exception of the one at 25 kW/m² had similar HRR throughout the flaming combustion phase, with the 40 kW/m² test having 60 kW/m² and 35 and 30 kW/m² having 50 kW/m² each, but the time variation was different. The 25 kW/m² test had the least heat release rate of about 10 kW/m² as expected because it did not ignite.

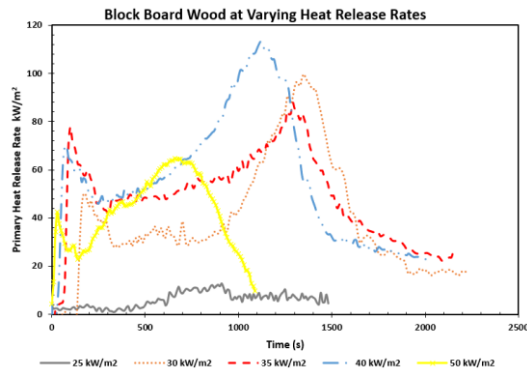
The primary HRR showed a different trend, with the 25 kW/m² having the lowest heat release rate followed by the 50 kW/m² test. The 40 kW/m² test had the highest peak heat release rate followed by the 30 kW/m² test but during the steady state burning phase, the 35 kW/m² test had the highest HRR of 53 kW/m² between 230-850 s. It is not clear why the results varied.



(a)



(b)



(c)

Figure 5-4 Heat Release Rates; Total HRR by O₂ Consumption (a), by Mass Loss Rate (b) and Primary Heat Release Rate (c)

The HRR by mass loss rate for the 50 kW/m² test was about 170 kW/m² between 170 to 600 s. The rest of the tests with the exception of the 25 kW/m² test had similar HRR throughout the flaming combustion or steady state burning phase with the 35 kW/m² test having 120 kW/m² while 40 and 30 kW/m² had 130 kW/m² each, but the time variation was different. The 25 kW/m² test had an average heat release rate of about 100 kW/m². The reason for the difference, from the lower values in Fig. 5-4a and b is that the evaluation of the HRR based on the mass loss rate effectively assumes complete combustion and release of all the available energy.

5.2 The Influence of Airflow Rate on Toxic Gas Emissions

The toxic gases were measured from the raw sampling point of the cone calorimeter using the heated FTIR, with the gas sampling system described in chapter 3. The toxic gases produced during the combustion of pine wood at varied airflow rates are compared and the results are presented in this section. Three (3) airflow rates were varied as mentioned in section 5.1.1 i.e. 59 kW/m²_{air}, 112 kW/m²_{air} and 174 kW/m²_{air}. Gases were analysed using the Gasmeter heated FTIR.

5.2.1 Toxic Gas Concentration

The FTIR results of some of the important toxic gases are presented in Fig. 5-5 as a function of time. The LC₅₀ toxic limits for CO, formaldehyde and HCN are

marked. There is no LC₅₀ limit for benzene, but the COSHH_{15min} limit for impairment of escape is 3 ppm and Fig. 5-5c shows concentrations over 100 times this level. Figure 5-5a shows that there were two peaks in CO: in the initial flaming combustion period up to 200 s and from 800 – 1200 s for the 59 kW/m²_{air} test, the first peak was 3% and the second 4% while the 112 kW/m²_{air} test had peaks of 1.6% and 2%. The 174 kW/m²_{air} test had lower peaks of <1%. Both peaks in CO occur at the same time the peaks in equivalence ratio occurred. In the same two-time periods Fig. 5-5b shows that there was an initial 4% peak in THC with the second 6% peak in THC at the same time as the second CO peak for the 59 kW/m²_{air} test and the 112 kW/m²_{air} having 2% and 4%. Again the 174 kW/m²_{air} test had <1% for both peaks. These are very high levels of CO (LC₅₀ and COSHH_{15min} threshold limits were exceeded) and unburned hydrocarbons with a very large energy content, that is released in the second stage combustion external to the chimney. Each individual hydrocarbon also showed the same two peaks in emissions as illustrated by the results for benzene in Fig. 5-5c, where the first flaming combustion peak was 1000 ppm and the second peak was 1300 ppm for the lowest airflow rate test and 450 ppm and 1200 ppm for the 112 kW/m²_{air} test. The highest airflow test produced much lower concentration of benzene of < 200 ppm. Formaldehyde emissions are shown as a function of time in Fig. 5-5d and this shows three peaks for all tests, the first two aligned with those for THC and the third peak was in the char combustion period.

The 174 kW/m²_{air} test showed much lower concentrations of most gases except for acrolein and formaldehyde where it was about a factor of 4 higher than the two tests during the first 100 s of the test. The low concentrations were as a result of the lean combustion exhibited during the test. The low airflow rate produced most of the toxic gases at high concentrations. On LC₅₀ basis, CO, formaldehyde and HCN concentration limits were exceeded for the 59 kW/m²_{air} test. For the 112 kW/m²_{air} test, only CO and HCN concentration limits were exceeded on an LC₅₀ basis. The 174 kW/m²_{air} test had CO and formaldehyde exceeding the toxic concentration limits on an LC₅₀ basis. Only the COSHH_{15 min} concentration limits for the impairment of escape was exceeded for all gases in all fires. This shows that the gases that are of importance to lethality are different from that of

impairment of escape. The results show that richer mixtures produce high concentration of toxic gases.

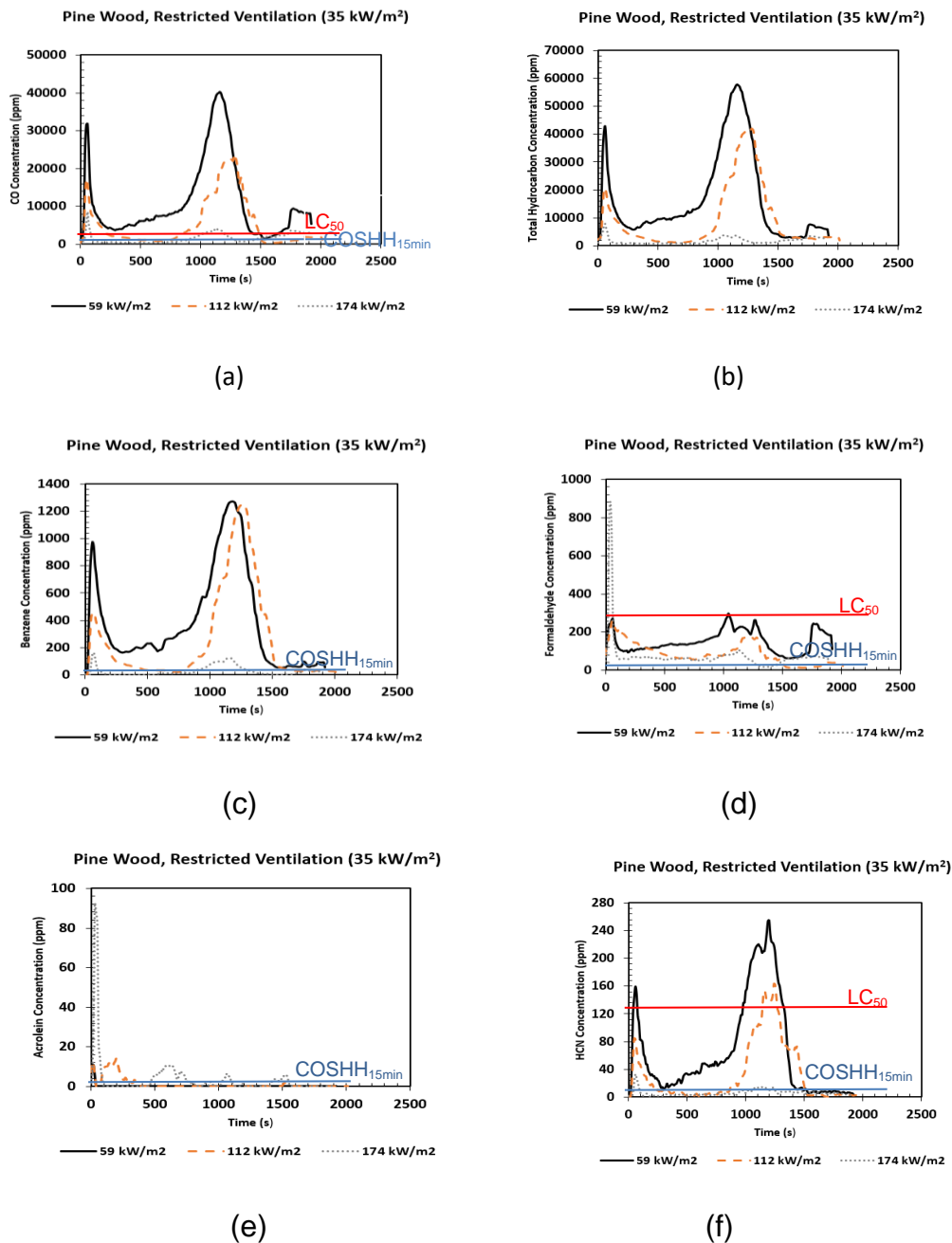


Figure 5-5 Toxic gas concentrations; CO (a), Total Hydrocarbon (b), Benzene (c), Formaldehyde (d), Acrolein (e) and Hydrogen Cyanide (f)

5.2.2 Total Fire Toxicity N on an LC₅₀ and COSHH 15min Basis

The total toxicity **N** for LC₅₀ and COSHH_{15min} are shown as a function of time in Fig. 5-6. Both methods of deriving **N** showed similar shapes of the dependence of **N** on time for all tests. Despite the differences in relative toxicity, the two

methods for calculating **N** locate the same time in the fire where the peak toxicity occurs. These results show that the pine wood at the lowest airflow rate had by far the highest total toxicity with an LC₅₀ of 16, followed by the 112 kW/m²_{air} with 9 while the highest airflow rate had an LC₅₀ of 5. The total **N** on COSHH_{15min} basis gives values of 1100 for the 59 kW/m²_{air} test, 830 for the 112 kW/m²_{air} test and 1380 for the 174 kW/m²_{air} test. This means that the toxic gases need to be diluted with fresh air by a factor of about 830-1380 before escape is not impaired and it has to be diluted by a factor of 5-16 before it doesn't kill anybody in 30 mins. All fires had two peaks of **N**, due to flaming combustion and these correspond to the periods where the heat release rates, mass loss rates and equivalence ratios were at their peak.

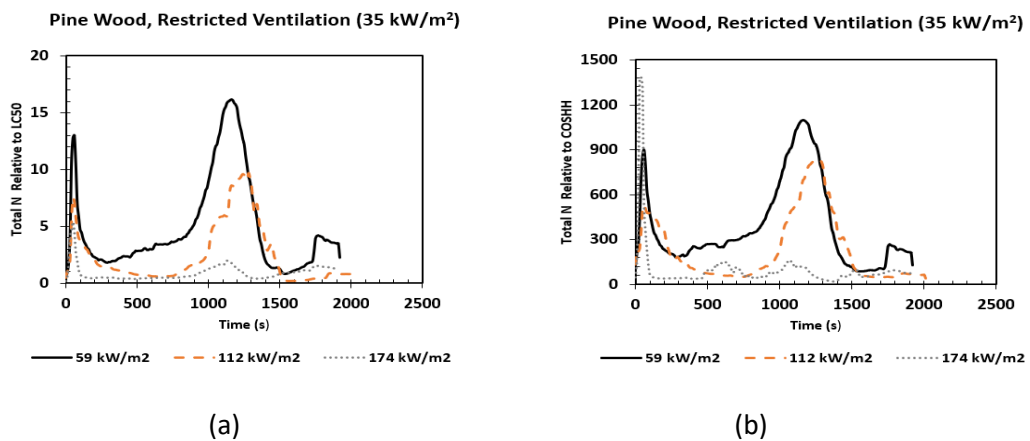
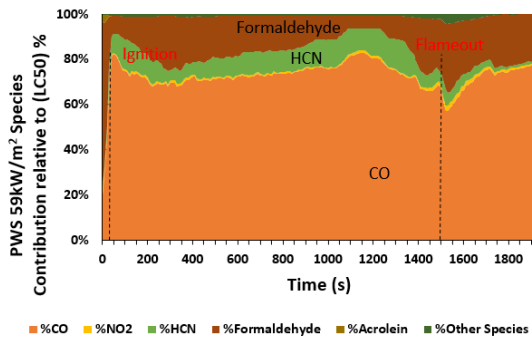


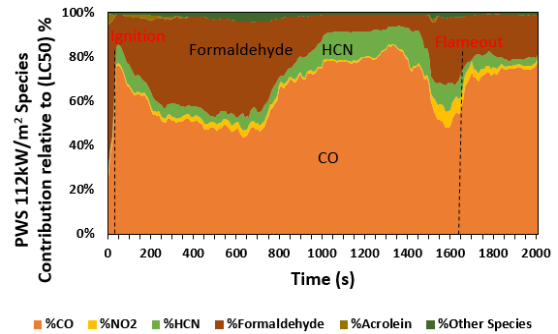
Figure 5-6 Total N relative to LC₅₀ (a) and COSHH_{15min} (b)

The major contribution to the total toxicity are shown on an LC₅₀ and COSHH_{15min} basis in Figs. 5-7 and 5-8 for the 3 pine wood tests. For 59 kW/m²_{air} the toxicity was dominated by CO, followed by formaldehyde and HCN on an LC₅₀ basis and formaldehyde, benzene, CO and HCN on a COSHH_{15min} basis. The contribution of acrolein was not more than 5% on LC₅₀ but was about 50% at the initial stage of the fire on a COSHH_{15min} basis. For the 112 kW/m²_{air}, the toxicity was dominated by CO, formaldehyde and HCN, on an LC₅₀ basis, but formaldehyde was more significant on COSHH_{15min} basis, followed by benzene, CO, acrolein and HCN. For the 174kW/m²_{air}, the toxicity was dominated by CO, formaldehyde HCN on an LC₅₀ basis, with < 10 % contribution of acrolein. However, acrolein was second most significant on COSHH_{15min} basis. The highest contribution was from formaldehyde, followed by acrolein, benzene, CO and HCN. Benzene also contributed significantly to the toxicity in these pinewood fires. For these pine

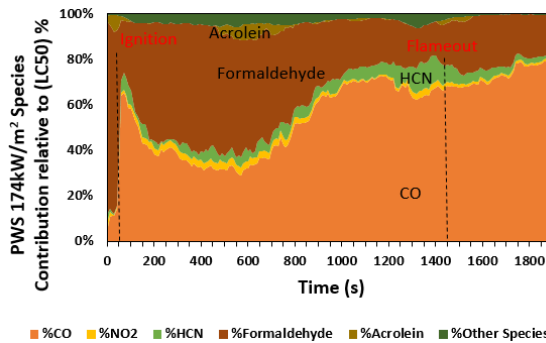
wood fires CO dominates in relation to death and for impairment of escape formaldehyde was more dominating.



(a)

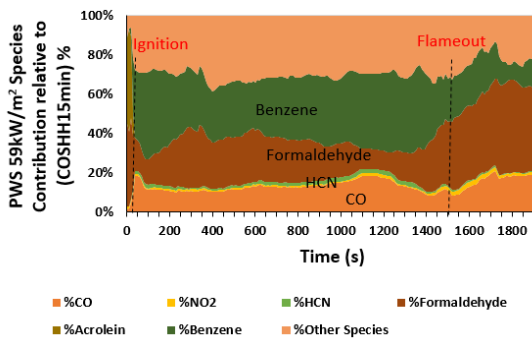


(b)

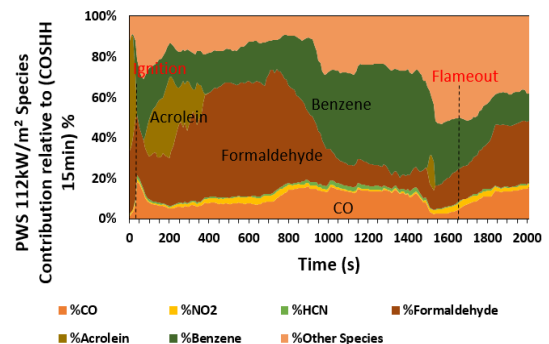


(c)

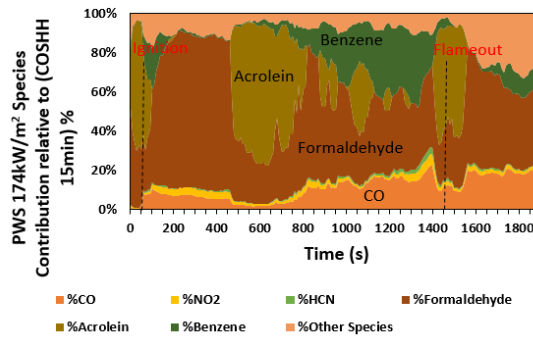
Figure 5-7 N-Gas Composition (LC₅₀) PWS; 59 kW/m²_{air} (a) 112 kW/m²_{air} (b) and 174 kW/m²_{air} (c)



(a)



(b)



(c)

Figure 5-8 N-Gas Composition (COSHH_{15min}) PWS; 59 kW/m²_{air} (a) 112 kW/m²_{air} (b) and 174 kW/m²_{air} (c)

5.2.3 Toxic Gas Yields

The toxic gas yields for the pine wood tests are presented in Fig. 5-9. Figure 5-9a shows that there were three peaks in the CO yield: in the initial flaming combustion period up to 200 s, the second flaming combustion phase from 800 – 1200 s and the smouldering combustion phase for the 59 kW/m²_{air} test, the first two peaks were about the same with a yield of 0.1 g/g and the third peak having the highest yield was 0.26 g/g while the 112 kW/m²_{air} test had peaks of 0.08 g/g, 0.15 g/g and 0.18 g/g. The 174 kW/m²_{air} test had 0.08 g/g during the initial combustion period, a lower peak of 0.03 g/g in the second phase and a much higher yield of 0.38 g/g during the smouldering combustion. The first two peaks in CO yield occur at the same time the peaks in equivalence ratio occurred. In the same time as the CO. Figure 5-9b shows that there was an initial 0.08 g/g peak in THC a second peak of 0.1 g/g and a third peak 0.12 g/g for the 59 kW/m²_{air} test and the 112 kW/m²_{air} having 0.05 g/g, 0.15 g/g and 0.17 g/g. The 174 kW/m²_{air} test had 0.08 g/g, 0.01 g/g and a high yield of 0.20 g/g during the smouldering phase. These are very high yields of CO and unburned hydrocarbons with a very large energy content. Each individual hydrocarbon also showed the same three peaks in yields as illustrated by the results for benzene in Fig. 5-9c, where the first flaming combustion peak was 0.009 g/g, the second peak was 0.01 g/g and the third was 0.006 g/g for the lowest airflow rate test and 0.006 g/g, 0.02 g/g and 0.009 g/g for the 112 kW/m²_{air} test. The highest airflow test produced much lower concentration of benzene of 0.002 g/g during the first two phases and 0.01 g/g in the third phase. Formaldehyde yields are shown as

a function of time in Fig. 5-9d and this shows two peaks for all tests, the first was at the initial combustion stage and the second peak was in the char combustion period. HCN yields were very low, which is as a result of the low nitrogen content in the pine wood.

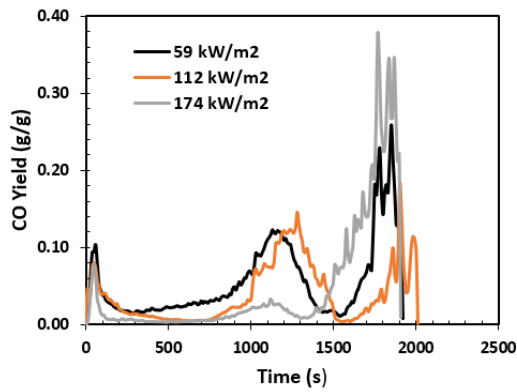
The 174 kW/m²_{air} test showed much lower yields of most gases except for acrolein and formaldehyde where it was about a factor of 4 higher than the two tests during the first 100 s of the test. For CO and the total hydrocarbon THC, the yields were higher than the two tests during the char burning period. The low yields were as a result of the lean combustion exhibited during the test. The low airflow rate produced high yields of most of the toxic gases. Table 5-3 shows a summary of the peak yields of the most important toxic gases.

Table 5-3 Toxic Gas Yields for Pine Wood Restricted Ventilation

Toxic Gas	Peak Yield and Time to Peak yield for Pine Wood		
	1 st Peak g/g	2 nd Peak g/g	3 rd Peak g/g
CO			
59 kW/m ² _{air}	0.1 (60 s)	0.1 (1240 s)	0.26 (1850 s)
112 kW/m ² _{air}	0.08 (60 s)	0.15 (1280 s)	0.18 (1900 s)
174 kW/m ² _{air}	0.08 (50 s)	0.03 (1140 s)	0.38 (1770 s)
THC			
59 kW/m ² _{air}	0.08 (60 s)	0.1 (1240 s)	0.12 (1850 s)
112 kW/m ² _{air}	0.05 (60 s)	0.15 (1280 s)	0.17 (1900 s)
174 kW/m ² _{air}	0.08 (50 s)	0.01 (1140 s)	0.20 (1770 s)
Acrolein			
59 kW/m ² _{air}	0.006 (10 s)	-	-
112 kW/m ² _{air}	0.001 (10 s)	-	-
174 kW/m ² _{air}	0.007 (30 s)	-	-
Formaldehyde			
59 kW/m ² _{air}	0.005 (10 s)	-	0.007 (1850 s)
112 kW/m ² _{air}	0.006 (10 s)	-	0.004 (1900 s)
174 kW/m ² _{air}	0.03 (30 s)	-	0.008 (1770 s)
Benzene			
59 kW/m ² _{air}	0.009 (60 s)	0.01 (1240 s)	0.006 (1850 s)
112 kW/m ² _{air}	0.006 (60 s)	0.02 (1280 s)	0.009 (1900 s)

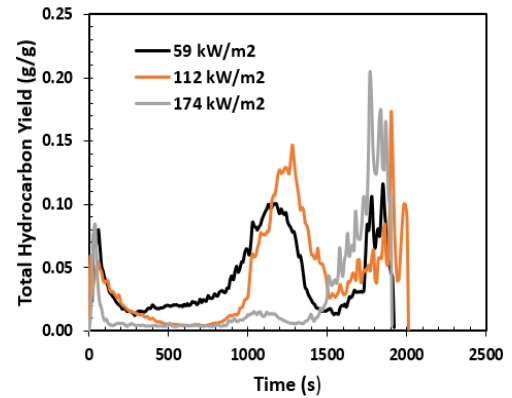
174 kW/m ² _{air}	0.002 (50 s)	0.002 (1140 s)	0.01 (1770 s)
HCN			
59 kW/m ² _{air}	0.0005 (60 s)	0.0007 (1190 s)	0.0002 (1780 s)
112 kW/m ² _{air}	0.0004 (60 s)	0.0009 (1240 s)	0.0003 (1900 s)
174 kW/m ² _{air}	0.0003 (50 s)	0.00009 (1140 s)	0.0005 (1780 s)

Pine Wood, Restricted Ventilation (35 kW/m²)



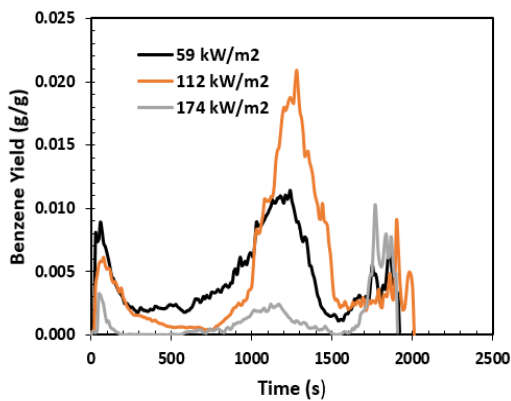
(a)

Pine Wood, Restricted Ventilation (35 kW/m²)



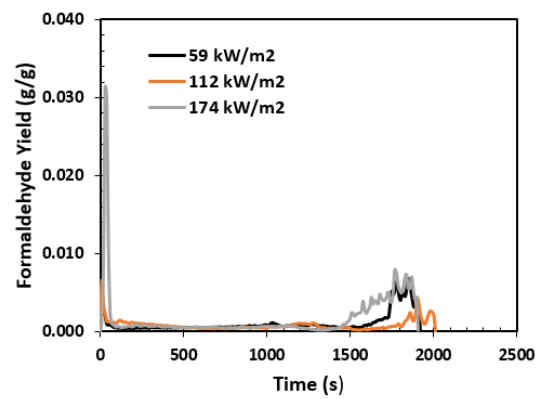
(b)

Pine Wood, Restricted Ventilation (35 kW/m²)



(c)

Pine Wood, Restricted Ventilation (35 kW/m²)



(d)

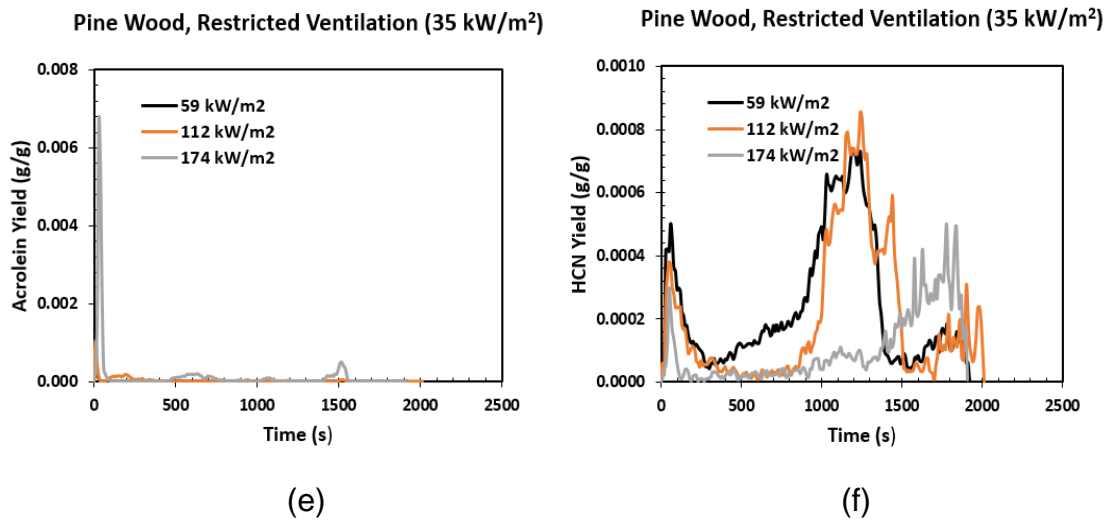


Figure 5-9 Toxic Gas Yields; CO (a), Total Hydrocarbon (b), Benzene (c), Formaldehyde (d), Acrolein (e) and Hydrogen Cyanide (f).

5.2.4 Combustion Efficiency and Heat Release Rate Correction

Figure 5-10 shows the combustion efficiency for the different pine wood tests. The test at the highest airflow rate had the highest yield of CO and unburnt total hydrocarbon (THC) during the smouldering or char burning phase, which led to a lower combustion efficiency of 60% at that period. During the initial flaming combustion, the efficiency was similar for all tests at about 88% efficiency. This is as a result of the low yield at that period. 59 and 112 kW/m² tests experienced a second drop in efficiency to about 84% (59 kW/m²) and 78% (112 kW/m²) before the char burning phase. The combustion efficiency increased to > 95% during the steady.

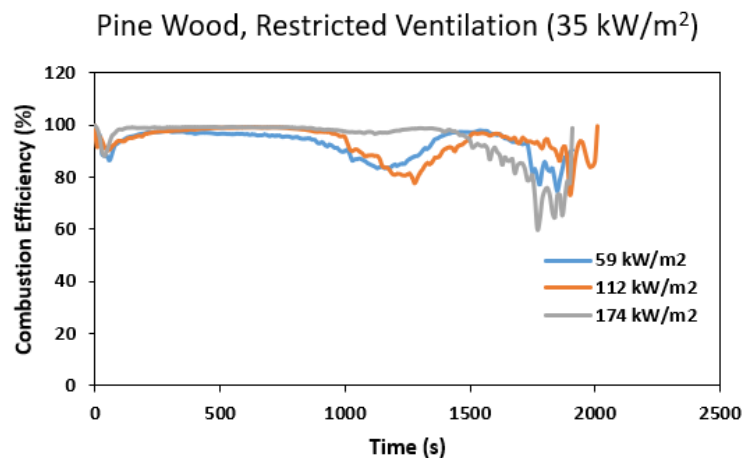
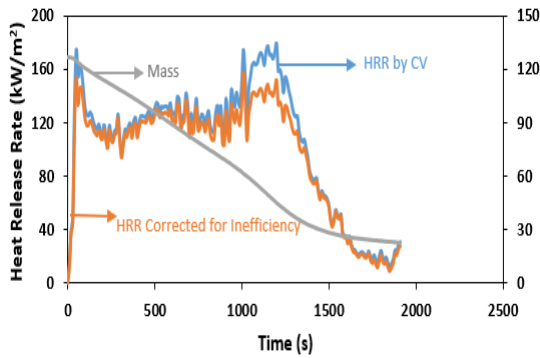


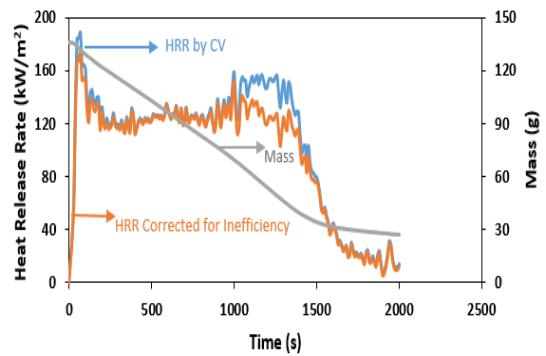
Figure 5-10 Combustion Efficiency for Pine Wood

Pine Wood , Restricted Ventilation (59 kW/m²air, 35 kW/m²)



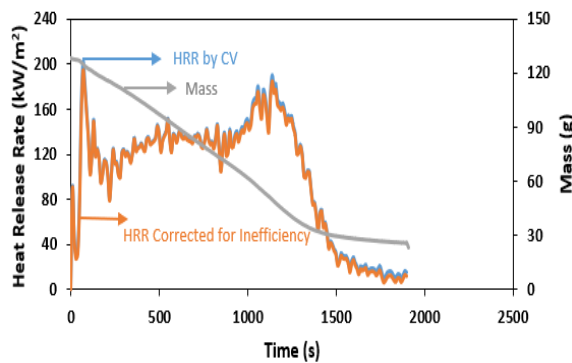
(a)

Pine Wood , Restricted Ventilation (112 kW/m²air, 35 kW/m²)



(b)

Pine Wood , Restricted Ventilation (174 kW/m²air, 35 kW/m²)



(c)

Figure 5-11 Mass, HRR based on the mass loss rate, adjusted HRR, based on inefficiency of combustion for; 59 kW/m² air (a) 112 kW/m² air (b) 174 kW/m² air (c)

The heat release rates corrected for inefficiencies are shown in Fig. 5-11. The difference between the corrected and the calculated was largely during the char burning phase where the yields of CO and unburnt total hydrocarbon were at their peak.

5.3 The Influence of Heat flux on Toxic Gas Emissions

In fire safety engineering a set of data on the toxic product yields of commercial products is required as a function of fire condition. Apart from the type of material, different parameters or conditions affect the yields of combustion products such as the fuel/air ratio; whether it is flaming or not; the stability of the flame; the temperature of the sample and the toxic effluent produced; the stability of the

decomposition conditions; and how the equipment interacts with the flames and the effluent [129]. It is therefore important to determine the yields and concentrations of toxic gases produced from different materials thermally decomposed under various fire conditions. In this section, the toxic gas emissions from block board wood at varying heat flux are presented. Varying the radiant heat fluxes allows for the measurement of toxicity dependent on the fire condition; flaming and non-flaming, complete and incomplete combustion. Incomplete combustion could be caused by insufficient oxygen or insufficient heat.

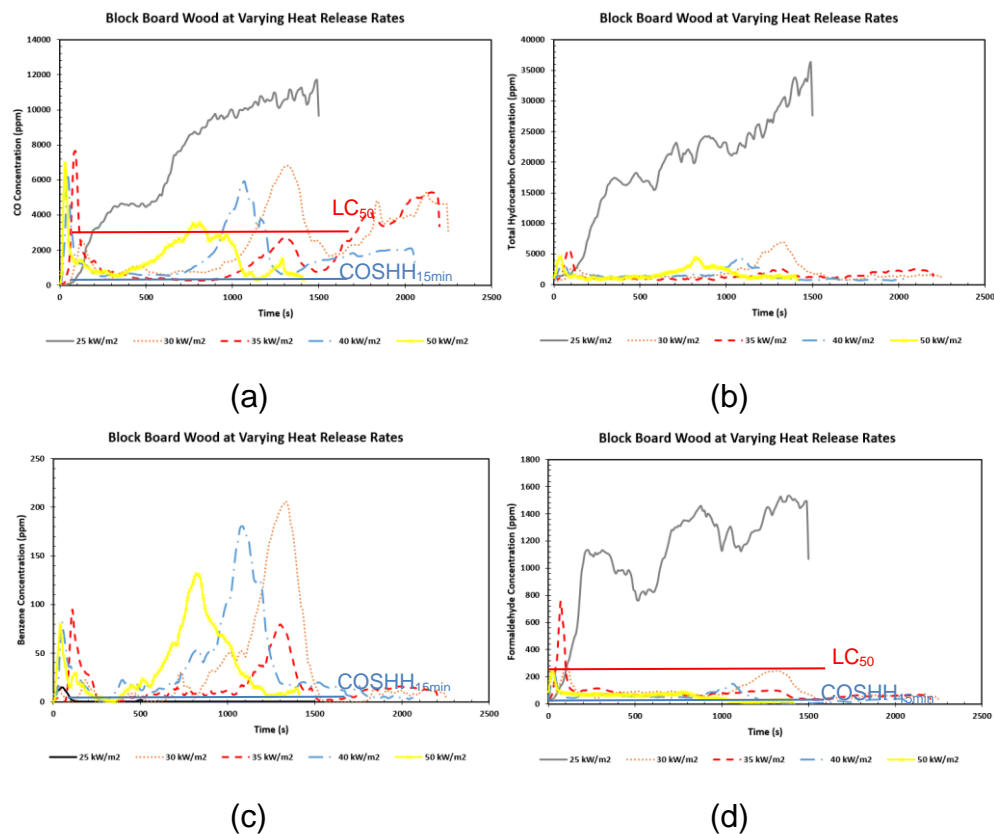
5.3.1 Toxic Gas Concentration

Carbon monoxide, a product of incomplete combustion is released in most fires especially compartment fires but the concentration may vary according to the condition of the fire and type of material. In these tests, the concentration of CO exceeded both the LC₅₀ and COSHH_{15min} toxicity limits. The 25 kW/m² test which did not ignite produced the highest concentration of CO as shown in Fig. 5-12a. Its failure to ignite resulted in the high values of CO obtained in the test. Figure 5-12a shows that there were more than two peaks in CO except for the 25 kW/m² test which did not ignite: in the initial flaming combustion period from 50-290 s, from 1030–1550 s and in the char burning phase. The LC₅₀ threshold limit was exceeded by a factor of 4 while that of COSHH_{15min} was exceeded by a factor of 60. For the 30 kW/m² test, the first peak was 2400 ppm and the second 6800 ppm. The third and fourth peaks occurred during the char burning. The 35 kW/m² test had the highest initial peak of 7650 ppm at 90 s just after ignition (85 s) and a second peak of 2600 ppm. The high initial peak was due to the rich combustion that occurred during the ignition delay period as shown in the equivalence ratio graph, and this led to the release of high CO. There was a third and a fourth peak with the fourth peak occurring in the char burning phase. The 40 kW/m² test had an initial combustion peak of 6300 ppm just after ignition and second peak of 5900 ppm and an increase in CO concentration at the char burning phase. The 50 kW/m² test had a CO peak of 7000 ppm just after ignition and a much lower second peak of 3500 ppm at 800 s with an increase in CO concentration at the char burning phase. The highest peaks in CO occur at the same time the peaks in equivalence ratio occurred. Figure 5-12b shows the total unburned

hydrocarbon against time. The peaks in THC occurred at the same time the CO concentration peaks occurred in all tests. Each individual hydrocarbon also showed the same two peaks in emissions as illustrated by the results for benzene in Fig. 5-12c.

Figure 5-12c shows that the LC₅₀ limit for the concentration of benzene obtained has not been exceeded, but it exceeds the COSHH_{15min} limit of toxicity. The 30 kW/m² test had the highest peak value of 200 ppm while the lowest concentration of 15 ppm was obtained in the 25 kW/m² test which occurred in the first 50 s of the test and reduced to zero afterwards. The 35, 40 and 50 kW/m² test had peaks of 98, 180 and 130 ppm respectively, with the 35 kW/m² having its highest peak during the ignition delay period while the 40 and 50 kW/m² test had their highest peaks during the second flaming stage. At low heat, as in the case of the 25 kW/m² test, the concentration of benzene was very low. This means that more heat is required to release benzene in fires.

Formaldehyde emissions are shown as a function of time in Fig. 5-12d and this shows two peaks for all tests except for the 25 kW/m² test. The two peaks aligned with those for THC.



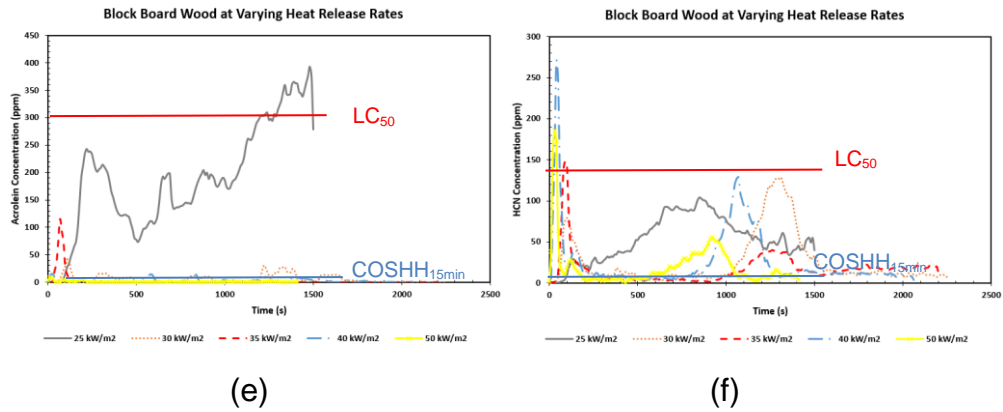


Figure 5-12 Toxic gas concentrations; CO (a), Total Hydrocarbon (b), Benzene (c), Formaldehyde (d), Acrolein (e) and Hydrogen Cyanide (f)

Formaldehyde exceeded its COSHH_{15min} toxicity limit of 2 ppm in all the tests. It also exceeded its LC₅₀ toxicity limit of 250 ppm in the 25, 30 and 35 kW/m² test respectively. The 25 kW/m² test produced the highest concentration of formaldehyde with a value of 1500 ppm followed by 35 kW/m² with a value of 760 ppm. The highest concentration in the 30, 35, 40 and 50 kW/m² tests occurred at the initial combustion stage. The highest peak value of 240 kW/m² was recorded in the 40 and 50 kW/m² test. These results show that the lower heating rates produced more formaldehyde than the higher heating rates.

Figure 5-12e shows the concentration of acrolein as a function of time for all tests and this is similar to what was obtained in formaldehyde, that is, 25 and 35 kW/m² tests having high peak values of 400 and 118 ppm respectively. The concentration of acrolein obtained in all the tests exceeded the COSHH_{15min} toxicity limit of 0.3 ppm. Only in the 25 kW/m² test was the LC₅₀ toxicity limit of 300 ppm exceeded. The high values obtained in the 25 kW/m² test is mainly due to low heat which caused incomplete combustion of the wood. The 35 kW/m² had more heat than the 30 kW/m² but produced higher acrolein concentration. This could be due to the much longer burning duration which allowed more acrolein to be released from the fire. The 40 and 50 kW/m² test had high heat and therefore higher fire temperature which burned fast, leading to a more efficient combustion and hence the low concentration of acrolein.

Hydrogen cyanide concentration against time for all tests is shown in Fig. 5-12f. The COSHH_{15min} toxicity limit of 10 ppm was exceeded in all tests. The 35, 40 and 50 kW/m² tests produced HCN which exceeded the LC₅₀ limit of 135 ppm.

Two peaks were observed in all tests except the 25 kW/m² test with most of the fires having the highest peak occurring at the initial flaming stage at the same period other toxic gases were released. These high values of hydrogen cyanide are as a result of the nitrogen content (0.93 %) in the block board wood as obtained from the elemental analysis. This nitrogen is a bit high for wood as natural wood contains about 0.3 % of nitrogen. This high nitrogen content could be as a result of how the wood was processed and the use of adhesives to stick the various layers together and hence the high concentration of HCN emitted. The high concentrations of toxic gases produced by the test that smouldered only is of great concern and suggests that low temperature fires are also a potential threat to people. This is in agreement with literature [50-52] where they mentioned that smouldering fires produce high yield of toxic species and can be lethal when produced for a long duration in enclosures or compartments.

5.3.2 Total Fire Toxicity N on an LC₅₀ and COSHH_{15min} Basis

The total toxicity **N** for LC₅₀ and COSHH_{15min} are shown as a function of time in Fig. 5-13. Both methods of deriving **N** showed similar shapes of the dependence of **N** on time for all tests. Despite the differences in relative toxicity, the two methods for calculating **N** locate the same time in the fire where the peak toxicity occurs. The 25 kW/m² which did not ignite had by far the highest total toxicity in terms of LC₅₀ and COSHH_{15min}. The **N** value relative to LC₅₀ value was 12 and the **N** value relative to COSHH_{15min} was 5200. The 35 kW/m² test was the next most toxic both in terms of LC₅₀ and COSHH_{15min} having values of 7 and 1630 respectively. The 30, 40 and 50 kW/m² tests had similar LC₅₀ value of 5 approximately. The total **N** on COSHH_{15min} basis gives values of 600 for the 30 kW/m² test, 307 for the 40 kW/m² test and 284 for the 50 kW/m² test. This means that the toxic gases need to be diluted with fresh air by a factor of about 284-5200 before escape is not impaired and it has to be diluted by a factor 5-12 before it doesn't kill anybody in 30 mins. The peaks of **N** in tests that ignited, correspond to the periods where the mass loss rates and equivalence ratios were at their peak. The two methods showed that the lowest heat flux which did not ignite produced the highest toxicity both in terms of lethality and impairment of escape.

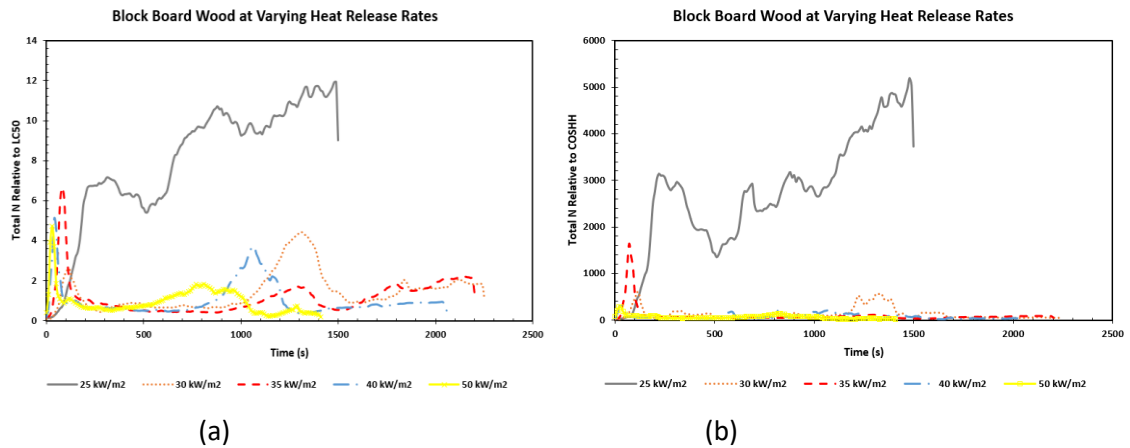


Figure 5-13 Total N relative to LC₅₀ (a) and COSHH_{15min} (b)

Figures 5-14 and 5-15 show the major contribution to the total toxicity on an LC₅₀ and COSHH_{15min} basis for the block board wood tests. The 25 kW/m² test was dominated by, formaldehyde followed by CO, acrolein and HCN on an LC₅₀ basis and acrolein, formaldehyde and benzene on a COSHH_{15min} basis. The contribution of CO and HCN was not more than 2% on a COSHH_{15min} basis throughout the combustion. The 30 kW/m² toxicity was dominated by CO, formaldehyde, HCN and acrolein on an LC₅₀ basis, but formaldehyde was more significant on COSHH_{15min} basis, followed by acrolein, CO and benzene. HCN contribution was about 5% on COSHH_{15min} basis. The 35 kW/m² toxicity was dominated by formaldehyde at the initial stage of the fire up to about 900 s but CO dominated from about 900 s till the end of the test on an LC₅₀ basis. This was followed by HCN with about 30% contribution. Acrolein contribution was < 10% and this was at the early stage of the combustion. However, on a COSHH_{15min} basis, formaldehyde dominated the toxicity, followed by CO, benzene and HCN. Acrolein was also significant but only at the early stage of the combustion. The 40 kW/m² test had CO, formaldehyde, HCN and acrolein dominating on an LC₅₀ basis, with < 10% contribution from acrolein. On COSHH_{15min} basis, formaldehyde dominated the toxicity followed by acrolein, CO, benzene and HCN. On an LC₅₀ basis, CO dominated the toxicity during the 50 kW/m² test followed by formaldehyde and HCN. Acrolein contribution was < 5%. On COSHH_{15min} basis, the highest contribution was from formaldehyde, followed by benzene, acrolein, CO and HCN. Just like the results obtained from pine wood tests, the block board wood tests showed that benzene was also a

significant contribution to the toxicity in block board fires. The different heating rates produced different toxic gases in terms of importance and concentration and these shows that different materials should be tested at different conditions to understand how they behave and the amount of toxic products they produce under such conditions.

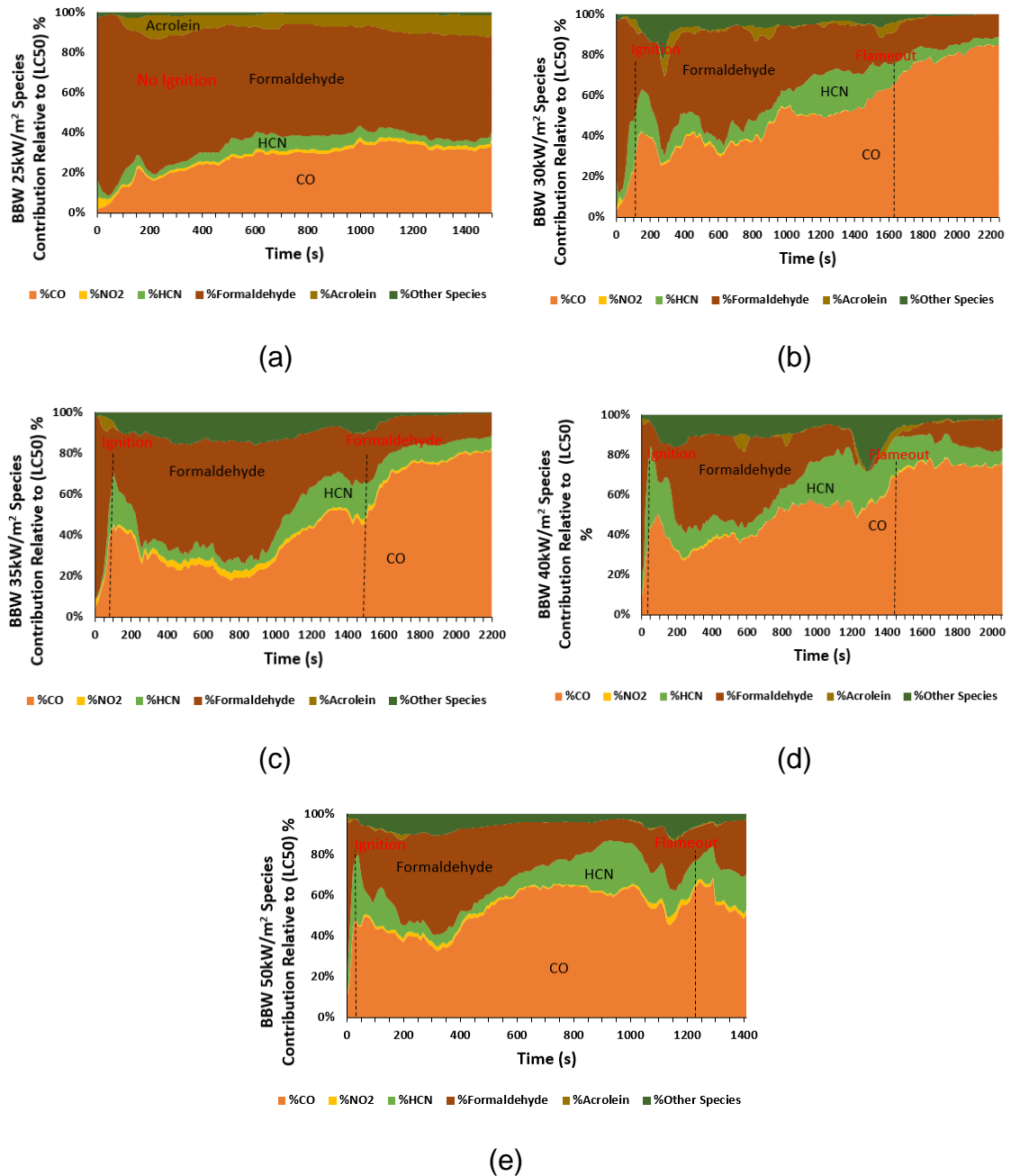


Figure 5-14 Species Contribution relative to (LC₅₀) BBW; 25 kW/m² (a) 30 kW/m² (b) 35 kW/m² (c) 40 kW/m² (d) and 50 kW/m² (e)

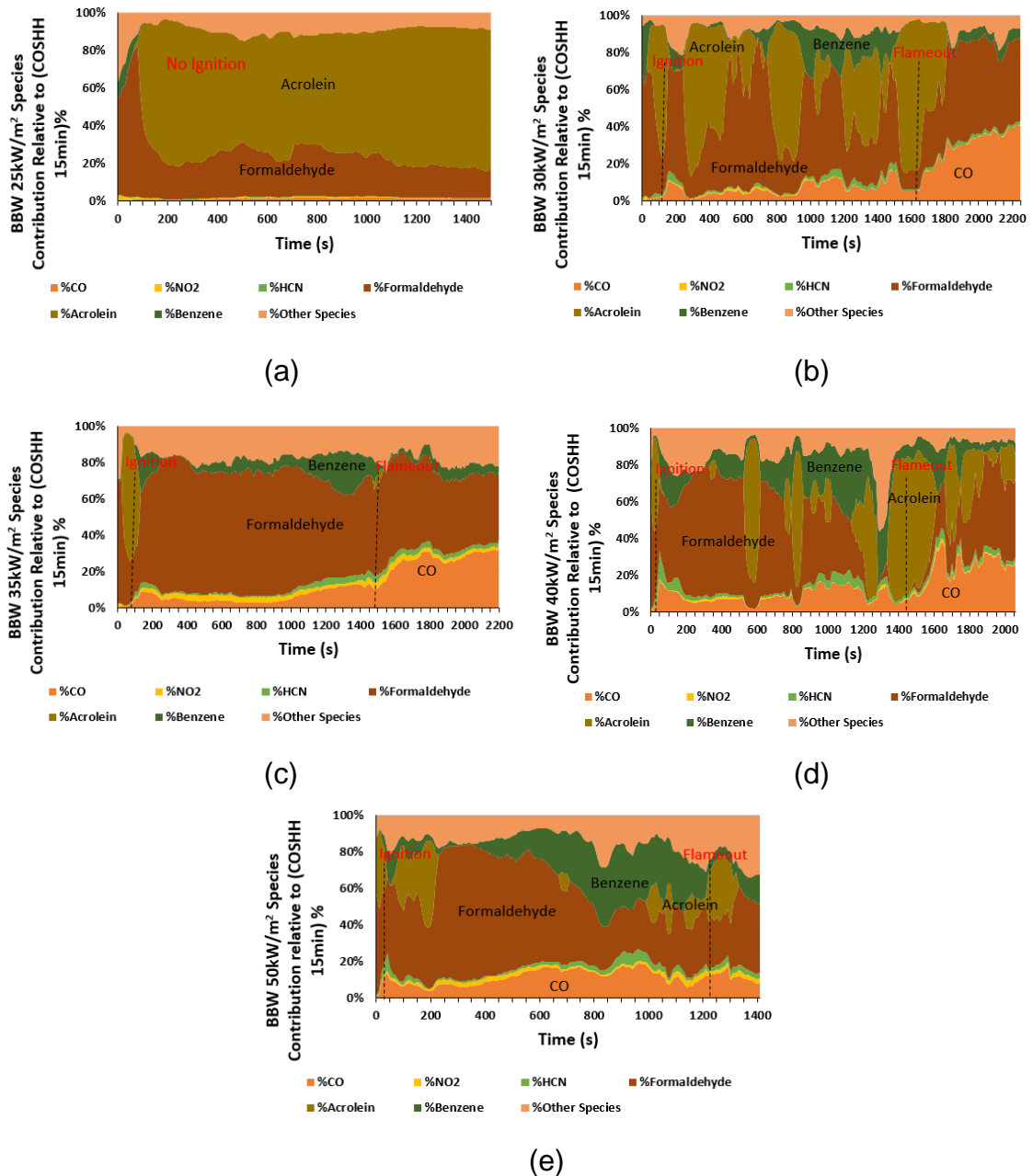


Figure 5-15 Species Contribution relative to (COSH_H 15min) BBW; 25 kW/m² (a) 30 kW/m² (b) 35 kW/m² (c) 40 kW/m² (d) and 50 kW/m² (e)

5.3.3 Toxic Gas Yields

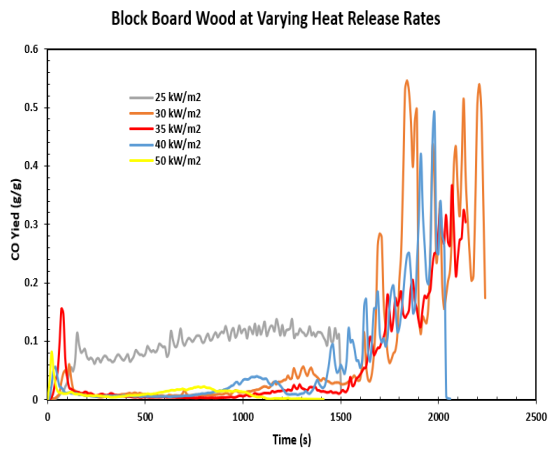
The toxic yields of the most important gases are presented in Fig. 5-16. The 25 kW/m² test which did not ignite produced its highest yield of CO (0.12 g/g) from 150 s to 1500 s as shown in Fig. 5-16a. Its failure to ignite resulted in the high values of CO obtained in the test. The rest of the tests produced their highest yields at the char burning phase with the exception of the 50 kW/m² test having its highest yield of 0.081 g/g during the ignition delay and a very low yield once

the wood ignited. Some of the yields showed that there were more than 2 peaks in some of the tests: in the initial flaming combustion period, a second peak during the second flaming combustion and a third peak during the char burning. The 30 kW/m² test had the highest CO initial peak of 0.06 g/g at 110 s just before ignition (110 s) and a second peak of 0.046 g/g and a much higher yield of 0.547 g/g during the char burning phase. The 35 kW/m² test had the highest CO initial peak of 0.155 g/g at 70 s just before ignition (85 s) and a second peak of 0.025 g/g and a much higher yield of 0.367 g/g during the char burning phase. The high initial peak was due to the rich combustion that occurred during the ignition delay period as shown in the equivalence ratio graph, and this led to the release of high CO. The 40 kW/m² test had an initial peak CO yield of 0.055 g/g just after ignition and second peak of 0.038 g/g and an increase in CO yield (0.489 g/g) at the char burning phase. The highest peaks in CO occur at the same time the peaks in equivalence ratio occurred. Figure 5-16b shows the total unburned hydrocarbon (THC) yield against time. The peaks in THC occurred at the same time as the CO concentration peaks occurred in all tests. Each individual hydrocarbon also showed the same peaks in emissions as illustrated by the results for benzene in Fig. 5-16c. The 25 kW/m² fire produced the highest yield of unburnt total hydrocarbon and other toxic gases as illustrated in Fig. 5-16. A summary of the most important toxic yields are given in Table 5-4.

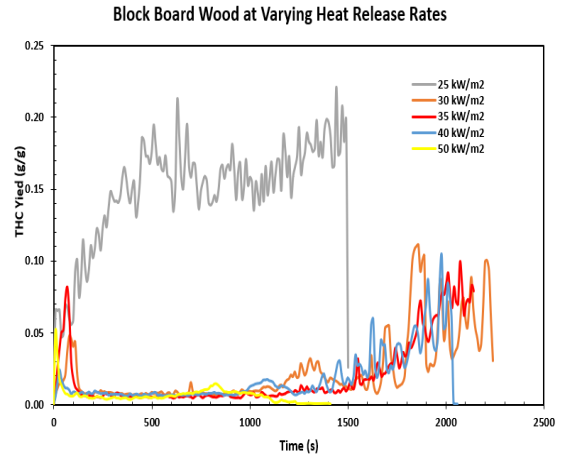
Table 5-4 Toxic Gas Yields for Pine Wood Restricted Ventilation

Toxic Gas	Peak Yield and Time to Peak yield for Pine Wood		
	1 st Peak g/g	2 nd Peak g/g	3 rd Peak g/g
CO			
25 kW/m ²	0.12 (150 s)	-	-
30 kW/m ²	0.06 (110 s)	0.046 (1320 s)	0.547 (1840 s)
35 kW/m ²	0.155 (70 s)	0.025 (1290 s)	0.367 (2070 s)
40 kW/m ²	0.055 (40 s)	0.038 (1060 s)	0.489 (1980 s)
50 kW/m ²	0.081 (20 s)	0.022 (800 s)	-
THC			
25 kW/m ²	0.17	0.17	0.17
30 kW/m ²	0.048 (80 s)	0.032 (1310 s)	0.111 (1860 s)
35 kW/m ²	0.08 (70 s)	0.009 (1320 s)	0.099 (2070 s)

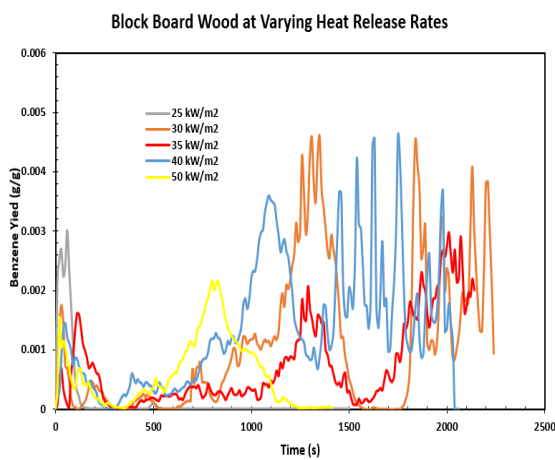
40 kW/m ²	0.024 (30 s)	0.017 (1080 s)	0.103 (1980 s)
50 kW/m ²	0.052 (10 s)	0.014 (830 s)	-
Acrolein			
25 kW/m ²	0.011 (220 s)	0.006 (680 s)	0.008 (1340 s)
30 kW/m ²	0.0023 (110 s)	0.0003 (1330 s)	0.0018 (1620 s)
35 kW/m ²	0.0068 (70 s)	-	-
40 kW/m ²	0.0004 (30 s)	-	0.001 (1450 s)
50 kW/m ²	0.0008 (10 s)	-	-
Formaldehyde			
25 kW/m ²	0.029 (190 s)	0.17	0.17
30 kW/m ²	0.011 (80 s)	0.0018 (1320 s)	0.01 (1850 s)
35 kW/m ²	0.024 (70 s)	-	0.005 (2030 s)
40 kW/m ²	0.004 (30 s)	0.001 (1060 s)	0.009 (1980 s)
50 kW/m ²	0.009 (10 s)	-	-
Benzene			
25 kW/m ²	0.003 (60 s)	-	-
30 kW/m ²	0.002 (30 s)	0.005 (1310 s)	0.005 (1840 s)
35 kW/m ²	0.0016 (110 s)	0.002 (1290 s)	0.0013 (1990 s)
40 kW/m ²	0.0015 (50 s)	0.004 (1100 s)	0.005 (1750 s)
50 kW/m ²	0.0015 (20 s)	0.002 (820 s)	-
HCN			
25 kW/m ²	0.0016 (120 s)	0.0013 (650 s)	-
30 kW/m ²	0.0031 (80 s)	0.0009 (1300 s)	0.0018 (1880 s)
35 kW/m ²	0.0026 (80 s)	0.00036 (1290 s)	0.0014 (2070 s)
40 kW/m ²	0.0024 (30 s)	0.0008 (1070 s)	0.0024 (1980 s)
50 kW/m ²	0.0024 (10 s)	0.0003 (940 s)	-



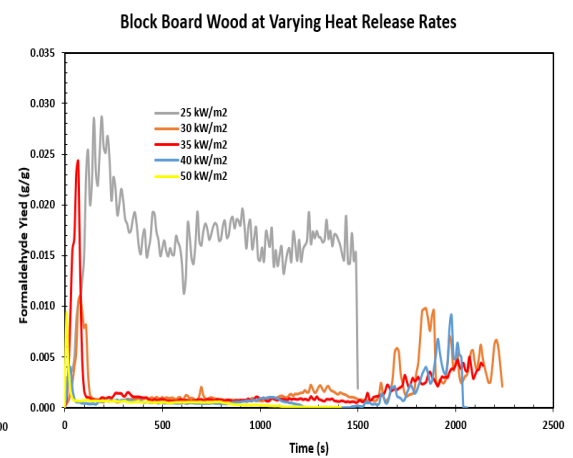
(a)



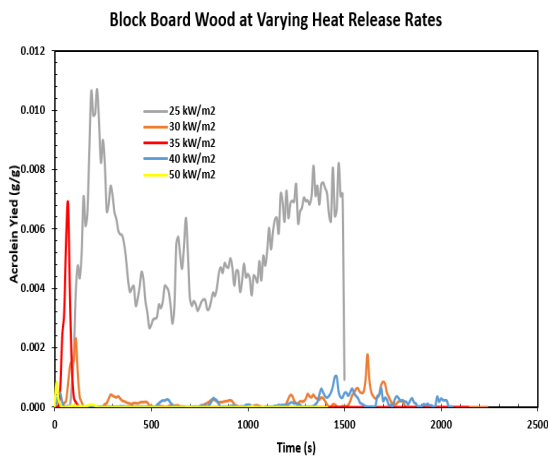
(b)



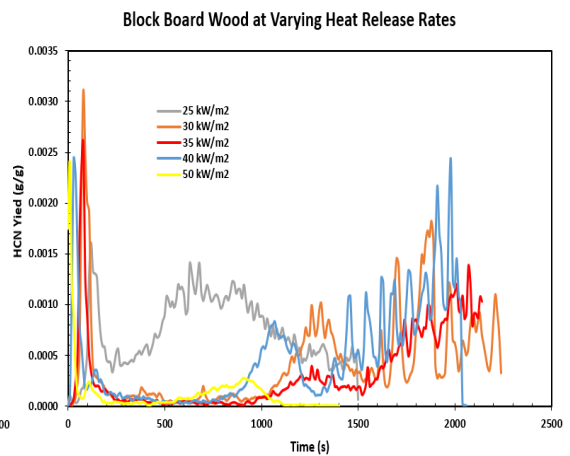
(c)



(d)



(e)



(f)

Figure 5-16 Toxic Gas Yields; CO (a), Total Hydrocarbon (b), Benzene (c), Formaldehyde (d), Acrolein (e) and Hydrogen Cyanide (f).

5.3.4 Combustion Efficiency and Heat Release Rate Correction

The combustion efficiency and heat release rates corrected for inefficiencies are presented in Figs. 5-17 and 5-18. The 25 kW/m² test had the lowest combustion efficiency because of the high release of unburnt hydrocarbons and CO which is an indication of incomplete combustion. The efficiency was about 77% throughout the period of smouldering as it did not ignite. The rest of the test had an almost 100% efficiency during the steady state combustion period, with a low efficiency during the smouldering or char burning phase.

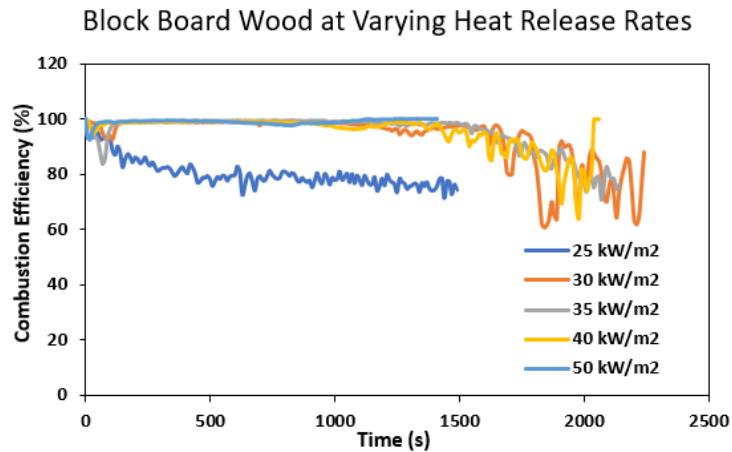
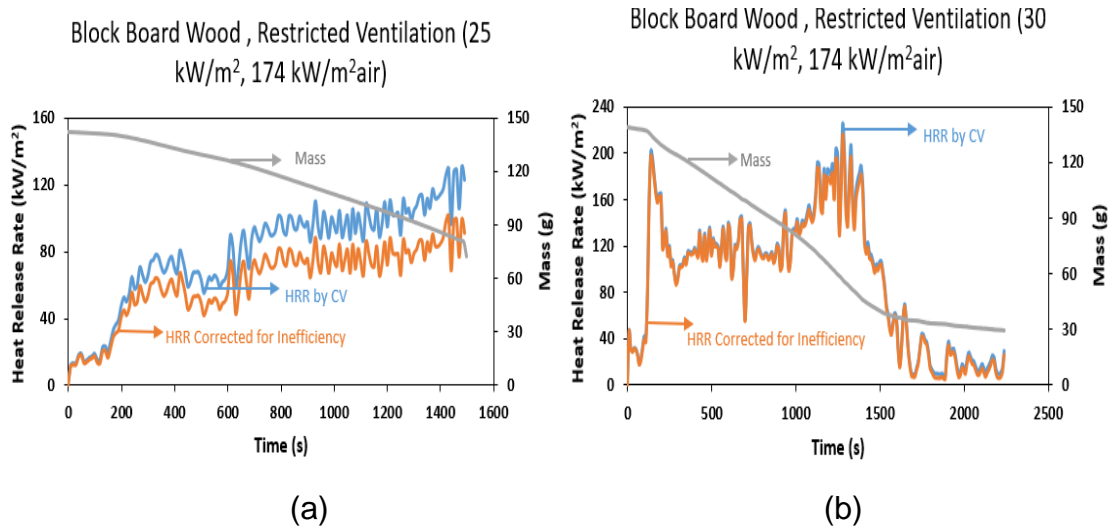


Figure 5-17 Combustion Efficiency for Block Board Wood



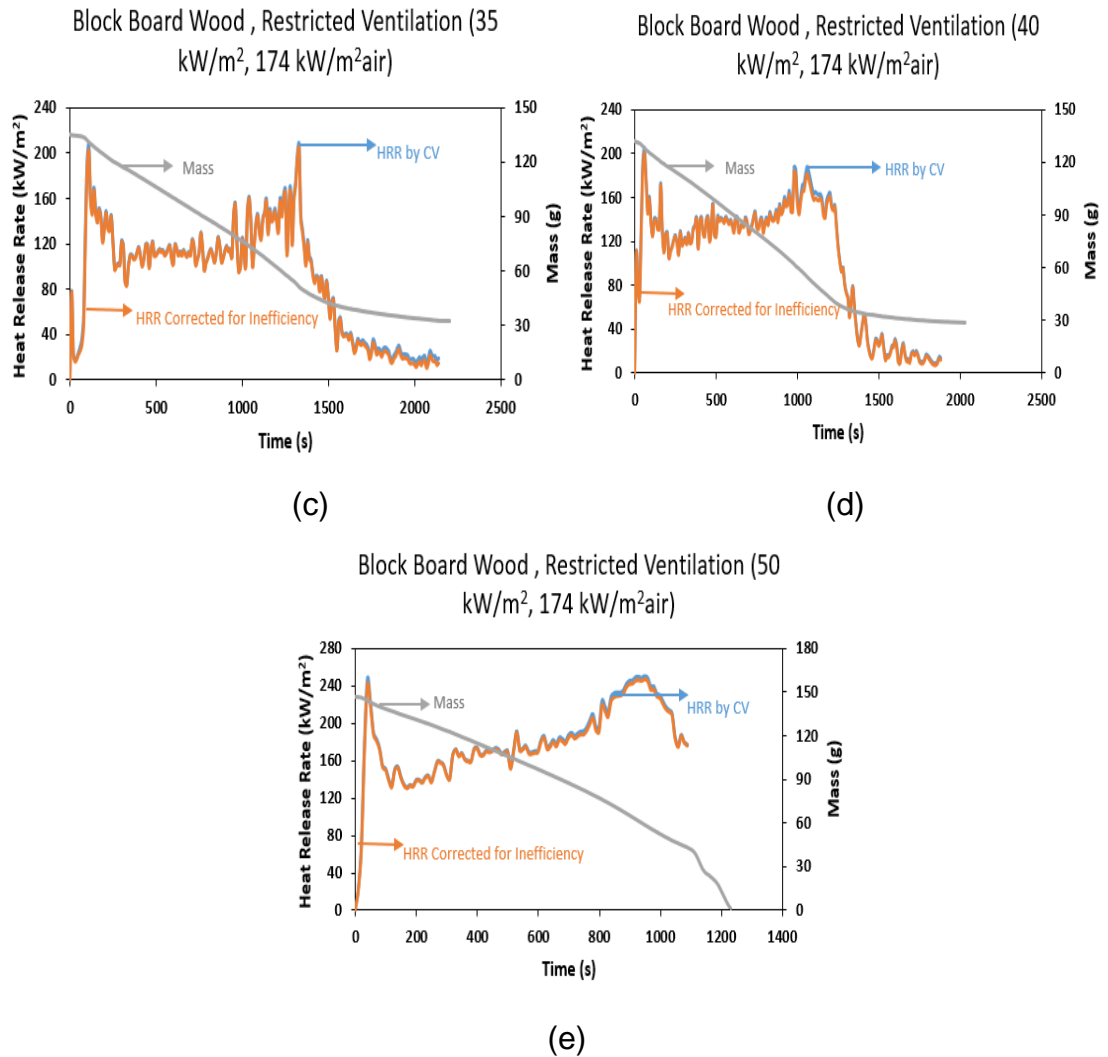


Figure 5-18 Mass, HRR based on the mass loss rate, adjusted HRR, based on inefficiency of combustion for; 59 kW/m² (a) 112 kW/m² (b) 174 kW/m² (c)

The heat release rates corrected for inefficiency did not show much difference from that calculated using the calorific value. This is as a result of the high efficiency experienced during the combustion. Only the test that smouldered (25 kW/m²) showed a significant difference in the two heat release rates, as a result of the high yield of CO and unburnt hydrocarbon produced

5.4 Particulate Emissions from Wood Samples in Controlled Atmosphere Cone Calorimeter

This section presents the particle size, number and mass concentrations obtained from the pine wood and block board tests. Comparisons are made to

show the effects of the various test conditions on the production of particles in fires.

5.4.1 Pine Wood

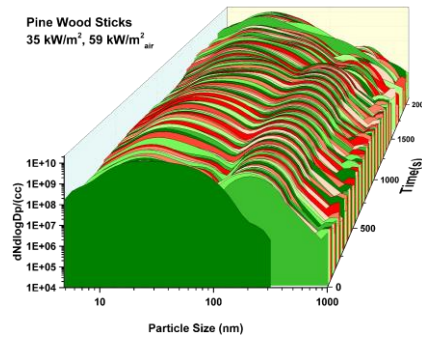
Particle number, mass concentrations and yields produced from pine wood fires at varying airflow rates of 59 kW/m²_{air}, 112 kW/m²_{air} and 174 kW/m²_{air} as described in Table 3-2, are compared in this section.

5.4.1.1 Particle Number Concentration

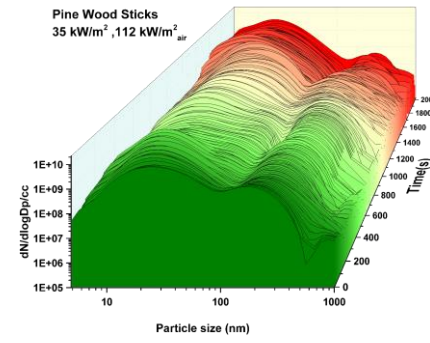
Figure 5-19 shows the number concentration and size distributions for the different airflow rates from the start of the tests to the end of sampling. Figure 5-20 shows some individual size distribution at defined times, which is easier to read the particle number. Size distributions were bimodal for all tests with one mode representing the nucleation mode and the other representing the accumulation mode. The nucleation mode was 20 nm for all tests and the accumulation mode was 200 nm. The initial particle size distribution during the ignition delay period of the 59 kW/m²_{air} test showed only Nano particles with a peak at 20 nm. These are likely to be liquid hydrocarbon aerosols and the high peak in THC in this period supports this. Once flaming combustion started there was a bimodal size distribution of nuclei particles centered on 20 nm and accumulation mode particles centered on 200 nm. The number based size distribution was reasonably consistent from 100 to 1500 s, which is the main flaming combustion period. There were differences in size distribution in the char burning phase of the fire, with a reduction in the number of accumulation mode particles. Particle concentrations were highest when the heat release was at its peak and gradually decreased after the flameout. The 112 kW/m²_{air} test in Fig. 5-19b showed a similar pattern but had a bimodal size distribution even before ignition took place. Particles were also 20 nm and 200 nm for the nucleation and accumulation mode. The 174 kW/m²_{air} test showed a different pattern at the start of the test, producing 1 x 10¹⁰/cc particles of the vaporised aerosols of 20 nm for 51 s (during the ignition delay). There was then a sudden decrease of the 20 nm particles after ignition as can be seen in Figs. 5-19c and 5-21 with < 1x 10⁸/cc and > 1x10⁸ /cc continued to be produced during the flaming combustion and increased to 1x10¹⁰ /cc when the heat release was at its peak but between

$1 \times 10^9/\text{cc}$ and $> 1 \times 10^8/\text{cc}$ particles were produced during the smouldering combustion. The 200 nm accumulation mode particles were produced throughout the flaming phase at $1 \times 10^9/\text{cc}$ and reduced to $>1 \times 10^8/\text{cc}$ during smouldering.

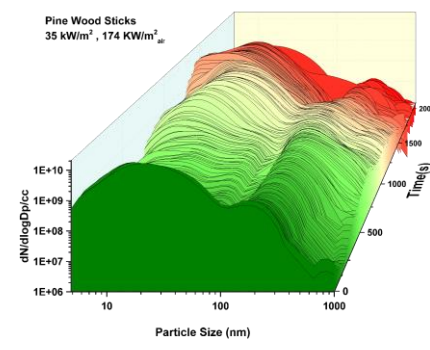
There have been relatively few previous measurement of particle size distribution in fires and none to the knowledge of the author in simulated or real compartment fires. Hertzberg et al [133, 151] used the Dekati ELPI aerodynamic particle size analyser to measure the particle number from 40 to 10 μm for a range of fire materials for the Purser furnace. At 200 nm the particle number varied from $10^5 - 10^8 / \text{cc}$, with the highest value for an unspecified wood. In the present work for $59 \text{ kW}/\text{m}^2_{\text{air}}$ pine wood, at 200 nm there were $10^9 / \text{cc}$ and the higher value is likely to be due to the simulation of a compartment fire using the modified cone calorimeter. Goo [155] has also used the ELPI aerodynamic size analyser for wood fires with the Purser steady state furnace method and reported particle number of $10^7 / \text{cc}$ at 200 nm, but the equivalence ratio of the tests were not given. These measurements are well below those in the present work. However, the Purser tube furnace method has a variable dilution ratio, which depends on the fire equivalence ratio that is simulated and varies between 5 and 25/1. If the measured particle number are corrected back to the concentration at the tube exit then they would increase by a factor of about ten and then be in better agreement with the present work. No measurements exist for particle number emissions from fires, to the knowledge of the author, in the 5-40 nm size range, which are responsible for the greatest health risks as it is this size of particles that accumulate in the alveolar regions of the lungs and for the finest particles penetrate into the blood stream. Figure 5-20a also compares the particle number distribution at different times during the test with tests from biomass pellets in a heater [154] for boilers and Euro 2 Diesel [192]. This shows that the present pine wood cone calorimeter compartment fire tests produced very high ultrafine particles compared to the diesel and the biomass pellets. The 20 nm size was about 100 times higher than that produced from the diesel or the biomass pellet. The accumulative mode was also at least a factor of 10 higher in number. This means that fine particles are produced in fires in much greater quantities than the more controlled combustion of diesel engines and biomass pellet heaters.



(a)

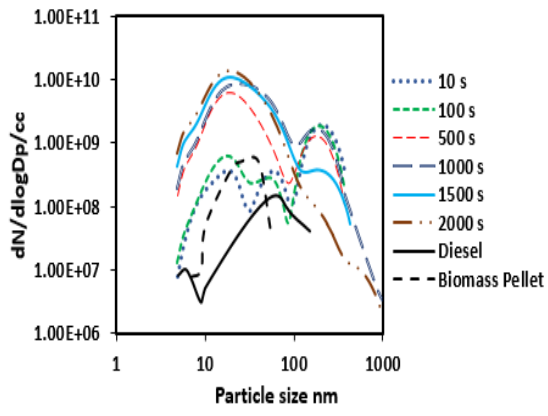


(b)

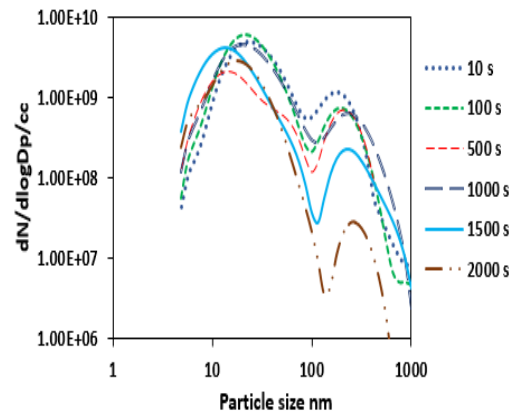


(c)

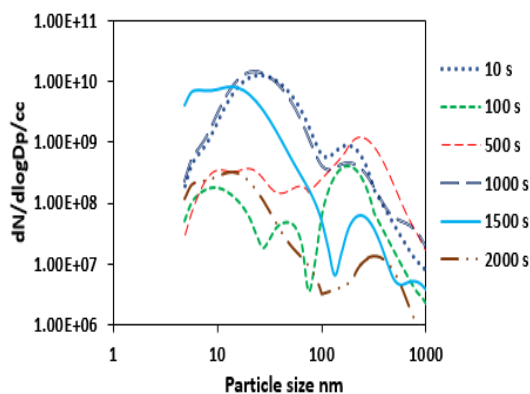
Figure 5-19 Particle Number and Size Distribution; 59 kW/m²_{air} (a) 112 kW/m²_{air} (b) and 174 kW/m²_{air} (c)



(a)



(b)



(c)

Figure 5-20 Particle Number and Size Distribution at Different times; 59 kW/m²_{air} Compared with Diesel [192] and Biomass Pellet [154] (a) 112 kW/m²_{air} (b) and 174 kW/m²_{air}

Figure 5-21 shows, as a function of time, the 20 nm and 200 nm sizes particle number, as characteristic of the nuclei and accumulative mode particles. The 20 nm nuclei particle number for the 59 kW/m²_{air} increased from 10⁹/cc to a peak of 10¹⁰/cc for the first 700 s. There was then a reduction by 30% from 700–1000 s and then an increase to 1.3 x 10¹⁰/cc just before the flame out. High 20 nm particles continued to be produced in the char burning phase, but there was a much reduced accumulative mode particle number. The 112 kW/m²_{air} test produced the 20 nm particle number at 7 x 10⁹/cc for the first 400 s and decreased to about 1.2 x 10⁹/cc. It then increased and reached a peak of 1.7 x 10¹⁰/cc at around 1400 s and then there was a decrease during the char burning phase.

The 174 kW/m²_{air} test produced the 20 nm particle number at 1 x 10¹⁰/cc during the ignition delay of 51 s, there was a significant reduction immediately after ignition to about 6 x 10⁷/cc for 100 s. It then increased gradually to a peak of 1.2 x 10¹⁰/cc from 900-1300 s with a much lower particle number during the char burning phase of 4 x 10⁷/cc. The 59 kW/m²_{air} test produced 200 nm accumulation mode particles at 1 x 10⁹/cc throughout the flaming phase and then reduced to <1 x 10⁸/cc in the smouldering phase of the combustion.

The 200 nm particles for the 112 kW/m²_{air} test were produced at 9 x 10⁸/cc throughout the flaming combustion but reduced to 4 x 10⁷/cc during the smouldering combustion phase. 1 x 10⁹/cc of 200 nm particles were produced from 170 - 670 s for the 174 kW/m²_{air} test and then reduced to about 4 x 10⁶/cc before the end of sampling. Particles in the range 30 nm – 100 nm had lower concentrations than the 20 nm particles.

The small size found in the present work is of great concern as that is where the greatest health hazard occurs. Particle number concentrations were highest when the heat release was at its peak and gradually decreased after the flameout. The aim of varying the inlet airflow was to investigate how it affects the production of particles and other toxic emissions. It was observed that the lowest airflow rate produced the highest number of particles both in the nuclei mode and the accumulation mode. Even though the highest airflow burned lean, the particle number produced is still high and of great concern.

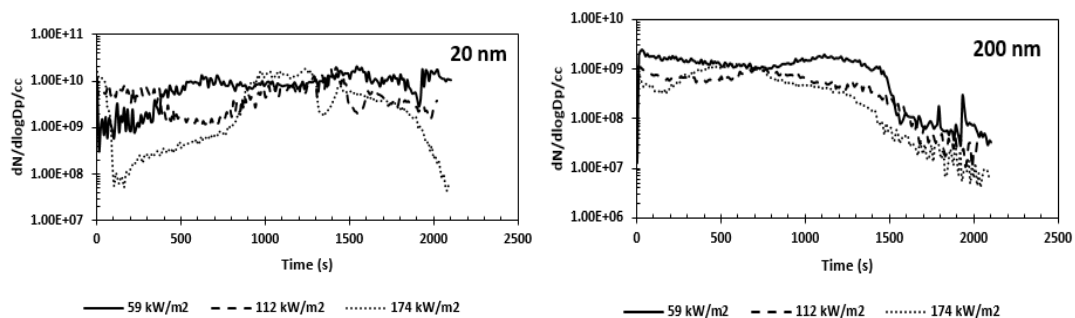
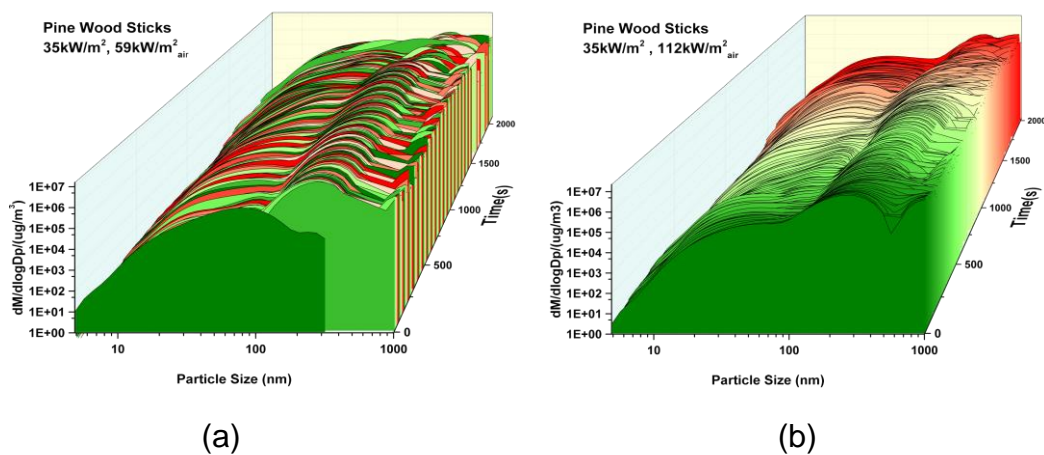


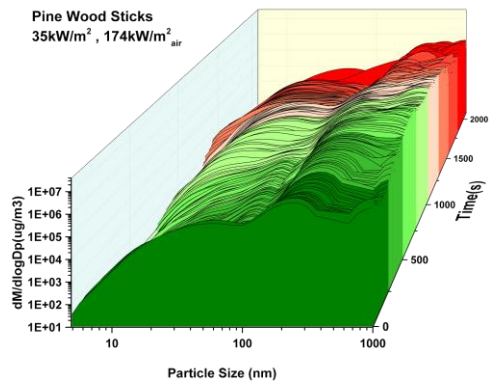
Figure 5-21 20 nm (a) and 200 nm (b) Particle Size Concentration as a Function of Time

5.4.1.2 Particle Mass Concentration

The equivalent mass distributions are shown in Figs 5-22 to 5-24. Figs. 5-22 and 5-23 show that there was less mass in the ultrafine particle region as compared to particles >100 nm, as expected, due to the particle volume and mass scaling with the cube of the particle diameter. Figure 5-24a shows that the 20 nm particle size had a mass of about 1 x 10⁵/μg/m³ (0.1 g/m³) and that the 200 nm mode had a mass of 1 x 10⁷/μg/m³ (10 g/m³) during the flaming phase of the combustion. It is also clear in Fig. 5-23 that there is more particle mass above the 1000 nm upper measurement range of the Combustion DMS500. In air

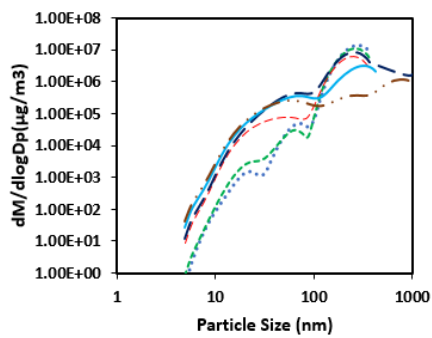
quality legislation for particulate emissions the European 24 hour limit for PM_{2.5} is 50 µg/m³ and the annual limit is 40 µg/m³. The 24 hour limit is a total particulate loading, for an average human breathing 10 m³ of air per day, of 0.5 mg/day. Exposure to the present pine wood fires would give a lung loading of 1 g per day of 20 nm particles and 100 g per day of 200 nm particles. For 20 nm particles this is 200 times the mass loading per day of PM₁₀ and for 200 nm particles it is 2000 times the fine particulate mass loading of a poor air quality day in terms of PM₁₀ air quality. The 112 kW/m²_{air} test produced the 20 nm particle mass at 3.2 x 10⁴ /µg/m³ for the first 400 s and decreased to about 5.6 x 10³/µg/m³. It then increased and reached a peak of 8.0 x 10⁴/µg/m³ at around 1400 s and then there was a decrease during the char burning phase. The 200 nm particle mass for the 112 kW/m²_{air} test was produced at 5 x 10⁶ /µg/m³ throughout the flaming combustion but reduced to 1 x 10⁵ /µg/m³ during the smouldering combustion phase. The 174 kW/m²_{air} test produced the 20 nm particle mass at 4 x 10⁴/µg/m³ during the ignition delay of 51 s, there was a significant reduction immediately after ignition to about 280/µg/m³ for 100s. It then increased gradually to a peak of 7 x 10⁴/µg/m³ from 900-1300 s with a much lower particle mass during the char burning phase of 200/µg/m³. 5 x 10⁶/µg/m³ of 200 nm particle mass was produced from 170 -670 s for the 174 kW/m²_{air} test and then reduced to about 2 x 10⁴/µg/m³ before the end of sampling. This represents a major health risk to people who breathe wood based particulates in fires. The situation will be worse for hydrocarbon based building products, as smoke yields are known to be about six times those for wood [82].



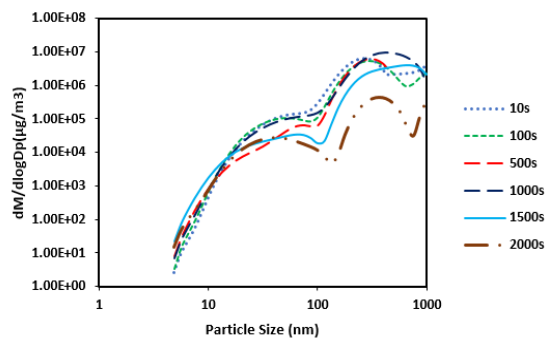


(c)

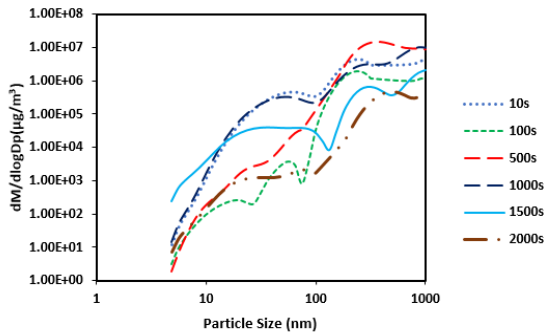
Figure 5-22 Particle Mass and Size Distribution; 59 kW/m²_{air} (a) 112 kW/m²_{air} (b) and 174 kW/m²_{air} (c)



(a)



(b)



(c)

Figure 5-23 Particle Mass and Size Distribution at Different times; 59 kW/m²_{air} (a) 112 kW/m²_{air} (b) and 174 kW/m²_{air} (c)

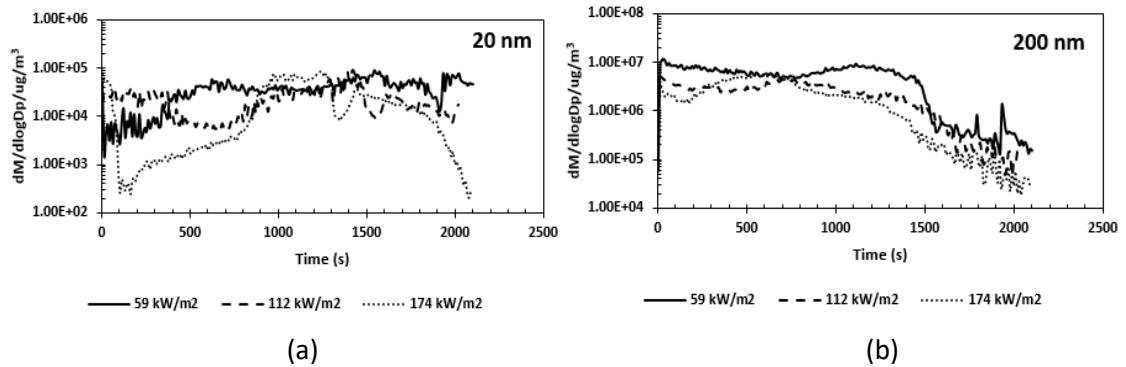


Figure 5-24 20 nm (a) and 200 nm (b) Particle Size Mass as a Function of Time

5.4.1.3 Particle Emission Index

Figure 5-25 shows the particle number for 20 nm and 200 nm particles as a function of the mass of wood burnt. This shows that for both particle sizes the particle number has a fairly constant relationship with the fuel mass burn rate. In the present work the air mass flow is constant so that the variation of equivalence ratio and mass burn rate in Fig. 5-1 are responsible for the trends in particle number. Only in the smoldering combustion phase of the fire were the trends in particle number different for 20 and 200 nm, with an increase in yield of 20 nm particles and a decrease with 200 nm particles. High yield of the 20 nm particles were produced in 59 and 112 kW/m²_{air} fires with the 20 nm particle for 59 kW/m²_{air} fire having a yield of about 3×10^{16} number/kg during the steady burning phase and a peak of 2.4×10^{17} number/kg during the char burning phase. The 112 kW/m²_{air} fire produced a similar 20 nm yield to that of the 59 kW/m²_{air} test at particles at 2.5×10^{16} number/kg during the steady burning phase and a peak of 2.4×10^{17} number/kg during the char burnout phase. The 174 kW/m²_{air} test produced a much higher yield as compared to the two richer mixtures, with the 20 nm particle having a yield of 3.7×10^{17} number/kg during the ignition delay and 3.1×10^{17} number/kg during the char burning phase. The 200 nm yield was lower than the 20 nm yield in all tests with the two lower airflow rates having a similar yield at steady state of about 5.0×10^{15} number/kg (59 kW/m²_{air}) and 4.0×10^{15} number/kg (112 kW/m²_{air}) and a much reduced yield during the char burnout phase. The highest airflow produced a 200 nm yield of about 9.5×10^{15} number/kg at steady state and again a much reduced yield during the char burning phase. The difference in the airflow greatly affected the production of

particles. The richer mixtures produced more particles both in the nucleation and the accumulation mode.

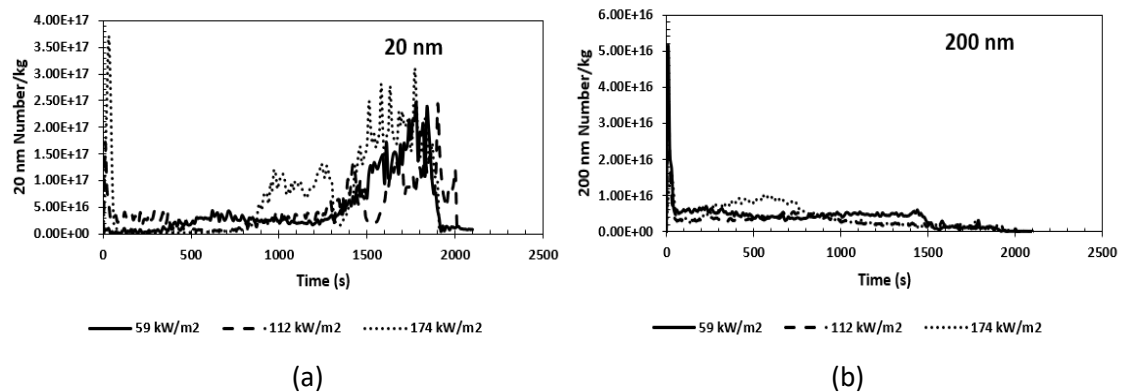


Figure 5-25 Particle Number per Mass of Fuel Burnt for 20 nm (a) and 200 nm (b) Particles

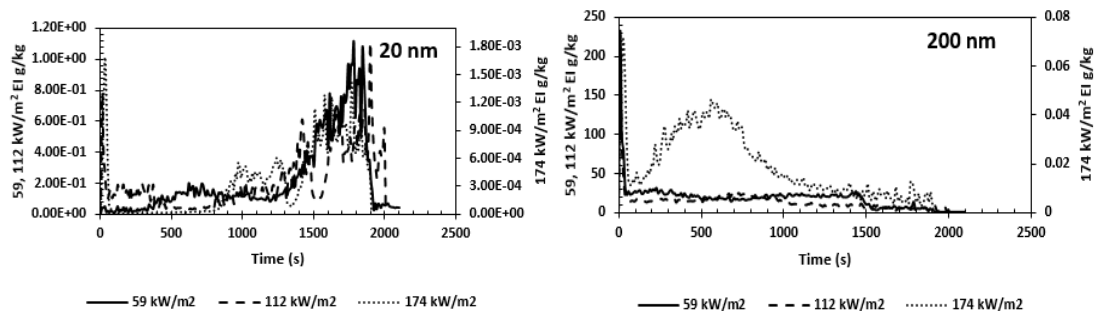


Figure 5-26 Particle Mass per Mass of Fuel Burnt for 20 nm (a) and 200 nm (b) Particles

The particle mass per unit mass of fuel burned shows the 20 nm particle for 59 kW/m² test having a yield of 0.04 g/kg during the ignition delay and 1.1 g/kg during the char burning phase while the 200 nm yield was about 232 g/kg during the ignition delay period, 21 g/kg during the steady state combustion and 5 g/kg during the char burning phase. The 112 kW/m²_{air} test however produced a 20 nm yield of about 0.77 g/kg during the ignition delay period and a much lower yield during the steady burning phase and a yield of 1.1 g/kg during the char burning phase while the 200 nm yield was as high as 178 g/kg at the ignition delay period, 17 g/kg at the steady state burning phase and 3 g/kg during the char burning phase. 174 kW/m²_{air} produced a 20 nm yield of about 0.02 g/kg during the ignition delay period and a much lower yield during the steady burning phase and a yield of 0.0014 g/kg during the char burning phase while the 200 nm yield was 0.07

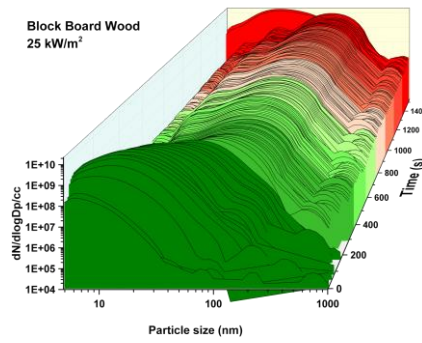
g/kg at the ignition delay period, 0.04 g/kg at the steady state burning phase and 0.008 g/kg during the char burnout phase. The time the peak particles were produced correspond to the time the heat release rate and mass burn rate were at their peak.

5.4.2 Block Board Wood

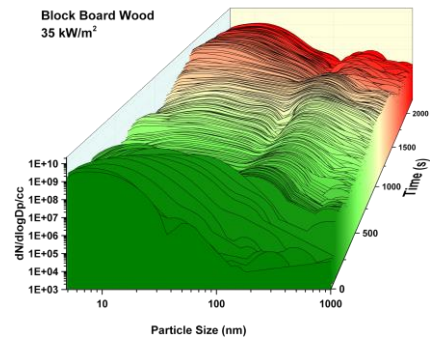
Particle number, mass concentrations and yields produced from block board wood fires at varying heat flux of 25 kW/m², 35 kW/m² and 50 kW/m² are compared in this section.

5.4.2.1 Particle Number Concentration

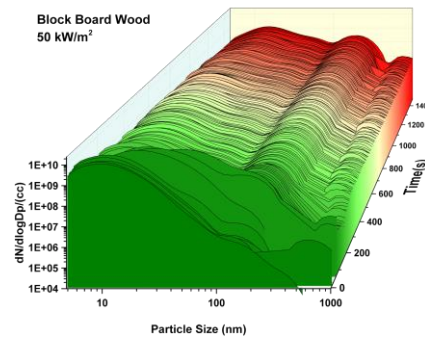
Figure 5-27 shows the particle number concentration as a function of size and time while Fig. 5-28 shows the particle concentration as a function of size at different times. The 25 kW/m² fire did not ignite as mentioned earlier. At the initial stage of the combustion, the 25 kW/m² test produced only nuclei particles of 10 nm size as shown in Fig. 5-28. At about 100 s, bimodal distribution of the particles was observed with the nuclei mode at 20 nm, with an average of 2.1×10^9 /cc and an accumulation mode at 100 nm with an average of 8.1×10^9 /cc. The accumulation mode particles were more than the nucleation mode particles in number. This is because smouldering fires are associated with low temperatures leading to heavy hydrocarbon compound and organic volatiles condensing out and adsorbing on the soot, forming larger sized particles through agglomeration. The 35 kW/m² test also produced only nuclei mode particles at the initial stage of the fire with a peak at 10 nm but once the wood sample ignited, there was a bimodal distribution of particles with the nuclei mode at 20 nm with a peak of 1.5×10^{10} /cc during the ignition delay, 7.1×10^8 /cc during the steady state combustion and a reduced particle number at the char burning phase. The accumulation mode centred at 200 nm with a particle number 3×10^8 /cc at the steady state burning phase. These nuclei particles formed at the initial stage of the combustion could be liquid hydrocarbon aerosols. The 50 kW/m² test produced bimodal distribution of particles with the nuclei mode centred at 10 nm with an average of 2.2×10^9 /cc and the accumulation mode centred at 200 nm with an average of 3.3×10^9 /cc.



(a)

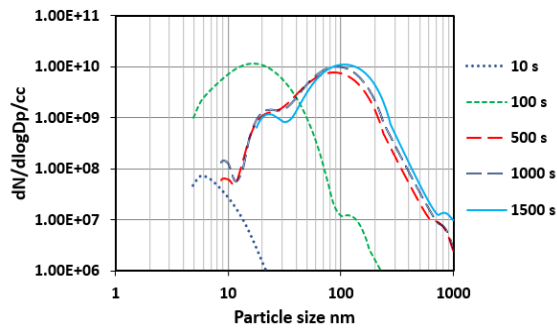


(b)

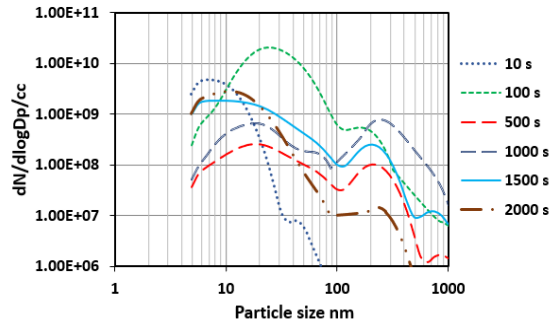


(c)

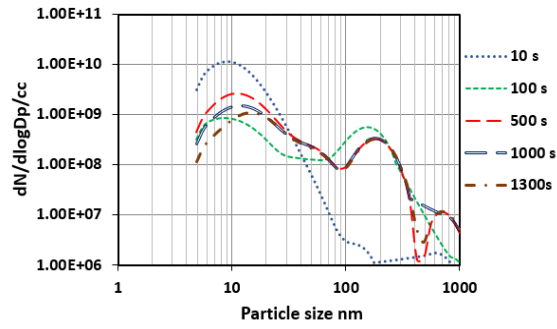
Figure 5-27 Particle Number and Size Distribution; 25 kW/m² (a) 35 kW/m² (b) and 50 kW/m² (c)



(a)

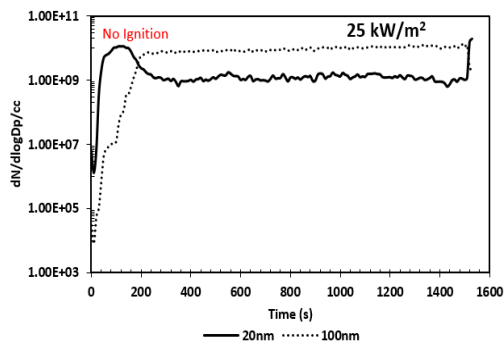


(b)

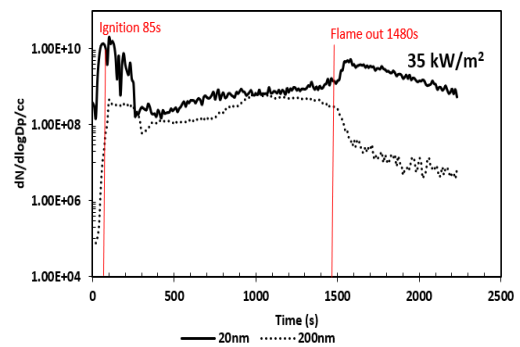


(c)

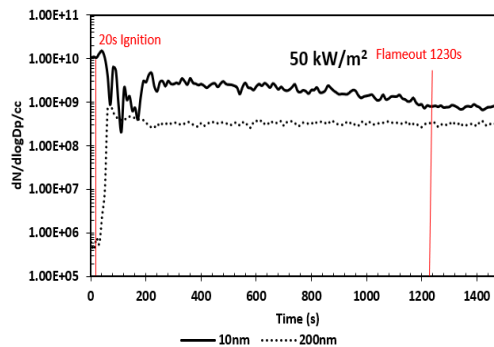
Figure 5-28 Particle Number and Size Distribution at Different times; 25 kW/m² (a) 35 kW/m² (b) and 50 kW/m² (c)



(a)



(b)



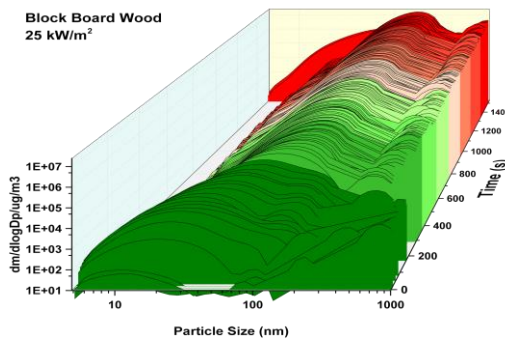
(c)

Figure 5-29 Nuclei and Accumulation mode sizes particle number for; 25 kW/m² (a) 35 kW/m² (b) and 50 kW/m² (c)

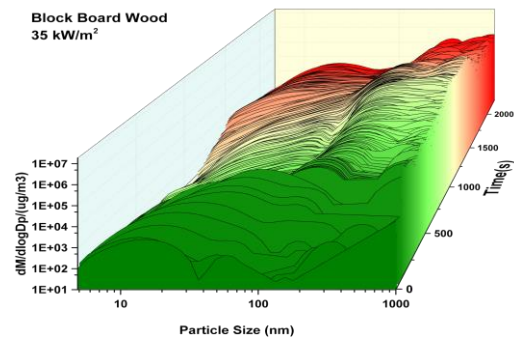
The results show that the irradiation level has a great influence on the particles produced in fires. The ultrafine particles and the accumulation mode particles differed for all the different heat flux applied.

5.4.2.2 Particle Mass Concentration

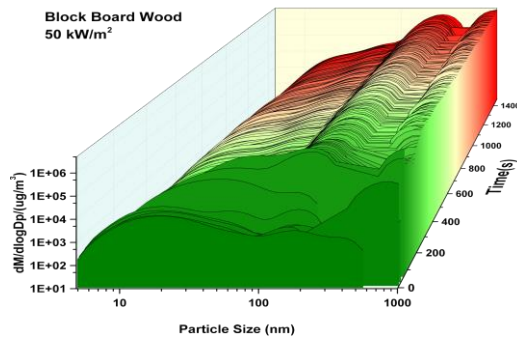
The mass concentrations for the block board wood tests are shown in Figs. 5-30 to 5-32. At the initial stage of the combustion, the particle mass for the 25 kW/m² test was dominated by nuclei particles size as can be seen in Figs. 5-30 and 5-31. This was because only the nuclei particles were produced at the initial stage. After 100 s, the 100 nm particles had the highest mass as expected due to the particle volume and mass scaling with the cube of the particle diameter. In the first 100 s, the 20 nm size produced a mass of $5 \times 10^4 \mu\text{g}/\text{m}^3$ ($0.05 \text{ g}/\text{m}^3$) and a fairly constant mass of $6 \times 10^3 \mu\text{g}/\text{m}^3$ ($0.006 \text{ g}/\text{m}^3$) afterwards. The 100 nm particle mass was about $4 \times 10^6 \mu\text{g}/\text{m}^3$ ($4 \text{ g}/\text{m}^3$). During the 35 kW/m² test 20 nm particle mass was highest during the ignition delay at $1 \times 10^5 \mu\text{g}/\text{m}^3$ ($0.1 \text{ g}/\text{m}^3$) which then reduced to $3 \times 10^3 \mu\text{g}/\text{m}^3$ ($0.003 \text{ g}/\text{m}^3$) during the steady state burning and increased in mass during the char burnout stage. The 200 nm mass was about $3 \times 10^6 \mu\text{g}/\text{m}^3$ ($3 \text{ g}/\text{m}^3$) at steady state but decreased to about $3 \times 10^4 \mu\text{g}/\text{m}^3$ ($0.03 \text{ g}/\text{m}^3$) during the char burnout. The 50 kW/m² test produced 10 nm particle mass of $1 \times 10^3 \mu\text{g}/\text{m}^3$ ($0.001 \text{ g}/\text{m}^3$) during the steady state burning and the char burnout while the 200 nm particle mass was about $1.5 \times 10^6 \mu\text{g}/\text{m}^3$ ($1.5 \text{ g}/\text{m}^3$) throughout the flaming and char burning phase.



(a)

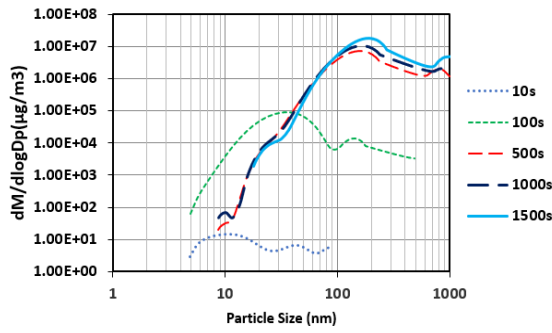


(b)

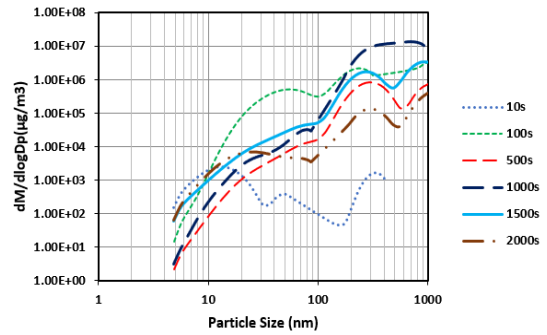


(c)

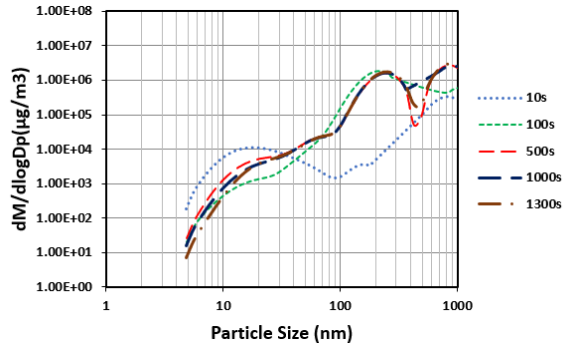
Figure 5-30 Particle Mass and Size Distribution; 25 kW/m² (a) 35 kW/m² (b) and 50 kW/m² (c)



(a)

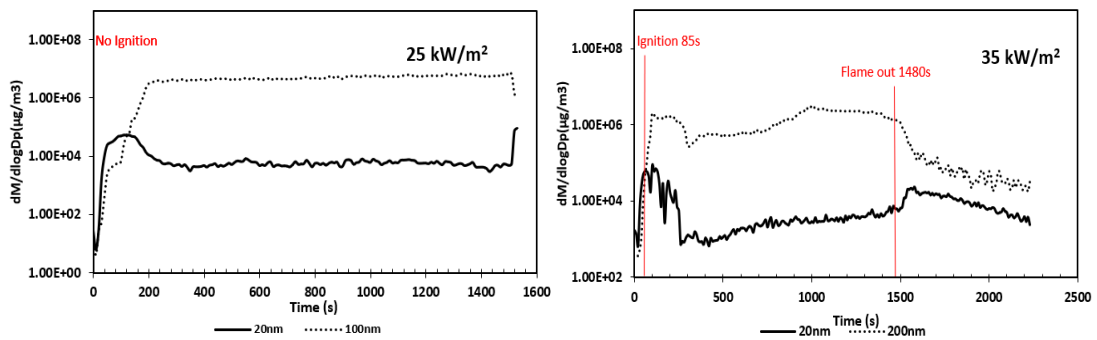


(b)



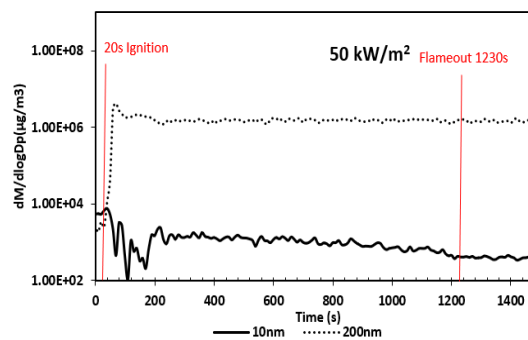
(c)

Figure 5-31 Particle Mass and Size Distribution at Different Times; 25 kW/m² (a) 35 kW/m² (b) and 50 kW/m² (c)



(a)

(b)



(c)

Figure 5-32 Nuclei and Accumulation Mode Sizes Particle Mass for; 25 kW/m² (a) 35 kW/m² (b) and 50 kW/m² (c)

The 50 kW/m² fire produced the lowest mass of both the nuclei and accumulation mode particles during the combustion.

5.4.2.3 Particle Emission Index

The particle yield or emission index for the nuclei and accumulation mode particles produced during the 3 tests at different heat flux is shown in Figs. 5-33 and 5-34. Figure 5-33 shows particle number for the nuclei and accumulation mode particles as a function of the mass of wood burnt. The 25 kW/m² test shows that the emission index for the 20 nm particles was highest in the first 100 s of the combustion, with a yield of 7.3×10^{17} number/kg while the 100 nm particle was about 1×10^{17} number/kg after the 100 s. The 35 kW/m² 20 nm particle yield was highest at 4.5×10^{17} number/kg during the ignition delay of 85 s and the char burnout phase while the 200 nm yield was highest at 6×10^{15} number/kg at the steady stage burning phase. The 50 kW/m² test produced 10 nm yield of $4.6 \times$

10^{17} number/kg during the ignition delay of 20 s and continued to produce the yield of 1.9×10^{16} number/kg afterwards. The 200 nm yield was lower at 4×10^{14} number/kg.

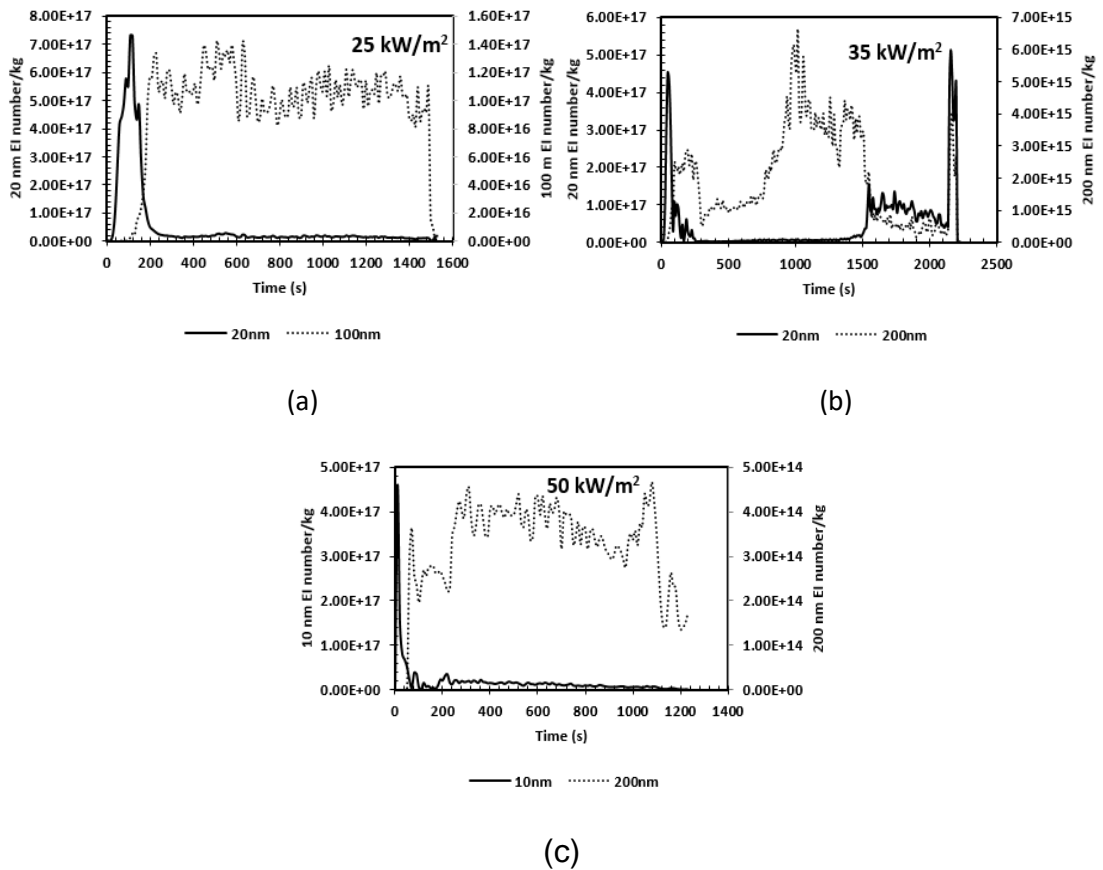
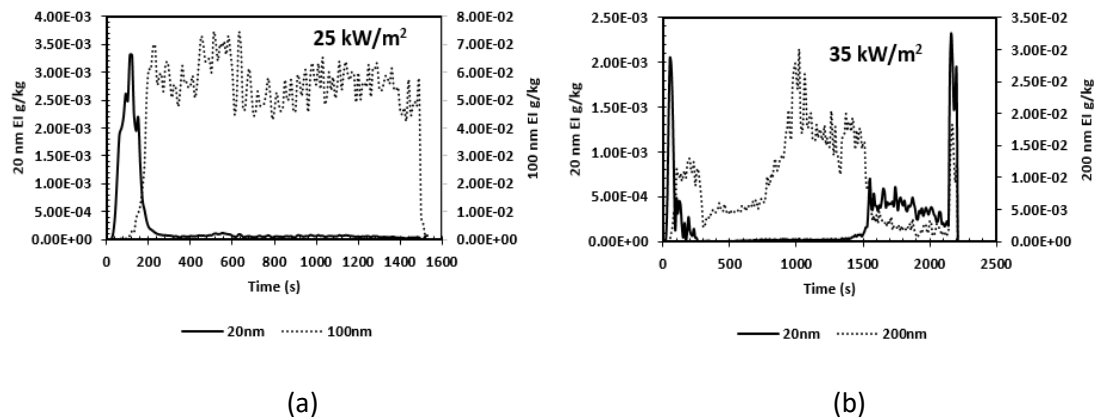
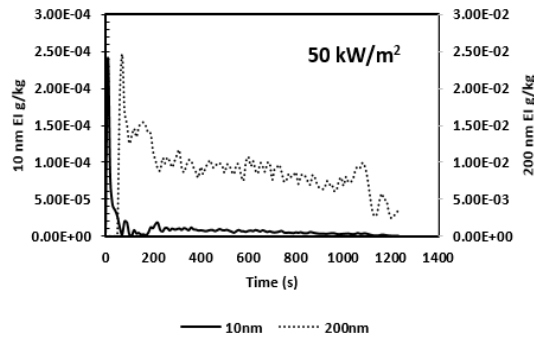


Figure 5-33 Particle Number per Mass of Fuel Burnt for nucleation mode and Accumulation mode particles for; 25 kW/m² (a) 35 kW/m² (b) and 50 kW/m² (c)





(c)

Figure 5-34 Particle Number per Mass of Fuel Burnt for nucleation mode and Accumulation mode particles for; 25 kW/m² (a) 35 kW/m² (b) and 50 kW/m² (c)

The particle mass per unit mass of fuel burned shows the 20 nm particle for 25 kW/m² test having a yield of 0.003 g/kg while the 100 nm yield was about 0.07 g/kg. The 35 kW/m² test however produced a 20 nm yield of about 0.002 g/kg during the ignition delay period and a much lower yield during the steady burning phase and a yield of 0.0004 g/kg during the char burning phase while the 200 nm yield was as high as 0.03 g/kg at the steady state burning phase, with a much lower yield during the char burnout stage. The 50 kW/m²_{air} produced a 10 nm yield of about 0.00024 g/kg during the ignition delay period and a much lower yield during the steady burning phase. The 200 nm yield was highest at 70 s into the combustion at 0.025 g/kg at the ignition delay period and an almost steady 0.008 g/kg afterwards.

The heat flux applied greatly affected the production of particles but despite the differences in the sizes and yields of particles produced, particles generated are a potential health hazard that may lead to the impairment of escape in the event of fire and subsequent death.

5.5 Comparison Between the Controlled Atmosphere Cone Calorimeter and the Freely Ventilated Setup

The cone calorimeter (ISO 5660) is designed to measure the heat release rate and flammability properties of materials. The cone calorimeter reproduces the oxidative pyrolysis stage (class 1b) and well ventilated flaming fires (class 2) classification of ISO 19706 [48]. The authors have adapted the standard cone

calorimeter [108] for direct raw gas analysis of the fire products at the outlet from the cone heater and used it with both free ventilation and restricted ventilation fires. The controlled atmosphere enclosure around the 100 mm square test fire in the cone calorimeter was used as a compartment fire with a metered air supply to the enclosure to generate a restricted ventilation fire, 3a classification of ISO 19706 [48]. It was operated with a controlled air supply designed to create rich combustion conditions that occur in air starved compartment fires. This section is based on the paper “Smoke Particle Size Distribution in Pine Wood Fires”[193].

5.5.1 Mass Loss and Heat Release Rates (HRR)

Compartment fires and freely ventilated fires are compared for the same pine wood test specimen at 35 kW/m² cone radiant heating and both had a gas sample for toxic gas and oxygen analysis taken as a raw heated mean gas sample from the chimney fitted on the cone exit. The results of the secondary combustion after air dilution beyond the chimney are not presented, apart from for the particle number analysis. Figure 5-35 shows that the ignition delay was much shorter for the restricted ventilation fire, due to the richer mixtures during the delay period, shown in Fig. 5-39, which have shorter ignition delays than the lean mixture for freely ventilated fires. Figure 5-35 shows the mass loss rate and total heat release rate for the primary combustion in the compartment. Both tests showed a mass loss rate at steady state of 0.07 g/s, with a much slower burn rate during the char burn phase from 1200 s. The two peaks in the mass burn rates will be shown to be associated with peaks in toxic gas emissions and in particulate emissions.

The oxygen mass consumption based heat release rate, shown in Fig. 5-35b, was computed from cone outlet chimney oxygen analysis, downstream of the FTIR. The wet based oxygen analysis (corrected for the water vapour removed based on the FTIR water analysis) is shown in Fig. 5-36. For the restricted ventilation fire, Fig. 5-35b shows that the HRR peaked immediately after ignition and remained steady at 50 kW/m², which was about one third of the freely ventilated fire where the steady state HRR was about 130 kW/m². This was due to the low combustion efficiency with high CO, H₂ and HC emissions in the restricted ventilation fire due to the low fire temperature. Figure 5-36 shows that for free ventilation there was always surplus oxygen in the fire with high oxygen

levels in the chimney. For the restricted ventilation fire the oxygen was close to zero for most of the time and combustion was completed in an external flame downstream of the chimney using the entrained oxygen from the dilution air.

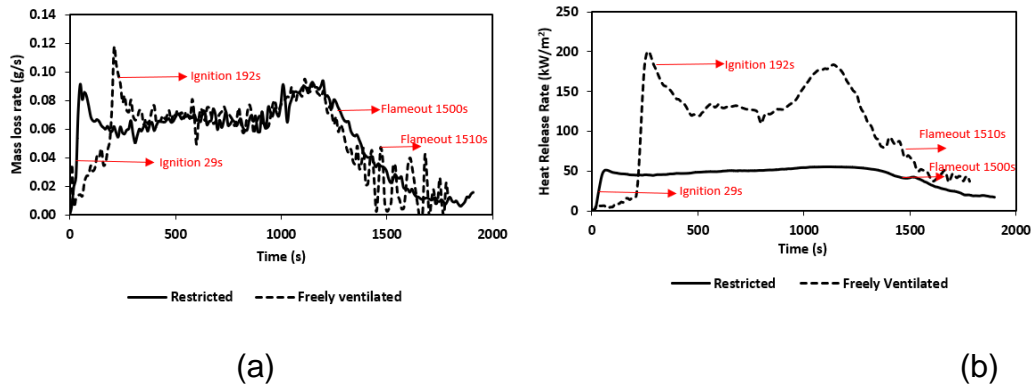


Figure 5-35 Mass loss rate (a) and primary heat release rate (b).

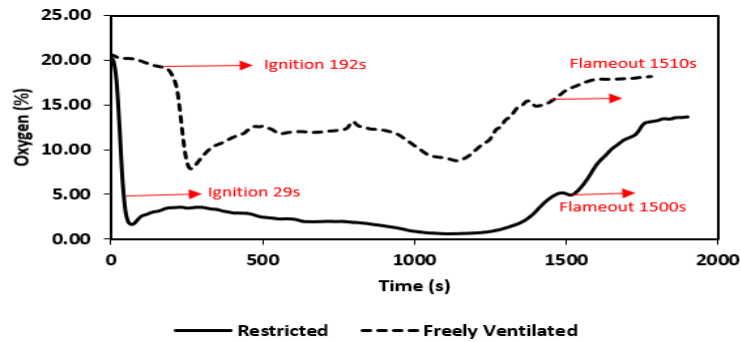


Figure 5-36 Oxygen in the cone outlet chimney

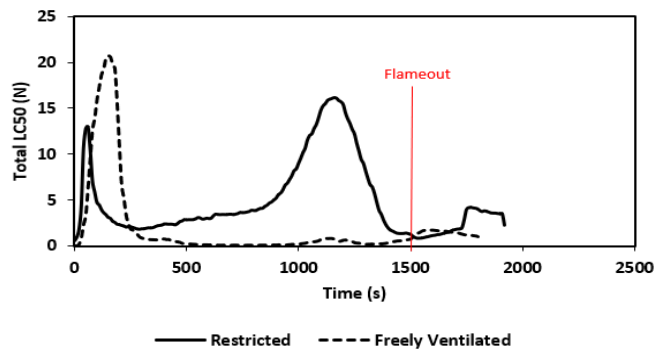


Figure 5-37 Total LC₅₀ FEC toxicity

5.5.2 Toxicity, CO, Hydrocarbon, Fire Equivalence Ratio and Combustion Efficiency

All the FTIR measured toxic gases were divided by the LC₅₀ limit and then summated to give the FEC total toxicity or N. This is shown as a function of time in Fig. 5-37, which shows both ventilations had a peak toxicity in the initial flaming

combustion phase, but for restricted ventilation there was a second large toxic peak just before the flame out and a second smaller peak for free ventilation. These two peaks in toxicity occurred at the same time as the two peaks in the mass burn rate in Fig. 5-35 and the two minimum in oxygen in Fig. 5-36. The CO and total hydrocarbon (HC) yields are compared for the two fire ventilation conditions in Fig. 5-38 and they had a similar shape to the total toxicity results. The fire mean equivalence ratio by carbon balance and the combustion efficiency computed from the energy content of CO and HC are shown in Fig. 5-39. The restricted ventilation fire had rich combustion with an equivalence ratio of 2.0 throughout the flaming period. In the burning period after the ignition delay the CO and HC yields were much higher for the restricted ventilation fire as a result of the rich combustion. The freely ventilated fire burned lean with an equivalence ratio of 0.4 for most of the flaming period. The CO and HC yields were very low once combustion started after the ignition delay, as expected from the lean combustion. During the ignition delay period the CO yield was almost 3 times higher and HC was about 7 times higher in the freely ventilated test. This was due to the long ignition delay period of 192 s compared to 29 s of ignition delay for the restricted fire, where the products of wood decomposition were present but not ignited. The free ventilation dispersed the products of thermal decomposition, reduced their concentration and delayed their auto-ignition.

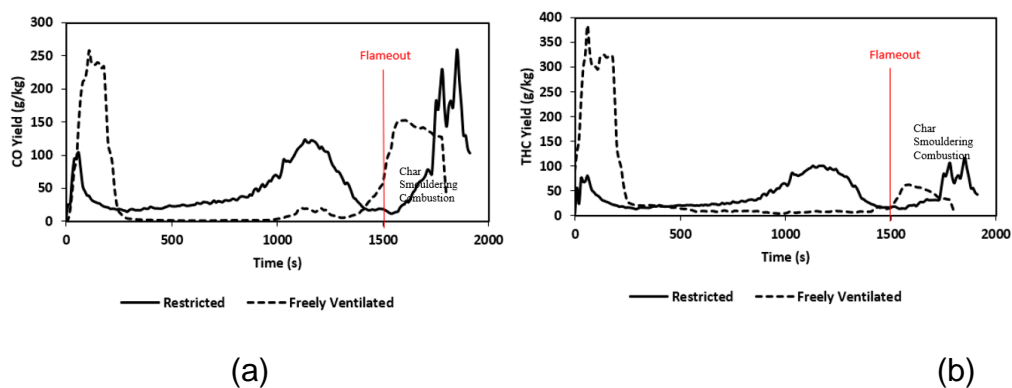


Figure 5-38 CO yield (a) and HC yield (b).

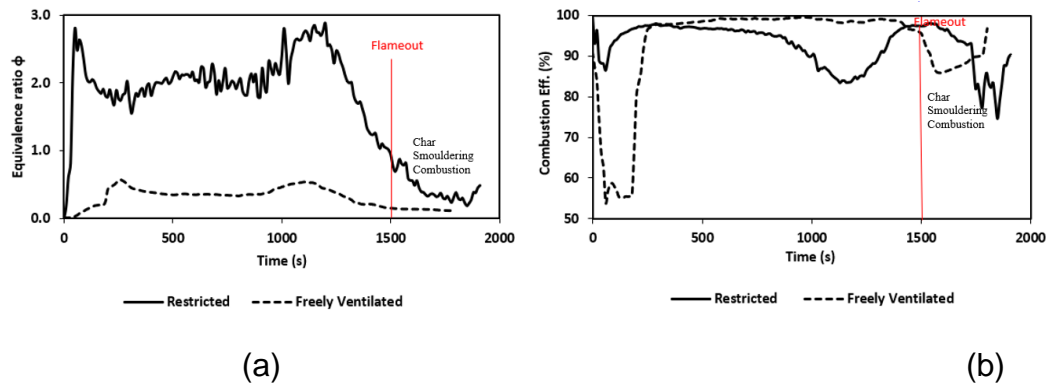


Figure 5-39 Equivalence ratio (a) and Combustion efficiency (b).

5.5.3 Particle Number Concentration

The particle number concentration as a function of size and time is shown in Fig. 5-40. A bimodal distribution of the particle sizes was observed indicating the nucleation mode and accumulation mode of the particle size distribution.

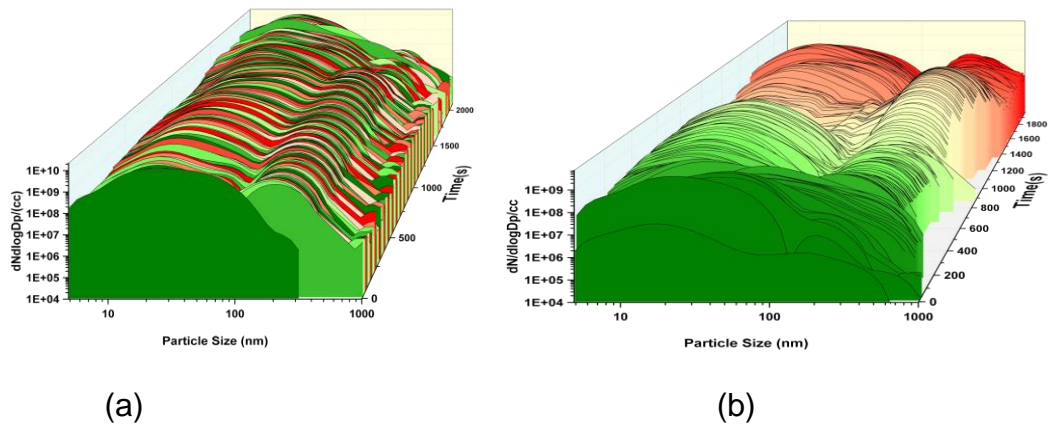


Figure 5-40 Particle number concentration and size distribution; (a) restricted (b) freely ventilated.

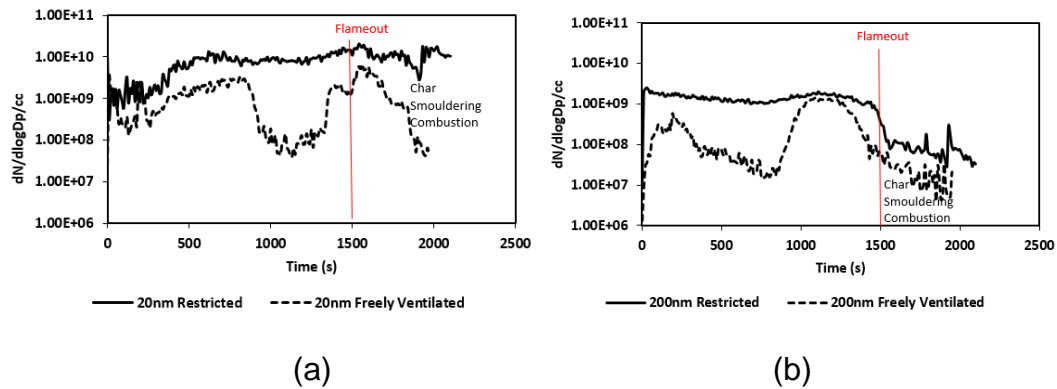


Figure 5-41 20 nm particle number concentration (a) and 200 nm particle number concentration (b).

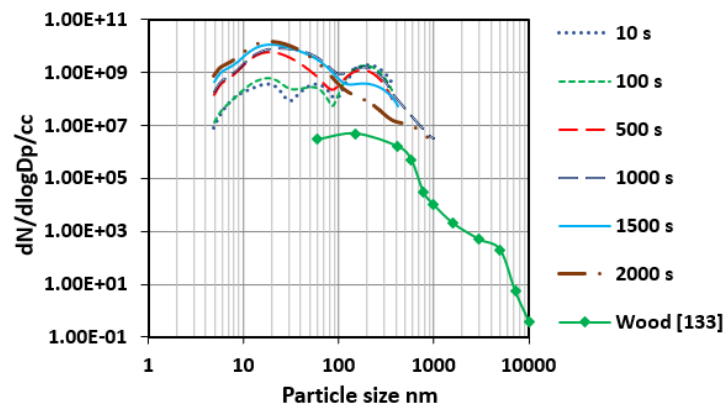
The nuclei mode for both ventilation conditions was found to peak at 20 nm and the accumulation mode at 200 nm. The number of particles for the two modes, 20 nm and 200 nm are compared in Fig. 5-40 as a function of time for both ventilation conditions. The particle concentrations were highest at the peak HRR of 50 and 130 kW/m² for the restricted and free ventilated fires. For both ventilations, the 20 nm particle number was 10⁶ higher than those at the roadside (1.8 x10⁴ to 3.4 x10⁴ /cm³) [186], where the health hazards are known to be high. The effect of restricting the fire ventilation was to increase the ultra-fine particle number, due to the richer mixtures generated, as shown in Fig. 5-39. However, even for free ventilation with lean combustion the particle number was high at 10⁵ times roadside levels [186] for 20 nm particles. These results show that ultra-fine particulate emissions in fires from wood burning are a potential serious toxic impairment of escape hazard and materials should be evaluated for their propensity to form ultra-fine particles in fires.

5.5.4 Particle Number Comparison

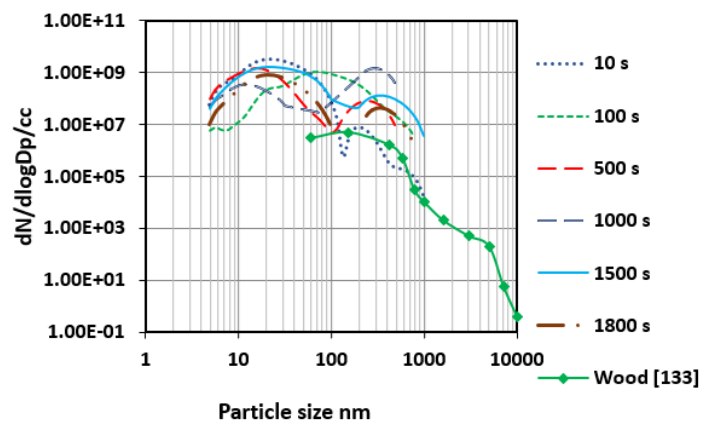
The particle number size distributions as a function of time in the fire are shown in Fig. 5-41 for freely and restricted ventilation fires. Both fires showed a nuclei mode with a peak at 20 nm and an accumulation mode at 200 nm. These two size ranges are shown as a function of time in Fig. 5-40. This shows that for restricted ventilation the particle numbers were higher than for free ventilation. However, the time dependency was different with fairly consistent peak numbers at 20 and 200 nm throughout the restricted ventilation fire. For the free ventilation fire there were two peaks in the particle number of both 20 and 200 nm particles.

These peaks in particle number coincide with the two peaks in HRR in Fig. 5-35b.

Relatively few investigations have been published on the particle size distribution in fires, especially in simulated compartment fires. Hertzberg and Blomqvist [133] used the low pressure impactor particle size analyser, the Dekati ELPI, to measure the particle number from 60 nm to 10 μm size range for different fire materials, using the standard cone calorimeter.



(a)



(b)

Figure 5-42 Comparison of particle number distribution with that of Hertzberg [133] using the ELPI aerodynamic size separation instrument for restricted (a) and freely ventilated (b).

Figure 5-42 shows a comparison between the pine wood test at both ventilation conditions with the unspecified ‘wood’ measured by Hertzberg and Blomqvist [133]. All their particle size distributions were monomodal. At 200 nm, Hertzberg

and Blomqvist [133] measured particle number of 10^6 /cm³. In the present pine wood work, at 200 nm there were 10^9 p/cm³ for the restricted condition and $10^8 - 10^9$ /cm³ for the free ventilation condition. These higher particle numbers for restricted ventilation were due to the richer mixtures where carbon formation occurs. The richer mixtures are also associated with high temperatures and therefore more soot particles are produced. The 5-60 nm size range of particles, which account for the greatest health risk, were not measured in Hertzberg's work for 'wood' [133]. This size range of particles accumulate in the alveolar regions of the lungs and penetrate into the blood stream [24-29]. The ELPI particle size analyser does not have the size resolution, below 50 nm where the greatest toxic particle hazard occurs and thus is not a good instrument for assessing particle size in fires. It is much better for larger particles >1 µm of interest in optical obscuration. Ultra-fine particles generated in the pine wood test was much higher than those found in the literature. These ultra-fine particles could be a significant cause of death and impairment of escape in fires

5.6 Summary

The controlled atmosphere cone calorimeter tests resulted in the following findings.

Pine Wood:

- The 174 kW/m²_{air} fire had a longer ignition delay because of the lean mixture.
- The 59 kW/m²_{air} and 112 kW/m²_{air}, combustion were rich or ventilation controlled throughout the flaming combustion phase, but were lean or fuel controlled in the char burning phase. The 174 kW/m²_{air} fire burned at stoichiometric at the beginning of the fire but burned lean throughout the steady burning phase.
- The 174 kW/m²_{air} test showed much lower concentrations of most gases except for acrolein and formaldehyde where it was about a factor of 4 higher than the two tests during the first 100 s of the test.
- For 59 kW/m²_{air}, the toxicity was dominated by CO > formaldehyde > HCN on an LC₅₀ basis and formaldehyde > benzene > CO > HCN on a COSHH_{15min} basis. The contribution of acrolein was not more than 5% on

an LC₅₀ but was about 50% at the initial stage of the fire on a COSHH_{15min} basis. For the 112 kW/m²_{air}, the toxicity was dominated by CO >formaldehyde >HCN on an LC₅₀ basis, but formaldehyde was more significant on COSHH_{15min} basis, followed by benzene, CO, acrolein and HCN. For the 174kW/m²_{air}, the toxicity was dominated by CO >formaldehyde >HCN on an LC₅₀ basis, with < 10% contribution of acrolein. However, acrolein was 2nd most significant on COSHH_{15min} basis.

- Most of the toxic gases produced high yields during the char burning or smouldering combustion phase.
- The lowest airflow produced the highest toxicity as a result of the rich mixture associated with incomplete combustion.
- It was observed that the lowest airflow rate produced the highest number of particles both in the nuclei mode and the accumulation mode as a result of the rich combustion. Even though the highest airflow burned lean, the particle number produced is still high and of great concern.

Block Board Wood:

- The minimum radiant heat flux for the auto-ignition of block board wood was 30 kW/m².
- The non-flaming, smouldering fire at 25 kW/m² was more toxic than flaming both in terms of lethality and impairment of escape.
- The toxicity of the fire sets in very early at a high concentration at the initial stage of the fire which is of great concern as that is when escape would be possible.
- The fire toxicity decreased with increasing radiant heat flux. The lower heat flux only pyrolysed the wood resulting in the partial oxidation of toxic gases while the higher heat flux resulted in an unrealistic clean burning behaviour.
- The adhesive used to glue the board together is responsible for high fire toxicity.

- The results show that the irradiation level has a great influence on the particles produced in fires. The ultrafine particles and the bigger particles differed for all the different heat flux applied.
- The 25 kW/m² test produced 20 nm and 100 nm particle sizes for the nuclei and accumulation modes, the 35 kW/m² test produced 20 nm and 200 nm and the 50 kW/m² test produced 10 nm and 200 nm.

Comparison Between the Controlled Atmosphere Cone Calorimeter and the Freely Ventilated Setup:

- The restricted ventilation fire had rich combustion with an equivalence ratio of 2.0 throughout the flaming period. The freely ventilated fire burned lean with an equivalence ratio of 0.4 for most of the flaming period.
- During the ignition delay period the CO yield was almost 3 times higher and hydrocarbon was about 7 times higher in the freely ventilated test. This is as a result of partial oxidation of gases at that period, generating products of incomplete combustion.
- The particle size distribution of pine wood was measured in real time under restricted and free ventilation condition showing a bimodal distribution of nucleation mode and agglomeration mode. The nucleation mode for both fires showed a peak of 20 nm on a number basis and a peak of 200 nm in the accumulation mode.
- More particles were generated in the restricted ventilation fire due to richer combustion.

The complexity of different materials makes overall comparison of their toxicity difficult due to wide differences in composition. The important factors that determine the toxicity of a material are the type of material, the ventilation condition and the heat flux. In the case of the wood materials tested, all the parameters play an important role in the emission of toxic gases and need be considered when testing for toxicity of combustion products.

Chapter 6 5m³ Compartment Test Results

Residential fires constitute the majority of fire fatalities and most fatalities are due to the inhalation of smoke [13]. There's therefore the need to have an effective assessment, measurement and quantification of toxic hazards from materials that are likely to be involved in residential fires, for effective development of safe building designs and safety strategies. This chapter presents results of experiments done on pine wood cribs in a 5m³ compartment constructed by the University of Leeds under different ventilation conditions. Different sizes of wood cribs were built and analysed for their toxic gas and particulate emissions using the heated FTIR and the Cambustion DMS 500 particle size analyser.

6.1 General Burning Characteristics

Three different sizes of pine wood cribs were built; the small wood crib, medium crib and large wood crib described in Table 3-8.

6.1.1 Small Wood Crib

Two tests were carried out at different ventilation conditions with the smallest wood crib. The load cell and the oxygen analyser provided insensible readings during the small crib test 1 experiments. As a result, the readings were ignored and therefore comparison made with test 2 was based on the available data. However, this section presents the analysis of the results available and the observations during the fire tests. Small crib 1 was tested with an air inlet area of 0.15 m² (fully open), equivalent to a K_{in} value of 5% while the small crib 2 was tested with an air inlet area of 0.00 m² (fully closed), equivalent to a K_{in} value of 0%. Both tests were ignited using ethanol as the accelerant.

6.1.1.1 Mass Loss Rate, Mean Ceiling Temperature and Heat Release Rate (HRR)

Figures 6-1a and b show the mass loss and mass loss rate as a function of time for the small crib 2. There was a high mass loss from the time of ignition to about 150 s and remained steady afterwards with a mass loss rate of < 1 g/s from 200 s during the smouldering phase. This indicates that the fire started lean with high intensity as shown by the heat release rate curve and the ceiling temperatures,

but because the air inlet was closed, the available oxygen was consumed quickly by the fire, resulting in an under ventilated fuel rich combustion.

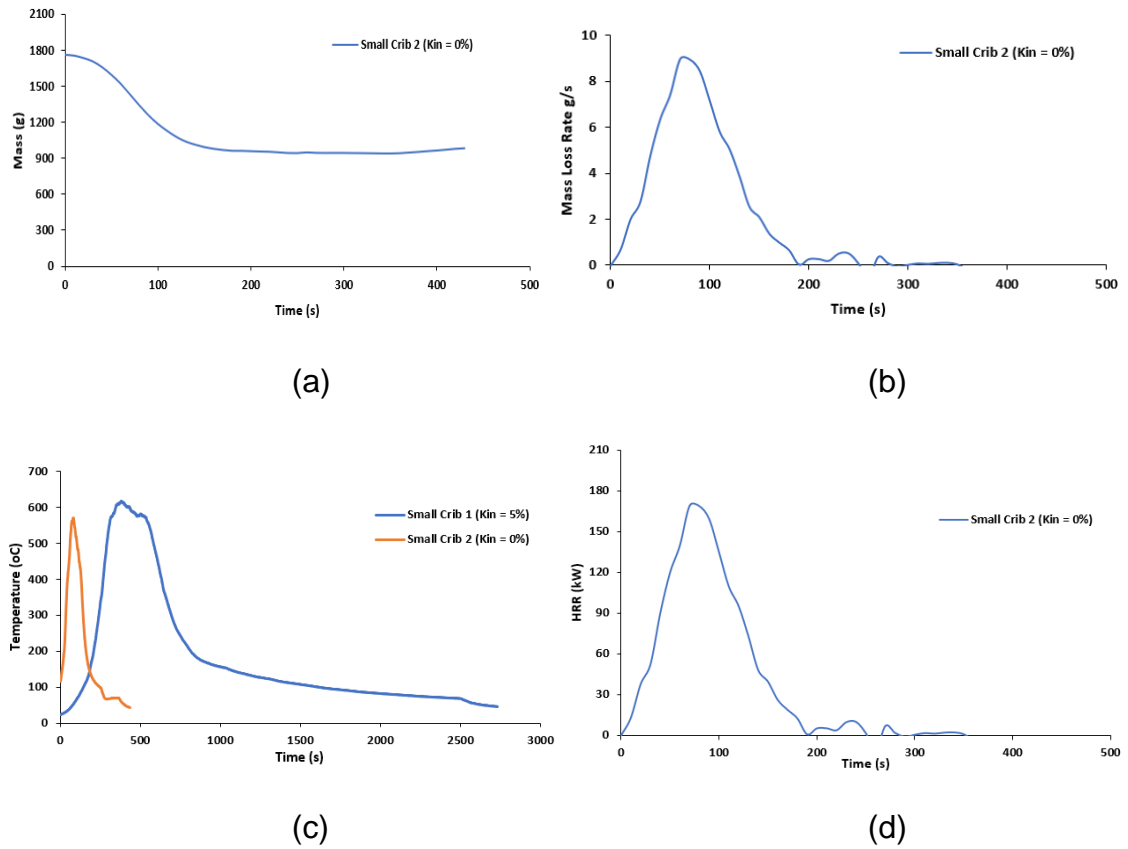


Figure 6-1 Mass Loss (a) Mass Loss Rate (b) Mean Ceiling Temperature (c) and Heat Release Rate HRR (d)

The mean ceiling temperature is compared for small crib 1 and 2 in Fig. 6-1c. Both crib fires had a high temperature at the initial stage of the fire, with the small crib 1 having a peak value of 620°C and the small crib 2 having a peak value of 560°C. This difference in temperature indicates that the ventilation has played an important role in limiting the temperature and the duration of the combustion in small crib 2 test. It was observed that there was a ceiling impingement at the time the ceiling temperature was at its peak for both tests as shown in Fig. 6-2. Mustafa et al. [89] burnt the same size of wood in a 1.6 m³ compartment under a controlled ventilation of 11ACH (air changes per hour) and a peak ceiling temperature of 350°C was obtained, while the peak heat release rate was 12 kW.

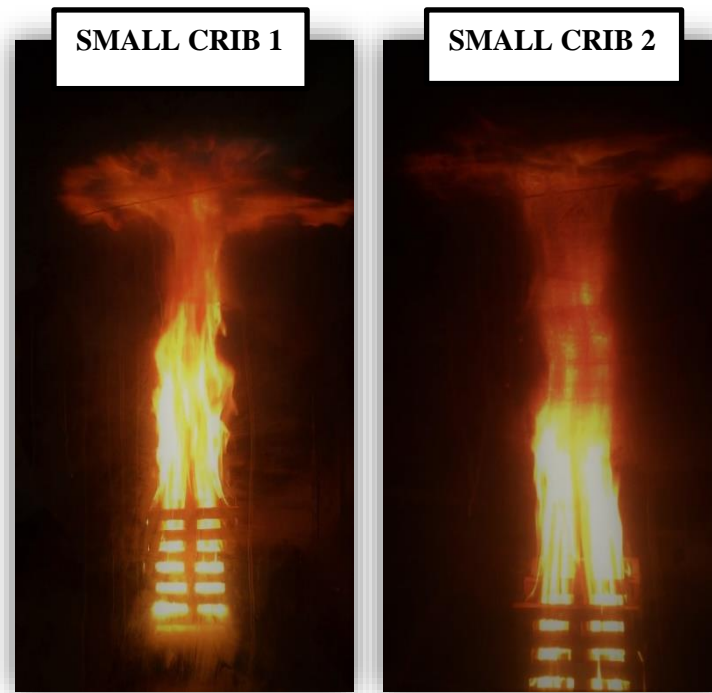


Figure 6-2 Picture Showing Ceiling Impingement during the Small crib Test

The small crib 1 mean ceiling temperature showed a steady burning between 300 s to 600 s with a rapid decrease in temperature of about 200°C afterwards and then to a minimum temperature of about 50°C. The low temperature was during the smouldering combustion in the final burning phase. The small crib 2 combustion was shorter due to limited ventilation, it self-extinguished before getting to the smouldering phase of the combustion. It reached a peak heat release rate of 170 kW when the combustion was well-ventilated and continued burning with lower burning rate and lower temperature before totally extinguishing without going through a smouldering phase.

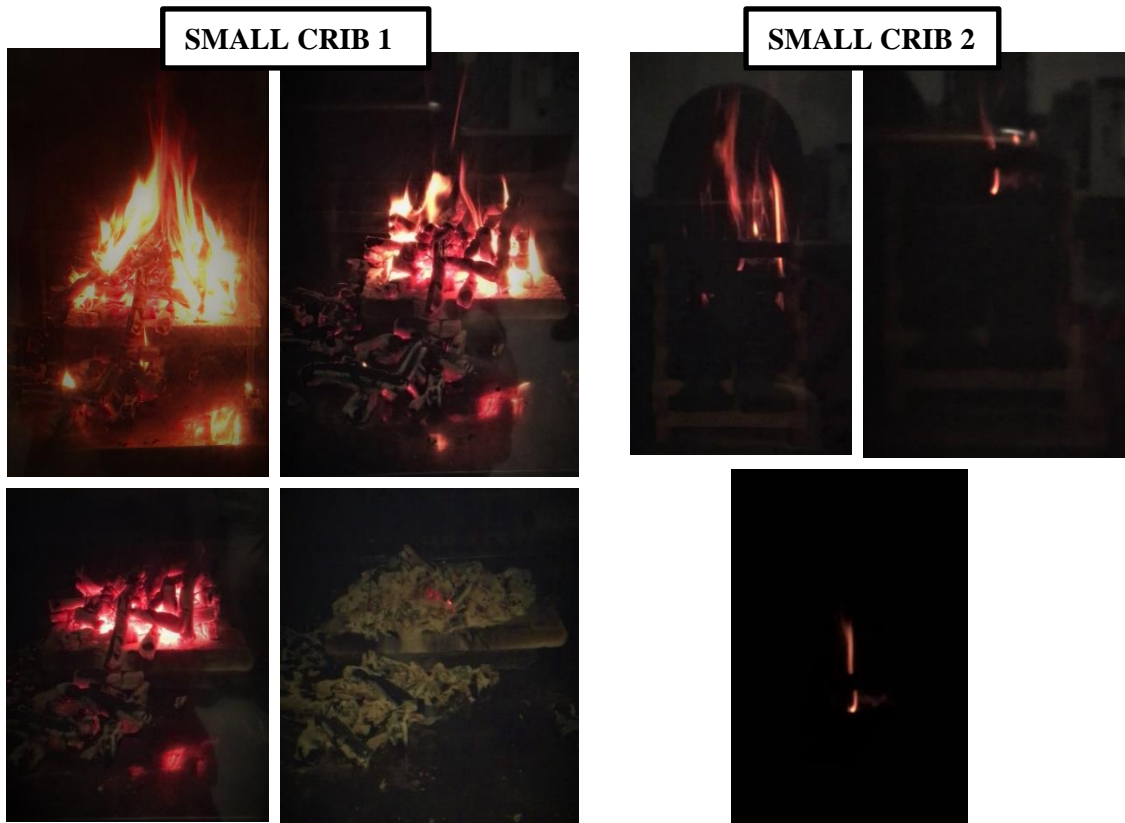


Figure 6-3 Picture showing the final stage of the small crib combustion

At the end of the test, only char and ashes were left as residue for small crib 1. However, only 44% of the total mass of small crib 2 was burnt with its structure still intact but with evidence of burn and char. Figure 6-4 shows the picture of the cribs at the end of the test, with small crib 2 indicating that there was a uniform spread of the flame from the centre to the edges before self-extinguishing.

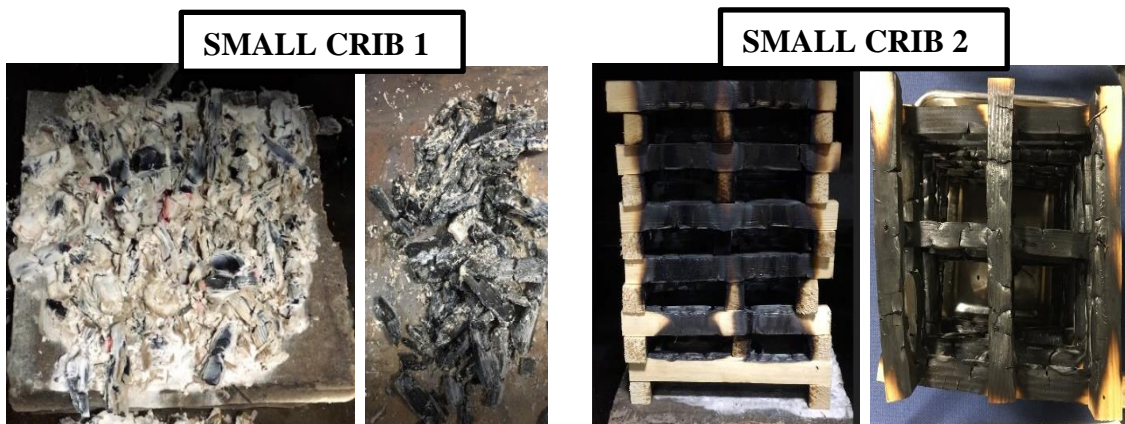


Figure 6-4 Residue after the Small Crib Tests

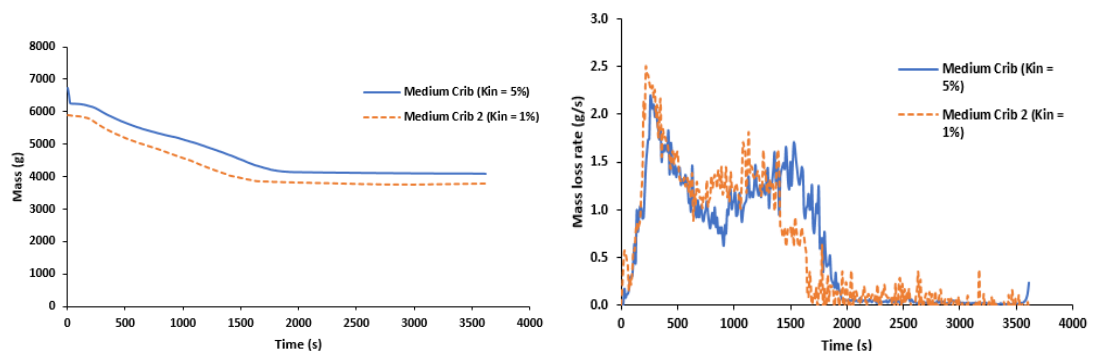
6.1.2 Medium Wood Crib

Two tests were carried out with the medium sized wood crib at ventilation rates of $K_{in} = 5\%$ (opening fully open) and $K_{in}=1\%$ (opening partially open). Ethanol, at 1% of the energy in pine, was used as an accelerant to ignite the fire. The results were compared and presented in this section.

6.1.2.1 Mass Loss Rate, Mean Ceiling Temperature, Oxygen. Equivalence Ratio and Heat Release Rate (HRR)

Figure 6-5 a shows the mass loss as a function of time with a gradual decrease in mass after the crib was ignited. Figures 6-5a and b show the mass loss and the mass loss rate as a function of time for the medium crib at two ventilation conditions ($k_{in}=5\%$ and 1%). A gradual decrease in mass loss was observed after ignition at 34 s for medium crib 1 and 42 s for medium crib 2 until around 2000 s and 1600 s respectively. The combustion continued with minimum burn rate until flameout occurred and smouldering combustion continued. The equivalence ratio (from carbon balance) in Fig. 6-5d for medium crib 1 and 2 was 0.5 during the period of maximum HRR of 42 kW and 48 kW at 400 s with a peak ceiling temperature of 400°C and 470°C. However, the fire then began to decay to a HRR of about 25 kW with an equivalence ratio of 0.7 for medium crib 1 and 0.6 for medium crib 2. This was due to the large mass of 6 kg of air in the compartment at the start of the fire.

The initial fire growth was a freely ventilated fire and then the effect of the restricted ventilation occurred with reduced HRR and richer mixtures. The fire continued to decay until flame out occurred at 7% oxygen and 170°C. There was then a long period of smouldering combustion with a HRR of about 1 kW.



(a)

(b)

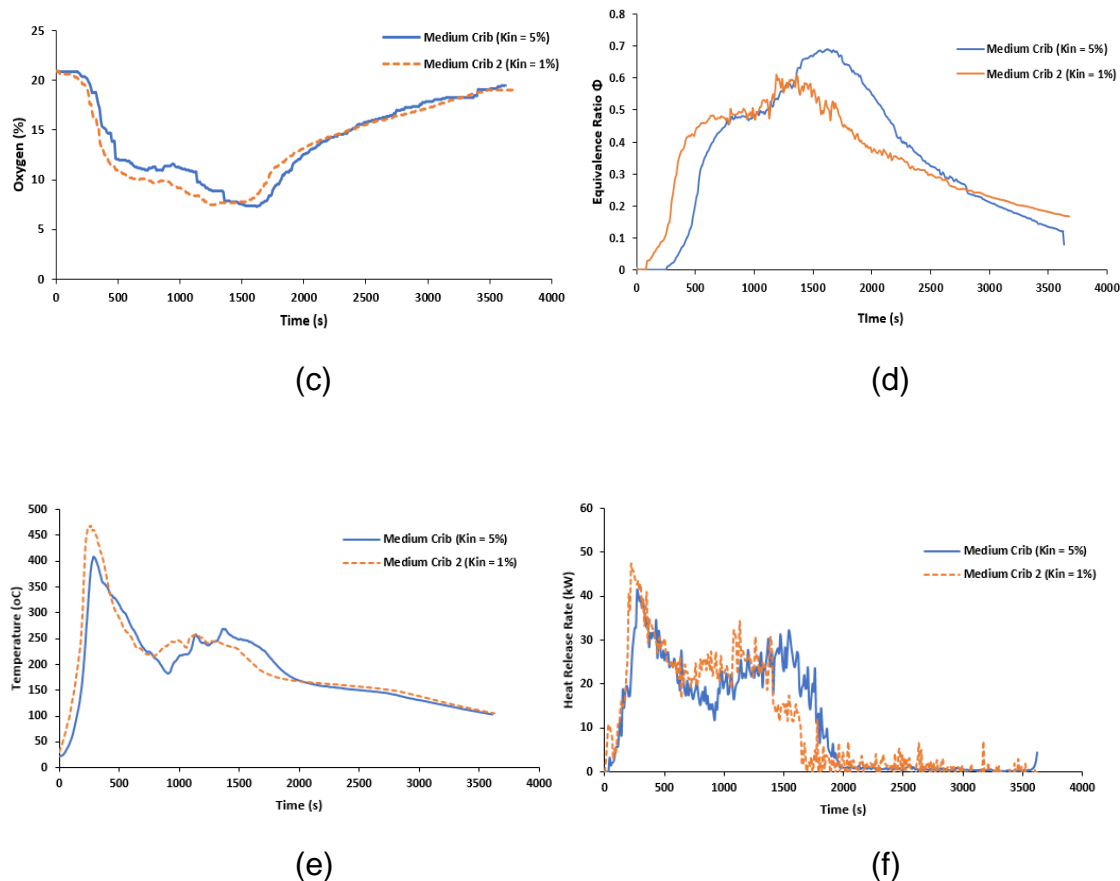


Figure 6-5 Mass Loss (a) Mass Loss Rate (b) Oxygen (c) Equivalence Ratio (d) Mean Ceiling Temperature (e) and Heat Release Rate HRR (f)

It was observed during the tests that the fire growth increased from around 800 s as shown on the graphs with increase in ceiling temperature, equivalence ratio, heat release rates and decrease in oxygen level. This occurred when the flame spread to the right corner of the crib in both cases.

Since the fires were ventilation-controlled, it was expected that the burning characteristics for medium crib 1 would be higher compared to medium crib 2 considering ventilation rate for medium crib 1 was higher. Instead, in this investigation, the opposite was observed. This is as a result of the mean air flow rate in the medium crib 1 (7.2 ACH air changes per hour) being lower than that of medium crib 2 (8.4 ACH air changes per hour). The difference in the results was not much even though the ventilation rates were different. This indicates that both the air inlet into the compartment K_{in} and exhaust outlet K_{out} controlled the air flow rate in the enclosure.

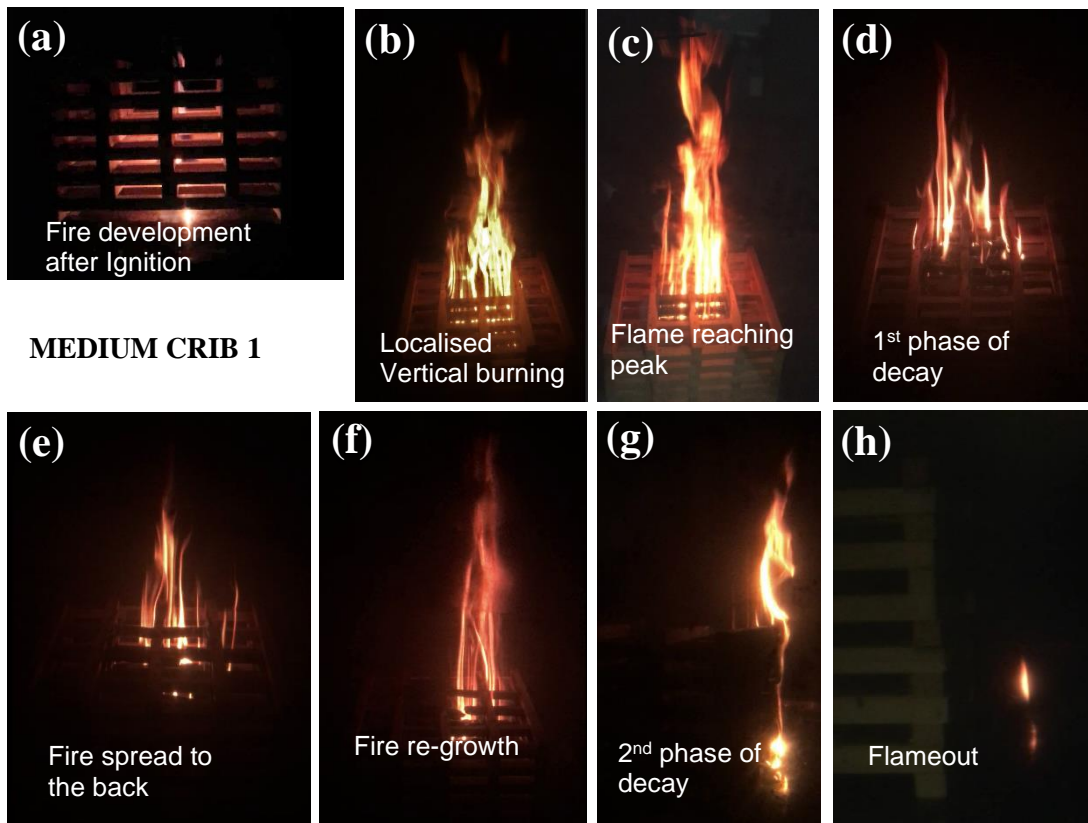


Figure 6-6 Fire development stages for medium crib 1

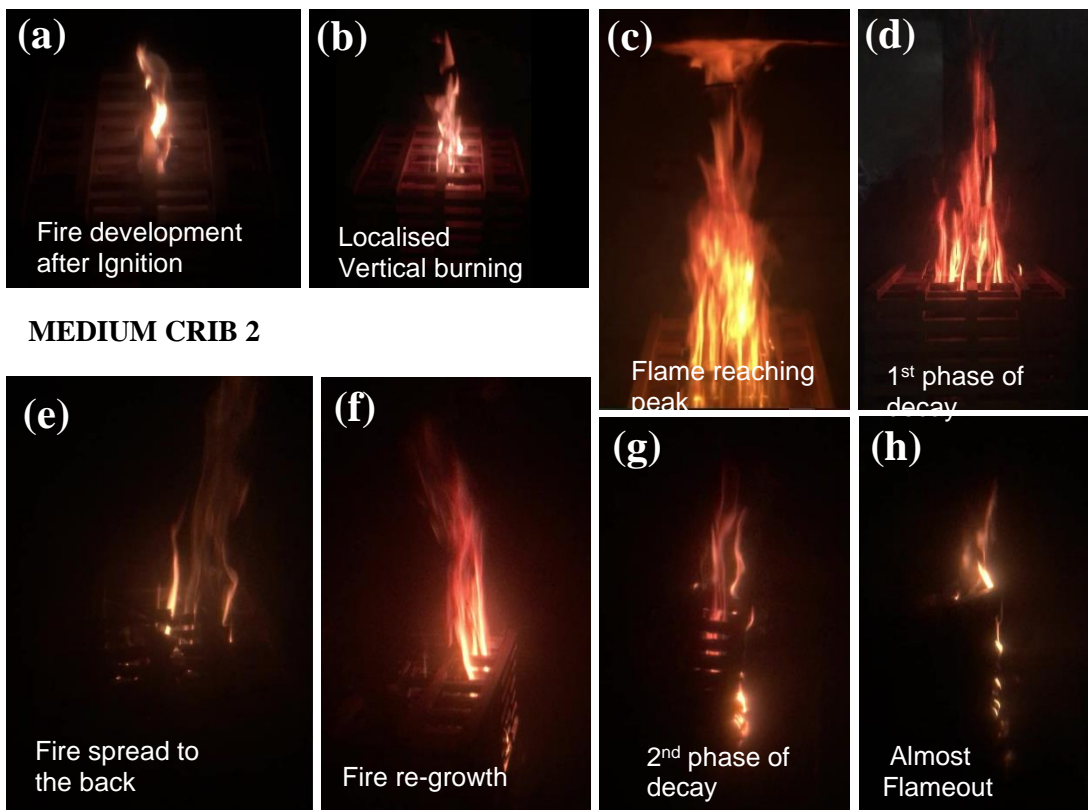


Figure 6-7 Fire development stages for medium crib 2

MEDIUM CRIB 1



MEDIUM CRIB 2

Figure 6-8 The Burnt Cribs

Figures 6-6 and 6-7 show the fire development stages for medium crib 1 and 2 tests. Figure 6-8 shows the burnt crib at the end of the tests with charcoal and ashes. The total mass burnt was 39% and 36% for crib 1 and 2 respectively. The pictures also show the growth of the fire in a vertical direction. Instead of horizontal and equal flame spread, the pattern of flame spread was from middle to the right corner at the back (as positioned in the compartment during the test) of the crib.

6.1.3 Large Wood Crib

The large wood crib of 400mm x 400mm x 497mm was made with 44 mm square construction pine wood and burned in the 5m³ compartment. Diesel (315.1 g), at 5% of the energy in the pine, was used as an accelerant to ignite the fire with a ventilation factor K_{in} of 5%, equivalent to 9 ACH (air changes per hour) mean air flow rate.

6.1.3.1 Mass Loss Rate, Mean Ceiling Temperature, Oxygen. Equivalence Ratio and Heat Release Rate (HRR)

Figures 6-9 a and b show the mass loss and the mass loss rate as a function of time. A gradual decrease in mass was observed throughout the test duration. Although it shows that 32% of the total mass was burnt, the large crib burnt completely at a low-temperature smouldering fire. The smouldering combustion

continued for 5 hours until all the crib was consumed. The day after the test the compartment was opened and only a small amount of ash was left.

The long duration of combustion led to the overheating of the load cell and therefore recorded unreliable data after a certain period of time. The mass, mass loss rate and the heat release rate data were estimated using the reliable data available.

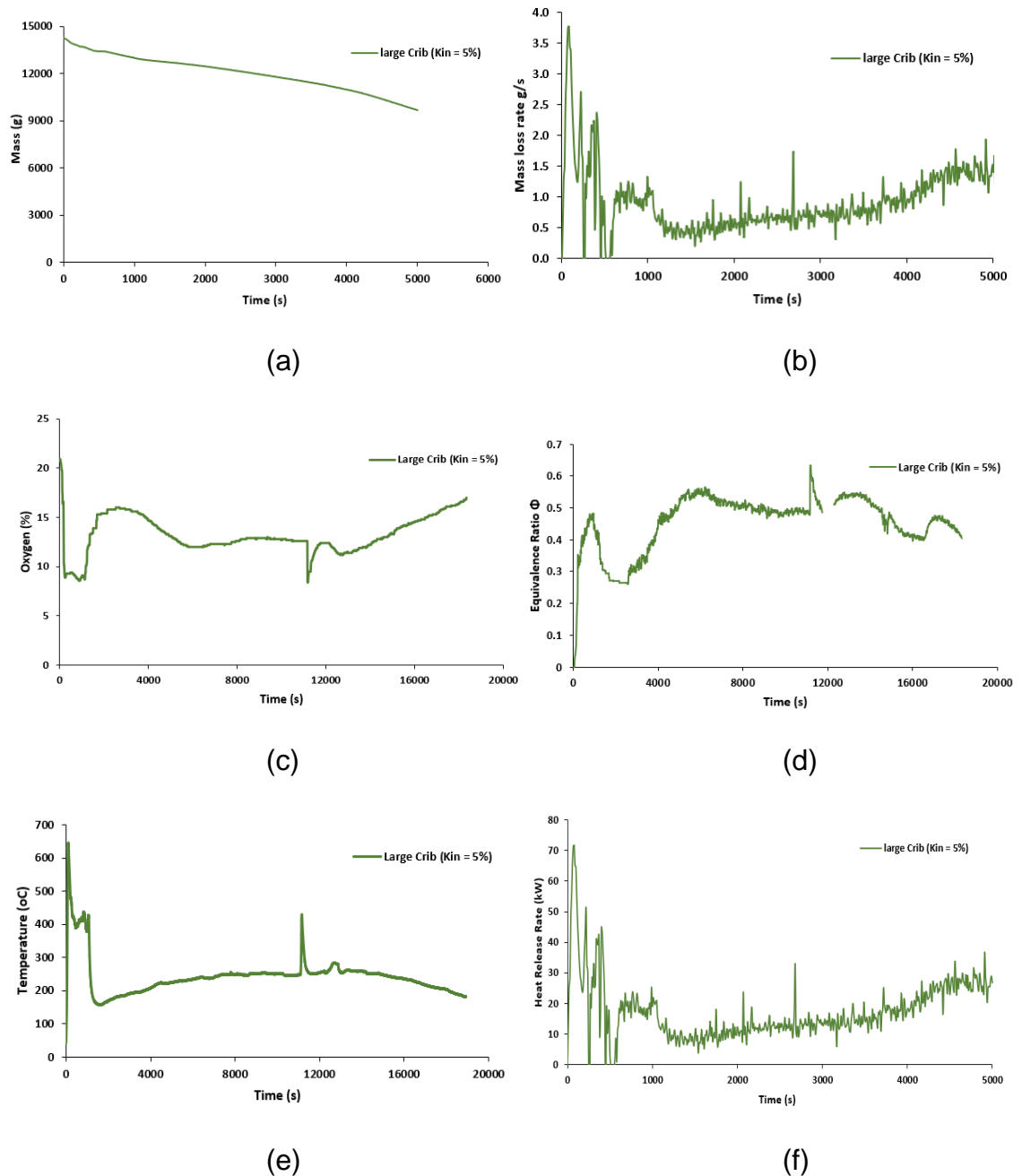


Figure 6-9 Mass Loss (a) Mass Loss Rate (b) Oxygen (c) Equivalence Ratio (d) Mean Ceiling Temperature (e) and Heat Release Rate HRR (f)

As mentioned above, the wood crib was ignited using diesel as an accelerant. The initial stage of the fire was entirely dominated by the diesel pool fire as evident from the strike of HRR in the enclosure at the initial stage shown in Fig. 6-9f. The flaming pool fire resulted in the decrease in the oxygen concentration and the rapid increase in the enclosure ceiling temperature reaching a peak of approximately 650°C. The fire extinguished when it ran out of diesel at about 1000 s but the heating of the crib as a result of the pool fire resulted in the smouldering of the crib which started at about 621 s and lasted for hours. Combustion was lean throughout as shown in Fig. 6-9d. During the smouldering combustion, the oxygen concentration increased and maintained a steady concentration of about 13%, in the same period the HRR was 15 kW.



Figure 6-10 Large Wood Crib Flaming Pool Fire

The compartment temperature however continued to increase steadily which led to an attempt in transition from smouldering to flaming combustion. This is evident in the sudden drop of oxygen concentration and at the same time an increase in the mean ceiling temperature at about 11000 s (3 hrs). The oxygen concentration dropped to < 10 % at that period, however the flame extinguished very fast and continued to smoulder until the whole crib was burnt to ashes as shown in Fig. 6-12.

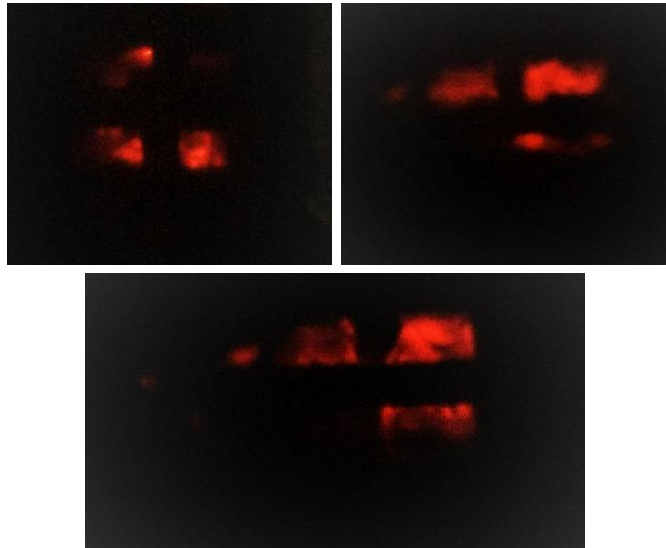


Figure 6-11 Large Wood Crib Smouldering Combustion



Figure 6-12 Char and Ashes at the end of the Large Crib Test

6.2 Toxic Gas Emissions from Wood Crib Tests

The analysis of the gas emissions presented in this section are only for the medium crib and large crib. The small crib, could not be analysed due to the blockage of the sample probe (about $\frac{3}{4}$ blockage) for collecting the smoke sample for the FTIR measurement. The data collected does not represent the well-ventilated flaming wood crib fire in the compartment. Data from 11700 s to 12400 s was excluded for the large crib, due to an error in the data.

Toxic gases were analysed on an LC₅₀ and COSHH_{15min} exposure level basis.

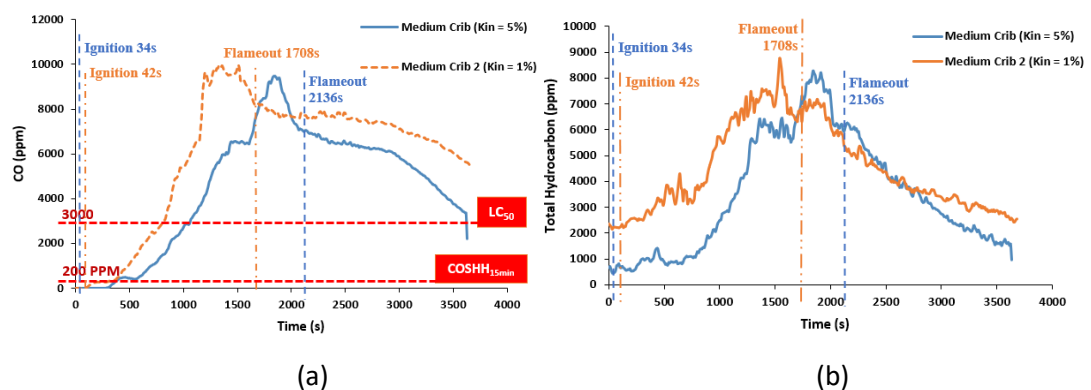
6.2.1 Medium Wood Crib

The toxic concentration for medium crib 1 and 2 were compared and presented in this section.

6.2.1.1 Toxic Gas Concentration

Figure 6-13 shows the most important toxic gas emissions, which had their highest concentration between 1500 s to 2000 s for medium crib 1 and 1000 s to 1500 s for medium crib 2 during the restricted ventilation phase of the fire. The transition from flaming to smouldering combustion with low oxygen concentration of < 10% was associated with the release of peak levels of toxic gases. The equivalence ratio was highest during this period, which explains that the richer the mixture, the higher the toxicity.

The main toxic gases were CO, formaldehyde and acrolein. Benzene was also found to be significant in this fire. This agrees with results obtained by the authors [88, 194] for a 1.6 m³ compartment fire. CO exceeded the LC₅₀ exposure limit by a factor of 3 while it exceeded the COSHH_{15min} exposure limit by a factor of 40. Formaldehyde also exceeded the exposure limits on both the LC₅₀ and COSHH_{15min} basis. Although acrolein did not exceed the LC₅₀ exposure limit, it exceeded the COSHH_{15min} limit by a factor of 5000. Medium crib 2 produced higher concentrations of the toxic gases than medium crib 1 except for HCN and benzene. Even though the compartment was considered well ventilated with lean combustion, high concentrations of toxic gases were produced in both tests that will lead to the impairment of escape and eventual death.



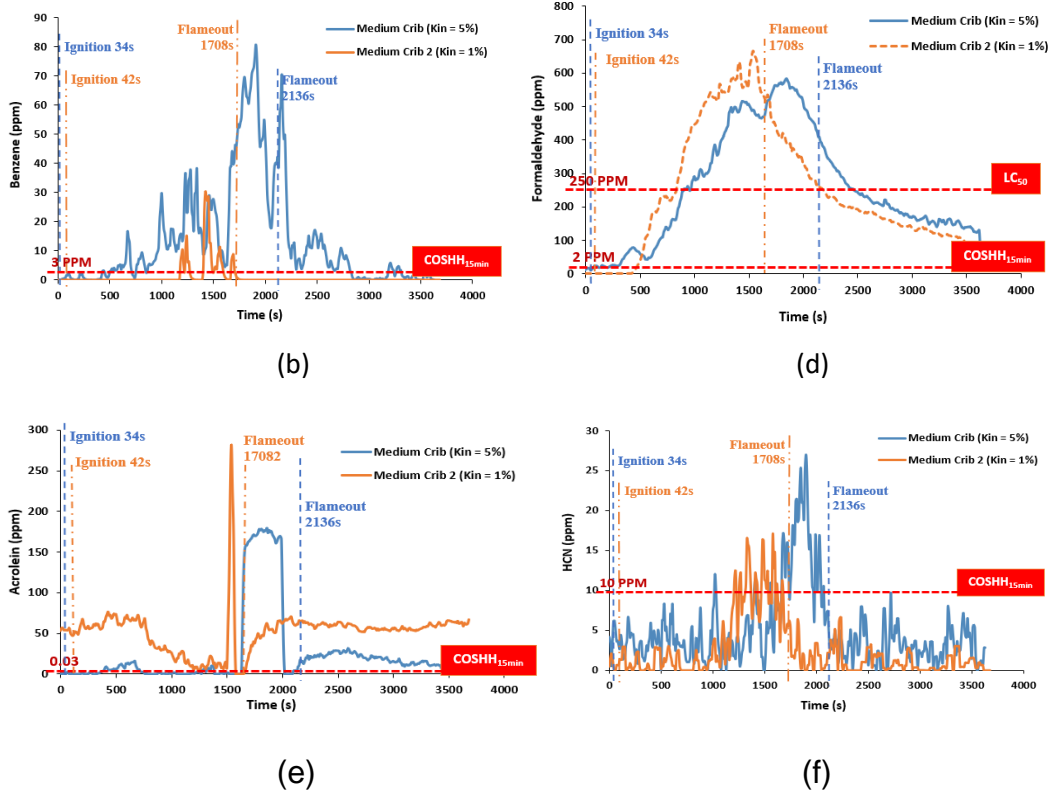


Figure 6-13 Toxic gas concentrations; CO (a), Total Hydrocarbon (b), Benzene (c), Formaldehyde (d), Acrolein (e) and Hydrogen Cyanide (f)

6.2.1.2 Total Fire Toxicity N on an LC₅₀ and COSHH_{15min} Basis

Figure 6-14 shows that the peak **N** for LC₅₀ was > 6 and the peak **N** on a COSHH_{15min} basis was > 2000, but they occurred at the same time in the transition from the flaming to smouldering combustion. The **N** values indicate that the toxic gases on escaping from the compartment would need to be diluted with air by a factor of > 2000 before escape was not impaired and by a factor of > 6 before deaths would not occur.

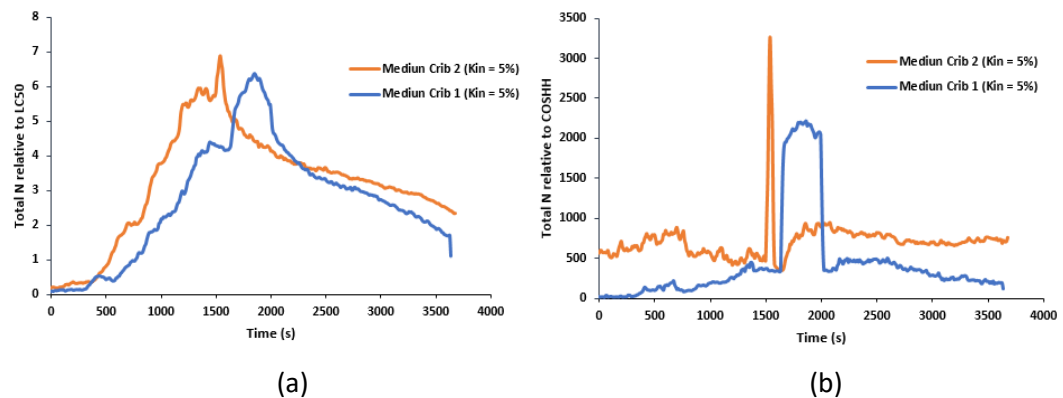


Figure 6-14 Total N relative to LC₅₀ (a) and COSHH_{15min} (b)

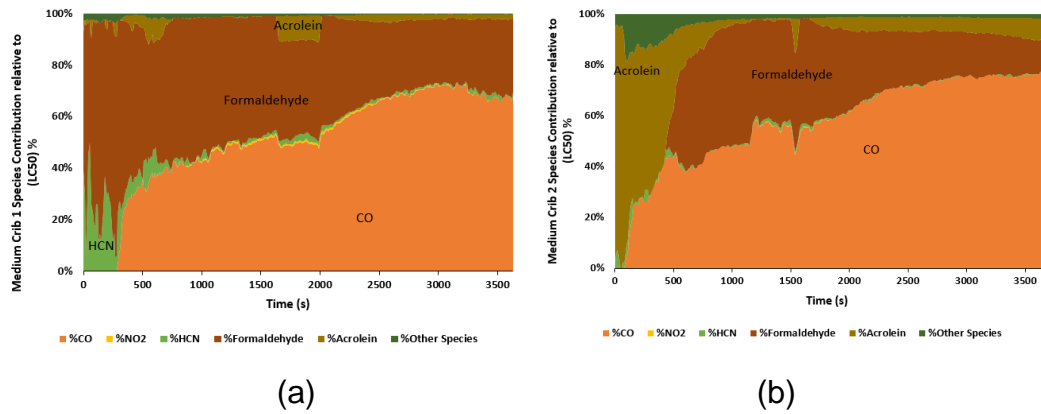


Figure 6-15 N-Gas Composition (LC₅₀) Medium Crib 1 (a) and Medium Crib 2 (b)

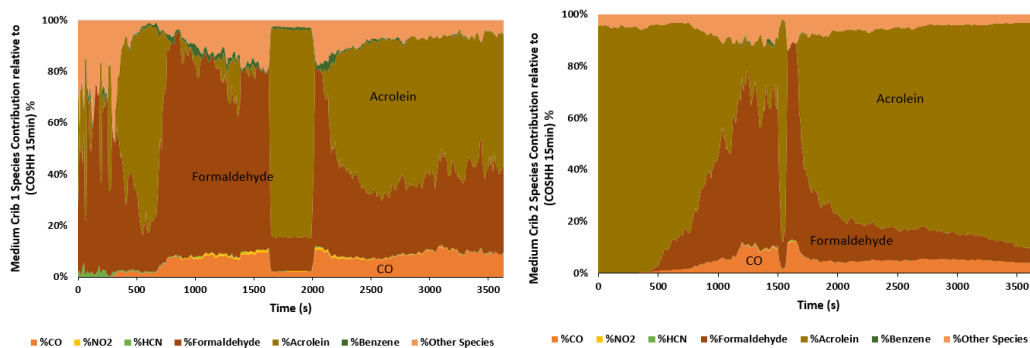


Figure 6-16 N-Gas Composition (COSHH_{15min}) Medium Crib 1 (a) and Medium Crib 2 (b)

Figure 6-15 and 6-16 show the major contribution to the total toxicity on an LC₅₀ and COSHH_{15min} basis. On an LC₅₀ basis the toxicity was dominated by CO, formaldehyde, acrolein and HCN for both tests while on a COSHH_{15min} basis formaldehyde, CO and benzene dominate for medium crib 1. Medium crib 2 was dominated by acrolein, formaldehyde and CO.

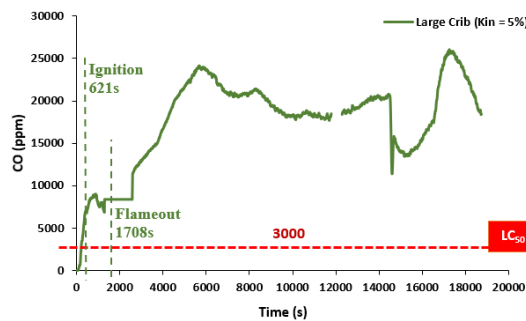
6.2.2 The Large Wood Crib

The analysis on the toxic gas emissions of the large wood crib are presented in this section.

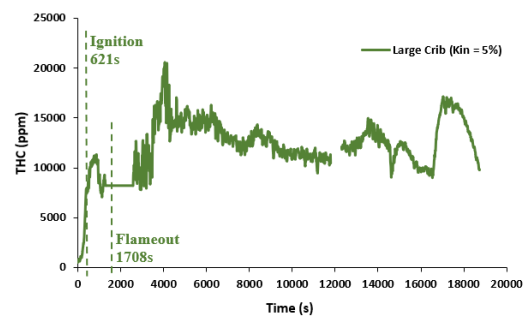
6.2.2.1 Toxic Gas Concentration

The large crib fire was a smouldering lean-combustion fire test. However, high concentration of toxic gases were generated as a result of the pyrolysis with partial oxidation of the gases. The toxic gases generated by this smouldering fire were double that generated by the flaming medium crib fires. Most of the

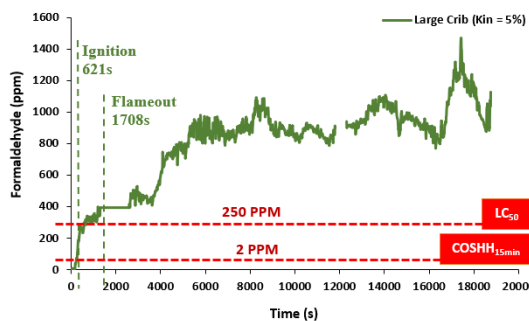
combustion products produced at the initial flaming stage were as a result of the pool fire. Toxic gases such as benzene and HCN were only high at the initial pool flaming stage but were very low after the flame out as shown in Fig. 6-17e and f. CO exceeded the LC_{50} limit by a factor of 8 and exceeded the $COSHH_{15min}$ limit by over a factor of 100. Formaldehyde was also significantly high, exceeding the limits on both LC_{50} and $COSHH_{15min}$ basis. Acrolein did not exceed the LC_{50} limit but exceeded the $COSHH_{15min}$ by over a factor of 10,000. These are irritants that not only affect the sensory organs, but also impair escape by slowing down the movement of people to a place of relative safety and eventually leading to death by being overcome by toxic gases.



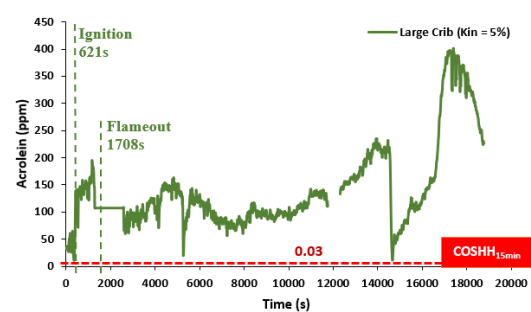
(a)



(b)



(c)



(d)

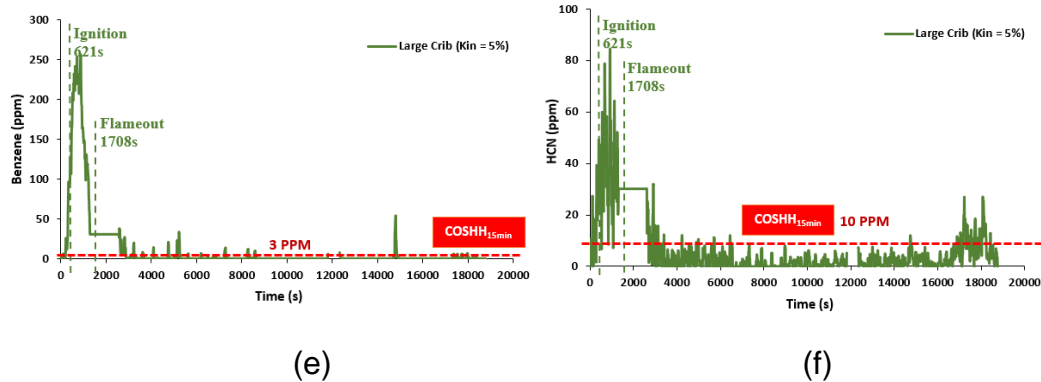


Figure 6-17 Toxic gas concentrations; CO (a), Total Hydrocarbon (b), Benzene (c), Formaldehyde (d), Acrolein (e) and Hydrogen Cyanide (f)

An important observation from the test was that as long as oxygen and fuel are available in a compartment, smouldering reaction will continuously take place, producing extremely toxic gases at high concentrations. The main toxic gases produced are CO, formaldehyde, acrolein and other unburnt hydrocarbons.

6.2.2.2 Total Fire Toxicity N on an LC₅₀ and COSHH_{15min} Basis

The total toxicity **N** for LC₅₀ and COSHH_{15min} are shown as a function of time in Fig.6-18. The **N** value relative to LC₅₀ value was an average of 10 with a peak of 16 around 18000 s and the **N** value relative to COSHH_{15min} was an average of 1500 with a peak of 4800 at about the same time. This means that the toxic gases need to be diluted with fresh air by a factor of about 4800 before escape is not impaired and it has to be diluted by a factor 16 before it doesn't lead to death in 30 mins. Both methods of calculating **N** located the same time in the fire where the peak toxicity occurs.

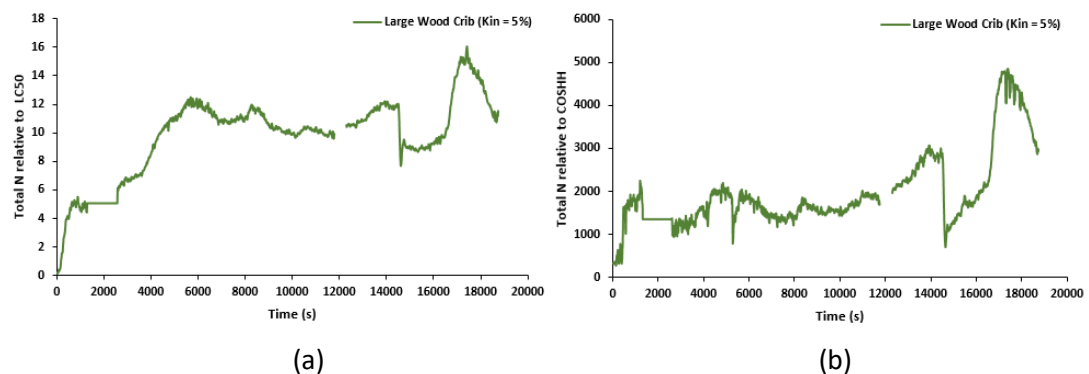


Figure 6-18 Total N relative to LC₅₀ (a) and COSHH_{15min} (b)

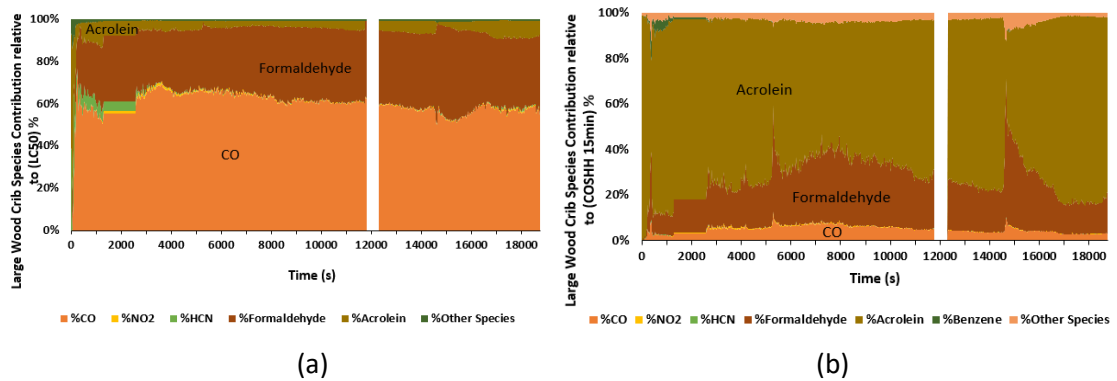


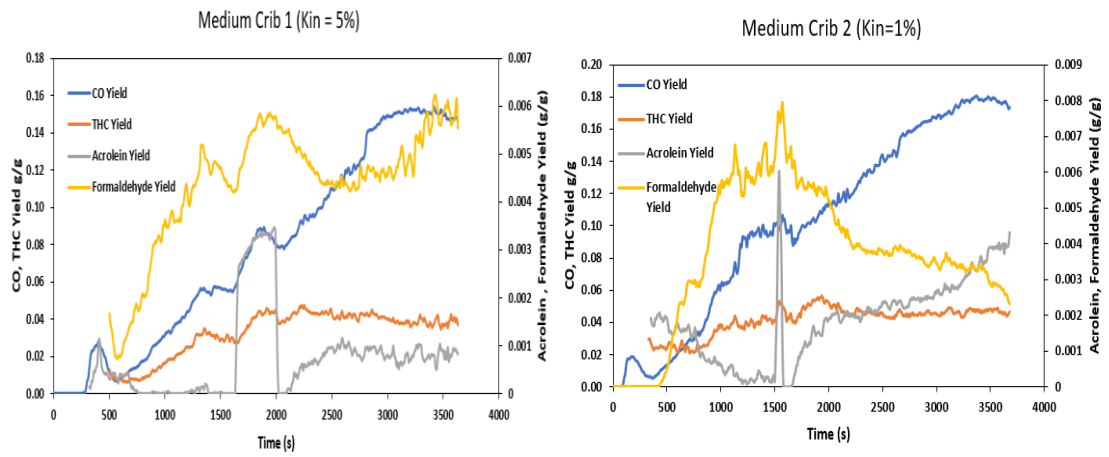
Figure 6-19 N-Gas Composition (LC₅₀) (a) and (COSHH_{15min}) (b)

The major contribution to the total toxicity are shown on an LC₅₀ and COSHH_{15min} basis in Figs. 6-19 a and b for the large wood crib. On an LC₅₀ basis, the toxicity was dominated by CO, followed by formaldehyde and acrolein while on a COSHH_{15min} basis, acrolein, formaldehyde and CO dominated. The dominating toxic gases were same on both basis but the emphasis and importance are different.

6.2.3 Toxic Gas Yields

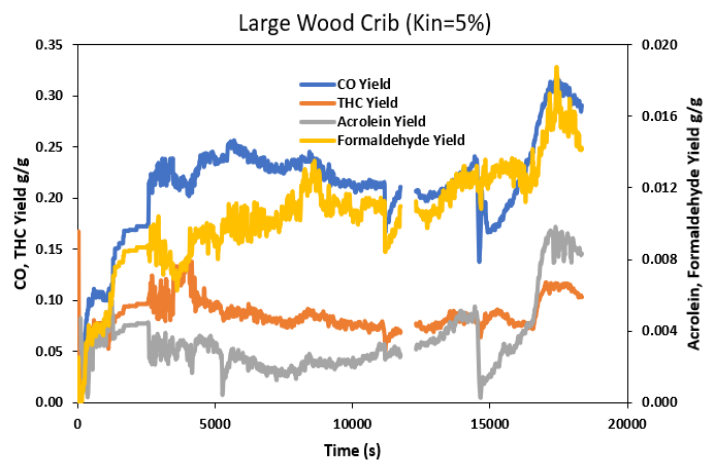
The toxic gas yields of the most important gases are presented in Fig. 6-20. These were obtained from measured gases by the heated FTIR. The lean non-flaming fires produced a higher yield of toxic gases than the flaming combustion. This was mainly due to pyrolysis with partial oxidation in the smouldering fire, which led to a high yield of the toxic gases. Even though the combustion was lean, the products of incomplete combustion were generated in high concentration.

The medium crib 1 test had a slightly lesser toxic yield than the medium crib 2, which was mostly influenced by the ventilation rate, affecting the fire conditions. Ideally, richer-combustion produces higher yield of toxic gases than the flaming combustion. However, the medium crib test showed a different trend, with the medium crib 1 having a richer mixture but lower yield of toxic gases compared to the medium crib 2. A possible reason for such rich-mixture, low yield could be the soot developed during the combustion of the wood acted as a catalyst to break CO₂ to CO and O resulting in high CO and an increase in oxygen [195].



(a)

(b)



(c)

Figure 6-20 Toxic Gas Yields; Medium Crib 1 (a), Medium Crib 2 (b) and Large Crib (c)

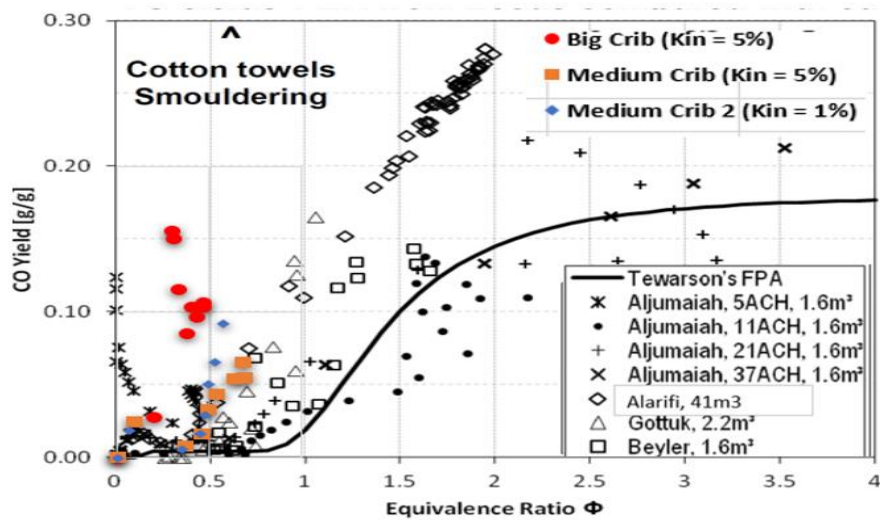


Figure 6-21 Comparison of CO Yield with Literature [87]

A comparison of the CO yield to that of Tewarson using the fire propagation apparatus shows that the wood yield in this work is higher at that equivalence ratio with lean combustion. This is so because of the smouldering combustion that occurred with the large crib causing the release of products of incomplete combustion and hence high yield of toxic gases especially when burned for a long duration as in the case of the large crib. A summary of the yields is given in Table 6-1, compared with test done by Alarifi et al. [196] on real fire test of wooden pallets in a bungalow.

Table 6-1 Toxic Gas Yields

Toxic Gas	Gas Peak Yield		
	Alarifi et al.	Medium Crib Test	Large Crib (average at steady state)
CO	0.24	0.15 – 0.18	0.25
Formaldehyde	0.012	0.06 – 0.08	0.012
Acrolein	0.005	0.0035 – 0.006	0.003
Total Unburnt Hydrocarbon	0.044	0.045 – 0.05	0.07

6.3 Particulate Emissions from Wood Crib Tests

This section presents the particle size, number and mass concentrations obtained from the wood crib tests. Particulate yield and concentration obtained from filter paper samples using a heated filter paper sampling system are also presented.

6.3.1 Small Wood Crib

6.3.1.1 Particle Number Concentration

The particle number concentration as a function of size and time for small crib 1 and 2 is shown in Figs. 6-22 and 6-23. A bimodal distribution of the particle sizes was observed indicating the nucleation mode and accumulation mode of the particle size distribution. The nuclei mode for the small crib 1 (fully open $K_{in}=5\%$) was found to peak at 20 nm. For the accumulation mode, the small crib 1 fire

peaked at 200 nm from 10 – 500 s and centred at 300 nm afterwards from around 800 s. The small crib 2 (closed $K_{in}=0$) had different peaks of the nuclei particles at different times but at the time the HRR was at its peak, around 100 s, the nuclei peak was 60 nm. However, the accumulation mode peaked at 250 nm throughout the combustion. Even though the small crib 2 fire was short, the analyser was allowed to sample for 1500 s. Small crib 2 produced more of the larger particles than small crib 1, which could be due to the limited ventilation in the compartment.

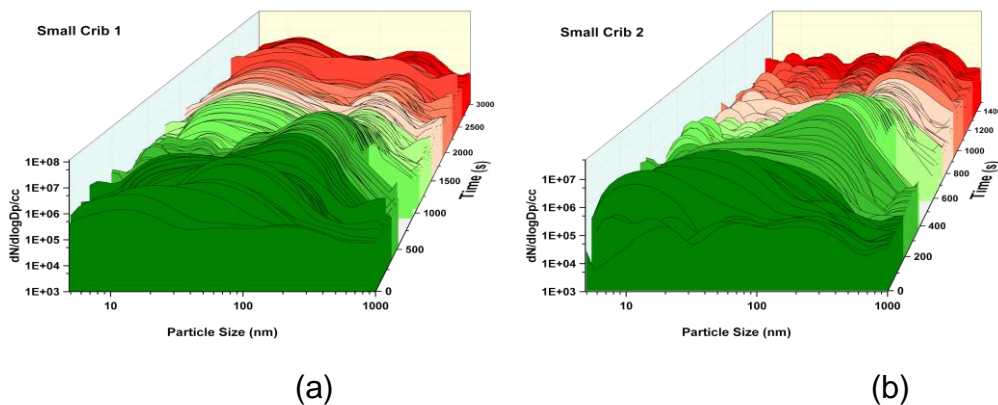


Figure 6-22 Particle Number and Size Distribution; Small Crib 1 (a) and 2 (b)

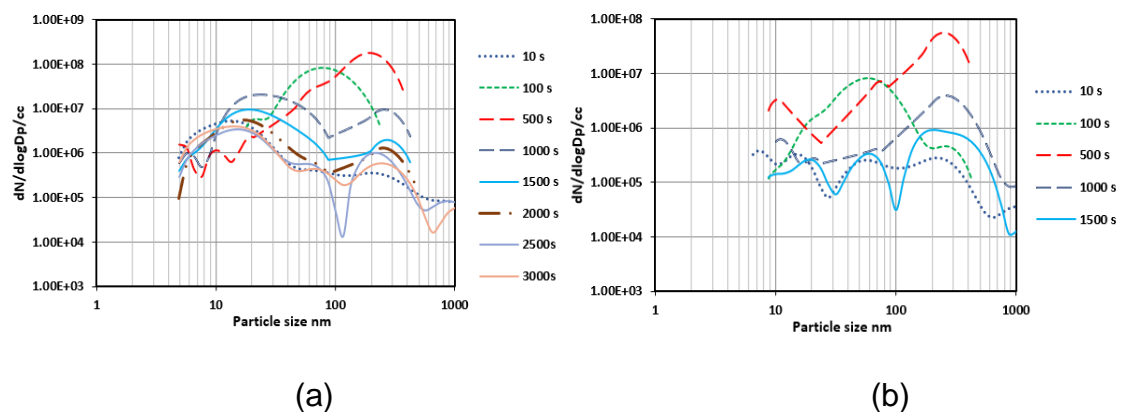


Figure 6-23 Particle Number and Size Distribution at Different times; Small Crib 1 (a) and 2 (b)

6.3.1.2 Particle Mass Concentration

The equivalent mass concentration is shown in Figs. 6-23 and 6-24. This shows that the larger particles had high mass concentration as compared to the ultrafine

particles. In terms of number, small particles in the nucleation mode constitute the majority of the particles.

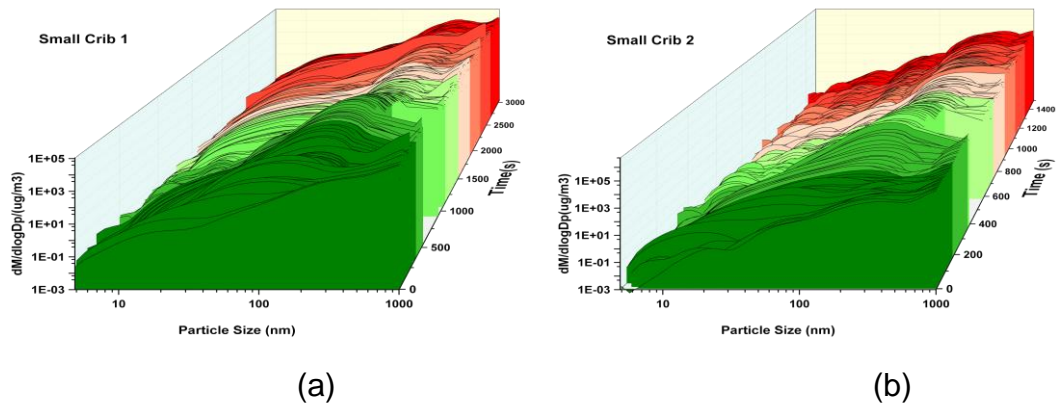


Figure 6-24 Particle Mass and Size Distribution; Small Crib 1 (a) and 2 (b)

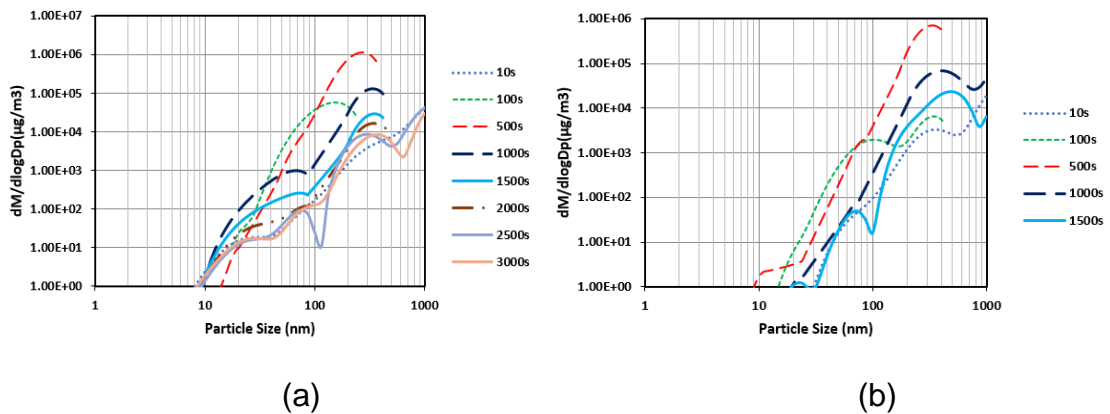


Figure 6-25 Particle Mass and Size Distribution at Different times; Small Crib 1 (a) and 2 (b)

The accumulation mode 300 nm for small crib 1 had a peak of $1 \times 10^6 \mu\text{g}/\text{m}^3$ ($1 \text{ g}/\text{m}^3$) while the peak for the accumulation mode of small crib 2 had a slightly lower mass concentration of $6.6 \times 10^5 \mu\text{g}/\text{m}^3$ ($0.7 \text{ g}/\text{m}^3$). Even though the compartment had limited ventilation in one of the tests, both fires produced particles that may lead to the impairment of escape and eventual death.

6.3.2 Medium Wood Crib

6.3.2.1 Particle Number Concentration

Figure 6-26 and 6-27 show the particle number concentrations as a function of particle size and time and the particle number concentrations at defined times. Figure 6-27a shows a bimodal distribution of the particle sizes but with less number concentration of the ultrafine particles centred at 20 nm. From the peak HRR phase to the stage where the flame was about to flame out, only the larger

particles centred at 200 nm were uniformly produced. However, at about 1500 s, where all toxic gases were at their peak, particles centred at 100 nm particle were produced at the highest concentration of 1.3×10^8 /cc.

Medium crib 2 fire test shown in Figure 6-25 and 6-26b, indicates different peaks at the beginning of sampling and towards the end of sampling. However, a bimodal distribution was observed indicating the nucleation and accumulation mode of particles formed from the time of ignition (42 s) to the flameout time (1708 s) having a peak of 20 nm and 100 nm at 4×10^5 /cc and 4.5×10^7 /cc. There was a uniform pattern of particle size distribution in this fire test through the burning duration but the highest concentration of particle number was during the fire decay phase.

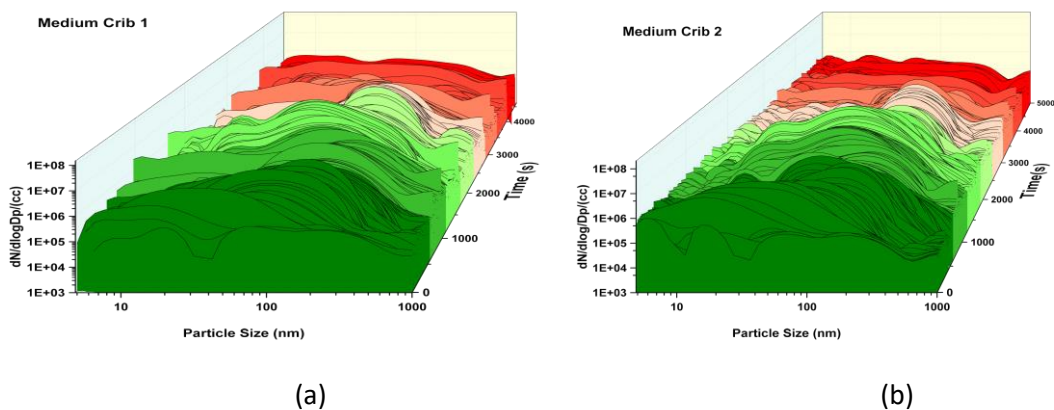


Figure 6-26 Particle Number and Size Distribution; Medium Crib 1 (a) and 2 (b)

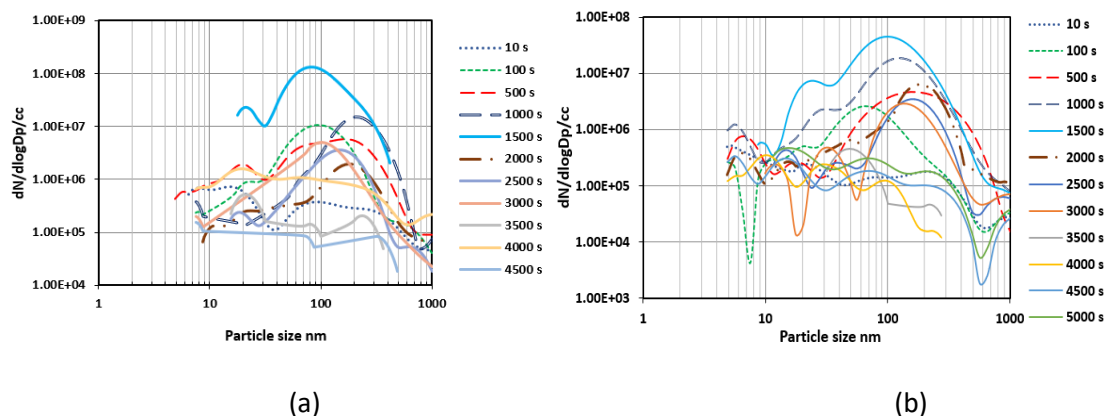


Figure 6-27 Particle Number and Size Distribution at Different times; Medium Crib 1 (a) and 2 (b)

6.3.2.2 Particle Mass Concentration

The equivalent mass concentration is given in Figs. 6-28 and 6-29. The mass concentration of the 200 nm particle size of medium crib 1 was a peak of $1.6 \times 10^5 \mu\text{g}/\text{m}^3$ and an average of $2.3 \times 10^4 \mu\text{g}/\text{m}^3$ while the mass concentration of the 100 nm particle size of the medium crib 2 was $3.3 \times 10^3 \mu\text{g}/\text{m}^3$.

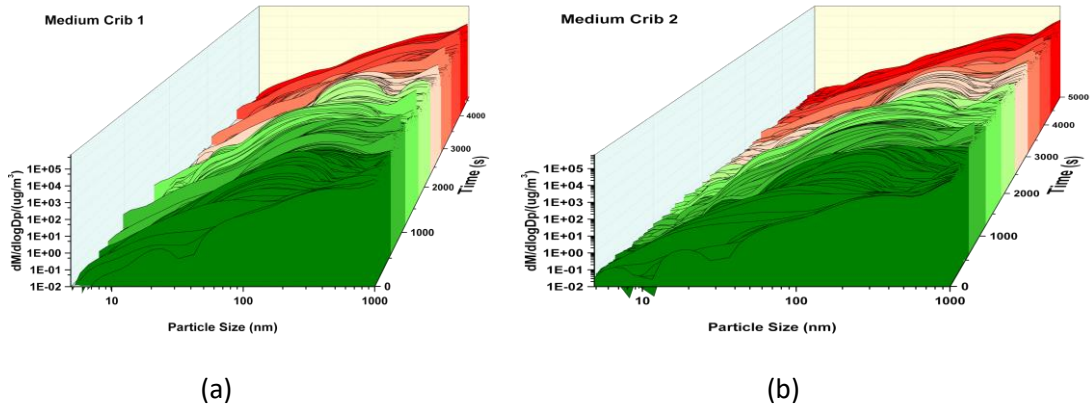


Figure 6-28 Particle Mass and Size Distribution; Medium Crib 1 (a) and 2 (b)

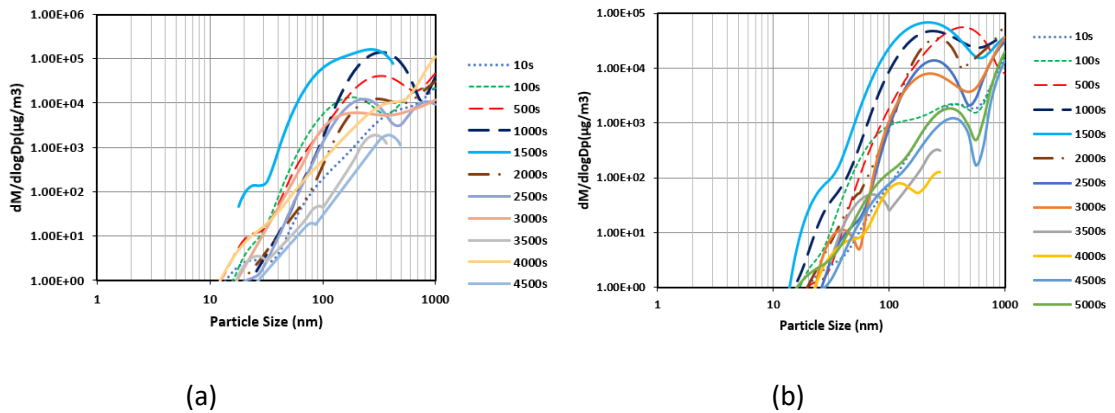


Figure 6-29 Particle Mass and Size Distribution at Different times; Medium Crib 1 (a) and 2 (b)

The mass concentration was highest with the larger particles. It can be observed that particles larger than 1000 nm were produced but that is above the (1000 nm) upper measurement range of the Cambustion DMS500.

6.3.3 Large Wood Crib

6.3.3.1 Particle Number Concentration

The large wood crib fire test produced a fairly constant distribution of particles from ignition and throughout the burning period. The smouldering combustion produced large particles at a high concentration compared to the flaming combustion. During the pool flaming combustion, only large particles of 200 nm size were produced as shown in Fig. 6-30b. Loo et al. [153] measured the soot concentrations of pool fires in a 1m³ mechanically ventilated compartment at 5 and 8 ACH (air changes per hour) and obtained a modal diameter of 200 nm. The 200 nm particle size had an average number concentration of 1 x 10⁷ number/cc.

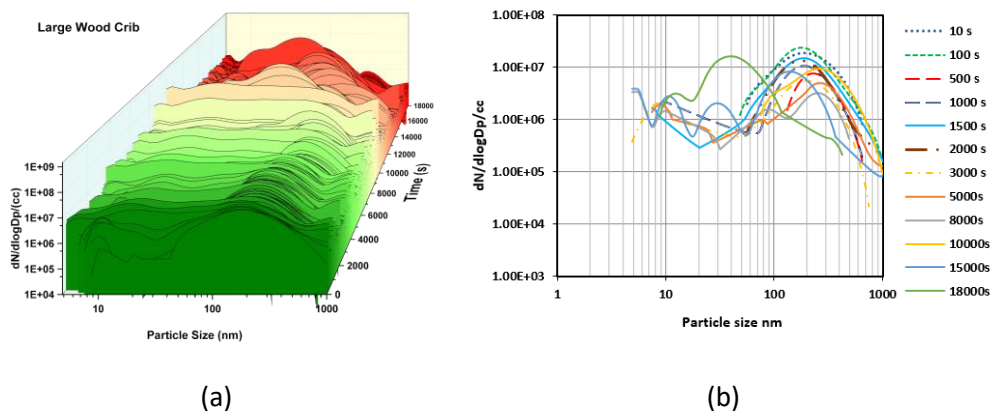


Figure 6-30 Large Crib Particle Number Concentration and Size Distribution at Different times

The fire development in the compartment tests did not show much influence on the production of particle number concentration and size distribution. The equivalence ratio also did not seem to have any effect on the particle generations since all the lean combustion seem to produce different particle sizes with different particle number concentration. However, one factor that had an effect on the concentration of particle number is the combustion scenario, the smouldering combustion produced a higher particle number concentration of the larger particles compared to the flaming combustion.

6.3.3.2 Particle Mass Concentration

The particle mass distribution is presented in Figures 6-31 a and b. The dominant modal size 200 nm produced an average of $4.5 \times 10^4 \mu\text{g}/\text{m}^3$ on mass basis.

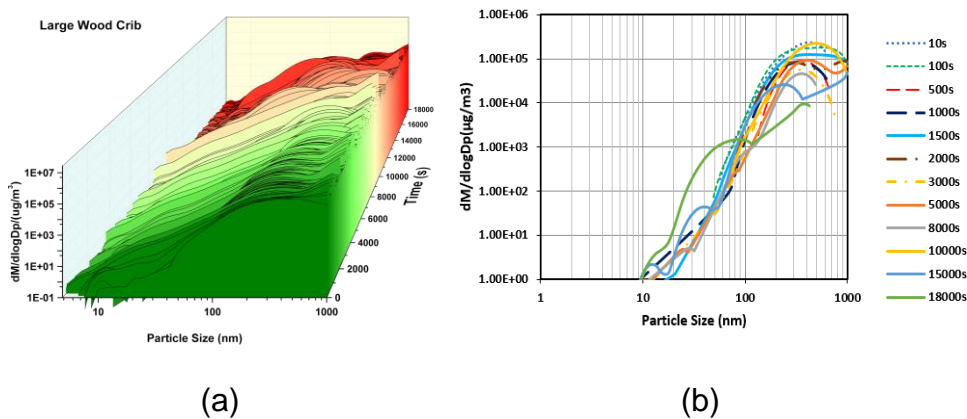


Figure 6-31 Large Crib Particle Mass Concentration (a) and Size Distribution at Different times (b)

6.3.4 Gravimetric Soot Sampling

Soot samples were collected on a filter paper using the Richard Oliver heated filter paper sampling equipment as described in chapter 3. The gravimetric soot mass concentrations and yield of medium crib 1, 2 and the large crib were compared and presented in Figures 6-32- 6-34.

6.3.4.1 Soot Particulate Mass Concentration

Soot samples collected for the duration of the tests were weighed after the tests to obtain the mass concentration. The total mass for medium crib 1 was $1 \text{ g}/\text{m}^3$, $1.23 \text{ g}/\text{m}^3$ for medium crib 2 and $2.37 \text{ g}/\text{m}^3$ for large wood crib but all tests have a similar maximum concentration of $0.25 \text{ g}/\text{m}^3$. The large wood crib produced the highest amount of soot compared to the two medium crib tests. The particle mass was also compared with other work done by Andrews et al [156] at 2.7 air changes per hour in Fig. 6-30. The present work shows a similar trend with the wood crib but the particle mass obtained was higher but comparable to the diesel mass concentration of $0.25 \text{ g}/\text{m}^3$. This could be as a result of the difference in the ventilation rate of 2.7 ACH as against the 7-8 ACH in the present work.

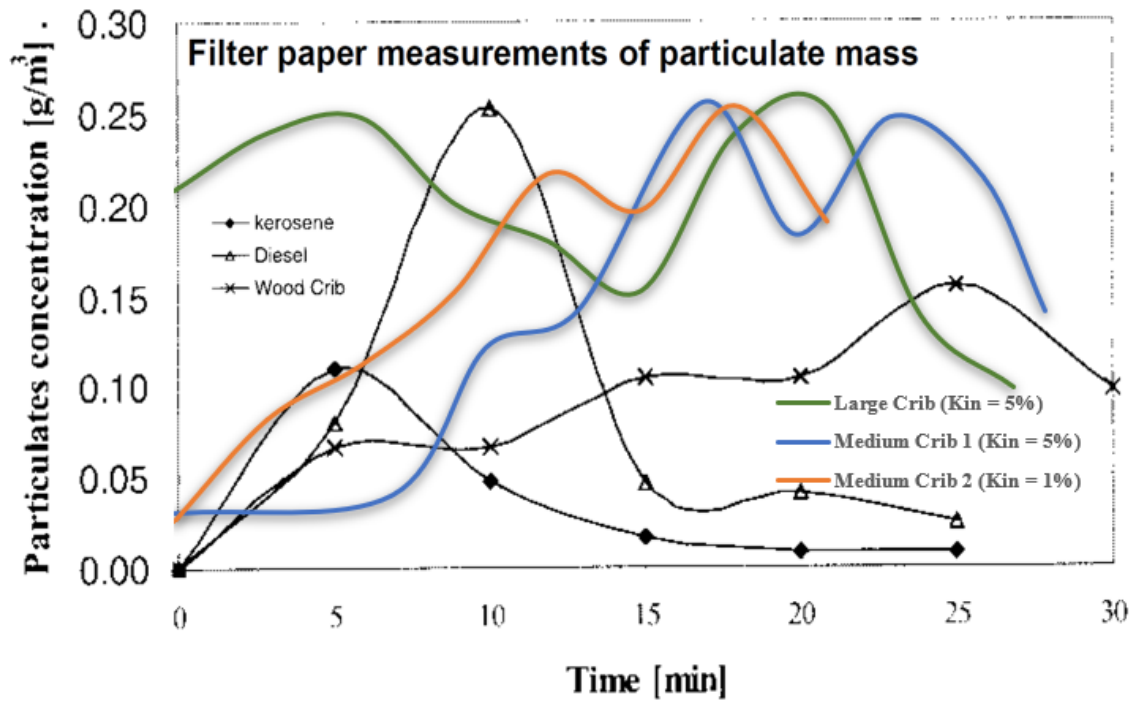


Figure 6-32 Comparison of Filter Paper Mass Concentration with Literature [156].

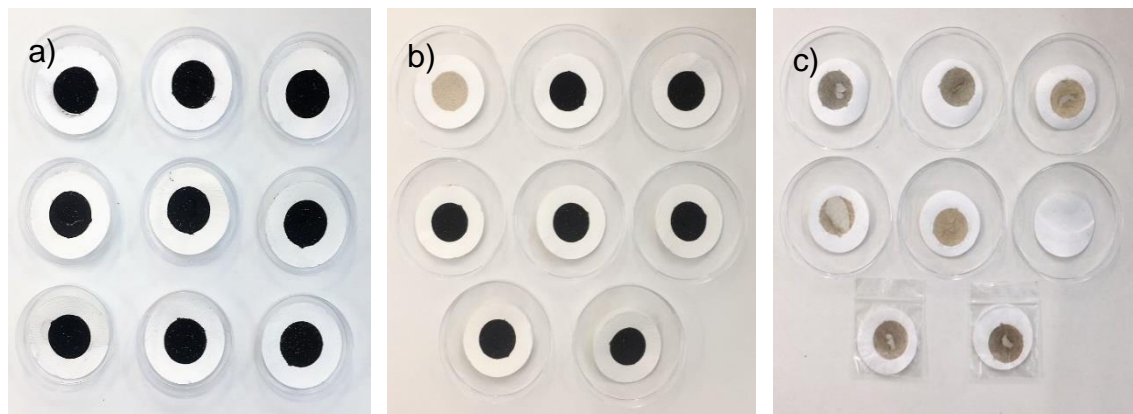


Figure 6-33 Soot Deposits on Filter Paper (a) medium crib 1 (b) medium crib 2 and (c) Large crib

6.3.4.2 Soot Particulate Yield

The soot particulate yield is shown as a function of the fire equivalence ratio in Fig. 6-34. It shows that the leaner combustion produced more soot. The mass of soot produced by medium crib 1 was lower than that produced by medium crib 2. This implies that the formation of soot is influenced by the ventilation factor as the combustion was leaner for the medium crib 2 than medium crib 1. The maximum yield for medium crib 1 was 2.6 g/kg and that of medium crib 2 was 5.3 g/kg.

The same Fig. 6-34 shows the soot yield for the large wood crib showing significant amount of yield collected before the ignition of wood, which was dominated by the pool fire soot. However, these tests show that the temperature has little effect on the generation of soot where the temperature of pool fire at the initial stage of the large crib fire was a lot higher than the temperature of medium crib 2 fire, but the soot yield was almost the same. The maximum yield for the large crib was found to be 5.7 g/kg.

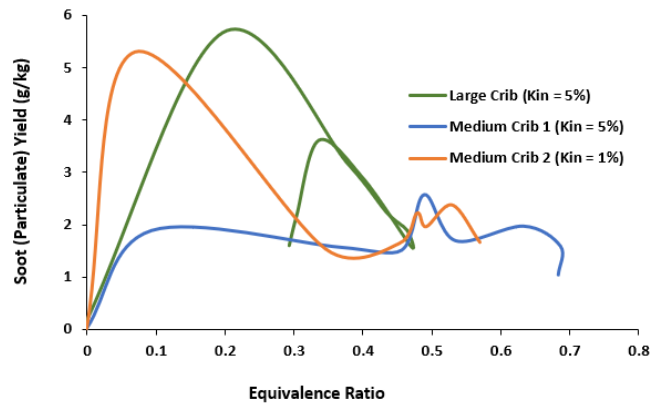


Figure 6-34 Soot Particulate Yield as a Function of Equivalence Ratio

The soot yield between 1000s to 1600s at the same temperature of 250°C showed that the smouldering combustion produced higher soot compared to flaming combustion having high oxygen concentration in the compartment. This shows that ventilation has more influence on the formation of soot compared to temperature.

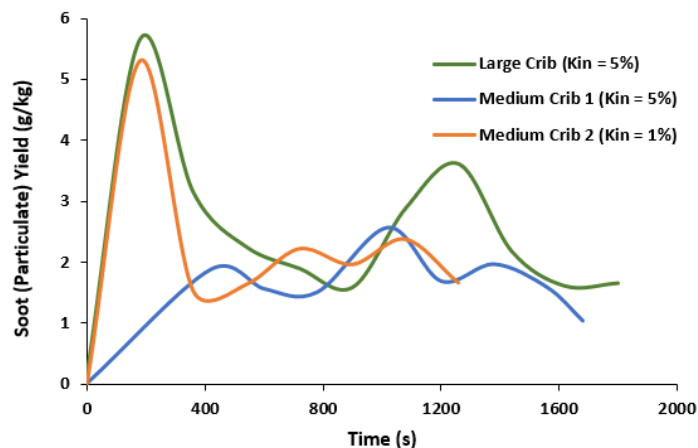


Figure 6-35 Soot Particulate as a Function of Time

6.4 SEM Analyses on Soot Samples

Two samples from the small wood crib 1 test ($K_{in} = 5\%$) were analysed using the scanning electron microscope SEM. This was done only to compare and verify the sizes obtained with that of the DMS500 particle size analyser, hence very few samples were analysed. Samples were taken from the smoke meter and the compartment window. The sizes obtained from the filter paper sampling equipment sample were in the range of 50 – 90 nm while the sizes obtained from the window sample were in the range of 40 – 85 nm. These sizes fall in the range of particles obtained by the DMS particle size analyser.

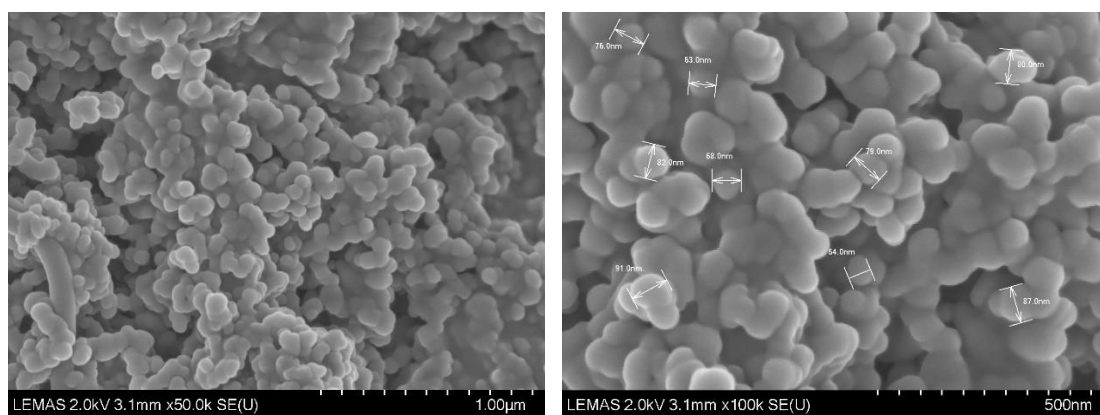


Figure 6-36 Small Crib 1 SEM Analysis on Smoke Meter Sample

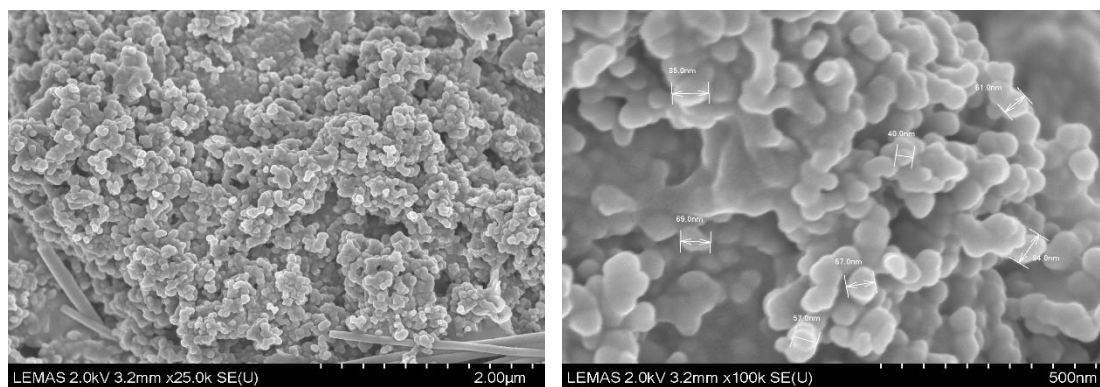


Figure 6-37 Small Crib 1 SEM Analysis on Window Sample

Comparing the SEM particle structure with that obtained by Perera and Litton [31] in Fig. 2-16 for Douglas fir shows similar morphology of particles but they [31] did not determine the size of the particles or the fractal aggregates from the SEM.

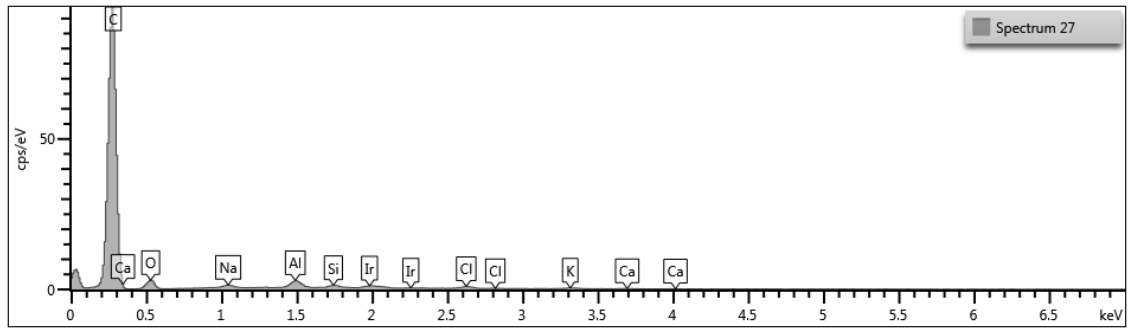


Figure 6-38 Small Crib 1 SEM Elemental Analysis on Smoke Meter Sample

Table 6-2 Small Crib 1 SEM Elemental Analysis on Smoke Meter Sample

Element	Wt%
C	89.94
O	7.89
Na	0.38
Al	0.83
Si	0.27
Cl	0.37
K	0.23
Ca	0.09
Total:	100

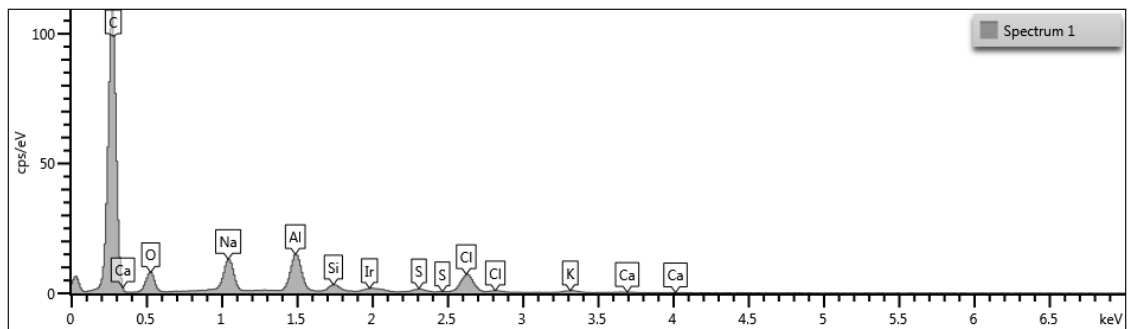


Figure 6-39 Small Crib 1 SEM Elemental Analysis on Window Sample

Table 6-3 Small Crib 1 SEM Elemental Analysis on Window Sample

Element	Wt%
C	81.47
O	9.78
Na	2.82
Al	2.7
Si	0.5
S	0.3
Cl	2.06
K	0.31
Ca	0.08

Figures 6-38 and 6-39 show the spectrum for the elemental analysis of the soot samples obtained from the filter paper sampling equipment and the compartment window. The soot from the filter paper sampler shows that about 90% of the soot sample is carbon, 8% oxygen and other trace elements while the soot collected from the window showed that about 81% of the soot sample is carbon and 9% oxygen, with other elements. The Aluminium in the sample is the aluminium stud on which the samples were placed for analyses and silicon is from the filter paper fibre.

6.5 Summary

The investigation on the fire toxicity and particulate emissions from pinewood crib fires in a 5m³ compartment resulted in the following findings:

- The burning of the small crib was influenced by the ventilation conditions. Small crib 2 self-extinguished due to the limited ventilation.
- The flow rate in the rig was controlled not only by the air inlet (K_{in}) but also the exhaust flow out (K_{out}) from the compartment.
- The equivalence ratio for the medium crib fire had no influence on the concentration of toxic gases produced and toxic gas yield. Medium crib 2 having leaner combustion than medium crib 1 generated the highest concentration of toxic gases and toxic yield throughout the burning process.

- The key toxic species for all wood crib fires were CO, acrolein, and formaldehyde.
- The smouldering fire was found to be more toxic and produced more soot than the flaming fire.
- The smouldering fires produced particle number concentrations higher than the flaming fires.
- The ventilation had more effect on the generation of soot than the temperature.
- The toxic gas yield for large wood crib fire compares well with full scale fire tests but for the medium crib fire the yield was lower.
- SEM analyses of filtered particulate samples showed sizes of particles within the range obtained by the DMS particle size analyser.

Chapter 7 Pool Fires

Pool fires are a potential hazard in many chemical and petrochemical industries, therefore understanding the nature of these fires is key to developing fire safety strategies and systems to mitigate the undesirable effects from pool fires. Pool fires do not happen frequently, but if they do, they have the tendency to cause a catastrophic damage both in terms of loss of lives and property and also environmental pollution. This Chapter presents the results of pool tests done on the cone calorimeter and the 5m³ compartment. Different pool sizes of diesel were burnt in the 5m³ compartment at varying ventilation rates. The burning characteristics and the toxic emissions (gaseous and particulate) are presented in this chapter.

7.1 Cone Calorimeter Pool Tests

Three pool tests (Diesel, lubricating oil and olive oil) were conducted using the freely ventilated setup of the cone calorimeter. 20 g of each fuel was burnt in a 100 x 100 mm tray and exposed to a radiant heat of 25 kW. In this section, the results of the mass loss, mass loss rate as a function of time, heat releases rate (HRR), equivalence ratio, oxygen concentration as a function of time and toxic gas analysis and yields are presented. Toxicity assessment was based on COSHH_{15min} and LC₅₀. The combustion period for each fuel is given in Table 7-1.

Table 7-1 Combustion Period

Fuel type	Ignition time (s)	Flameout time (s)	Burning duration (s)
Diesel	164	493	329
Lubricating oil	288	766	478
Olive oil	904	1291	387

7.1.1 General burning Characteristics: Mass Loss, Mass Loss Rate, Heat Release Rates, Equivalence Ratio and Oxygen

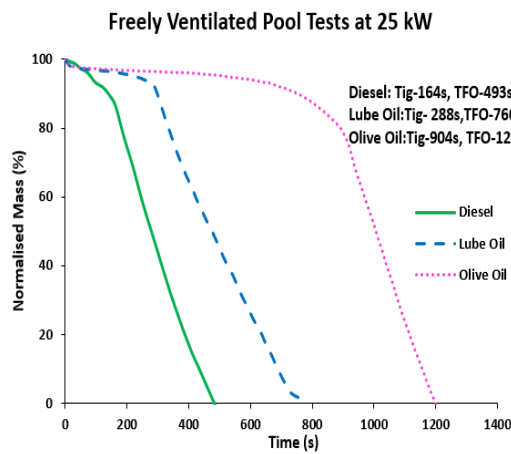
Figure 7.1a and b show the mass loss and the mass loss rate of the 3 pool tests from the beginning of the test to the end. This shows that diesel was the fastest to ignite at 164 s while olive oil took the longest time to ignite at 904 s. This difference in ignition delay can be connected to the difference in flash point of each liquid fuels with diesel having a flash point of 71°C [197], lubricating oil 340°C [198] and olive oil 437°C [198]. The flash point of a liquid hydrocarbon is the temperature to which it must be heated to emit sufficient flammable vapor to flash when brought into contact with an ignition source [199]. The temperature of a flammable mixture must be at or above the flash point before it burns. If the temperature is below this point then the vapor mixture will not burn, even in the presence of an ignition source [200]. The ignition source must be of sufficiently high temperature and must also contain sufficient energy to ignite the fuel even when the material is above its flash point. The minimum energy varies with type of gas and concentration; for hydrocarbon vapours it is low, for high flash point liquids, such as diesel and fuel oil, it is much higher [200].

Diesel has the lowest flash point of 71°C [197] amongst all the fuels. During the ignition delay period, the fuel vaporised due to exposure to the heat but the rate at which each fuel vaporised differed, resulting in longer ignition delay in some fuels than others. Therefore the mass of fuel lost before the fuels ignited is different for each fuel. About 4 g of olive oil was lost before it ignited because it was exposed to the heat for a very long time and therefore vaporised for long time compared to the diesel and the lubricating oil. It was observed from Fig. 7-1b that the diesel fuel had the highest mass loss rate, followed by olive oil and the lubricating oil. The average mass loss rates for the fuels are 0.053 g/s for diesel, 0.041 g/s for the lubricating oil and 0.054 for the olive oil. The diesel and the olive oil had similar mass loss rate with the olive oil having a slightly higher mass loss rate.

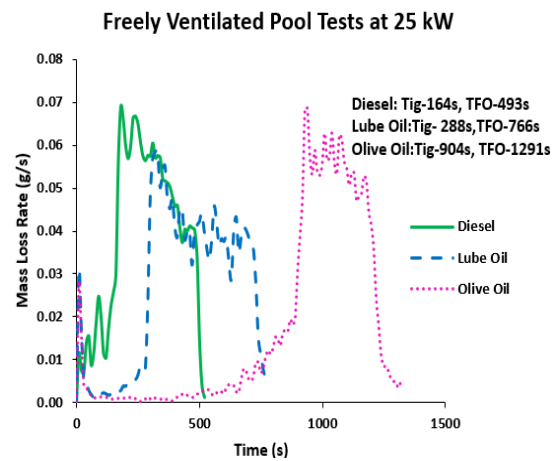
The equivalence ratio in Fig. 7-1c showed that the combustion was lean at the initial stage of the fire until the ignition time when the fire became very rich showing an evidence of confinement even though the experiment was freely ventilated. It will be shown that these rich mixtures were associated with the

release of toxic gases that are a potential hazard to people. The diesel had a peak equivalence ratio of > 5 during the flaming combustion while the other two fuels had above 2 during the flaming combustion.

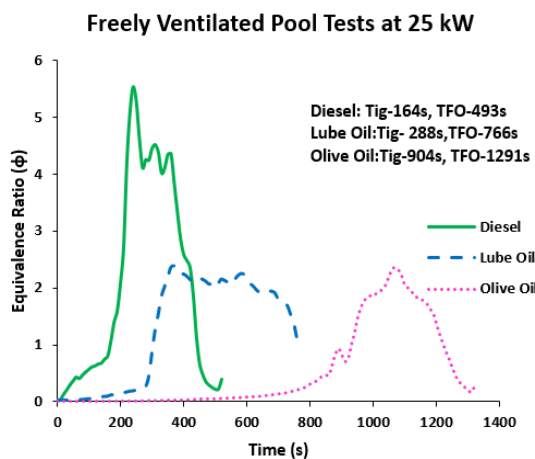
The heat release rate calculated based on mass loss rate is shown in Fig. 7-1d. The HRR for each fuel was highest when the combustion was richest and the mass loss rate was highest. The diesel fuel had the highest heat release rate with a peak HRR of about 320 kW/m^2 followed by olive oil with about 280 kW/m^2 and lubricating oil with about 250 kW/m^2 . There was a drop in oxygen level at the maximum HRR period as shown in Fig. 7-1e.



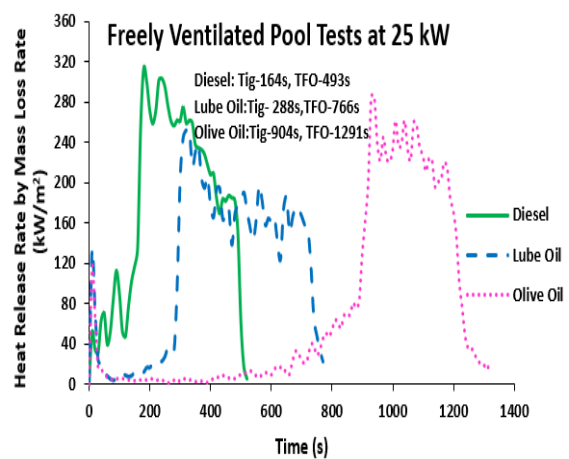
(a)



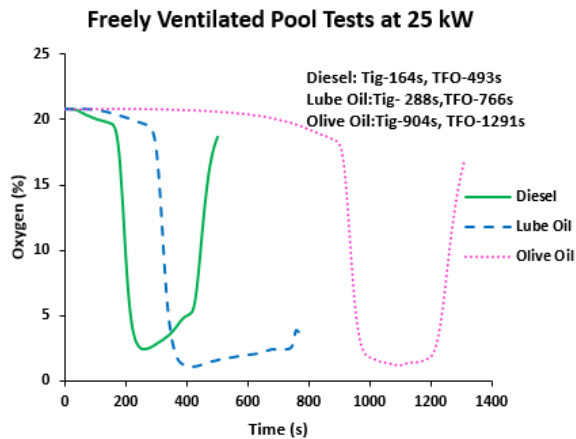
(b)



(c)



(d)

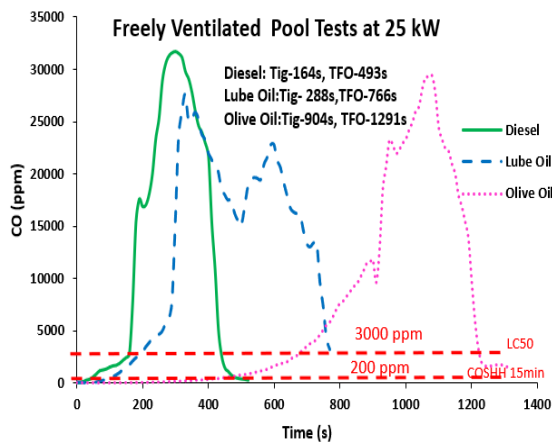


(e)

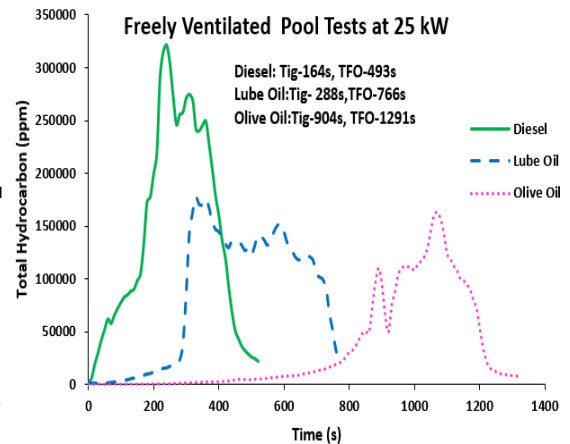
Figure 7-1 Normalised Mass Loss (a) Mass Loss Rate (b) Equivalence Ratio (c) Heat Release Rate HRR (d) and Oxygen (e)

7.2 Toxic Gas Concentrations from Cone Calorimeter Pool Fires

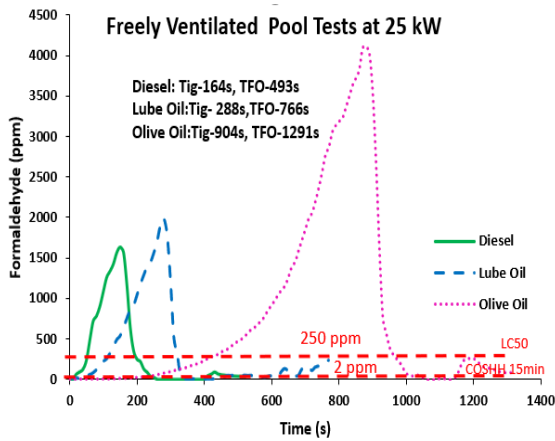
The most important toxic gases from the three pool tests are compared in Fig. 7.2. The main hydrocarbons of toxic significance were benzene, trimethylbenzene (TMB) and naphthalene for all the pool fires. The other major toxic gases generated in the fires were oxygenated hydrocarbons in the form of aldehydes and acidic gases such as acetic acid. In the diesel, lubricating oil and olive oil fires, formaldehyde and acrolein were the main toxic gases of this type and the combination of these gases are those referred to as irritant and acidic gases by those caught breathing these types of toxic gases. High concentrations of the gases with the exception of formaldehyde and acrolein were released during the flaming combustion period and when the HRR was at its peak for all the test fires due to the rich mixture at that stage of the fire. Formaldehyde and acrolein were produced during the ignition delay period. The olive oil with the longest ignition delay period produced the highest concentration of formaldehyde and acrolein, exceeding both the LC_{50} and the $COSHH_{15min}$ limits. All the toxic gases released exceeded the LC_{50} and $COSHH_{15min}$ limits of lethality and impairment of escape, only the LC_{50} limit for benzene was not exceeded. CO limit was exceeded by about 10 times on an LC_{50} basis and was exceeded by about 150 times on a $COSHH_{15min}$ basis.



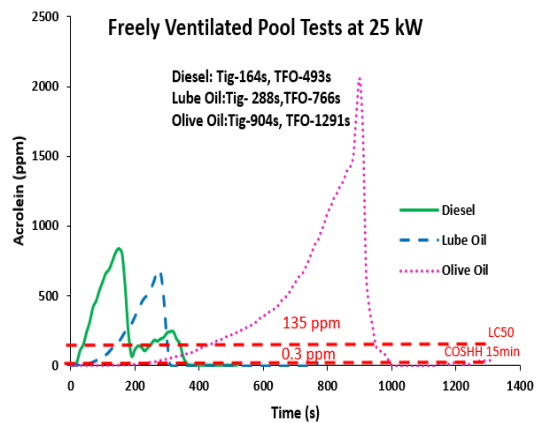
(a)



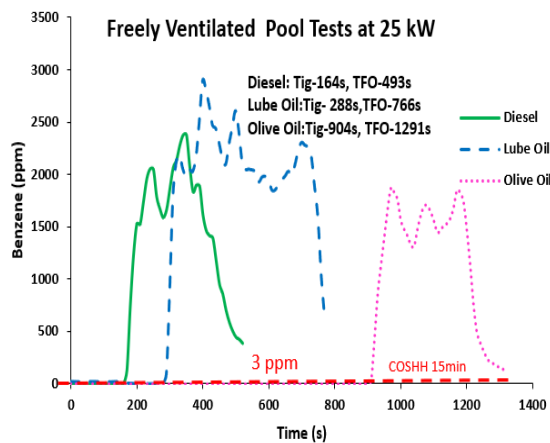
(b)



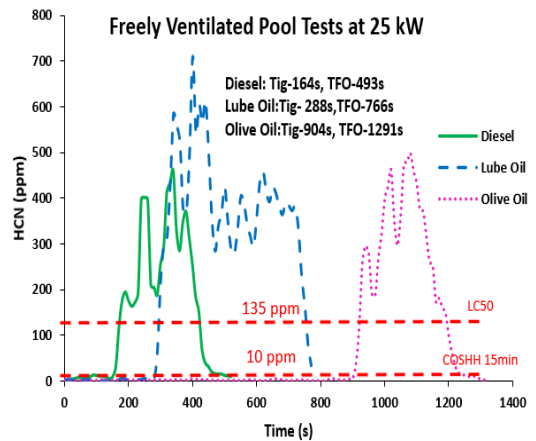
(c)



(d)



(e)



(f)

Figure 7-2 Toxic gas concentrations; CO (a), Total Hydrocarbon (b), Benzene (c), Formaldehyde (d), Acrolein (e) and Hydrogen Cyanide (f)

7.2.1 Total Fire Toxicity N on an LC₅₀ and COSHH 15min Basis

The total toxicity **N** for the three pool samples is shown in Fig. 7-3 as a function of time. The results show similar variation of **N** with time for the COSHH_{15min} and LC₅₀ toxic assessments. Lethal levels of 30-minute exposure toxicity were produced in these pool fires and the COSHH_{15min} toxicity levels indicate that the concentrations would impair escape for the entire duration of the fire even though the fire burnt lean for most of the time. The diesel fire produced toxic gases at a much earlier stage than the two other fuels. Olive oil took a long time before high concentration of the toxic gases were produced and this was between 600 – 1200 s. The dilution required to prevent 30-minute LC₅₀ exposure levels from being lethal was about 13-27 indicating that people exposed to these gases would be at risk of death. Impairment of escape would be a much more significant effect as these toxic gases need to be diluted by about 10 000 for diesel fire and over 5000 for lubricating oil and over 20 000 for olive oil before these gases would not impair escape. From these values, it shows that olive oil produced by far the most toxic gases even though it took longer to ignite.

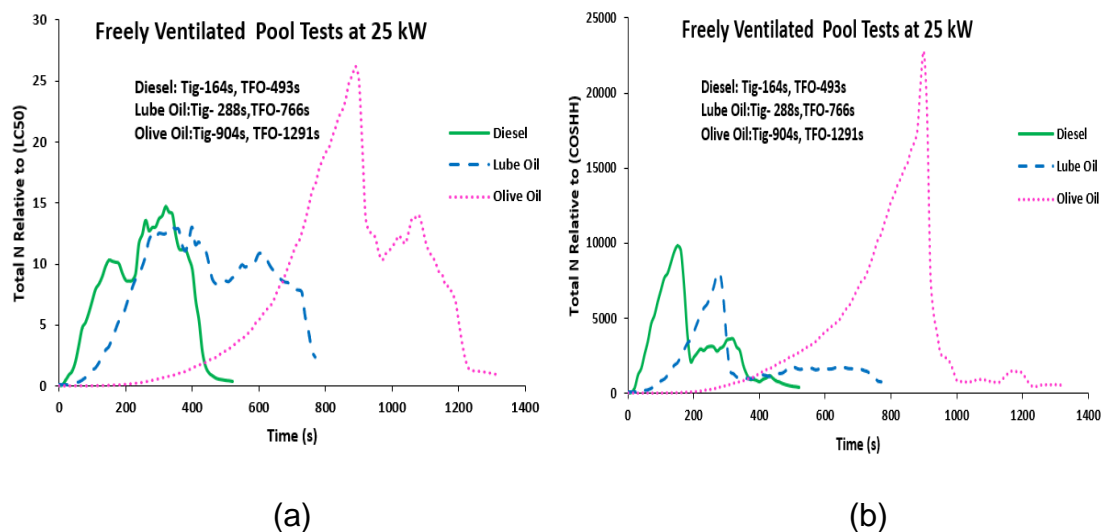
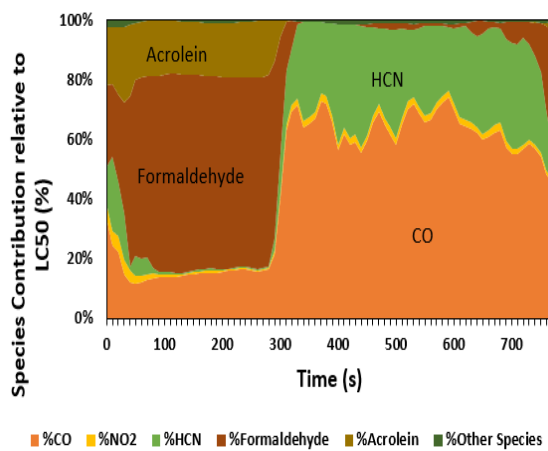


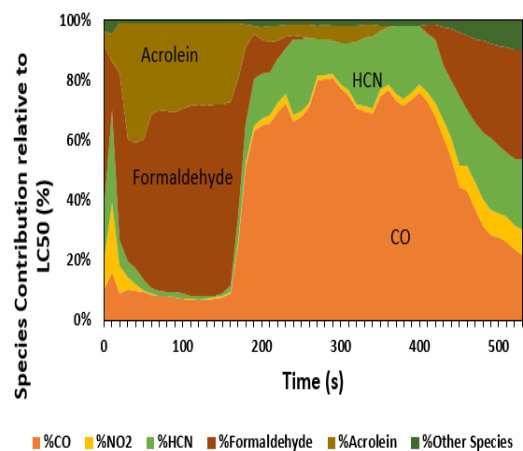
Figure 7-3 Total N relative to LC₅₀ (a) and COSHH_{15min} (b)

Figures 7-4 and 7-5 show the major contribution to the total toxicity on an LC₅₀ and COSHH_{15min} basis for the pool tests. The diesel test was dominated by, CO followed by formaldehyde, HCN and acrolein on an LC₅₀ basis and acrolein, benzene, TMB, CO and formaldehyde on a COSHH_{15min} basis. The contribution of CO and formaldehyde was not more than 10% on a COSHH_{15min} basis throughout the combustion. The lubricating oil toxicity was dominated by CO,

formaldehyde, acrolein and HCN on an LC₅₀ basis, but acrolein was more significant on COSHH_{15min} basis, followed by benzene, TMB, formaldehyde and CO. HCN contribution was less than 5% on COSHH_{15min} basis. The olive oil toxicity was dominated by formaldehyde and acrolein at the initial stage of the fire up to about 900 s but CO dominated from about 900 s till the end of the test on an LC₅₀ basis. This was followed by HCN with about 30% contribution. Acrolein contribution was > 20% and this was at the early stage of the combustion. However, on a COSHH_{15min} basis, acrolein dominated the toxicity, followed by benzene, formaldehyde, TMB and CO. HCN contribution to the total toxicity was < 5% and this occurred only at the flaming stage of the combustion. These results are comparable to those obtained by Andrews et.al [178] on pool fires from diesel pool fire. Even though the different pool fires produced the same types of toxic gases, there was a variation in the toxic gases produced in terms of importance and concentration and this shows that different materials should be tested at different conditions to understand how they behave and the amount of toxic products they produce under such conditions.



(a)



(b)

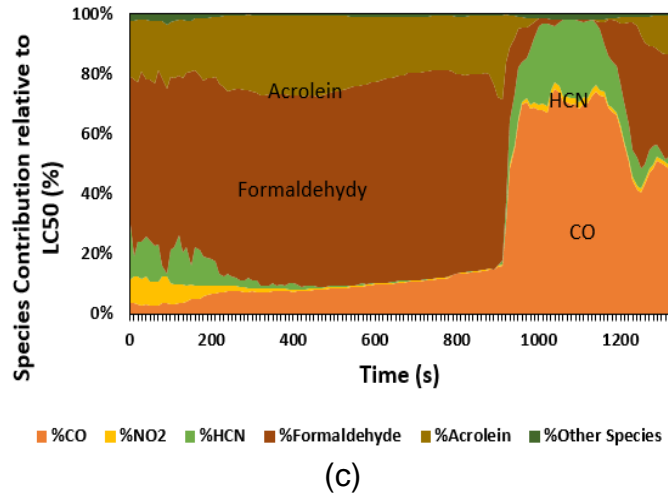
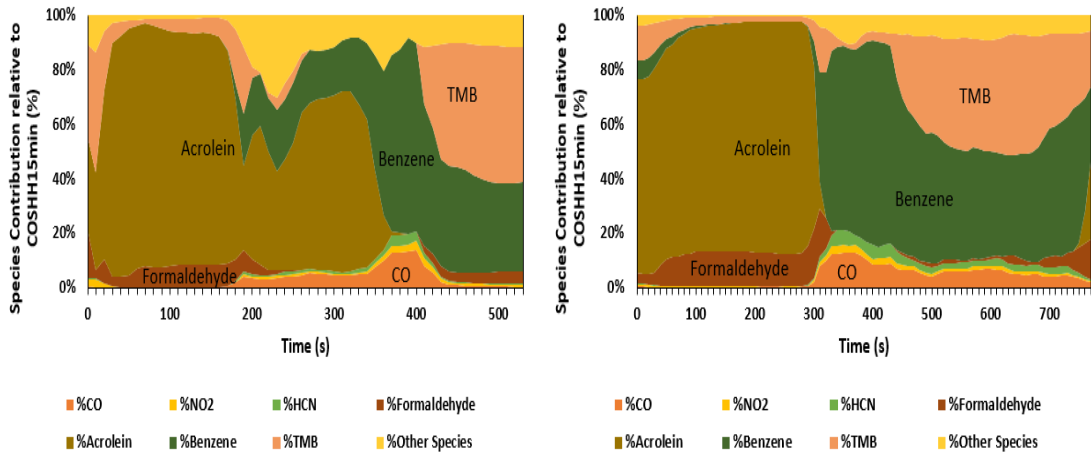


Figure 7-4 Species Contribution (LC₅₀); Diesel (a) Lube oil (b) Olive oil (c)



(a)

(b)

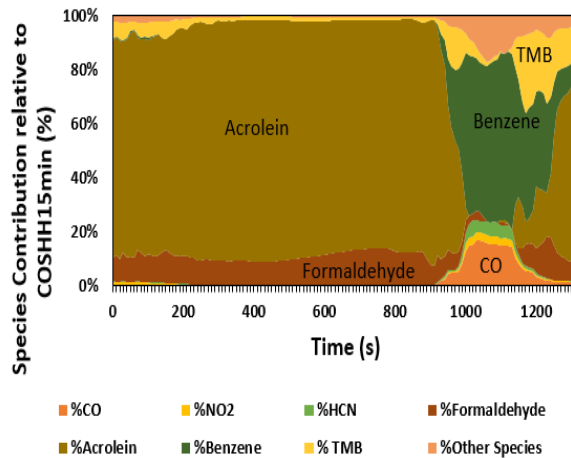


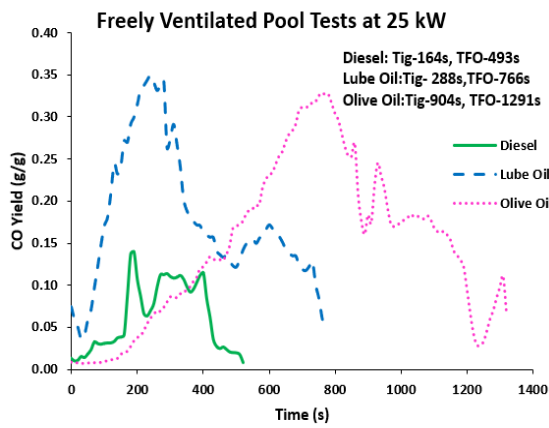
Figure 7-5 Species Contribution (COSHH_{15min}); Diesel (a) Lube oil (b) Olive oil (c)

7.2.2 Toxic Gas Yields

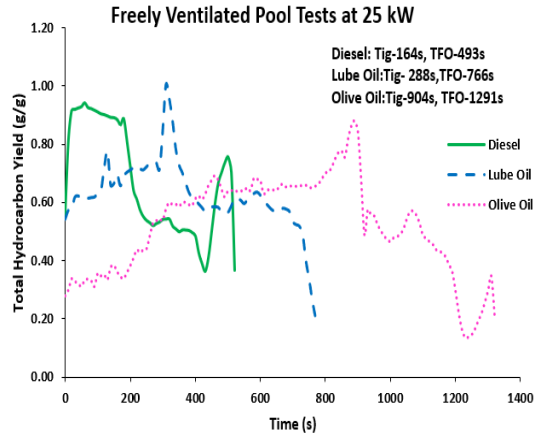
The yields of the important gases are shown as a function of time in Fig. 7-6 for the three pool tests. Diesel produced its peak CO of 0.14 g/g at 180 s, when the fire was rich and the mass loss rate and HRR were at their peak. Lubricating oil and olive oil produced their peak CO yield during the ignition delay period at 240 s (0.35 g/g) for lubricating oil and at 760 s (0.33 g/g) for olive oil. A fairly constant yield of the unburnt total hydrocarbon was observed for diesel (0.94 g/g) in the first 180 s of the test and another peak just at flameout time. The lubricating and olive oils showed a similar trend with their peak yields just about the ignition time with the lube oil having a peak yield of 1 g/g and olive oil 0.88 g/g. Acrolein and formaldehyde peak toxic yields were also produced during the ignition delay periods for all the pool fires, with olive oil producing the highest yield of both gases. The benzene yield was highest during the flaming combustion of the pool fires where the richer mixtures were formed and the oxygen level was at its minimum. This was much lower for the olive oil. HCN yield was produced throughout the combustion period but was highest during the flaming combustion, with the lube oil having the highest HCN yield and diesel having the lowest HCN yield. The yields are very high for both lean and rich mixtures for all the fuels. The high yields of CO and THC are due to inefficient combustion. Even though the diesel burnt richer than all fuels, the highest yield of CO and THC was not produced by diesel and same happened with the rest of the toxic gases. A summary of the peak yields and the time to reach the peak yield are presented in table 7-2.

Table 7-2 Toxic Gas Yields

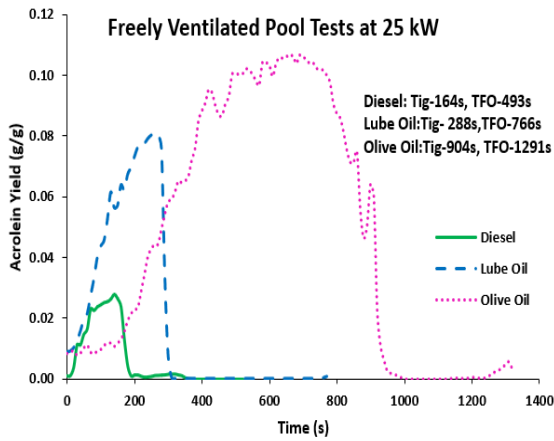
Toxic Gas	Peak Yield and Time to Peak yield		
	Diesel g/g	Lube Oil g/g	Olive oil g/g
CO	0.14 (180 s)	0.35 (240 s)	0.33 (760 s)
THC	0.94 (0-180 s)	1 (310 s)	0.88 (890 s)
Acrolein	0.03 (140 s)	0.08 (270 s)	0.11 (660 s)
Formaldehyde	0.03 (140 s)	0.122 (270 s)	0.18 (720 s)
Benzene	0.06 (490 s)	0.06 (320-720 s)	0.04 (1190 s)
HCN	0.001 (190-380 s)	0.005 (400 s)	0.003 (940-1100 s)



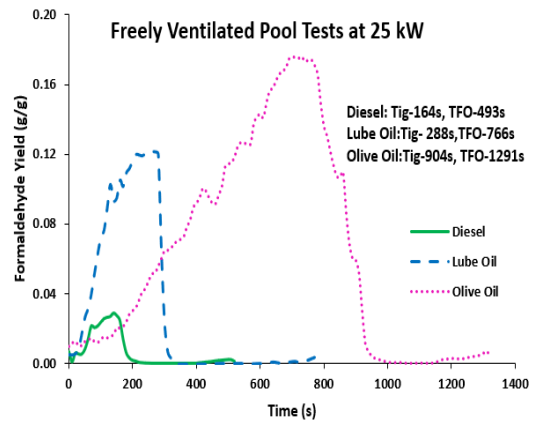
(a)



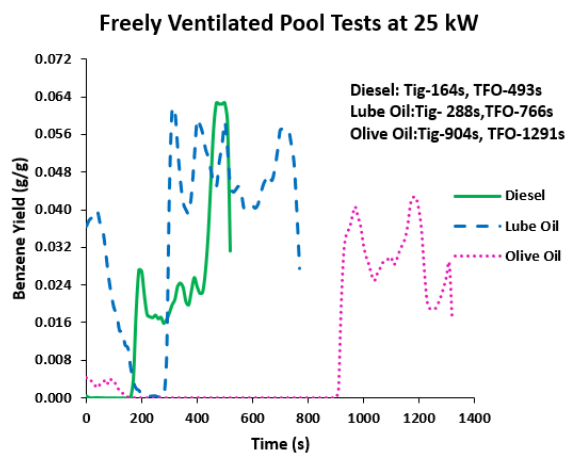
(b)



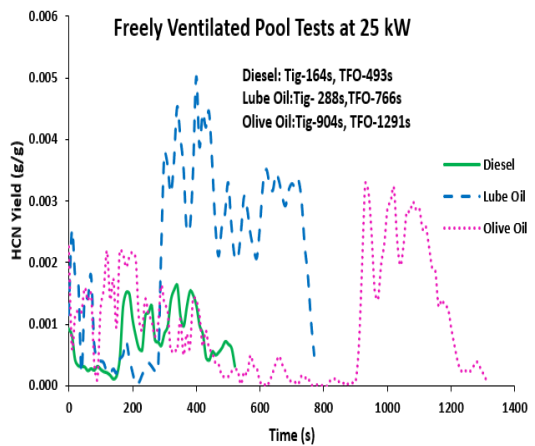
(c)



(d)



(e)



(f)

Figure 7-6 Toxic gas yields; CO (a), Total Hydrocarbon (b), Acrolein (c), Formaldehyde (d), Benzene (e) and Hydrogen Cyanide (f)

7.2.3 Combustion Efficiency and Heat Release Rate Correction

The combustion efficiency was determined by summing the CO and THC yields using the calorific value of CO and taking HC as methane. This is shown in Fig.7-7. For the diesel pool rich combustion fire the combustion efficiency was $< 20\%$ during the ignition delay and increased to $> 60\%$ after the first 164 s following autoignition, when the HRR was still increasing. For the lube oil and the olive oil, the CO and HC emissions were also very high, resulting in very low combustion efficiencies of $<< 20\%$, once the fire had a significantly rich overall equivalence ratio. The combustion efficiency deteriorates as a result of the equivalence ratio becoming richer as the fire develops, as shown in Fig. 7-1c. The combustion efficiency increased to about 80% following autoignition of the sample and flaming combustion.

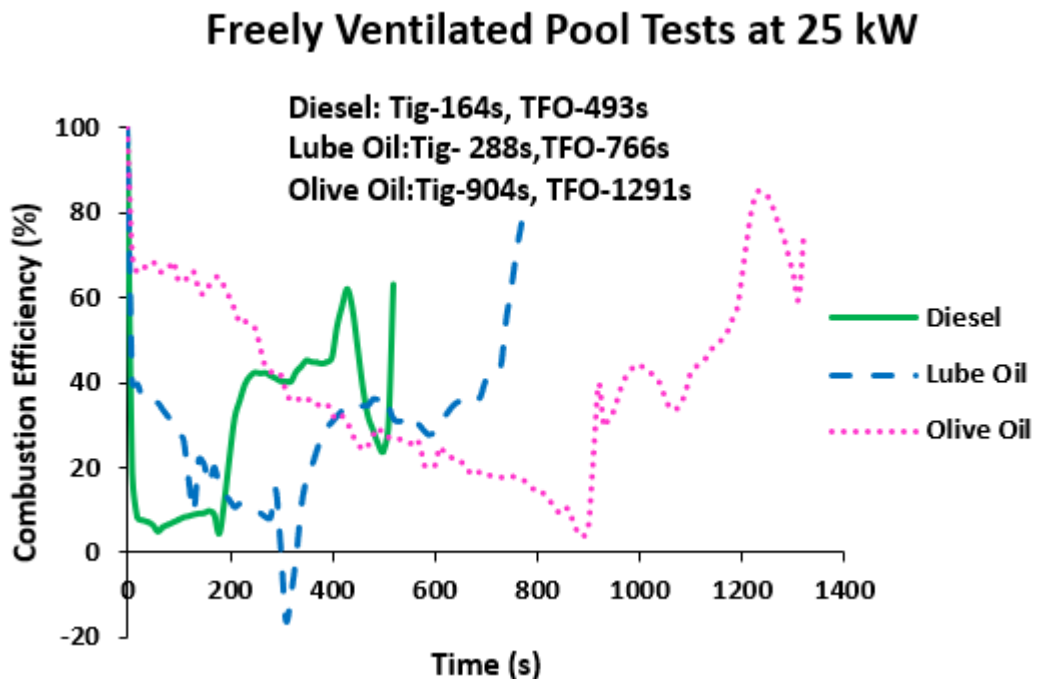


Figure 7-7 Combustion Efficiency

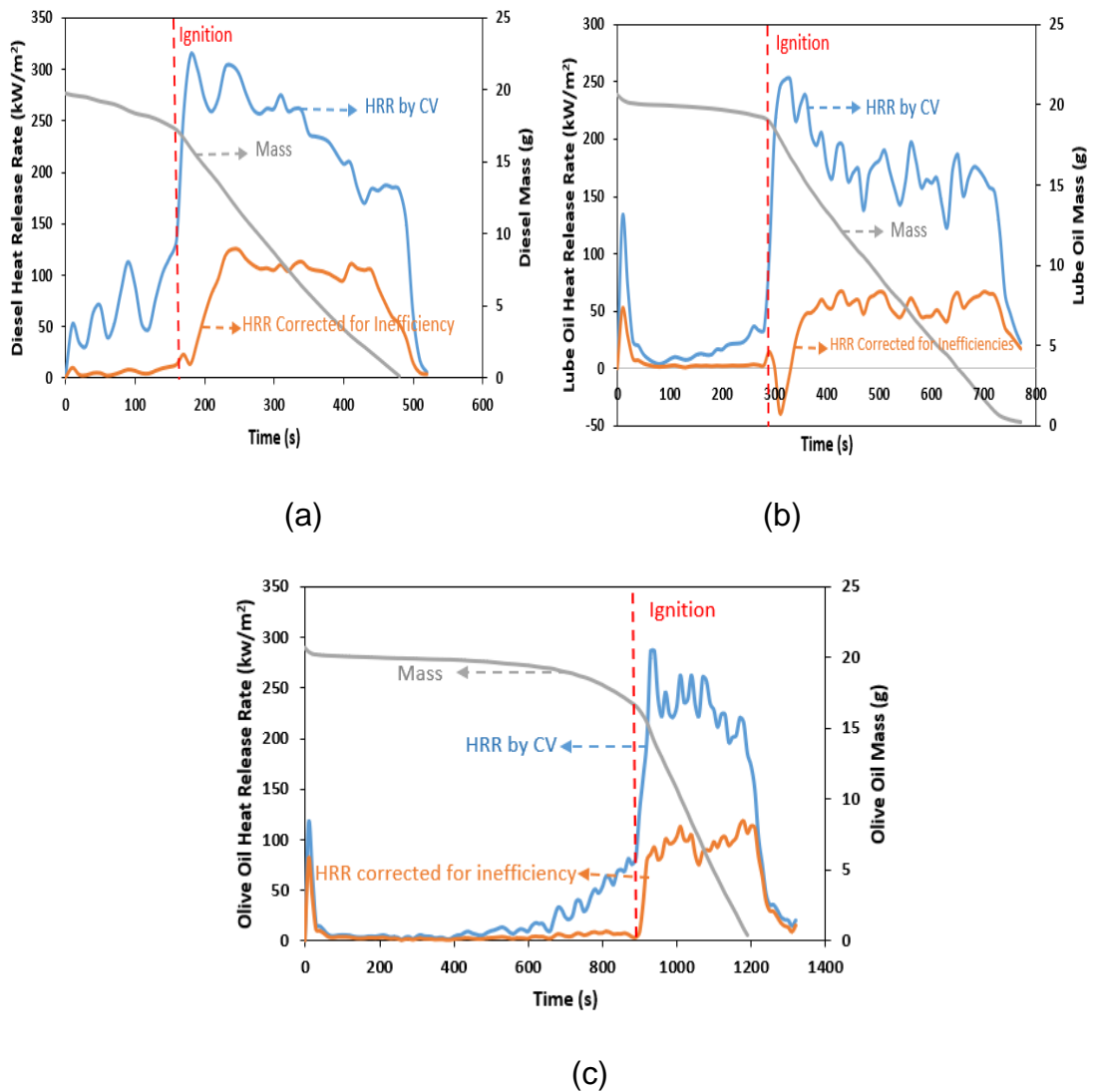


Figure 7-8 Mass, HRR based on the mass loss rate, adjusted HRR, based on inefficiency of combustion for; Diesel (a) Lube oil (b) and olive oil (c)

The mass loss rate and calorific value (CV) based heat release rate (HRR) for the three fuels is shown in Fig. 7-4. This heat release rate by mass loss rate assumes complete combustion and release of all the available energy. CO, total hydrocarbons THC (unburnt hydrocarbons) and soot are all indication of incomplete combustion and therefore unreleased energy, which is measured as the combustion inefficiency. For soot yields to be significant, they need to be > 1%.

The present work did not determine the soot yield, the combustion efficiency was determined based on the CO and total hydrocarbons using procedures used for engine emissions [107]. Aljumaiah et al. [88] showed that in under-ventilated wood crib fires, total hydrocarbons (unburnt hydrocarbon) were particularly significant in correctly evaluating the heat release rate HRR.

The CO and total hydrocarbon yields in Fig. 7-6 a and b were used in the present work to correct the heat release rate HRR shown in Fig.7-8. The heat release rate by mass loss rate showed an over estimation of the corrected heat release by about 2 times in all the pool fires.

7.3 5m³ Pool Tests

Eight tests were conducted to investigate the influence of different ventilation and pool size on toxicity and particulate emissions. Table 7-3 summarises the experiments and the conditions they were carried out.

Table 7-3 Summary of the 5m³ Pool Tests

Test	Pool size (mm)	Pool area (m ²)	K _{in} (%)	K _{out} (%)	Fuel mass (g)	Mean pool depth (mm)	Fuel burn out	Burning duration (s)	(min)
Test 1	100*100	0.010	5	0.62	102.9	12.25	Yes	1674	27'54"
Test 2	200*200	0.040	5	0.62	301.8	8.98	Yes	915	14'49"
Test 3	465*465	0.216	5	0.62	801.2	4.42	Yes	580	9'40"
Test 4	1000*705	0.705	5	0.62	2401.8	4.06	Yes	1161	19'21"
Test 5	200*200	0.040	0	0.62	241.6	7.19	No	958	15'58"
Test 6	200*200	0.040	5	0.14	317.3	9.44	Yes	1185	19'45"
Test 7	465*465	0.216	1	0.14	495.6	2.73	No	420	7'
Test 8	200*200	0.040	1	0.14	320	9.52	Yes	1294	21'34"

*Note: 1. Test 6, Test 7 and Test 8 were done with an installed outlet orifice plate.
 2. Test 5, total fuel load was 301.8 g with 241.6 g burnt and 60.2 g unburnt
 3. Test 7, total fuel load was 1695 g with 495.6 g burnt and 1199.4 g unburnt

In some of the tests, the glass window was either totally covered by soot or the insulation door had to be closed because of severe radiation, therefore, the flameout stage of the fire could not be observed. For these tests, the flameout

time was obtained by observing the change in fuel tray temperature or the increase in oxygen level.

Comparing 200 mm ($K_{in}=5\%$) without the orifice plate and 200 mm ($K_{in}=5\%$) with orifice plate, having the same inlet area and pool size, the burning duration of the test without the orifice plate was about 15 min while that of the test with an outlet orifice plate was more than 19 min. This significant difference indicates that the orifice played a significant role in the burning pattern of the fuel. Test 200 mm ($K_{in}=5\%$) without the orifice plate burnt out quicker because air was drawn into the fire rig to support the burning, after restricting the area of the outlet, the air supply of the fire became lower which led to a longer burning duration. However, comparing 200 mm ($K_{in}=5\%$) test and 200 mm ($K_{in}=1\%$) test, indicated that the burning duration was not significantly affected by the K_{in} factor. Hence, it can be concluded that the ventilation during the combustion process was mainly controlled by compartment exit. Furthermore, an increase in the mass of the pool can increase the burning duration but the low ventilation rate could also lead to air starvation and an early flameout before all the fuel is consumed.

7.3.1 The Effect of Pool Size

The 400 mm ($K_{in}=1\%$) test and 200 mm ($K_{in}=1\%$) having the same ventilation factor $K_{in} = 1\%$ but different pool sizes were compared to investigate the effect of pool size on fires and toxic emissions. Table 7-4 shows a summary of the general burning characteristics.

Table 7-4 The Average Results of the Tests with Different Pool Fire Size

Test	Pool size (mm)	Ave. Mass Loss (g/s)	Ave. AFR	Airflow Rate (g/s)	HRR-O2 (kW)	Unit HRR (kW/m ²)
Test 7 (400 mm ($K_{in}=1\%$))	465	1.18	12.88	15.20	45.60	211.09
Test 8 (200 mm ($K_{in}=1\%$))	200	0.25	36.09	9.02	27.07	676.67

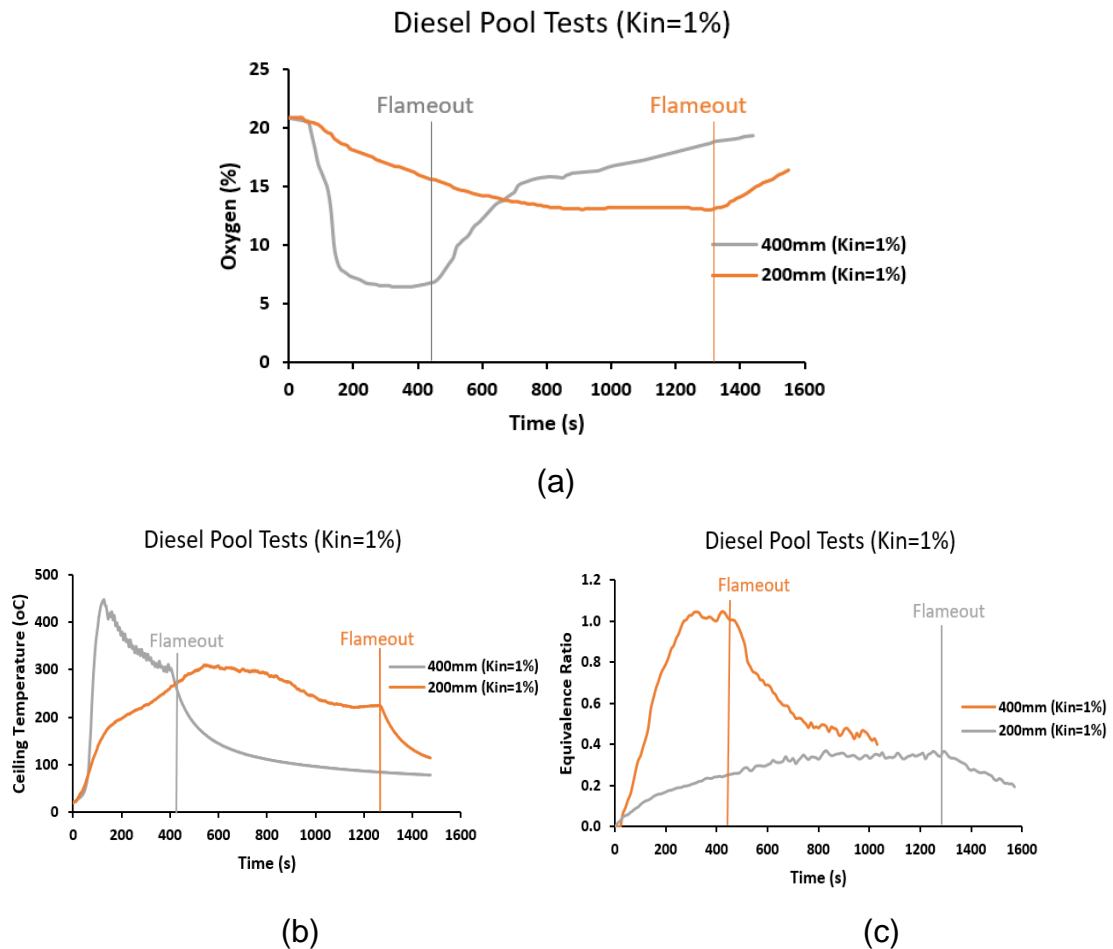


Figure 7-9 Oxygen (a) Ceiling Temperature (b) and Equivalence Ratio (c) for tests with different pool fire size

The flameout time for the bigger fire was faster than the small fire. The air flow rate of 400 mm ($K_{in}=1\%$) test was 15.2 g/s, equivalent to 9 ACH (Air changes per hour), while 200 mm ($K_{in}=1\%$) test had 5.6 ACH. Within the period of combustion, 400 mm ($K_{in}=1\%$) test had the oxygen drop down to almost 5% even though it was short while 200 mm ($K_{in}=1\%$) test was $< 15\%$. The trays used for the tests were not completely flat with the exception of 100 mm² pool tray. Therefore with the consumption of fuel and reduction in fuel depth, it was observed that after the initial burning period, the fire moved to a corner. This will result in the actual burning surface being less than the pool size during the later burning period and therefore the realistic heat release rate (HRR) per surface area would be higher than the values presented in Table 7-4.

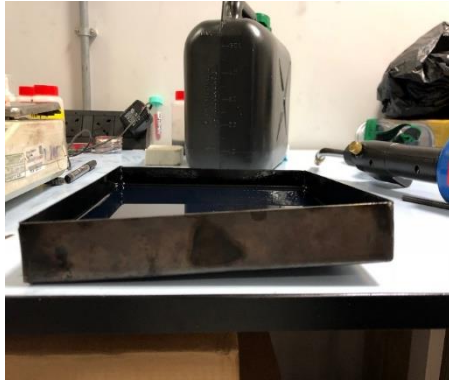


Figure 7-10 200 x 200 mm pool tray

Figure 7-11 Fire burning at the corner

Figure 7-9 showed that 400 mm ($K_{in}=1\%$) test burnt faster than 200 mm ($K_{in}=1\%$) test because of its high burning surface but only about 30% of the fuel was burnt. A rapid increase in temperature was observed once the fuel was ignited but was restricted by the air supply from the outside at around 170 s in both tests. The 400 mm ($K_{in}=1\%$) test had a peak ceiling temperature of 450°C while 200 mm ($K_{in}=1\%$) test had a peak temperature of 300°C. These temperatures are low compared to the work of Aljumaiah et al. [85] conducted in a 1.6 m³ compartment where the temperature was up to 500°C.

The equivalence ratio showed that both fires were lean but 400 mm ($K_{in}=1\%$) reached a stoichiometric combustion condition at steady state. At about a ceiling temperature of 440°C, a pulsing phenomenon (shown in Fig. 7-12) was observed with 400 mm ($K_{in}=1\%$) (the big pool) where smoke was seen pulsing out of the air inlet at regular intervals, lasting for about 4 mins until flameout. This is as a result of the pressure difference generated from the increase in temperature, thereby pushing the smoke out of the compartment and preventing air from going into the compartment. The insufficient air supply into the compartment lowered the flame temperature, reducing the pressure difference and allowing the air to flow into the compartment again. This pulsing phenomenon was also observed by Alarifi [87] in a large room fire with a closed door, where smoke was seen pulsing out from the 3 mm door gap at the bottom.

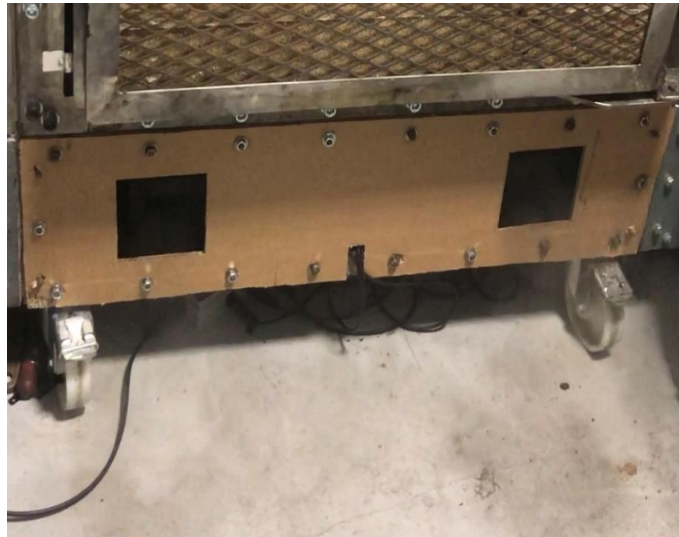
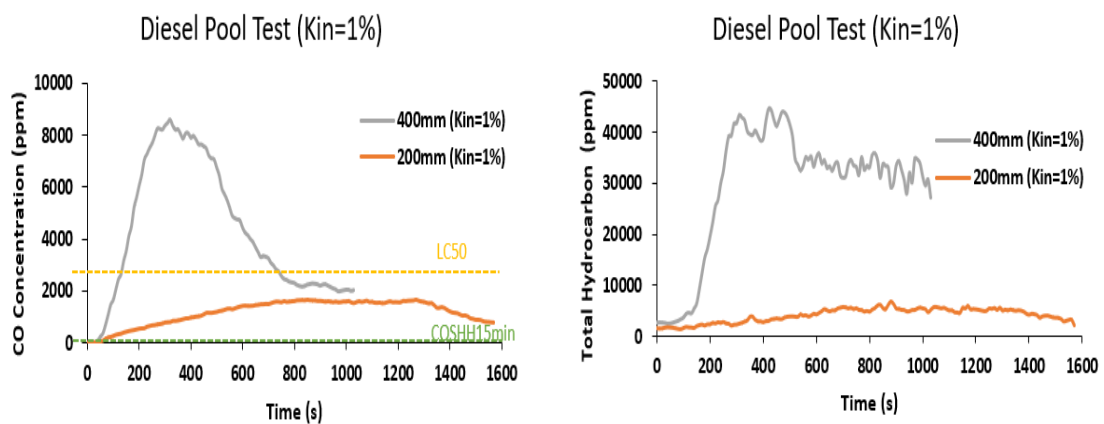


Figure 7-12 Pulsing Phenomenon (400 mm ($K_{in}=1\%$) Test)

7.3.1.1 Toxic Gas Concentrations

Some of the important toxic gases are presented in Fig. 7-13 as a function of time. The bigger pool (400 mm) had higher concentrations of all the toxic gases than the smaller pool (200 mm). There was an increase in toxic concentration as the temperature increased. Acrolein concentration was high before ignition and was eventually consumed during the combustion process. On LC_{50} basis CO, formaldehyde and acrolein concentration limits were exceeded for the bigger pool (400 mm) fire but none of the LC_{50} limits for 200 mm ($K_{in}=1\%$) was exceeded. Only the $COSHH_{15\text{ min}}$ concentration limits for the impairment of escape was exceeded for all gases in both fires. This shows that impairment of escape would be a more significant threat to people.



(a)

(b)

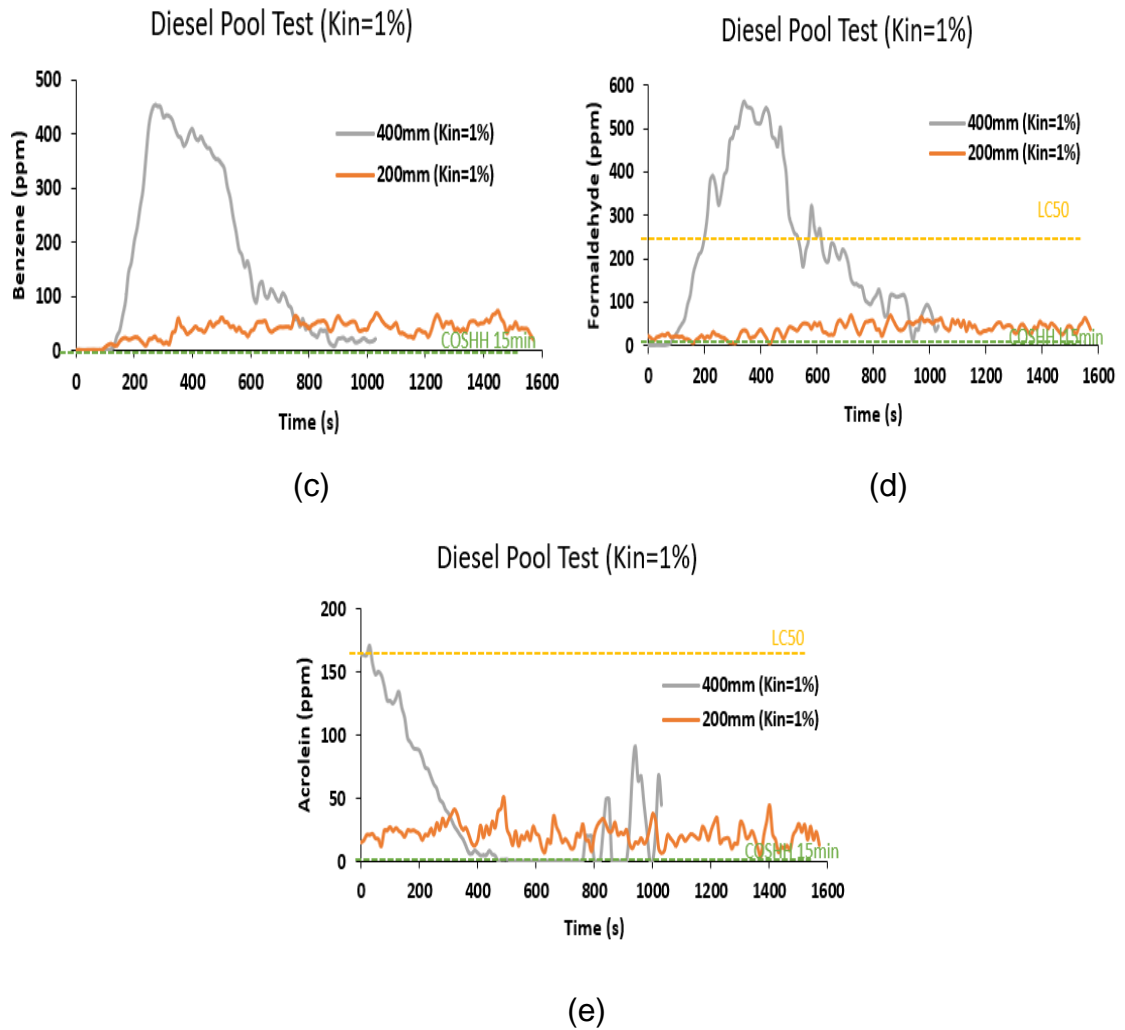


Figure 7-13 Toxic Gas concentrations; CO (a) THC (b) Benzene (c) Formaldehyde (d) Acrolein (e)

7.3.1.1.1 Total Toxicity N on an LC₅₀ and COSHH_{15min} Basis

The total toxicity **N** for the 400 mm ($K_{in}=1\%$) and 200 mm ($K_{in}=1\%$) tests are shown in Fig. 7-3 as a function of time. The results show similar variation of **N** with time for the COSHH_{15min} and LC₅₀ toxic assessments. Lethal levels of 30-minute exposure toxicity were produced in these pool fires and the COSHH_{15min} toxicity levels indicate that the concentrations would impair escape for the entire duration of the fire even though the fire burned lean for most of the time. The bigger diesel fire (400 mm ($K_{in}=1\%$)) produced most of its toxic gases during the flaming combustion while the smaller pool (200 mm ($K_{in}=1\%$)) was fairly constant across the combustion period. The dilution required to prevent 30-minute LC₅₀

exposure levels from being lethal was about 6 for the 400 mm ($K_{in}=1\%$) test while it is just above 1 for 200 mm ($K_{in}=1\%$) test indicating that people exposed to the gases emitted from the 400 mm ($K_{in}=1\%$) test would be at risk of death while that of 200 mm ($K_{in}=1\%$) test is at a safe level. Impairment of escape would be a much more significant effect as these toxic gases need to be diluted by over 1500 for diesel fire 400 mm ($K_{in}=1\%$) test and over 500 for diesel fire 200 mm ($K_{in}=1\%$) test before these gases would not impair escape. From these values, it shows that 400 mm ($K_{in}=1\%$) test produced by far the most toxic gases.

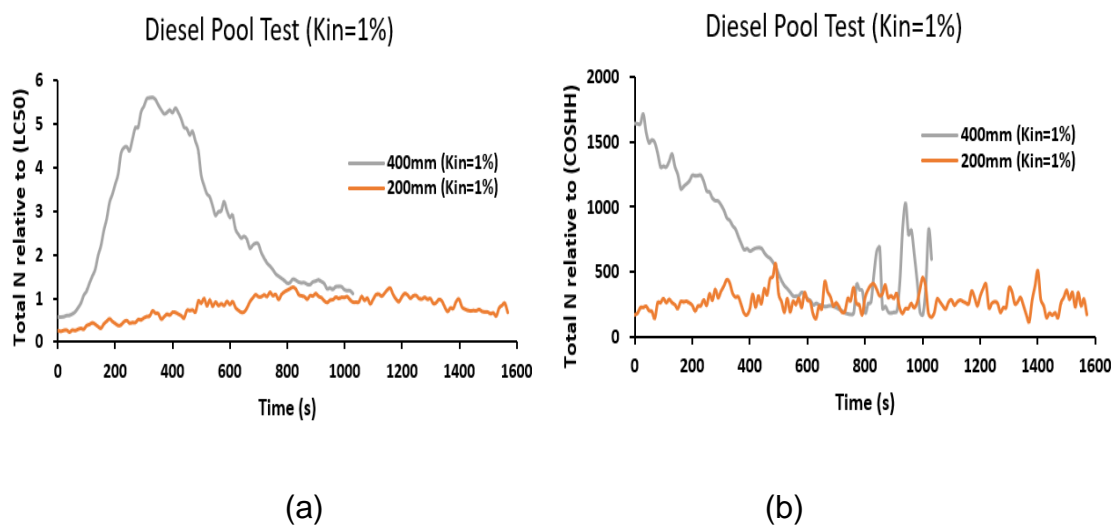


Figure 7-14 Total N relative to LC_{50} (a) and $COSHH_{15min}$ (b)

Figures 7-15 and 7-16 show the major contribution to the total toxicity on an LC_{50} and $COSHH_{15min}$ basis for diesel 400 mm ($K_{in}=1\%$) test and 200 mm ($K_{in}=1\%$) test. The 400 mm ($K_{in}=1\%$) test was dominated by CO followed by formaldehyde, acrolein and HCN on an LC_{50} basis and acrolein, formaldehyde, TMB, benzene and CO on a $COSHH_{15min}$ basis. The contribution of CO was less than 10% on a $COSHH_{15min}$ basis throughout the combustion. The 200 mm ($K_{in}=1\%$) test toxicity was dominated by CO, HCN, formaldehyde and acrolein on an LC_{50} basis, but acrolein was more significant on $COSHH_{15min}$ basis, dominating about 80% of the total toxicity followed by formaldehyde with about 10% and benzene and CO with less than 5%. These results are comparable to those obtained from the cone calorimeter in this work but the concentration of the gases and the order of importance varies. Even though the same type of pool was tested and the fires produced the same types of toxic gases, there was a variation in the toxic gases produced in terms of importance and concentration and these shows that the

size of the pool plays a vital role in the emission and concentration of toxic gases under such conditions.

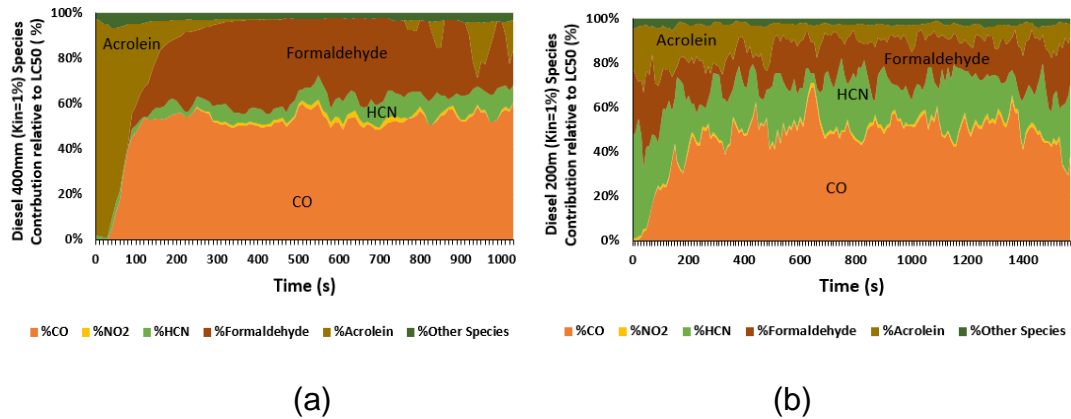


Figure 7-15 Species Contribution (LC₅₀); Diesel 400 mm (K_{in}=1%) Test (a) and 200 mm (K_{in}=1%) Test (b)

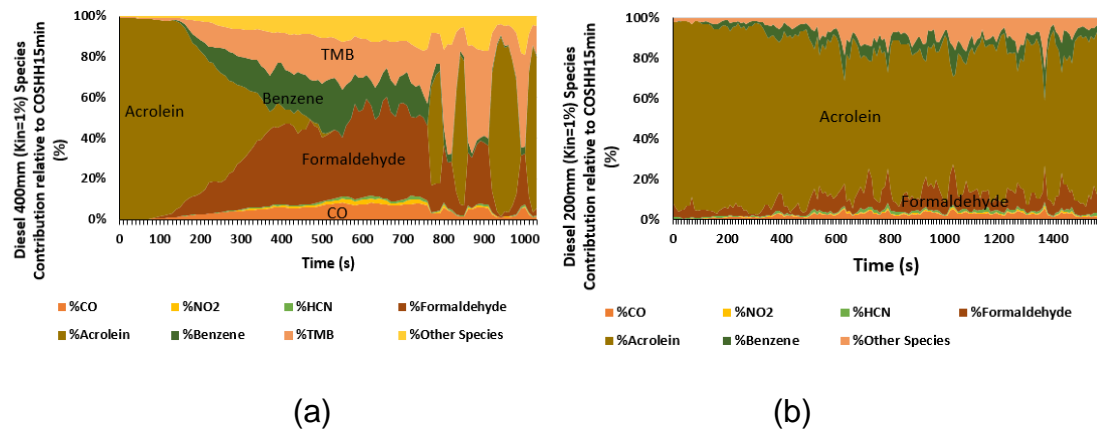
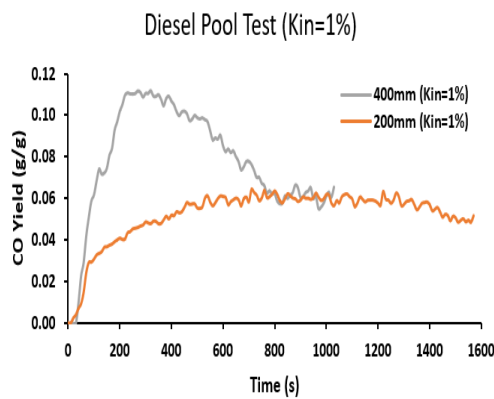


Figure 7-16 Species Contribution (COSHH_{15min}); Diesel 400 mm (K_{in}=1%) Test (a) and 200 mm (K_{in}=1%) Test (b)

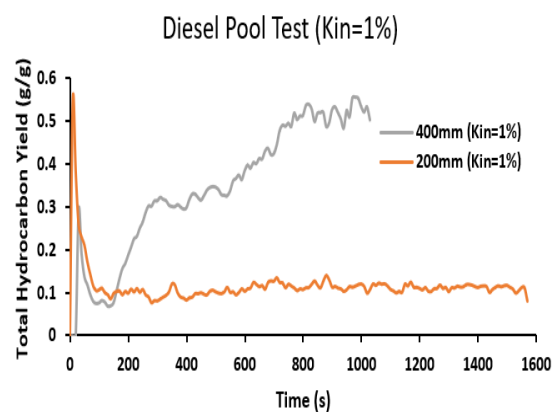
7.3.1.2 Toxic Gas Yield and Combustion Efficiency

The yields of the important gases are shown as a function of time in Fig. 7-17 for the 2 pool tests. The peak CO yield for the big fire (400 mm (K_{in}=1%)) was 0.11 g/g while that of 200 mm (K_{in}=1%) was 0.06 g/g during the steady state burning phase. The CO yield in 400 mm (K_{in}=1%) was found to be higher than other materials analysed by Tewerson [84]. Figure 7-19 compares 400 mm (K_{in}=1%) with the CO yields from Aljumaiah’s pool fire tests [85]. The yield was much lower than what was obtained by Aljumaiah for all his pool tests. This is because of the much leaner mixture obtained in the present work. The present diesel tests had higher acrolein yield, but lower CO and formaldehyde yields.

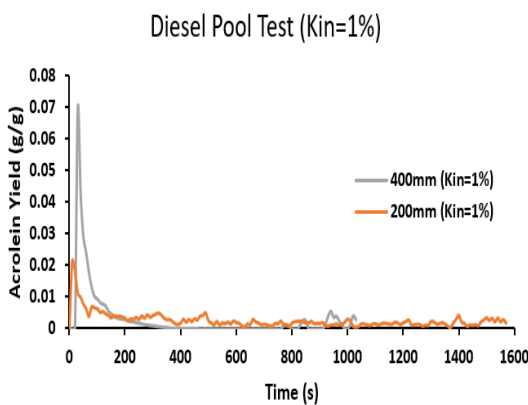
The combustion efficiency of the bigger pool (400 mm ($K_{in}=1\%$)) decreased as fire developed and remained at about 65% during the steady burning phase. The smaller pool (200 mm ($K_{in}=1\%$)) however, had a fairly constant combustion efficiency of around 85% throughout the burning period. The generation of high yield of CO, total Hydrocarbon (Unburnt hydrocarbon) and soot by the bigger pool led to the inefficient combustion during the test. Pool fires release a large amount of unburnt hydrocarbons and soot which tend to lower the efficiency of the combustion. The size of the bigger pool meant longer burning and high release of soot and unburnt hydrocarbons and hence low combustion efficiency.



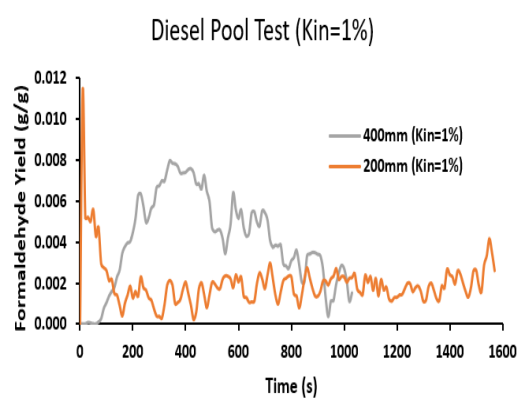
(a)



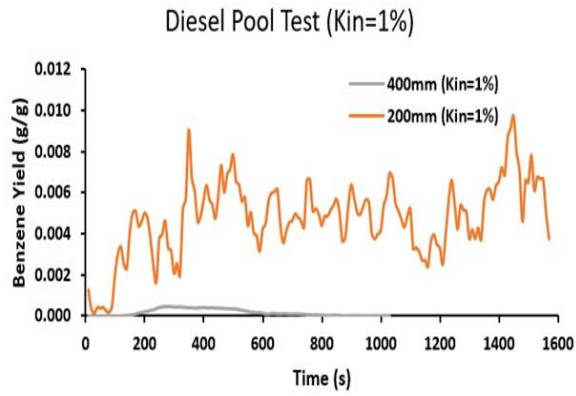
(b)



(c)



(d)



(e)

Figure 7-17 Toxic gas yields; CO (a), Total Hydrocarbon (b), Acrolein (c), Formaldehyde (d), Benzene (e) and Hydrogen Cyanide (f)

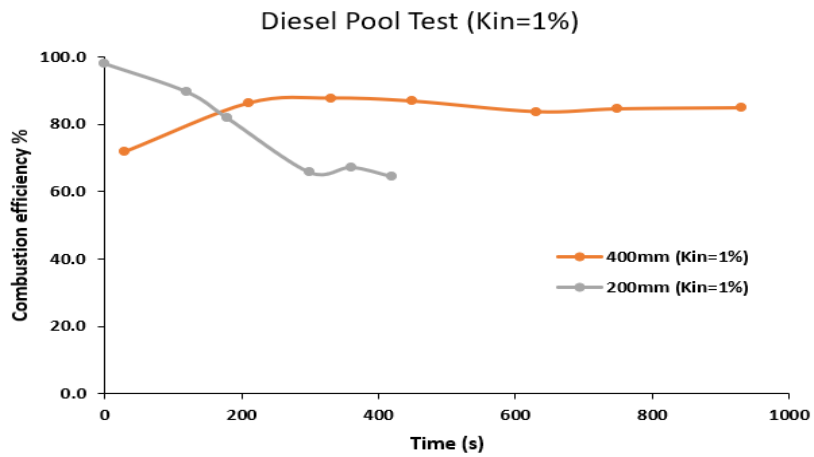


Figure 7-18 Combustion Efficiency

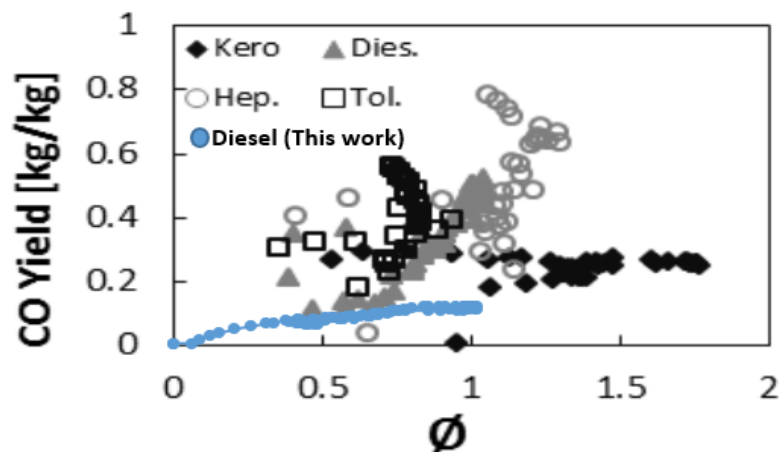


Figure 7-19 CO Yield Comparison with Aljumaiah's [85]

7.3.1.3 Particulate Emissions

The particle number concentration as a function of size and time for 400 mm ($K_{in}=1\%$) and 200 mm ($K_{in}=1\%$) is shown in Fig.7-20. A dilution ratio of 30 was obtained through repeated wood crib tests to correct the particulate concentration for dilution and was assumed to be constant for all the tests conducted in this compartment. The bigger pool (400 mm ($K_{in}=1\%$)) showed a relatively even distribution on particle number from the beginning of the test but higher concentration of the larger particles was obtained towards the end of sampling. The smaller pool (200 mm ($K_{in}=1\%$)) produced a fairly constant distribution of the particles from around 100 s until the end of sampling. However, both pool sizes had about three different number concentration peaks centred at approximately 10 nm, 60 nm and 200 nm. The first two sizes of particles are nanoparticles within the range which presents a hazard to the human health.

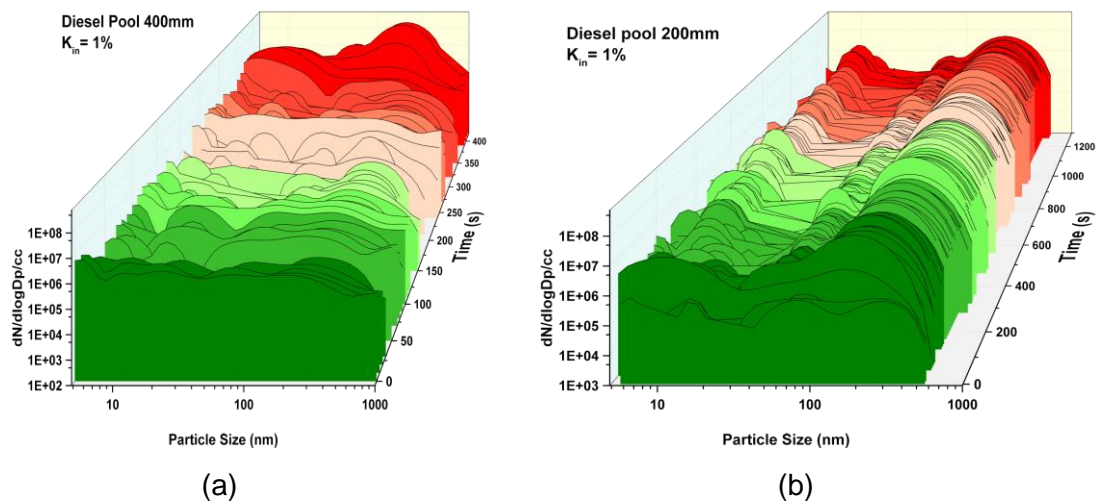


Figure 7-20 Particle Number and Size Distribution; 400 mm ($K_{in}=1\%$)Test (a) and 200 mm ($K_{in}=1\%$)Test (b)

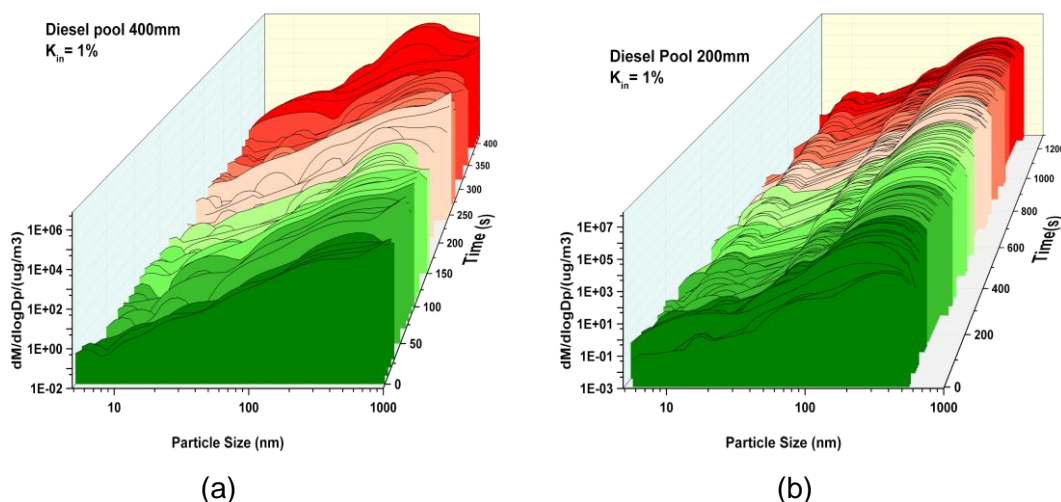


Figure 7-21 Particle Number and Size Distribution; 400 mm ($K_{in}=1\%$)Test (a) and 400 mm ($K_{in}=1\%$)Test (b)

The equivalent mass distribution is shown in Fig. 7-21 as a function of size and time. The mass concentration was highest with the larger particles. It can be observed that particles larger than 1000 nm were produced by 400 mm ($K_{in}=1\%$) but in 200 mm ($K_{in}=1\%$), particles larger than 500 nm were not produced. Particles larger than 1000 nm are above the 1000 nm upper measurement range of the Cambustion DMS500 and therefore could not be measured.

7.3.1.3.1 Soot Yield

The gravimetric soot sampling system using a smoke meter was used to collect soot samples on a filter paper and the soot yield determined. The soot sample from the walls of the compartment was also collected as described in chapter 3. The fire temperature greatly affected the formation of soot as the fire with the lower temperature (small pool, 200 mm ($K_{in}=1\%$)) generated more soot than the higher temperature fire (bigger pool, 400 mm ($K_{in}=1\%$)). The soot yield estimated from the soot deposits of the internal compartment walls was compared with the one discharged from the chimney and it was found that about 30% of the total soot emission remained inside the compartment. The total soot yield obtained by summing the deposited soot yield and the discharged soot yield was found to be 0.0931 g/g (93.1 g/kg) for 465 mm pool (400 mm ($K_{in}=1\%$)) and 0.2858 g/g (285.8 g/kg) for 200 mm (200 mm ($K_{in}=1\%$)) while the average soot yields were 0.005 g/g and 0.031 g/g respectively. The yield obtained from 400 mm ($K_{in}=1\%$) falls within the range obtained at University of Leeds for enclosed diesel fire, which is

between 10 to 200 g/kg. From Tewarson's yield data for wood and plastic, the diesel yield in this work compares well with the soot yield for flexible polyurethane. The result for the big fire test is also similar to the work of Andrews et al. [156] on diesel at 2.7 air changes/hour. This diesel soot result is higher than other liquid fuels (Ethyl alcohol and heptane) obtained by Quintiere [201].

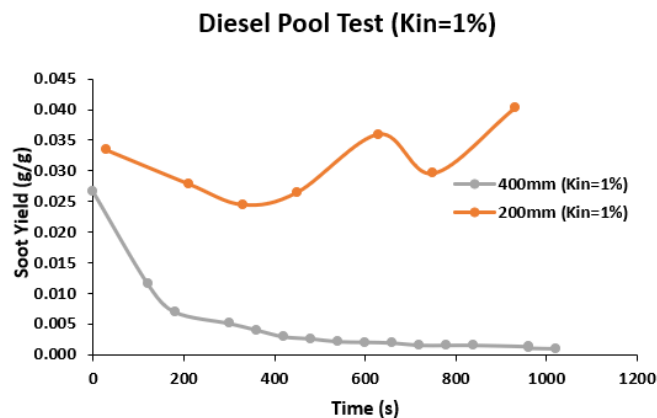


Figure 7-22 The Discharged Soot Yield for Tests 7 and 8

Table 7-5 Total Soot Yield

Test	Total Soot Yield (g/kg)	
	Deposited	Discharged
400 mm ($K_{in}=1\%$)	19.2	73.9
200 mm ($K_{in}=1\%$)	67.6	218.2

7.3.2 The Effect of Ventilation

Test 6 (200 mm ($K_{in}=1\%$)) and 8 (200 mm ($K_{in}=1\%$)) with the same pool size of 200 x 200 mm but having different ventilation factor $K_{in} = 5\%$ and 1% were compared to investigate the effect of ventilation on the pool fires and toxic emissions. Table 7-6 shows a summary of the general burning characteristics.

Table 7-6 The Average Results of the Burning Characteristics at Different Ventilation

Test	Ventilation Factor (K_{in})	Average Mass Loss Rate (g/s)	Average Air-to-Fuel-Ratio	Air Flow Rate (g/s)	HRR- O_2 (kW)	Unit HRR (kW/m ²)
Test 6 (200 mm ($K_{in}=5\%$))	5%	0.27	34.99	9.45	28.34	708.55
Test 8 (200 mm ($K_{in}=1\%$))	1%	0.25	36.09	9.02	27.07	676.67

The fire with the high ventilation factor, (200 mm ($K_{in}=5\%$)) burned faster than the low ventilation factor test (200 mm ($K_{in}=1\%$)) but not significantly. A mean airflow rate of 9 g/s translating to about 5.6 ACH was obtained. A mean heat release rate HRR based on the oxygen consumed was found to be 28 kW for 200 mm ($K_{in}=5\%$) and 27 kW for 200 mm ($K_{in}=1\%$). In general, the difference in ventilation factor did not make any significant difference in the fires as the air supply into the compartment was mainly controlled by the air outflow. Since the K_{out} (ventilation outlet) was fixed and influenced the inlet air, increasing the air inlet by a factor of 5 only made a small change of 0.43 g/s to the airflow rate. This was unexpected as it is expected that there would be a significant difference in the burning behaviour of the fires.

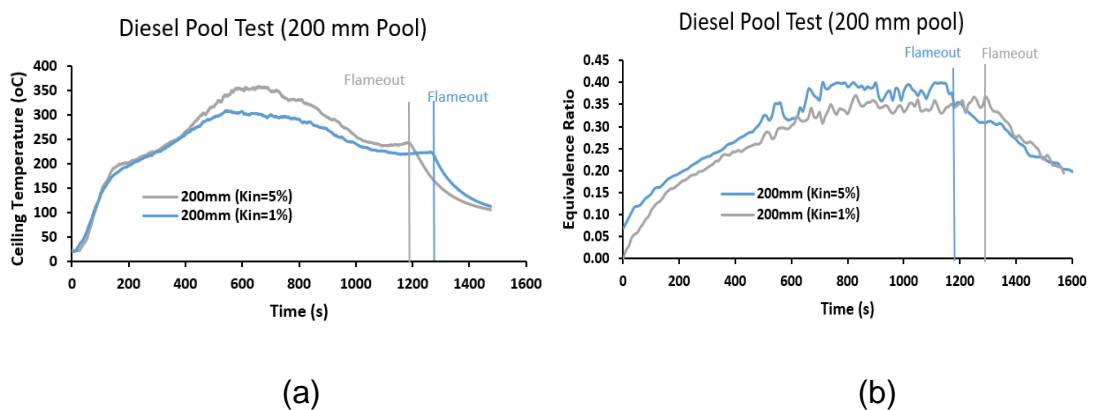


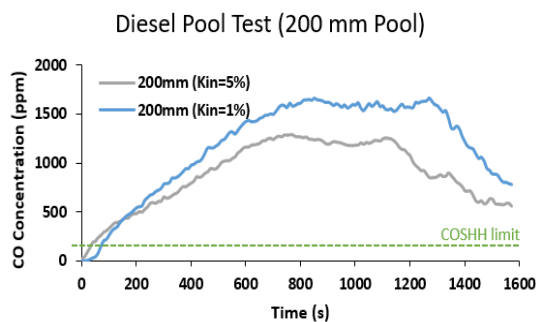
Figure 7-23 Ceiling Temperature (a) and Equivalence Ratio (b)

The two fires with different ventilation factors had a similar development within 170 s of the initial burning stage. 200 mm ($K_{in}=1\%$) had a peak ceiling temperature of 300°C at about 550 s while 200 mm ($K_{in}=5\%$) reached a ceiling

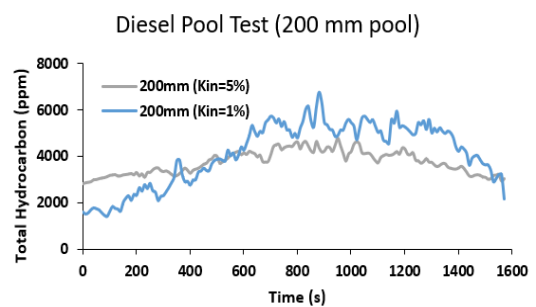
temperature of about 350°C at approximately the same time before decaying after a short steady burning period. The equivalence ratio was 0.4 (200 mm ($K_{in}=5\%$)) and 0.35 (200 mm ($K_{in}=1\%$)) indicating that both fires burned lean. These lean fires will be shown to have produced low concentrations of toxic gases considering the size of the pool.

7.3.2.1 Toxic Gas Concentrations

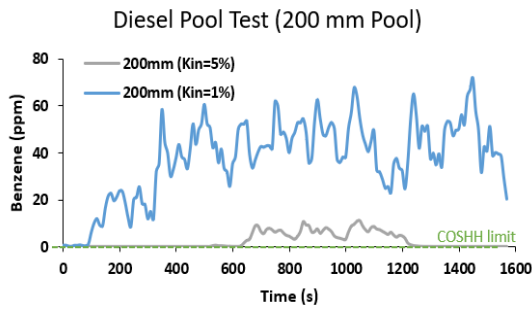
Figure 7-24 shows the most important toxic gases compared as a function of time obtained from the FTIR. The CO concentration of 200 mm ($K_{in} = 5\%$) reached a peak of 1200 ppm and that of 200 mm ($K_{in} = 1\%$) was 1600 ppm indicating that the CO concentration increased with low ventilation. The total hydrocarbon concentrations followed a similar trend to that of CO, with the low ventilation test having a higher concentration. Benzene and formaldehyde were very low in 200 mm ($K_{in} = 5\%$) and was for a short period of time during the steady burning period. The 200 mm ($K_{in} = 1\%$) however produced the two species throughout the duration of the test. This suggests that the low ventilation fire produced higher concentrations of benzene and formaldehyde. In contrast, acrolein had a higher concentration in the initial burning stage and decay period. Acrolein was produced at a fairly constant rate in 200 mm ($K_{in}=1\%$) at about 20 ppm while 200 mm ($K_{in}=5\%$) produced higher acrolein than 200 mm ($K_{in}=1\%$) test, with its highest concentration during the initial burning phase (80 ppm) and the decay phase (60 ppm). This shows that acrolein might be easier generated under low temperature conditions. On an LC_{50} basis, none of the toxic gases exceeded the toxic limit but all gases exceeded the COSHH_{15min} limit. This indicates that these tests are not lethal but will impair escape when exposed to them in the event of a fire occurring.



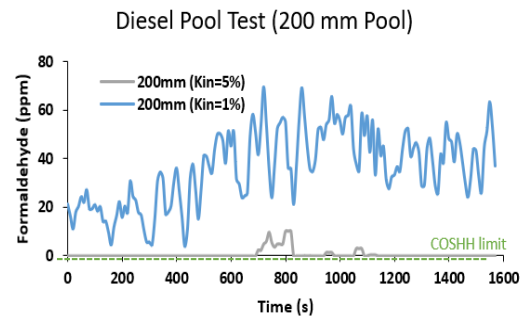
(a)



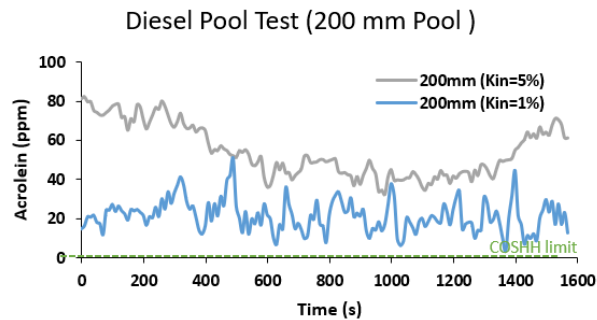
(b)



(c)



(d)



(e)

Figure 7-24 Toxic Gas Concentrations; CO (a) THC (b) Benzene (c) Formaldehyde (d) and Acrolein (e)

7.3.2.1.1 Total Toxicity N on an LC_{50} and $COSHH_{15min}$ Basis

The total toxicity N for the 200 mm ($K_{in}=5\%$) and 200 mm ($K_{in}=1\%$) is shown in Fig. 7-25 as a function of time. The total toxicity N relative to LC_{50} shows that the lethality of the smoke increased with the development of the fire. The N for 200 mm ($K_{in}=1\%$) is just above 1 and that of 200 mm ($K_{in}=5\%$) is < 1 indicating that both fires are not lethal to people, even though the test with the low ventilation had a higher N . Unlike LC_{50} , the $COSHH_{15min}$ results show that the fire with higher ventilation (200 mm ($K_{in}=5\%$)) places people more at risk of being impaired during escape than the low ventilation test (200 mm ($K_{in}=1\%$)). This is as a result of the high concentration of acrolein produced in 200 mm ($K_{in}=5\%$). Impairment of escape would be a much more significant effect as these toxic gases need to be diluted by over 800 for diesel fire 200 mm ($K_{in}=5\%$) and over 500 for diesel fire 200 mm ($K_{in}=1\%$) before these gases would not impair escape.

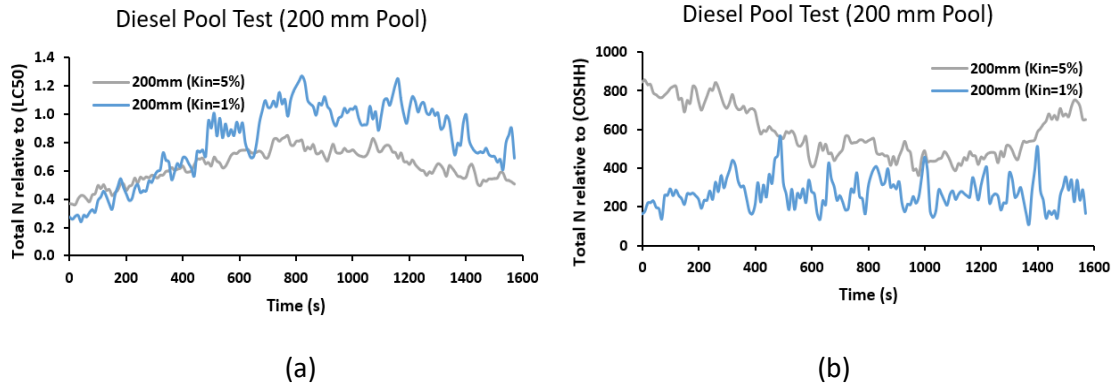


Figure 7-25 Total N relative to LC₅₀ (a) and COSHH_{15min} (b)

The most dominant toxic species for 200 mm ($K_{in}=5\%$) are presented in Fig. 7-26. The graphs for 200 mm ($K_{in}=1\%$) were presented in section 7.3.1.1.1. In the initial burning stage, acrolein was the most dominant toxic species but as the fire developed, CO became the most dominant toxic gas with HCN also contributing to the lethality. Formaldehyde was more significant in the fires with low ventilation (200 mm ($K_{in}=1\%$)), but showed no dominance with the high ventilation fire (200 mm ($K_{in}=5\%$)). On COSHH_{15min} basis, acrolein was the most dominant and important species in both tests, with over 80% contribution.

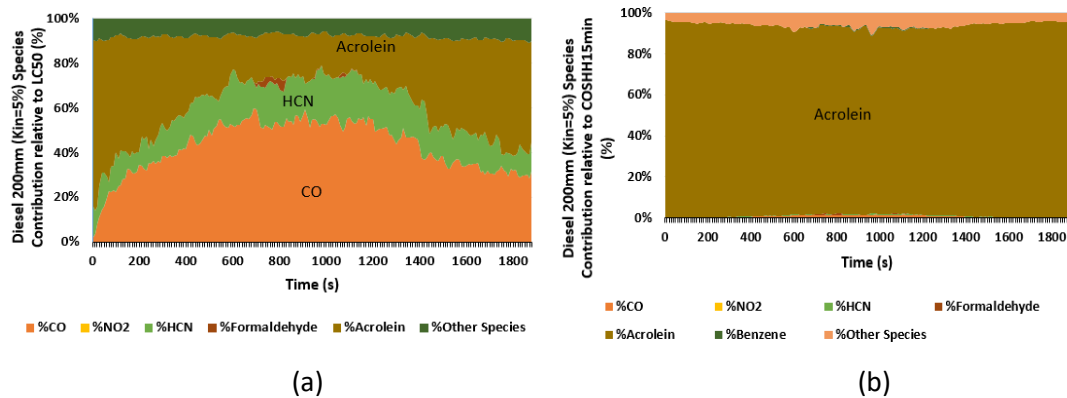


Figure 7-26 Species Contribution Diesel 200 mm ($K_{in}=5\%$) Test; LC₅₀ (a) and COSHH_{15min} (b)

7.3.2.2 Toxic Gas Yield

The yield comparison of the important gases are shown as a function of time in Fig. 7-27 for the 2 pool tests. The peak CO yield for 200 mm ($K_{in}=5\%$) was 0.04 g/g while that of 200 mm ($K_{in}=1\%$) was 0.06 g/g during the steady state burning

phase. Except for acrolein, all the toxic yields were higher in 200 mm ($K_{in}=1\%$). Comparing the CO yield at steady state with Tewarson's yield for well ventilated fire $\phi < 1$ of building materials, it was found that the CO yields were similar to polystyrene and PVC test, but much higher than ethyl alcohol and heptane tests. Total hydrocarbon yields were similar in the two tests.

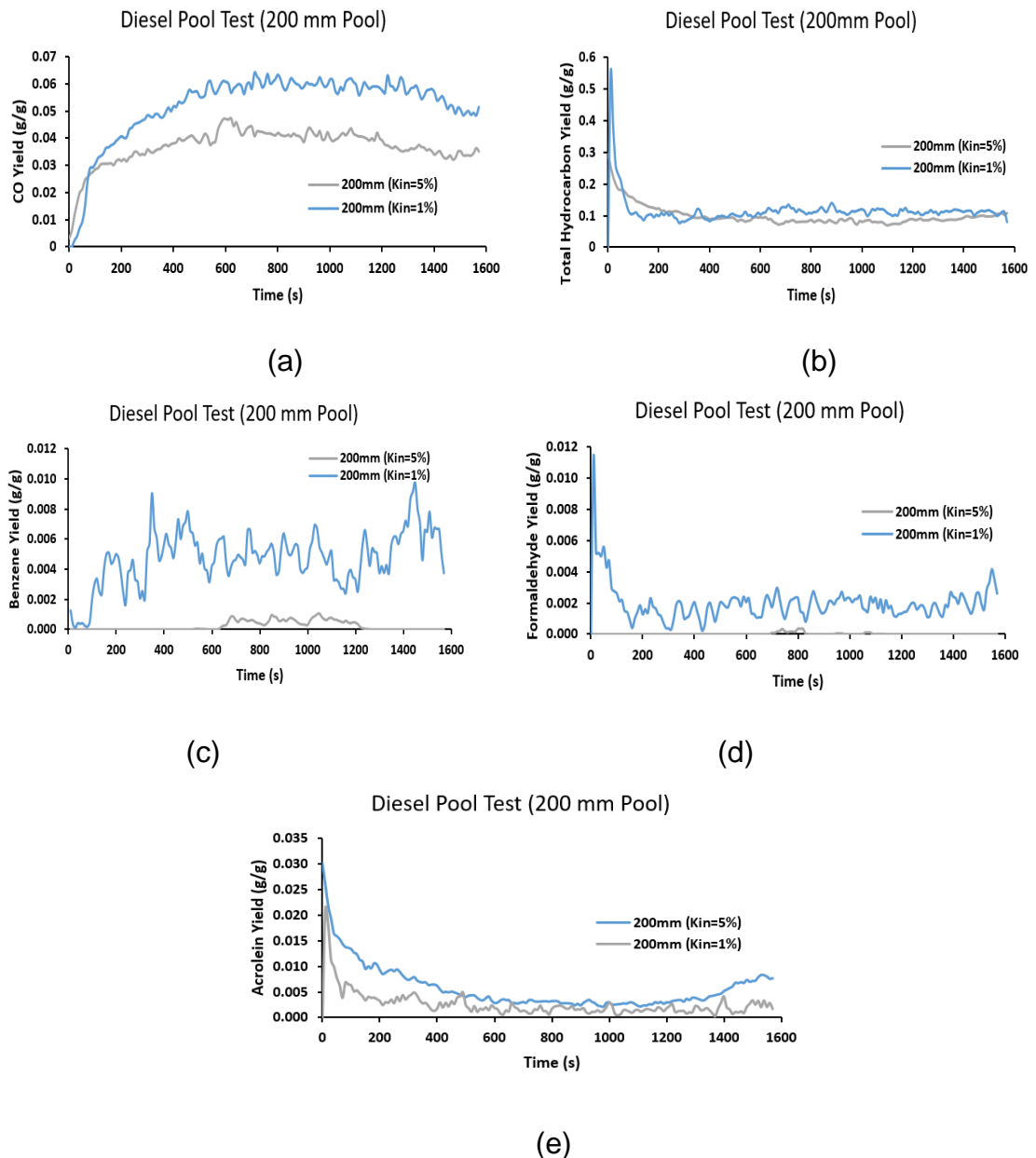


Figure 7-27 Toxic Gas Yields for tests with different ventilation factor; CO (a) THC (b) Benzene (c) Formaldehyde (d) and Acrolein (e)

7.3.2.3 Particulate Emissions

The number concentration and mass concentrations for 200 mm ($K_{in}=5\%$) are presented in Fig. 7-28 as a function of size and time. Three different peaks of

particle distribution was observed, with the nuclei mode peak centred at 10 nm and 60 nm while the accumulation mode centred at 200 nm. The shapes of the particle size distribution were almost same for both tests with 200 mm pool. The particle number concentration and sizes for the two tests was compared at 200 s and 600 s in Fig. 7-29. It was observed that the number concentration of the particles was influenced by ventilation condition, with the higher ventilation fire producing more particles.

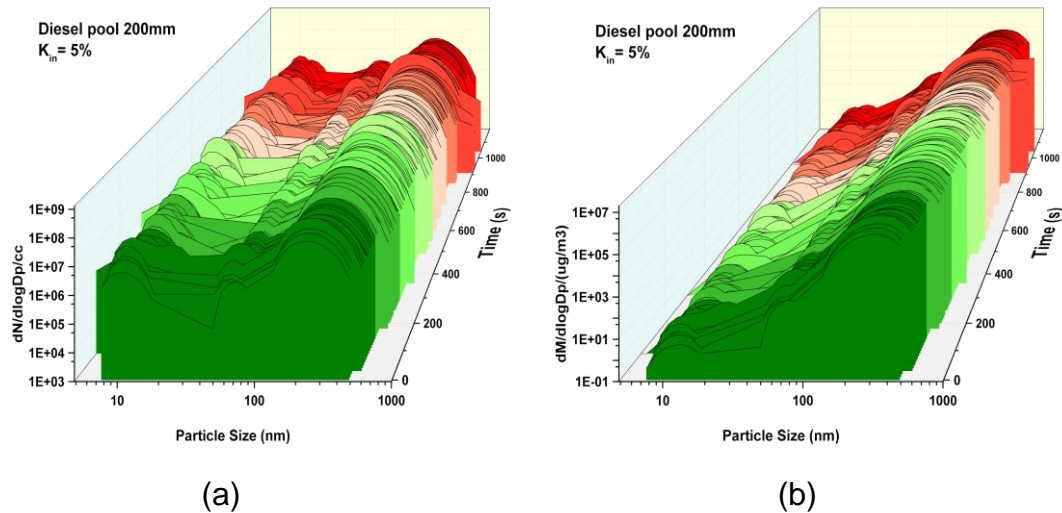


Figure 7-28 200 mm ($K_{in}=5\%$) Test Particle Number and Size Distribution (a) and Mass Concentration (b)

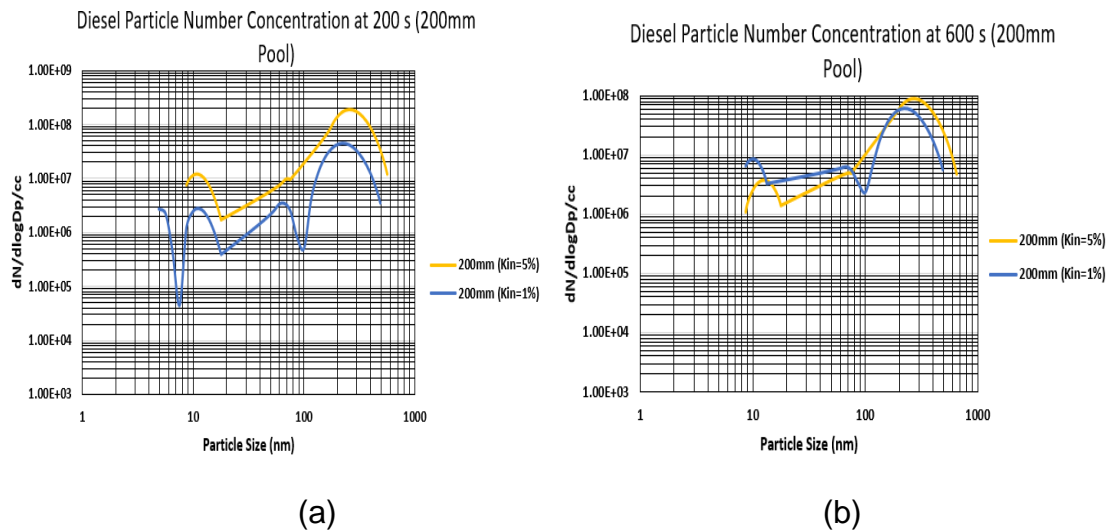


Figure 7-29 Comparison of Particle Number and Size Distribution at Different times; 200 s (a) and 600 s (b)

7.3.2.3.1 Soot Yield

The total soot yield discharged from the compartment in 200 mm ($K_{in} = 5\%$) could not be determined because there were insufficient filter papers. The total soot yield discharged from compartment therefore remained unknown. Comparing the amount of soot deposited, the test with low ventilation 200 mm ($K_{in} = 1\%$) had higher soot emission than that at a higher ventilation 200 mm ($K_{in} = 5\%$).

Table 7-7 Total Soot Yield Comparison

Test	Total Soot Yield (g/kg)	
	Deposited	Discharged
Test 6 (200 mm ($K_{in} = 5\%$))	23.5	-
Test 8 (200 mm ($K_{in} = 1\%$))	67.6	218.2

7.4 Tests without Orifice Plate

There were problems with the analysers and the load cell in some of the tests. The orifice plate had a great impact on the burning of the fuel and therefore only the reliable results are presented without the orifice plate.

Table 7-8 The Average Results of the Burning Characteristics of Tests Without Orifice Plate

Test	Pool size (mm)	Ventilation Factor (K_{in})	Average Mass Loss Rate (g/s)	HRR-Mass Loss (kW)
Test 1	100x100	5%	0.06	2.80
Test 2	200x200	5%	0.33	15.04
Test 3	465x465	5%	1.38	63.00
Test 4	700x1000	5%	2.07	94.33
Test 5	200x200	0%	0.25	11.50

The mean mass loss rate are presented because of the failure of the load cell during the test. The larger pool burned faster than the rest of the pool sizes at the same ventilation rate. The heat release rate HRR was calculated based on the average mass loss rate obtained and this was presented without correcting for combustion inefficiency, hence the actual HRR would be less than the values presented.

Diesel Pool Tests without Orifice Plate

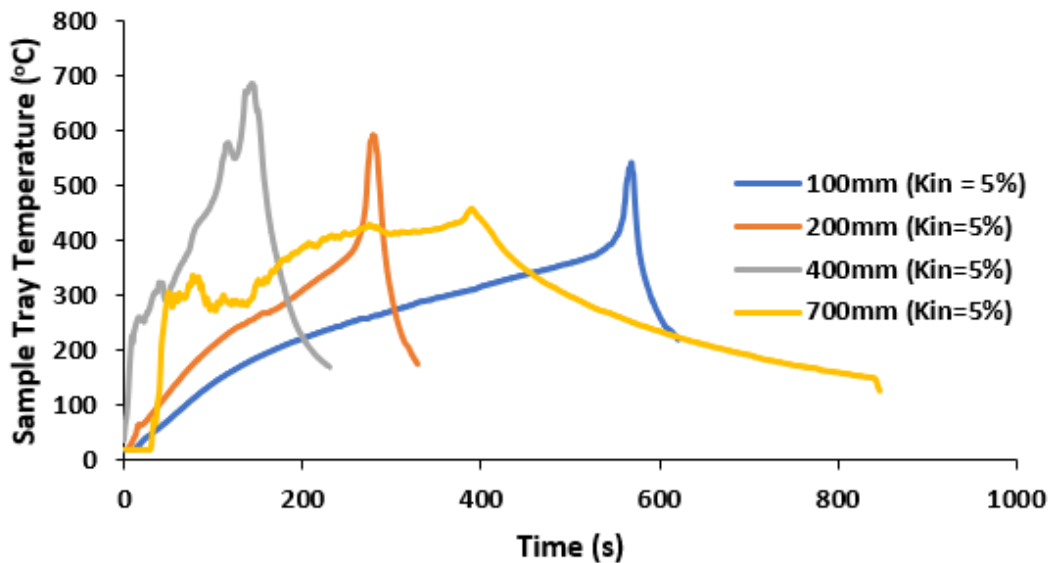


Figure 7-30 Sample Tray Temperatures as a Function of Time

Figure 7-30 shows the temperatures of sample tray for the four tests without orifice plate with the same ventilation factor ($K_{in}=5\%$). They had a similar profile with a rapid rise in temperature at the initial burning period but then decreased for some time with a sharp increase when the temperature got to approximately 360°C . The significant rise in temperature at about 360°C is as a result of the diesel fractions exceeding their boiling point, thereby increasing the hydrocarbon vapours that combust [16] and release large amount of energy.

7.4.1 Toxic Gas Concentrations

The test without the orifice plate had the problem of air suction from the chimney therefore diluting the gases with air. The gases sampled by the FTIR was diluted, which underestimated the overall toxicity. This is not a true representative of the toxic gases emitted and the hazards they can cause. The total toxicity **N** relative to LC_{50} and $\text{COSHH}_{15\text{min}}$ are compared in Fig. 7-31 for the 4 tests with the same ventilation factor. This showed a very low total toxicity which underestimates the actual toxic hazard that these gases may cause. Even though the biggest size of pool was higher in total toxicity it is still very low considering the size of the pool.

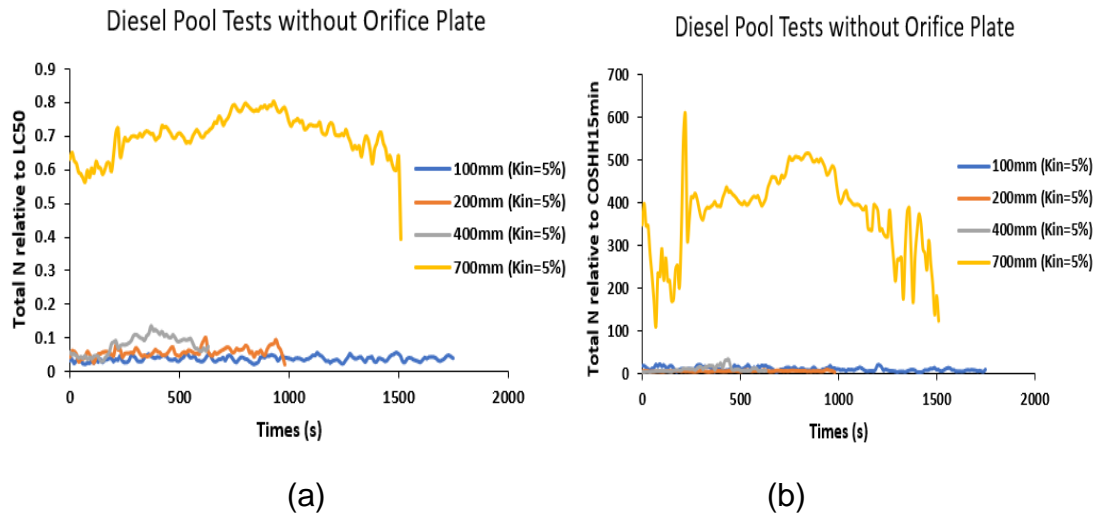


Figure 7-31 Total N relative to LC₅₀ (a) and COSHH_{15min} (b)

7.4.2 Soot Deposit

The yields of soot deposited on the walls of the compartment are presented in Table 7-9. The first three tests showed an increase in soot yield with increase in the size of the pool. The biggest pool however had a very low yield.

Table 7-9 Yield of Soot Deposited on the Walls of the Compartment

Test	Yield of Soot Deposited (g/kg)
100 mm ($K_{in}=5\%$)	6.36
200 mm ($K_{in}=5\%$)	28.75
400 mm ($K_{in}=5\%$)	36.79
700 mm ($K_{in}=5\%$)	8.12

7.5 SEM Analyses on Soot Samples

Two samples from the diesel pool 200 mm ($K_{in}= 0\%$) test were analysed using the scanning electron microscope SEM. Samples were taken from the smoke meter and the compartment window. The sizes obtained from the smoke meter sample were in the range of 17 – 85 nm while the sizes obtained from the window sample were in the range of 40 – 80 nm. These sizes fall in the range of particles obtained by the DMS particle size analyser.

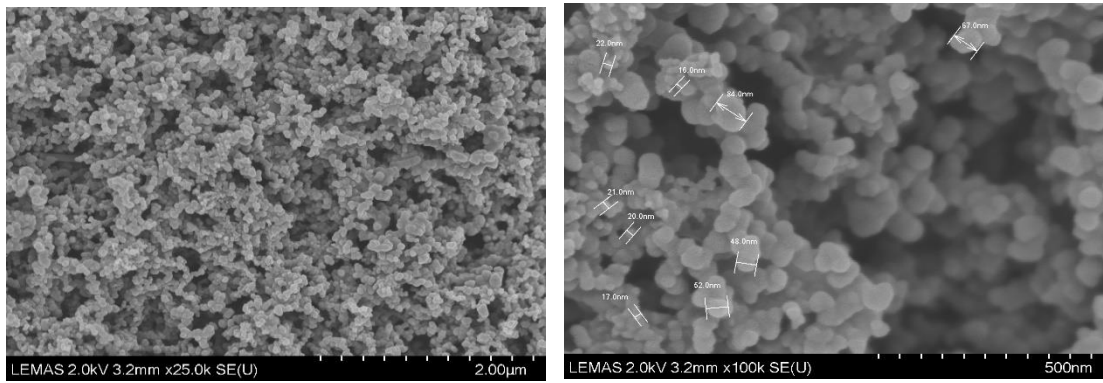


Figure 7-32 Diesel Pool 200 mm ($K_{in}=0\%$) SEM Analysis on Smoke Meter Sample

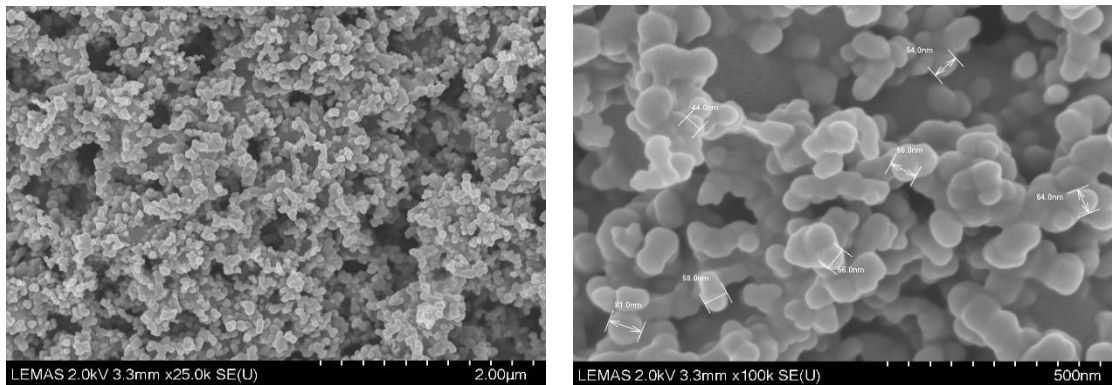


Figure 7-33 Diesel Pool 200 mm ($K_{in}=0\%$) SEM Analysis on Window Sample

Comparing the SEM results with that of wood in Figs. 6-36 and 6-37, the sizes obtained from the wood samples were larger than that obtained from the diesel. The smoke meter soot sample sizes ranged from 50-90 nm for wood and 17-85 nm for diesel while that of the window sample was 40-85 nm for the wood crib and 40-80 nm for the diesel. The morphology was quite similar, having similar particle structure and agglomerates.

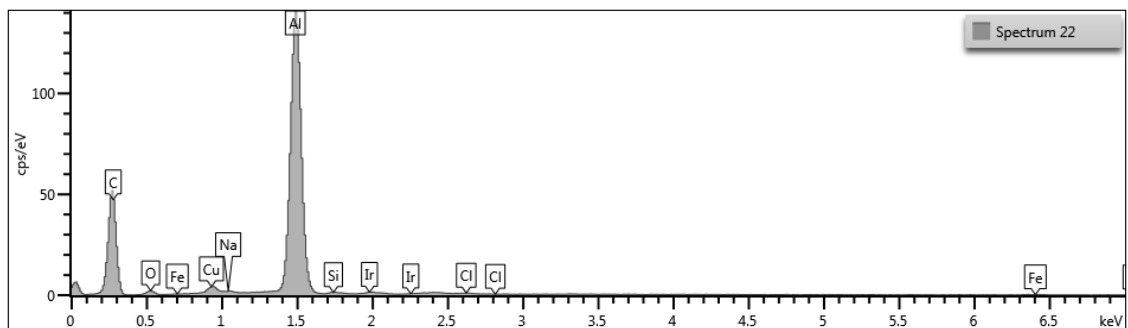


Figure 7-34 Diesel Pool 200 mm ($K_{in}=0\%$) SEM Elemental Analysis on Smoke Meter Sample

Table 7-10 Diesel Pool 200 mm ($K_{in}=0\%$) SEM Elemental Analysis on Smoke Meter Sample

Element	Wt%
C	70.57
O	2.29
Na	0.16
Al	24.73
Si	0.16
Cl	0.11
Fe	0.3
Cu	1.68
Total:	100

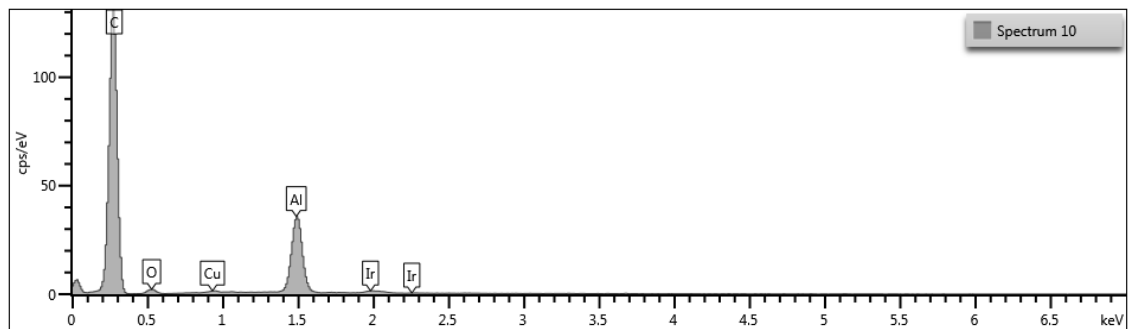


Figure 7-35 Diesel Pool 200 mm ($K_{in}=0\%$) SEM Elemental Analysis on Window Sample

Table 7-11 Diesel Pool 200 mm ($K_{in}=0\%$) SEM Elemental Analysis on Window Sample

Element	Wt%
C	89.35
O	3.08
Al	7.11
Cu	0.46
Total:	100

Figures 7-34 and 7-35 show the spectrum for the elemental analysis of the soot samples obtained from the smoke meter and the compartment window. The soot from the smoke meter shows that about 70% of the soot sample is carbon, 2%

oxygen and other trace elements while the soot collected from the window showed that about 89% of the soot sample is carbon and 3% oxygen, with other elements. The aluminium in the sample is the aluminium stud on which the samples were placed for analyses.

7.6 Summary

The test on pool fires on the cone calorimeter and the 5m³ compartment resulted in the following findings

Cone Calorimeter Pool Test:

- The flash point of the fuels played an important role in the ignition of the fuel. Olive oil with higher flash point took longer time to ignite at the same irradiation.
- The equivalence ratio showed that the combustion was lean at the initial stage of the fire but became very rich showing an evidence of confinement even though the experiment was freely ventilated.
- Diesel had the highest mass loss rate compared to lubricating oil and olive oil.
- In the diesel, lubricating oil and olive oil fires, formaldehyde and acrolein were the main irritant toxic gases. CO and HCN were the main asphyxiants. Benzene and trimethylbenzene were the hydrocarbons of toxic significance.
- The dilution required to prevent 30-minute LC₅₀ exposure levels from being lethal was about 13-27 indicating that people exposed to these gases would be at risk of death. Impairment of escape would be a much more significant effect as these toxic gases need to be diluted by about 10 000 for diesel fire and over 5000 for lubricating oil and over 20 000 for olive oil before these gases would not impair escape.
- Olive oil was by far the most toxic of the 3 pool fires.
- For all 3 pool fires, CO dominated the toxicity on an LC₅₀ basis. However, on a COSHH_{15min} basis, acrolein dominated the toxicity.

5m³ Compartment Pool Test

- The ventilation was mainly controlled by the compartment outflow instead of the air inflow.
- The equivalence ratio showed that these fires were lean.
- The ceiling temperatures were between 300°C to 450°C, which is lower than typical compartment fires temperatures due to the ventilation restriction.
- A smoke pulsing phenomenon was observed in the big pool test with low ventilation due to the pressure difference.
- CO and unburnt total hydrocarbon were produced at high concentrations during the fires. Benzene and formaldehyde were more easily produced in the lower ventilation fires. Unlike other species which all had higher concentration and yield at the steady burning period, acrolein was formed at low temperature during the initial burning and decay stages.
- In terms of lethality, low ventilation fire was more lethal than the high ventilation fires but less hazardous in terms of impairment of escape. While the fire with large fuel load was more hazardous both in terms of lethality and impairment of escape.
- CO dominated the toxicity on an LC₅₀ basis while acrolein dominated on a COSHH_{15min} basis.
- Soot yield produced ranged from 0.003 g/g to 0.040 g/g.
- The low temperature fires generated more soot and the amount of soot deposited on the walls of the compartment contributed significantly to the soot yield, which was approximately 30% of the total soot emission.
- Diesel produced higher soot yield than other materials in the literature such as wood and heptane.
- Nanoparticles in sizes hazardous to health were generated in all the fires centred in the range of 10–200 nm with peak concentration of 10⁷–10⁸/cc.
- SEM analyses showed sizes of particles within the range obtained by the DMS particle size analyser.

Chapter 8 Conclusions and Future Work

8.1 Main Findings and Conclusions

From the review of fire statistics and literature it was concluded that the death-toll as a result of smoke inhalation is still unacceptably high with a greater understanding needed of the type and yield of toxic gases for different materials under different fire ventilation conditions. The hazard of particulate emissions from fires has not received much investigation. Importantly, there exists a gap in the knowledge of size distribution and emission factors/yields of the smoke/soot particles generated in fires, especially compartment fires.

This research investigated and measured particulates and toxic gases produced in vitiated and freely ventilated fires and also investigated the capability of various fuel loads found in compartments/buildings to generate particulates using the University of Leeds 5m³ rig test facility, the standard cone calorimeter and the controlled atmosphere cone calorimeter.

Ultra-fine particles in the range of 5-40 nm, in high enough concentrations to potentially be a significant cause of death and impairment of escape in fires were generated in all fires and these concentrations were much higher than those previously reported in the literature. To the knowledge of the author, this is one of the first reported studies in this range of particle sizes in fire. The main gaseous species were found to agree with those reported in the literature and these were analysed in detail and ranked in terms of lethality and irritancy.

The composition of the various materials was responsible for the type of toxic gases emitted. Plywoods of different compositions tested, produced different concentrations and yields of toxic gases. Other wood materials tested also had different concentration and yields of the toxic gases produced. Large amount of soot particles and toxic gases were produced by the pool fires due to the high release of unburnt hydrocarbons.

Ventilation also played an important role in the production of toxic gases and particulates. More ultrafine particles were produced with the richer mixtures compared to the lean mixtures and high concentration and yield of toxic gases were found with the restricted ventilation fires. Variation of heat flux showed that

the fire toxicity decreased with increasing radiant heat flux. The lower heat flux only pyrolysed the wood resulting in the partial oxidation of toxic gases while the higher heat flux resulted in an unrealistic clean burning behaviour. The results show that the irradiation level has a great influence on the particles produced in fires. The ultrafine particles and the bigger particles differed for all the different heat flux applied.

The complexity of different materials makes overall comparison of their toxicity difficult due to wide differences in composition. The important factors that determined the toxicity of the materials tested were the type of material, the ventilation condition and the heat flux. All the parameters played an important role in the emission of toxic gases and therefore need to be considered when testing for toxicity of various combustion products.

The modified cone calorimeter in combination with a heated FTIR and DMS 500 particle size analyser, was found to be a good technique for the realistic determination of toxic gases and particulate emissions under different controlled ventilation conditions.

8.2 Recommendations and Future Work

The four plywoods had different compositions indicating that the manufacturing processes were different and hence released different concentrations of the toxic gases. It would be useful to analyse the glue lines of the bonded woods to ascertain the chemical composition of the adhesives used to know how they contributed to the overall toxicity.

Another recommendation would be to further investigate other composite materials, in order to assess their propensity to produce any critical toxicant and particulates which may increase the overall toxic effect if any. This will provide suitable data for computer modellers and help in design, fire risk assessments and strategy.

Future work on testing of wood samples and pool fires on the cone calorimeter should include the use of thermocouples, placed in the samples, or thermal imaging camera to measure the temperature of the sample at the point of ignition. That will give the temperature at which the material ignites.

The modified cone calorimeter proved to be a good technique for realistic determination of particle size distributions in biomass combustion and pool fires when used with the FTIR and the DMS 500 analysers. However, the DMS 500 particle size analyser measures sizes ranging from 5-1000 nm and particles measured showed there is more particle mass above the 1000 nm upper measurement range. Another analyser such as the ELPI which are able to analyse particle up to 10 μm should be used in conjunction with the DMS 500 to measure other sizes outside the DMS range.

The 5m³ compartment is good for different types of fire testing but requires further modification to the apparatus and the methodology, which include:

- Using a cooling mechanism to cool the load cell which prevents overheating of the load cell affecting the measurement of the mass loss of the fire test.
- Using forced air supply instead of the natural ventilation which makes it more difficult to analyse the results and investigate the fire. To simulate the air supply condition in realistic fire scenario, natural air supply was used in this work. However, it makes it more difficult for analysis and to investigate the fire.
- Installing a longer chimney, to take care of the backflow of air reaching the position of sample probes and diluting the fire gases.

A further investigation on the soot samples collected on filter papers is required to determine the polycyclic aromatic hydrocarbons (PAHs) present in the soot using GC/MS.

References

- [1] G.E. Hartzell, Overview of combustion toxicology, *Toxicology*, 115 (1996) 7-23.
- [2] H.L. Kaplan, A.F. Grand, G.E. Hartzell, Toxicity and the smoke problem, *Fire Safety Journal*, 7 (1984) 11-23.
- [3] R. Gilbey, Rosepark Revisited, in: *Fire Risk Management*, The Fire Protection Association, Gloucestershire, 2012.
- [4] J. Lockett, 'GASSED TO DEATH' Grenfell Tower victims 'may have been poisoned by CYANIDE gas from burning insulation boards' in: Sun, News Group Newspapers Limited London, 2017.
- [5] Home Office, Fire and rescue incident statistics: England, year ending March 2019, in, 2019.
- [6] D.A. Purser, 3 - Hazards from smoke and irritants, in: *Fire Toxicity*, Woodhead Publishing, 2010, pp. 51-117.
- [7] D.A. Purser, Combustion Toxicity, in: e.a. M.J. Hurley (Ed.) *SFPE handbook of fire protection engineering*, Springer, New York, 2016, pp. 2207-2307.
- [8] A.A. Stec, Fire toxicity – The elephant in the room?, *Fire Safety Journal*, 91 (2017) 79-90.
- [9] FEMA, Civilian Fire Fatalities in Residential Buildings (2011-2013), in, FEMA: Emmitsburg, Maryland.
- [10] J. Giebułtowicz, M. Rużycka, P. Wroczyński, D.A. Purser, A.A. Stec, Analysis of fire deaths in Poland and influence of smoke toxicity, *Forensic Science International*, 277 (2017) 77-87.
- [11] Great Britain. Central Office of, A guide to the Furniture and Furnishings (Fire) (Safety) Regulations, Department of Trade and Industry, London, 1995.
- [12] D.A. Purser, R.L. Maynard, Chapter 1 Overview of Combustion Toxicology, in: *Toxicology, Survival and Health Hazards of Combustion Products*, The Royal Society of Chemistry, 2016, pp. 1-10.
- [13] Home Office, Fire and rescue incident statistics: England, year ending March 2018, in, London, 2018.
- [14] D.K. Shen, M.X. Fang, W.K. Chow, IGNITION OF WOOD-BASED MATERIALS BY THERMAL RADIATION, *International Journal on Engineering Performance-Based Fire Codes*, 8 (2006) 69-83.
- [15] B. Persson, M. Simonson, Fire Emissions into the Atmosphere, *Fire Technology*, 34 (1998) 266-279.
- [16] G.A. Chamberlain, The Hazards Posed by Large-Scale Pool Fires in Offshore Platforms, in: *ICHEME Symposium*, 1995, pp. 213-226.
- [17] L.T. Cowley, A.D. Johnson, I. Steel Construction, B. Great, Health, E. Safety, Oil and gas fires : characteristics and impact, H.M.S.O., London, 1992.
- [18] Geocaching, The Cleveland Fire of 1929, in, USA, 2012.
- [19] A.O. Mirkhah, Lessons from the Past: MGM Grand Fire, in: *FIREHOUSE*, 2010.
- [20] S. Duff, Remembering Piper Alpha disaster, in: BBC News, BBC Scotland, Scotland, 2008.
- [21] HSE, Buncefield: Why did it happen? , in: C.o.M.A.H. COMAH (Ed.), 2011.
- [22] K.M. Butler, G.W. Mulholland, Generation and Transport of Smoke Components, in, Kluwer Academic Publishers, Boston, 2004, pp. 149-176.
- [23] R.D. Daniels, T.L. Kubale, J.H. Yiin, M.M. Dahm, T.R. Hales, D. Baris, S.H. Zahm, J.J. Beaumont, K.M. Waters, L.E. Pinkerton, Mortality and cancer incidence in a pooled cohort of US firefighters from San Francisco, Chicago and Philadelphia (1950-2009), *Occupational and Environmental Medicine*, 71 (2014) 388-397.
- [24] A. Violi, Effects of Combustion-Generated Nanoparticles on Cellular Membranes, *Combustion Science and Technology*, 188 (2016) 769-775.
- [25] C.A. Pope, R.L. Verrier, E.G. Lovett, A.C. Larson, M.E. Raizenne, R.E. Kanner, J. Schwartz, G.M. Villegas, D.R. Gold, D.W. Dockery, Heart rate variability associated with particulate air pollution, *American Heart Journal*, 138 (1999) 890-899.

- [26] J.S. Lighty, J.M. Veranth, A.F. Sarofim, Combustion aerosols: factors governing their size and composition and implications to human health, *Journal of the Air & Waste Management Association* (1995), 50 (2000) 1565-1618.
- [27] A. Seaton, D. Godden, W. MacNee, K. Donaldson, Particulate air pollution and acute health effects, *The Lancet*, 345 (1995) 176-178.
- [28] A. Peters, H.E. Wichmann, T. Tuch, J. Heinrich, J. Heyder, Respiratory effects are associated with the number of ultrafine particles, *American journal of respiratory and critical care medicine*, 155 (1997) 1376-1383.
- [29] A. Kocbach Bølling, J. Pagels, K.E. Yttri, L. Barregard, G. Sallsten, P.E. Schwarze, C. Boman, Health effects of residential wood smoke particles: the importance of combustion conditions and physicochemical particle properties, *Particle and Fibre Toxicology*, 6 (2009) 29.
- [30] A. Tewarson, Smoke Emissions In Fires, in: B. Karlsson (Ed.) FIRE SAFETY SCIENCE–PROCEEDINGS OF THE NINTH INTERNATIONAL SYMPOSIUM, INTERNATIONAL ASSOCIATION FOR FIRE SAFETY SCIENCE, Karlsruhe, Germany, 2009, pp. pp. 1153-1164.
- [31] I.E. PERERA, C.D. LITTON, A Detailed Study of the Properties of Smoke Particles Produced from both Flaming and Non-Flaming Combustion of Common Mine Combustibles, in: M. Spearpoint (Ed.) FIRE SAFETY SCIENCE-PROCEEDINGS OF THE TENTH INTERNATIONAL SYMPOSIUM, INTERNATIONAL ASSOCIATION FOR FIRE SAFETY SCIENCE, University of Maryland, 2011, pp. 213-226.
- [32] Y. Tsuchiya, J.F. MATHIEU, Heat, CO and Smoke Release Rates of Plywood under a Depleted Oxygen Atmosphere: An Experimental Study using an OSU Heat Release Rate Apparatus, in: G. Cox, B. Langford (Eds.) FIRE SAFETY SCIENCE-PROCEEDINGS OF THE THIRD INTERNATIONAL SYMPOSIUM, University of Edinburgh, Scotland, 1991, pp. 605-614.
- [33] M. Barakat, J.-M. Souil, C. Breillat, J.-P. Vantelon, V. Knorre, F.-X. Rongère, Smoke data determination for various types of fuel, *Fire Safety Journal*, 30 (1998) 293-306.
- [34] B.S. Haynes, H. Jander, H.G. Wagner, Optical Studies of Soot-Formation Processes in Premixed Flames, *Berichte der Bunsengesellschaft für physikalische Chemie*, 84 (1980) 585-592.
- [35] Government, The Building Regulations 2010 : fire safety : approved document B. Vol. 1, Dwellinghouses, 2006 edition incorporating 2010 and 2013 amendments. ed., NBS RIBA Enterprises, London, 2013.
- [36] BS 9999:2017 - Fire safety in the design, management and use of buildings. Code of practice, 2017.
- [37] BS 476-10:2009 - Fire tests on building materials and structures. Guide to the principles, selection, role and application of fire testing and their outputs, 2008.
- [38] BS ISO 12136:2011: Reaction to fire tests. Measurement of material properties using a fire propagation apparatus, in, British Standards Institute, 2011.
- [39] D. Drysdale, An introduction to fire dynamics, 2nd ed., Wiley, New York, 1998.
- [40] N. Boonmee, J.G. Quintiere, Glowing and flaming autoignition of wood, *Proceedings of the Combustion Institute*, 29 (2002) 289-296.
- [41] R.O. Carvel, FIRE SIZE IN TUNNELS, in: School of the Built Environment, Division of Civil Engineering, Heriot-Watt University, Edinburgh, 2004, pp. 348.
- [42] L. Forest Products, Wood handbook: wood as an engineering material, in, The Laboratory, Madison, Wis, 2010.
- [43] T. Steinhaus, S. Welch, R. Carvel, J. Torero, Large-scale pool fires, *Thermal Science*, 11 (2007) 101-118.
- [44] K.S. Mudan, Thermal radiation hazards from hydrocarbon pool fires, *Progress in Energy and Combustion Science*, 10 (1984) 59-80.
- [45] J.A. Koski, L.A. Gritzo, L.A. Kent, S.D. Wix, Actively Cooled Calorimeter Measurements and Environment Characterization In a Large Pool Fire, *Fire and Materials*, 20 (1996) 69-78.
- [46] F.M. Liang, W.K. Chow, S.D. Liu, Preliminary Studies on Flashover Mechanism in Compartment Fires, *Journal of Fire Sciences*, 20 (2002) 87-112.

- [47] R.W. Fitzgerald, *Building Fire Performance Analysis*, in, Wiley, USA, 2004, pp. 54.
- [48] BS ISO 19706:2011: *Guidelines for assessing the fire threat to people*, in, British Standards Institute, 2012.
- [49] D.A. Purser, Chapter 2 *Fire Types and Combustion Products*, in: *Toxicology, Survival and Health Hazards of Combustion Products*, The Royal Society of Chemistry, 2016, pp. 11-52.
- [50] G. Rein, *Smoldering Combustion*, Springer, 2016.
- [51] A.A. Stec, T.R. Hull, *Assessment of the fire toxicity of building insulation materials*, *Energy & Buildings*, 43 (2011) 498-506.
- [52] J. Quintiere, M. Birky, F. McDonald, G. Smith, *An Analysis of Smoldering Fires in Closed Compartments and Their Hazard Due to Carbon Monoxide*, in: M.D. National Bureau Of Standards Gaithersburg (Ed.), 1982.
- [53] BS EN 60695-7-1:2010: *Fire hazard testing. Toxicity of fire effluent. General guidance*, in, British Standards Institute, 2010.
- [54] G.E. Hartzell, *Criteria and methods for evaluation of toxic hazard*, *Fire Safety Journal*, 12 (1987) 179-182.
- [55] T.R. Hull, A.A. Stec, 1 - *Introduction to fire toxicity*, in: *Fire Toxicity*, Woodhead Publishing, 2010, pp. 3-25.
- [56] S.I. consultants, *Tenability Limit*, in, SHEVS IFT consultants Pte Ltd, Singapore, 2015.
- [57] C.P.T. Coalition, *SMOKE Cyanide and Carbon Monoxide: The Toxic Twins of Smoke Inhalation*, in, Indianapolis, 2009.
- [58] D.A. Purser, in: P.J. DiNenno (Ed.) *SFPE Handbook of Fire Protection Engineering*, National Fire Protection Association, Quincy, MA, 2008, pp. 2-96 - 92-193.
- [59] S.E. Manahan, *Environmental chemistry*, CRC Press, Boca Raton, Fla;London;, 2010.
- [60] Y. Alarie, *Toxicity of Fire Smoke*, *Critical Reviews in Toxicology*, 32 (2002) 259-289.
- [61] ISO 13571:2007, *Life -threatening components of fire - Guidelines for the estimation of time available for escape using fire data*, in, BSI, 13571:2007.
- [62] D.A. Purser, *Toxic Assessment of Combustion Products*, in: P.J. Dinenno (Ed.) *SFPE Handbook of Fire Protection Engineering*, National Fire Protection Association, Quincy, MA, 2002, pp. 2-83-82-171.
- [63] P. Blomqvist, *Emissions from Fires Consequences for Human Safety and the Environment*, in: *Fire Safety Engineering*, Lund University, Lund, Sweden, 2005, pp. 129.
- [64] G. Andrews, J. Ledger, H. Phylaktou, *Pool fires in a low ventilation enclosure*, in: *INSTITUTION OF CHEMICAL ENGINEERS SYMPOSIUM SERIES*, Institution of Chemical Engineers; 1999, 2000, pp. 171-184.
- [65] G. Andrews, J. Ledger, H.N. Phylaktou, *Enclosed Pool Fires in Low Ventilation Enclosures: Flame Temperatures and Global Heat Loss Using Gas Analysis*, in: M. Curtat (Ed.) *Proceedings of the Sixth International Symposium on Fire Safety Science*, International Association for Fire Safety Science, Poitiers, 2000, pp. 591-602.
- [66] G.E. Andrews, J. Ledger, H.N. Phylaktou, *The Gravimetric Determination of Soot Yields in Enclosed Pool Fires*, in: *3rd International Colloquia on Explosions in Reactive Systems*, Windermere, 2000.
- [67] C.J. Wiecek, *Carbon Monoxide Generation and Transport from Compartment Fires*, in: *Mining and Minerals Engineering*, Virginia Polytechnic Institute and State University, Blackburg, VA, 2003.
- [68] Y. Utiskul, *Theoretical and Experimental study on Fully Developed Compartment Fires*, in: *Fire Protection Engineering*, College Park, University of Maryland, 2005.
- [69] Y. Utiskul, J.G. Quintiere, *Generalizations on Compartment Fires from Small-scale Experiments for Low Ventilation Conditions*, in: D. Gottuk, B.Y. Lattimer (Eds.) *Proceedings of the Eighth International Symposium on Fire Safety Science*, International Association for Fire Safety Science, Beijing, 2005.

- [70] Y. Utiskul, J.G. Quintiere, A.S. Rangwala, B.A. Ringwelski, K. Wakatsuki, T. Naruse, Compartment fire phenomena under limited ventilation, *Fire Safety Journal*, 40 (2005) 367-390.
- [71] M. Bundy, H. Anthony, J. Erik, C.K. Sung, H.K. Gwon, B.L. David, NIST Technical Note 1483: Measurements of Heat and Combustion Products in Reduced-Scale Ventilation-Limited Compartment, in, NIST Technical Notes. United States Department of Commerce, Gaithersburg. NIST, 2007.
- [72] G.H. Ko, A. Hamins, M. Bundy, E.L. Johnsson, S.C. Kim, D.B. Lenhart, Mixture fraction analysis of combustion products in the upper layer of reduced-scale compartment fires, *Combustion and Flame*, 156 (2009) 467-476.
- [73] G.E. Andrews, B. Daham, M.D. Mmolawa, S. Boulter, J. Mitchell, G. Burrell, J. Ledger, W. Gunamusa, R.A. Boreham, H.N. Phylaktou, Toxic Emissions from Air Starved Fires, in: A.o.F.S. Science (Ed.) 8th Symposium on Fire Safety Science, 2005, pp. 1035-1046.
- [74] O. Sugawa, K. Kawagoe, Y. Oka, Burning behavior in a poor-ventilation compartment fire — ghosting fire —, *Nuclear Engineering and Design*, 125 (1991) 347-352.
- [75] M.J. Peatross, C.I. Beyler, Thermal Environment Prediction in Steel Bounded Pre-Flashover Compartment Fires, in: Fifth International Symposium on Fire Safety Science 1997, pp. 415-426.
- [76] L. Audouin, J.M. Such, J.C. Malet, C. Casselman A Real Scenario for a Ghosting Flame, in: Fire Safety Science-Proceedings of the Fifth International Symposium International Association for Fire Safety Science, 1997, pp. 1261 -1272
- [77] D.T. Gottuk, R.J. Roby, C.L. Beyler, A study of carbon monoxide and smoke yields from compartment fires with external burning, *Symposium (International) on Combustion*, 24 (1992) 1729-1735.
- [78] D.T. Gottuk, R.J. Roby, M.J. Peatross, C.I. Beyler, Carbon Monoxide Production in Compartment Fires, *Fire Protection Engineering*, 4 (1992) 133-150.
- [79] C.M. Fleischmann, A.R. Parkes, Effects Of Ventilation On The Compartment Enhanced Mass Loss Rate, in: IAFSS Symposiums, 1997, pp. 415-426.
- [80] Y. Ohmiya, T. Tanaka, T. Wakamatsu, A Room Fire Model for Predicting Fire Spread by External Flames, *Fire Science and Technology*, 18 (1998) 11-21.
- [81] D.A. Purser, ASET and RSET: addressing some issues in relation to occupant behaviour and tenability, in: D. Evans (Ed.) Proceedings of the Seventh International Symposium on Fire Safety Science,, International Association for Fire Safety Science,, Worcester, 2003, pp. 10.3801/IAFSS.FSS.3807-3891.
- [82] A. Tewarson, Generation of Heat and Chemical Compounds in Fires, in: SFPE handbook of fire protection engineering, National Fire Protection Association, Bethesda, Md;Quincy, Mass;, 2002, pp. 3/83-83/161.
- [83] W.M. Pitts, The global equivalence ratio concept and the formation mechanisms of carbon monoxide in enclosure fires, *Progress in Energy and Combustion Science*, 21 (1995) 197-237.
- [84] A. Tewerson, Generation of Heat and Chemical Compounds in Fires, in: P.J. DiNenno (Ed.) SFPE handbook of fire protection engineering, National Fire Protection Association, Bethesda, Md;Quincy, Mass;, 2002, pp. 3/83-83/161.
- [85] O.A.O. Aljumaiah, Combustion products from ventilation controlled fires: toxicity assessment and modelling, in, University of Leeds, PhD, Leeds, 2012.
- [86] C.L. Beyler, Development and Burning of a Layer of Products of Incomplete Combustion Generated by a Buoyant Diffusion Flame, Harvard University, 1983.
- [87] A.A.S. Alarifi, Compartment fire toxicity: measurements and aspects of modelling, in, University of Leeds, PhD, Leeds 2016.
- [88] O. Aljumaiah, G.E. Andrews, H.N. Phylaktou, B.G. Mustafa, H. Al-Qattan, V. Shah, Air Starved Compartment Wood Crib Fire Heat Release and Toxic Gas Yields, in: Fire Safety Science - Proceedings of the Tenth International Symposium, International Association for Fire Safety Science, 2011, pp. 1263-1276.

- [89] B.G. Mustafa, G.E. Andrews, H.N. Phylaktou, A. Al-Shammri, V. Shah, Impact of Wood Fire Load on Toxic Emissions in Ventilation Controlled Compartment Fires, in: IFireSS - International Fire Safety Symposium, Coimbra, Portugal, 2015.
- [90] Y. Tsuchiya, CO/CO₂ Ratios in Fire in: FIRE SAFETY SCIENCE-PROCEEDINGS OF THE FOURTH INTERNATIONAL SYMPOSIUM, International Association for Fire Safety Science, 1994, pp. pp. 515-526.
- [91] Y. Tsuchiya, Chemical Modeling of Fire Gases, *Journal of Fire Sciences*, 13 (1995) 214-223.
- [92] R.S. Spindt, Air-Fuel Ratios from Exhaust Gas Analysis, in, SAE International, 1965.
- [93] S.H. Chan, An exhaust emissions based air-fuel ratio calculation for internal combustion engines, ARCHIVE: Proceedings of the Institution of Mechanical Engineers, Part D: Journal of Automobile Engineering 1989-1996 (vols 203-210), 210 (1996) 273-280.
- [94] ISO 8718, Reciprocating Internal Combustion Engines - Exhaust Emission Measurement - Part 1:Test-bed Measurement of Gaseous and Particulate Exhaust Emissions in, BSI, 8178-1:2006.
- [95] C. Huggett, Estimation of rate of heat release by means of oxygen consumption measurements, *Fire and Materials*, 4 (1980) 61-65.
- [96] B. Karlsson, J.G. Quintiere, Enclosure fire dynamics, 1 ed., CRC Press, Boca Raton, FL, 2000.
- [97] H.C. Tran, R.H. White, Heat Release from Wood Wall Assemblies Using Oxygen Consumption Method in: G.L. Nelson (Ed.) *Fire and Polymers: Hazards Identification and Prevention*, Proceedings of 197th national meeting of the American Chemical Society, American Chemical Society, Dallas, TX. Washington, DC, 1990, pp. 411-428.
- [98] J.J. Brenden, F.L. Browne, Heat of combustion of the volatile pyrolysis products of fire-retardant-treated ponderosa pine, 1964.
- [99] B.Z. Dlugogorski, J.R. MAWHINNEY, V.H. DUC, The Measurement of Heat Release Rates by Oxygen Consumption Calorimetry in Fires Under Suppression, in: *Fire Safety Science-Proceedings of the Fourth International Symposium*, International Association for Fire Safety Science, 1994, pp. 877-888.
- [100] W.M. Pitts, An algorithm for estimating CO formation in enclosed fires, in: *Fire Safety Science-Proceedings of the Fifth International Symposium*, 1997, pp. 536-546.
- [101] T.R. Hull, R.E. Quinn, I.G. Areri, D.A. Purser, polymer degradation and stability, 77 (2002) 235-242.
- [102] PD ISO/TS 19700:2016: Controlled equivalence ratio method for the determination of hazardous components of fire effluents. Steady-state tube furnace, in, British Standards Institute, 2016.
- [103] BS 7990:2003: Tube furnace method for the determination of toxic product yields in fire effluents, in, British Standards Institute, 2003.
- [104] D.T. Gottuk, B.Y. Lattimer, Effect of Combustion Conditions on Species Production, in: SFPE handbook of fire protection engineering, National Fire Protection Association, Bethesda, Md;Quincy, Mass;, 2002.
- [105] A. Tewarson, Fully developed enclosure fires of wood cribs, *Symposium (International) on Combustion*, 20 (1985) 1555-1566.
- [106] B. Forell, A methodology to assess species yields of compartment fires by means of an extended global equivalence ratio concept. 2007, in: Institut fur Baustoffe, Massivbau und Brandschutz, University of Braunschweig, Germany, 2007.
- [107] H. Li, G.E. Andrews, B. Daham, M. Bell, J. Tate, K. Ropkins, Impact of Traffic Conditions and Road Geometry on Real World Urban Emissions Using a SI Car, in, SAE International, 2007.
- [108] BS ISO 5660-1:2015: Reaction-to-fire tests. Heat release, smoke production and mass loss rate. Heat release rate (cone calorimeter method) and smoke production rate (dynamic measurement), in, British Standards Institute, 2015.

- [109] S.T. McKenna, T.R. Hull, The fire toxicity of polyurethane foams, *Fire Science Reviews*, 5 (2016) 3.
- [110] V. Babrauskas, W.H. Twilley, M. Janssens, S. Yusa, A cone calorimeter for controlled-atmosphere studies, *Fire and Materials*, 16 (1992) 37-43.
- [111] M. Christy, R. Patrella, J. Penkala, Controlled-atmosphere cone calorimeter, *Fire and Polymers II: Materials and Tests for Hazard Prevention*, 599 (1995) 498-517.
- [112] G.W. Mulholland, M.L. Janssens, S. Yusa, W.H. Twilley, V. Babrauskas, The Effect of Oxygen Concentration on CO and Smoke Produced by Flames, in: *Fire Safety Science: Proceedings of the 3rd International Symposium*, 1991, pp. 585-594.
- [113] R.V. Petrella, N. Batho, The controlled-atmosphere cone calorimeter – an improved tool for fire testing of materials., in: *Fire and Materials, 1st International Conference*, Washington D.C, USA, 1992, pp. 311-321.
- [114] J.E. Leonard, P.A. Bowditch, V.P. Dowling, Development of a controlled-atmosphere cone calorimeter, *Fire and Materials*, 24 (2000) 143-150.
- [115] E. Mikkola, Effects of Oxygen Concentration on Cone Calorimeter Results, in: *6th International Conference (Interflam 93)*, Interscience Communications, Oxford, UK, 1993, pp. 49-56.
- [116] J. Hietaniemi, R. Kallonen, E. Mikkola, Fires at Chemical Warehouses, in: *Research Notes 1810*, VTT – Technical Research Center of Finland, Finland, 1997.
- [117] J. Hietaniemi, R. Kallonen, E. Mikkola, Burning characteristics of selected substances: production of heat, smoke and chemical species, *Fire and Materials*, 23 (1999) 171-185.
- [118] C. Gomez, A. Zalkin, M.L. Janssens, Using the Cone Calorimeter for Quantifying Toxic Potency, in: *12th. International Fire Science & Engineering Conference (Interflam '10)*, Nottingham, UK, 2010.
- [119] M.L. Janssens, C. Gomez, Enclosure effects on burning behavior in the cone calorimeter, in: *21st Annual Conference on Recent Advances on Flame Retardancy of Polymeric Materials*, Stanford, CT/USA, 2010.
- [120] C. Gomez, M.L. Janssens, A. Zalkin, Measuring yields of toxic gases from materials during different stages of fire development, in: *Fire and Materials 2011*, Interscience Communications Ltd, San Francisco, USA, 2011.
- [121] D. Marquis, Multi-scale characterisation and modelling of the fire behaviour of a composite for application in ship building, in: *Ecole des Mines de Nantes*, Nantes, FRA, 2010.
- [122] D.M. Marquis, E. Guillaume, A. Camillo, M. Pavageau, T. Rogaume, Usage of Controlled-Atmosphere Cone Calorimeter to Provide Input Data for Toxicity Modelling, in: *Fire and Materials 2011*, Interscience Communications Ltd., San Francisco, CA, USA, 2011.
- [123] E. Guillaume, D.M. Marquis, C. Chivas, Experience plan for controlled-atmosphere cone calorimeter by Doehlert method, *Fire and Materials*, 37 (2013) 171-176.
- [124] D. Marquis, E. Guillaume, D. Lesenechal, Accuracy (Trueness and Precision) of Cone Calorimeter Tests with and Without a Vitiated Air Enclosure, in: Elsevier Ltd, 2013, pp. 103-119.
- [125] M. Werrel, J.H. Deubel, S. Krüger, A. Hofmann, U. Krause, The calculation of the heat release rate by oxygen consumption in a controlled-atmosphere cone calorimeter: Heat release rate in a controlled-atmosphere cone calorimeter, *Fire and Materials*, 38 (2014) 204-226.
- [126] A. Irshad, Gasification Burning of Biomass, in, PhD, University of Leeds, 2017.
- [127] BS ISO 13344:2015: Estimation of the lethal toxic potency of fire effluents, in, British Standards Institute, 2016.
- [128] ISO 13571, Life-threatening components of fire -- Guidelines for the estimation of time available for escape using fire data, in, British Standard Institute, 2007.
- [129] T.R. Hull, 12 - Bench-scale generation of fire effluents, in: *Fire Toxicity*, Woodhead Publishing, 2010, pp. 424-460.

- [130] P. Blomqvist, T. Hertzberg, H. Tuovinen, K. Arrhenius, L. Rosell, Detailed determination of smoke gas contents using a small-scale controlled equivalence ratio tube furnace method, *Fire and Materials*, 31 (2007) 495-521.
- [131] A.A. Stec, T.R. Hull, J.A. Purser, D.A. Purser, Comparison of toxic product yields from bench-scale to ISO room, *Fire Safety Journal*, 44 (2009) 62-70.
- [132] A.A. Stec, T.R. Hull, K. Lebek, Characterisation of the steady state tube furnace (ISO TS 19700) for fire toxicity assessment, *Polymer Degradation and Stability*, 93 (2008) 2058-2065.
- [133] T. Hertzberg, P. Blomqvist, Particles from fires—a screening of common materials found in buildings, *Fire and Materials*, 27 (2003) 295-314.
- [134] I.M. Kennedy, Models of soot formation and oxidation, *Progress in Energy and Combustion Science*, 23 (1997) 95-132.
- [135] S. Léonard, G.W. Mulholland, R. Puri, R.J. Santoro, Generation of CO and smoke during underventilated combustion, *Combustion and Flame*, 98 (1994) 20,IN23-34,IN24.
- [136] ISO 29904:2013, Fire Chemistry - Generation and Measurement of Aerosols, in, Switzerland, 2013.
- [137] N.Y. Rojas, Diesel exhaust system influences on transient particulate emissions and particle size distribution: cold start and fast acceleration particulate mass emissions and particle size distribution changes through a practical exhaust system, PhD, University of Leeds, Leeds 2001.
- [138] A.Y.P. Wardoyo, Biomass Burning: Particle Emissions, Characteristics, and Airborne Measurements, in: School of Physical and Chemical Sciences, PhD, Queensland University of Technology, Queensland, 2007, pp. 218.
- [139] M.D. Hays, C.D. Geron, K.J. Linna, N.D. Smith, J.J. Schauer, Speciation of gas-phase and fine particle emissions from burning of foliar fuels, *Environmental Science & Technology*, 36 (2002) 2281-2295.
- [140] P.M. Fine, G.R. Cass, B.R.T. Simoneit, Chemical Characterization of Fine Particle Emissions from Fireplace Combustion of Woods Grown in the Northeastern United States, *Environmental Science & Technology*, 35 (2001) 2665-2675.
- [141] P.M. Fine, G.R. Cass, B.R.T. Simoneit, Chemical Characterization of Fine Particle Emissions from the Fireplace Combustion of Woods Grown in the Southern United States, *Environmental Science & Technology*, 36 (2002) 1442-1451.
- [142] J.D. McDonald, B. Zielinska, E.M. Fujita, J.C. Sagebiel, J.C. Chow, J.G. Watson, Fine Particle and Gaseous Emission Rates from Residential Wood Combustion, *Environmental Science & Technology*, 34 (2000) 2080-2091.
- [143] E. Hedberg, A. Kristensson, M. Ohlsson, C. Johansson, P.-Å. Johansson, E. Swietlicki, V. Vesely, U. Wideqvist, R. Westerholm, Chemical and physical characterization of emissions from birch wood combustion in a wood stove, *Atmospheric Environment*, 36 (2002) 4823-4837.
- [144] P. Fardell, E. Guillaume, 11 - Sampling and measurement of toxic fire effluent, in: *Fire Toxicity*, Woodhead Publishing, 2010, pp. 385-423.
- [145] T. Nussbaumer, C. Czasch, N. Klippel, L. Johansson, C. Tullin, Particulate Emissions from Biomass Combustion in IEA Countries. Survey on Measurements and Emission Factors, in, International Energy Agency (IEA) Bioenergy Task 32 and Swiss Federal Office of Energy (SFOE), Zurich, 2008.
- [146] W.C. Hinds, *Aerosol technology: properties, behavior, and measurement of airborne particles*, Wiley, New York;Chichester;, 1982.
- [147] *Cambustion, DMS500 Fast Particulate Spectrometer with Heated Sample Line High Ratio Diluter User Manual*, in, Cambridge, 2011.
- [148] P. Le Canut, M.O. Andreae, G.W. Harris, F.G. Wienhold, T. Zenker, Airborne studies of emissions from savanna fires in southern Africa: 1. Aerosol emissions measured with a laser optical particle counter, *Journal of Geophysical Research: Atmospheres*, 101 (1996) 23615-23630.

- [149] R.K. Chakrabarty, H. Moosmüller, M.A. Garro, W.P. Arnott, J. Walker, R.A. Susott, R.E. Babbitt, C.E. Wold, E.N. Lincoln, W.M. Hao, Emissions from the laboratory combustion of wildland fuels: Particle morphology and size, *Journal of Geophysical Research - Atmospheres*, 111 (2006) D07204.
- [150] S. Hosseini, Q. Li, D. Cocker, D. Weise, A. Miller, M. Shrivastava, J.W. Miller, S. Mahalingam, M. Princevac, H. Jung, Particle size distributions from laboratory-scale biomass fires using fast response instruments, *Atmos. Chem. Phys.*, 10 (2010) 8065-8076.
- [151] T. Hertzberg, P. Blomqvist, M. Dalene, G. Skarping, Particles and Isocyanates from fires, in: S.S.N.T.a.R. Institute (Ed.) *Brandforsk project 324-021*, SP Swedish National Testing and Research Institute, Borås, Sweden, 2003.
- [152] P. Blomqvist, M.S. McNamee, A.A. Stec, D. Gylestam, D. Karlsson, u. Stockholms, f. Naturvetenskapliga, k. Institutionen för analytisk, Detailed study of distribution patterns of polycyclic aromatic hydrocarbons and isocyanates under different fire conditions, *Fire and Materials*, 38 (2014) 125-144.
- [153] A.S.X. Loo, A. Coppalle, J. Yon, P. Aîné, Time-dependent smoke yield and mass loss of pool fires in a reduced-scale mechanically ventilated compartment, *Fire Safety Journal*, 81 (2016) 32-43.
- [154] M.A. Altaher, G.E. Andrews, B.M. Gibbs, S.A. Hadavi, H. Li, E. Jones, M. Mercer, Comparison of Gaseous and Particulate Emissions from Wood Pellet and Oil Fired Combustion for the same Heat Input, in: *The 10th European Conference on Industrial Furnaces and Boilers (INFUB-10)*, Porto, Portugal, 2015.
- [155] J. Goo, Study on the real-time size distribution of smoke particles for each fire stage by using a steady-state tube furnace method, *Fire Safety Journal*, 78 (2015) 96-101.
- [156] G.E. Andrews, B. Daham, M.D. Mmolawa, S. Boulter, J. Mitchell, J. Ledger, W. Gunamusa, R.A. Boreham, H.N. Phylaktou, Toxic Gases Emissions from Air Starved Fires, in: A.o.F.S. Science (Ed.) *8th Symposium on Fire Safety Science*, 2005.
- [157] D.A. Purser, 8 - Application of human and animal exposure studies to human fire safety, in: *Fire Toxicity*, Woodhead Publishing, 2010, pp. 282-345.
- [158] Y. Tsuchiya, K. Sumi, Evaluation of the toxicity of combustion products, *Fire and flammability*, (1972) 356-362.
- [159] B.C. Levin, New research avenues in toxicology: 7-gas N-gas model, toxicant suppressants, and genetic toxicology, *Toxicology*, 115 (1996) 89-106.
- [160] V. Babrauskas, Fire safety improvements in the combustion toxicity area: is there a role for LC50 tests?, *Fire and Materials*, 24 (2000) 113-119.
- [161] V. Babrauskas, R.G. Gann, B.C. Levin, M. Paabo, R.H. Harris, R.D. Peacock, S. Yusa, A methodology for obtaining and using toxic potency data for fire hazard analysis, *Fire Safety Journal*, 31 (1998) 345-358.
- [162] D. Purser, Validation of additive models for lethal toxicity of fire effluent mixtures, *Polymer Degradation and Stability*, 97 (2012) 2552-2561.
- [163] D.A. Purser, J.A. Purser, HCN Yields and Fate of Fuel Nitrogen for Materials under Different Combustion Conditions in the ISO 19700 Tube Furnace and Large-scale Fires in: *9th International Symposium on Fire Safety Science*, International Association for Fire Safety Science University of Karlsruhe, Germany, 2008, pp. 1117-1128.
- [164] V. Babrauskas, B.C. Levin, R.G. Gann, M. Paabo, R.H. Harris, R.D. Peacock, Toxic Potency measurement for Fire Hazard Analysis, in: *Special Publication 827*, National Institute of Standards and Technology. NIST, Gaithersburg, MD, 1991.
- [165] H.L. Kaplan, G.E. Hartzell, Modeling of Toxicological Effects of Fire Gases: I. Incapacitating Effects of Narcotic Fire Gases, *Journal of Fire Sciences*, 2 (1984) 286-305.
- [166] A.A. Stec, 15 - Estimation of toxicity during burning of common materials, in: *Fire Toxicity*, Woodhead Publishing, 2010, pp. 541-558.

- [167] D.A. Purser, Toxic product yields and hazard assessment for fully enclosed design fires, *Polymer International*, 49 (2000) 1232-1255.
- [168] EH40/2005, *Workplace Exposure Limits*, in, 2005.
- [169] G.E. Andrews, Fire Combustion Products and Toxicity as a Function of Ventilation Conditions, in, University of Leeds, 2008.
- [170] OSHA, Permissible Exposure Limits – Annotated Tables, in, US Department of Labor, Washington.
- [171] ACGIH, 6th edition of the Documentation of the Threshold Limit Values and Biological Exposure Indices, in, ACGIH, Cincinnati, 1997.
- [172] NIOSH, NIOSH respirator selection logic, in: P.H.S. U.S. Department of Health and Human Services, Centers for Disease Control (Ed.), National Institute for Occupational Safety and Health, DHHS (NIOSH), Cincinnati, OH, 2004.
- [173] N.R. Council, Acute Exposure Guideline Levels for Selected Airborne Chemicals. 2015:, in, The National Academies Press, 2015.
- [174] D.A. Purser, J.L. McAllister, Assessment of Hazards to Occupants from Smoke, Toxic Gases, and Heat, in: e.a. M.J. Hurley (Ed.) *SFPE handbook of fire protection engineering*, Springer, New York, 2016, pp. 2308-2428.
- [175] ISO, BS ISO 13344:2015: Estimation of the lethal toxic potency of fire effluents, in, British Standards Institute, 13344:2015.
- [176] G.E. Andrews, S. Boulter, G. Burell, M. Cox, B. Daham, H. Li, H.N. Phylaktou, Toxic Gas Measurements Using FTIR for Combustion of COH Materials in Air Starved Enclosed Fires, in: Third European Combustion Meeting ECM, 2007.
- [177] P. Blomqvist, M.S. McNamee, A.A. Stec, D. Gylestam, D. Karlsson, Characterisation of Fire Generated Particles, in: BRANDFORSK project, SP Technical Research Institute of Sweden, Sweden, 2010.
- [178] G.E. Andrews, B. Daham, M.D. Mmolawa, S. Boulter, J. Mitchell, G. Burrell, J. Ledger, W. Gunamusa, R.A. Boreham, H.N. Phylaktou, FTIR Investigations of Toxic Gases in Air Starved Enclosed Fires, in: D.a.L.B.Y. Gottuk (Ed.) 8th International Symposium on Fire Safety Science, International Association for Fire Safety Science, Beijing, 2006.
- [179] C.R. Shaddix, Correcting Thermocouple Measurements for Radiation Loss, in: 33rd National Heat Transfer Conference, Albuquerque, NM, 1999.
- [180] A.A. Alarifi, J. Dave, H.N. Phylaktou, O.A. Aljumaiah, G.E. Andrews, Effects of fire-fighting on a fully developed compartment fire: Temperatures and emissions, *Fire Safety Journal*, 68 (2014) 71-80.
- [181] A.A. Alarifi, H.N. Phylaktou, G.E. Andrews, Heated Raw Gas Sampling with Heated FTIR Analysis of Toxic Effluents from Small and Large Scale Fire Tests, in: 10th Asia-Oceania Symposium on Fire Science and Technology, IAFSS, Tsukuba, Japan, 2015.
- [182] M. Janssens, Calorimetry, in: P.J. DiNenno (Ed.) *SFPE Handbook of Fire Protection Engineering*, National Fire Protection Association, Quincy, MA, 2002, pp. 3-38.
- [183] D.A. Purser, Toxic Assessment of Combustion Products, in: P.J. Dinenno (Ed.) *SFPE Handbook of Fire Protection Engineering*, National Fire Protection Association, Quincy, MA, 2002, pp. 2-83-82-171.
- [184] G.E. Hartzell, Engineering analysis of hazards to life safety in fires: the fire effluent toxicity component, *Safety Science*, 38 (2001) 147-155.
- [185] D.A. Purser, J.A. Purser, HCN Yields and Fate of Fuel Nitrogen for Materials under Different Combustion Conditions in the ISO 19700 Tube Furnace and Large-Scale Fires, in: 9th International Symposium on Fire Safety Science, International Association for Fire Safety Science, University of Karlsruhe, Germany, 2008, pp. 1117-1128.
- [186] J.J.N. Lingard, E.L. Agus, D.T. Young, G.E. Andrews, A.S. Tomlin, Observations of urban airborne particle number concentrations during rush-hour conditions: analysis of the number

- based size distributions and modal parameters, *Journal of environmental monitoring* : JEM, 8 (2006) 1203.
- [187] V. Babrauskas, *Ten Years of Heat Release Research with the Cone Calorimeter*, 1993.
- [188] B. Scharrel, T.R. Hull, *Development of fire-retarded materials—Interpretation of cone calorimeter data*, *Fire and Materials*, 31 (2007) 327-354.
- [189] K.W. Flecknoe-Brown, K. Livkiss, P. Van Hees, *Experimental and Numerical Investigation on Fire Behaviour of Foam/Fabric Composites*, in: 15th International Conference, *Fire and Materials*, Interscience Communications, San Francisco, USA, 2017, pp. 240-253.
- [190] H.E.j. Moran, *Effectiveness of Water Mists for Protection from Radiant Heat Ignition*, in: *NRL Report 5439*, US Naval Research Laboratory, Washington, 1960.
- [191] H. Shoub, E.W. Bender, *Radiant Ignition of Wall Finish Materials in Small Home*, in: *NBS 8172*, National Bureau of Standards, Washington, DC, 1964.
- [192] H. Li, A. Lea-Langton, G.E. Andrews, M. Thompson, C. Musungu, *Comparison of Exhaust Emissions and Particulate Size Distribution for Diesel, Biodiesel and Cooking Oil from a Heavy Duty DI Diesel Engine*, in, *SAE International*, 2008.
- [193] B. Mustafa, M. Mat Kiah, G. Andrews, H. Phylaktou, H. Li, *Smoke Particle Size Distribution in Pine Wood Fires*, in, *Saint-Petersburg Polytechnic University Press*, 2019, pp. 930-939. ISBN 978-935-7422-6498-7429.
- [194] O. Aljumaiah, G.E. Andrews, A. Abdullahi, B.G. Mustafa, H.N. Phylaktou, *Wood Crib Fires under High Temperature Low Oxygen Conditions*, in: D. Bradley, G. Makhviladze, V. Molkov (Eds.) *6th International Seminar on Fire and Explosion Hazards*, Research Publishing, Leeds, United Kingdom, 2010, pp. 1044-1055.
- [195] D.A. Purser, A.A. Stec, T.R. Hull, 2 - *Fire scenarios and combustion conditions*, in: *Fire Toxicity*, Woodhead Publishing, 2010, pp. 26-47.
- [196] A. Alarifi, H.N. Phylaktou, G.E. Andrews, J. Dave, O. Aljumaiah, *Toxic Gas Emissions from a Timber-Pallet-Stack Fire in a Full-Scale Compartment*, Springer, 2017.
- [197] C.L. Mealy, M.E. Benfer, D.T. Gottuk, *FIRE DYNAMICS AND FORENSIC ANALYSIS OF LIQUID FUEL FIRES* in, *Hughes Associates, Inc*, Baltimore, 2011.
- [198] J.M. Kuchta, R.J. Cato, *Ignition and Flammability Properties of Lubricants*, *SAE Transactions*, 77 (1968) 1008-1020.
- [199] R.D. Grace, *Chapter Four - Special Conditions Problems and Procedures in Well Control*, in: R.D. Grace (Ed.) *Blowout and Well Control Handbook (Second Edition)*, Gulf Professional Publishing, Boston, 2017, pp. 121-209.
- [200] I. Sutton, *Chapter 4 - Consequence and likelihood analysis*, in: I. Sutton (Ed.) *Process Risk and Reliability Management*, William Andrew Publishing, Oxford, 2010, pp. 191-276.
- [201] J.G. Quintiere, *Principles of Fire Behavior*, Delmar Publishers, 1998.